

*Ph.D. thesis*

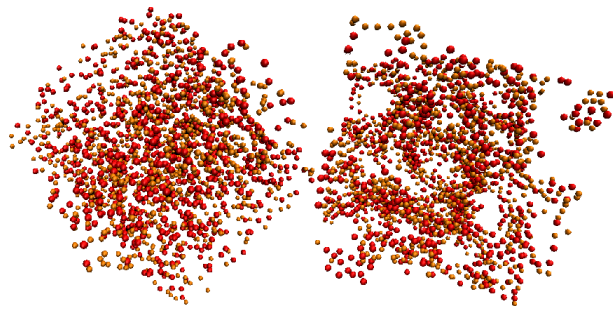
---

---

**Viscous liquid dynamics in and out of equilibrium**  
*from isomorphous curves in the phase diagram to effective  
temperatures in ageing*

---

---



Nicoletta Gnan

Supervisor: Thomas B. Schrøder

*Danish National Research Foundation Centre "Glass and Time",  
IMFUFA, Department of Science, Systems and Models,  
Roskilde University, Denmark*



---

## Abstract

This doctoral thesis has eight companion papers.

The main part of the work is based on the study of strongly correlating liquids and isomorphs. It is shown the existence of a class of liquids for which it has been observed a strong correlation between the fluctuations of the potential energy and of the virial at constant volume. This class of liquids is called “strongly correlating liquids” (SCLs). These liquids are characterized by two important numbers: the coefficient  $R$  that quantifies the correlation (strong correlation corresponds to  $R > 0.9$ ) and  $\gamma$  that corresponds to the slope resulting from plotting the fluctuations of the virial against those of the potential energy.

A perfect correlation is trivially found in soft-spheres whose potential is an inverse power-law (IPL); in such case the potential energy is proportional to the virial through a factor given by  $\gamma = n_{IPL}/3$  where  $n_{IPL}$  is the exponent of the inverse power-law. For other SCLs instead an explanation of the strong correlation is given if the pair potential can be approximated with an *extended inverse power-law* (eIPL), i.e. an inverse power-law plus a linear term. In this approximation, the correlation is explained by the fact that only the inverse power-law term contributes to the fluctuations and therefore to strong correlation.

In this work it is shown that SCLs inherits to good approximation a number of properties from IPLs. In particular simulations show that SCLs surprisingly inherit scale invariance, i.e. state points with the same  $\rho^\gamma/T$  have a number of thermodynamic, dynamic and structural properties that are the same in scaled units. The curves identified by the relation above are characterized by state points having proportional Boltzmann factors and are called “isomorphs”. An extended theoretical and numerical investigation has been done to test the isomorph properties which can be found not only at equilibrium but even in the aging regime. The equations of isomorphs for generalized Lennard-Jones systems are derived and for this case it is shown that the shape of isomorphs depends only on the exponents of the potential and not on its parameters.

To investigate the properties of isomorphs in the glassy state the fluctuation dissipation relation (FDR) is used showing that the glassy line defined by the effective temperature calculated via the FDR is an isomorph. Moreover it is shown that from a single aging experiment (i.e. from a temperature/density jump) it is possible to predict with a very good approximation the effective temperatures of all the aging experiments that can be performed.

Part of the thesis is dedicated to the energy landscape approach for the study of supercooled liquids. In particular the attention is focused on the evolution in time of the probability distribution function (PDF) of inherent states (IS) energy during temperature jumps from low to high temperatures. It is shown that small systems exhibit a double peak distribution of metabasins energy in analogy with the trap model. For large systems instead this effect is smeared out and the time evolution of the PDF suggests that the big system can be thought as a superposition of weakly interacting subsystems having - on average - the same mean value and the same variance of the PDF of the large system.

---

### Abstract in Danish

Denne Ph.D afhandling har otte ledsagende artikler.

Hovedparten af dette arbejde omhandler stærkt korrelerende væsker og isomorfer. Afhandlingen viser eksistensen af en klasse af væsker hvor man har observeret stærke korrelationer mellem fluktuationerne af den potentielle energi og virialet (den konfigurationelle del af tryk ket) ved konstant volume. Denne klasse af væsker betegnes "stærkt korrelerende væsker" (SKVs). Disse væsker er karakteriseret ved to vigtige tal: korrelations koefficienten  $R$  der er et mål for selve korrelationen (stærk korrelation svarer til  $R > 0.9$ ) og  $\gamma$  der svarer til hældningen af plottet mellem fluktuationerne af den potentielle energi mod virialet.

En perfekt korrelation er trivielt fundet i såkaldte "soft-spheres" hvis potentiale er en invers potens funktion (IPF); i dette tilfælde er den potentielle energi proportional med virialet gennem en faktor givet ved  $\gamma = n_{IPF}/3$  hvor  $n_{IPF}$  er eksponenten af den inverse potens funktion. For andre (SKVs) kan den stærke korrelation forklares hvis par potentialet kan approksimeres ved en *udvidet invers potens funktion* (uIPF) d.v.s. en invers potens funktion plus et lineært led. I denne approksimation er korrelationen forklaret ved at det kun er den inverse potens funktion der bidrager til fluktuationerne og derfor den stærke korrelation.

I dette arbejde er det vist at SKVs nedarver, til en god tilnærmelse, en række egenskaber fra IPFs. Simulationer viser specifikt at SKV overraskende nedarver skala invarians, d.v.s. tilstands punkter med samme  $\rho^\gamma/T$  har en række termodynamiske, dynamiske og strukturelle egenskaber der er ens i skalerede enheder. Kurverne der beskriver denne relation er karakteriseret ved at have proportionelle Boltzmann faktorer og er kaldet "isomorfer". En gennemgribende teoretisk og numerisk undersøgelse er udført for at teste disse isomorfers egenskaber som eksisterer under ligevægt og ude af ligevægt. Ligningerne for isomorfer for generaliserede Lennard-Jones systemer er udledt og for dette tilfælde er det vist at isomorfernes form kun afhænger af eksponenterne af potentialet og ikke af konstanterne der indgår.

For at undersøge isomorfernes egenskaber i glastilstanden er fluktuations dissipation relationen (FDR) brugt til at vise at glas linjen defineret ved den effektive temperatur, beregnet via FDR, er en isomorf. Udover er det vist at det er muligt ud fra et enkelt ældnings eksperiment (d.v.s fra et temperatur eller densitets hop) at forudsige, med god præcision, den effektive temperatur af alle ældnings eksperimenter der kan foretages.

En del af denne afhandling er dedikeret til analyse af underafkølede vokser via det potentielle energi-landskab. Specielt er fokus rettet mod tidsudviklingen af sandsynligheds fordelinger af såkaldte "inherent energies" ved hop fra lav til høj temperatur. Det er vist at små systemer udviser en dobbel energi distribution af metabassinger i analogi med "trap" modellen. For store systemer er denne effekt udvisket og tidsudviklingen af sandsynlighedsfordelingen antyder at store systemer er en superposition af stærkt vekselvirkende under-systemer der har - i gennemsnit - den samme gennemsnits værdi og samme varians af sandsynligheds fordelingen som det store system.

# Preface

This work is based on the research carried out as a Ph.D. student in the Danish national research foundation centre for viscous liquid dynamics “Glass and Time”. The Ph.D. program lasted three years: it was initiated May 1st 2007 and the thesis was submitted April 29th 2010. The thesis consists of six chapters. The aim of each chapter is to guide the reader through the understanding of the papers listed below. Parts of the papers are elaborated in the chapters while some other parts are not discussed here: the reader can however integrate the reading consulting the papers at the end of the thesis.

## Papers

This is a list of the companion papers reprinted at the end of the thesis.

**Paper I** Nicholas P. Bailey, Ulf R. Pedersen, Nicoletta Gnan, Thomas B. Schröder, Jeppe C. Dyre, *Pressure-energy correlations in liquids. I. Results from computer simulations.* J. Chem. Phys. **129**, 184507,(2008).

**Paper II** Nicholas P. Bailey, Ulf R. Pedersen, Nicoletta Gnan, Thomas B. Schröder, Jeppe C. Dyre, *Pressure-energy correlations in liquids. II. Analysis and consequences.* J. Chem. Phys. **129**, 184508, (2008).

**Paper III** Thomas B. Schröder, Nicholas P. Bailey, Ulf R. Pedersen, Nicoletta Gnan, Jeppe C. Dyre, *Pressure-energy correlations in liquids. III. Statistical mechanics and thermodynamics of liquids with hidden scale invariance.* J. Chem. Phys. **131**, 234503, (2009).

**Paper IV** Nicoletta Gnan, Thomas B. Schröder, Ulf R. Pedersen, Nicholas P. Bailey, Jeppe C. Dyre, *Pressure-energy correlations in liquids. IV. “Isomorphs” in liquid state diagrams.* J. Chem. Phys. **131**, 234504, (2009).

**Paper V** Thomas B. Schröder, Nicoletta Gnan, Nicholas P. Bailey, Ulf R. Pedersen, Jeppe C. Dyre, *Pressure-energy correlations in liquids. V. “Isomorphs” in generalized Lennard-Jones systems.* arXiv:1004.5142 (2010).

**Paper VI** Ulf R. Pedersen, Nicoletta Gnan, Nicholas P. Bailey, Thomas B. Schröder, Jeppe C. Dyre, *Strongly correlating liquids and their isomorphs.* arXiv:1004.1182 (2010).

**Paper VII** Christian Rehwald, Nicoletta Gnan, Andreas Heuer, Thomas B. Schröder, Jeppe Dyre and Gregor Diezemann, *Aging effects manifested in*

*the potential energy landscape of a model glassformer.* arXiv:1004.4738 (2010).

**Paper VIII** Nicoletta Gnan, Claudio Maggi, Thomas B. Schröder, Jeppe C. Dyre, *Predicting the effective temperature of a glass.* Phys. Rev. Lett. **104**, 125902 (2010).

## Acknowledgments

First I would like to thank my supervisor Thomas Schröder for having had the patience of proofreading the whole thesis...thanks a lot Thomas!

Then I would like to thank all the members of the “Glass and Time” group: the professors and associate professors Jeppe Dyre, Tage Christensen, Niels Boye Olsen, Kristine Niss and Søren Toxvaerd, the post-docs Nicholas Bailey and Bo Jakobsen, the graduated Ph.D. students Albena Nielsen and Ulf Pedersen, the Ph.D. students Tina Hecksher, Jon Papini, Ditte Gundermann, Lasse Boehling (thanks for the Danish translation of the abstract!) and Trond Ingebrigsten, the IT specialist Heine Larsen and the technical staff Ib Høst Pedersen, Ebbe H. Larsen, Torben Rasmussen and Preben Olsen. A special thank to Kirsten Høffding for the help with bureaucracy. I also would like to thank to the “curly hair women in science” association and more in general all the guys at the IMFUFA department: Neslihan Saglanmak, Gitte Jensen, Tomas Hecksher, Mario Sanchez, Luna Lomonaco, Morten Andersen and Frank Vinther.

Finally I would like to thank my family for the huge moral support and Claudio Maggi for having shared this adventure with me.

# Contents

<b>Preface</b>	<b>v</b>
Papers . . . . .	v
Acknowledgments . . . . .	vi
<b>Contents</b>	<b>vii</b>
<b>1 Introduction</b>	<b>1</b>
1.1 From liquids to glasses . . . . .	1
1.2 Simulations of liquids and supercooled liquids . . . . .	5
1.3 Outline of the thesis . . . . .	8
<b>2 Strongly correlating liquids</b>	<b>11</b>
2.1 Potential energy - virial fluctuations and their correlation . . . . .	11
2.1.1 The parameter $\gamma$ . . . . .	12
2.2 Causes of strong correlation . . . . .	14
2.2.1 A trivial case: the soft-spheres potential . . . . .	14
2.2.2 The extended inverse power-law potential . . . . .	15
2.3 Which systems are strongly correlating? . . . . .	19
2.3.1 A case of negative correlation: the square-well system . . . . .	21
2.3.2 Competition between different interactions: the water case . . . . .	24
<b>3 Density scaling of strongly correlating liquids and isomorphs</b>	<b>29</b>
3.1 Inheritance of scaling properties by generalized IPL potentials . . . . .	29
3.1.1 Density scaling for IPL potentials . . . . .	29
3.2 Hidden scale invariance for Strongly correlating liquids . . . . .	33
3.3 Definition of isomorphs . . . . .	34
3.4 How to identify isomorphs . . . . .	36
3.5 Isomorph properties . . . . .	39
3.5.1 Statistical thermodynamics of isomorphs . . . . .	39
3.6 Static equilibrium properties . . . . .	41
3.7 Equilibrium dynamics . . . . .	44
3.8 A breakdown of the isomorph theory: the WCA potential . . . . .	47
3.9 Equations of isomorphs in the U-W plane . . . . .	55
3.10 The <i>master</i> isomorph . . . . .	58
3.11 Equation of state of generalized Lennard-Jones potentials . . . . .	60

<b>4</b>	<b>Aging in strongly correlating liquids</b>	<b>65</b>
4.1	Temperature down-jumps in the $U$ - $W$ phase diagram . . . . .	65
4.2	Temperature and density jumps in the $U$ - $W$ phase diagram . .	66
4.3	Aging in the energy landscape . . . . .	72
4.3.1	The PEL approach . . . . .	72
4.4	Aging in the PEL after temperature down-jumps and up-jumps	73
<b>5</b>	<b>FDR in strongly correlating liquids</b>	<b>81</b>
5.1	The quest for an extra parameter . . . . .	81
5.2	FDT and its generalization . . . . .	83
5.3	Measuring the effective temperature in simulations . . . . .	85
5.4	Predicting the effective temperature in strongly correlating liquids	89
5.5	Equivalence between crunches and quenches . . . . .	90
<b>6</b>	<b>Outlook</b>	<b>99</b>
	<b>Appendix</b>	<b>101</b>
<b>A</b>	<b>Invariance of the Liouville operator</b>	<b>101</b>
<b>B</b>	<b>Harmonic oscillator coupled to a system</b>	<b>103</b>
<b>C</b>	<b>Equivalent formulations of FDT</b>	<b>107</b>
C.1	Energy bond formulation . . . . .	107
C.2	Creep function formulation of FDT . . . . .	108
C.3	Equivalence of the formulations . . . . .	108
<b>D</b>	<b>The Lennard-Jones Gaussian</b>	<b>111</b>
	<b>Bibliography</b>	<b>115</b>
	<b>Papers</b>	<b>125</b>
	Paper I . . . . .	127
	Paper II . . . . .	141
	Paper III . . . . .	161
	Paper IV . . . . .	179
	Paper V . . . . .	197
	Paper VI . . . . .	205
	Paper VII . . . . .	217
	Paper VIII . . . . .	233

# Chapter 1

## Introduction

### 1.1 Equilibrium and off-equilibrium: from liquids to glasses

When a liquid is cooled below the melting temperature  $T_m$  a first order phase transition occurs: the liquid turns into a crystal. A naive way of describing liquids and crystals (or solids in general) comes from everyday life where it is well known that liquids are able to flow while solids are not. In physics the ability of flowing is related to a quantity called *viscosity*<sup>1</sup>[Mauro *et al.* (2009), Dyre (2006), Angell (1995)] that can be measured in real and computer experiments. Thus we can characterize the two states in terms of the viscosity: a liquid has a low viscosity while a solid has a large resistance to flow, i.e. high viscosity.

However it is well known from both experimental and simulation results that under certain conditions the liquid does not crystallize below  $T_m$ , but it enters into a metastable phase known as *supercooled* phase [Elliot (1983), Debenedetti (1996)]. Although the thermodynamic stable state in that temperatures region is the crystal, none of the observables that we measure can tell us if the system is in a metastable state since it is still possible to equilibrate the liquid and the standard thermodynamic approach still applies to it. Thus we will refer to the metastable state as an equilibrium state to distinguish that from the off-equilibrium properties of liquids.

An explanation for the occurring of the metastable state can be traced back into the classical nucleation theory [Volmer & Weber (1926), Becker & Doring (1935), Cavagna (2009), Schmelzer (2005)]. According to that the Gibbs free energy change  $\Delta G(R)$  due to the formation of a crystal nucleus of size  $R$  is given by two terms: a free energy density difference  $\delta g$  between the metastable phase and the crystal stable phase and a second term that represents the energy cost for building an interface  $\sigma$  between the liquid and the solid phases:  $\Delta G(R) = \sigma R^{d-1} - \delta g R^d$  (here  $d$  is the dimensionality of the system). Below a given value of  $R$  the interface value dominates and therefore the nuclei formed are

---

<sup>1</sup>Generally the viscosity is defined in terms of shear stress and shear strain. Consider a parallel and uniform flow. We can think of applying a small force (shear) along the x-axis whose consequence is to produce a velocity gradient  $\dot{\gamma} = \partial v / \partial y$  (shear strain) among the layers of the fluid. The fluid responds to the shear strain giving rise to a shear stress  $\sigma$  proportional to the strain :  $\sigma = \eta \dot{\gamma}$  where  $\eta$  is the viscosity.

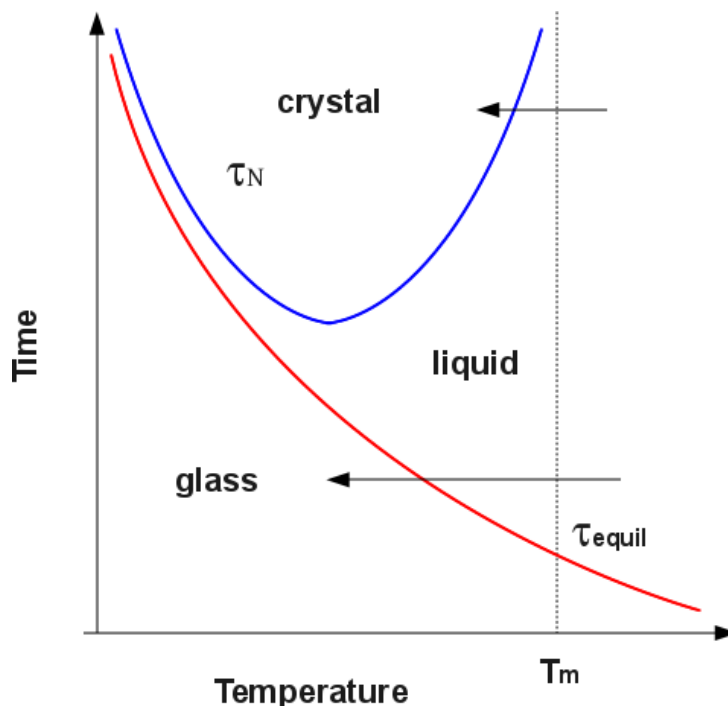


Figure 1.1: nucleation characteristic time  $\tau_N$  and relaxation time of the liquid  $\tau_{equil}$  as a function of temperature  $T$ . According to the classical nucleation theory the characteristic nucleation time must diverge at the melting temperature and at  $T = 0$ . Note that if the cooling rate is too small then the nucleation curve will be crossed and the liquid will turn into a crystal. To avoid nucleation and require the equilibrium condition for the liquid below  $T_m$  during the cooling procedure, the nucleation line should be avoided and the liquid relaxation time's curve has not to be crossed. If the equilibrium curve is crossed than the system appears frozen since has no time to relax: the liquid has become a glass.

not stable. Only when the volume term takes over the interface term then a stable nucleus can be formed: this situation occurs for a critical value of the size of the nucleus  $R_c$  corresponding to the value of  $R$  that maximizes the the Gibbs free energy change. It is possible to define a characteristic nucleation time  $\tau_N = \tau_0 \exp(\frac{\Delta G(R_c)}{k_B T})$  associated to  $R_c$ . This means that - all the times that the cooling rate is faster than the nucleation rate - the nucleation process can be avoided and the system remains a liquid even below  $T_m$  (see fig. 1.1).

Thus the nucleation curve gives informations on how to avoid the crystal formation. Lets consider now the case in which crystallization is avoided and the system is cooled with a constant cooling rate. We can again make use of the viscosity to describe what happens to the supercooled liquid. When the system is brought down to the deep supercooled regime the viscosity increases enormously within a small decrease of temperature. This corresponds to the situation in which the relaxation time of the supercooled liquid is of the order

of the observation time (for a high temperature liquid instead the relaxation time is much smaller than the experimental time). It is natural to wonder what happens to the system if we keep cooling it until the relaxation time exceeds the experimental time window i.e. when the  $\tau_{equil}$  curve of fig. 1.1 is crossed. When this happens the system looks frozen in a liquid-like state since it has no time to respond to the temperature change. The system is then *out-of-equilibrium* and the phenomenon observed is called *glass transition* since the liquid becomes a *glass*. The temperature associated to the glass transition is the *glass transition temperature*  $T_g$ . Note that this is not a thermodynamic transition as in the case of the crystal but rather a *dynamic transition* and  $T_g$  can be considered as a reference temperature introduced for experimental reasons [Moynihan *et al.* (1974)]. How do we characterize a glass? From the phenomenology of the glass transition described above a glass behaves like a mechanically stable off-equilibrium system. This means that a glass shows some properties of the crystalline state (the mechanical rigidity) but - on the other hand - it differs from the crystal since it has a disordered structure at the molecular level like in liquids.

The arrested phase is a consequence of the fact that the system has no time to explore the entire phase space: it remains instead trapped in one part of it as in the case of the crystal. This condition is called *non-ergodicity*. It is important to remark that both the crystal and the glass are non-ergodic states but - while the crystal represents a thermodynamic equilibrium state<sup>2</sup> - the glass is off-equilibrium.

Our first definition of the solid state (and then of the glass) involved the viscosity. This quantity is also useful for classifying structural glasses in two main different categories introduced by A. Angell [Angell (1985)]. If we plot in fact the logarithm of the viscosity as a function of  $T_g/T$  we note that two main behaviors of the viscosity appear. The first one is smooth, i.e. the viscosity increase can be described through an exponential. Viscous liquids with this behavior are termed *strong* liquids (i.e. they form strong glasses). When the behavior departs from an exponential law the viscous liquid is called *fragile*.<sup>3</sup>

This classification is important for showing the different sensitivity of liquids structure to changes in temperature; in particular fragile liquids whose viscosity is described by the Volger-Fulcher law  $\eta = A \exp[B/(T - T_0)]$  have a structure that is sensitive to changes in temperature compared to the structure of strong glasses characterized by an Arrhenius law for the viscosity  $\eta = A \exp[E/k_B T]$  [Debenedetti & Stillinger (2001), Hecksher *et al.* (2008)].

If the main feature of glassiness is to have a disordered arrested phase then glassy behavior can be encountered in many different systems, sometimes quite different from the structural glasses (i.e. mainly atomic and molecular glasses) whose behavior we described so far. We can find indeed a big variety of glassformers that can be divided in - mainly - three different categories:

1. “Hard ” (structural) glasses: characterized by a large viscosity. Examples of this category are silica and inorganic molecular glasses, metallic glasses, polymers etc...

<sup>2</sup>i.e. the system is in the minimum of its thermodynamic potential.

<sup>3</sup> In both cases the glass transition temperature is the temperature at which the viscosity is  $10^{13} Poise$ .

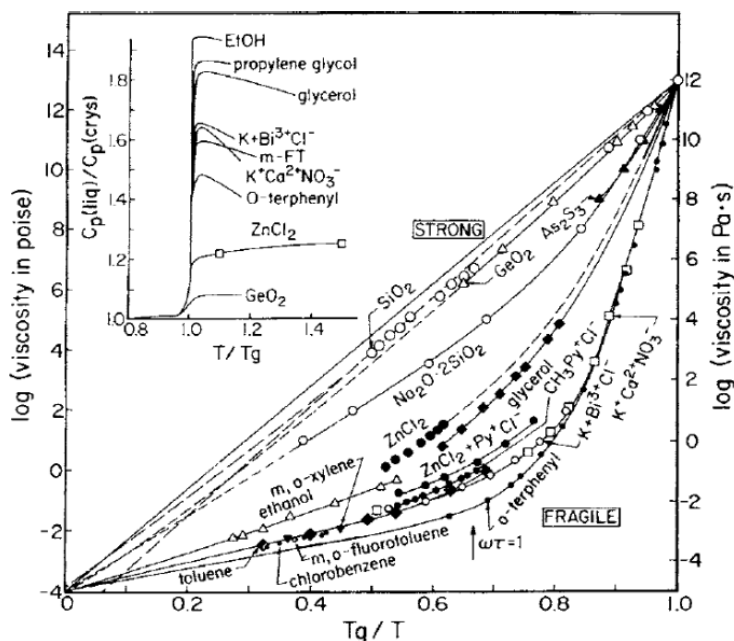


Figure 1.2: Logarithm of the viscosity as a function of the inverse of the temperature. The plot is known as the *Angell's plot*. The scope of this plot is to show that supercooled liquids behave in mainly two different way while approaching the glass transition temperature. A first category is given by the *strong liquids* characterized by Arrhenius behavior of the viscosity  $\eta$  while liquids of the second class (i.e. fragile liquids) have the viscosity behavior that can be fitted by the Volger-Fulcher equation (see the text). If we define the apparent activation energy as  $E = d \ln(\eta) / d(1/T)$  then we find that - while in strong liquids the activation energy is independent of  $T$  - it increases when  $T$  decreases for fragile liquids. Figure taken from reference [Dyre (2006)].

2. "soft " glasses: characterized by a small viscosity. Soft glasses can be foams, granulars, colloidal suspensions, emulsions, etc...
3. Other kind of glasses for which does not make sense to define the viscosity: spin glasses, orientational glasses, etc...

In this thesis we will deal mainly with hard glasses and soft glasses leaving the interesting category of spin systems out of the discussion.

Even though glassiness is a well known state of matter a complete understanding of it represents an open challenge in condensed matter physics. Then we could wonder what is the best way to characterize glasses. The main approaches for understanding and characterizing the glassy state are two: the first one consists of understanding the slowing down mechanism studying thermodynamic, dynamic and structural properties of supercooled liquids. The second root corresponds in developing an off-equilibrium statistical mechanics approach introducing an extra parameter in the definition of the thermodynamic potentials. We will present both the approaches in this thesis.

## 1.2 Simulations of liquids and supercooled liquids

Computer simulations are a powerful tool for probing microscopical behavior of liquids and supercooled liquids. As in real experiments, also in simulations a number of control parameters can be set in order to study static and dynamic quantities of the system. For instance in this work most of the simulations have been performed fixing the volume  $V$ , the number of particles  $N$  and controlling the temperature  $T$  through a thermostat. In statistical mechanics this would correspond to study the *canonical ensemble* for which a thermodynamic approach is well defined [Frenkel & Smith (2002)]. Alternatively we can think of controlling the total energy instead of the temperature (NVE simulations) or the pressure instead of the volume (NpT simulations). The main advantage respect to experiments is that in simulations it is possible to follow the trajectory of each particle (even within a time window that is of hundreds of ns). This allow to define some suitable observables for probing the average single particle dynamics. Examples are the self-intermediate scattering function  $F_s(\mathbf{q}, t) = \langle e^{i\mathbf{q} \cdot (\mathbf{r}_n(t) - \mathbf{r}_n(0))} \rangle$  (i.e the density-density correlation function in the wave vector space, see fig. 1.3) and the mean square displacement  $\langle \Delta \mathbf{r}^2 \rangle = \langle |\mathbf{r}_i(t) - \mathbf{r}_i(0)|^2 \rangle$  (i.e. the velocity-velocity correlation function, see fig. 1.4). In both cases the index  $i$  corresponds to the  $i$ -th particle and the average is performed over all the particles in the system. At high temperature (i.e. in the stable liquid state) the dynamics is well described by a gaussian (Fickian) process. The mean square displacement displays two different behaviors corresponding to two different regimes: the first regime represents the ballistic motion - i.e. the free motion of a particle - occurring for distances much smaller than the interparticle distance. In this region the mean square displacement is a quadratic function in time. The second regime corresponds to the Fickian diffusion. In fact if the distribution of particles displacement  $G_s(\Delta \mathbf{r}, t) = \exp(-|\Delta \mathbf{r}|^2/4Dt)/(4\pi Dt)^{3/2}$  is an isotropic gaussian process ( $D$  is the diffusion constant) then from the mean square displacement follows a simple diffusion expression:  $\langle \Delta \mathbf{r}^2 \rangle = \int d(\Delta \mathbf{r}) G_s(\Delta \mathbf{r}, t) \Delta \mathbf{r}^2 = 6Dt$ . Hence in this case the mean square displacement is linear in time. The self-intermediate scattering function shows the same informations of the mean square displacement since  $F_s(q, t) = \int d(\Delta \mathbf{r}) G_s(\Delta \mathbf{r}, t) e^{i\mathbf{q} \cdot \Delta \mathbf{r}} = \exp(-q^2 Dt)$ . Moreover an important quantity that can be extracted from  $F_s(q, t)$  is the relaxation time  $\tau$  which is roughly a measure of the time that a particle takes to move more than the interparticle distance.  $\tau$  is related to the diffusion constant through a simple dispersion relation:  $\tau = q^{-2} D^{-1}$ . The crossover between the liquid and a supercooled liquid is marked by the emergence of a plateau indicating a slowing down of the particles motion and a separation of the time scales. It is well established that this plateau corresponds to the so called *cage effect* i.e. particles are “caged” by the surrounding particles and are forced to rattle inside a limited space for a long time instead of diffusing. The emergence of the plateau is accompanied by a change in the shape of the self-intermediate scattering function that is no longer an exponential function but becomes to a good approximation a stretched exponential  $F_s(q, t) \sim \exp[-(t/\tau)^\beta]$ . Moreover the dispersion relation is not valid anymore because of the break down of the Gaussian approximation and thus the relaxation process and the diffusion *decouple*. This is a direct consequence of the fact that the dynamics is no longer homogeneous but becomes *heterogeneous* [Berthier & Biroli (2009)].

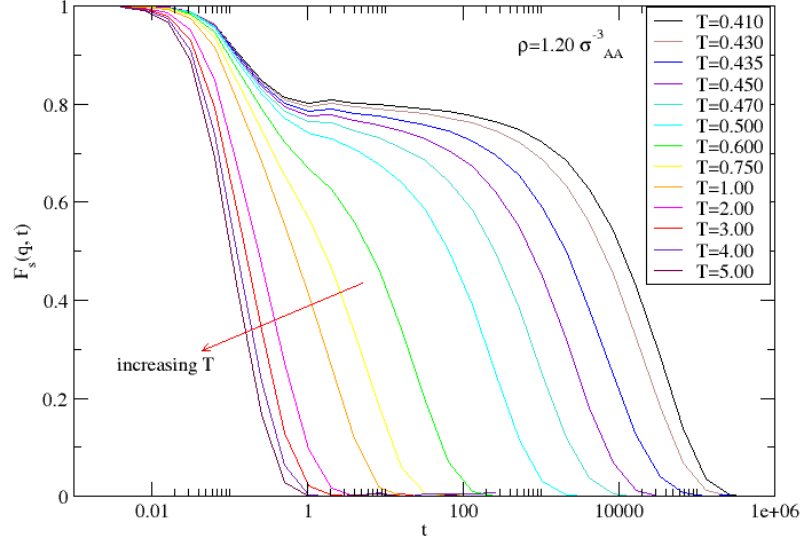


Figure 1.3: Self-intermediate scattering function  $F_s(\mathbf{q}, t) = \langle e^{i\mathbf{q} \cdot (\mathbf{r}_n(t) - \mathbf{r}_n(0))} \rangle$  for one specie of the Kob-Andersen binary Lennard-Jones system [Kob & Andersen (1994)]. The figure shows the big difference in the shape of the function going from a stable liquid state to the metastable supercooled liquid state. The main difference is given by the developing of a plateau indicating that the particles are caged by other particles (see the text). Another important feature is the change of the shape of the curves from an exponential  $F_s(\mathbf{q}, t) = Ae^{-t/\tau}$  to a stretched exponential  $F_s(\mathbf{q}, t) = Ae^{-(t/\tau)^\beta}$  indicating that the distribution probability of the displacement is no longer gaussian (i.e. homogeneous) but becomes heterogeneous.

An important difference between the liquid and the supercooled liquid in fact is that in the latter large spatial fluctuations of the dynamics appear. This means that in some parts of the system there are groups of particles moving very little, while in other regions their displacements after some time can be larger than the average (see fig. 1.5). This spatially varying motion can be quantified by a four-point susceptibility resulting from integrating the correlation function of the mobility field  $f(\mathbf{r}, t) = \sum_i f_i(t) \delta(\mathbf{r} - \mathbf{r}_i)$  (where  $f_i(t) = \exp[i\mathbf{q} \cdot (\mathbf{r}_i(t) - \mathbf{r}_i(0))]$ ):  $\chi_4(\mathbf{q}, t) = \int d\mathbf{r} \langle \delta f(\mathbf{0}, t) \delta f(\mathbf{r}, t) \rangle = N[\langle f^2(\mathbf{q}, t) \rangle - F_s^2(\mathbf{q}, t)]$  where  $f(\mathbf{q}, t) = (1/N) \sum_{j=1}^N \exp[i\mathbf{q} \cdot (\mathbf{r}_j(t) - \mathbf{r}_j(0))]$  (and  $F_s(\mathbf{q}, t) = \langle f(\mathbf{q}, t) \rangle$ ). This function contains informations about the typical fluctuation of the correlation function around its average value and provides the (time-dependent) size of the regions with a correlated dynamics. The four-point susceptibility defined in this way reveals the growth of fluctuations in the dynamics reaching a maximum at  $t \simeq \tau_\alpha$  and decaying to zero for  $t \rightarrow \infty$  as

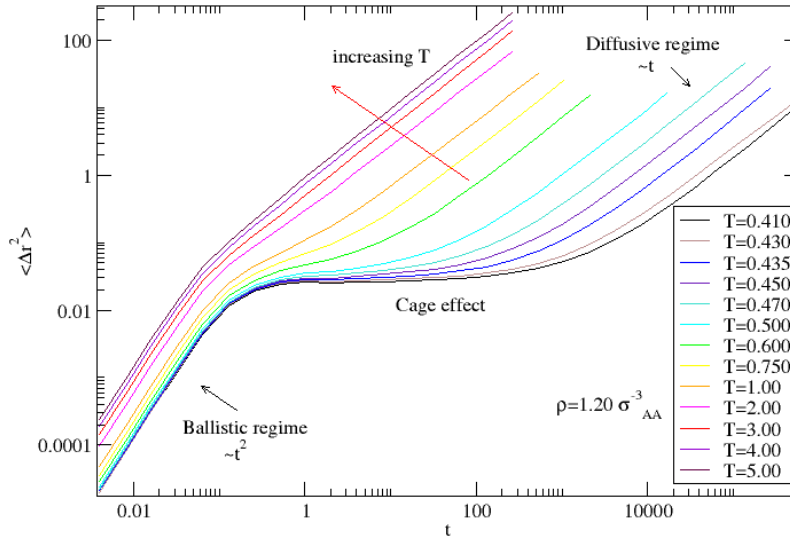


Figure 1.4: mean square displacement  $\langle \Delta \mathbf{r}^2 \rangle = \langle |\mathbf{r}_i(t) - \mathbf{r}_i(0)|^2 \rangle$  for one specie of the Kob-Andersen binary Lennard-Jones system [Kob & Andersen (1994)]. As in the case of the self-intermediate scattering function (see fig.1.3) a plateau appears in the crossover between the liquid and the supercooled liquid. In this case it is easy to identify the three different regimes characterizing particles motion: ballistic, caged and diffusive regime.

the system gets fully rearranged and all the particles have equally moved along large distances (see fig. 1.6) [Hurley & Harrowell (1995), Bennemann *et al.* (1999), Donati *et al.* (2002), Whitelam *et al.* (2004)].

So far we have discussed properties of supercooled liquids. At the beginning of this digression on glass-forming liquids it was stressed that if the observation time is much smaller than the relaxation time, the system appears frozen. In this case what we observe is an out-of-equilibrium system whose description through statistical thermodynamics still remains a challenge. The main feature of the off-equilibrium behavior of liquids is given by *aging*. During aging time translational invariance (TTI) does not hold anymore and the fluctuation-dissipation theorem is violated [Crisanti & Ritort (2003)]. A Consequence of TTI is that all the dynamic properties depend on the observation time that is usually called “waiting time”  $t_w$ . Figure 1.7 shows the self-intermediate scattering function at different times after a temperature down-jump (also called quench). Soon after the quench (i.e. for small waiting times  $t_w$ ) the system is more fluid than what we would get at longer times since particles still move; that is because the system is working its way to equilibrium. This evolution towards equilibrium is what we call aging. At longer waiting times - when

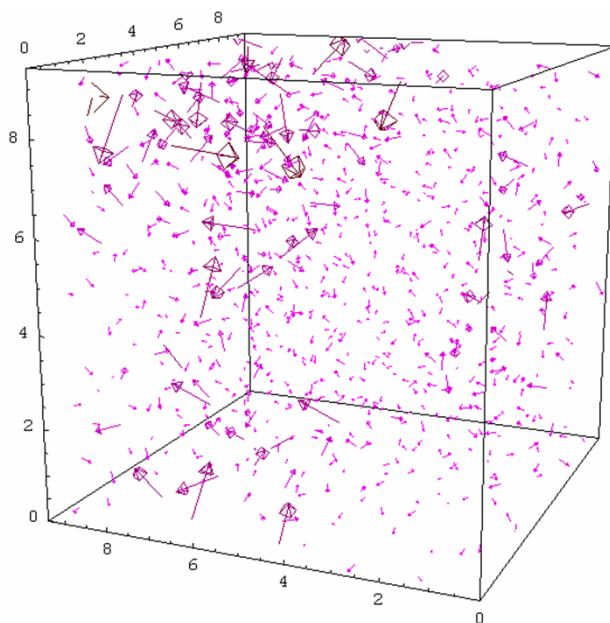


Figure 1.5: Particle displacement field for a Kob-Andersen binary Lennard-Jones at  $T = 0.45$  and  $\rho = 1.2$ . Clearly the dynamics is heterogeneous.

the *age* of the system is increased - the relaxation becomes too slow and the system appears frozen at that time scale. In order to observe aging two time quantities as the  $F_s(\mathbf{q}, t)$  of fig. 1.7 are necessary since, single time quantities like the potential energy are not sensitive to aging.

In this framework equilibrium thermodynamics does not work and in order to describe out-of-equilibrium systems through an extended thermodynamic approach we need an extra parameter which has the meaning of an effective temperature  $T_{eff}$ . This temperature can be for instance calculated via the generalized fluctuation-dissipation relation [Crisanti & Ritort (2003)] but the role that plays this parameter, i.e. the possibility that  $T_{eff}$  is a real temperature that can be measured directly in some way, is not yet established [Leuzzi (2009)].

### 1.3 Outline of the thesis

In chapter 2 it is shown the existence of a number of liquids that exhibit a strong correlation between the fluctuations of potential energy  $U$  and virial  $W$  (i.e. the configurational part of the pressure) in the NVT ensemble. These liquids are called strongly correlating liquids. The origin of the strong correlation is investigated and explained. Some counterexamples are also included in the discussion at the end of the chapter. In chapter 3 is discussed the “hidden” scale invariance that strongly correlating liquids inherits from inverse power-law potentials. This is the direct consequence of the existence of curves in the phase diagram along which a number of structural, dynamic and thermody-

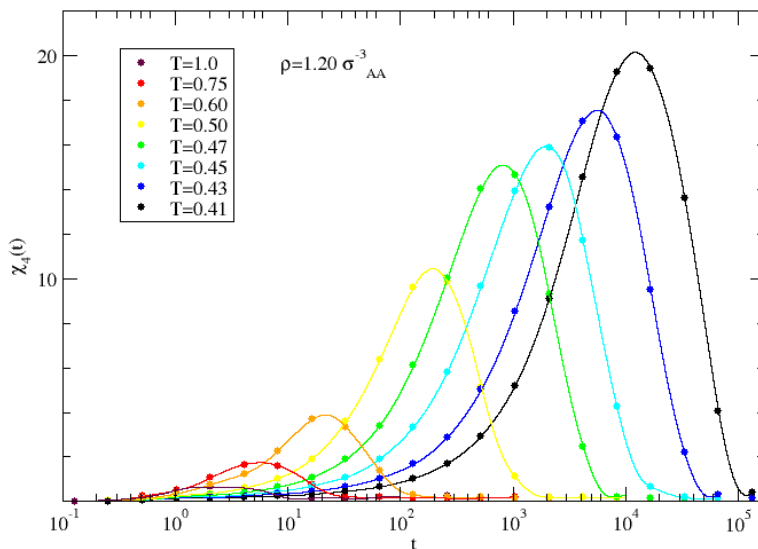


Figure 1.6: time dependence of the four-point susceptibility  $\chi_4$  at different temperatures for a Kob-Andersen binary Lennard-Jones. It reveals that the dynamics becomes more and more spatially heterogeneous as the temperature decreases.

dynamic properties are invariant. These curves are called “isomorphs”. Except for soft-spheres (characterized by an inverse power-law potential), isomorphs are only an approximation in strongly correlating liquids. In the chapter we test how good is the approximation via numerical simulations. Some counterexamples are included in the discussion. At the end of the chapter a set of equations that define isomorphs in the  $U$ - $W$  plane are derived and a comparison between analytical predictions and simulation results is done. Aging properties of strongly correlating liquids are discussed in the first part of chapter 4 while the second part is dedicated to the study of the evolution of the inherent-states energy probability distribution function during temperatures up-jumps and down-jumps. Simulation results for systems with different sizes are described through the Gaussian trap model and through the use of a demarcation energy which separates frozen states from the equilibrated ones. In chapter 5 the discussion about off-equilibrium dynamics in strongly correlating liquids continues. In the chapter - after having introduced the fluctuation-dissipation relation (FDR) - results from simulations are presented. The results explain why the effective temperature calculated via FDR depends only on the density of the final state that the system wants to reach after cooling (quench) or densification (crunch). The reason is that for strongly correlating liquids it is possible to produce equivalent quenches and crunches by using the isomorphs

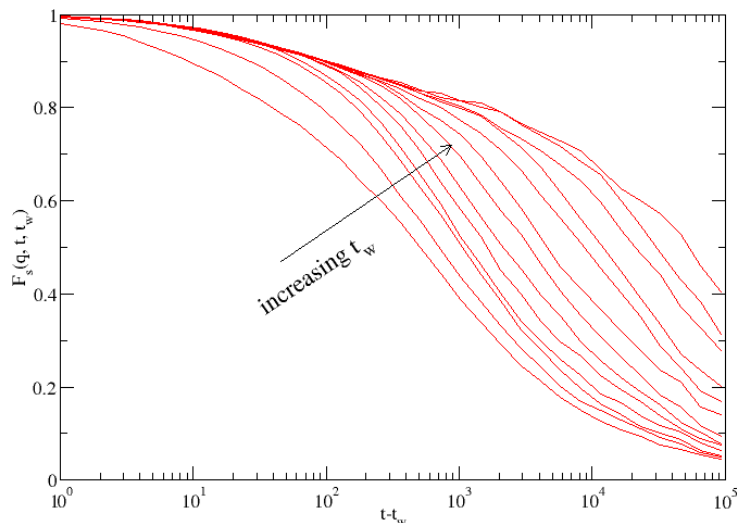


Figure 1.7: Monte Carlo (MC) aging dynamics of the Kob-Andersen binary Lennard-Jones system. The two-times self-intermediate scattering function is shown for different waiting times. The system is quenched at  $t = 0$  from  $T = 4.0$  to  $T = 0.4$  and the correlation function is evaluated at  $t_w = 0, 16, 64, 128, 256, 512, 1024, 2048, 4096, 8192, 16384, 32768$  and  $65536$  MC steps. The number density of the system is  $\rho = 1.2$ .

aging properties. It is also shown that it is possible to predict the effective temperature of all the produced glasses by doing only one aging experiment. Other considerations on the effective temperature are done at the end of the chapter. In particular it is shown that the effective temperature gives informations on the basins in the energy landscape explored during aging since these are of the same kind of those explored by the system when it is in equilibrium with a temperature  $T = T_{eff}$ . The last chapter is an outlook.

This work shows a number of scientific results which are the product a joint collaboration with the co-authors of the papers included at the end of the thesis. Therefore I could not avoid to include in the thesis some results which are not my personal contribution to the research projects. In fact when I started the Ph.D. program, researchers in the “Glass and Time” group were already working on strongly correlating liquids. My first project was to investigate the correlation in colloids with a short range square well attraction and to understand the weak correlation in hydrogen bonding liquids like water. After that I moved my attention to isomorphs. Most of the simulation results on isomorphs showed in the thesis are the result of this study. During the Ph.D. I have been also interested in out-of-equilibrium dynamics of strongly correlating liquids. I have studied their aging properties and I worked also on the distribution of the inherent states energies during up-jumps and down-jumps for a large Lennard-Jones system. I spent the last part of the Ph.D. developing a new way for investigating glassy properties of strongly correlating liquids. This has been done by using the effective temperature to characterize out-of-equilibrium dynamics of these systems.

## Chapter 2

# Strongly correlating liquids

In this chapter we discuss the properties of a class of liquids whose behavior is simpler than other liquids. We will refer to liquids belonging to this class as *strongly correlating liquids*.

### 2.1 Potential energy - virial fluctuations and their correlation

It is well known that in any thermodynamic system there are variables that fluctuate and some other that do not. For instance if the system is made of  $N$  particles and has fixed volume  $V$  and temperature  $T$  we expect that the total energy  $E$  and the pressure  $p$  are the main fluctuating quantities. Fluctuations are important in thermodynamics since from them it is possible to calculate different observables of the system under consideration. In the case of energy and pressure, we know that from their fluctuations we can calculate the specific heat at constant volume  $C_V = (\partial E / \partial T)_V$ , the isothermal compressibility  $\kappa_T = -V^{-1}(\partial V / \partial p)_T$  and the isochoric pressure coefficient  $\beta_V = (\partial p / \partial T)_V$  through relations that involve the variance of both  $E$  and  $p$  [Allen & Tildesley (1987)]:

$$\langle \Delta E^2 \rangle = k_B T^2 C_V$$

$$\langle \Delta p^2 \rangle = \frac{k_B T}{V} \left( \frac{2Nk_B T}{3V} + \langle p \rangle - \kappa_T^{-1} + \frac{X}{V} \right)^1$$

and their covariance

$$\langle \Delta p \Delta E \rangle = k_B T^2 V \beta_V.$$

If we indicate energy-pressure instantaneous values as respectively,  $E(t)$  and  $p(t)$  and their mean value as  $\langle E \rangle$  and  $\langle p \rangle$ , then  $\Delta E = E(t) - \langle E \rangle$  and  $\Delta p = p(t) - \langle p \rangle$  are the fluctuations appearing in the expressions above.

Both energy and pressure are the result of a kinetic contribution and a configurational term that depends only on the positions of particles. We can then rewrite energy and pressure in the following way:

---

<sup>1</sup>X is called hypervirial and is not a thermodynamic quantity.

$$E(t) = \frac{3}{2}Nk_B T(t) + U(t) \quad (2.1)$$

$$p(t)V = Nk_B T(t) + W(t) \quad (2.2)$$

From eq. (2.1) and (2.2) it is easy to identify the configurational part of  $E$  and  $p$ , i.e. the potential energy  $U$  and the virial  $W$ .

What do we expect from the instantaneous fluctuations of  $U$  and  $W$ ? In principle no relation suggests a correlation between these two variables. Quite surprising instead it was shown [Pedersen *et al.* (2008a), Paper I] that - for a number of liquids - fluctuations of virial and potential energy are instantaneously correlated, i.e. if we plot  $\Delta W(t)$  together with  $\Delta U(t)$  as a function of time (see fig. 2.1 (a)) the instantaneous fluctuations of virial and potential energy follow each other.

To better investigate such correlation we need a quantity to characterize precisely how much a liquid is strongly correlating. We then define the correlation coefficient  $R$  as:

$$R = \frac{\langle \Delta W \Delta U \rangle}{\sqrt{\langle (\Delta W)^2 \rangle \langle (\Delta U)^2 \rangle}}. \quad (2.3)$$

$R$  is a normalized parameter due to the Cauchy-Schwarz relation [Abramowitz & Stegun (1972)] thus it cannot be greater than 1. Therefore we say that a liquid is strongly correlating if  $|R| > 0.9$ . Here we express  $R$  through its absolute value since for a small number of liquids the correlation coefficient defined in eq. (2.3) is negative. Although a negative correlation coefficient appears mostly in cases of almost zero correlation, i.e. for non strongly correlating liquids, we have found also the case of a system with high negative correlation. We will discuss this particular case in section 2.3.1.

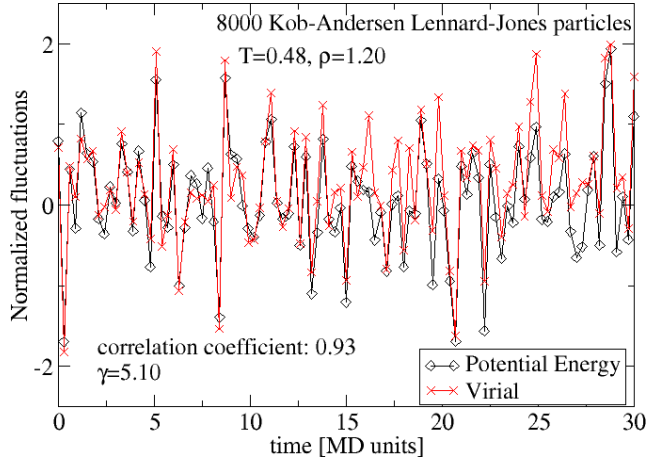
### 2.1.1 The parameter $\gamma$

If we plot  $W(t)$  against  $U(t)$  an elongated ellipse appears if the liquid is strongly correlating (fig.2.1 (b)); it means that to a good approximation  $W(t)$  and  $U(t)$  are proportional through a proportionality coefficient  $\gamma$  that can be found by fitting the ellipse.

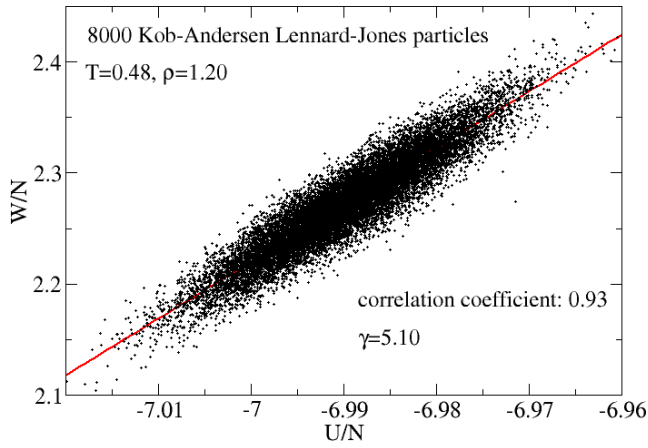
In Paper I, Paper II and Paper III,  $\gamma$  is defined as the ratio between the variances of virial and potential energy:

$$\gamma \equiv \sqrt{\frac{\langle (\Delta W)^2 \rangle}{\langle (\Delta U)^2 \rangle}}. \quad (2.4)$$

Indeed this is not the only way of defining  $\gamma$ . In fact for characterizing the strong correlation between  $U$  and  $W$  three different expressions for  $\gamma$  are valid - apparently - in an equal way. In fact - instead of the ratio between the standard deviations as in eq. (2.4) - we can consider the slope calculated from the linear regression principle when  $W$  is plotted against  $U$ . In this case  $\gamma$  would be  $\gamma_1 = (\langle \Delta W \Delta U \rangle) / (\langle (\Delta U)^2 \rangle)$ . Note that  $\gamma_1$  is the result of having chosen  $U$  as independent variable. We could also do the opposite, i.e. to let  $W$  be the independent variable; in this case we would get a third expression for the slope  $\gamma$ , i.e.  $\gamma_3 = (\langle (\Delta W)^2 \rangle) / (\langle \Delta W \Delta U \rangle)$ . The three  $\gamma$ s are related one to another:



(a)



(b)

Figure 2.1: (a) Instantaneous normalized fluctuations of virial and potential energy for the Kob-Andersen binary Lennard Jones system (KABLJ)[Kob & Andersen (1994)]. It is remarkable how the fluctuations of the two quantities follow each other. For these fluctuations it is possible to define a correlation coefficient whose expression is in eq. (2.3). The value obtained for the correlation is 0.93, so the liquid is strongly correlating as explained in the text. (b) Potential energy per particle against virial per particle for the KABLJ evaluated at the same state point of (a). When the system is strongly correlating an elongated ellipse appears. From the ellipse we can calculate the slope  $\gamma$  of eq. (2.7) between  $U$  and  $W$  through the linear regression principle.

$$\gamma_1 = R\gamma_2 = R^2\gamma_3 \quad (2.5)$$

where  $\gamma_2$  is the  $\gamma$  defined in eq. (2.4). In the case of 100%  $UW$  correlation (i.e.  $|R| = 1$ ) the three  $\gamma$ s coincide. For a strongly correlating liquid instead  $\gamma_1$ ,  $\gamma_2$  and  $\gamma_3$  are only close to each other. Another expression that relates the three  $\gamma$ s is

$$\gamma_1 \leq \gamma_2 \leq \gamma_3. \quad (2.6)$$

The relation (2.6) is valid only in case of positive strong correlation. Under this assumption there is no difference between the  $\gamma$ s except for the fact that two of them -  $\gamma_1$  and  $\gamma_3$  - depends on the choice of the dependent and independent variables. Then a first reasonable choice would be to preserve the symmetry between  $U$  and  $W$  choosing  $\gamma_2$  as definition of  $\gamma$ . If we want to include the case of negative strong correlation, then we suddenly note that eq. (2.6) is not valid anymore since  $\gamma_1$  and  $\gamma_3$  become negative, while  $\gamma_2$  continues to be positive. Thus  $\gamma_2$  does not reflect the change in the sign of the correlation and therefore  $\gamma_2$  is not the most appropriate  $\gamma$  to use for embracing all the possible cases of correlations. Apart from this consideration it is also true that the requirement of symmetry between the potential energy and the virial is not necessary. In fact the two quantities do not play the same role in statistical thermodynamics, e.g. the potential energy enters into the Boltzmann factor while the virial does not have the same *primary* role. We will show in section 3.4 that the best  $\gamma$  to use is

$$\gamma = \frac{\langle \Delta W \Delta U \rangle}{\langle (\Delta U)^2 \rangle}. \quad (2.7)$$

## 2.2 Causes of strong correlation

### 2.2.1 A trivial case: the soft-spheres potential

Consider  $N$  identical particles interacting with an inverse power-law potential (IPL)  $v(r_{ij})$ . Particles with this kind of interaction are also called *soft-spheres* [Hoover *et al.* (1970), Hoover & Ross (1971), Hoover *et al.* (1971)] and their total potential energy is:

$$U^{(IPL)}(r) = \sum_{i<j} v(r_{ij}) = \sum_{i<j} A_{ij} r_{ij}^{-n}. \quad (2.8)$$

By definition the virial is given by [Hansen & McDonald (2006)]

$$W^{(IPL)}(r) = -\frac{1}{3} \sum_{i<j} r_{ij} \frac{dv(r_{ij})}{dr_{ij}} = \sum_{i<j} w(r_{ij}). \quad (2.9)$$

Since  $v'(r_{ij}) = -nv(r_{ij})/r_{ij}$ , from simple algebra it is straightforward to find that for soft-spheres

$$W^{(IPL)}(r) = \frac{n}{3} \sum_{i<j} r_{ij} \frac{v(r_{ij})}{r_{ij}} = \frac{n}{3} \sum_{i<j} v(r_{ij}), \quad (2.10)$$

i.e.

$$W^{(IPL)}(r) = \frac{n}{3}U^{(IPL)}(r). \quad (2.11)$$

Equation (2.11) shows that for soft-spheres the proportionality between  $W$  and  $U$  is an exact relation and therefore the system is 100% correlated. Note that in the soft-spheres case  $\gamma = n/3$ , i.e.  $\gamma$  is related to the exponent  $n$  of the inverse power-law potential of eq. (2.8). Hence we find that the correlation is intrinsically related to the shape of the potential, that for an inverse power-law potential corresponds to a totally repulsive interaction.

What happens when the system has a different interaction potential?

### 2.2.2 The extended inverse power-law potential

In figure 2.1 (a) the fluctuations of virial and potential energy are shown for a binary mixture interacting with a Lennard-Jones (LJ) pair potential:

$$U^{(LJ)}(r) = \sum_{\alpha,\beta} \sum_{i<j} v_{\alpha\beta}(r_{ij}) = 4\epsilon_{\alpha\beta} \left[ \left( \frac{\sigma_{\alpha\beta}}{r_{ij}} \right)^{12} - \left( \frac{\sigma_{\alpha\beta}}{r_{ij}} \right)^6 \right] \quad (2.12)$$

where  $\alpha = \{A, B\}$  and  $\beta = \{A, B\}$  are indexes representing the possible type of the interacting particles (type A or B) of size  $\sigma_{AA} = 1$  and  $\sigma_{BB} = 0.88$  with  $\epsilon_{AA} = 1$ ,  $\epsilon_{BB} = 1$  and  $\epsilon_{AB} = 0.5$ .  $r_{ij}$  is the pair distance. The choice of the mixture (80% A particles and 20% B particles), the parameters defined above and the cut-off of the interaction at  $r_c = 2.5$ <sup>2</sup> are peculiar of the well known Kob-Andersen binary Lennard-Jones (KABLJ) [Kob & Andersen (1994)]. The virial associated to this potential is:

$$W^{(LJ)}(r) = \sum_{\alpha,\beta} \sum_{i<j} w_{\alpha\beta}(r_{ij}) = 8\epsilon_{\alpha\beta} \left[ 2 \left( \frac{\sigma_{\alpha\beta}}{r_{ij}} \right)^{12} - \left( \frac{\sigma_{\alpha\beta}}{r_{ij}} \right)^6 \right] \quad (2.13)$$

For the sake of clarity lets drop for a moment the indexes  $\alpha$  and  $\beta$  and consider only the interactions between particles of type A.

In the case of the LJ potential the exact relation for soft-spheres in eq. (2.11) does not hold (in fact the virial in eq. (2.13) is not directly proportional to the potential energy in eq. (2.12)). Then why is the system still strongly correlating? One could think that - since in soft-spheres the repulsion between close encounters gives rise to the correlation - also in the LJ potential the correlation is originated by the repulsive term dominating over the attractive one in a given range of temperatures and densities. If this conjecture is true than we would have  $W^{(LJ)}(t) \approx 4U^{(LJ)}(t)$  where the factor 4 comes from

---

<sup>2</sup>in molecular dynamics simulations usually a cut-off is introduced in the interaction i.e. the potential is truncated at a given value  $r_c$  beyond which the interaction is 0. This is a common approximation that is done in short range potentials like the KABLJ since the main contribution to the total potential energy (and forces) is at distances shorter than the chosen cut-off. This allow to save computational time but leads to have approximated thermodynamics properties. For the KABLJ potential a spherical cut-off is applied. Moreover the potential is smoothed in order to have continuous forces at the cut-off distance. In this case a third degree polynomial is added in the range  $r_1 < r < r_c$  in order to ensure this continuity. We will discuss this procedure with more details in section 3.8.

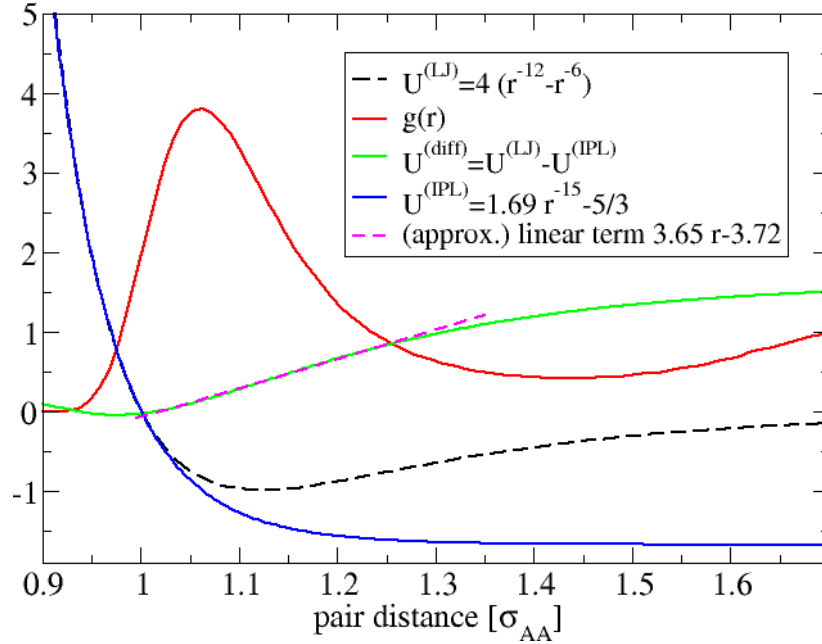


Figure 2.2: The figure shows the KABLJ potential  $U^{(LJ)}$  (for A particles only) together with the radial distribution function  $g(r)$ . In the region where the potential is repulsive - corresponding to the left part of the first peak of the  $g(r)$  - a good approximation of the interaction is given by an effective inverse power-law potential  $U^{IPL}$  with an exponent given by  $n = 3\gamma \approx 15$  where  $\gamma$  is the slope formed by plotting the potential energy against the virial as shown in fig. 2.1 (b). However the main contribution to the pair interaction is around the first peak of the  $g(r)$  which corresponds to the interactions around the minimum of the potential. Then the effective inverse power-law is not the best approximation for the potential since it does not take into account the interactions around the minimum. In the figure is plotted the difference  $U^{(diff)}$  between  $U^{(LJ)}$  and  $U^{(IPL)}$ . Note that in the region of the first peak of the  $g(r)$   $U^{(diff)}$  is well approximated by a linear term and after the first peak the difference is almost constant. Then a better expression for the approximated potential is an *extended* inverse power-law (eIPL) i.e. an inverse power-law plus a linear term.

considering as leading term the repulsive part  $r^{-12}$  of the LJ potential, and therefore  $\gamma = n/3 = 12/3$  as for the soft-spheres case. In fig. 2.1 (b) is found instead  $\gamma = 5.1$ . This would correspond to a power-law with exponent  $n \approx 15$  instead of 12 as conjectured. What is the reason of this discrepancy? The answer to that is given by looking at fig. 2.2.

There the radial distribution function  $g(r)$  is plot together with the pair potential  $U^{LJ}(r)$  of the KABLJ for particles of type A. From the  $g(r)$  we know that the main contribution to the virial and to the potential energy comes from interactions occurring at distances around the first peak of the  $g(r)$ , i.e. at distances corresponding to pair interactions placed around the minimum of the potential. This means that both the repulsion and the attraction play a

role in almost equal way in the emerging of the correlation. Moreover if we try to interpolate the LJ potential with an inverse power-law in the region corresponding to the left side of the  $g(r)$  (i.e. the region to the left of the minimum of the potential) the exponent  $n$  that we find is bigger than 12 and therefore  $\gamma = n/3$  is in good agreement with the value extrapolated from fig. 2.1(b). Actually it is possible to estimate the exponent of the inverse power-law that best fits the repulsive part of the potential. Paper II shows one way of estimating such exponent in the case of a single component Lennard-Jones potential (SCLJ). The procedure used is the following: the Lennard-Jones potential can be written as the sum of an inverse power-law potential and a rest

$$U^{(LJ)} = U^{(IPL)} + U^{(diff)}; \quad (2.14)$$

similarly the same decomposition can be done for the virial  $W^{(LJ)} = W^{(IPL)} + W^{(diff)}$ . The exponent of  $U^{(IPL)}$  that we want to know can be chosen by minimizing the variances  $\langle(\Delta U^{(diff)})^2\rangle$  and  $\langle(\Delta W^{(diff)})^2\rangle$ . Since there is no unique way to estimate the exponent  $n$  of the inverse power-law by fitting, we only want to show that using  $n \simeq 3\gamma$  (with  $\gamma$  evaluated in fig. 2.1 (b)) we obtain a reasonable interpolation of the Lennard-Jones potential. Figure 2.3 shows the interpolation of the KABLJ potential with two different IPL potentials: one with exponent  $n = 12$  and the other with  $n = 3\gamma \approx 15$ . Between the two, the interpolation with the second IPL is the best confirming that colliding pairs feels an interaction different from  $r^{-12}$  since the attraction makes the repulsion steeper. Summarizing - on a first approximation - LJ particles feel an effective potential (due to the presence of both attraction and repulsion) that is an IPL with exponent  $n = 3\gamma$  and therefore is called *effective* inverse power-law.

The effective inverse power-law cannot be the whole explanation since it is a good description only for short distances, i.e. for  $r \leq r_0^3$ , instead we know from the first peak of the radial distribution function that most of interactions take place in a larger region overcoming the minimum of the potential where the inverse power-law explanation cannot be valid. Moreover in Paper I it is shown that the correlation survives even at zero pressure where most of the interactions are around the minimum of the Lennard-Jones potential. We have then to take into account also the part of the potential acting at distances longer than  $r_0$ . Figure 2.2 shows the two terms of the potential in which the Lennard-Jones can be decomposed according to eq. (2.14). Looking at the difference between the effective inverse power-law and the total potential - i.e.  $U^{(diff)}$  - we note that in the region corresponding to the first peak of the  $g(r)$ ,  $U^{(diff)}$  can be approximated with a straight line and for longer distances  $U^{(diff)} \simeq const$ . Adding these extra terms in the approximation of the Lennard-Jones potential allow us to take into account all the possible interactions among particles. We call the approximated Lennard-Jones potential *extended* inverse power-law potential (eIPL):

$$U^{(LJ)} \simeq U^{(eIPL)} = Ar^{-n} + B + Cr. \quad (2.15)$$

Which role plays the linear term in the strong correlation? Lets consider as example the case of a one-dimensional liquid in a fixed volumes  $L$ . For simplicity we allow only nearest neighbors interactions. Consider now the case in which

---

<sup>3</sup> $r_0$  is the interparticle distance where the potential is zero.

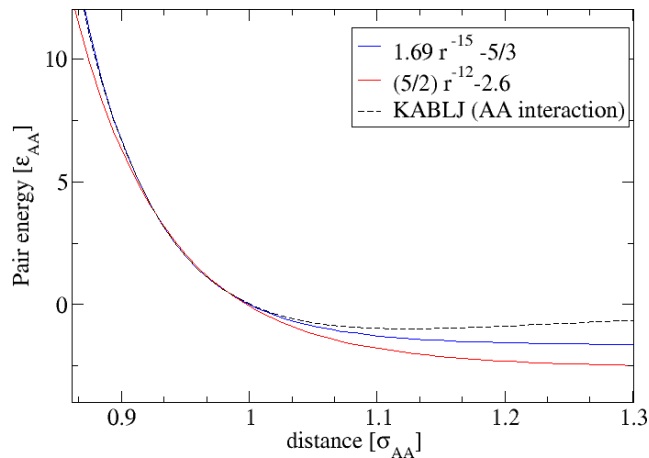


Figure 2.3: Interpolation of the KABLJ potential (for  $A$  particles) with two different inverse power-law potentials with exponent  $n$  respectively equal to 12 and 15. The exponent 12 corresponds to the repulsive term in the expression of the LJ, but the matching with the repulsive part of the potential is not good since the attractive term makes the repulsion steeper. The exponent  $n = 15$  corresponds to  $3\gamma$  where  $\gamma$  is the slope estimated in fig. 2.1 (b). The good matching with the repulsive part indicates that particles during collisions experience an effective interaction of the form of an inverse power-law. That is why we call it *effective* inverse power-law.

one particle performs a small displacement in order to be closer to one of the two possible neighbors: the bond length with this neighbor gets shorter but at the same time the particle gets far from the other neighbor thus having a bond length with it longer than before. That means that the total bond length among the three particles remains constant. We can think to have these local displacements for all the particles in the one-dimensional liquid. It is important to stress that the displacement is something local since affects only the nearest neighbors interaction distances. When we sum up all the local displacements, the shorter bond lengths will compensate the longer ones:

$$\sum_{i < j} r_{ij} = L. \quad (2.16)$$

If we have an interacting potential given by a linear term plus a constant and we want to calculate its fluctuations in the one-dimensional liquid then we have:

$$\Delta U_{1D} = \sum_{ij} \Delta(Ar_{ij} + b) = \Delta(AL + Nb) = 0. \quad (2.17)$$

Then a linear term in the potential does not contribute to the fluctuations of the potential energy because of the volume constraint. Of course when we move to the three-dimensional case things are not so easy anymore but we can still propose some arguments that support the one-dimensional picture also when we move to three dimensions (a careful analysis of the fluctuations of the

linear term in the extended inverse power-law potential can be found in Paper II).

Summarizing we have shown that the linear term in the extended inverse power-law potential does not contribute significantly to the fluctuations of potential energy and virial. This is thanks to the volume constraint and the locality of the fluctuations as explained above. This is not surprising if one consider that the effective IPL potential alone is a good approximation even at almost zero pressure when most of interactions occurs in the minimum of the potential or in the Lennard-Jones crystal (see Paper II).

### 2.3 Which systems are strongly correlating?

In the previous sections we have described the case of strong correlation in the KABLJ liquid. Indeed strong correlation has been observed in a wide class of liquids (see Paper I). Figure 2.4 shows the numerator and the denominator of the correlation coefficient defined in eq. (2.3) in units of pressure (i.e. both divided by  $k_B TV$ ) in order to have extensive quantities of 13 different liquids. If the correlation is strong than the the points should lay close to the dashed line. No correlation means having points on the bottom part of the plot. The upper part instead is forbidden because of the Cauchy-Schwarz inequality for the correlation coefficient. From fig. 2.4 is clear that a number of liquids - among which there are also molecular liquids - are strongly correlating. Those liquids have mainly van der Waals type of interactions, except for a model of colloidal particles, a model with exponential repulsion and models of metals. On the other hand there is a bunch of liquids whose correlation is poor: these are methanol and water, i.e. hydrogen bonding liquids.

Apart from simulation results for different liquid models, the correlation coefficient of supercritical Argon has been estimated from experimental data. We stressed at the beginning of the chapter that the variance of virial and potential energy as well as their covariance are related to thermodynamic observable through their fluctuations<sup>4</sup>. In the case of Argon no internal degree contributes to the fluctuations then energy and virial are those of an ideal gas for which the following relations hold:

$$\langle(\Delta U)^2\rangle/Nk_B T^2 = c_V - \frac{3}{2}k_B = c_V^{conf} \quad (2.18)$$

$$\langle(\Delta W)^2\rangle/k_B T = Nk_B T + \langle W \rangle - V\kappa_T + \langle X \rangle \quad (2.19)$$

$$\langle\Delta W \Delta U\rangle/k_B V T^2 = \beta_V - Nk_B/V = \beta_V^{conf} \quad (2.20)$$

where  $X = \sum_{i<j} r w'(r_{ij})$  is the hypervirial and it cannot be measured since it is not a thermodynamic quantity. However it is still possible to subtract it off from the equations by making use of a reference state point and then making the approximation (verified by our simulations) that along an isochore  $X - X_{ref} \approx (n/3)(W - W_{ref})$ , where  $n$  is the exponent of an inverse power-law. If we define

---

<sup>4</sup>the relation is given by the fluctuation-dissipation theorem. see e.g. [Smit & Frenkel (2001)]

## 2. STRONGLY CORRELATING LIQUIDS

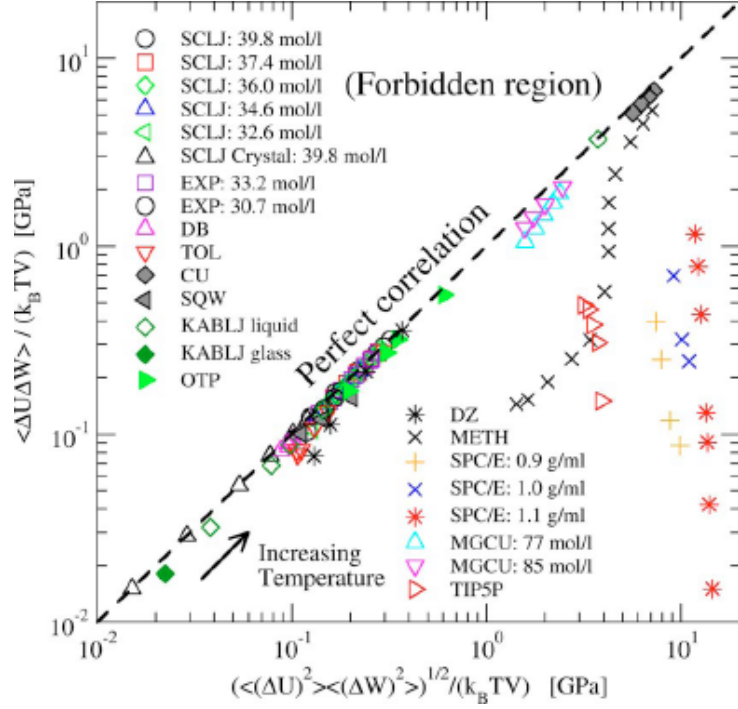


Figure 2.4: Check of  $UW$  strong correlation for a number of liquids. On the x-axis the numerator of the correlation coefficient  $R$  defined in eq. (2.3) is plotted against the denominator on the y-axis. Both quantities are expressed in units of pressure in order to be comparable among different systems. If the liquid is strongly correlating then it should lay close to the diagonal corresponding to perfect correlation. The simulated systems are the single component Lennard-Jones liquids (SCLJ), a model with exponential repulsion (EXP), an asymmetric dumbbell model (DB), a toy model for toluene using the UA-OPLS parameters (TOL) [Jorgensen *et al.* (1984)], a model of pure Cu with a many body potential (CU) [Jacobsen *et al.* (1987), Jacobsen *et al.* (1996)], a binary mixture of particles with hard-core repulsion and square-well attraction (SQW) [Zaccarelli *et al.* (2002), Zaccarelli *et al.* (2004)], a Kob-Andersen binary Lennard-Jones system [Kob & Andersen (1994)], an ortho-terphenyl model suggested by Lewis and Wahnström [Wahnström (1991)] (OTP), a single component glassformer suggested by Dzugutov [Dzugutov (1992)] (DZ), a model of methanol using GROMOS parameters [van Gunsteren *et al.* (1996)] (METH), a three-site model of water [Berendsen *et al.* (1987)] (SPC/E), a model of  $Mg_{85}Cu_{15}$  [Bailey *et al.* (2004)] (MGCU) and a five-site model of water [Mahoney & Jorgensen (2000)] (TIP5P).

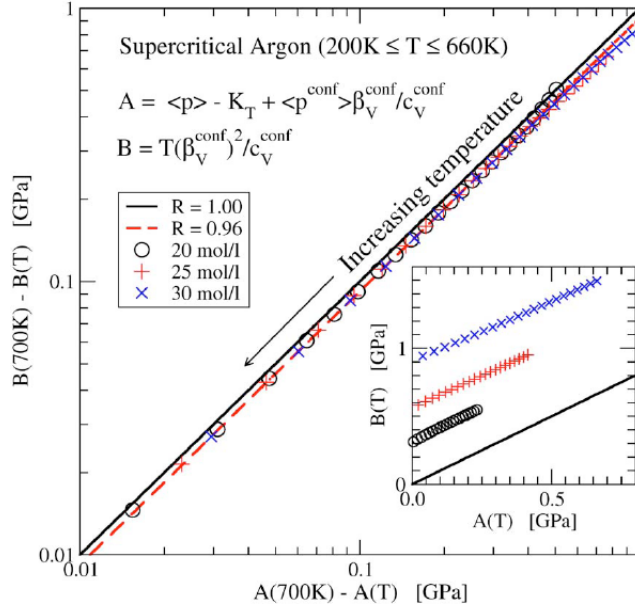


Figure 2.5: Experimental data of supercritical Argon at three different densities. Data from NIST database [Lemmon *et al.* (2005)]. The correlation coefficient found is  $R = 0.96$ . The inset shows the comparison with the soft-spheres case for which  $A(T) = B(T)$ . Figure is also shown in Paper II and in reference [Pedersen *et al.* (2008a)].

$B(T) = T(\beta_V^{\text{conf}})^2 / c_V^{\text{conf}}$  and  $A(T) = \langle p \rangle - \kappa_T + (\langle p \rangle^{\text{conf}} \beta_V^{\text{conf}} / c_V^{\text{conf}})$  - where  $\langle p \rangle^{\text{conf}} = \langle p \rangle - (Nk_B T / V)$  - then the correlation coefficient becomes:

$$R_{WU} \approx \sqrt{\frac{B(T) - B(T_{ref})}{A(T) - A(T_{ref})}}. \quad (2.21)$$

Figure 2.5 shows data from supercritical Argon [Lemmon *et al.* (2005)] close to the diagonal. The correlation coefficient is  $R = 0.96$  showing that strong correlation exists also in nature.

In the next subsection we will discuss the case of particular systems whose behavior is different from the Lennard-Jones case. In particular we will show the case in which the system is strongly correlating but the correlation is negative and the more general case of no correlation in hydrogen bonding liquids.

### 2.3.1 A case of negative correlation: the square-well system

In this chapter we have defined a correlation coefficient  $R$  that can assume also negative values. This is to take into account the rare but still possible case of negative strong correlation observed for a model of hard-core colloidal particles interacting with a short range attractive square-well (SW) [Sciortino (2002), Zaccarelli *et al.* (2002), Zaccarelli *et al.* (2004)]. In the case of colloidal particles there are two parameters that can be tuned to explore the whole phase diagram: the temperature  $T$  and the packing fraction  $\phi = (\pi/6)\rho\sigma^3$  where  $\rho$  is

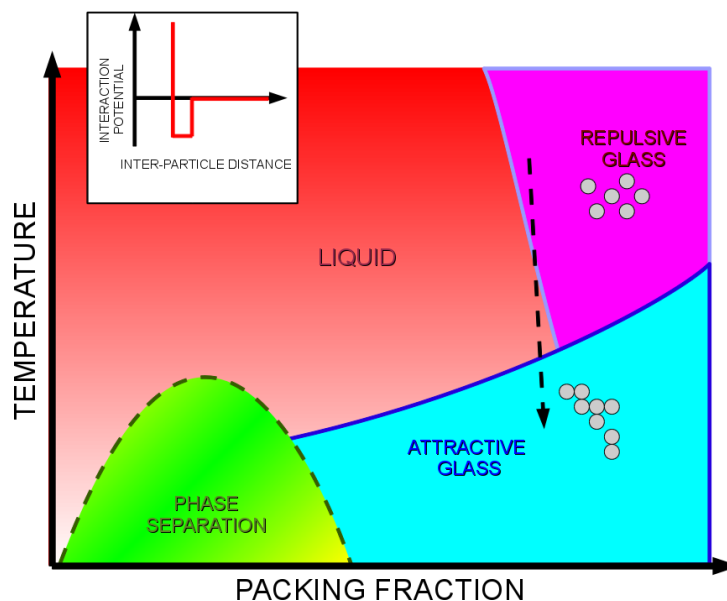


Figure 2.6: Sketch of the phase diagram of SW particles when the width of the attractive well is much smaller than the particle diameter. The phase diagram shows two different glass lines: the repulsive glass line associated to a disordered “hard-spheres” like phase and an attractive glass line resulting from the arrest due to the fact that particles are trapped in their own wells. Finally at low packing fractions and temperatures a phase separation region appears. The dashed arrow shows that is possible to go from the repulsive glass to the liquid state and to the attractive glass just lowering the temperature.

the number density and  $\sigma$  is the diameter of the colloidal particles [Foffi *et al.* (2004)]. This system has been widely studied in the last years showing an interesting phase diagram when the attractive range becomes small compared to the size of the particle. Here we use a well width of  $3\%\sigma$ .

The phase diagram is sketched in fig. 2.6. The most interesting feature is the appearing of a reentrance in the isodiffusivity curve that separates the liquid phase from the glassy state and that gives rise to two different kind of glasses. At high packing fraction and high temperature the glass transition occurs mainly for entropic reasons: the system then behaves like an hard-sphere system and the disordered arrested phase is called *repulsive glass*. The interesting feature of the reentrance is that it is possible to go from the repulsive glassy state to the liquid state just lowering the temperature (which is really counterintuitive) and from the liquid to a new glass called *attractive glass* just continuing to lower the temperature (see the dashed black arrow in fig. 2.6). Zaccarelli *et al.* [Zaccarelli *et al.* (2002)] have shown that structural and dynamic properties of repulsive and attractive glass are very different. In the repulsive glass the repulsion of the hard-core term is dominant, while lowering the temperature the attraction becomes a competitive force and it eventually dominates for very low temperatures. Under this conditions particles are not trapped in the cages made by the surrounding particles (like in the hard-spheres

case) but rather into each other attractive well. This competition between attraction and repulsion makes the SW system interesting to study from the point of view of the  $UW$  correlation. For discontinuous potentials the algorithm to use for the simulation is quite different from the one of continuous potentials. The interaction in fact is built through a number of discrete events avoiding to integrate the equation of motions as it is usually done in molecular simulations. This kind of dynamics is called event driven dynamics [Rapaport (2004)] and corresponds basically to the same algorithm for simulating hard spheres systems [Alder & Wainwright (1959)] but with a larger variety of events generated by the existence of the attractive well in the potential. At each step the algorithm detects which particles are involved in a given event and which kind of event is. Four different events can be detected: (1) “collisions” between particles, (2) “trapping” of a particles into a mutual well, (3) “bounces” i.e. when particles hit the boundary of the well and are pushed back and (4) “escaping” of particles from the mutual well. Since we are dealing with a number of instantaneous events the corresponding instantaneous virial would be a sum of delta functions in time which is clearly not well suited for the analysis of correlations. To obtain a well defined virial we need to average over the time. It was Rapaport [Rapaport (2004)] who introduced the time averaged virial defined as:

$$W = \frac{1}{3\Delta t} \sum_e m_e \mathbf{r}_e \cdot \Delta \mathbf{v}_e \quad (2.22)$$

where “ $e$ ” corresponds to a given event,  $\Delta t$  is the time window along which the virial is averaged and  $\mathbf{r}_e$  and  $\Delta \mathbf{v}_e$  are respectively the relative position and the change of the relative velocity of two particles participating to a given event. The time averaged potential energy is more simple to define. In fact the potential energy  $U$  is the number of bonds formed by all particles (with a minus sign). It means that  $U$  increases (negatively) if there is a trapping event while it decreases only in the case of an escaping event. Then the time averaged  $U$  is just the sum of these events occurring within the time  $\Delta t$ .

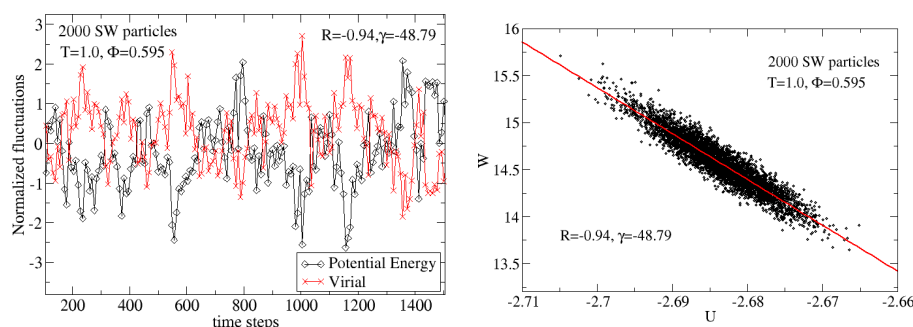


Figure 2.7: Fluctuations of virial and potential energy for a system of hard core colloidal particles interacting with a short range square-well potential. At high temperatures and packing fractions strong correlation appears. Fluctuations are averaged over  $1/10$  of the relaxation time  $\tau_\alpha = 76.5$  of the potential energy-virial correlation function as explained in the text.

The mechanism giving rise to negative correlation is the following: at high packing fraction the biggest contribution to the virial is given by collisions

## 2. STRONGLY CORRELATING LIQUIDS

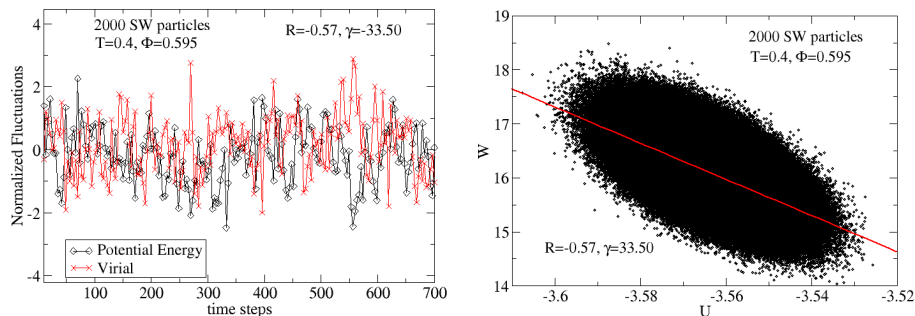


Figure 2.8: Same plot of fig. 2.7 but for a high packing fraction and low temperature state. Here the correlation is clearly lost even though the fluctuations have been averaged over  $1/10$  of the relaxation time  $\tau_\alpha = 30.0$  of the potential energy-virial correlation function.

which is the only event that increases positively the virial. The number of collisions occurring in a time  $\Delta t$  are proportional to the colliding pairs, i.e. to the pair bonds that are anticorrelated to the energy. Figure 2.7 and 2.8 show the  $UW$  correlation at high packing fraction and temperature (i.e. in the hard-sphere type regime) and at high packing fraction and low temperature (i.e. in the attractive well regime). Clearly the system remains correlated only at high temperatures while the correlation is lost in the region dominated by the attraction. In both cases collisions are the most likely event since the packing fraction is the same. Then we have to look at the second more likely event that at high temperatures are trapping and escaping (in equal weight), while at low temperatures is the bounce against the well boundary. All these events brings a negative contribution to the virial - which does not tell us too much on the resulting correlation. The explanation has to be found in the potential energy fluctuations instead. In fact events occurring at high temperature allow the potential energy to fluctuate together with the virial (leaving a well or entering into it corresponds to an increase or a decrease the potential energy) while at low temperatures the fluctuations of  $U$  are more inhibited because of the bounces that do not bring any contribution to it.

As it is stressed in Paper I a better strong correlation is achieved if the average is performed over long times. This is done to allow only the relevant time scales to contribute to the strong correlation. The right average time can be found looking at fig. 2.9 (a) and fig. 2.9 (b). In the two plots autocorrelation functions of potential energy and virial are represented together with the absolute value of cross-correlation between  $U$  and  $W$ . To be sure to remove the fast time scales in the correlation it is enough to chose as average time  $1/10$  of the relaxation time of the cross-correlation function.

### 2.3.2 Competition between different interactions: the water case

Water is the most famous example of network forming liquid [Stanley *et al.* (1998), Mishima & H.E. (1998), Debenedetti (1996), Poole *et al.* (1992), Kohl *et al.* (2005), Speedy & Angell (1976)] . It is well known that water exhibits

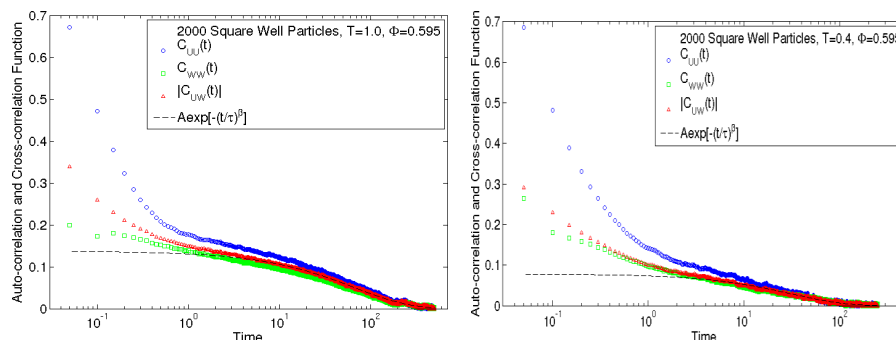


Figure 2.9: Correlation functions of virial and potential energy together with the absolute value of their cross-correlation function for two different states of the SW system. In both cases the slow relaxation of the cross-correlation function has been interpolated with a stretched exponential in order to extract the relaxation time.

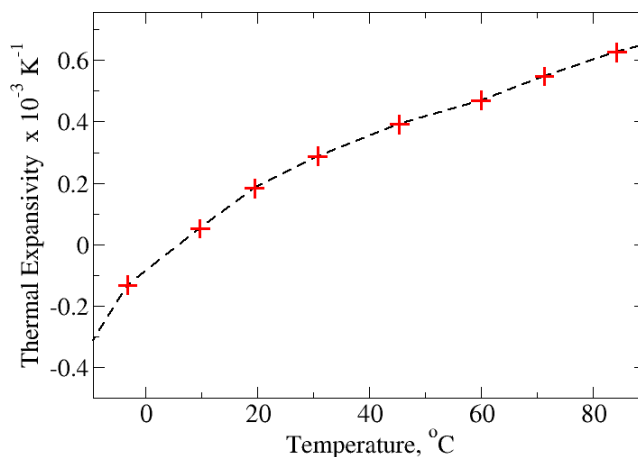


Figure 2.10: Thermal expansivity of water. The curve has a zero in correspondence of the density maximum at  $T=4^\circ\text{C}$ . The thermal expansivity is related to the isochoric pressure coefficient  $\beta_V$  that is connected to the covariance of pressure and energy through the fluctuation dissipation theorem. If we consider only its configurational part - which is related to the numerator of the correlation coefficient  $R$  in eq. (2.3) - when  $\beta_V^{conf} = 0$  then  $R$  is zero as well.

density anomalies: a density maximum at  $4^\circ\text{C}$  and a less famous density minimum at around  $-41^\circ\text{C}$  [Brovchenko *et al.* (2003)]. Both the anomalies are ensured by the fact that the isochoric pressure coefficient  $\beta_V = (\partial p / \partial T)_V$  is zero. The last relation can be understood from the behavior of thermal expansivity of water  $\alpha_p = (1/V)(\partial V / \partial T)_p$  which is zero for  $T = 4^\circ\text{C}$  [Kell (1975)] as shown in fig. 2.10.

Since  $\alpha_p$  reflects the change of the volume correspondent to a temperature change, clearly the density slightly increases going from high  $T$  to low  $T$  until it reaches a maximum value and it decreases after it.  $\alpha_p$  is related to  $\beta_V$  by the following relation:

## 2. STRONGLY CORRELATING LIQUIDS

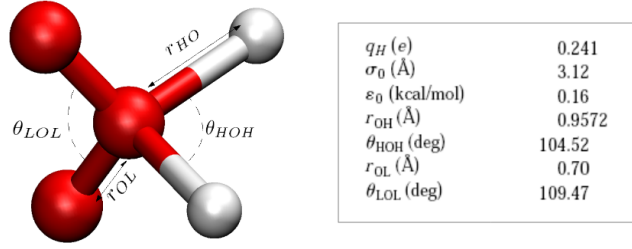


Figure 2.11: schematic picture of a molecule of tip5p water.

$$\alpha_p = \frac{1}{V} \left( \frac{\partial V}{\partial T} \right)_p = -\frac{1}{V} \left( \frac{\partial p}{\partial V} \right)_T^{-1} \left( \frac{\partial p}{\partial T} \right)_V = \beta_V \kappa_T \quad (2.23)$$

where  $\kappa_T = -(1/V)(\partial V/\partial p)_T$  is the isothermal compressibility and is related to the fluctuations of the volume  $\langle(\Delta V)^2\rangle_{NpT}$  at constant pressure<sup>5</sup>. It follows that - to ensure  $\alpha_p$  to be zero -  $\beta_V$  must be zero as well in correspondence to the density maximum. Here we are interested in the configurational part of the isochoric pressure coefficient, i.e.  $\beta_V^{conf}$  since it is related to the covariance of virial and potential energy  $\langle\Delta W \Delta U\rangle$  through the fluctuation dissipation theorem (see eq. (2.20)). Therefore  $\beta_V^{conf}$  is connected to the numerator of the correlation coefficient  $R$  in eq. (2.3). We then expect to have  $R = 0$  when  $\beta_V^{conf} = 0$ , i.e. close to the density maximum.<sup>6</sup> For investigating the correlation in water we have simulated a five-site model of water (TI5P) which reasonably well reproduces the density maximum [Mahoney & Jorgensen (2000), Mahoney & Jorgensen (2001), Vega & Abascal (2005)].

This model has a lone pair of oxygens and their potential is modeled with a Lennard-Jones while hydrogens interact with a Coulomb potential:

$$E_{ab} = \sum_{ij} \frac{q_i q_j e^2}{r_{ij}} + 4\varepsilon_0 \left[ \left( \frac{\sigma_{OO}}{r_{OO}} \right)^{12} - \left( \frac{\sigma_{OO}}{r_{OO}} \right) \right] \quad (2.24)$$

where the value of the parameters are shown in fig. 2.11.

We know already that the coulomb term is an IPL with  $n = 1$ , i.e. is 100% correlated; we want then to investigate the correlation of the Lennard-Jones part. To do that we had to separate its contribution from the total potential, using for instance the instantaneous radial distribution functions of oxygens  $g_{OO}(r, t)$  to calculate both  $W(t)$  and  $U(t)$  as follow:

$$U_{LJ}(t) = (4\pi\rho N_O/2) \int v_{ij}^{(LJ)}(r) g_{OO}(r, t) r^2 dr \quad (2.25)$$

$$W_{LJ}(t) = (4\pi\rho N_O/2) \int w_{ij}^{(LJ)}(r) g_{OO}(r, t) r^2 dr \quad (2.26)$$

<sup>5</sup> $\kappa_T \propto \langle(\Delta V)^2\rangle_{NpT}$  ensures that the isothermal compressibility is not zero at the density maximum.

<sup>6</sup>we do not have  $R = 0$  in correspondence of the density maximum because we are considering only the configurational part of the isochoric pressure coefficient  $\beta_V^{conf} = \beta_V - k_B(N/V)$ . Thus  $\beta_V$  vanishes exactly at the density maximum but the absence of the kinetic term in  $\beta_V^{conf}$  makes the correlation coefficient vanish at a slightly higher temperature.

Which systems are strongly correlating?

<b>T</b> <b>°C</b>	<b>Density</b> <b>(g/cm<sup>3</sup>)</b>	<b>-E</b> <b>(Kcal/N mol)</b>	<b>Cp</b> <b>(cal/K mol)</b>	<b>Δ H</b> <b>(Kcal/mol)</b>
-37.5	0.97312 ± 0.00258	11.74 ± 0.0206	20.12638	12.2102 ± 0.0206
-25.0	0.98733 ± 0.00105	11.32 ± 0.0084	45.88653	11.809 ± 0.0084
-12.5	1.00029 ± 0.00067	10.86 ± 0.0053	40.70098	11.3784 ± 0.0053
0.0	1.00715 ± 0.00033	10.49 ± 0.0027	33.63934	11.0374 ± 0.0027
12.5	1.00758 ± 0.00021	10.18 ± 0.0017	31.26966	10.7477 ± 0.0017
25.0	1.00319 ± 0.00024	9.89 ± 0.0019	29.19173	10.4864 ± 0.0019
37.5	0.99574 ± 0.00018	9.62 ± 0.0015	27.35955	10.2403 ± 0.0015
50.0	0.98512 ± 0.00015	9.36 ± 0.0012	26.67767	10.0047 ± 0.0012
62.5	0.97398 ± 0.00015	9.11 ± 0.0021	26.03611	9.7784 ± 0.0021
75.0	0.95993 ± 0.00011	8.86 ± 0.0008	25.43161	9.5665 ± 0.0008

Table 2.1: Thermodynamic values of TIP5P water around the density maximum. NpT simulations with p=1atm.

<b>T (°C)</b>	<b>R</b>
-25.0	0.9992
-12.5	0.9990
0.0	0.9989
12.5	0.9986
25.0	0.9982
37.5	0.9979
50.0	0.9978
62.5	0.9977

Table 2.2: Correlation coefficient of the Lennard-Jones potential in water. The densities at which  $R$  has been evaluated are shown in table 2.1.

where  $w_{ij}^{(LJ)} = -(1/3)rv_{ij}^{(LJ)}(r)$ . The value of the correlation coefficient for the Lennard-Jones around the density maximum is shown in table (2.2).

Clearly the tip5p potential is a sum of two strongly correlating terms, i.e.  $W_c = (1/3)U_c$ <sup>7</sup> and  $W_{LJ} \simeq \gamma U_{LJ} + W_{LJ}^0$ . However it is surprising to see how the two interactions destroy the correlation. The reason is that the two terms have different proportionality constants (i.e.  $(1/3)$  and  $\gamma \approx 4.5$ ). In fact if we write the total potential energy and virial we have:

$$U = U_{LJ} + U_c \quad (2.27)$$

and

$$W = W_{LJ} + W_c \simeq W_{LJ}^0 + \gamma U_{LJ} + \frac{1}{3}U_c. \quad (2.28)$$

Hence  $U$  and  $W$  would be correlated only if  $\gamma \simeq (1/3)$  but this is not the case and therefore the liquid is not strongly correlating.

<sup>7</sup> $U_c$  and  $W_c$  are the potential energy and virial of the coulomb interaction.

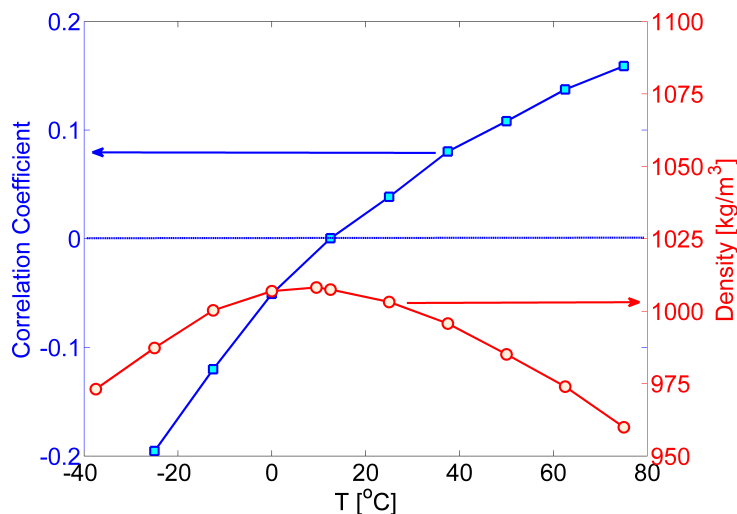


Figure 2.12: Correlation coefficient and density as a function of temperature for tip5p water (2560 molecules). Densities are chosen to give an average pressure of  $1 \text{ atm}$ .

Figure 2.12 shows the correlation coefficient together with the density maximum for the tip5p water model at ambient pressure. The correlation is weak everywhere and - as predicted from the behavior of  $\beta_V^{conf}$  - it becomes zero for a value slightly higher than the density maximum temperature ( $\sim 12 \text{ }^\circ\text{C}$ ). Interesting to note is that after being zero, the correlation coefficient becomes negative: this is still a consequence of the behavior of  $\alpha_p$  that becomes negative soon after having crossed the density maximum. The correlation will be zero and positive again at very low temperatures after having crossed the density minimum.

Summarizing, the competing interactions in water destroy the correlation even though the virial and the potential energy of the separated interactions are strongly correlating. without looking at the correlation this can be predicted from thermodynamics properties of water that ensure the system to have zero correlation in correspondence of a density maximum or minimum. The poor correlation of water appears not only in all hydrogen-bonding liquids but all the time that there are different length-scales interactions or whenever orientational bonds are introduced in the liquid.

## Chapter 3

# Density scaling of strongly correlating liquids and isomorphs

### 3.1 Inheritance of scaling properties by generalized IPL potentials

In the previous chapter we have stated that there is a connection between Lennard-Jones (LJ) liquids and liquids interacting with an inverse power-law (IPL) potential. It was shown indeed that the Lennard-Jones potential can be rewritten as an inverse power-law plus a rest  $U^{(rest)} = U^{(LJ)} - U^{(IPL)}$ . The term  $U^{(rest)}$  can be approximated around the first peak of the radial distribution function by a linear term that does not contribute to the fluctuations of virial and potential energy. Here we show that there is something more connecting the LJ and the IPL potential: this is the inheritance of some properties that can be explained with the existence of curves in the phase diagram along which some thermodynamic, dynamic and structural quantities are invariant.

#### 3.1.1 Density scaling for IPL potentials

Consider the free energy  $F$  of a system of soft-spheres. For convenience we can rewrite it as the sum of two terms :  $F_{IPL} = F_{id,IPL} + F_{ex,IPL}$ , where  $F_{id,IPL} = -Nk_B T \ln(\rho \Lambda^3)$  is the free energy of an ideal gas <sup>1</sup> and  $F_{ex,IPL}$  is the excess free energy due to the fact that particles are interacting. Lets focus on  $F_{ex,IPL}$ ; its definition in the canonical ensemble is:

$$e^{-\beta F_{ex,IPL}} = \frac{1}{V^N} \int d\mathbf{r}_1 \dots d\mathbf{r}_N e^{-\beta U(\mathbf{r}_1, \dots, \mathbf{r}_N)} \quad (3.1)$$

where  $\beta = 1/k_B T$ . From Klein's theorem [Klein (1919), Berlin & Montroll (1952)] if  $U(\lambda \mathbf{r}_1, \dots, \lambda \mathbf{r}_N) = \lambda^\mu U(\mathbf{r}_1, \dots, \mathbf{r}_N)$ , i.e. if  $U(\mathbf{r}_1, \dots, \mathbf{r}_N)$  is an homogeneous function of degree  $\mu$ , then we have

$$F_{ex} = Nk_B T \phi(\rho^{-\mu/3}/T). \quad (3.2)$$

A generic IPL potential  $U_{IPL} = \sum_{i < j} A_{ij} r_{ij}^{-n}$  has degree  $-n$ . In this case eq. (3.2) becomes:

---

<sup>1</sup>note that  $\rho$  is the number density and  $\Lambda$  is the de Broglie wavelength

### 3. DENSITY SCALING OF STRONGLY CORRELATING LIQUIDS AND ISOMORPHS

$$F_{ex, IPL} = Nk_B T \phi(\rho^{n/3}/T). \quad (3.3)$$

Note that in NVT simulations  $\rho$  and  $T$  are the parameters used for determining a state point. This means that we can find a number of states with different  $\rho$  and  $T$  that maintain the ratio  $\rho^{n/3}/T$  constant. The locus of points where  $\rho^{n/3}/T = Const$  describes a curve along which the free energy and other observables are invariant. In fact, since a number of variables are functions of  $F_{ex, IPL}$  or functions of its first or second derivatives, we can show that they satisfy as well the *density scaling* relation  $\rho^{n/3}/T = Const$  [Roland *et al.* (2006)]. In Paper III a list of these thermodynamic quantities is presented. Here we show, as example, the case of the excess entropy. Since  $S_{ex} = -(\partial F_{ex}/\partial T)_V$  we have

$$S_{ex, IPL} = -Nk_B \phi(\rho^{n/3}/T) + Nk_B \frac{\rho^{n/3}}{T} \phi'(\rho^{n/3}/T) \quad (3.4)$$

$$= Nk_B f_1(\rho^{n/3}/T). \quad (3.5)$$

This is true also for the potential energy ( $U_{IPL} = F_{ex, IPL} - TS_{ex, IPL}$ ), the virial ( $W_{IPL} = -V(\partial F_{ex, IPL}/\partial V)_T$ ), the specific heat ( $c_{V, IPL}^{ex} = \frac{-T}{V}(\partial^2 F_{ex, IPL}/\partial T^2)_V$ ), etc... It is important to stress that not only thermodynamic variables are invariant along the curve defined by  $\rho^{n/3}/T = Const$ . For instance it is possible to show that the dynamics satisfy the density scaling as well. In MD simulations the dynamics is obtained by integrating at each time step Newton's equations for finding the position of each particle  $\mathbf{r}_i(t)$  ( $i = 1, \dots, N$ ) at time  $t$ . If  $\mathbf{r}_i(t)$  is the solution of Newton's equations at time  $t$  for the state point  $(T_0, \rho_0)$ , i.e.

$$m_i \ddot{\mathbf{r}}_i(t) = -\nabla_{\mathbf{r}_i} \sum_{i < j} A_{ij}(\mathbf{r}_i - \mathbf{r}_j)^{-n}, \quad (3.6)$$

then we can show that also  $\mathbf{r}_i^{(1)}(t) = \alpha \mathbf{r}_i(\lambda t)$  is a solution for the state point  $(T_1 = T_0 \alpha^2 \lambda^2, \rho_1 = \rho_0/\alpha^3)$  when  $\alpha^{-n+2} = \lambda^2$ . In fact we have that

$$m_i \ddot{\mathbf{r}}_i^{(1)}(t) = -\nabla_{\mathbf{r}_i^{(1)}} \sum_{i < j} A_{ij}(\mathbf{r}_i^{(1)} - \mathbf{r}_j^{(1)})^{-n} \quad (3.7)$$

$$m_i \alpha \lambda^2 \ddot{\mathbf{r}}_i(\lambda t) = -\frac{1}{\alpha} \nabla_{\mathbf{r}_i^{(1)}} \sum_{i < j} A_{ij}(\alpha \mathbf{r}_i - \alpha \mathbf{r}_j)^{-n} \quad (3.8)$$

$$= -\alpha^{-(n-1)} \nabla_{\mathbf{r}_i^{(1)}} \sum_{i < j} A_{ij}(\mathbf{r}_i - \mathbf{r}_j)^{-n} \quad (3.9)$$

is a solution as eq. (3.6) only if  $\alpha \lambda^2 = \alpha^{-(n+1)}$ . Moreover this implies that the two state points satisfy the density scaling relation:

$$\begin{aligned} \frac{\rho_0^{n/3}}{T_0} &= \alpha^2 \lambda^2 \frac{(\rho_1 \alpha^3)^{n/3}}{T_1} \\ &= \frac{\rho_1^{n/3}}{T_1}. \end{aligned} \quad (3.10)$$

From the calculation illustrated above it is straightforward to derive other relations connecting the two state points and involving different quantities. For instance, since  $T_1 = \alpha^{-n}T_0$  then

$$\frac{U_{IPL}(\mathbf{r}_1^{(1)}, \dots, \mathbf{r}_N^{(1)})}{T_1} = \frac{U_{IPL}(\mathbf{r}_1, \dots, \mathbf{r}_N)}{T_0} \quad (3.11)$$

i.e. the Boltzmann factors are the same for the two configurations. This is an important result that we will use later for introducing the concept of isomorphs. We can obtain further connections between the two state points introducing the probability distribution of the configuration space:

$$\begin{aligned} P_{IPL}(\mathbf{r}_1, \dots, \mathbf{r}_N) &= \frac{e^{-U_{IPL}(\mathbf{r}_1, \dots, \mathbf{r}_N)/k_B T}}{\frac{1}{V^N} \int d\mathbf{r}_1 \dots d\mathbf{r}_N e^{-U_{IPL}(\mathbf{r}_1, \dots, \mathbf{r}_N)/k_B T}} \\ &= e^{-(U_{IPL}(\mathbf{r}_1, \dots, \mathbf{r}_N) - F_{ex, IPL})/k_B T}. \end{aligned} \quad (3.12)$$

Moreover we define the reduced positions as

$$\rho_1^{1/3} \mathbf{r}_1 = \rho_0^{1/3} \mathbf{r} = \tilde{\mathbf{r}} \quad (3.13)$$

since the two states are related by the equation  $\mathbf{r}_1 = \alpha \mathbf{r}$  where  $\alpha = (\rho_0/\rho_1)^{1/3}$ . We can write now the reduced probability distribution for the state  $(\rho_1, T_1)$ :

$$\begin{aligned} P^{(1)}(\tilde{\mathbf{r}}_1, \dots, \tilde{\mathbf{r}}_N) &= \frac{e^{-\beta_1 \rho_1^{-N/3} U_{IPL}(\rho_1^{1/3} \mathbf{r}_1^{(1)}, \dots, \rho_1^{1/3} \mathbf{r}_N^{(2)})}}{\frac{1}{N^N} \int d\rho_1 \mathbf{r}_1^{(1)} \dots d\rho_1 \mathbf{r}_N^{(1)} e^{-\beta_1 \rho_1^{-N/3} U_{IPL}(\rho_1^{1/3} \mathbf{r}_1^{(1)}, \dots, \rho_1^{1/3} \mathbf{r}_N^{(1)})}} \\ &= \frac{e^{-\beta_1 \rho_1^{-N/3} U_{IPL}(\tilde{\mathbf{r}}_1, \dots, \tilde{\mathbf{r}}_N)}}{\frac{1}{N^N} \int d\tilde{\mathbf{r}}_1 \dots d\tilde{\mathbf{r}}_N e^{-\beta_1 \rho_1^{-N/3} U_{IPL}(\tilde{\mathbf{r}}_1, \dots, \tilde{\mathbf{r}}_N)}} \end{aligned} \quad (3.14)$$

since  $T_1 = \alpha^{-n}T_0$  then  $T_1 \rho_1^{-n/3} = T_0 \rho_0^{-n/3}$ . Substituting the last relation into eq. (3.14) we get:

$$\begin{aligned} P^{(1)}(\tilde{\mathbf{r}}_1, \dots, \tilde{\mathbf{r}}_N) &= \frac{e^{-\beta_1 \rho_1^{-N/3} U_{IPL}(\tilde{\mathbf{r}}_1, \dots, \tilde{\mathbf{r}}_N)}}{\frac{1}{N^N} \int d\tilde{\mathbf{r}}_1 \dots d\tilde{\mathbf{r}}_N e^{-\beta_1 \rho_1^{-N/3} U_{IPL}(\tilde{\mathbf{r}}_1, \dots, \tilde{\mathbf{r}}_N)}} \\ &= \frac{e^{-\beta_0 \rho_0^{-N/3} U_{IPL}(\tilde{\mathbf{r}}_1, \dots, \tilde{\mathbf{r}}_N)}}{\frac{1}{N^N} \int d\tilde{\mathbf{r}}_1 \dots d\tilde{\mathbf{r}}_N e^{-\beta_0 \rho_0^{-N/3} U_{IPL}(\tilde{\mathbf{r}}_1, \dots, \tilde{\mathbf{r}}_N)}} = P^{(2)}(\tilde{\mathbf{r}}_1, \dots, \tilde{\mathbf{r}}_N). \end{aligned} \quad (3.15)$$

Then the reduced probability distribution is the same for the two state points. From eq. (3.15) is easy now to show that the radial distribution function and all the higher order equilibrium probability distributions are invariant for the two state points when reduced units are used. In fact the general expression of a higher order particle probability distribution is

### 3. DENSITY SCALING OF STRONGLY CORRELATING LIQUIDS AND ISOMORPHS

$$\begin{aligned}
g_{IPL}^{(n,1)}(\mathbf{r}_1^{(1)}, \dots, \mathbf{r}_n^{(1)}) &= \frac{V^{(1)n} N!}{N^n (N-n)!} \frac{\int d\mathbf{r}_{n+1}^{(1)} \dots d\mathbf{r}_N^{(1)} e^{-U_{IPL}(\mathbf{r}_1^{(1)}, \dots, \mathbf{r}_N^{(1)})/k_B T_1}}{\int d\mathbf{r}_1^{(1)} \dots d\mathbf{r}_N^{(1)} e^{-U_{IPL}(\mathbf{r}_1^{(1)}, \dots, \mathbf{r}_N^{(1)})/k_B T_1}} \\
&= \frac{N!}{N^n (N-n)!} \frac{1}{V^{(1)N-n}} \int d\mathbf{r}_{n+1}^{(1)} \dots d\mathbf{r}_N^{(1)} e^{-(U_{IPL}(\mathbf{r}_1^{(1)}, \dots, \mathbf{r}_N^{(1)}) - F_{1,ex})/k_B T_1} \\
&= \frac{N!}{N^n (N-n)!} \frac{1}{V^{(1)N-n}} \int d\mathbf{r}_{n+1}^{(1)} \dots d\mathbf{r}_N^{(1)} P_{IPL}(\mathbf{r}_1^{(1)}, \dots, \mathbf{r}_N^{(1)}).
\end{aligned} \tag{3.16}$$

Since we know that the reduced probability distribution is the same for the two state points then we can rewrite eq. (3.16) in reduced units:

$$\begin{aligned}
g_{IPL}^{(n,1)}(\tilde{\mathbf{r}}_1, \dots, \tilde{\mathbf{r}}_n) &= \frac{N!}{N^n (N-n)!} \frac{N^{-N} \rho_1^{-(N-n)}}{V_1^{(N-n)}} \int d\tilde{\mathbf{r}}_1 \dots d\tilde{\mathbf{r}}_N P(\tilde{\mathbf{r}}_1, \dots, \tilde{\mathbf{r}}_N) \\
&= \frac{N!}{N^n (N-n)!} N^N \int d\tilde{\mathbf{r}}_1 \dots d\tilde{\mathbf{r}}_N P(\tilde{\mathbf{r}}_1, \dots, \tilde{\mathbf{r}}_N) = g_{IPL}^{(n,2)}(\tilde{\mathbf{r}}_1, \dots, \tilde{\mathbf{r}}_n).
\end{aligned} \tag{3.17}$$

The general idea is that all state points satisfying the same equation of motion belong to the same density scaling curve. It follows that the state point  $(T_1, \rho_1)$  can be achieved from  $(T_0, \rho_0)$  by a simple scaling of positions.

Moreover one can consider any autocorrelation function with relaxation time

$$\tau_A = \frac{\int_0^\infty \langle A(0)A(t) \rangle dt}{\langle A^2 \rangle} \tag{3.18}$$

where

$$\langle A(0)A(t) \rangle = \int P(\mathbf{r}_1, \dots, \mathbf{r}_N) A(\mathbf{r}_1, \dots, \mathbf{r}_N) e^{-i\mathcal{L}t} A(\mathbf{r}_1, \dots, \mathbf{r}_N). \tag{3.19}$$

Using the fact that  $e^{-i\tilde{\mathcal{L}}^{(1)}\tilde{t}^{(1)}} = e^{-i\tilde{\mathcal{L}}\tilde{t}}$  (see appendix A) then it is possible to show that

$$\tau_A^{(1)} = \lambda \tau_A = \frac{\rho_0^{-1/3} \sqrt{1/T_0}}{\rho_1^{-1/3} \sqrt{1/T_1}} \tau_A. \tag{3.20}$$

If we define the characteristic thermal time as  $t_c = \rho^{-1/3} \sqrt{m/k_B T}$  we have that the relaxation times of two state points with the same scaling parameters are the same when are divided by their characteristic time:

$$\tau_A^{(1)}/t_c^{(1)} = \tau_A/t_c^{(0)}. \tag{3.21}$$

Following the same approach it is possible to demonstrate that the diffusion coefficient  $D$  is invariant if divided by its characteristic value  $D_c = \rho^{-2/3}/t_c$ .

Summarizing we have shown that for *IPL* potentials there exist some curves identified by the density scaling relation  $\rho^{(n/3)}/T = Const$  along which all the state points have a number of thermodynamic quantities that are invariant, as well as structure and dynamics if expressed in characteristic (or reduced) units. These state points have microscopic configurations that differ only by a simple scaling of positions and more importantly have same Boltzmann factors. We call such curves *isomorphs* (see Paper IV) and we will discuss the consequences of their existence in the next section.

### 3.2 Hidden scale invariance for Strongly correlating liquids

In section (2.2) we have shown how the LJ potential can be rewritten as the sum of an inverse power-law and a rest that can be approximated with a linear term and a constant. Therefore we can write a generalized LJ interaction in the following way:

$$v_{ij} = \varepsilon_{ij} \left( \frac{\sigma_{ij}}{r_{ij}} \right)^{-n} + v_{ij}^{diff}(r_{ij}) \quad (3.22)$$

where  $U^{diff}(\mathbf{r}_1, \dots, \mathbf{r}_N) = \sum_{i < j} v_{ij}^{diff} \simeq f(V)$  to a good approximation and the exponent  $n = 3\gamma$ . Following an analogous approach to the one presented in the previous section we identify the excess free energy of the system:

$$e^{-\beta F_{ex}} = \int d\mathbf{r}_1 \dots d\mathbf{r}_N e^{-[U_{IPL}(\mathbf{r}_1, \dots, \mathbf{r}_N) + U_{diff}]/k_B T} \quad (3.23)$$

$$\simeq e^{-f(V)/k_B T} \int d\mathbf{r}_1 \dots d\mathbf{r}_N e^{-U_{IPL}(\mathbf{r}_1, \dots, \mathbf{r}_N)/k_B T}. \quad (3.24)$$

It follows that

$$F_{ex} \simeq f(V) + F_{ex,IPL} = f(V) + Nk_B T \phi(\rho^{n/3}/T). \quad (3.25)$$

We recall that in the IPL case  $F_{ex,IPL}/T$  is constant for all the state points satisfying the density scaling relation  $\rho^{n/3}/T = const$ . Equation (3.25) shows that this is not the case for the LJ because of the presence of the extra term  $f(V)$ . In the previous section we have said that a number of thermodynamic properties are invariant since they are defined via the excess free energy, so - according to eq. (3.25) - we could expect that in the case of the LJ the invariance is lost. Luckily this is not generally true. Consider for instance the excess entropy  $S_{ex} = (-\partial F_{ex}/\partial T)_V$ ; for the LJ potential it can be expressed as

$$S_{ex} \simeq (-\partial F_{ex,IPL}/\partial T)_V = Nk_B f_1(\rho^{n/3}/T). \quad (3.26)$$

Then the excess entropy still satisfy the invariance even though the excess free energy does not. Among several thermodynamic properties that can be obtained from the excess free energy only some of them are still invariant. In

### 3. DENSITY SCALING OF STRONGLY CORRELATING LIQUIDS AND ISOMORPHS

fact those quantities containing the extra contribution from the  $f(V)$ -term do not “inherit” the IPL scaling. Moreover, using the same arguments of section (3.1.1) it is possible to show that the invariance of structure and dynamics survive for the LJ liquid. Paper III shows a comparison between LJ invariants and those of the IPL potential. Note that in the LJ the Boltzmann factors are not invariants. In fact given two configurations (1) and (2) satisfying a density scaling relation we have:

$$e^{-U(\mathbf{r}_1^{(1)}, \dots, \mathbf{r}_N^{(1)})} = e^{-U_{IPL}(\mathbf{r}_1^{(1)}, \dots, \mathbf{r}_N^{(1)})/k_B T_1} e^{-U_{diff}^{(1)}/k_B T_1} \quad (3.27)$$

$$= e^{-U_{IPL}(\mathbf{r}_1^{(2)}, \dots, \mathbf{r}_N^{(2)})/k_B T_2} e^{-U_{diff}^{(1)}/k_B T_1} \frac{e^{-U_{diff}^{(2)}/k_B T_2}}{e^{-U_{diff}^{(2)}/k_B T_2}} \quad (3.28)$$

$$= \frac{e^{-U_{diff}^{(1)}/k_B T_1}}{e^{-U_{diff}^{(2)}/k_B T_2}} e^{-U(\mathbf{r}_1^{(2)}, \dots, \mathbf{r}_N^{(2)})}, \quad (3.29)$$

i.e. the Boltzmann factors are proportional through a constant that depends on the state points.

If  $U^{(diff)} \simeq f(V)$  is a good approximation (as in the case where  $U^{(diff)}$  is given by a linear term plus a constant), then we should be able to find approximated state points having proportional Boltzmann factors. The curves identified by these points satisfy the hidden<sup>2</sup> scale invariance [Schröder *et al.* (2009)] characterizing strongly correlating liquids. We call such curves *isomorphs*.

### 3.3 Definition of isomorphs

Consider two state points (1) and (2) with temperatures  $T_1$  and  $T_2$  and densities  $\rho_1$  and  $\rho_2$ . Moreover consider for these two state points any microscopic configuration for which is possible to define the reduced coordinates

$$\tilde{\mathbf{r}}_i \equiv \rho^{1/3} \mathbf{r}_i; \quad (3.30)$$

it follows that  $\tilde{\mathbf{r}}_i^{(1)} = \tilde{\mathbf{r}}_i^{(2)}$ . We say that the two state points are *isomorphic* if, for all the physically relevant configurations, they have proportional Boltzmann weights:

$$e^{-U(\mathbf{r}_1^{(1)}, \dots, \mathbf{r}_N^{(1)})/k_B T_1} = C_{12} e^{-U(\mathbf{r}_1^{(2)}, \dots, \mathbf{r}_N^{(2)})/k_B T_2}. \quad (3.31)$$

We recall the fact that only for IPL potentials isomorphs exist. We will show however that for strongly correlating liquids the existence of isomorphs is a good approximation. Note that the isomorph definition does not refer to the quantities characterizing strongly correlating liquids, i.e. the correlation coefficient  $R$  and the slope  $\gamma$ . Then the reader could think that other liquids which are not strongly correlating might have isomorphs. We can prove indeed that the existence of isomorphs is strictly related to the fact that the system is strongly correlating. To show this consider two microscopic configurations

<sup>2</sup>we use the word “hidden” because the connection with IPL potentials and the role of  $U^{(diff)}$  were unknown so far.

infinitesimally close with the same reduced coordinates. An infinitesimal variation of the reduced coordinates is given by:

$$\delta\tilde{\mathbf{r}}_i = \frac{1}{3}\rho^{-2/3}(d\rho)\mathbf{r}_i + \rho^{1/3}\delta\mathbf{r}_i. \quad (3.32)$$

For the two infinitesimally close configurations considered above  $\delta\tilde{\mathbf{r}}_i = 0$  since they have the same reduced coordinates. Equation (3.32) becomes zero when  $\delta\mathbf{r}_i = -(1/3)(1/\rho)(d\rho)\mathbf{r}_i = -(1/3)(d\ln\rho)\mathbf{r}_i$ . Consider now the variation of the potential energy associated to the two configurations:

$$\begin{aligned} \delta U &= \sum_i \delta\mathbf{r}_i \cdot \nabla_{\mathbf{r}_i} U = -\frac{1}{3}(d\ln\rho) \sum_i \mathbf{r}_i \cdot \nabla_{\mathbf{r}_i} U \\ &= (d\ln\rho)W, \end{aligned} \quad (3.33)$$

where we have used the virial definition in eq. (2.9). Moreover if the two infinitesimally close configurations are isomorphic then from eq. (3.31) we get:

$$\delta\left(\frac{U}{T}\right) = \frac{\delta U}{T} - \frac{U\delta T}{T^2} = \frac{(d\ln\rho)W - U(d\ln T)}{T} = \text{Const.} \quad (3.34)$$

If we introduce now the difference  $\Delta$  between two relevant configurations of the same state point, from eq. (3.34) we have that  $\Delta\delta(U/T) = 0$ , i.e.

$$\frac{(d\ln\rho)\Delta W - \Delta U(d\ln T)}{T} = 0, \quad (3.35)$$

$$\Delta W = \frac{d\ln T}{d\ln\rho} \Delta U \quad \Rightarrow \quad \gamma = \frac{d\ln(T)}{d\ln(\rho)}. \quad (3.36)$$

We have found that if a system has isomorphs then the fluctuations of potential energy and virial are correlated. Moreover eq. (3.36) tells us what is the expression for  $\gamma$  along an isomorph. We will come back to this point later. In Paper IV it is shown that also the opposite is valid, i.e. if the liquid is strongly correlating than it has isomorphs. The idea is basically the following: if the liquid is strongly correlating then  $\Delta W = \gamma\Delta U$  holds to a good approximation. Inserting the last expression into eq.(3.35) we get:

$$\Delta\delta\left(\frac{U}{T}\right) = \frac{(d\ln\rho)\gamma\Delta U - \Delta U(d\ln T)}{T}. \quad (3.37)$$

If temperature and density are changed in order that  $d\ln T = \gamma d\ln\rho$  then the equation above is zero or  $\delta(U/T) = \text{const.}$  which is the condition for having isomorphs.

It is important to stress that all these considerations are made in the case of 100% correlation. When the liquid is not 100% correlated these remain a qualitative explanation supported by simulations. We will see in fact that isomorphs are a very good approximation in some Lennard-Jones liquids, while there are cases of strongly correlating liquids having high correlation coefficient but a deviation from a good scaling.

### 3.4 How to identify isomorphs

If the eIPL approximation is good for strongly correlating liquids then we should be able to identify state points of approximated isomorphs through the density scaling relation  $\rho^{n/3}/T = \text{Const}$  as in the case of the IPL potential, where  $n/3$  is replaced by  $\gamma$  when the correlation is not 100%. In the previous section we have also shown what is the expression of  $\gamma$  along an isomorph, i.e.  $\gamma = d\ln(T)/d\ln(\rho)$ . How can we rewrite  $\gamma$  in terms of fluctuations of potential energy and virial? For instance we can use the fact that the excess isochoric specific heat  $C_v^{ex}$  is invariant along an isomorph (see Paper IV). This means that the difference in the specific heat between two isomorphous points is zero. Then a small displacement along an isomorph corresponds to a small change in density and temperature that maintains  $C_v^{ex}$  constant:

$$0 = dC_v^{ex} = \left( \frac{\partial C_v^{ex}}{\partial \ln(\rho)} \right)_T d\ln(\rho) + \left( \frac{\partial C_v^{ex}}{\partial \ln(T)} \right)_\rho d\ln(T). \quad (3.38)$$

To satisfy this invariance we need that  $(\partial C_v^{ex}/\partial \ln(\rho))_T = -(\partial C_v^{ex}/\partial \ln(T))_\rho$ . Lets start looking at the first term. Using the fluctuation dissipation theorem we can rewrite  $C_v^{ex}$  through the fluctuations of the potential energy:

$$\begin{aligned} \left( \frac{\partial C_v^{ex}}{\partial \ln(\rho)} \right)_T &= \left( \frac{\partial \langle (\Delta U)^2 \rangle / k_B T^2}{\partial \ln(\rho)} \right)_T \\ &= \frac{2}{k_B T^2} \langle \Delta U \left( \frac{\partial \Delta U}{\partial \ln(\rho)} \right)_T \rangle - \frac{\langle (\Delta U)^2 \rangle}{k_B T^4} \left( \frac{\partial T^2}{\partial \ln(\rho)} \right)_{C_v^{ex}} \\ &= \frac{2}{k_B T^2} \langle \Delta U \Delta W \rangle - \frac{2}{k_B T^2} \langle (\Delta U)^2 \rangle \left( \frac{\partial \ln(T)}{\partial \ln(\rho)} \right)_{C_v^{ex}} \\ &= \frac{2}{k_B T^2} \langle \Delta U \Delta W \rangle - \frac{2}{k_B T^2} \langle (\Delta U)^2 \rangle \gamma. \end{aligned} \quad (3.39)$$

$$(3.40)$$

Note that we used eq.(3.33) to evaluate  $(\partial \Delta U / \partial \ln(\rho))_T$ . For the second term we have:

$$\begin{aligned}
 \left( \frac{\partial C_v^{ex}}{\partial \ln(T)} \right)_\rho &= \left( \frac{\langle (\Delta U)^2 \rangle / k_B T^2}{\partial \ln(T)} \right)_\rho \\
 &= \frac{2}{k_B T^2} \langle \Delta U \left( \frac{\partial \Delta U}{\partial \ln(T)} \right)_\rho \rangle - \frac{2 \langle (\Delta U)^2 \rangle}{k_B T^2} \\
 &= \frac{2}{k_B T^2} \langle \Delta U \left( \frac{\partial \Delta U}{\partial \ln(\rho)} \right)_T \left( \frac{\partial \ln(\rho)}{\partial \ln(T)} \right)_{C_v^{ex}} \rangle - \frac{2 \langle (\Delta U)^2 \rangle}{k_B T^2} \\
 &= \frac{2}{k_B T^2} \langle \Delta U \Delta W \rangle \frac{1}{\gamma} - \frac{2}{k_B T^2} \langle (\Delta U)^2 \rangle = 0.
 \end{aligned} \tag{3.41}$$

$$(3.42)$$

We finally get:

$$\begin{aligned}
 0 = dC_v^{ex} &= \left( \frac{\partial C_v^{ex}}{\partial \ln(\rho)} \right)_T d \ln(\rho) + \left( \frac{\partial C_v^{ex}}{\partial \ln(T)} \right)_\rho d \ln(T) \\
 &= \frac{2}{k_B T^2} \langle \Delta U \Delta W \rangle d \ln(\rho) - \frac{2}{k_B T^2} \langle (\Delta U)^2 \rangle \gamma d \ln(\rho) \\
 &\quad + \frac{2}{k_B T^2} \langle \Delta U \Delta W \rangle \frac{1}{\gamma} d \ln(T) - \frac{2}{k_B T^2} \langle (\Delta U)^2 \rangle d \ln(T)
 \end{aligned} \tag{3.43}$$

which is satisfied only if

$$\gamma = \frac{\langle \Delta U \Delta W \rangle}{\langle (\Delta U)^2 \rangle} \tag{3.44}$$

i.e. only if  $\gamma$  is the slope calculated via the linear regression principle when  $W(t)$  is plotted against  $U(t)$ . Now it is possible to understand why in chapter 2 we have assumed that eq.(3.44) was a reasonable choice for  $\gamma$ : only this  $\gamma$  satisfies the density scaling invariance of fundamental thermodynamic quantities as the excess specific heat (in Paper IV the same derivation of  $\gamma$  is shown using the excess entropy).

Another problem related to  $\gamma$  is the fact that for strongly correlating liquids  $\gamma$  is slightly state point dependent. This problem is particularly important in simulations when we want to find approximated isomorphic state points. A slightly state point dependent  $\gamma$  means that the density scaling relation holds only locally. We can then find good approximated isomorphic points only if those state points are close enough to assume that  $\gamma$  is constant in that range of temperatures and densities. Thus, if we simulate a state point to which is associated a given  $\gamma = \gamma_1$  we can still find a close isomorphic point using the relation  $\rho_1^{\gamma_1}/T_1 = \rho_2^{\gamma_1}/T_2$ . We can then iterate the procedure using as new  $\gamma$  the slope calculated in state point 2 - i.e  $\gamma_2$  - to find a third state point close

### 3. DENSITY SCALING OF STRONGLY CORRELATING LIQUIDS AND ISOMORPHS

to state point 2 (and less close to state point 1 but still isomorphic to it) which satisfies the relation  $\rho_2^{\gamma_2}/T_2 = \rho_3^{\gamma_2}/T_3$ . The values of some isomorphic state points evaluated according to the above procedure are reported in table (3.1).

$T^*$	$\rho(\sigma_{AA}^{-3})$	$\mathbf{R}$	$\gamma$
0.795	1.318	0.975	4.964
0.707	1.288	0.967	5.018
0.628	1.258	0.957	5.110
0.557	1.228	0.950	5.138
0.490	1.198	0.942	5.182
0.431	1.168	0.919	5.200
0.847	1.291	0.973	4.983
0.752	1.261	0.967	5.043
0.665	1.231	0.959	5.108
0.586	1.201	0.944	5.130
0.515	1.171	0.930	5.191
0.450	1.141	0.904	5.212

Table 3.1: Two sets of isomorphic state points for the KABLJ. Each point has been evaluated using a local version of the density scaling relation as explained in the text. This is due to the fact that  $\gamma$  is not constant along an isomorph but is slightly state point dependent.

An even more accurate estimation of isomorphic points is done by using an algorithm that exploits informations on two known isomorphic state points to find another one. Suppose that we want to find the state point  $i + 1$  and we know state points  $i$  and  $i - 1$ . Equation (3.36) implies that

$$\gamma_i = \frac{\ln T_{i+1} - \ln T_{i-1}}{\ln \rho_{i+1} - \ln \rho_{i-1}} \quad (3.45)$$

from which follows that

$$\frac{(\rho_{i+1})^{\gamma_i}}{T_{i+1}} = \frac{(\rho_{i-1})^{\gamma_i}}{T_{i-1}}. \quad (3.46)$$

We can then start finding two isomorphic state points using the simpler relation  $(\rho_{i-1})^{\gamma_{i-1}}/T_{i-1} = (\rho_i)^{\gamma_{i-1}}/T_i$  and then we can continue the search according to the algorithm of eq. (3.45).

A third way of finding isomorphic points in simulations is given by the *direct isomorph check*. This check uses directly the definition of isomorphs in eq. (3.31), i.e. checks the proportionality of the Boltzmann factors of two isomorphic points. Consider then two isomorphic states 1 and 2. Since the Boltzmann factors are proportional then the relevant configurations of state 1 (i.e. the microscopic configurations having a large Boltzmann weight) are the same (in reduced units) of state 2. Once we know one or more of this relevant configurations we can proceed in the following way: suppose we know state 1 and only the density of state 2. We can take many different configurations of state 1, calculate the potential energy  $U_1 = U(\mathbf{r}_1^{(1)}, \dots, \mathbf{r}_N^{(1)})$  and scale the positions of all the particles in order to achieve the density of state 2. For

those new configurations we then calculate the new potential energy  $U_2 = U((\rho_1/\rho_2)^{1/3}(\mathbf{r}_1^{(1)}, \dots, \mathbf{r}_N^{(1)}))$ . If exists an isomorphic state point at the density  $\rho_2$  then the energies  $U((\rho_1/\rho_2)^{1/3}(\mathbf{r}_1^{(1)}, \dots, \mathbf{r}_N^{(1)})) = U(\mathbf{r}_1^{(2)}, \dots, \mathbf{r}_N^{(2)})$  are those of its relevant configurations. According to eq.(3.31) if we plot  $U_1$  against  $U_2$  we get a line whose slope  $m$  is the ratio between the temperatures of the two isomorphic state points. Since we know  $T_1$  then  $T_2 = m \cdot T_1$ . If the points are approximated isomorphic points as in the Lennard-Jones case, instead of a line we will get a scatter plot of energies as it is shown in fig. 3.1(a). Figure 3.1(b) shows the same procedure but starting from state 2. If the two points were not isomorphic the temperature resulting from the slope of the scatter plot in fig. 3.1(b) would have been different from  $T_1$ .

## 3.5 Isomorph properties

### 3.5.1 Statistical thermodynamics of isomorphs

In Paper IV a number of thermodynamic properties satisfying the scale invariance are enumerated. Here we show for some of them why the invariance holds by using the definition of isomorphs.

Let start considering the excess term of the relevant thermodynamic potential in the NVT ensemble, i.e. the excess Helmotz free energy  $F_{ex}$ :

$$e^{-\beta F_{ex}} = \int \frac{d\mathbf{r}_1}{V} \dots \frac{d\mathbf{r}_N}{V} e^{-\beta U(\mathbf{r}_1, \dots, \mathbf{r}_N)}. \quad (3.47)$$

For the free energy the same equation that relates the Boltzmann factors holds:

$$e^{-\beta F_{1,ex}} = C_{12} e^{-\beta F_{2,ex}}. \quad (3.48)$$

If we solve eq. (3.31) for  $C_{12}$  and insert it into eq.(3.48) we get:

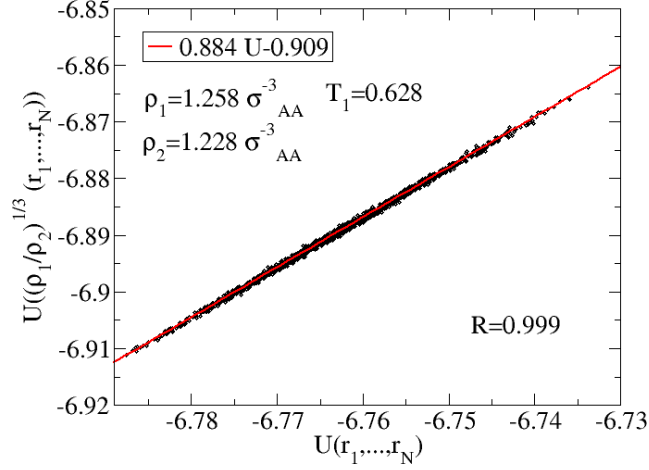
$$\frac{F_{1,ex} - U(\mathbf{r}_1^{(1)}, \dots, \mathbf{r}_N^{(1)})}{T_1} = \frac{F_{2,ex} - U(\mathbf{r}_1^{(2)}, \dots, \mathbf{r}_N^{(2)})}{T_2}. \quad (3.49)$$

We use now the same arguments of section 3.1.1 and we express  $(F_{ex} - U(\mathbf{r}_1, \dots, \mathbf{r}_N))/T = P(\mathbf{r}_1, \dots, \mathbf{r}_N)$  in reduced units. The result is that

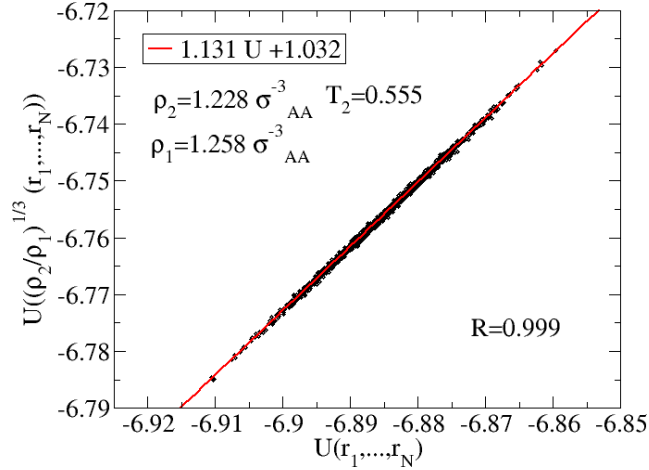
$$P(\tilde{\mathbf{r}}_1, \dots, \tilde{\mathbf{r}}_N) = \exp[-\beta(U(\tilde{\mathbf{r}}_1, \dots, \tilde{\mathbf{r}}_N) - \tilde{F}_{ex})] = const. \quad (3.50)$$

Using the same procedure we can derive many thermodynamic properties. For instance in the previous section we have used the invariance of the excess isochoric specific heat  $C_V^{ex}$  to obtain the expression of the slope  $\gamma$  in terms of fluctuations of the potential energy and the virial. We can here demonstrate the invariance of  $C_V^{ex}$ . Consider again the state point 1. Its isochoric specific heat can be expressed in terms of potential energy variance:  $C_V^{ex,(1)} = \langle(\Delta U_1)^2\rangle/k_B T_1^2$ . We define a new variable  $X = U/k_B T$ , then  $C_V^{ex,(1)} = k_B \langle(\Delta X_1)^2\rangle$ . We want to evaluate  $\Delta X = X - \langle X \rangle$  and show that is the same for two isomorphic state points showing automatically that  $C_V^{ex,(1)} = C_V^{ex,(2)}$ . From eq.(3.31) we know that  $(U_1/k_B T_1) = (U_2/k_B T_2) + \ln(C_{12})$ , i.e.  $X_1 = X_2 + \ln(C_{12})$ . It follows that  $\langle X_1 \rangle = \langle X_2 \rangle + \ln(C_{12})$  as well. Therefore

### 3. DENSITY SCALING OF STRONGLY CORRELATING LIQUIDS AND ISOMORPHS



(a)



(b)

Figure 3.1: Direct isomorph check for two state points of the KABLIJ. (a) The plot is the result of the following procedure: for each simulated configuration of state 1 the total energy  $U(\mathbf{r}_1, \dots, \mathbf{r}_N)$  is evaluated. Afterwards the configurations are scaled to a new density  $\rho_2$  of state 2 and the new energy  $U((\rho_1/\rho_2)^{1/3}(\mathbf{r}_1, \dots, \mathbf{r}_N))$  is calculated. According to eq. (3.31) the slope formed by the two energies should give the ratio  $m = (T_1/T_2)$ . Knowing  $T_1 = 0.628$  we find  $T_2 = 0.555$ . (b) Same procedure of (a) but starting now from the state  $(\rho_2, T_2)$  with  $T_2$  evaluated in (a). From the slope  $m = T_1/T_2$  we get  $T_1 = 0.628$  as expected in case of isomorphic points.

$$X_1 - \langle X_1 \rangle = X_2 + \ln(C_{12}) - \langle X_2 \rangle - \ln(C_{12}) = X_2 - \langle X_2 \rangle \quad (3.51)$$

i.e.  $\Delta X_1 = \Delta X_2$  and consequently  $C_V^{ex,(1)} = k_B \langle (\Delta X_1)^2 \rangle = k_B \langle (\Delta X_2)^2 \rangle = C_V^{ex,(2)}$ .

$T^*$	$\rho(\sigma_{AA}^{-3})$	$c_v^{ex}$
0.847	1.291	2.023
0.752	1.261	1.980
0.665	1.231	2.068
0.586	1.201	1.906
0.515	1.171	1.833
0.450	1.141	1.934

Table 3.2: excess isochoric specific heat per particle along an isomorph.

Many other thermodynamic invariants are reported in paper Paper IV. Here we briefly recall some of them

- The excess entropy defined as  $S_{ex} = \frac{1}{V^N} \int d\mathbf{r}_1 \dots d\mathbf{r}_N P(\mathbf{r}_1, \dots, \mathbf{r}_N) \ln P(\mathbf{r}_1, \dots, \mathbf{r}_N)$  is invariant along an isomorph. The requirement of constant entropy along isomorphs means that these curves are *configurational* adiabats. In  $U - W$  plane the thermodynamic relation  $TdS = dE + pdV$  is replaced by  $dU = Wd\ln(\rho)$  along an isomorph. This also tells us that the change of energy along an isomorph is controlled only by the density.
- The configurational entropy  $S_c$  defined as  $k_B \ln(\mathcal{N})$  - where  $\mathcal{N}$  is the density of states - is invariant along an isomorph. This is a consequence of the fact that the energy landscape of two isomorphic points are the same except for a scaling and a shifting factor according to eq.(3.31). A sketch of the two energy landscapes is depicted in fig. 3.5.1.

### 3.6 Static equilibrium properties

A comparison between theory and simulations is possible when equilibrium static properties of isomorphs are considered. From theory we can prove that reduced radial distribution functions - as well as higher order equilibrium particle probability distributions - are invariant along an isomorph. According to what we have shown in eq. (3.16) for IPL potentials, here the result is basically the same. Consider this time the second order radial distribution function  $g(r) = g(\mathbf{r}_1, \mathbf{r}_2)$  defined as follow:

$$g(\mathbf{r}_1, \mathbf{r}_2) = \frac{N!}{N^2(N-2)!} P(\mathbf{r}_1, \mathbf{r}_2) \quad (3.52)$$

where

$$P(\mathbf{r}_1, \mathbf{r}_2) = \frac{(1/V^{N-2}) \int e^{-\beta U(\mathbf{r}_1, \dots, \mathbf{r}_N)} d\mathbf{r}_3 \dots d\mathbf{r}_N}{(1/V^N) \int e^{-\beta U(\mathbf{r}_1, \dots, \mathbf{r}_N)} d\mathbf{r}_1 \dots d\mathbf{r}_N}. \quad (3.53)$$

### 3. DENSITY SCALING OF STRONGLY CORRELATING LIQUIDS AND ISOMORPHS

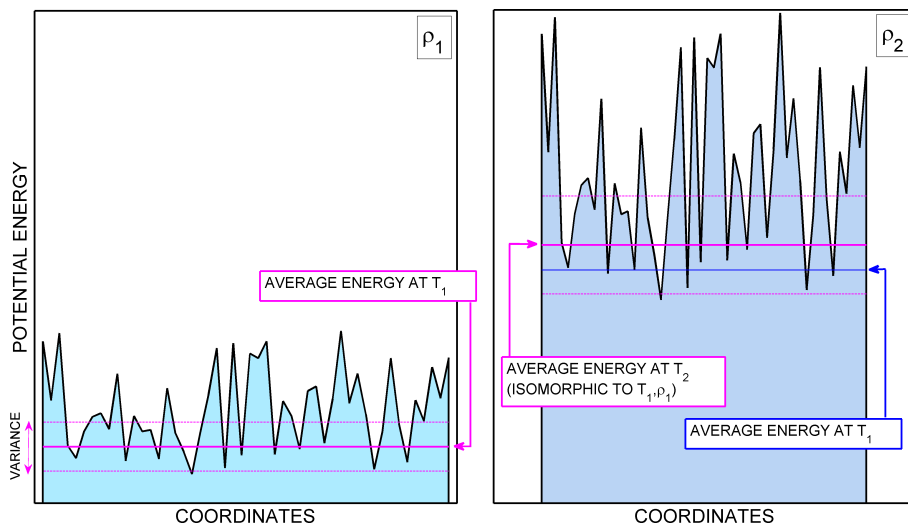


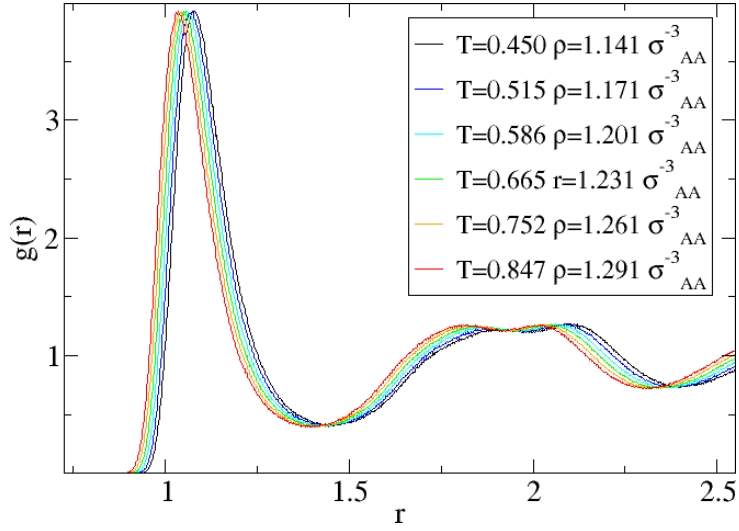
Figure 3.2: Sketch of the scaling of the potential energy landscape for a strongly correlating liquid. The 3N-dimensional energy surface is only shifted and scaled when the density is changed from  $\rho_1$  to  $\rho_2 (> \rho_1)$ . The average energy and its variance at  $(T_1, \rho_1)$  are indicated in the left figure (purple lines). The average energy of  $(T_2, \rho_2)$  isomorphous to  $(T_1, \rho_1)$  scales and shifts as the overall energy landscape as shown in the right figure by the purple lines. Note instead that if the point is not isomorphous as for instance  $(T_1, \rho_2)$  the average energy does not scale as in the isomorph case (blue line).

If we express everything in reduced units, for two isomorphous state points we have

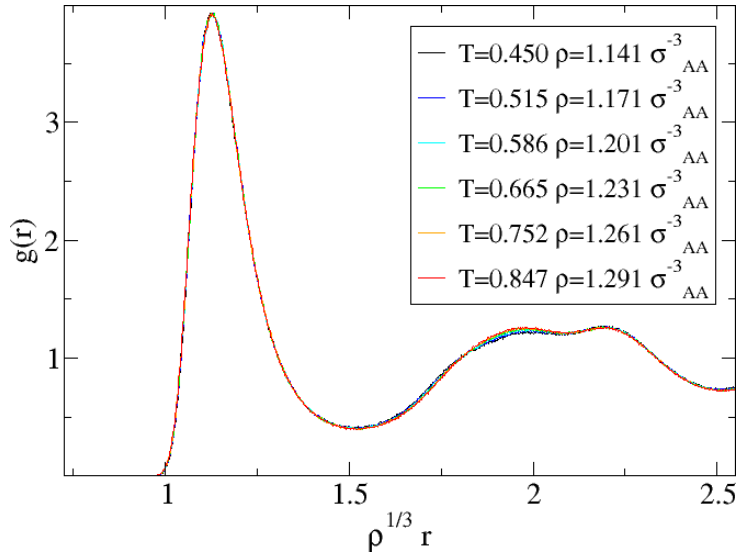
$$g^{(1)}(\rho_1^{1/3} r) = g^{(2)}(\rho_2^{1/3} r) \quad (3.54)$$

since  $\tilde{P}(\mathbf{r}_1, \mathbf{r}_2)$  is the same.

For testing this theoretical statement for a strongly correlating liquid we report here results from molecular dynamics simulations of the KABLJ system. The procedure that we have applied for searching for isomorphous points is the one described in section (3.4) : given a reference point  $(U(T_*, \rho_*), W(T_*, \rho_*))$  with a certain  $\gamma$ , we look for a new state  $(U(T, \rho), W(T, \rho))$  satisfying the relation  $\rho_*^\gamma / T_* = \rho^\gamma / T$ . Figure (3.6)(a) shows the radial distribution function of particles  $A$  (the largest particles in the KABLJ) for various isomorphous state points. Each state point has a density difference of 3% with the closest point covering a total density change of 18% while the total temperature change is of almost a factor 2. Note that - as predicted - the radial distribution functions are not invariant if they are not reported as a function of the reduced distances, but when this is done (fig. (3.6)(b)) the scaling is almost perfect. In Paper IV we report the scaled radial distribution functions also of particles  $B$ . In that case there is a larger deviation from the perfect scaling than in the case of particles  $A$ , a demonstration of the fact that isomorphs are an approximation for this liquid.



(a)



(b)

Figure 3.3: (a) Radial distribution functions (A particles) of a set of isomorphic points. The total density change is 18% while the temperatures change of a factor 2.(b) when the  $g(r)$ s are plotted in reduced distances the collapse into a single curve is almost perfect. This confirms the validity of the relation in eq. (3.54) for the KABLJ.

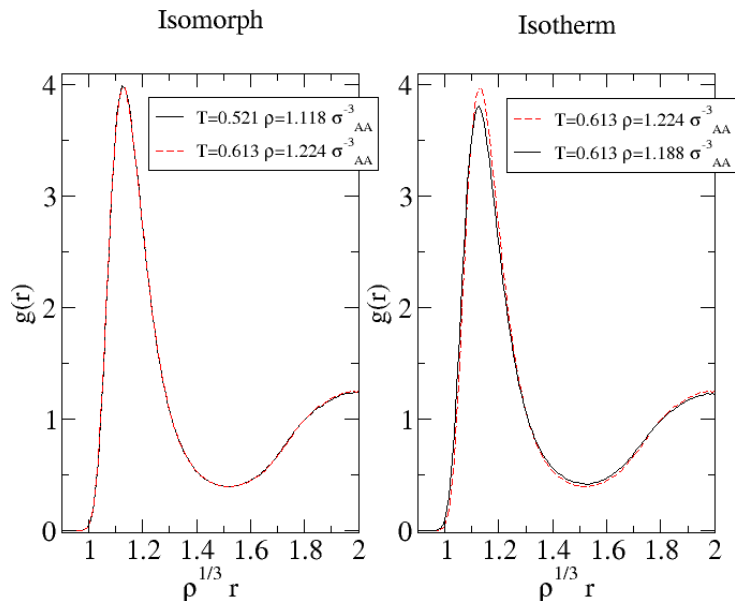


Figure 3.4: Comparison among reduced  $g(r)$  (A particles) for two isomorph points and those for two isothermal points of the KAB LJ system. Note that one of the isothermal points is also one of the isomorph points. From the figure it is clear that the good collapse observed also in fig. 3.6 is not an artifact due to the poor sensitivity of the  $g(r)$  to a density and temperature change, but is a real phenomenon that occurs only for isomorph points.

It is well known that the radial distribution function is not a very sensitive observable in the sense that it does not change significantly for small changes in densities and temperatures (except when a phase transition occurs). We wonder then what happens if we compare the reduced radial distribution functions of isomorph points with those of isothermal points: which has the best scaling? The situation is shown in fig. (3.6). There we show the comparison of the scaling of the first peaks of the reduced radial distribution functions for two isomorph state points and for two isothermal points (where one of the isothermal points is also one of the isomorph points of the nearby figure). It is clear from the two plots that the isomorph scaling is a significant property that has nothing to do with the small sensitivity of the radial distribution function.

### 3.7 Equilibrium dynamics

In section (3.1.1) we have shown that for IPL potentials the Newtonian dynamics satisfies the density scaling relation and therefore reduced Newtonian dynamics is invariant along an isomorph.

In the previous section we have already used the term “reduced” units. In those cases we have always dealt with reduced positions. In addition there exist also natural reduced units for time and energy as it is shown in Table 3.3. The argument of section (3.1.1) refers to the so called *NVE* dynamics. Our simulations

Quantity	Newtonian dynamics	Brownian dynamics	Monte Carlo dynamics
Energy units ( $E_0$ )	$k_B T$	$k_B T$	$k_B T$
Length units ( $l_0$ )	$\rho^{-1/3}$	$\rho^{-1/3}$	$\rho^{-1/3}$
Time units ( $t_0$ )	$\sqrt{(m/k_B T)}/\rho^{1/3}$	$1/\rho^{2/3}\mu k_B T$	$\tau(\rho^{-1/3}\delta_{max})$

Table 3.3: Reduced units. Note that the time units depends on which dynamics we are considering. For Monte Carlo dynamics the relaxation time depends on  $\delta_{max}$ , i.e. the maximum distance that a particle can cover during one Monte Carlo step. Then to get a reduced time we have to set a reduced  $\delta_{max}$  at the beginning of the simulation.

instead are performed mostly in the canonical ensemble corresponding to NVT Newtonian dynamics. To maintain the temperature of the system constant in simulations we want the particle velocities to be controlled by a thermostat. In our simulations we use the Nosé-Hoover thermostat [Nosé (1984)]. This can be basically implemented by adding an extra term in the force - a friction term -  $\zeta \dot{\mathbf{r}}_i$  where the friction coefficient is controlled by a first order differential equation  $\dot{\zeta} = (1/M) [(\sum_i p_i^2/2m_i)/(3N+1)k_B T_{bath} - 1]$  where  $M$  is a thermal inertial parameter which determines the rate of heat transfer and that can be considered as a thermostat time constant. If we include this extra term in Newton's equation it is possible to show that the equation becomes invariant when written in reduced units (see Paper IV). As a consequence of the invariance of the NVT dynamics we expect to have same time dependent correlation functions along an isomorph when expressed in reduced units as well as reduced transport coefficients, like the diffusion constant  $D$  that can be extracted from the mean square displacement. Figure (3.5) (b) shows the self-intermediate scattering functions of particles  $A$  in reduced units for seven different isomorph points of the KABLJ system.

Also in this case we have a very good superposition. Again to appreciate the scaling we can compare the reduced self-intermediate scattering functions for two isomorph points and those of two isothermal state points. The results are shown in fig. 3.5. The quality of the scaling here is even more striking than in the case of the radial distribution functions in fig. 3.6.

Since the mean square displacement is the velocity-velocity correlation function, we expect a good scaling as well as it is shown in fig. (3.7). Moreover the diffusion constant can be evaluated from the mean square displacement since in the diffusive regime we have that  $\langle \Delta r^2 \rangle = 6Dt$ , then from fig. (3.7) (b) we get that the reduced diffusion coefficient  $\tilde{D} = \rho^{1/3} \sqrt{m/k_B T} D$  is invariant along an isomorph.

We have stated many times that only strongly correlating liquids have isomorphs. We expect that in liquids with small correlation coefficient - like water - it is not possible to find isomorph points. Thus we have investigated water using two different strategies. In the first one we suppose that water has isomorphs. Then all the points with the same reduced diffusion constant should have the same structure, dynamics etc... Figure 3.7 shows a set of isochoric points at two different densities and for them we have plotted the logarithm of the inverse reduced diffusion constant  $D^*$  as a function of  $1/T$ . The two sets

### 3. DENSITY SCALING OF STRONGLY CORRELATING LIQUIDS AND ISOMORPHS

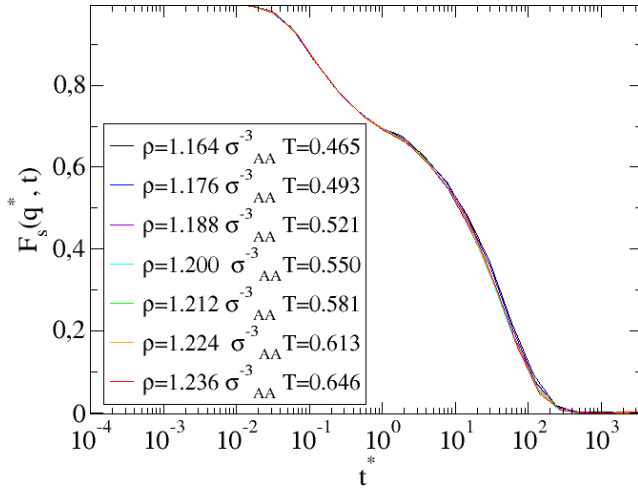


Figure 3.5: Reduced self-intermediate scattering function  $F_s(q^*, t)$  (A particles) for a set of isomorphous state points of the KABLJ system. The collapse is very good. The plot confirms that the dynamics is the same along an isomorph: it means that the state points have not only the same relaxation time but the all shape of the  $F_s(q^*, t)$  must coincide. Data of Thomas Schröder.

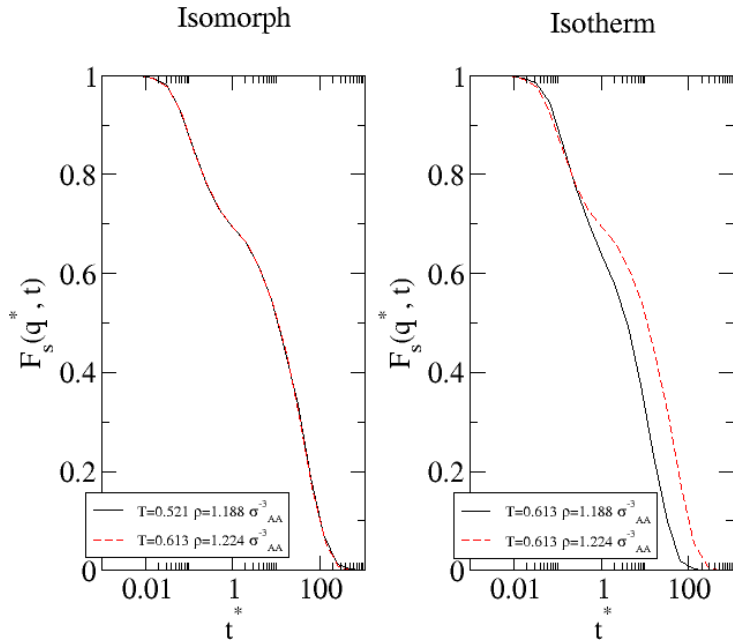


Figure 3.6: Comparison of the reduced self-intermediate scattering function  $F_s(q^*, t)$  (A particles) for two isomorphous points and two isothermal points of the KABLJ system. As in the case of the radial distribution function the scaling appears only along an isomorph.

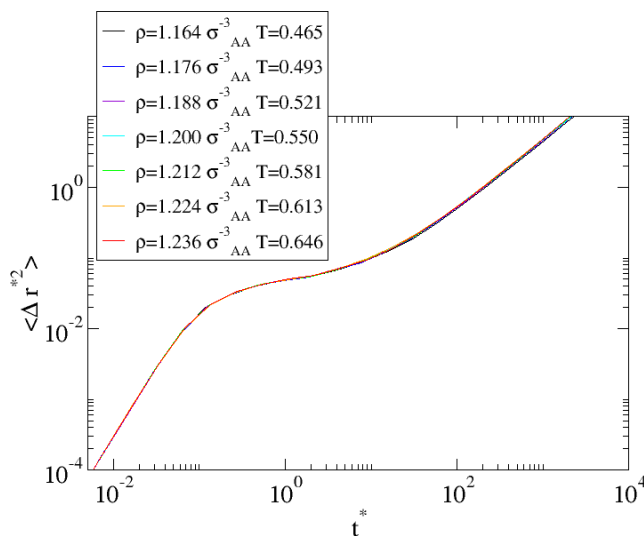


Figure 3.7: Reduced mean square displacement (A particles) for a set of isomorph points of the KABLJ system. A very good collapse is found. A consequence of the scaling is that the reduced diffusion constant that can be estimated in the diffusive regime of the mean square displacement -  $D^* = \langle \Delta r^{*2} \rangle / 6t^*$  - is the same for all the isomorph points. Data of Thomas Schröder.

of data have been interpolated with polynomial functions in order to find two points having the same  $D^*$ . The intersection of the two curves defines these two points. If the two states are isomorph then the structure should be the same in reduced units. The result is shown in fig. 3.9. Clearly the structure of the two points is completely different confirming that isomorphs do not exist in non strongly correlating liquids.

Another way for looking for isomorph points in water is to use the direct isomorph check. The results are shown in fig. 3.10 (a) and (b). Starting from state  $(T_1, \rho_1)$  we have evaluated the potential energy of configurations that a state point  $(T^*, \rho_2)$  (where  $T^*$  is unknown) would have if its relevant configurations (in reduced units) were equal to those of  $(T_1, \rho_1)$ . The slope  $m$  between these new energies and those of  $(T_1, \rho_1)$  when they are plotted against each other gives the value  $T^* = mT_1 = T_2$ . If  $(T_1, \rho_1)$  and  $(T_2, \rho_2)$  were isomorph then we would expect to find the temperature  $T_1$  by making the direct check but starting from  $(T_2, \rho_2)$ . Instead what we find is something very different as shown in fig. 3.10: clearly SPC water has no isomorphs.

### 3.8 A breakdown of the isomorph theory: the WCA potential

So far we have used the KABLJ potential to show how the isomorph approximation works well in strongly correlating liquids. In this framework the reader maybe got the idea that the more the liquid is strongly correlating the more the isomorph approximation is good. Unfortunately this turned out to be a

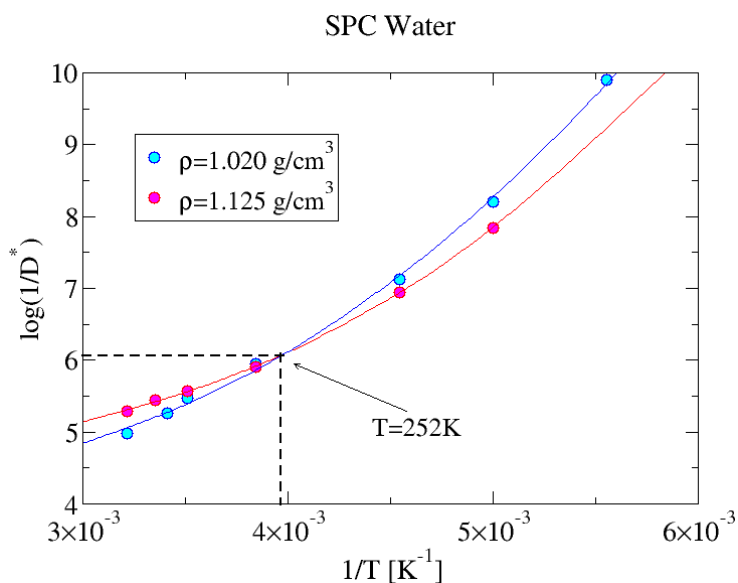


Figure 3.8: Logarithm of the inverse reduced diffusion constant  $D^*$  as a function of the inverse temperature for two sets of isochoric points in SPC water [Berendsen *et al.* (1987)]. The points have been interpolated with two polynomial curves. The intersection of the curves identifies two state points with the same  $D^*$ .

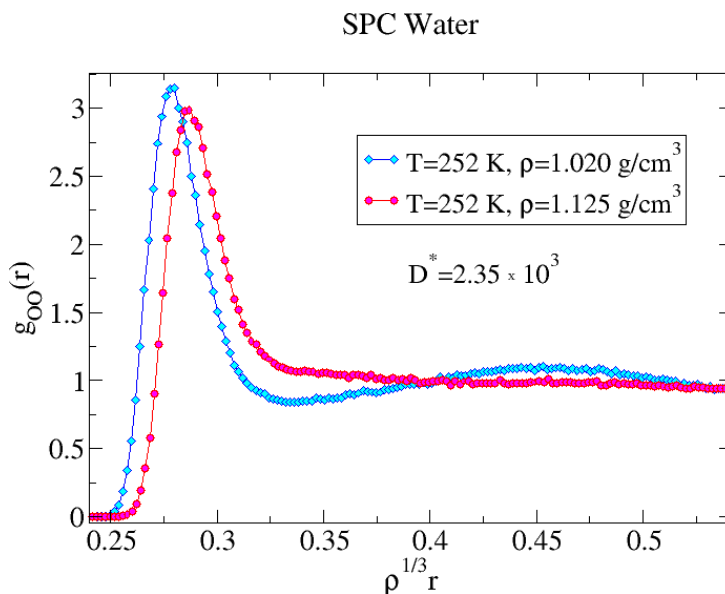


Figure 3.9: Oxygen-oxygen radial distribution functions for two points having the same reduced diffusion constant. If the points were isomorphic then they would have had the same structure in reduced units and therefore identical radial distribution functions. Clearly this is not the case.

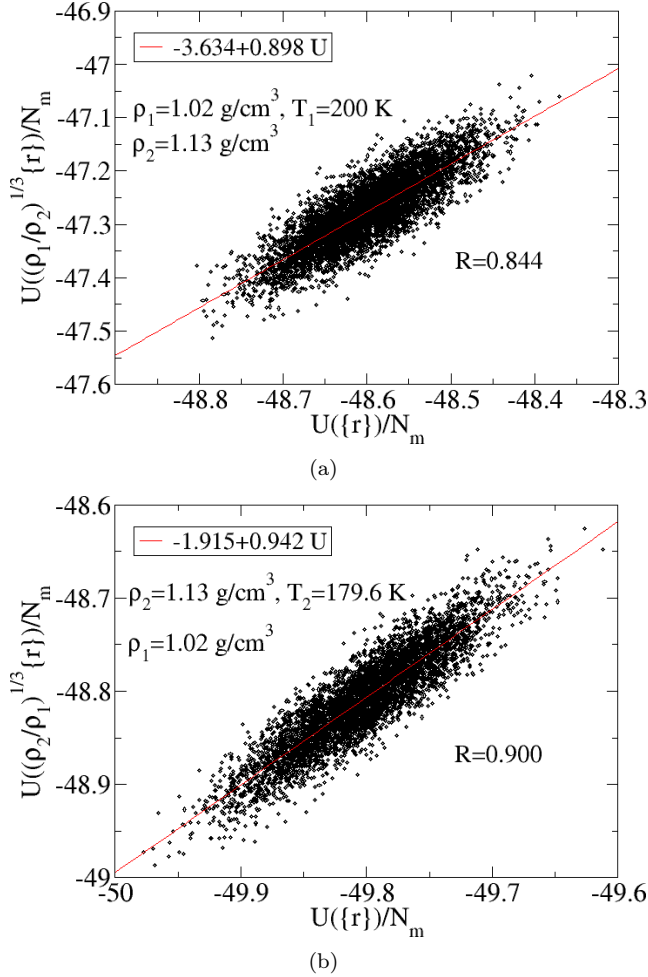


Figure 3.10: Direct isomorph check for SPC water [Berendsen *et al.* (1987)].  $N_m$  is the number of water molecules. The procedure for finding hypothetical isomorph points is the same explained in section 3.4. (a) from the potential energy of configurations belonging to  $(T_1 = 200K, \rho_1 = 1.02g/cm^3)$  a rescaled energy is evaluated from the corresponding rescaled configurations with a density  $\rho_2$ . Afterwards from the slope of the scatter plot a temperature  $T_2 = 179.6K$  associated to  $\rho_2$  is found. (b) same procedure of (a) but starting from  $(T_2 = 179.6K, \rho_2 = 1.13g/cm^2)$  with  $T_2$  evaluated in (a). From the slope of the scatter plot we find  $T_1 = 169.2K$  different from  $T_1$  in (a); it means that the relevant scaled configurations of state 1 are not relevant for state 2 and consequently the two states are not isomorphic.

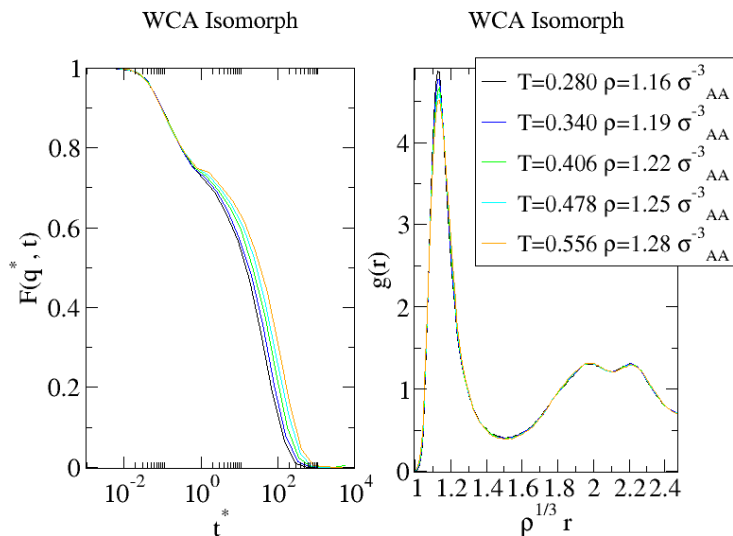


Figure 3.11: scaled self-intermediate scattering functions for the binary WCA. The points have been found using the algorithm in eq. (3.45). Clearly the scaling is not perfect as it is in the case of the KABLJ.  $\gamma$  varies between  $\gamma = 6.30$  (at  $(T = 0.556, \rho = 1.28)$ ) and  $\gamma = 7.85$  (at  $(T = 0.28, \rho = 1.16)$ ). A comparison between the scaling of the WCA and that of different Lennard-Jones liquids is shown in fig. 3.14.

wrong picture as shown by the case of the Weeks-Chandler-Andersen potential (WCA) [Andersen *et al.* (1971), Heyes & Okumura (2006), Ahmed & Sadus (2009)]. The WCA potential is defined as

$$v(r) = 4\varepsilon\left[\left(\frac{\sigma}{r}\right)^{12} - \left(\frac{\sigma}{r}\right)^6\right] - \varepsilon \quad r < r_c \quad (3.55)$$

$$= 0 \quad r \geq r_c \quad (3.56)$$

where  $r_c = 2^{1/6}\sigma$  is the cut-off corresponding to the minimum of the Lennard-Jones potential. This is a totally repulsive potential with discontinuous forces at  $r = r_c$ . It was shown in reference [Berthier & Tarjus (2009)] that this system does not satisfy the density scaling relation even though the correlation is higher than in the KABLJ. It was also noted in reference [Coslovich & Roland (2009)] that  $\gamma$  varies very much on the same density range in which the  $\gamma$  of the corresponding LJ system is almost constant. Here we try to investigate the problem that makes the WCA so different from strongly correlating liquids discussed so far.

We have simulated the WCA version of the KABLJ potential (i.e. we have cut the KABLJ at  $r_c = 2^{1/6}\sigma_{\alpha\beta}$ ) and we have tried to find isomorphic state points using the density scaling relation in the form of the algorithm in eq.(3.45). The results for the scaled self-intermediate scattering functions and the scaled radial distribution functions are shown in fig. 3.11.

It is clear that - despite the high correlation coefficient ( $0.972 < R < 0.981$ ) and the accuracy in seeking for isomorphic state points - the scaling of both

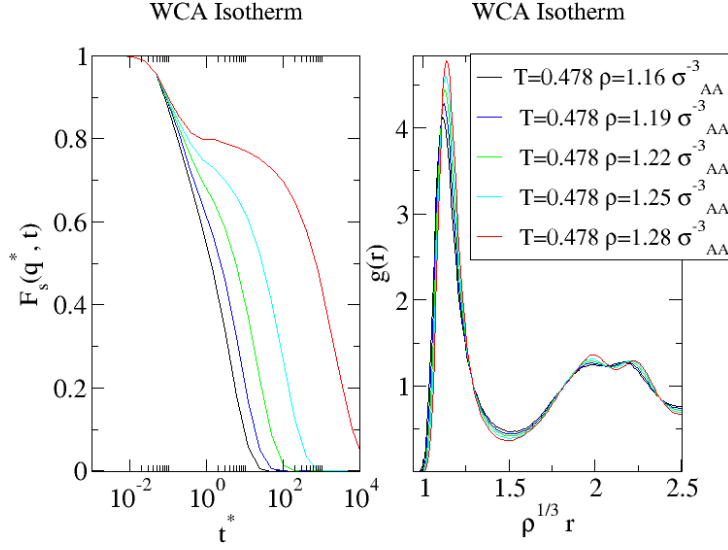


Figure 3.12: scaled self-intermediate scattering functions and radial distribution functions for a set of isothermal state points at  $T = 0.478$  having the same densities of points in fig.3.11.

the self-intermediate scattering functions and the radial distribution functions is not as good as it is for the KABLJ. Although a clear deviation from the perfect scaling is observed we have that this deviation is significantly smaller compared to the change of the self-intermediate scattering function and of the reduced radial distribution function along an isochore and an isotherm (see fig. 3.12 and fig. 3.13).

We naturally wonder what causes such departure from the perfect scaling. A possible problem could be the discontinuity of the forces at the cut-off distance. To avoid discontinuous forces the potential can be “smoothed” i.e. a polynomial term is added in order to guarantee continuity up to the third derivative of the potential (we are ensuring that also the derivatives of the forces are continuous). If the polynomial term is  $S(r) = (A/3)(r - r_1)^3 - (B/4)(r - r_1)^4 - C$  then

$$v(r) = v_{WCA}(r) - C \quad r < r_1 \quad (3.57)$$

$$= v_{WCA}(r) - S(r) \quad r_1 \leq r < r_c \quad (3.58)$$

$$= 0 \quad r \geq r_c \quad (3.59)$$

where  $A$ ,  $B$  and  $C$  are found imposing the following constraints:

$$S(r_1) = 0 \quad (3.60)$$

$$S'(r_1) = 0 \quad (3.61)$$

$$S(r_c) = -F_{WCA}(r_c) \quad (3.62)$$

$$S'(r_c) = -F'_{WCA}(r_c). \quad (3.63)$$

The results of the smoothing are shown in the isomorph check of fig. (3.15). As explained in section 3.4, in fig. 3.15 (left panel) from state  $(T_1, \rho_1)$  the

### 3. DENSITY SCALING OF STRONGLY CORRELATING LIQUIDS AND ISOMORPHS

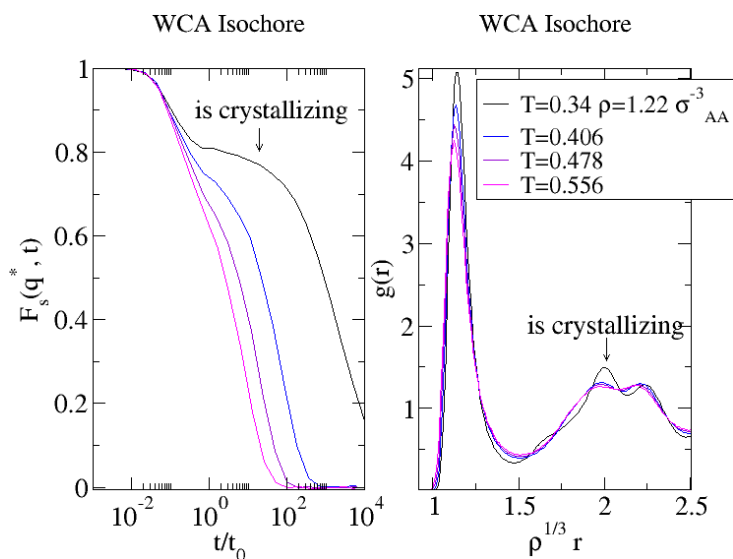


Figure 3.13: scaled self-intermediate scattering functions and radial distribution functions for a set of isochoric points at  $\rho = 1.22\sigma_{AA}^{-3}$  having the same temperatures of points in fig.3.11. Note that crystallization occurs at  $T = 0.34$ .

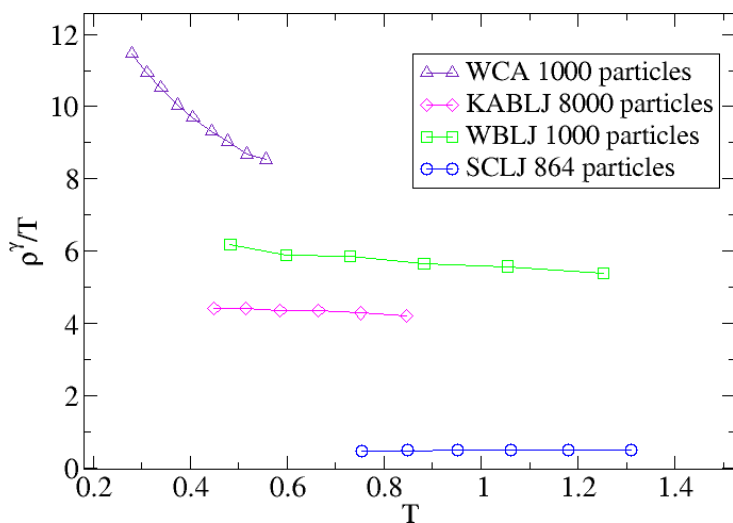


Figure 3.14: Comparison among isomorphous points of four systems. For all the different Lennard-Jones systems state points have been found using the local version of the density scaling relation as explained in section 3.4. The points of the WCA system instead have been evaluated according the more accurate algorithm of eq. (3.45). If the points satisfy the density scaling equation  $\rho^\gamma/T = Const.$  then each set of state points should lay on a horizontal straight line. This is true in the Lennard-Jones cases while there is a clear deviation for the WCA.

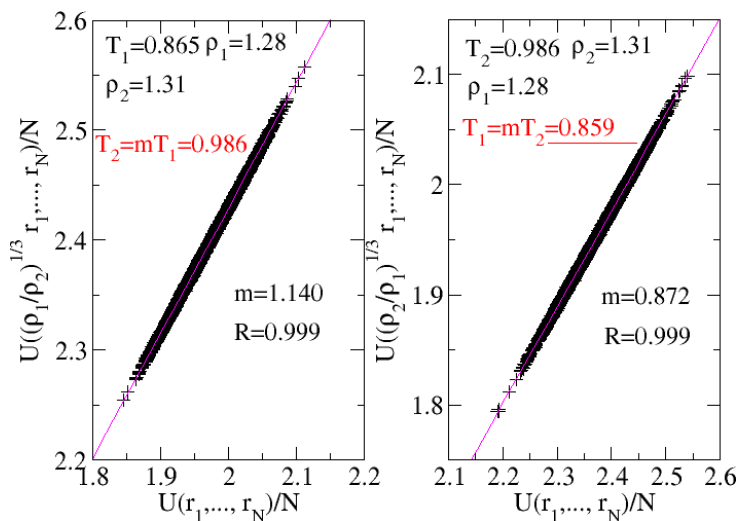


Figure 3.15: Double direct isomorph check after the WCA potential has been smoothed. The different temperature found in the left panel than the expected  $T_1 = 0.865$  is a proof that smoothing the potential does not solve the deviation from the perfect scaling in the WCA.

energies of new configurations belonging to another state at density  $\rho_2$  are evaluated. These should be the relevant configurations for that state if it is isomorphic to  $(T_1, \rho_1)$ . From the slope of fig. 3.15 (left panel)  $T_2$  is evaluated and the all procedure is repeated starting from  $(T_2, \rho_2)$ . If the two points are isomorphic then the new temperature calculated in fig. 3.15 (right panel) should be  $T_1$ . Instead the temperature we find is slightly different. This discrepancy is the proof that smoothing the potential does not solve the problem for the WCA system.

The problem instead could be given by the fact that the cut-off of the potential is in the the first peak of the  $g(r)$  cutting-off some relevant interactions that are important for the existence of isomorphic states (see fig. 3.16).

If this is the problem than it should happens all the times that we cut the potential of a strongly correlating liquids with isomorphs close to the interparticle distance. For investigating this possibility we studied an inverse power-law potential  $v(r) = (\sigma/r)^{18} - (\sigma/r_c)^{18}$  at two different cut-offs:  $r_c = 2^{1/6}\sigma$  and  $r_c = 2.5\sigma$ . What we expect is that for the short cut-off, the shift term interferes in the correlation forcing the inverse power-law to be less than 100% correlated. That is in fact what can be seen in fig. 3.17 (left panel). For the large cut-off instead the system continues to be 100% correlated and the slope is exactly  $n/3 = 6$  (see fig. 3.17 right panel).

Starting from a common state point, for both the cut-offs we have used the isomorph direct check to find isomorphic points and we have tested the scaling for the reduced radial distribution functions as shown in fig. 3.18.

For the standard cut-off the collapse between the two radial distribution functions is perfect as expected from a 100% correlating liquid. Instead when the cut-off is moved to  $r_c = 2^{1/6}\sigma$ , a deviation from the perfect scaling is observed. Then the cut-off ruins the perfect correlation in the IPL but even

### 3. DENSITY SCALING OF STRONGLY CORRELATING LIQUIDS AND ISOMORPHS

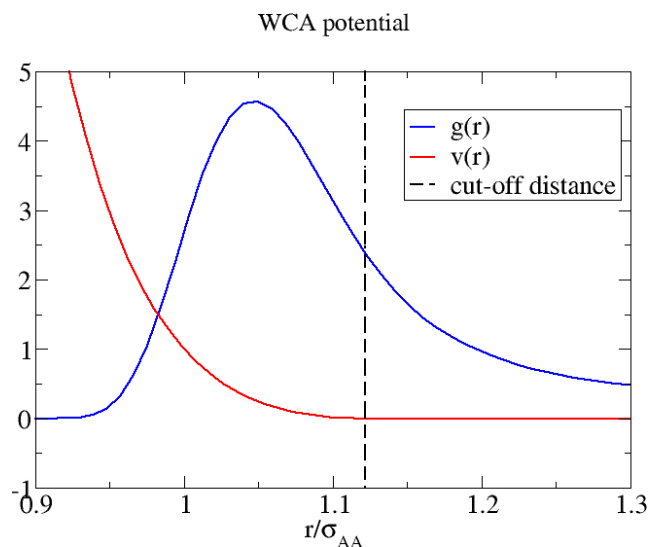


Figure 3.16: radial distribution function  $g(r)$  together with the WCA potential. The cut-off of the potential is at  $r_c = 2^{1/6}\sigma_{AA}$  i.e. inside the first peak of the  $g(r)$ . The presence of the cut-off in that region could remove from the dynamics some important interactions for a good isomorph scaling.

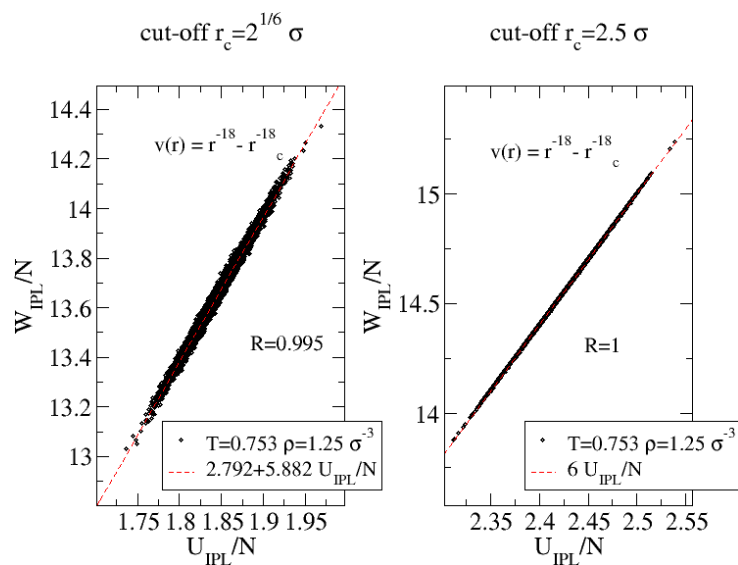


Figure 3.17: Correlation for an IPL potential cut at  $r_c = 2^{1/6}\sigma$  and  $r_c = 2.5\sigma$ .

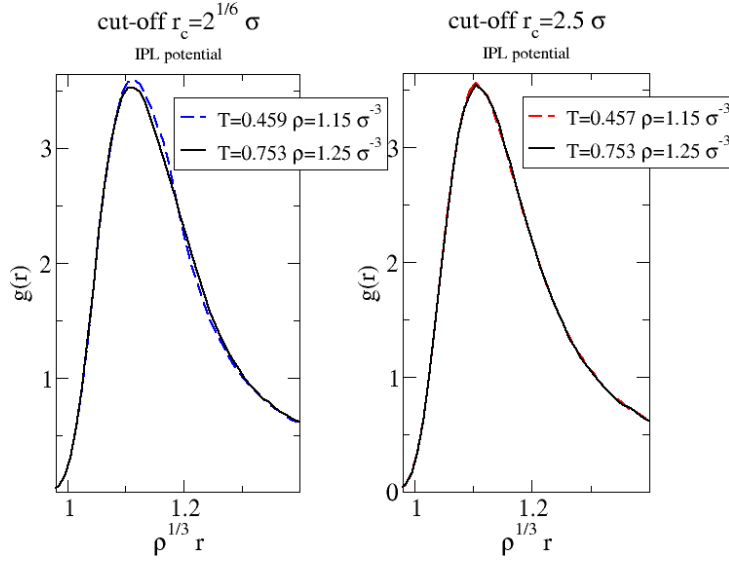


Figure 3.18: scaled radial distribution functions for an IPL potential cut at  $r_c = 2^{1/6}\sigma$  and  $r_c = 2.5\sigma$ . While the scaling is perfect when  $r_c = 2.5\sigma$ , a deviation from the perfect collapse is observed when  $r_c = 2^{1/6}\sigma$ .

more the perfect scaling since fig. 3.18 (right panel) shows a deviation from the isomorph scaling larger than what we have observed in the KABLJ. We expect then the the scaling in the WCA is ruined as well by the cut-off. This is something that our theory on isomorphs cannot predict since no statements on the cut-off (that is something that we artificially introduce in simulations) are needed. Anyway the analysis done above does not explain why the WCA has higher correlation coefficient than the KABLJ but a worse scaling. A qualitative explanation could be given by fig. 3.19. It shows three plots for three different systems of the correlation between single particle energy and virial. The bad correlation of the SCL and of the KABLJ does not surprise much. In fact in Paper III we stated many times that strong correlation is a collective effect and cannot be traced back in the single pair virial and potential energy correlation. Surprising is instead the correlation of the WCA which is very high. This explains its strong correlation. It seems that the cut-off removes some important interactions that give rise to a good scaling in strongly correlating liquids; these interactions are those that inhibit the correlation at the level of single pairs and turn it into a collective effect. Once these interactions are removed the single pair correlation is restored but the good scaling is lost.

### 3.9 Equations of isomorphs in the U-W plane

So far we have used the density scaling relation for finding isomorphic points in simulations. This relation is only an approximated procedure that we no longer need if we are not looking for state points but we want only to know

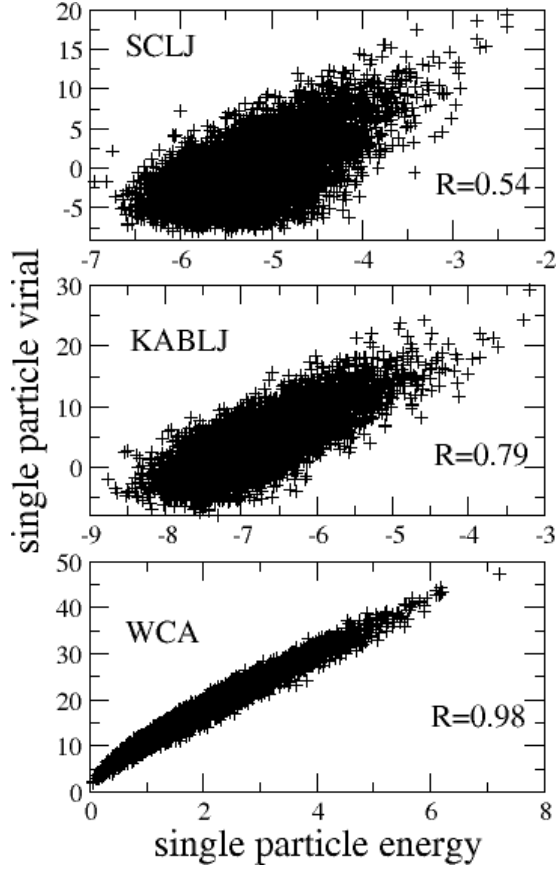


Figure 3.19: single particle virial and potential energy for the SCLJ, the KABLJ and the WCA potential. The SCL (864 particles) has been simulated at the state ( $T = 80K, \rho = 34.6mol/l$ ) in Argon units, the KABLJ (8000 particles) at the state ( $T = 0.586, \rho = 1.200$ ) and the WCA (1000 particles, MC simulation) at the state ( $T = 0.753, \rho = 1.253$ ).

the shape of an isomorph in the  $U$ - $W$  phase diagram. In this diagram in fact we are able to derive a set of equations defining isomorphic points only by assuming that isomorphs exist (the same problem is discussed in Paper V). Consider a generalized Lennard-Jones pair interaction, i.e. a sum of inverse power-law potentials (if we substitute  $m$  and  $n$  with 12 and 6 we get back the standard 12-6 Lennard-Jones potential used so far)

$$v_{ij}(r_{ij}) = v_{ij}^{(m)} + v_{ij}^{(n)}, \quad v_{ij}^{(k)} \equiv \varepsilon_{ij}^{(k)} \left( \frac{\sigma_{ij}^{(k)}}{r_{ij}} \right)^k. \quad (3.64)$$

We can write the total potential energy and virial

$$U = U_m + U_n, \quad U_k \equiv \sum_{i>j} v_{ij}^{(k)}(r_{ij}) \quad (3.65)$$

$$W = \frac{m}{3}U_m + \frac{n}{3}U_n, \quad (3.66)$$

and we can solve the equations above for  $(U_m, U_n)$ :

$$U_m = \frac{-3W + nU}{n - m} \quad (3.67)$$

$$U_n = \frac{3W - mU}{n - m}. \quad (3.68)$$

We now use the fact that all the configurations along an isomorph have the same reduced coordinates, i.e.  $\rho_1^{1/3}r^{(1)} = \rho_2^{1/3}r^{(2)} = \tilde{r}$ . Moreover we identify the potential energy and the virial of a state point along an isomorph using the following notation:  $U_k(T, \rho)_{isomorph} = U_k(\Gamma, \rho)$  where  $\Gamma = \rho^{k/3}/T$ . Denoting with “\*” a reference state point the isomorph scaling implies:

$$\begin{aligned} \frac{U_m(\Gamma_*, \rho)}{\rho^{m/3}} &= \frac{1}{\rho^{m/3}} \sum_{i>j} \varepsilon_{ij}^{(m)} \left( \frac{\sigma_{ij}^{(m)}}{\tilde{r}_{ij}\rho^{-1/3}} \right)^m \\ &= \frac{1}{\rho^{m/3}\rho^{-m/3}} \sum_{i>j} \varepsilon_{ij}^{(m)} \left( \frac{\sigma_{ij}^{(m)}}{r_{ij}\rho^{*1/3}} \right)^m \\ &= \frac{1}{\rho^{*m/3}} \sum_{i>j} \varepsilon_{ij}^{(m)} \left( \frac{\sigma_{ij}^{(m)}}{r_{ij}} \right)^m = \frac{U_m(\Gamma_*, \rho^*)}{\rho^{*m/3}} = \frac{U_m^*}{\rho^{*m/3}}, \end{aligned} \quad (3.69)$$

i.e. for a given state point belonging to the same isomorph of the reference state the rescaled potential energy (i.e the energy divided by the density) is equal to the one of the reference point. If we define  $\tilde{\rho} = \rho/\rho^*$ , we can also rewrite eq.(3.69) as

$$U_m(\Gamma_*, \rho) = \left( \frac{\rho}{\rho^*} \right)^{m/3} U_m^* = \tilde{\rho}^{m/3} U_m^*. \quad (3.70)$$

If we combine eq.(3.65), eq.(3.66) and eq.(3.70) we obtain an expression that defines isomorphs in the  $U$ - $W$  plane:

$$U = \tilde{\rho}^{m/3} U_m^* + \tilde{\rho}^{n/3} U_n^* \quad (3.71)$$

$$W = \frac{m}{3} \tilde{\rho}^{m/3} U_m^* + \frac{n}{3} \tilde{\rho}^{n/3} U_n^*. \quad (3.72)$$

For the 12 – 6 Lennard-Jones potential the equations above become:

$$\frac{U}{\tilde{\rho}^2} = U_{12}^* \tilde{\rho}^2 + U_6^* \quad (3.73)$$

$$\frac{W}{4\tilde{\rho}^2} = U_{12}^* \tilde{\rho}^2 + \frac{1}{2} U_6^*. \quad (3.74)$$

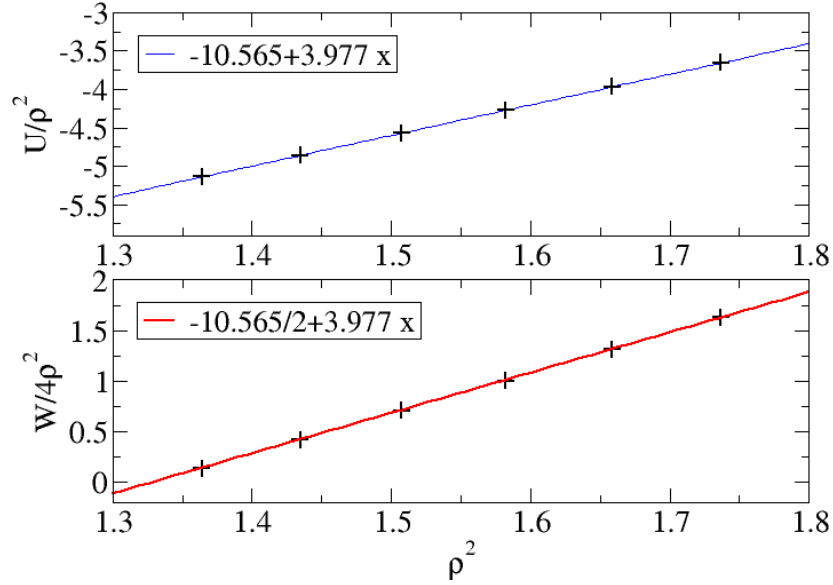


Figure 3.20: Comparison between simulations and theoretical predictions: if  $U/\tilde{\rho}^2$  is plotted as a function of  $\tilde{\rho}^2$  the data from simulations of the KABLJ should lay on a line according to eq. (3.73). This is shown in the upper plot where all the points are interpolated with a linear fit. The slope and the intercept of the fit give, respectively,  $U_{12}^*$  and  $U_6^*$ . We use these two values for drawing the line in the lower plot which therefore is not a fit. All the points match the line, which confirms the prediction in eq. (3.74).

We can now check the validity of these equations by comparing them with the results obtained from simulations.

Figure 3.20 (a) shows the first theory check. According to eq. (3.73) isomorphous points should lay on a straight line if  $U/\tilde{\rho}^2$  is plot as a function of  $\tilde{\rho}^2$ . The slope and the intercept of the fit done in the upper panel of fig. 3.20 give respectively  $U_{12}^*$  and  $U_6^*$ . We can use these values for testing eq. (3.74). In the lower panel of fig. 3.20 a line is drawn using the parameters extracted from the previous fit. The line matches the points meaning that there is a good agreement between the theoretical results in eq. (3.73) and eq. (3.74) and simulations.

We are now able to draw an isomorph curve in the  $U$ - $W$  diagram as it is shown in fig. 3.21. The full lines come from eq. (3.73) and eq. (3.74) while the scatter plots are simulation results from two sets of isomorphous points of the KABLJ system. The agreement between theory and simulations is good even for values of virial very close to zero.

### 3.10 The *master* isomorph

It is important to stress that eq. (3.73) and eq. (3.74) depend only on the exponents 12 and 6 but not on the parameters of the potential. This means that all the 12-6 Lennard-Jones potentials, i.e. single component LJ, multi

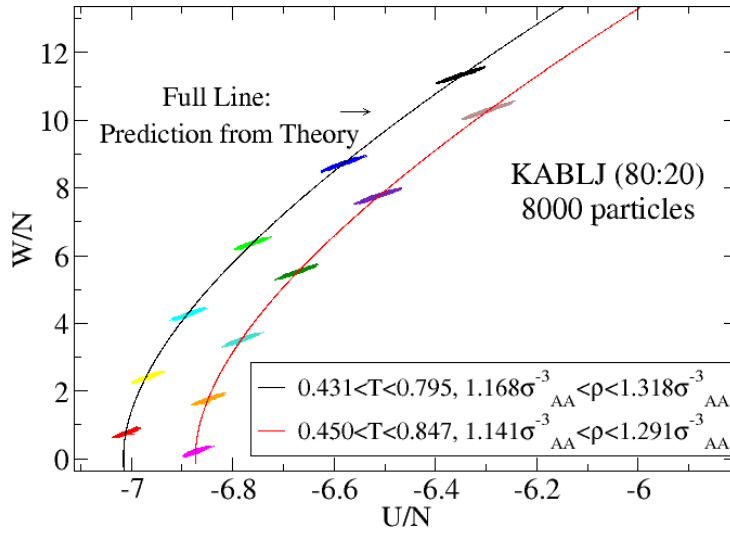


Figure 3.21: Isomorphs in the  $U$ - $W$  phase diagram. the full lines correspond to the predictions of eq. (3.73) and eq. (3.74) while the ellipses are the scatter plots coming from MD simulations of the KABLJ. Note that the very good comparison between simulations and theory holds also close to zero virial.

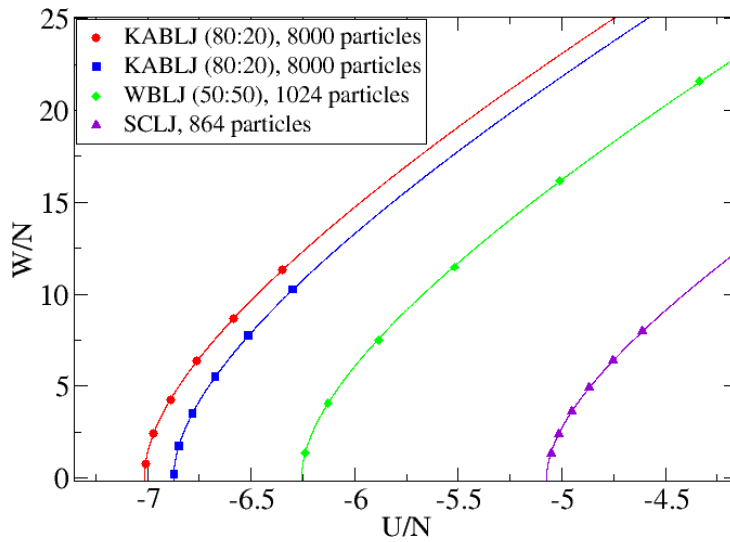


Figure 3.22: four different sets of isomorph points belonging to three different LJ systems.

### 3. DENSITY SCALING OF STRONGLY CORRELATING LIQUIDS AND ISOMORPHS

component LJ, polydispersed LJ, etc., have all the same isomorphs shape. Here we show that given a reference point we can scale isomorphs into a curve which is the same for all the scaled isomorphs belonging to 12-6 LJ systems. Consider again the equations defining an isomorph in the  $U$ - $W$  plane (eq.(3.73) and eq.(3.74)). We can solve the equations respect to  $\tilde{\rho}^2$  and  $\tilde{\rho}^4$ :

$$\tilde{\rho}^2 = -\frac{W - 4U}{2U_6^*} = \frac{W - 4U}{W^* - 4U^*} \quad (3.75)$$

and

$$\tilde{\rho}^4 = \frac{W - 2U}{2U_{12}^*} = \frac{W - 2U}{W^* - 2U^*} \quad (3.76)$$

where we have used also eq.(3.67) and eq. (3.68). We choose as a reference point ( $W^* = W_0^*, U^* = 0$ ). If we substitute  $W_0^*$  to  $W^*$  and 0 to  $U^*$  in eq.(3.75) and then we insert it into eq.(3.76) we find an expression for  $W_0^*$ :

$$W_0^* = \frac{(W - 4U)^2}{W - 2U}. \quad (3.77)$$

Note that  $W_0^*$  is the only number that identifies the isomorph to which it belongs. Solving eq.(3.77) for  $W/W_0^*$  we find:

$$\frac{W}{W_0^*} = \frac{(8U/W_0^* + 1) \pm \sqrt{(8U/W_0^* + 1)^2}}{2} \quad (3.78)$$

that gives real solutions only for  $U/W_0^* \geq (-1/8)$ . Equation (3.78) tells that the master isomorph is a rotated parabola in the  $UW$  plot. If this prediction is right then we should be able to scale isomorphs of different 12-6 LJ systems onto the same curve. Figure 3.22 shows simulation results for three different Lennard-Jones systems: two sets of isomorphic points belong to the KABLJ, one set to the SCLJ and the last set to the Wahnström binary Lennard-Jones (WBLJ) [Wahnström (1991)]. The very good scaling of different sets of isomorphic points into a unique curve is shown in fig. 3.23. Note the consistency with what we have derived from the theory, i.e. that to zero scaled virial corresponds a scaled energy of  $-(1/8)$ .

#### 3.11 Equation of state of generalized Lennard-Jones potentials

If we put together the equations describing the strong correlation between  $U$  and  $W$  and the density scaling relation we have not enough informations for writing down an equation of state for strongly correlating liquids in the  $U$ - $W$  phase diagram. The extra information comes from Rosenfeld and Tarazona [Rosenfeld & Tarazona (1998)] who derived - through a density functional theory argument - an expression describing the potential energy along an isochore:

$$U(\rho^*, T) = U_0 + \alpha T^{3/5} \quad (3.79)$$

where  $U_0$  and  $\alpha$  are parameters depending only from the density  $\rho^*$ .

The validity of this equation has been confirmed many times in different models, and in fig.3.11 we report the case of the KABLJ.

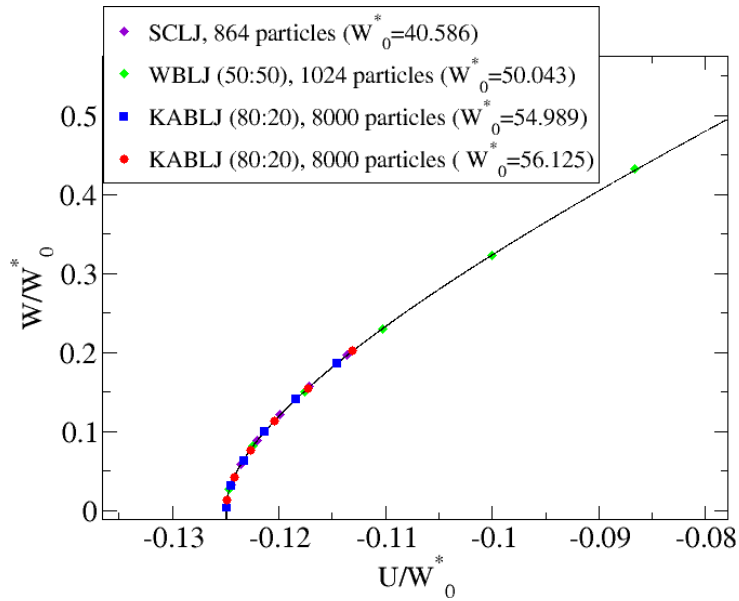


Figure 3.23: The master isomorph. The curve is the result of the collapse of different isomorphs shown in fig. (3.22). This means that the isomorphs shape is independent from the parameters characterizing the different potentials but it only depends on the kind of potential used, i.e. in this case a 12-6 LJ potential.

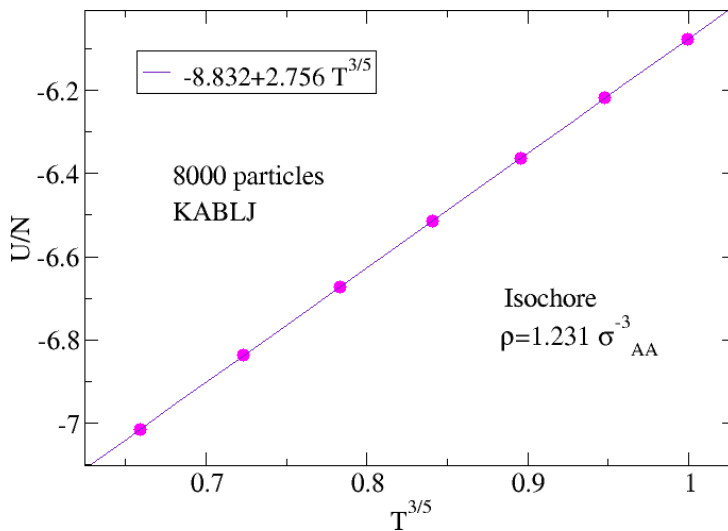


Figure 3.24: Rosenfeld and Tarazona scaling [Rosenfeld & Tarazona (1998)] for a set of isochoric points of the KABLJ.

### 3. DENSITY SCALING OF STRONGLY CORRELATING LIQUIDS AND ISOMORPHS

With eq. (3.79) we have all the ingredients for building an equation of state for generalized Lennard-Jones systems. The equations we need are the following:

$$T^*(\rho, T) = T\tilde{\rho}^{-\gamma}, \quad \tilde{\rho} \equiv \frac{\rho}{\rho^*} \quad (3.80)$$

$$U^*(\rho, T) = U_0 + \alpha T^{3/5} \quad (3.81)$$

$$W^*(\rho, T) = W_0 + \gamma U^*(\rho, T). \quad (3.82)$$

The idea is to map any state point  $(\rho, T, U, W)$  into a reference isochore defined by the density  $\rho^*$ . To do that we can use eq.(3.67) and (3.68) together with the three equations defined previously:

$$U_m^*(\rho, T) = \frac{-3W^*(\rho, T) + nU^*(\rho, T)}{n - m} = \frac{-3W_0^* + (n - 3\gamma)U^*(\rho, T)}{n - m} \quad (3.83)$$

$$U_n^*(\rho, T) = \frac{3W^*(\rho, T) - mU^*(\rho, T)}{n - m} = \frac{3W_0^* - (m - 3\gamma)U^*(\rho, T)}{n - m}. \quad (3.84)$$

If now we use the definition of isomorphs in the  $U$ - $W$  plane (i.e. eq.(3.74) and eq.(3.73)) we obtain an expression for the potential energy and the virial of the state point  $(\rho, T, U, W)$ :

$$U(\rho, T) = \tilde{\rho}^{n/3}U_n^*(\rho, T) + \tilde{\rho}^{m/3}U_m^*(\rho, T) \quad (3.85)$$

$$W(\rho, T) = \frac{n}{3}\tilde{\rho}^{n/3}U_n^*(\rho, T) + \frac{m}{3}\tilde{\rho}^{m/3}U_m^*(\rho, T). \quad (3.86)$$

The resulting equation of state contains four parameters  $(W_0, \gamma, U_0, \alpha)$  that we have to estimate. A possible way of finding the parameters is the following: for two non-isomorphic state points we use eq. (3.85) and eq. (3.86) to get  $U^*$  and  $W^*$  at two different reference densities. Afterwards we insert the two sets of  $U^*$  and  $W^*$  into eq. (3.82) in order to get  $W_0$  and  $\gamma$  and in eq.(3.81) to get  $U_0$  and  $\alpha$ . This procedure has been applied for the SCLJ. The resulting equation of state is shown in fig. 3.25.

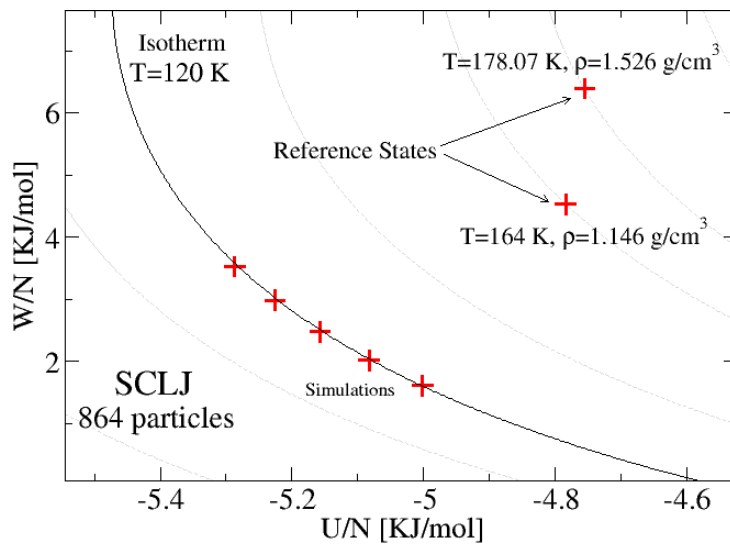


Figure 3.25: Equation of state for the SCLJ in the  $U$ - $W$  diagram.



## Chapter 4

# Aging in strongly correlating liquids

So far we have discussed only equilibrium properties of strongly correlating liquids. We have seen that we can completely describe Lennard-Jones systems also in the  $U$ - $W$  plane using the equation of state that we have derived through the definition of isomorphs. Unfortunately when the system is off-equilibrium we have no thermodynamic approach that allow us to completely describe it. Does it maintain its strong correlation? How does the system behave when temperature and density are suddenly changed? In this chapter we will discuss the aging behavior of strongly correlating liquids and we will show some interesting features that can be explained again in terms of isomorphs.

### 4.1 Temperature down-jumps in the $U$ - $W$ phase diagram

We said many times that the Lennard-Jones potential can be roughly approximated with an inverse power-law potential. We also said that the volume constraint plays an important role in this approximation. Then once the volume is fixed strong  $UW$  correlation appears in a wide range of temperatures and densities. No assumption on equilibrium has to be done in order to obtain such correlation, therefore we expect to have strong correlation even when the system is out-of-equilibrium.

Figure 4.1 shows the aging behavior of the KABLJ in the  $U$ - $W$  phase diagram when - from an equilibrium state point - its temperature is dropped down to a value corresponding to another isochoric state. The equilibration path followed by the system corresponds to the straight line connecting the two isochoric points: it means that  $W \simeq \gamma U + W_0$  during the all aging process and therefore strong correlation holds. Note that in equilibrium, isochoric states describe an almost straight line in the  $U$ - $W$  diagram: the same line that connects the initial and final points in the aging process.<sup>1</sup> We have then found that during a temperature down-jump strongly correlating liquids age along the isochore which - in the  $U$ - $W$  plane is a straight line and therefore  $\Delta W(t) \simeq \gamma \Delta U(t)$  holds during aging.

---

<sup>1</sup>As a consequence the slope  $\gamma$  entering in the correlation is almost constant along an isochore (see table 4.1).

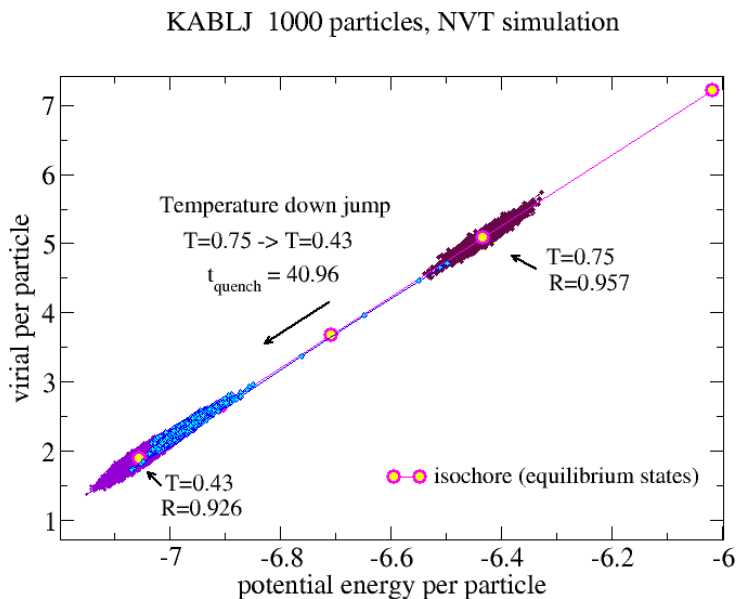


Figure 4.1: Temperature down-jump of the KABLJ along an isochore ( $\rho = 1.201$ ) in the  $U$ - $W$  plane. The scatter plot of virial and potential energy for the starting and final equilibrium points are colored differently (maroon and purple) from the aging process (blue). The virial and the potential energy remain correlated during the aging: it means that the aging pattern followed by the system is a straight line which also corresponds to an isochore in the  $U$ - $W$  plane (the pink dots are equilibrium isochoric points).

One could wonder what happens to non strongly correlating liquids during aging. Consider again water as example. Figure 4.2 shows the aging pattern of SPC water [van Gunsteren *et al.* (1996)] in the  $U$ - $W$  plane during a temperature down-jump at constant volume. An isochore is drawn to show to the reader the difference between the equilibrium and off-equilibrium isochoric pattern. From the figure it follows that - in the case of water - the system explores different states during the aging following a path that is much more complicated than in strongly correlating liquids.

## 4.2 Temperature and density jumps in the $U$ - $W$ phase diagram

In this section we will use the concept of isomorphs to better understand the out-of-equilibrium behavior of strongly correlating liquids. A first experiment that we can perform is shown in the inset of fig. 4.3(a).

The scatter plots of potential energy and virial are shown for four different state points labeled with numbers. States 1, 3 and 4 are isochoric while states 1 and 2 are isomorphous. At time zero the system in the equilibrium states 1, 3 and 4 is brought off-equilibrium thanks to a change of temperature and density, and starts aging towards state 2. In fig. 4.3 (a) the relaxation of the potential energy is shown for the three aging experiments. In the case of the

$T^*$	$\gamma$
0.41	5.1833
0.42	5.2054
0.43	5.1728
0.45	5.1940
0.47	5.1542
0.50	5.1778
0.60	5.1446
0.75	5.1629
1.00	5.0882
2.00	4.8768

Table 4.1: Temperature dependence of  $\gamma$  in the KABLJ for isochoric state points with  $\rho = 1.20$ . Note that when the temperature becomes high  $\gamma$  suddenly decreases towards  $\gamma \sim 4$  since the particles experience most of the time the very repulsive part of the KABLJ potential, i.e.  $\sim r^{-12}$ .

$3 \rightarrow 2$  jump and the  $4 \rightarrow 2$  jump a clear relaxation towards an equilibrium value (dashed line) occurs. Surprising instead is the aging behavior of the potential energy after the  $1 \rightarrow 2$  jump: the system seems to have reached the equilibrium instantaneously. Figure 4.3 (b) shows the potential energy behavior during the first instants after the isomorphic  $1 \rightarrow 2$  jump. Initially the system is in equilibrium at the state point 1. At a given time the length of the simulation box is changed in order to achieve the density of state 2. The overshoot at the first time step is a consequence of the abrupt change of the box size. In fact particles inside the simulation box find a bigger volume to occupy instantaneously and after the first instant they find themselves in equilibrium in the new state as shown by the potential energy. This is a consequence of the fact that isomorphic state points have the same reduced relevant configurations. It means that microscopic relevant configurations of one state - if rescaled to a new density - are also relevant for the corresponding isomorphic point. We have already discuss it when we have talked about the direct isomorph check in section 3.4. As stated in Paper IV we can summarize this aging property as follows:

- *A jump between two isomorphic state points starting from equilibrium takes the system instantaneously to equilibrium. This is because the normalized Boltzmann probability factors for microscopic configurations with same reduced coordinates are identical for the two systems. Thus isomorphs are predicted to be a kind of “wormholes” in the phase diagram along which one can jump instantaneously from equilibrium to equilibrium, even when the states are characterized by long relaxation times.*

A second aging experiment is illustrated in the inset of fig. 4.4. The system - initially in two isomorphic equilibrium states (1 and 2) - is brought out-of-equilibrium after a change of temperature (and density in the case of state 1) and starts aging towards state 3 that has the same volume of state 2.

Figure 4.4 show the relaxation of the potential energy after the two aging experiments. It is surprising how - despite the different starting energies -

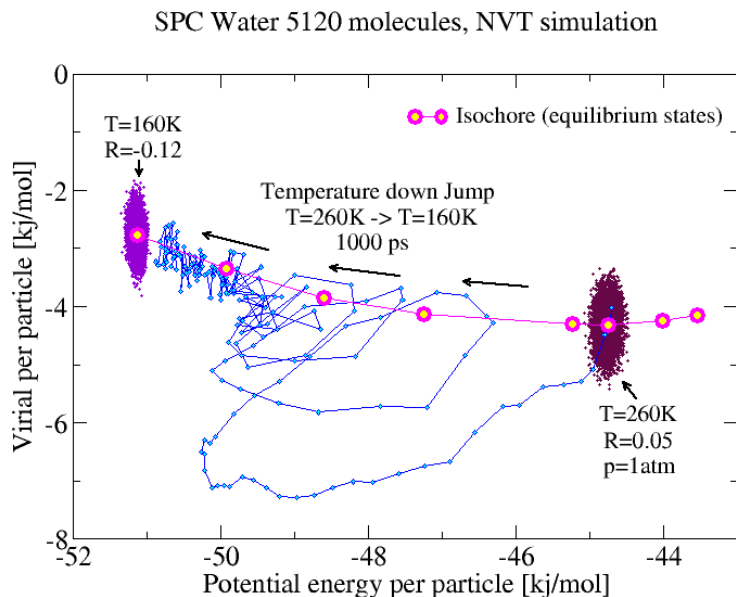


Figure 4.2: Potential energy and virial of SPC water during a temperature down-jump at constant volume ( $\rho = 1.020\text{g}/\text{cm}^3$ ). The initial state was first prepared in order to have a volume corresponding to an average pressure of 1 atm. A number of isochoric state points at equilibrium are plotted (pink circles) to compare the equilibrium path with the off-equilibrium one (blue curve).

the relaxation pattern for the two aging experiments is the same. This is a consequence of the fact that the system in state 1 - instead of relaxing towards 3 along an unknown path - prefers to move along the following relaxation path: it first jumps instantaneously on the isomorphous state having the right final density - i.e. state 2 - and then it relaxes along the right isochore towards state 3. Then - since the jump between isomorphous points is instantaneous - the pattern followed in the  $1 \rightarrow 3$  jump is the same of that in the  $2 \rightarrow 3$  jump. Thus whenever there is a transition from one state on an isochore to another state on a different isochore an isomorphous jump is involved. This can be seen also in fig. 4.3 for the transition  $3 \rightarrow 2$ . Note that the potential energy in state 3 is slightly above the potential energy in state 2. However when the aging starts the relaxing potential energy of the  $3 \rightarrow 2$  jump approaches the equilibrium line from below. The explanation is that the system in state 3 first jumps on the isomorphous point having the same density of state 2 but a lower potential energy and then it starts moving along the isochore, towards state 2.

In Paper IV the properties of this second aging experiment are summarized as follow:

- *Jumps from any two isomorphous state points to a third state point lead to the same aging behavior for all physical quantities.*

A third and final aging experiment that we want to present is sketched in fig. 4.5: given two isomorphous points 1 and 2 we perform for both of them a

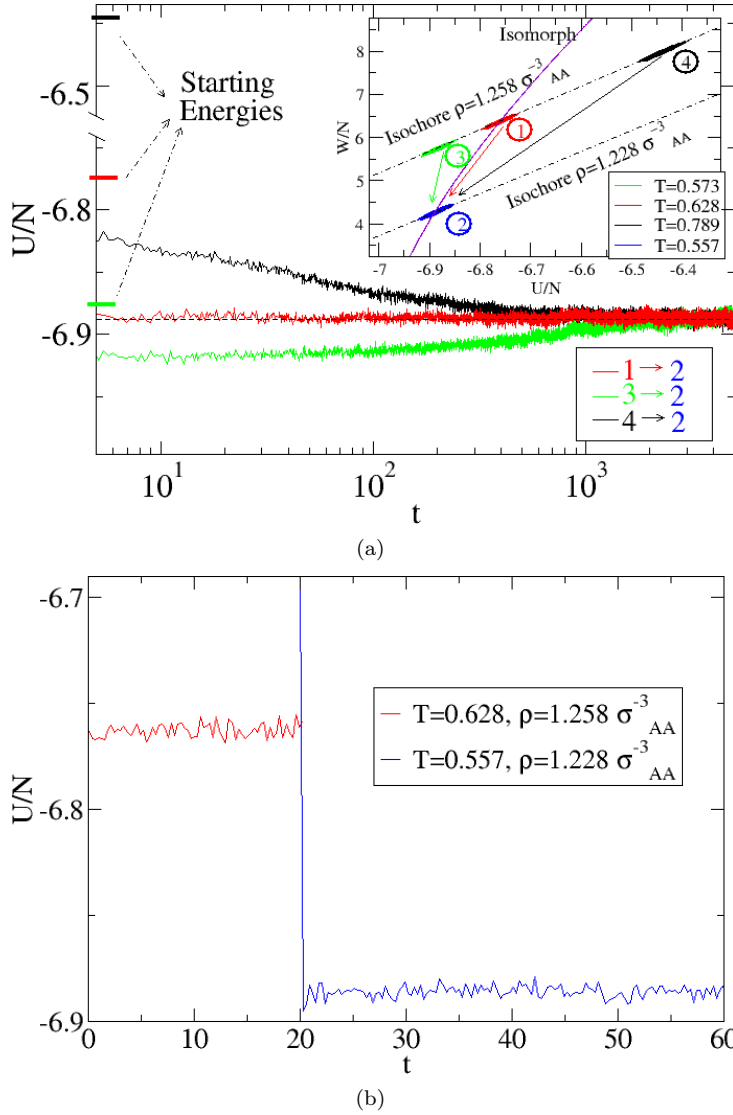


Figure 4.3: (a) Relaxation of the KABLJ potential energy for three different aging experiments. The situation is sketched in the subplot: for three isochoric state points at  $\rho = 1.258\sigma_{AA}^{-3}$  both temperatures and densities are changed to the values ( $T = 0.557, \rho = 1.228\sigma_{AA}^{-3}$ ) corresponding to a state point isomorph to one of the initial points (i.e. the point ( $T = 0.628, \rho = 1.258\sigma_{AA}^{-3}$ )). The starting mean energies for the three states are indicated in the plot. While for the two non isomorph jumps the aging of the potential energies is observed, for the isomorph jump instead no relaxation occurs: the potential energy is instantaneously at equilibrium. This surprising behavior is a consequence of the fact that the two state points have proportional Boltzmann factors. (b) The potential energy before and after the isomorph jump illustrated in (a). The time has been shifted in order to not display negative times. The system is in equilibrium at ( $T = 0.628, \rho = 1.258\sigma_{AA}^{-3}$ ). At  $t = 20$  (in LJ units) the length of the simulation box has been instantaneously increased to a value corresponding to  $\rho = 1.228\sigma_{AA}^{-3}$  and also the temperature has been changed to the final value  $T = 0.557$ . The overshoot in the potential energy is the consequence of the abrupt density change: since the particles positions were not rescaled they instantaneously occupy the larger box and their new positions correspond to a new equilibrium configuration (after the overshoot the the potential energy oscillates already around its equilibrium value).

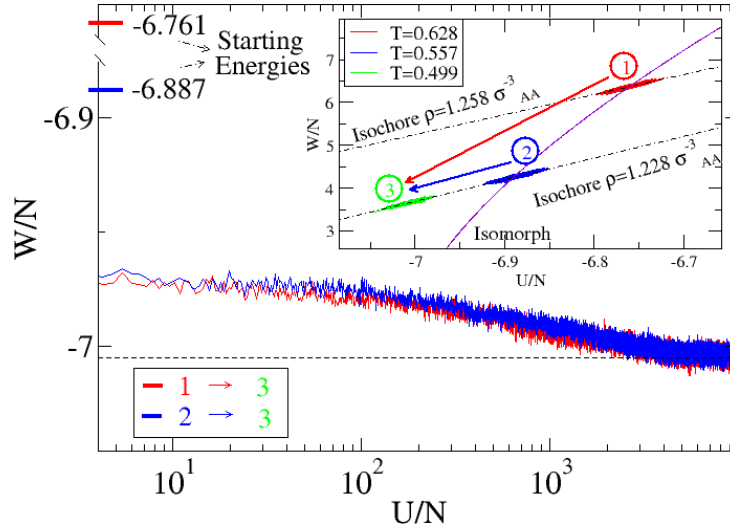


Figure 4.4: Relaxation of the KABLJ potential energy for two different aging experiments. The situation is sketched in the subplot: the system in the two isomorphic state points ( $T_1 = 0.628, \rho_1 = 1.258\sigma_{AA}^{-3}$ ) and ( $T_2 = 0.557, \rho_1 = 1.228\sigma_{AA}^{-3}$ ) is brought out-of-equilibrium after a change of temperatures and density (only for  $(T_1, \rho_1)$ ). The final values of  $T$  and  $\rho$  (i.e.  $(T = 0.499, \rho = 1.228)$ ) correspond to the state  $(T_3, \rho_3)$  isochoric to  $(T_2, \rho_2)$ . Starting equilibrium energies are also included in the plot. Even though the initial potential energies are different, a common relaxation pattern appears for the two aging experiments. This is because the system in  $(T_1, \rho_1)$  first jumps instantaneously on the isomorph state having the right final density and then it relaxes towards the final state.

temperature down-jump to other two isomorphic state points 3 and 4. Here we have chosen the case in which the final isomorphic points are in the glassy state but this is not mandatory for what we want to show.

Figure 4.6 shows the relaxation of potential energy and virial after the two temperature jumps in a Monte Carlo (MC) simulation of the KABLJ system. In the figure the initial and final states are not present. The figure shows that all the state points visited by the system during the  $1 \rightarrow 3$  jump and the  $2 \rightarrow 4$  jump are connected by an isomorph at each time. This means that the system aging along the  $1 \rightarrow 3$  pattern can instantaneously jump on the other aging pattern ( $2 \rightarrow 4$ ), wait some time, and jump back without perturbing its aging process (see the dashed red lines in fig. 4.5).

All the aging properties above are the starting point for discussing the glassy behavior of strongly correlating liquids. In fact in the next chapter we will show that - using these properties - it is possible to characterize the glassy state and to make more predictions on the off-equilibrium system behavior.

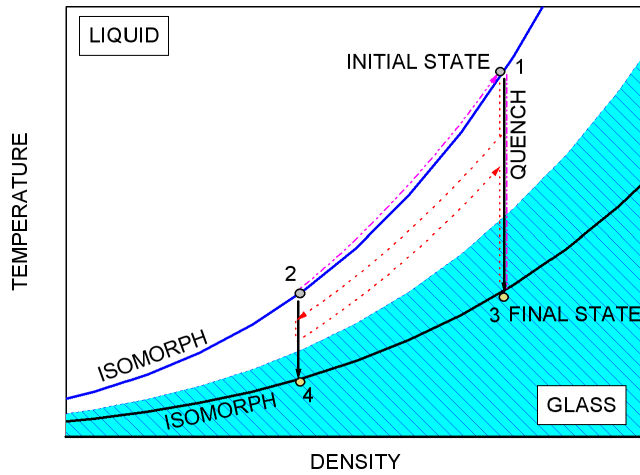


Figure 4.5: Sketch of the following aging experiment: for two isomorph points (1 and 2) a temperature down-jump (also called quench) is performed down to other two state points (3 and 4) belonging to the same isomorph. During the aging the off-equilibrium states of the two quenches are always connected by isomorphs, meaning that the system of the  $1 \rightarrow 3$  jump can instantaneously jump on the isomorph to the state of the  $2 \rightarrow 4$  jump and then go back without affect its aging process (dashed red arrows).

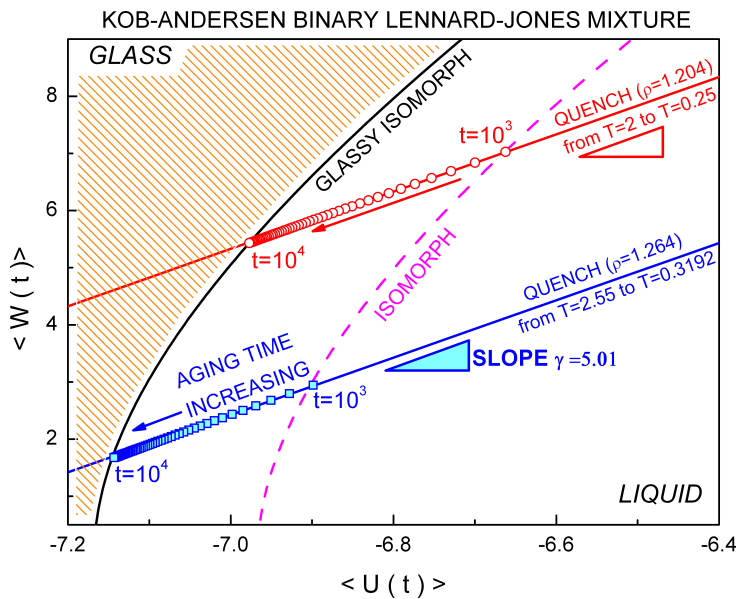


Figure 4.6: Relaxation of the potential energy and the virial after two temperature jumps (Monte Carlo simulation of the KABLJ system). Note that the relaxation pattern is a straight line in the  $U$ - $W$  phase diagram as discussed previously in this chapter. For two different waiting times ( $t_w = 10^3$  and  $t_w = 10^4$  MC steps) we show that the two aging paths are always connected by isomorphs.

### 4.3 Aging in the energy landscape

#### 4.3.1 The PEL approach

PEL (potential energy landscape) is the potential energy  $U(\mathbf{r}^N)$  of a system of  $N$  particles (then  $U(\mathbf{r}^N)$  depends on  $3N$  coordinates) [Kauzmann (1948), Martinez & C.A. (2001), Wales (2004)]. In this work we have already encountered the potential energy landscape when we were discussing all the isomorph properties (see chapter 3). In that case we sketched the PEL as a rough landscape full of local maxima and minima of different depths. In this picture to each local minimum (which is also called inherent state) corresponds a *basin*, i.e. the locus of points connected to the minimum by a steepest descendant path [Sciortino (2005)]. During the dynamics the system jumps back and forth between adjacent basins until it leaves the region. These collection of basins are embedded into what is called a *metabasin* (MB) [Doliwa & Heuer (2003)]. The idea of describing the PEL through basins and metabasins was first introduced by Stillinger and Weber [Stillinger & Weber (1982), Stillinger & Weber (1984), Stillinger & Weber (1935)]. In this framework it is possible to map the true dynamics of a liquid into the inherent states (IS) dynamics. To understand that lets assume to have a one dimensional landscape in which each basin can be approximated with a parabola. During the IS dynamics portions of a given basin are explored since the system has a *vibrational* energy  $\varepsilon_{vib}$ . Each point explored in the PEL corresponds to a configuration of the system in the true dynamics. Thus the exploration of a basin corresponds to the situation in which particles vibrates around their “equilibrium positions” and the configurations assumed by the system are close to each other. If we remove the vibrational energy the system in the PEL will sit on the bottom of the basin - the inherent state - corresponding to the equilibrium configuration in the true dynamics having energy  $\varepsilon_{IS}$  [Schröder *et al.* (2000)]. When a “flow event” occurs - i.e. a consistent rearrangement of a portion of particles force them to vibrate around a new equilibrium position - in the energy landscape the system has moved to another basin after having crossed a “barrier” or having slid down from a “saddle” separating the two minima (see fig. 4.7).

Metabasins energy instead seems to be connected to the primary relaxation of the system, i.e. when the system in its true dynamics has completely lost memory of its initial state.

In the last decade the interest in the IS dynamics and its connection with the true dynamics is enormously increased <sup>2</sup> as well as its connection with the aging dynamics in a system [Bouchaud *et al.* (1998), Saika-Voivod & Sciortino (2004)]. In particular a lot of effort has been done in trying to understand the primary relaxation mechanism from the properties of the PEL. In this contest there is a growing evidence that IS and MB energies are relevant for the determination of the activation energies during the relaxation process [Dyre (1995)].

In the next section we will study the response of the system after a temperature jump using the PEL approach. In particular we will show the evolution

---

<sup>2</sup>see for instance references [Keyes (1997), Li & Keyes (1999), Keyes (1994), Gezelter *et al.* (1997), Bembenek & Laird (2001), Donati *et al.* (2000), La Nave *et al.* (2001), La Nave *et al.* (2000), Angelani *et al.* (2000), Broderix *et al.* (2000), Cavagna (2001), Angelani *et al.* (2002), Angelani *et al.* (2003)]

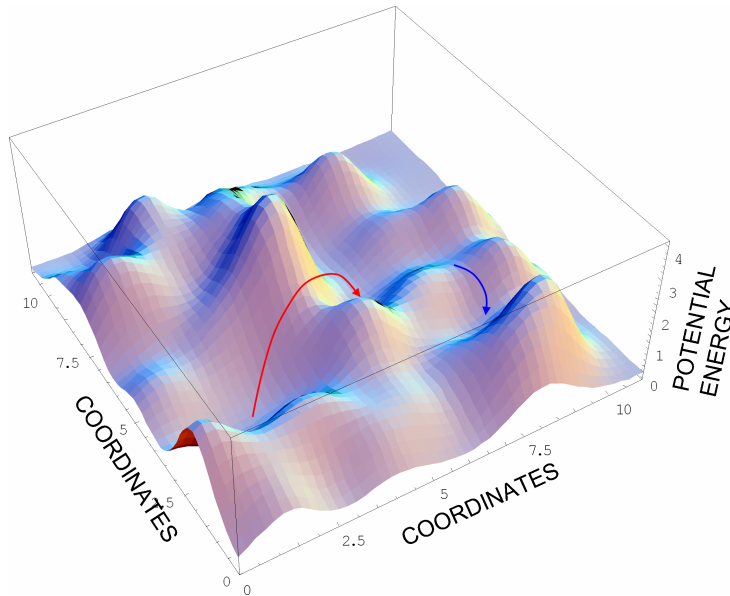


Figure 4.7: Sketch of the relaxation mechanisms in the energy landscape. Stationary points can be “stable” (minima) and “unstable” (saddles). The “saddles” are characterized by having at least one negative Hessian eigenvalue. If the system is trapped into a minimum it can reach another stationary point by crossing a barrier (red arrow). If the system is on a saddle point it can also slide down - towards another stationary point - along the direction with negative eigenvalues of the saddle (blue arrow).

of the IS energy distribution during the aging and we will try to describe the results using the Gaussian trap model [Monthus & Bouchaud (1996)]. More details can be found in Paper VII.

#### 4.4 Aging in the PEL after temperature down-jumps and up-jumps

It is well known that the Gaussian trap model can capture the relevant features of the energy landscape of a simulated glassy system [Heuer (2008), Denny *et al.* (2003)]. We will show here its predictions for the probability distribution of the IS energy during temperature down-jumps and up-jumps. Saika-Voivod and Sciortino [Saika-Voivod & Sciortino (2004)] studied already the IS energy distribution after a temperature down-jump. They found that the mean IS energy  $\langle e_{IS} \rangle$  was monotonically dropping down to its final equilibrium value while the width of the distribution was decreasing and then increasing again during the aging process. The Gaussian trap model captures the same main features of a system during a temperature down-jump. The model is a very simple version of an energy landscape: it consists of a collection of states (or traps) and the temporal evolution of the population in the traps is determined by the master equation

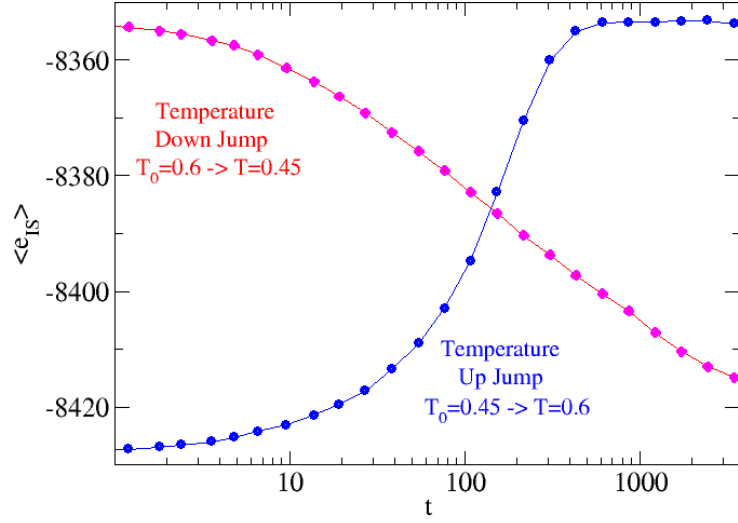


Figure 4.8: Evolution of the mean energy during a temperature down-jump from  $T = 0.6$  to  $T = 0.45$  and the reverse up-jump for a KABLJ of 1000 particles. The density of the system is  $\rho = 1.2\sigma_{AA}^{-3}$ . The plot is the result of an average over 1200 different aging experiments.

$$\dot{p}_T(\varepsilon, t) = -\kappa_T(\varepsilon)p_T(\varepsilon, t) + \rho(\varepsilon) \int d\varepsilon' \kappa_T(\varepsilon')p_T(\varepsilon', t) \quad (4.1)$$

where  $\kappa_T(\varepsilon) \propto e^{\varepsilon/T}$  is the escape rate and  $\rho(\varepsilon)$  is the density of states and is chosen to be Gaussian. When a change in temperature from  $T_0$  to  $T$  (with  $T_0 > T$ ) is done, the mean energy evolution is described by the following equation:

$$E_T(t) = \int d\varepsilon \varepsilon p_T(\varepsilon, t). \quad (4.2)$$

Since for infinite times  $p(\varepsilon, t \rightarrow \infty) = p_T^{eq}$  where

$$p_T^{eq}(\varepsilon) = \frac{1}{\sqrt{2\pi}\sigma} e^{-(\varepsilon - \bar{\varepsilon}_T)^2 / 2\sigma^2} \quad \bar{\varepsilon}_T = \beta\sigma^2, \quad (4.3)$$

we find that  $E(t=0) = E_{T_0}^{eq} = -\beta_0\sigma^2$ , the final value is  $E(\infty) = E_T^{eq} = -\beta\sigma^2$  and during the aging  $E_T(t)$  changes monotonically between the two extremes. This prediction is consistent with the results found by Saika-Voivod and Sciortino during a temperature down-jump. The same kind of prediction can be done for the mean energy and variance during a temperature up-jump. Figure 4.8 and fig. 4.9 shows the evolution of the mean energy  $\langle e_{IS} \rangle$  and the variance  $\langle \Delta\sigma^2 \rangle$  during a temperature up-jump and a temperature down-jump for the KABLJ. In the case of the mean energy both the curves are monotone as expected but not symmetric [Angell *et al.* (2000)]. There is no reason anyway to expect them to be symmetric: this reflects the fact that we are far from the linear response regime where the symmetry between the curves is required.

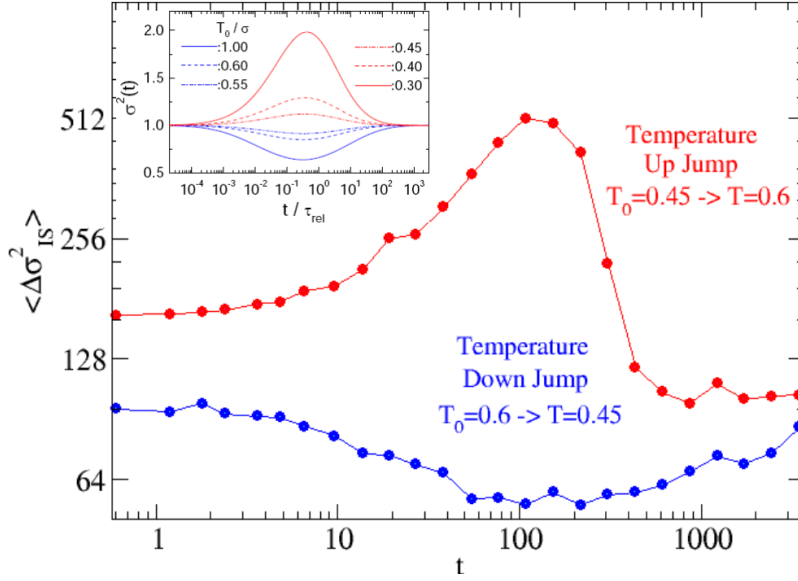


Figure 4.9: Evolution of the variance of the IS energy distribution during a temperature down-jump from  $T = 0.6$  to  $T = 0.45$  and the reverse up-jump. The system studied is the KABLJ with 1000 particles and density  $\rho = 1.2\sigma_{AA}^{-3}$ . Clearly the two events are very different: in the case of an up-jump the variance increases in time corresponding to a broadening of the distribution of the IS energy. The opposite happens - with a smaller magnitude- during the temperature down-jump. The inset shows the predictions of the trap model for up-jumps (red curves) and down-jumps (blue curves).

Consider now the evolution of the IS energy distribution after a temperature down-jump. Figure 4.10 shows the evolution of  $p_T(\varepsilon, t)$  obtained solving numerically the master equation in eq. (4.1) [Diezemann (2005)]. Another way of finding the evolution of  $p_T(\varepsilon, t)$  is to make the following approximation: we define the *demarcation* energy through  $\kappa_T(\varepsilon_D) = 1/t = \kappa_\infty e^{\varepsilon_D/k_B T}$ , i.e.

$$\varepsilon_D = -\beta^{-1} \ln(\kappa_\infty). \quad (4.4)$$

Then the demarcation energy corresponds to a sort of threshold energy below which (i.e. for  $\varepsilon < \varepsilon_D$ ) states are frozen at time  $t$  and above which (i.e.  $\varepsilon > \varepsilon_D$ ) states have reached equilibrium<sup>3</sup> [Dyre (1995), Dyre (1987) and Arkhipov *et al.* (1979)]. This allow us to make some considerations. We can assume that the equilibrium population of frozen states diminishes as  $p_{T_0}^{eq}(\varepsilon) e^{-\kappa_T(\varepsilon)t}$  while the final population of states increases according to  $p_T^{eq}(\varepsilon)(1 - e^{-\kappa_T(\varepsilon)t})$ . Thus we have

$$p_T^{ap}(\varepsilon, t) = N(t)^{-1} [p_{T_0}^{eq}(\varepsilon) e^{\kappa(\varepsilon)t} + p_T^{eq}(\varepsilon)(1 - e^{\kappa(\varepsilon)t})] \quad (4.5)$$

<sup>3</sup>this is a consequence of the activated dynamics.

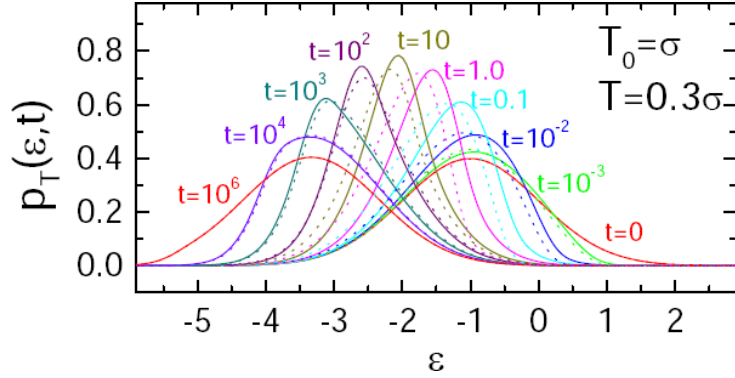


Figure 4.10: Evolution of  $p_T(\varepsilon, t)$  at different waiting times after a temperature down-jump. The full lines are obtained integrating numerically the master equation in eq. (4.1). The dashed lines are instead the solutions of the approximated distribution  $p_T^{ap}(\varepsilon, t)$  found using the concept of demarcation energy (see eq.(4.5)). Results from Gregor Diezemann. The same figure can be found in Paper VII.

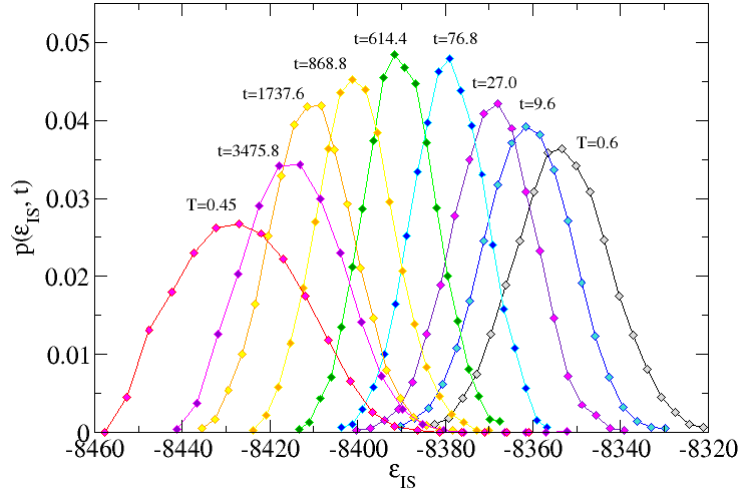


Figure 4.11: Evolution of  $p_T(\varepsilon_{IS}, t)$  at different waiting times after a temperature down-jump ( $T = 0.6 \rightarrow T = 0.45$ ) for the KABLI system with 1000 particles. The distribution at each time has been obtained after having performed 1200 different aging experiments. The results are consistent with the prediction of the Gaussian trap model.

where  $N(t) = \int d\varepsilon p_T^{ap}(\varepsilon, t)$  is a normalization constant. The very good agreement with the numerical solution of the master equation in fig. 4.10 gives us a simple interpretation of the temporal evolution of the distribution.

$p_{T_0}^{eq}(\varepsilon)$  corresponds to the distribution of the frozen states while  $p_T^{eq}(\varepsilon)$  is the one of the relaxed states and they are both Gaussian. The different weights on the distributions give rise to a narrowing of  $p_T(\varepsilon, t)$  during the evolution, as we can observe in fig. 4.10 but also from simulation results in fig. 4.11.

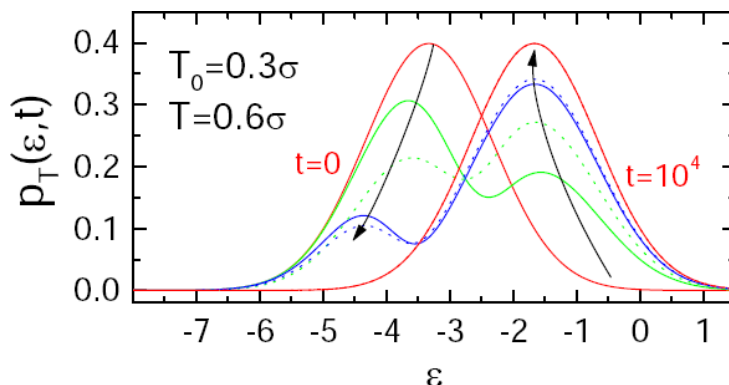


Figure 4.12: Evolution of  $p_T(\varepsilon, t)$  at different waiting times after a temperature up-jump. The full lines are obtained integrating numerically the master equation in eq. (4.1). The dashed lines are instead the solutions of the approximated distribution  $p_T^{ap}(\varepsilon, t)$  found using the concept of demarcation energy (see eq.(4.5)). Results from Gregor Diezemann. The same figure can be found in Paper VII.

A completely different solution of the trap model appears for a temperature up-jump. In this case we start from a low energy distribution then we expect that most of the low energy states are trapped for long times while the high energy states on the right tail relax quickly. The result of this behavior is the splitting of the initial peak into two peaks, one made of trapped states and the other one made of relaxed states (see fig. 4.12).

Despite the variances in fig. 4.9 and the mean energies of fig. 4.8 are well described by the Gaussian trap model, the evolution of the IS energy distribution is instead quite different. Figure 4.13 shows the evolution of  $p_T(\varepsilon, T)$  for the KABLJ system.

There no double peak appears: instead the increasing of the variance and its maximum in fig. 4.9 correspond to a smearing out of the distribution (as if the two peaks were mixed together) and a consecutive narrowing. We could argue that the Gaussian trap model is too simplistic to capture all the features of the KABLJ system. Indeed we can think at the KABLJ as a superposition of some weakly coupled subsystems having - on average - the same  $\langle \varepsilon_{IS} \rangle$  and  $\langle \Delta \sigma_{IS}^2 \rangle$ . This means that properties like the evolution of the mean energy and of the variance are reflected in the big system but other effects - like the bimodality - are smeared out because of the superposition of the subsystems. In Paper VII it is shown that already with two subsystems the double peak effect is washed out. Moreover we have to take into account that the return probability - i.e. the probability of jumping back to the initial  $IS$  after some transitions - is non zero. In the trap model instead the return probability is zero, therefore we should run our simulation under the same conditions. Thus we can consider transitions between MB instead of IS transitions for which the return probability is almost zero.

Under this conditions we have simulated a small KABLJ system (65 particles) and we have looked at the evolution in time of  $p(e_{MB})$ . After having been sure that the system could be described by the Gaussian trap model during a

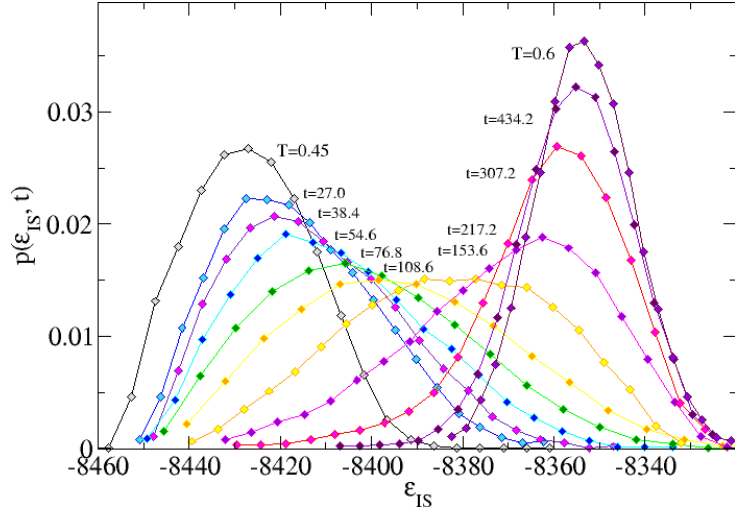


Figure 4.13: Evolution of  $p_T(\varepsilon_{IS}, t)$  at different waiting times after a temperature up-jump ( $T = 0.45 \rightarrow T = 0.6$ ) for a KABLJ system of 1000 particles. The distribution at each time has been obtained after having performed 1200 different aging experiments. Even though no double peak distribution appears - as predicted from the Gaussian trap model - the result is still consistent with that if we interpret it as a superposition of the aging distributions of weakly coupled subsystems.

temperature down-jump, a temperature up-jump was performed at the same temperatures used for the big system. The result is shown in fig. 4.14. In this case we really observe a two peak distribution as predicted by the Gaussian trap model.

Summarizing we have tried to qualitatively rationalize the results from the Gaussian trap model and from simulations in terms of demarcation energy. In the case of the Gaussian trap model in fact it is possible to define a probability distribution of the states that approximates well the evolution of the real probability distribution satisfying eq. (4.1) during both a temperature down-jump and a temperature up-jump. The comparison with simulations shows that the Gaussian trap model captures the main features of small KABLJ systems when the MB energy distribution is considered but fails in describing the evolution of the IS energy distribution after an up-jump for big systems. This is not a big failure since the smearing out of the distribution can be interpreted as a superposition of the two peaks distribution predicted in the Gaussian trap model and observed in the small system. The lack of bimodality is caused by a superposition of weakly coupled subsystems that washes out the two peaks contribution.

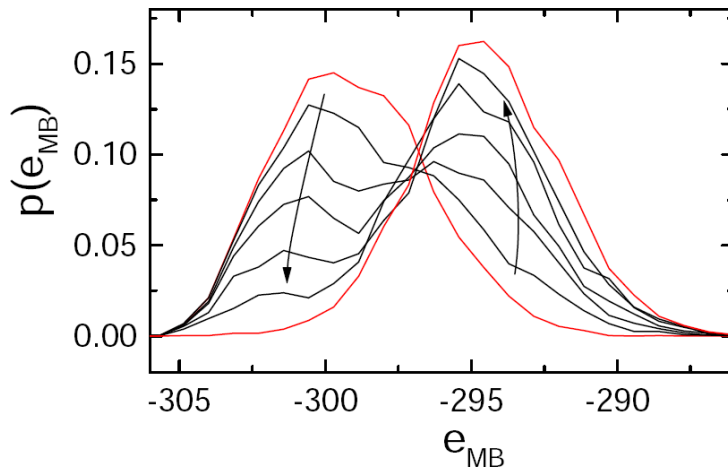


Figure 4.14: Evolution of  $p_T(e_{MB}, t)$  at different waiting times after a temperature up-jump ( $T = 0.45 \rightarrow T = 0.6$ ) for a KABLJ system of 65 particles. The red lines correspond to the equilibrium distributions. Simulations performed by Christian Rehwald. The same figure can be found in Paper VII.



## Chapter 5

# Fluctuation-dissipation relation in out-of-equilibrium strongly correlating liquids

In this chapter we will discuss the off-equilibrium glassy behavior of strongly correlating liquids. Before that we will introduce the subject discussing the idea that an extra parameter is needed for describing out-of-equilibrium systems. This parameter has the meaning of an effective temperature  $T_{eff}$  associated to the slow degrees of freedom in the aging supercooled liquid. As we will see there are a number of different ways of defining  $T_{eff}$ . In this chapter we will focus on the definition of the effective temperature related to the fluctuation-dissipation relation (FDR).  $T_{eff}$  will be our tool for investigating the glassy properties of strongly correlating liquids showing again that this class of liquids behaves in a simpler way than other liquids even out-of-equilibrium.

### 5.1 The quest for an extra parameter

In a large variety of cases condensed matter is found out-of-equilibrium. This motivates the effort made in understanding the principles governing non equilibrium processes. The main problem in studying these processes is the lack of a thermodynamic description that can capture out-of-equilibrium features as well as it does with equilibrium properties of liquids. When a system is brought out-of-equilibrium it starts aging; as a consequence its fundamental dynamic properties look different depending on the observation time (also known as *waiting time* or *aging time*). A way to take into account the aging features of the system is by inserting the time dependence in an extra parameter that enters in the new thermodynamic approach and that acts as an *effective* temperature [Crisanti & Ritort (2003), Leuzzi (2009), Cugliandolo (2004)]. This extra parameter should keep track of the whole history of the system [Nieuwenhuizen (1997), Leuzzi & Nieuwenhuizen (2007)].

Moreover we know that when a liquid is aging down to the glassy state, a separation of time scales occurs. For instance we can think of a high temperature liquid that is put in contact with a thermal bath having a very low temperature: the doom of the liquid is to turn into a glass. In this situation we usually have a number of fast degrees of freedom that are instantaneously in

equilibrium with the thermal bath and a number of slow modes on a larger time scale to which is associated the “age” of the system. Since we want the effective temperature to keep track of this age it is straightforward to connect  $T_{eff}$  to the slow modes. We can then think this modes to be - on a large time scale  $t$  - in a “quasi” equilibrium situation with a temperature  $T_{eff}(t)$  mentioned above.

If one extra parameter is enough to describe the non-equilibrium behavior of liquids it is possible to generate an extended thermodynamic approach better known as “two temperature thermodynamics” [Reiss (1997), Gutzow & Schmelzer (1995), Leuzzi & Nieuwenhuizen (2007)] whose main laws are:

- first law

$$dE = \delta Q + \delta W = TdS_{vib} + T_{eff}dS_c - pdV \quad (5.1)$$

- heat exchange

$$\delta Q \equiv TdS_{vib} + T_{eff}dS_c \quad (5.2)$$

- Second law

$$\delta Q \leq TdS_{tot} = Td(S_{vib} + S_c) \Rightarrow (T_{eff} - T)dS_c \leq 0, \quad (5.3)$$

where  $S_c$  and  $S_{vib}$  are the configurational and the vibrational entropy and  $T_{eff}$  is the intensive conjugate variable of  $S_c$ .

How can we define and measure the effective temperature? In the literature we can find different approaches from which is possible to define an effective temperature. The most fruitful definitions of the effective temperature in the physics of structural glasses come from the *fluctuation-dissipation relation* [Cugliandolo & Kurchan (1993), Cugliandolo & Kurchan (1994), Parisi (1997)] and the *inherent structure formalism* [Sciortino (2005), Sciortino & Tartaglia (2001)]. For many years a deep interest was focused on the concept of fictive temperature as well <sup>1</sup> [Narayanaswamy (1971), Moynihan *et al.* (1976)], but it is well known that this is not a real thermodynamic parameter, thus we will not discuss this approach here. If we include also spin-glasses then the number different definitions for the effective temperature increases. What is important to stress here is that - if we want  $T_{eff}$  to be the right parameter that enters in the two temperature thermodynamics - all its different definitions must give the same result. Moreover we should be able to build a thermometer that could measure the effective temperature as was conjectured in references [Cugliandolo *et al.* (1997)] and [Kurchan (2005)] in the case of  $T_{eff}$  defined through the fluctuation dissipation relation (see appendix B). Unfortunately in real experiments (as well as in simulations) a direct measure of  $T_{eff}$  is not possible yet, moreover the effective temperature measured in complicated systems like colloids seems to depend crucially on the quantities studied [Bellon *et al.* (2001), Jabbari-Farouji *et al.* (2007), Maggi *et al.* (2010)], ruling out the possibility of considering  $T_{eff}$  as a true thermodynamic parameter. However this does not mean that we cannot still find a class of liquids in which  $T_{eff}$  is the only extra parameter necessary for describing their off-equilibrium behavior. For instance strongly correlating liquids seem to be described during aging by a single extra parameter [Pedersen *et al.* (2008b)]. Moreover it

<sup>1</sup>the fictive temperature is the temperature at which the glass would be in thermal equilibrium.

was found by Sciortino et al. [Sciortino & Tartaglia (2001)] that the effective temperature defined with the inherent structure formalism and the one defined in the fluctuation-dissipation relation are, to a good approximation, the same for Lennard-Jones liquids. This encouraged us to use the effective temperature as a tool for characterizing the glassy behavior of strongly correlating liquids. This study is illustrated in the next sections.

## 5.2 The fluctuation dissipation theorem and its generalization out-of-equilibrium

The most famous derivation of the fluctuation dissipation theorem was formulated by Onsager [Onsager (1931a), Onsager (1931b)] through the *regression principle*. His formulation states that: *the relaxation of macroscopic non-equilibrium disturbances is governed by the same laws as the regression of spontaneous microscopic fluctuations in a system at equilibrium*. To understand the statement above suppose to introduce a perturbation  $\varepsilon(t) = \varepsilon\Theta(t)$  into state 1 in equilibrium with a thermal bath of temperature  $T$ . This perturbation is coupled to the observable  $B(\mathcal{C})$ <sup>2</sup> in order that the total energy in the presence of the perturbation is:

$$E_\varepsilon(\mathcal{C}) = E(\mathcal{C}) - \varepsilon B(\mathcal{C}). \quad (5.4)$$

To monitor the effect of the perturbation on the system we can look at the evolution of the mean value  $\langle A(t) \rangle_\varepsilon$  of the variable  $A(\mathcal{C})$  during the transient from state 1 to a new equilibrium state 2. The expectation value of  $\langle A(t) \rangle_\varepsilon$  is

$$\langle A(t) \rangle_\varepsilon = \sum_{\mathcal{C}, \mathcal{C}_0} A(\mathcal{C}) P_\varepsilon(\mathcal{C}, t | \mathcal{C}_0, 0) P_0(\mathcal{C}_0), \quad (5.5)$$

where  $P_\varepsilon(\mathcal{C}, t | \mathcal{C}_0, 0)$  is the conditional probability of evolution from the initial configuration and  $P_0(\mathcal{C}_0)$  is the probability distribution of the system in a given configuration  $\mathcal{C}_0$ :

$$P(\mathcal{C}) = \frac{\exp[-\beta E(\mathcal{C})]}{\sum_{\mathcal{C}} \exp[-\beta E(\mathcal{C})]}. \quad (5.6)$$

The regression principle says that the conditional probability in the presence of the perturbation is equivalent to that of a spontaneous equilibrium fluctuation in the new state. Since the state 2 has a new energy that includes the presence of the perturbation, we can rewrite the conditional probability in eq. (5.5) as

$$P_\varepsilon(\mathcal{C}, t | \mathcal{C}_0, 0) = P_0(\mathcal{C}, t | \mathcal{C}_0, 0) \exp[\beta \varepsilon (B(\mathcal{C}) - B(\mathcal{C}_0))] \quad (5.7)$$

where  $P_0(\mathcal{C}, t | \mathcal{C}_0, 0)$  is the spontaneous fluctuation conditional probability in state 1 and  $\exp[\beta \varepsilon (B(\mathcal{C}) - B(\mathcal{C}_0))]$  is the correction due to the presence of the field. Then the right hand side of eq. (5.7) corresponds to the spontaneous fluctuation in the state 2. Inserting eq. (5.7) into eq. (5.5) we get

---

<sup>2</sup> $B(\mathcal{C})$  means the observable  $B$  associated to a given configuration  $\mathcal{C}$ .

$$\begin{aligned}
 \langle A(t) \rangle_\varepsilon - \langle A \rangle_0 &= \beta\varepsilon \sum_{\mathcal{C}, \mathcal{C}_0} A(\mathcal{C}) [B(\mathcal{C}) - B(\mathcal{C}_0)] P_0(\mathcal{C}_0) \\
 &= \beta\varepsilon [\langle A(t)B(t) \rangle_0 - \langle A(t)B(0) \rangle_0]
 \end{aligned} \tag{5.8}$$

If we define the correlation function  $C_{A,B}(t, t') = \langle A(t)B(t') \rangle$  and the susceptibility  $\chi_{A,B}(t) = \lim_{\varepsilon \rightarrow 0} (\langle A(t) \rangle_\varepsilon - \langle A \rangle_0) / \varepsilon$  we can rewrite eq. (5.8) as:

$$\chi_{A,B}(t, t') = \beta \int_0^t \frac{\partial C_{A,B}(t, t')}{\partial t'} dt' \tag{5.9}$$

or

$$\frac{\partial \chi_{A,B}(t, t')}{\partial t'} = \frac{1}{T} \frac{\partial C_{A,B}(t, t')}{\partial t'}. \tag{5.10}$$

Equation (5.10) is the differential form of the fluctuation-dissipation theorem. In appendix C alternative derivations using the energy bond formalism and the creep function formulation are presented and are shown to be equivalent to eq. (5.10).

We can extend the FDT in the out-of-equilibrium regime if we do some considerations. The most important thing that we have to take into account is aging: when the system ages the time translational invariance does not hold anymore and all the correlation functions and susceptibilities start to depend on the waiting time  $t'$  of the system. Moreover the FDT is violated. Under these conditions it is still possible to rewrite both the correlation functions and the susceptibilities as the sum of two contributions [Crisanti & Ritort (2003)]:

$$\chi(t, t') = \chi_{st}(t - t') + \chi_{ag}(t, t') \tag{5.11}$$

i.e. a stationary term and an aging one. Moreover the aging term satisfies the so called ‘‘full aging’’, i.e. has the following scaling behavior [Kob & Andersen (1994)]:

$$\chi_{ag}(t, t') = \hat{\chi}(t/t'). \tag{5.12}$$

In the full aging scenario FDT is violated depending on the ratio  $(t - t')/t'$ . In particular

- If  $(t - t')/t' \ll 1$   
then  $C(t, t') \simeq C_{st}(t - t')$  and the FDT holds

$$\frac{\partial C_{st}(t - t')}{\partial t'} = T \frac{\partial \chi_{st}(t - t')}{\partial t'} \tag{5.13}$$

- If  $(t - t')/t' \gg 1$   
then  $C(t, t') \simeq C_{ag}(t, t')$  and the FDT does not hold but a more general relation which takes into account the FDT violation can be written

$$\frac{\partial C_{ag}(t, t')}{\partial t'} = T_{eff}(t') \frac{\partial \chi_{ag}(t, t')}{\partial t'} \tag{5.14}$$

where  $T_{eff}$  is the effective temperature of the discussion in section 5.1.

Thus if we want to put together the two cases we can write a general formulation of the FDT that is called *fluctuation-dissipation relation* (FDR):

$$\frac{\partial C_{A,B}(t,t')}{\partial t'} = \frac{T}{X_{A,B}(t,t')} \frac{\partial \chi_{A,B}(t,t')}{\partial t'} \quad (5.15)$$

where  $X_{A,B}(t,t') = -(1/T)(\partial \chi_{A,B}(t,t')/\partial C_{A,B}(t,t'))|_{t'=fixed, C_{A,B}(t,t')=const}$  is the fluctuation dissipation ratio. Then for  $(t-t')/t' \ll 1$   $|X_{A,B}(t,t')| = 1$  and FDT is recovered while for  $(t-t')/t' \gg 1$   $|X_{A,B}(t,t')| = T/T_{eff}(t,t')$  the violation of FDT is taken into account through  $T_{eff}$ .

Usually for structural glasses  $T_{eff}$  takes two values:  $T$  and  $T_{eff}(t')$  where  $T_{eff}(t') > T$ . The effective temperature reflects the separation of time scales into the system: the fast degrees of freedom are instantaneously at equilibrium with the bath temperature  $T$  on a time scale of order of  $(t-t')/t' \ll 1$  while the slow degrees of freedom are in a “quasi equilibrium” situation with a temperature  $T_{eff}(t,t')$  for time scales of the order of  $(t-t')/t' \gg 1$ . From eq. (5.15) it is clear that the easiest way of measuring the effective temperature is through the slope formed by the correlation and the susceptibility as it shown in the so called FD-plot in fig. (5.1).

### 5.3 Measuring the effective temperature in simulations

In the past a big number of simulations have been performed for calculating the effective temperature in model of liquids via the FDR [Hansen & Yip (1995), Parisi (1997) I, Parisi (1997) II, Kob & Andersen (1995b) I, Kob & Andersen (1995a) II, Kob & Barrat (1999), Sciortino & Tartaglia (2001), Di Leonardo *et al.* (2000)]. In all these works the standard technique employed is the following: two parallel simulations are run starting from the same configuration. A time  $t_0 = 0$  the system is brought out-of-equilibrium for instance dropping instantaneously the temperature in both the simulations and it is let aging until a given time  $t$  which is fixed. Afterwards at time  $t' < t$  in one of the two simulations a small external field  $\varepsilon$  conjugated to a variable  $B(t')$  is introduced. In the other non equilibrium simulation instead the correlation function between the physical observable  $A(t')$  and  $B(t')$  is evaluated:

$$C(t,t') = \langle A(t)B(t') \rangle_0, \quad (5.16)$$

where the subscript “0” indicates that the system is not affected by any external field. Note that - since the system is aging - we have to perform many of these quenches and repeat the procedure in order to get a good statistics. In the simulation with the external field applied we have to calculate the response to the field  $\chi(t,t')$ . We can exploit the fact that the field is small for using an approximated definition of  $\chi(t,t')$ :

$$\chi(t,t') \approx \frac{[\langle A(t) \rangle - \langle A(t) \rangle_0]}{\varepsilon}. \quad (5.17)$$

Note that  $\chi(t,t')$  is implicitly dependent on  $t'$  because of the external field perturbing the system. In order to build the FD plot, this procedure must be repeated for many different waiting times  $t'$ . It follows that this kind of simulation is very time consuming. In the past - in order to save some computational

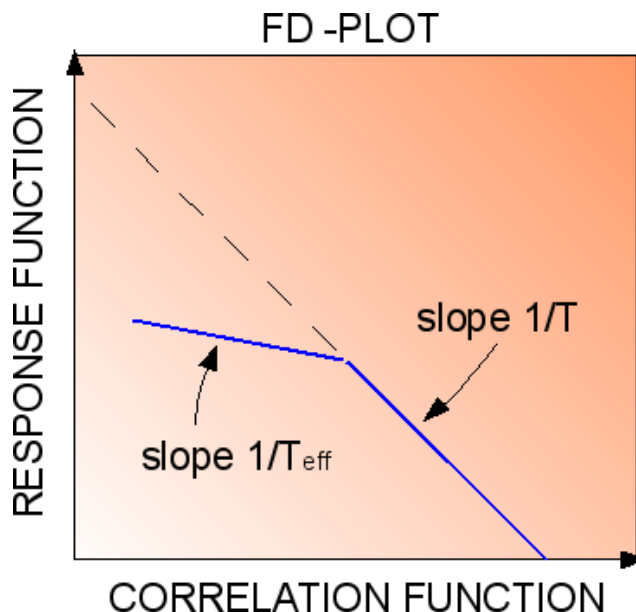


Figure 5.1: Fluctuation-dissipation plot. The two slopes give informations on the effective temperatures of fast and slow degrees of freedom. The fast degrees of freedom of the correlation function and the response are instantaneously at equilibrium with the temperature of the bath  $T$ . In this case FDT holds and the first slope is equal to  $1/T$ . For longer time scales both correlation and response cannot equilibrate; when  $(t - t')/t' \gg 1$  (where  $t'$  is the waiting time) their slow degrees of freedom are in a sort of quasi equilibrium with an effective temperature  $T_{eff}$ . FDT does not hold anymore but it is replaced by a more general expression shown in eq. (5.15). This new relation predicts that the slope formed by the correlation and the response at long waiting times is  $1/T_{eff}$ .

time - instead of fixing  $t$  and calculating  $\chi(t, t')$  and  $C(t, t')$  for different waiting times,  $t'$  was fixed and  $\chi(t, t')$  and  $C(t, t')$  calculated for different  $t$ . This corresponds in replacing  $\partial t'$  with  $\partial t$  in the differential expression of the FDR (eq. (5.15)) and it can be done only if  $X_{A,B}(t, t')$  is not an explicit function of  $t$  and  $t'$  [Berthier (2007)]. In the case of Lennard-Jones liquids the two methods give two  $T_{eff}$  that differ only of the 20% but in other systems (included spin systems and colloids) the result can be much different. Moreover there is always the problem of the applied field that has to be small enough to avoid non linear effects in the system, but a small field corresponds to longer simulations in order to get a better statistics.

A much easier way to calculate  $T_{eff}$  from the FD-plot exists and was developed by L. Berthier [Berthier (2007)]. The idea is the following: consider a Monte Carlo simulation of the liquid that we want to study. Every time that a particle has to move the Monte Carlo step generates a trial configuration  $C'_t$  that has to be accepted or refused according to an acceptance rate  $A_{C_t \rightarrow C'_t}$ . The transition probability  $W_{C_t \rightarrow C'_t}$  is given by the probability that the trial

configuration  $\mathcal{C}'_t$  at time  $t$  will be the new configuration at time  $t + 1$  plus the probability that it will be instead rejected:

$$W_{\mathcal{C}_t \rightarrow \mathcal{C}'_t} = \delta_{\mathcal{C}_{t+1}, \mathcal{C}'_t} A_{\mathcal{C}_t \rightarrow \mathcal{C}'_t} + \delta_{\mathcal{C}_{t+1}, \mathcal{C}'_t} (1 - A_{\mathcal{C}_t \rightarrow \mathcal{C}'_t}).^3 \quad (5.18)$$

If we define the probability of a trajectory  $k$  from time  $t'$  to time  $t$  as

$$P_k(t \rightarrow t') = \prod_{t''=t'}^{t-1} W_{\mathcal{C}_{t''}^k \rightarrow \mathcal{C}_{t''+1}^k} \quad (5.19)$$

where  $\mathcal{C}_t^k$  is the configuration visited at time  $t$  in the trajectory  $k$ , we can write the correlation function  $\langle A(t)B(t') \rangle_0$  as :

$$\langle A(t)B(t') \rangle_0 = \frac{1}{N} \sum_{k=1}^N A_k(t) B_k(t') P_k(t \rightarrow t'). \quad (5.20)$$

More complicated is the evaluation of the susceptibility  $\chi(t, t')$ :

$$\begin{aligned} \chi(t, t') &= \lim_{\varepsilon \rightarrow 0} \frac{[\langle A(t) \rangle - \langle A(t) \rangle_0]}{\varepsilon} = \frac{\partial \langle A(t) \rangle}{\partial \varepsilon} \Big|_{\varepsilon \rightarrow 0} = \frac{\partial}{\partial \varepsilon} \left[ \frac{1}{N} \sum_{k=1}^N A_k(t) P_k(t \rightarrow t') \right] \\ &= \frac{1}{N} \sum_{k=1}^N \frac{\partial A_k(t)}{\partial \varepsilon} P_k(t \rightarrow t') + \frac{1}{N} \sum_{k=1}^N A_k(t) \frac{\partial (\prod_{t''=t'}^{t-1} W_{\mathcal{C}_{t''}^k \rightarrow \mathcal{C}_{t''+1}^k})}{\partial \varepsilon}. \end{aligned} \quad (5.21)$$

In the first term of eq. (5.21)  $A_k(t)$  does not depend on the field  $\varepsilon$  hence the derivative is zero. Only the second term survives. Moreover we note that :

$$\prod_{t''=t'}^{t-1} W_{\mathcal{C}_{t''}^k \rightarrow \mathcal{C}_{t''+1}^k} = \exp \left[ \sum_{t''=t'}^{t-1} \ln(W_{\mathcal{C}_{t''}^k \rightarrow \mathcal{C}_{t''+1}^k}) \right]. \quad (5.22)$$

If we insert eq. (5.22) into eq. (5.21), then we have to calculate something like  $(\partial \exp[f(\varepsilon)] / \partial \varepsilon) = f'(\varepsilon) \exp[f(\varepsilon)]$  :

$$\begin{aligned} \chi(t, t') &= \frac{1}{N} \sum_{k=1}^N A_k(t) \sum_{t''=t'}^{t-1} \frac{\partial}{\partial \varepsilon} \ln(W_{\mathcal{C}_{t''}^k \rightarrow \mathcal{C}_{t''+1}^k}) \exp \left[ \sum_{t''=t'}^{t-1} \ln(W_{\mathcal{C}_{t''}^k \rightarrow \mathcal{C}_{t''+1}^k}) \right] \\ &= \frac{1}{N} \sum_{k=1}^N A_k(t) R(t \rightarrow t') P_k(t \rightarrow t') = \langle A_k(t) R(t \rightarrow t') \rangle_0, \end{aligned} \quad (5.23)$$

where  $R(t \rightarrow t') = \sum_{t''=t'}^{t-1} \frac{\partial}{\partial \varepsilon} \ln(W_{\mathcal{C}_{t''}^k \rightarrow \mathcal{C}_{t''+1}^k})$ . Hence the susceptibility is expressed through an unperturbed average. It easy to show that we do not need

<sup>3</sup>  $\delta_{\mathcal{C}_{t+1}, \mathcal{C}'_t}$  is the Kronecker delta related to the possibility that at time  $t + 1$  the new configuration  $\mathcal{C}$  is the trial configuration  $\mathcal{C}'$  generated at time  $t$ .

to apply any external field into the system but we can run a single unperturbed MC simulation where the only extra effort is to update at each time the value of  $R(t \rightarrow t')$ . To show that consider a Monte Carlo simulation with the Metropolis acceptance rate [Metropolis *et al.* (1953)]. Let  $V$  be the potential energy and  $B(t)$  the dynamic variable (whose correlation function with  $A(t)$  is the quantity that we want to study). We define  $r_{t \rightarrow t+1} = \partial \varepsilon \ln(W_{\mathcal{C}_t \rightarrow \mathcal{C}_{t+1}})$ . We need to calculate  $r_{t \rightarrow t+1}$  at each time since  $R(t \rightarrow t') = \sum_{t''=t'}^{t-1} r_{t'' \rightarrow t''+1}$ . To do that we can run an unperturbed Monte Carlo simulation in which at each time we normally reject or accept trial configurations; moreover at the same time we also evaluate the transition probability  $W_{\mathcal{C}_t \rightarrow \mathcal{C}_{t+1}}$  that a given trial configuration would have in the presence of an external field. We recall that in a MC simulation we can have different cases according to the Metropolis rule:

- If  $V(\mathcal{C}'_t) \leq V(\mathcal{C}_t)$   
then  $\mathcal{C}_{t+1} = \mathcal{C}'_t$  (the configuration is accepted)
- If  $V(\mathcal{C}'_t) \geq V(\mathcal{C}_t)$  then a random number  $M$  is extracted
  - If  $M < \exp[-(1/T)(V(\mathcal{C}'_t) - V(\mathcal{C}_t))]$   
then  $\mathcal{C}_{t+1} = \mathcal{C}'_t$  (the configuration is accepted)
  - If  $M \geq \exp[-(1/T)(V(\mathcal{C}'_t) - V(\mathcal{C}_t))]$   
then  $\mathcal{C}_{t+1} = \mathcal{C}_t$  (the configuration is rejected).

Using the scheme above we try now to evaluate  $r_{t \rightarrow t+1}$ . Remember that in the presence of an external field the modified potential energy is  $V(\mathcal{C}_t) - \varepsilon B(\mathcal{C}_t)$ .

- If  $V(\mathcal{C}'_t) \leq V(\mathcal{C}_t)$   
then  $\mathcal{C}_{t+1} = \mathcal{C}'_t$ . It means that  $W_{\mathcal{C}_t \rightarrow \mathcal{C}_{t+1}} = 1$  and  $r_{t \rightarrow t+1} = \partial \varepsilon \ln(W_{\mathcal{C}_t \rightarrow \mathcal{C}_{t+1}}) = 0$  in the biased dynamics (i.e. in the presence of the field).
- If  $V(\mathcal{C}'_t) \geq V(\mathcal{C}_t)$  then a random number  $M$  is extracted
  - If  $M < \exp[-(1/T)(V(\mathcal{C}'_t) - V(\mathcal{C}_t))]$   
then  $\mathcal{C}_{t+1} = \mathcal{C}'_t$  the configuration is accepted in the biased dynamics. This time the transition probability is given by the difference between the biased energies:

$$W_{\mathcal{C}_t \rightarrow \mathcal{C}_{t+1}} = \exp[-(1/T)(\Delta V_{\mathcal{C}_t \rightarrow \mathcal{C}'_t} - \varepsilon \Delta B_{\mathcal{C}_t \rightarrow \mathcal{C}'_t})]. \quad (5.24)$$

As a consequence we get  $r_{t \rightarrow t+1} = (1/T)[B(\mathcal{C}'_t) - B(\mathcal{C}_t)]$ .

- If  $M \geq \exp[-(1/T)(V(\mathcal{C}'_t) - V(\mathcal{C}_t))]$   
then  $\mathcal{C}_{t+1} = \mathcal{C}_t$  the configuration is rejected in the biased dynamics. The probability for the configuration to be rejected is  $1 - W_{\mathcal{C}_t \rightarrow \mathcal{C}_{t+1}}$ . It follows that  $r_{t \rightarrow t+1} = (B(\mathcal{C}'_t) - B(\mathcal{C}_t))/[T(1 - \exp[-(1/T)(V(\mathcal{C}'_t) - V(\mathcal{C}_t))])]$ .

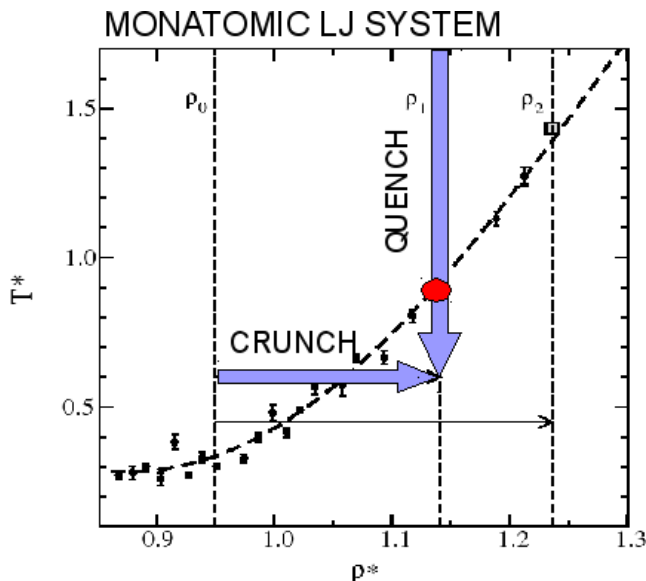


Figure 5.2: Glass transition in a monatomic Lennard-Jones system. The points on the line are identified from the crossover of the potential energy as a function of temperature. In the plot are also reported some effective temperatures calculated through FDR (the big empty square and the red dot). The important thing to note is the following: if a crunch and a quench are performed from two different state points to a final common state, the effective temperature measured will be the same. In the plot the red dot corresponds to the effective temperature calculated from the crunch and quench underlined by arrows. The original plot can be found in reference [Di Leonardo *et al.* (2000)].

In the next sections we will show the results applying this method on a KABLJ. In our study  $T_{eff}$  is used as a tool for characterizing the glassy behavior of the system and - more in general - of strongly correlating liquids. The properties that we will discuss below have helped us also to explain the findings in past works which have remained unsolved so far.

#### 5.4 Predicting the effective temperature in strongly correlating liquids

Dropping the temperature in a liquid (i.e. making a quench) is not the only way for turning it into a glass. The other option is to perform a “crunch” i.e. to increase the density of the system by squeezing the particles in a smaller volume. What happens is that particles have no space to relax in an equilibrium situation and the system gets arrested. Also in this case is possible to calculate the effective temperature via the FDR. In a work done by R. Di Leonardo *et al.* [Di Leonardo *et al.* (2000)], both quench and crunch procedures are applied on a monatomic Lennard-Jones in order to calculate  $T_{eff}$ .

Figure 5.2 shows the glass line in the monatomic Lennard-Jones identified from

the crossover in the temperature dependence of equilibrium potential energy. Among these points there are also some points corresponding to the effective temperature measured via FDR during crunches and quenches. The surprising result obtained by the authors of the paper is sketched in fig. 5.2. Suppose to perform a quench from a given state point to a final point in the glassy state. During the aging the system is so arrested that - at a given time -  $T_{eff}$  can be measured. the point  $(T_{eff}, \rho_1)$  corresponds to the red dot in the figure. After the quench, a crunch is performed from another initial state point to the same final state point used in the quench. In doing both the quench and the crunch the authors found something interesting: the effective temperatures measured were the same. In the paper they do not explain why this happens but they argue that the effective temperature depends only on the final density. Here we will show that an explanation for such behavior can be found in the fact that the monatomic Lennard-Jones is a strongly correlating liquid. The results that we will present can be found also in Paper VIII.

### 5.5 Equivalence between crunches and quenches

To understand why a crunch should be equivalent to a quench in a strongly correlating liquid we have to recall the aging properties discussed in section 4.2. In particular we are interested in the result obtained from the second aging experiment where the liquid - starting from two isomorphic state points 1 and 2 - was aging towards a common final state point 3. State 2 had the same density of state 3 (see fig. 4.4) while state 1 had both different temperature and density. We found that the relaxation patterns in the  $1 \rightarrow 3$  jump and in the  $2 \rightarrow 3$  jump were the same since the system in state 1 first performed an isomorphic instantaneous  $1 \rightarrow 2$  jump in order to achieve the right final density and then slowly relaxed towards state 3 only adjusting its temperature (and therefore relaxing exactly like state 2). Then all the time that we perform a crunch in a strongly correlating liquid, the system jumps instantaneously on its isomorphic point having the right final density and then it adjusts the temperature as if the crunch was instead a quench. Figure 5.3 shows exactly the situation illustrated now for two isomorphic points in which the system is forced to relax towards the same final (glassy) state through a quench and a crunch. Since the relaxation is identical in the two processes we expect to measure the same correlation functions and responses (in reduced units) and therefore to have the same FD-plot and same  $T_{eff}$  (see the subplot in fig. 5.3). Hence in strongly correlating liquids a quench is equivalent to a crunch and that explains the results found by Di Leonardo et al. as shown in fig. 5.3.

Crunching or quenching the system from two isomorphic state points is not the only way to obtain the same FD-plot (in reduced units). Another way consists in using the third aging property explained in section 4.2 which says that for two jumps  $(T_1, \rho_1) \rightarrow (T_3, \rho_3)$  and  $(T_2, \rho_2) \rightarrow (T_4, \rho_4)$  between mutually isomorphic initial and final states (i.e.  $(\rho_1^\gamma/T_1) = (\rho_2^\gamma/T_2)$  and  $(\rho_3^\gamma/T_3) = (\rho_4^\gamma/T_4)$ ) the relaxation pattern of the two jumps can be connected at each time with an isomorph. It means that the system in the two aging experiments follows the same path in the reduced configuration space since correlation functions and responses in the two jumps are the same when plotted in reduced units. To show that we have performed another quench from a state point  $(T_1, \rho_1)$  iso-

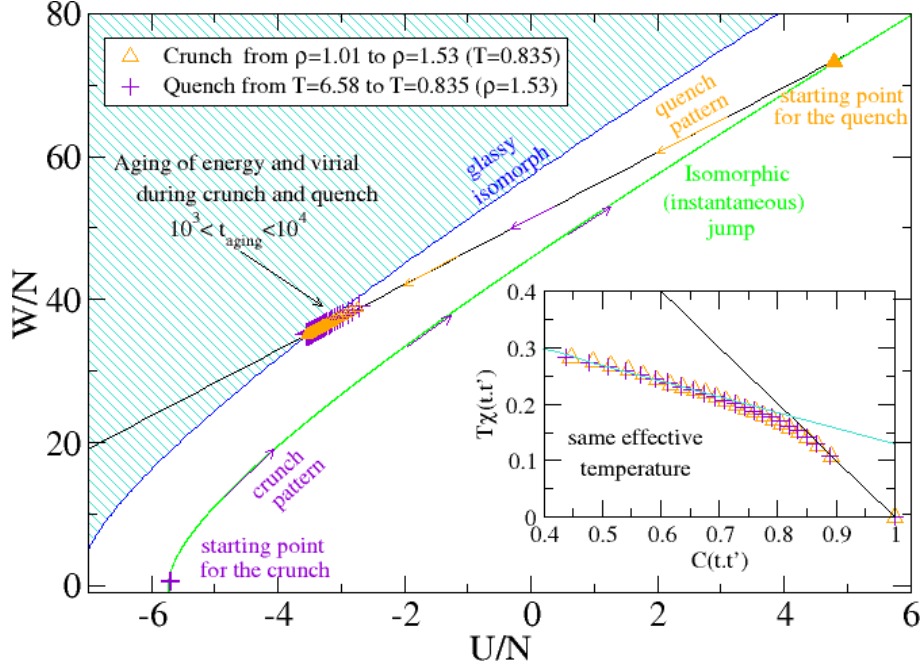


Figure 5.3: A crunch is performed from a state point (purple cross) towards a final point in the glassy state. The relaxation pattern is the following: the system jumps instantaneously on the isomorphic point (orange triangle) having the final density that it has to achieve and then it changes temperature towards the final temperature as if the crunch has been turned into a quench. We can think then to perform a quench from the point identified by the orange triangle towards the same final state of the crunch. For what has been shown in section 4.2 regarding the aging properties of isomorphic points, the relaxation pattern of the quench is the same of the crunch and the correlation functions and responses measured are the same (in reduced units), i.e. the FD-plot is the same and consequently the effective temperature. For the simulations we have used the KABLJ (1000 particles). The crunch is from  $(T = 0.835, \rho = 1.01)$  to  $(T = 0.835, \rho = 1.53)$ . The quench is from  $(T = 6.58, \rho = 1.53)$  to  $(T = 0.835, \rho = 1.53)$ . This is a MC simulation in which the correlation functions and the responses have been evaluated with the method introduced by Berthier and explained in section 5.3. In the MC simulation we have used has reference maximum displacement  $\delta_{max}$  the one suggested in reference [Berthier & Kob (2007)] and adjusted at different densities using the relation  $\delta_{max,2} = (\rho_1/\rho_2)^{1/3} \delta_{max,1}$  in order to obtain correlation functions and responses in reduced units of length and time.

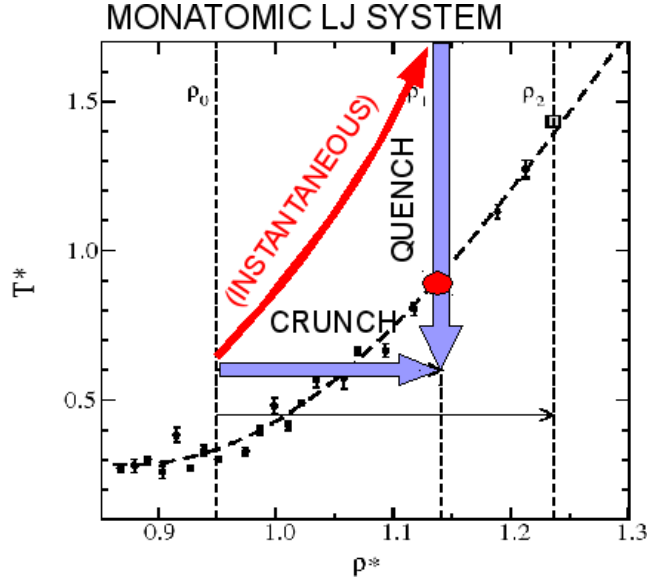


Figure 5.4: Same plot of fig. 5.2 but here it is shown why quench and crunch are equivalent. The instantaneous jump between isomorphic points turns the crunch into an equivalent quench from its isomorphic state point down to the same final state. The original plot can be found in the reference [Di Leonardo *et al.* (2000)].

morphic to the two state points of fig. 5.3 down to a state  $(T_3, \rho_3)$  isomorphic to the final glassy state of the previous example that we will call  $(T_4, \rho_4)$ . To find the initial and final states we have used always the same  $\gamma$  corresponding to the slope obtained from the fluctuations of  $U$  and  $W$  of the initial state in the quench of fig. 5.3  $(T_2, \rho_2)$ . In fact is not possible to use the equilibrium fluctuations of  $U$  and  $W$  in the glassy state to find isomorphic points but we can use the fact that along the isochore connecting  $(T_2, \rho_2)$  and  $(T_4, \rho_4)$ ,  $\gamma$  is almost constant. Then we can use that  $\gamma$  for finding  $(T_3, \rho_3)$  from  $(T_4, \rho_4)$ . The result is shown in fig. 5.6.

The last example allow us to make some considerations. Since the reduced units dynamics is the same for the two “isomorph-connected” jumps described previously, their violation factors  $X(t, t') = (T/T_{eff}(t, t'))$  are identical (see fig. 5.6). We call

$$X_3(t, t') = \frac{T_3}{T_{eff,3}(t, t')} \quad (5.25)$$

and

$$X_4(t, t') = \frac{T_4}{T_{eff,4}(t, t')} \quad (5.26)$$

the violation factors associated to the jumps  $(T_1, \rho_1) \rightarrow (T_3, \rho_3)$  and  $(T_2, \rho_2) \rightarrow (T_4, \rho_4)$ . Moreover we know that

$$\frac{\rho_3^\gamma}{T_3} = \frac{\rho_4^\gamma}{T_4}. \quad (5.27)$$

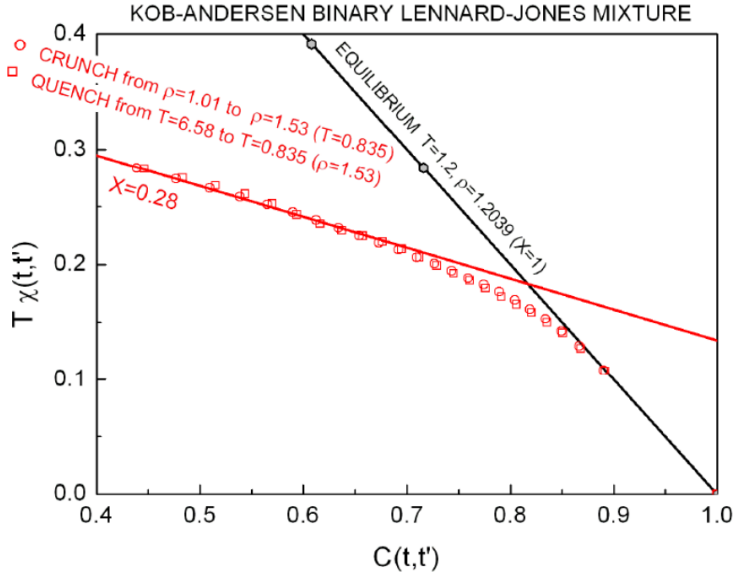


Figure 5.5: FD-plots for the crunch and the quench described in fig. 5.3. The plots have fixed  $t = 10^4$  MC steps and different waiting times. The correlation function used is  $C(t, t') = \langle A(t)B(t') \rangle$  where  $A_{\mathbf{k}}(t'') = N^{-1} \sum_j \eta_j \exp(i\mathbf{k} \cdot \mathbf{r}_j(t''))$  and  $B_{\mathbf{k}}(t'') = N[A_{\mathbf{k}}(t'') + A_{-\mathbf{k}}(t'')]$ . The response has been evaluated according the Berthier's method in section 5.3. For more informations see Paper VIII.

Inserting eq. (5.25) and eq. (5.26) in eq. (5.27) we find the following expression:

$$\frac{\rho_3^\gamma}{T_{eff,3}(t, t')} = \frac{\rho_4^\gamma}{T_{eff,4}(t, t')}. \quad (5.28)$$

This implies that

$$\frac{\rho^\gamma}{T_{eff}(t, t')} = Const. \quad (5.29)$$

Equation (5.29) identifies the dynamic glass transition curve in the  $(\rho, T)$  plane defined by the FDR effective temperatures with an isomorph<sup>4</sup>. This is a very important relation because defines the form of the glass line in strongly correlating liquids. A direct consequence is that we just need to calculate the effective temperature in one off-equilibrium jump (it could be a crunch, a quench or even a crunch-quench) and we will automatically know the effective temperatures of all the jumps that at each time are connected by isomorphs to the first jump. The single jump required is needed to find the constant *Const* that enters in eq. (5.29) and that characterizes the glassy line<sup>5</sup>. We then need

<sup>4</sup>Note the the standard definition of the glass line is where the relaxation time reaches a certain high value and therefore usually the time dependent effective temperature is used to mark such line.

<sup>5</sup>note that the glassy line in eq. (5.29) depends on the time at which the effective temperature is calculated.

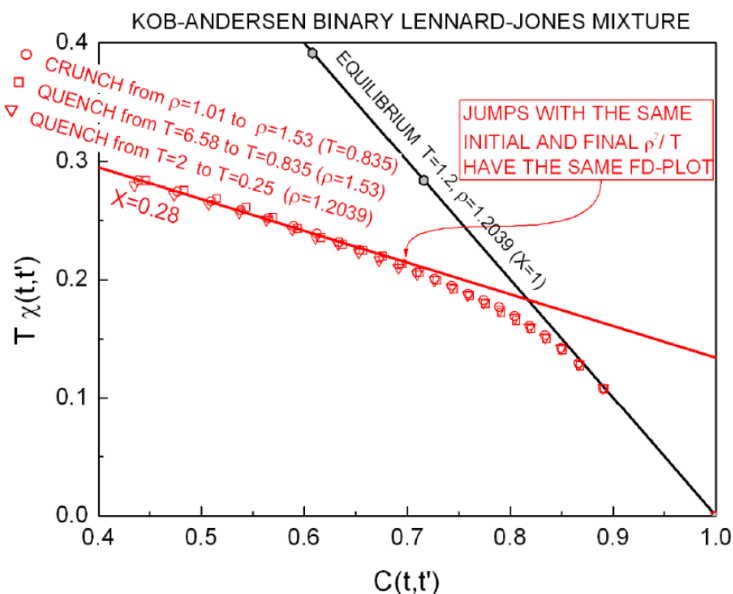


Figure 5.6: Equivalent FD-plots are found not only in equivalent crunches and quenches but also in jumps from isomorphic state points to isomorphic state points. We consider here an extra jump:  $(T = 2, \rho = 1.2039) \rightarrow (T = 0.25, \rho = 1.2039)$ . In this case  $(T = 2, \rho = 1.2039)$  is isomorphic to both  $(T = 6.58, \rho = 1.53)$  and  $(T = 0.835, \rho = 1.01)$ . Moreover  $(T = 0.25, \rho = 1.2039)$  is isomorphic to  $(T = 0.835, \rho = 1.53)$  then we expect that the two quenches and the crunch follow the same path in the configuration space (in reduced units) according to the third aging property of section 4.2. Note that having the same FD-plot does not mean to have the same  $T_{eff}$  but only the same violation factor  $X(t, t') = (T/T_{eff}(t, t')) = 0.28$ . In the equivalent crunch and quench  $T = 0.835$  (i.e. the final temperature) is the same (i.e.  $T_{eff}$  is the same) while in the new crunch  $T = 0.25$  and therefore  $T_{eff}$  is different.

$\gamma$  and one  $T_{eff}$  to insert in eq. (5.29) and that can be found by doing - for instance - a quench. Moreover we can drop the constraint on only “isomorph-connected” jumps. In fact it is well known [Kob & Barrat (1999), Berthier (2007)] that in a jump - if the starting state corresponds to a “warm liquid state” (i.e. low viscous state) and the final state is in the linear regime where  $X(t, t') = T/T_{eff}(t, t')$  (with constant  $T_{eff}$ ) - then  $T_{eff}$  is independent from the initial and final state and eq. (5.29) holds very well for all the off-equilibrium jumps occurring in that region. Figure 5.7 shows a number of FD-plots for different densities and temperatures. The slopes of the full straight lines have been predicted using eq. (5.29). On the contrary if our prediction holds, then all the effective temperatures extracted from the FD-plots should belong to the same glassy line as shown in fig. (5.8).

The simple aging properties discussed here are valid only for strongly correlating liquids. To show that we have simulated the non-equilibrium dynamics of the non strongly correlating “monatomic Lennard-Jones Gaussian” (LJG)

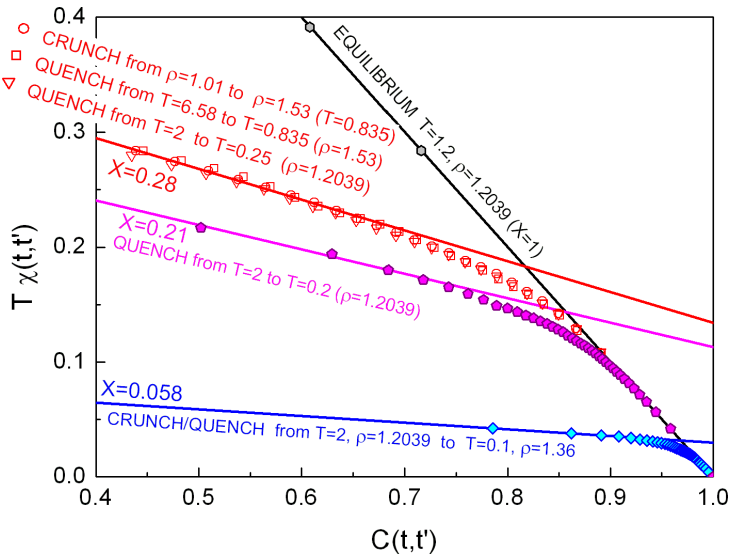


Figure 5.7: FD-plots for several density/temperature jumps. Simulation details are explained in the caption of fig. 5.5. The full lines have the slope predicted from eq. (5.29) and are adjusted only by a vertical shift to fit the data.

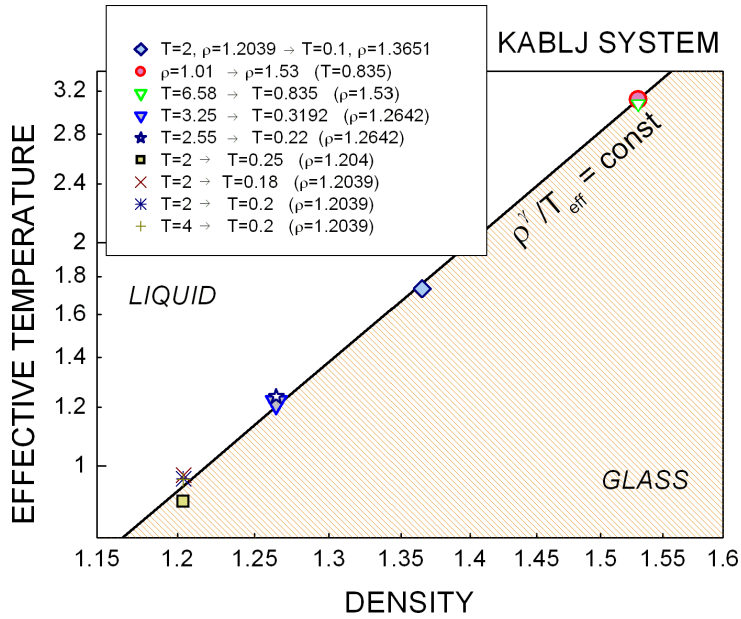


Figure 5.8: Effective temperature as a function of density on a log-log scale. The full line is the glass defined by one single off-equilibrium jump from which we can extract  $T_{eff}$  and  $\rho$  entering in eq. (5.29) while the points on the line corresponds to the effective temperatures calculated from the FD-plots of several density/temperature jumps. It is clear that the prediction stated in the text holds well.

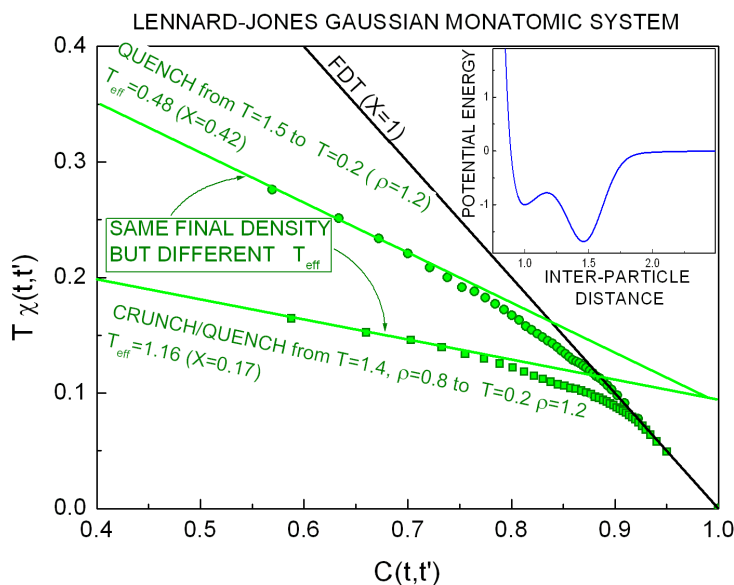


Figure 5.9: FD-plots for two off-equilibrium jumps of the monatomic Lennard-Jones Gaussian. The inset shows the potential of the model. The different FD-plots are a proof of the fact that simple aging properties exist only in strongly correlating liquids.

model [Van Hoang & Odagaki (2008)]. Informations on the MC simulations of this system are found in appendix D. For this system we have calculated the effective temperatures of two off-equilibrium jumps from two different state points to the same final state. The results are shown in fig. 5.9. If the system were strongly correlating then we would have expected to have the same FD-plots: clearly this is not the case.

We now come back to the discussion started in section 5.1 regarding the meaning of the effective temperature as a thermodynamic parameter. Which informations can we extract from the knowledge of the effective temperature? An example is given in fig. 5.10. The plot is obtained using the following procedure: for different quenches we evaluate the effective temperature at  $t = 10^4$  MC steps. At that time we also evaluate the mean IS energy of the system through a conjugate gradient minimization procedure. Since  $T_{eff} > T$  we are able most of the times to equilibrate easily the system at  $T_{eff}$  because it is still in the liquid phase. Since this is the case for all the quenches performed, we evaluate the mean IS energy of the equilibrium state points with a temperature equal to  $T_{eff}$ . When we plot off-equilibrium IS energies and equilibrium IS energies we find that for strongly correlating liquids the two energies are the same. This means that the aging pattern of a strongly correlating liquids is well defined and goes through a series of states that can be also visited at equilibrium (and  $T_{eff}$  tells us which are these states). This is also suggested in reference [Sciortino & Tartaglia (2001)]. Thus  $T_{eff}$  is a good physical quantity for strongly correlating liquids since it is an instrument for getting informations on the shape of the basins in the energy landscape.

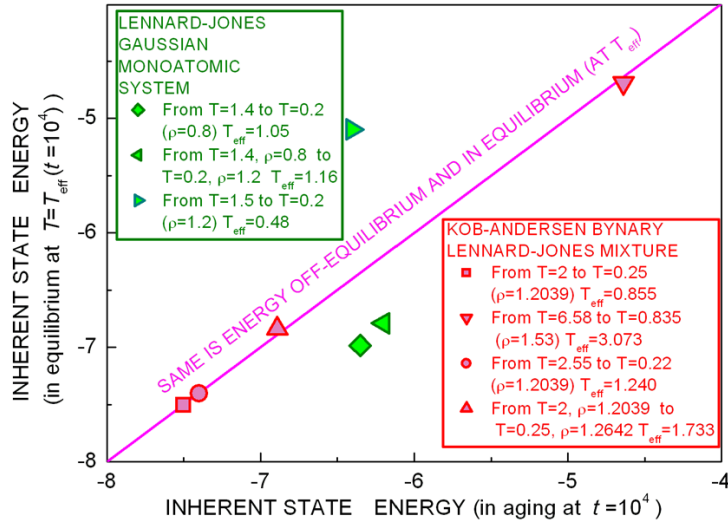


Figure 5.10: Comparison between the average IS energies at equilibrium with  $T = T_{eff}$  and out-of-equilibrium evaluated at the same time  $t$  in which  $T_{eff}$  is calculated after a temperature jump via FDR. Data are for the KABLJ and for the LJG. For The KABLJ the IS energies are the same and this indicates that during aging, at time  $t$ , the system visits basins with the same depth of those of system at equilibrium at  $T = T_{eff}$ . The energy value of the LJG are scaled of a factor 2.5 for an easier comparison with the KABLJ energies.

Summarizing we have shown that aging properties of isomorphs illustrated in section 4.2 explain why the effective temperature depends only on the final density. In fact when there are isomorphs it is always possible to produce equivalent density/temperature transformations which give the same FD-plot in reduced units. Thanks to these informations we have found that also the effective temperature satisfies the density scaling relation  $\rho^\gamma/T_{eff}$ , i.e. the glass line defined by  $T_{eff}$  is an isomorph. In this framework we only need to know the effective temperature from the result of one single aging simulation for predicting the effective temperatures of all the possible glasses that we can produce. Moreover for strongly correlating liquids the effective temperature gives informations on the average IS type that the system can visit off-equilibrium since is the same kind of IS that the system visits at equilibrium with a specific temperature:  $T = T_{eff}$ . Therefore  $T_{eff}$  has a good physical meaning (at least for strongly correlating liquids) even though is not established if it could also play the role of a thermodynamic temperature in an off-equilibrium thermodynamic description.



## Chapter 6

# Outlook

This chapter provides some perspectives of the studies presented in the thesis. A list of open questions is shown as a support for future research projects.

- 1 . In chapter 3 we have shown that properties of strongly correlating liquids can be explained with the existence of isomorphs. Moreover we know from chapter 2 that not only atomic systems belong to the class of strongly correlating liquids, but also molecular liquids like ortho-terphenyl and toluene. It would be interesting to investigate the isomorph properties for these systems and derive - as it was done for the 12-6 Lennard-Jones - equations which define isomorphs in the  $U$ - $W$  plane.
- 2 . In the last few years there has been a growing interest related to the “jamming transition”. According to that different systems like molecular glasses, colloids and granulars are jammed into a unique state when the temperature, the inverse of packing fraction and the shear stress tend to zero. Starting from the jamming points all these systems get different if different parameters are tuned. It follows that glasses unjam when the temperature is raised, colloids unjam when the packing fraction is lowered and foams unjam when the shear stress gets higher. The phase diagram that should collect all these informations is called jamming phase diagram [Liu & Nagel (1998)]. It would be interesting to study what happens to strong correlation when the part of the phase diagram ruled by temperature and shear stress is explored, i.e. in case of off-equilibrium liquids in a stationary state. Does strong correlation survive? Moreover it would be valuable to investigate if for strongly correlating liquids there is a relation between temperature and strain rate of the same kind of that between density and temperature (i.e. the density scaling).
- 3 . In chapter 3 we have discussed the particular case of the binary WCA system. We showed that this system is strongly correlating (with a correlation coefficient higher than in the case of the KABLJ) but the presence of the cut-off inside the first peak of the radial distribution function causes a bad isomorph scaling. This point should be investigated further.
- 4 . A natural consequence of the study on isomorphs is to identify isomorphic points in real experiments. As it is discussed in Paper IV there are already some experimental evidences of the existence of isomorphs. For

## 6. OUTLOOK

---

instance K. Ngai *et al.* [Ngai *et al.* (2005)] showed that only the average relaxation time determines the shape of the dielectric loss peak in an experiment at constant temperature and pressure. This “isochronal” superposition should work only for strongly correlating liquids since the dielectric spectrum should be an isomorph invariant. This means that we are able to find experimentally isomorphic points following this method. It would be interesting then to study the aging properties illustrated in chapter 4 via temperature/pressure jumps. This is an on-going work of the glass and time group.

- 5 . As discussed in chapter 5 and in Paper VIII the effective temperature  $T_{eff}$  defined via the fluctuation-dissipation relation has some remarkable scaling properties in strongly correlating liquids. Moreover we have shown that  $T_{eff}$  locates the equilibrium inherent states that the system visits in aging. This scenario is found to breakdown for non strongly correlating systems. In this context it would be important to understand more precisely why an off-equilibrium strongly correlating liquid has to age through equilibrium states and why a non strongly correlating liquid has a very different relaxation pattern. Computer simulations and theoretical works might clarify these issues.
- 6 . Recently we have found that a quite striking correlation exists between the non-ergodicity factor  $f_k$  and the violation factor  $X$  in a strongly correlating glassy system. In fact they are connected through the following relation:

$$X = \alpha \frac{(1 - f_k)}{f_k} \quad (6.1)$$

where  $\alpha$  is a parameter. Interestingly a similar situation is found in some spin systems where this correlation expresses some topological properties of the free-energy landscape in the replica symmetry breaking (RSB) approach [Young (1998)]. In particular for a spherical  $p$ -spin model [Castellani & Cavagna (2005), Horner *et al.* (1993)] we have that:

$$X = (p - 2) \frac{(1 - q)}{q} \quad (6.2)$$

where  $p$  is the number of interacting neighbors and  $q$  is the “overlap” parameter [Castellani & Cavagna (2005)]. Since it is possible to show that in spin-systems the violation factor is related to the complexity of the system (i.e. the number of states with a given depth), if we understand the relation between  $q$  and  $f_k$  we could have information on the topology of the energy landscape visited by the strongly correlating liquid.

## Appendix A

# Invariance of the Liouville operator

Here we show how the Liouville operator - which controls the temporal evolution of an observable - is invariant for IPL potentials when it is expressed in reduced units. Consider the two state points of section (3.1.1):  $(T_0, \rho_0)$  and  $(T_1 = T_0 \alpha^2 \lambda^2, \rho_1 = \rho_0 / \alpha^3)$ .  $\mathbf{r}_i(t)$  and  $\mathbf{r}_i^{(1)}(t) = \alpha \mathbf{r}_i(\lambda t)$  are both solutions of Newton's equation when  $\alpha^{-(n+2)} = \lambda^2$ . If we want to express positions and velocities in reduced units we have to use the following relations:

$$\mathbf{r}_i \rho^{1/3} = \mathbf{r}_i^{(1)} \rho_1^{1/3} = \tilde{\mathbf{r}}_i, \quad (\text{A.1})$$

$$t \sqrt{T_0 \rho_0^{1/3}} = t^{(1)} \sqrt{T_1 \rho_1^{1/3}} = \tilde{t} \quad (\text{A.2})$$

and

$$\mathbf{v}_i \rho_0^{-2/3} \sqrt{T_0} = \mathbf{v}_i^{(1)} \rho_1^{-2/3} \sqrt{T_1} = \tilde{\mathbf{v}}_i. \quad (\text{A.3})$$

Consider now an observable  $A$ . We can associate to it a dynamic correlation function defined as [Hansen & McDonald (2006)]

$$\langle A(0)A(t) \rangle = \int P(\mathbf{r}_1, \dots, \mathbf{r}_N) A(\mathbf{r}_1, \dots, \mathbf{r}_N) e^{-i\mathcal{L}t} A(\mathbf{r}_1, \dots, \mathbf{r}_N) d\mathbf{r}_1 \dots d\mathbf{r}_N, \quad (\text{A.4})$$

where  $i\mathcal{L}$  is the Liouville operator

$$i\mathcal{L} = \sum_i \left[ \frac{\partial H}{\partial \mathbf{p}_i} \frac{\partial}{\partial \mathbf{r}_i} - \frac{\partial H}{\partial \mathbf{r}_i} \frac{\partial}{\partial \mathbf{p}_i} \right] \quad (\text{A.5})$$

and  $H$  is the Hamiltonian of the system. Since in this case the observable depends only on the position, the Liouville operator reduces to  $i\mathcal{L} = \sum_i \frac{\partial H}{\partial \mathbf{p}_i} \frac{\partial}{\partial \mathbf{r}_i}$ . The Hamiltonian for a system interacting with an inverse power-law potential is given by

$$H = \sum_i \frac{\mathbf{p}_i^2}{2m} + U_{IPL}(\mathbf{r}_1, \dots, \mathbf{r}_N). \quad (\text{A.6})$$

Inserting eq.(A.6) into eq.(A.5) we can write the Liouville operator applied to one of the two state points in reduced units

$$\begin{aligned}
 i\tilde{\mathcal{L}}\tilde{t} &= \sum_i \rho_0^{-2/3} T_0 \frac{\mathbf{p}_i}{m} \frac{\partial}{\partial \mathbf{r}_i} t \\
 &= \sum_i \frac{\tilde{\mathbf{p}}_i}{m} \frac{\partial}{\partial \tilde{\mathbf{r}}_i} \tilde{t} \\
 &= \sum_i \rho_1^{-2/3} T_1 \frac{\mathbf{p}_i^{(1)}}{m} \frac{\partial}{\partial \mathbf{r}_i^{(1)}} t^{(1)} \\
 &= i\tilde{\mathcal{L}}^{(1)}\tilde{t}^{(1)}.
 \end{aligned} \tag{A.7}$$

Hence we have found that  $i\mathcal{L}^{(1)}t^{(1)}$  is equal to  $i\mathcal{L}t$  if expressed in reduced units.

## Appendix B

# Harmonic oscillator coupled to a system

We here briefly discuss the “gedanken” experiment described in reference [Kurchan (2005)] to show how a thermometer coupled to a system can measure directly the effective temperature on its response time scale. Consider a one dimensional system in equilibrium with an energy  $E$  and a harmonic oscillator linearly coupled to it. Figure B.1 shows a schematic drawing of the experiment. We can use as observable of the system the Fourier transform of the density  $\rho_k = \int \cos(kx)\rho(x,t)dx$ . The total energy (system plus harmonic oscillator) will be

$$E_{tot} = E + x\rho_k + \frac{p_x^2}{2} + \frac{\omega^2 x^2}{2} \quad (\text{B.1})$$

where  $x$  is the oscillator coordinate which is coupled to the density of the system and  $p_x$  and  $\omega$  are, respectively, the momentum and the frequency of the oscillator.

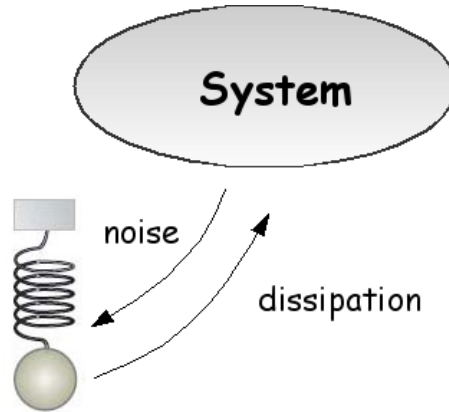


Figure B.1: A harmonic oscillator with frequency  $\omega$  is weakly coupled to a system. The harmonic oscillator is pumped with the energy that collects from the fluctuations of the system’s variable coupled to it and it dissipates this energy through the echo of the feedback reaction on the system.

We can now solve the harmonic oscillator for  $x$  if we consider the coupling as a small perturbation, and after that we can obtain the expression of  $\rho_k$  if we think of  $x$  as a field acting linearly on the system.

For the harmonic oscillator we have

$$\ddot{x} = -\omega x - \rho_k, \quad (\text{B.2})$$

and using linear response theory we can calculate the action of the oscillator on  $\rho_k$ :

$$\rho_k = [\rho_k]_0 + \int_{-\infty}^t dt' \frac{\partial \chi}{\partial t'} x(t'). \quad (\text{B.3})$$

$\chi(t - t')$  is the susceptibility and it measures how much  $\rho_k$  responds on average at time  $t$  to a small perturbation at time  $t'$ . Summarizing the harmonic oscillator feels the coupling term  $x\rho_k$  as a noise which pumps energy into it, while the system feels the presence of the oscillator through  $x$  as an external field which acts as a feedback reaction.

We can now write the total equation of motion for the harmonic oscillator:

$$\ddot{x} = -\omega x + [\rho_k]_0 + \int_{-\infty}^t dt' \frac{\partial \chi}{\partial t'} x(t'). \quad (\text{B.4})$$

Equation (B.4) has the form of a Langevin equation because there is a noise and the integral can be interpreted as a friction term. Thus the oscillator takes up energy from the fluctuations of  $\rho_k$  (that are measured by the autocorrelation function  $C(t - t') = \langle [\rho_k]_0(t)[\rho_k]_0(t') \rangle$ ), and dissipates it through the echo of its feedback on the system (which is proportional to  $\chi(t - t')$ ). It is possible to show that these two effects give the right energy of the oscillator using the equipartition theorem. If we define  $C(\omega)$  the Fourier transform of  $C(t - t')$  and  $\chi(\omega)$  the Fourier transform of  $\chi(t - t')$  it is possible to prove that:

$$\frac{1}{2}\omega^2 \langle x^2 \rangle = \langle E_{osc} \rangle = \frac{\omega \operatorname{Re}[C(\omega)]}{2 \operatorname{Im}[\chi(\omega)]} \quad (\text{B.5})$$

and using the equipartition theorem that

$$T(\omega) = \langle E_{osc} \rangle = \frac{\omega \operatorname{Re}[C(\omega)]}{2 \operatorname{Im}[\chi(\omega)]}. \quad (\text{B.6})$$

The last expression represents the fluctuation dissipation theorem. Thus when our thermometer (the oscillator) is coupled to a thermal bath (the system) it measures the temperature suggested by the fluctuation dissipation theorem. Note that the thermometer responds on a timescale  $1/\omega$ . At equilibrium the effective temperature corresponds to the temperature of the bath. When the system is brought out of equilibrium the fluctuation dissipation theorem does not hold anymore but a more general relation connects the effective temperature with correlation and response. In this case the effective temperature corresponds to the temperature of the slow degrees of freedom and usually is higher than the bath temperature. The out of equilibrium version of eq. (B.6) is:

$$T(\omega, t_w) = \frac{\omega \operatorname{Re}[C(\omega, t_w)]}{2 \operatorname{Im}[\chi(\omega, t_w)]}, \quad (\text{B.7})$$

---

where now the correlation and the response function depend also on  $t_w$  because of the lack of time translational invariance (TTI). In the case of two time scales systems like structural glasses, if the thermometer takes energy from the high frequency degrees of freedom it will measure the bath temperature again. To have a thermometer measuring the effective temperature - i.e. the temperature of the slow degrees of freedom - its frequency must be  $\omega \sim 1/t_w$  i.e. has to respond on a time scale of the order of the waiting time (i.e. of the order of the age of the system). This makes difficult to measure  $T_{eff}$ . To solve this problem we need an ensemble of small thermometers [Cugliandolo & Kurchan (1999)] but this does not solve the problem of how we can operatively measure the effective temperature.



## Appendix C

# Equivalent formulations of FDT

Here we present an alternative derivation of the FDT using the “energy bond” and the creep function formulation. Moreover we show that the alternative definitions are equivalent to the differential form of the FDT:

$$k_B T \partial_{t'} \chi_{A,B}(t, t') = -\partial_{t'} C_{A,B}(t, t'). \quad (\text{C.1})$$

### C.1 Energy bond formulation

The energy bond formalism provides a description of the interaction of a system with its surrounding [Paynter (1961), Christiansen (1971)]. An energetic interaction between the system and the surrounding defines an energy bond.

An energy bond has an “effort”  $e(t)$  (it can be for instance the voltage  $V$ ) and a “flow”  $f(t)$  (e.g. the current flow  $J$ ). The product  $e(t) \cdot f(t)$  is the rate of energy transferred from the surrounding to the system per unit time. We also define the “displacement” variable  $q$  (that could correspond to the charge in the example above) and the time integrated flow  $\dot{q} = f(t)$ . Suppose that we can control the effort variable, which is the analogous of an external field applied to the system. The flow response to the applied field is:

$$\langle f(t) \rangle_e = \beta \int_0^\infty \langle f(0) f(\tau) \rangle_0 e(t - \tau) d\tau \quad (\text{C.2})$$

where  $\langle \dots \rangle_0$  means that the average is performed under equilibrium conditions, i.e.  $e = 0$ . Equation (C.2) is the definition of the FDT in this formulation. It can happen to have more than one bond. Then the FDT formulation becomes

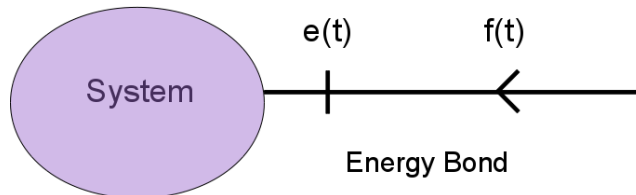


Figure C.1: Abstract energy bond

$$\langle f(t) \rangle_e = \beta \sum_{j=1}^N \int_0^\infty \langle f_i(0) f_j(\tau) \rangle_0 e_j(t - \tau) d\tau \quad (\text{C.3})$$

where  $N$  is the number of bonds.

## C.2 Creep function formulation of FDT

Another way of defining the FDT is through the following method. Suppose that we can control the external field  $e(t) = e_0 \theta(t)$  and we want to know what is the change in the displacement variable after the field has been applied. We can define the the creep function  $J(t) \equiv \langle \Delta q(t) \rangle_e / e_0$  (where  $\Delta q(t) = q(t) - q(0)$ ) and the expression of FDT is

$$J(t) = \frac{\langle \Delta q^2(t) \rangle_0}{2k_B T}. \quad (\text{C.4})$$

## C.3 Equivalence of the formulations

Lets start from the formulation in eq. (C.4). Since  $\dot{q} = f$  i.e.

$$\Delta q(t) \equiv \int_0^t f(\tau) d\tau, \quad (\text{C.5})$$

then

$$\begin{aligned} \frac{d\langle \Delta q(t) \rangle_e}{dt} &= \langle f(t) \rangle_e = \frac{1}{k_B T} \int_0^t \langle f(0) f(\tau) \rangle_0 e_0 \theta(t - 0) d\tau \\ &= \frac{e_0}{k_B T} \int_0^t d\tau \langle f(0) f(\tau) \rangle_0. \end{aligned} \quad (\text{C.6})$$

We evaluate now the equilibrium average of

$$\Delta q(t)^2 = \int_0^t \int_0^t dt' dt'' f(t') f(t''), \quad (\text{C.7})$$

i.e.

$$\langle \Delta q^2(t) \rangle_0 = \int_0^t \int_0^t dt' dt'' \langle f(t') f(t'') \rangle_0 \quad (\text{C.8})$$

and

$$\begin{aligned} \frac{d\langle \Delta q^2(t) \rangle_0}{dt} &= 2 \int_0^t d\tau \langle f(t) f(\tau) \rangle_0 \\ &= 2 \int_0^t d\tau \langle f(0) f(\tau) \rangle_0 \end{aligned} \quad (\text{C.9})$$

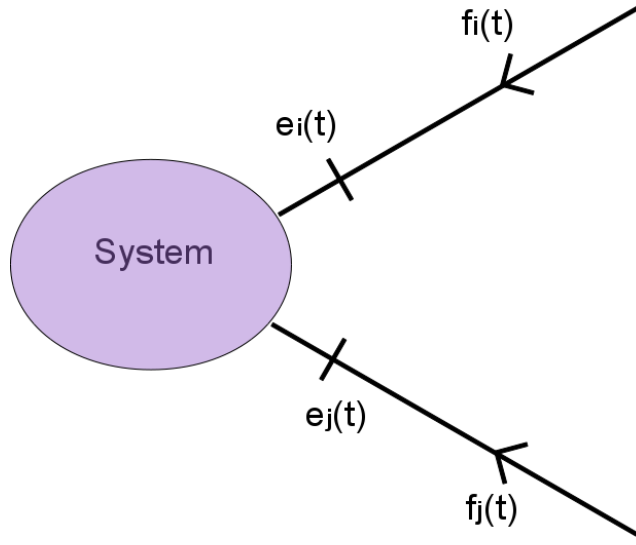


Figure C.2: Case with two bonds

for TTI. Summarizing we have that

$$\begin{aligned} \frac{d\langle\Delta q(t)\rangle_e/e_0}{dt} &= \langle f(t)\rangle_e \\ &= \frac{1}{k_B T} \int_0^t d\tau \langle f(t)f(\tau)\rangle_0 = \frac{1}{2k_B T} \frac{d\langle\Delta q^2(t)\rangle_0}{dt} \end{aligned} \quad (\text{C.10})$$

i.e. we have proved the equivalence between eq. (C.2) and eq. (C.4).

Consider now the case in which the system has two bonds.

The field applied to the  $j$  variable is  $\neq 0$  while the one of the  $i$  variable is zero and therefore we will use this variable to build the response to the field. The FDT definition in eq. (C.4) becomes:

$$\frac{\langle\Delta q_i(t)\rangle_e}{e_j} = \frac{1}{2k_B T} \langle\Delta q_i(t)\Delta q_j(t)\rangle_0 \quad (\text{C.11})$$

$$= \frac{1}{2k_B T} (2\langle q_i(0)q_j(0)\rangle - 2\langle q_i(0)q_j(t)\rangle) = -\frac{1}{k_B T} \langle q_i(0)\Delta q_j(t)\rangle_0. \quad (\text{C.12})$$

If now we make the analogy between the displacement variables and the observables entering in eq. (C.1) we have:

- $q_i(t) \rightarrow A(t)$
- $q_j(t) \rightarrow B(t)$ .

By definition we recognize that  $\chi(0, t) = \langle\Delta A\rangle/h = \langle\Delta q_i(t)\rangle_e/e_j$  (note that  $h$  is the external field). Finally we have

### C. EQUIVALENT FORMULATIONS OF FDT

---

$$k_B T \chi_{A,B}(0, t) = -\langle A(0) \Delta B(t) \rangle_0 \quad (\text{C.13})$$

$$k_B T \partial_t \chi_{A,B}(0, t) = -\partial_t \langle A(0) B(t) \rangle_0 = -\partial_t C_{A,B}(0, t) \quad (\text{C.14})$$

i.e. eq. (C.2) is equivalent to eq. (C.1).

## Appendix D

# The Lennard-Jones Gaussian

The pair potential of the monatomic Lennard-Jones Gaussian is

$$v(r_{ij}) = \varepsilon \left\{ \left( \frac{\sigma}{r_{ij}} \right)^{12} - 2 \left( \frac{\sigma}{r_{ij}} \right)^6 - \varepsilon_0 \exp \left[ -\frac{(r_{ij} - r_0)^2}{2\sigma_0^2} \right] \right\} \quad (\text{D.1})$$

i.e. is a Lennard-Jones with a Gaussian term which gives rise to an extra well in the potential (see fig. D.1). The parameters value are the same of reference [Van Hoang & Odagaki (2008)], i.e.  $r_0 = 1.47$ ,  $\varepsilon_0 = 1.50$ , and  $\sigma_0^2 = 0.02$ .

The competition of the two wells at different length scales destroys the correlation as it is shown in fig. D.2.

In the literature MC simulations of the LJG do not exist. We had then to set up the simulation from the beginning. In this procedure it is important to choose correctly the maximum displacement size  $\delta_{max}$  that will be used at each MC step. To do that we have used the same procedure presented in reference [Berthier & Kob (2007)], i.e we have chosen  $\delta_{max}$  which minimizes the relaxation time  $\tau_\alpha$  of the self-intermediate scattering function. Figure D.3 (a) shows that for a given  $\delta_{max}$  the behavior of the self-intermediate scattering

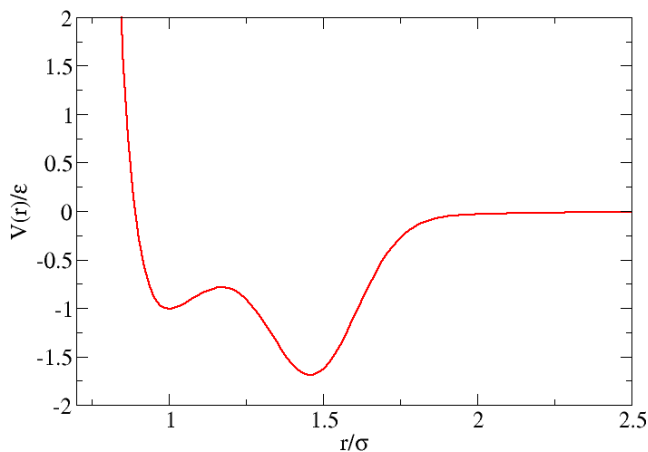


Figure D.1: shape of the LJG pair potential.

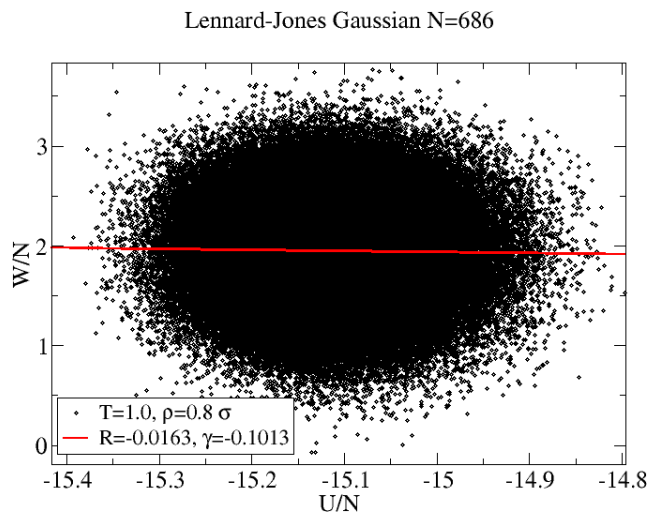
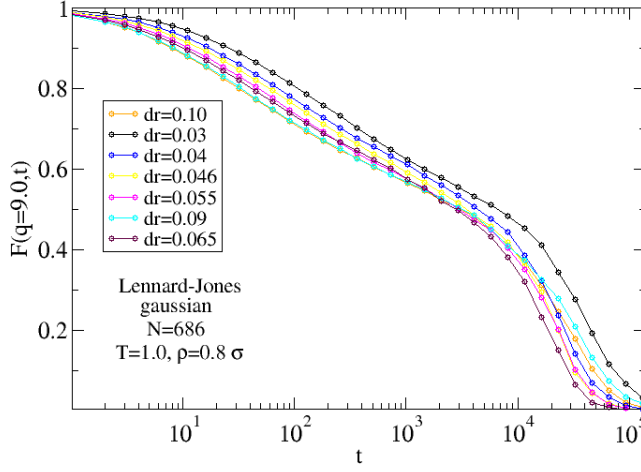


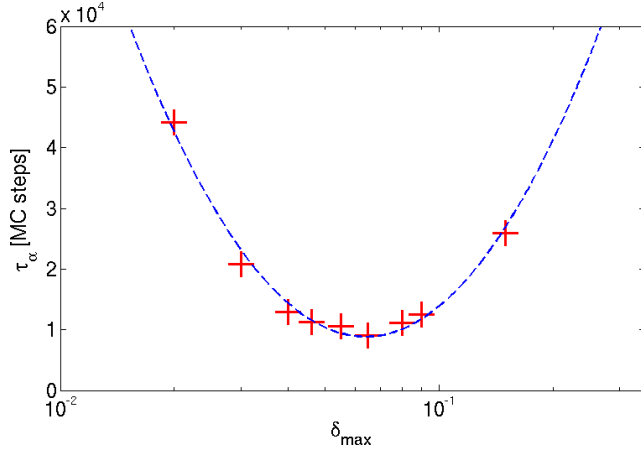
Figure D.2: Instantaneous  $U$  and  $W$  for the LJG at  $(T = 1, \rho = 0.8)$ . Clearly the system is not strongly correlating and this is because of the presence of the second well that introduces an extra interaction into the dynamics competing with the one of the Lennard-Jones.

function can be very different. In fig. D.3 (b) the different relaxation times as a function of  $\delta_{max}$  are collected and interpolated with a parabola in order to find the minimum of the curve: we have chosen  $\delta_{max} = 0.065$  at the state point  $(T = 1.0, \rho = 0.8)$ .

In reference [Van Hoang & Odagaki (2008)] only the radial distribution functions and mean square displacements (msd) are shown. This is enough for a rough comparison between the two dynamics. Figure D.4 shows the msd from reference [Van Hoang & Odagaki (2008)] (full line) at  $(T = 1, \rho = 0.8)$  and the one found from the MC dynamics with  $\delta_{max} = 0.065$ . Since MD steps and MC steps are not the same, to have a good collapse we have scaled the times of the our mean square displacement as done in reference [Berthier & Kob (2007)] for the KABLJ system. The good collapse at long times means that the MC dynamics captures the features of the slow dynamics of system.



(a)



(b)

Figure D.3: (a) Self-intermediate scattering functions at  $(T = 1, \rho = 0.8)$  for different  $\delta_{max}$ . The wave vector chosen is in correspondence with the first peak of the structure factor  $S(q)$ . According to reference [Berthier & Kob (2007)] the most realistic dynamics is given by  $\delta_{max}$  which minimizes the relaxation time  $\tau_{alpha}$ . (b) Relaxation time of the self-intermediate scattering functions in (a) as a function of  $\delta_{max}$ . The relaxation time has been estimated as the time at which the functions assume the value  $1/e$ . The points have been interpolated with a parabola in order to find the minimum value. We have chosen to use  $\delta_{max} = 0.065$ .

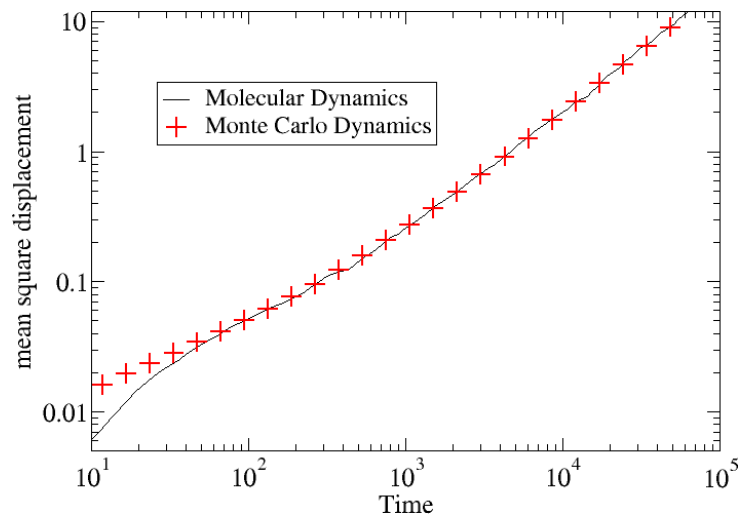


Figure D.4: Comparison between the msd of the MD dynamics from reference [Van Hoang & Odagaki (2008)] and our MC dynamics with  $\delta_{max} = 0.065$ . Both the two msd have been evaluated at  $(T = 1, \rho = 0.8)$ . Since MD steps and MC steps are different we have scaled the time axes for the MC plot of an arbitrary scaling factor in order to obtain a good collapse.

# Bibliography

- Abramowitz, M., & Stegun, I. A. 1972. *Handbook of Mathematical Functions with Formulas, Graphs, and Mathematical Tables, 9th printing*. New York: Dover.
- Ahmed, A., & Sadus, R.J. 2009. Phase diagram of the Weeks-Chandler-Andersen potential from very low to high temperatures and pressures. *Phys. rev. e.*, **80**, 061101.
- Alder, B.J., & Wainwright, T.E. 1959. Studies in molecular dynamics. I. General method. *J. chem. phys.*, **31**, 459.
- Allen, M. P., & Tildesley, D. J. 1987. *Computer Simulations of Liquids*. Oxford Science Publications.
- Andersen, H. C., Weeks, J. D., & Chandler, D. 1971. Relationship between hard-sphere fluid and fluids with realistic repulsive forces. *Physical review a: Atomic, molecular, and optical physics*, **4**(4), 1597.
- Angelani, L., Di Leonardo, R., Ruocco, G., Scala, A., & Sciortino, F. 2000. Saddles in the Energy Landscape Probed by Supercooled Liquids. *Phys. rev. lett.*, **85**, 5356.
- Angelani, L., Di Leonardo, R., Ruocco, G., Scala, A., Sciortino, F., & Cavagna, A. 2002. Quasisaddles as relevant points of the potential energy surface in the dynamics of supercooled liquids. *J. chem. phys.*, **116**, 10297.
- Angelani, L., Ruocco, G., Sampoli, M., & Sciortino, F. 2003. Comment on "Quasisaddles as relevant points of the potential energy surface in the dynamics of supercooled liquids". *J. chem. phys.*, **118**, 5265.
- Angell, K. Ngai, K., McKenna, G., McMillan, P., & Martin, S. 2000. Relaxation in glassforming liquids and amorphous solids. *J. appl. phys*, **88**, 3113.
- Angell, C. A. 1985. Relaxations in complex systems. *Pages 3–11 of: Ngai, K. L., & Wright, G. B. (eds), Strong and fragile liquids*. Washington, D. C.: U.S. GPO.
- Angell, C. A. 1995. Formation of glasses from liquids and biopolymers. *Science*, **267**, 1924.
- Arkhipov, V., Iovu, M., Rudenko, A., & Shutov, S. 1979. *Phys. status solidi (a)*, **54**, 67.

## BIBLIOGRAPHY

---

- Bailey, N. P., Schiotz, J., & Jacobsen, K. W. 2004. Simulation of Cu-Mg metallic glass: Thermodynamics and structure. *Physical review b: Condensed matter and materials physics*, **69**(14).
- Becker, R., & Doring, W. 1935. Kinetic treatment of germ formation in super-saturated vapour. *Annalen der Physik*, **24**(8), 719–752.
- Bellon, L., Ciliberto, S., & Laroche, C. 2001. *Europhys. lett.*, **53**, 511.
- Bembenek, S. D., & Laird, B. B. 2001. Instantaneous normal mode analysis of amorphous and supercooled silica. *J. chem. phys.*, **114**, 2340.
- Bennemann, C., Donati, C., Baschnagel, J., & Glotzer, S.C. 1999. Range of correlated motion in a polymer melt on cooling towards the glass transition. *Nature*, **399**, 246.
- Berendsen, H. J. C., Grigera, J. R., & Straatsma, T. P. 1987. The missing term in effective pair potentials. *Journal of physical chemistry*, **91**(24), 6269–6271.
- Berlin, T.H., & Montroll, E.W. 1952. On the free energy of a mixture of ions: An extension of Kramers' theory. *J. chem. phys.*, **20**, 75.
- Berthier, L. 2007. Efficient measurement of linear susceptibilities in molecular simulations: Application to aging supercooled liquids. *Phys. rev. lett.*, **98**, 220601.
- Berthier, L., & Biroli, G. 2009. Glasses and Aging: A Statistical Mechanics Perspective. *Encyclopedia of complexity and systems science*, *springer*.
- Berthier, L., & Kob, W. 2007. The Monte Carlo dynamics of a binary Lennard-Jones glass-forming mixture. *J. phys: Condens. matter*, **19**, 205130.
- Berthier, L., & Tarjus, G. 2009. Nonperturbative Effect of Attractive Forces in Viscous Liquids. *Phys. rev. lett.*, **103**, 170601.
- Bouchaud, J. P., Cugliandolo, L., & Mezard, M. 1998. *in: Spin Glasses and Random Fields*. World Scientific, Singapore.
- Broderix, K., Bhattacharya, K. K., Cavagna, A., Zippelius, A., & Giardinà, I. 2000. Energy Landscape of a Lennard-Jones Liquid: Statistics of Stationary Points. *Phys. rev. lett.*, **85**, 5360.
- Brovchenko, I., Geiger, A., & Oleinikova, A. 2003. Multiple liquid-liquid transitions in supercooled water. *J. chem. phys.*, **118**, 9873.
- Castellani, T., & Cavagna, A. 2005. Spin-glass theory for pedestrians. *Journal of statistical mechanics: Theory and experiment*, **P05012**.
- Cavagna, A. 2001. Fragile vs. strong liquids: A saddles-ruled scenario. *Europhys. lett.*, **53**, 490.
- Cavagna, A. 2009. Supercooled liquids for pedestrians. *Physics reports*, **476**, 51.
- Christiansen, P.V. 1971. *Semiotik og Systemegenskaber*. IMFUFA Roskilde Text N. 22, Roskilde.

- 
- Coslovich, D., & Roland, C. M. 2009. Density scaling in viscous liquids: From relaxation times to four-point susceptibilities. *J. chem. phys.*, **131**, 151103.
- Crisanti, A., & Ritort, F. 2003. Violation of the fluctuation-dissipation theorem in glassy systems: basic notions and numerical evidence. *J. phys. a*, **36**, R181.
- Cugliandolo, L., & Kurchan, J. 1999. Thermal properties of slow dynamics. *Physica a*, **263**, 242.
- Cugliandolo, L. F., & Kurchan, J. 1993. Analytical solution of the off-equilibrium dynamics of a long-range spin-glass model. *Phys. rev. lett.*, **71**, 173.
- Cugliandolo, L. F., & Kurchan, J. 1994. On the out-of-equilibrium relaxation of the Sherrington-Kirkpatrick model. *J. phys. a*, **27**, 5749.
- Cugliandolo, L.F. 2004. *Slow Relaxations and nonequilibrium dynamics in condensed matter, Course 7: Dynamics of Glassy Systems*. Springer Berlin / Heidelberg.
- Cugliandolo, L.F., Kurchan, J., & Peliti, L. 1997. Energy flow, partial equilibration, and effective temperatures in systems with slow dynamics. *Phys. rev. e*, **55**, 3898.
- Debenedetti, P. 1996. *Metastable Liquids: Concepts and Principles*. Princeton Univ. Press.
- Debenedetti, PG, & Stillinger, FH. 2001. Supercooled liquids and the glass transition. *Nature*, **410**(6825), 259–267.
- Denny, R., Reichman, D., & Bouchaud, J. 2003. Trap Models and Slow Dynamics in Supercooled Liquids. *Phys. rev. lett.*, **90**, 025503.
- Di Leonardo, R., Angelani, L., Parisi, G., & Ruocco, G. 2000. Off-equilibrium effective temperature in monatomic Lennard-Jones glass. *Phys. rev. lett.*, **84**, 6054.
- Diezemann, G. 2005. Aging in a free-energy landscape model for glassy relaxation. *J. chem. phys.*, **123**, 204510.
- Doliwa, B., & Heuer, A. 2003. What Does the Potential Energy Landscape Tell Us about the Dynamics of Supercooled Liquids and Glasses?. *Phys. Rev. Lett.*, **91**, 235501.
- Donati, C., Sciortino, F., & Tartaglia, P. 2000. Role of Unstable Directions in the Equilibrium and Aging Dynamics of Supercooled Liquids. *Phys. rev. lett.*, **85**, 1464.
- Donati, C., Franz, S., Glotzer, S.C., & Parisi, G. 2002. Theory of non-linear susceptibility and correlation length in glasses and liquids. *Journal of non-crystalline solids*, **307**, 215.
- Dyre, J. C. 1987. Master-equation approach to the glass transition. *Phys. rev. lett.*, **58**, 792.

## BIBLIOGRAPHY

---

- Dyre, J.C. 1995. Energy master equation: A low-temperature approximation to bässler's random-walk model. *Phys. rev. b*, **51**, 12276.
- Dyre, Jeppe C. 2006. Colloquium: The glass transition and elastic models of glass-forming liquids. *Reviews of modern physics*, **78**(3), 953–972.
- Dzugutov, M. 1992. Glass-formation in a simple monatomic liquid with icosahedral inherent local order. *Physical review a: Atomic, molecular, and optical physics*, **46**(6), R2984–R2987.
- Elliot, S.R. 1983. *Physics of Amorphous Materials*. London: Longman Group Ltd.
- Foffi, G., Sciortino, F., Zaccarelli, E., & Tartaglia, P. 2004. Dynamical arrest in dense short-ranged attractive colloids. *J. phys.: Condensed matter*, **16**, S3791–S3806.
- Frenkel, D., & Smith, B. 2002. *Understanding Molecular Simulations 2nd edition*. Academic Press.
- Gezelter, J. D., Rabani, E., & Berne, B.J. 1997. Can Imaginary Instantaneous Normal Mode Frequencies Predict Barriers to Self-Diffusion? *J. chem. phys.*, **107**, 4618.
- Gutzow, I., & Schmelzer, J. 1995. *The vitreous states*. Springer.
- Hansen, J. P., & Yip, S. 1995. Molecular dynamics investigations of slow relaxations in supercooled liquids. *Transp. theory stat. phys.*, **24**, 1149.
- Hansen, Jean-Pierre, & McDonald, I.R. 2006. *Theory of simple liquids*. third edn. Academic Press.
- Hecksher, T., Nielsen, A.I., Olsen, N.B., & Dyre, J.C. 2008. Little evidence for dynamic divergences in ultraviscous molecular liquids. *Nature phys.*, **4**, 737.
- Heuer, A. 2008. Exploring the potential energy landscape of glass-forming systems: from inherent structures via metabasins to macroscopic transport. *J. phys.: Condens. mat.*, **20**, 373101.
- Heyes, D.M., & Okumura, H. 2006. Equation of state and structural properties of the Weeks-Chandler-Andersen fluid. *J. chem. phys.*, **124**, 164507.
- Hoover, W. G., & Ross, M. 1971. Statistical Theories Of Melting. *Contemporary physics*, **12**(4), 339.
- Hoover, W. G., Roos, M, Johnson, K. W., Henderson, D, Barker, J. A., & Brown, B. C. 1970. Soft-sphere equation of state. *Journal of chemical physics*, **52**(10), 4931.
- Hoover, W. G., Gray, S. G., & Johnson, K. W. 1971. Thermodynamic Properties of Fluid and Solid Phases force Inverse Power Potentials. *Journal of chemical physics*, **55**(3), 1128.
- Horner, H., Crisanti, A., & Sommers, H.-J. 1993. The spherical p-spin interaction spin glass model: The dynamics. *Zeitschrift fur physik b*, **92**, 257.

- 
- Hurley, M.M., & Harrowell, P. 1995. Kinetic Structure of a 2-Dimensional Liquid. *Phys. rev. e*, **52(2)**, 1694.
- Jabbari-Farouji, S., Mizuno, D., Atakhorrani, M., MacKintosh, F.C., Schmidt, C.F., Eiser, E., Wegdam, G.H., & Bonn, D. 2007. Fluctuation-Dissipation Theorem in an Aging Colloidal Glass. *Phys. rev. lett.*, **98**, 108302.
- Jacobsen, K. W., Nørskov, J. K., & Puska, M. J. 1987. Interatomic Interactions In The Effective-Medium Theory. *Physical review b: Condensed matter and materials physics*, **35(14)**, 7423–7442.
- Jacobsen, K. W., Stoltze, P., & Nørskov, J. K. 1996. A semi-empirical effective medium theory for metals and alloys. *Surface science*, **366(2)**, 394–402.
- Jorgensen, W. L., Madura, J. D., & Swenson, C. J. 1984. Optimized intermolecular potential functions for liquid hydrocarbons. *Journal of the american chemical society*, **106(22)**, 6638–6646.
- Kauzmann, A.W. 1948. The nature of the glassy state and the behavior of liquids at low temperatures. *Chem. rev.*, **43**, 219.
- Kell, G.S. 1975. Density, thermal expansivity, and compressibility of liquid water from 0 to 150C: Correlations and tables for atmospheric pressure and saturation reviewed and expressed on 1968 temperature scale. *J. chem. eng. data*, **20(1)**, 97.
- Keyes, T. 1994. Unstable modes in supercooled and normal liquids: Density of states, energy barriers and self-diffusion. *J. chem. phys.*, **101**, 5081.
- Keyes, T. 1997. Random energy model for dynamics in supercooled liquids: N dependence. *J. phys. chem.*, **101**, 2921.
- Klein, O. 1919. . *Medd. vetenskaps akad. nobelinst.*, **5**, 1.
- Kob, W., & Andersen, H. C. 1995a. Testing Mode-Coupling Theory for a Supercooled Binary Lennard-Jones Mixture .2. Intermediate Scattering Function and Dynamic Susceptibility. *Physical review e: Statistical, nonlinear, and soft matter physics*, **52(4, Part B)**, 4134–4153.
- Kob, W., & Andersen, H. C. 1995b. Testing mode-coupling theory for a supercooled binary Lennard-Jones mixture I: The van Hove correlation function. *Physical review e: Statistical, nonlinear, and soft matter physics*, **51(5)**, 4626–4641.
- Kob, W., & Andersen, H.C. 1994. Scaling behavior in the  $\beta$ -relaxation regime of a supercooled Lennard-Jones mixture. *Physical review letters*, **73(10)**, 1376–1379.
- Kob, W., & Barrat, J.P. 1999. Fluctuation-dissipation ratio in an aging Lennard-Jones glass. *Europhys. lett.*, **46**, 637.
- Kohl, I., Bachmann, L., & Mayer, E. Hallbrucker, A. Loerting T. 2005. Water Behaviour: Glass transition in hyperquenched water? . *Nature*, **435**, E1.
- Kurchan, J. 2005. In and out of equilibrium . *Nature*, **433**, 222.

## BIBLIOGRAPHY

---

- La Nave, E., Scala, A., Starr, F. W., Sciortino, F., & Stanley, H. E. 2000. Instantaneous Normal Mode Analysis of Supercooled Water. *Phys. rev. lett.*, **84**, 4605.
- La Nave, E., Scala, A., Starr, F. W., Sciortino, F., & Stanley, H. E. 2001. Dynamics of supercooled water in configuration space. *Phys. rev. e.*, **64**, 036102.
- Lemmon, E. W., McLinden, M. O., & Friend, D. G. 2005. Thermophysical properties of fluid systems. In: Linstrom, P. J., & Mallard, W. G. (eds), *Chemistry webbook, nist standard reference database number 96*. Gaithersburg MD, 20899: National Institute of Standards and Technology.
- Leuzzi, L. 2009. A stroll among effective temperatures in aging systems: limits and perspectives. *Journal of non-crystalline solids*, **355**, 686.
- Leuzzi, L., & Nieuwenhuizen, T.M. 2007. *Thermodynamic of the glassy state*. Taylor and Francis.
- Li, W. X., & Keyes, T. 1999. Instantaneous normal mode theory of diffusion and the potential energy landscape: Application to supercooled liquid CS<sub>2</sub>. *J. chem. phys.*, **111**, 5503.
- Liu, A.J., & Nagel, S.R. 1998. Nonlinear dynamics: Jamming is not just cool any more. *Nature*, **396**, 21.
- Maggi, C., Di Leonardo, R., Dyre, J.C., & Ruocco, G. 2010. Generalized fluctuation-dissipation relation and effective temperature in off-equilibrium colloids. *Phys. rev. b*, **81**, 104201.
- Mahoney, M. W., & Jorgensen, W. L. 2000. A five-site model for liquid water and the reproduction of the density anomaly by rigid, nonpolarizable potential functions. *Journal of chemical physics*, **112**(20), 8910–8922.
- Mahoney, M. W., & Jorgensen, W. L. 2001. Diffusion constant of the TIP5P model of liquid water. *J. chem. phys.*, **114**, 363.
- Martinez, L.M., & C.A., Angell. 2001. A thermodynamic connection to the fragility of glass-forming liquids. *Nature*, **410**, 663.
- Mauro, J.C., Yue, Y., Ellison, A.J., Gupta, P. K., & Allan, D.C. 2009. Viscosity of glass-forming liquids. *PNAS*, **24**, 19780.
- Metropolis, N., Rosenbluth, A.W., Rosenbluth, M.N., Teller, A.H., & Teller, E. 1953. Equations of State Calculations by Fast Computing Machines. *J. chem. phys.*, **21**, 1087.
- Mishima, O., & H.E., Stanley. 1998. The relationship between liquid, supercooled and glassy water. *Nature*, **396**, 329.
- Monthus, C., & Bouchaud, J.-P. 1996. Models of traps and glass phenomenology. *J. phys. a: Math. gen.*, **29**, 3847.
- Moynihan, C. T., Easteal, A.J., Wilder, J., & Tucker, J. 1974. Dependence of the glass transition temperature on heating and cooling rate. *J. phys. chem.*, **78**, 2673.

- 
- Moynihan, C. T., Macedo, P. B., Montrose, C. J., Gupta, P. K., Debolt, M. A., Dill, J. F., Dom, B. E., Drake, P. W., Eastal, A. J., Elterman, P. B., Moeller, R. P., Sasabe, H., & Wilder, J. A. 1976. Structural relaxation in vitreous materials. *Annals of the new york academy of sciences*, **279**(Oct 15), 15–35.
- Narayanaswamy, O.S. 1971. A Model of Structural Relaxation in Glass. *J. am. ceram. soc.*, **54**, 491.
- Ngai, K.L., Casalini, R., Capaccioli, S., Paluch, M., & Roland, C.M. 2005. Do Theories of the Glass Transition, in which the Structural Relaxation Time Does Not Define the Dispersion of the Structural Relaxation, Need Revision? *J. phys. chem. b*, **109**, 17356.
- Nieuwenhuizen, T.M. 1997. Ehrenfest Relations at the Glass Transition: Solution to an Old Paradox. *Phys. rev. lett.*, **79**, 1317.
- Nosé, S. 1984. A Molecular-Dynamics Method for Simulations in the Canonical Ensemble. *Molecular physics*, **52**(2), 255–268.
- Onsager, L. 1931a. Reciprocal relations in irreverdible processe. i. *Physical review*, **37**, 405.
- Onsager, L. 1931b. Reciprocal relations in irreverdible processe. ii. *Physical review*, **38**, 2265.
- Parisi, G. 1997. Off-Equilibrium Fluctuation-Dissipation Relation in Fragile Glasses. *Phys. rev. lett.*, **79**, 3660.
- Parisi, G. 1997. Short-time aging in binary glasses. *Journal of physics a*, **30**, L765.
- Paynter, H. 1961. *Analysis and Design of Engineering Systems*. MIT, Cambridge.
- Pedersen, Ulf R., Bailey, Nicholas P., Schrder, Thomas B., & Dyre, Jeppe C. 2008a. Strong Pressure-Energy Correlation in van der Waals Liquids. *Physical review letters*, **100**(Jan 11), 015701–015704.
- Pedersen, U.R., Christensen, Schroder, T.B., & Dyre, J. C. 2008b. Feasibility of a single-parameter description of equilibrium viscous liquid dynamics. *Phys. rev. e*, **77**, 011201.
- Poole, P.H., Sciortino, F., Essmann, U., & Stanley, H.E. 1992. Phase behaviour of metastable water. *Nature*, **360**, 324.
- Rapaport, D.C. 2004. *The art of molecular dynamics simulation. 2nd edition*.
- Reiss, H. 1997. *Methods of thermodynamics*. New York: Dover.
- Roland, C. M., Bair, S., & Casalini, R. 2006. Thermodynamic scaling of the viscosity of van der Waals, H-bonded, and ionic liquids. *Journal of chemical physics*, **125**(12).
- Rosenfeld, Y., & Tarazona, P. 1998. Density functional theory and the asymptotic high density expansion of the free energy of classical solids and fluids . *Mol. phys.*, **95**, 141.

- Saika-Voivod, I., & Sciortino, F. 2004. Distributions of inherent structure energies during aging. *Phys. rev. e*, **70**, 041202.
- Schmelzer, J. 2005. *Nucleation theory and applications*. Wiley-Vch.
- Schröder, T. B., Pedersen, U.R., Bailey, N.P., & Dyre, J.C. 2009. Hidden scale invariance in molecular van der Waal liquids: A simulation study. *Phys. rev. e*, **80**, 041502.
- Schröder, T. B., Sastry, S., Dyre, J.C., & Glotzer, S.C. 2000. Crossover to potential energy landscape dominated dynamics in a model glass-forming liquid. *J. Chem. Phys.*, **112**, 9834.
- Sciortino, F. 2005. Potential energy landscape description of supercooled liquids and glasses. *Journal of statistical mechanics: Theory and experiment*, **P05015**.
- Sciortino, F., & Tartaglia, P. 2001. Extension of the Fluctuation-Dissipation Theorem to the Physical Aging of a Model Glass-Forming Liquid. *Phys. rev. lett.*, **86**, 107.
- Sciortino, Francesco. 2002. One liquid two glasses. *Nature materials*, **1**.
- Smit, Berend, & Frenkel, Daan. 2001. *Understanding Molecular Simulation: from Algorithms to Applications*. Second edn. Academic Press; 2nd edition (October 15, 2001).
- Speedy, R. J., & Angell, C. A. 1976. Isothermal compressibility of supercooled water and evidence for a thermodynamic singularity at -45 C. *J. chem. phys.*, **65**, 851.
- Stanley, H.E., Buldyrev, S.V., Mishima, O. Sadr-Lahijany, M. R. Scala A., & Starr, F.W. 1998. Unsolved mysteries of water in its liquid and glassy phases. *J. phys.: Condens. matter*, **12**, A403.
- Stillinger, F.H., & Weber, T.A. 1935. Packing Structures and Transitions in Liquids and Solids . *Science*, **267**.
- Stillinger, F.H., & Weber, T.A. 1982. Hidden structure in liquids. *Phys. rev. a.*, **25**, 978.
- Stillinger, F.H., & Weber, T.A. 1984. Packing Structures and Transitions in Liquids and Solids. *Science*, **225**, 983.
- van Gunsteren, W. F., Billeter, S. R., Eising, A. A., Hunenberger, P. H., Kruger, P., Mark, A. E., Scott, W. R. P., & Tironi, I. G. 1996. *Biomolecular simulation: The GROMOS96 manual and user guide*. vdf Hochschulverlag AG an der ETH Zurich and BIOMOS b.v., Zurich, Groningen.
- Van Hoang, V., & Odagaki, T. 2008. Glasses of simple liquids with double-well interaction potential. *Physica b: Condensed matter*, **403**, 3910.
- Vega, C., & Abascal, J.L.F. 2005. Relation between the melting temperature and the temperature of maximum density for the most common models of water. *J. chem. phys.*, **123**, 144504.

- 
- Volmer, M, & Weber, A. 1926. Germ-formation in oversaturated figures. *Zeitschrift für physikalische chemie–stochiometrie und verwandtschaftslehre*, **119**(3/4), 277–301.
- Wahnström, G. 1991. Molecular-Dynamics Study of a Supercooled 2-Component Lennard-Jones System. *Physical review a: Atomic, molecular, and optical physics*, **44**(6), 3752–3764.
- Wales, D.J. 2004. *Energy Landscapes*. Cambridge University Press.
- Whitelam, S., Berthier, L., & Garrahan, J. P. 2004. Dynamic criticality in glassforming liquids. *Phys. rev. lett.*, **92**, 18.
- Young, A.P. (ed). 1998. *Spin glasses and random fields*. World Scientific.
- Zaccarelli, E, Foffi, G, Dawson, K. A., Buldyrev, S. V., Sciortino, F, & Tartaglia, P. 2002. Confirmation of anomalous dynamical arrest in attractive colloids: A molecular dynamics study. *Physical review e: Statistical, nonlinear, and soft matter physics*, **66**(4, Part 1).
- Zaccarelli, E, Sciortino, F, & Tartaglia, P. 2004. Numerical study of the glass-glass transition in short-ranged attractive colloids. *Journal of physics: Condensed matter*, **16**(42, Sp. Iss. SI), S4849–S4860. Workshop on Structural Arrest Transitions in Colloidal Systems with Short-Range Attractions, Messina, ITALY, DEC 17-20, 2003.



# Papers



## Pressure-energy correlations in liquids. I. Results from computer simulations

Nicholas P. Bailey,<sup>a)</sup> Ulf R. Pedersen, Nicoletta Gnan, Thomas B. Schröder, and Jeppe C. Dyre

*DNRF Center "Glass and Time," IMFUFA, Department of Sciences, Roskilde University, P.O. Box 260, DK-4000 Roskilde, Denmark*

(Received 3 July 2008; accepted 25 August 2008; published online 14 November 2008)

We show that a number of model liquids at fixed volume exhibit strong correlations between equilibrium fluctuations of the configurational parts of (instantaneous) pressure and energy. We present detailed results for 13 systems, showing in which systems these correlations are significant. These include Lennard-Jones liquids (both single- and two-component) and several other simple liquids, neither hydrogen-bonding liquids such as methanol and water, nor the Dzugutov liquid, which has significant contributions to pressure at the second nearest neighbor distance. The pressure-energy correlations, which for the Lennard-Jones case are shown to also be present in the crystal and glass phases, reflect an effective inverse power-law potential dominating fluctuations, even at zero and slightly negative pressure. An exception to the inverse power-law explanation is a liquid with hard-sphere repulsion and a square-well attractive part, where a strong correlation is observed, but only after time averaging. The companion paper [N. P. Bailey *et al.*, *J. Chem. Phys.* **129**, 184508 (2008)] gives a thorough analysis of the correlations, with a focus on the Lennard-Jones liquid, and a discussion of some experimental and theoretical consequences. © 2008 American Institute of Physics. [DOI: 10.1063/1.2982247] [Two typos on pages 1 and 2 corrected]

### I. INTRODUCTION

Physicists are familiar with the idea of thermal fluctuations in equilibrium. They also know how to extract useful information from them, using linear response theory.<sup>1–4</sup> These methods started with Einstein's observation that the specific heat in the canonical ensemble is determined by the magnitude of energy fluctuations. In any thermodynamic system some variables are fixed and some fluctuate. The magnitude of the variances of the latter, as well as their mutual covariances, determines the thermodynamic "response" parameters.<sup>1</sup> For example, in the canonical ( $NVT$ ) ensemble, pressure  $p$  and energy  $E$  fluctuate; the magnitude of pressure fluctuations is related to the isothermal bulk modulus  $K_T \equiv -V(\partial p / \partial V)_T$ , that of the energy fluctuations to the specific heat at constant volume  $c_V \equiv T(\partial S / \partial T)_V$ , while the covariance  $\langle \Delta p \Delta E \rangle$  is related<sup>4</sup> to the thermal pressure coefficient  $\beta_V \equiv (\partial p / \partial T)_V$ . If the latter is nonzero, it implies a degree of correlation between pressure and energy fluctuations. There is no obvious reason to suspect any particularly strong correlation, and to the best of our knowledge none has ever been reported. However, in the course of investigating the physics of highly viscous liquids by computer simulation, we noted strong correlations between pressure and energy equilibrium fluctuations in several model liquids, also in the high temperature, low-viscosity state. These included the most studied of all computer liquids, the Lennard-Jones system. Surprisingly, these strong correlations survive crystallization, and they are also present in the glass phase. "Strong" here and henceforth means a correlation coefficient of order

0.9 or larger. In this paper we examine several model liquids and detail which systems exhibit strong correlations and which do not. In the companion paper<sup>5</sup> (referred to as Paper II) we present a detailed analysis of the correlations for the single-component Lennard-Jones (SCLJ) system, and discuss some consequences.

Specifically, the fluctuations that are in many cases strongly correlated are those of the configurational parts of pressure and energy. The (instantaneous) pressure  $p$  and energy  $E$  have contributions both from particle momenta and positions as follows:

$$p = Nk_B T(\mathbf{p}_1, \dots, \mathbf{p}_N)/V + W(\mathbf{r}_1, \dots, \mathbf{r}_N)/V, \quad (1)$$

$$E = K(\mathbf{p}_1, \dots, \mathbf{p}_N) + U(\mathbf{r}_1, \dots, \mathbf{r}_N),$$

where  $K$  and  $U$  are the kinetic and potential energies, respectively. Here  $T(\mathbf{p}_1, \dots, \mathbf{p}_N)$  is the "kinetic temperature,"<sup>4</sup> proportional to the kinetic energy per particle. The configurational contribution to pressure is the virial  $W$ , which is defined<sup>4</sup> by

$$W = -\frac{1}{3} \sum_i \mathbf{r}_i \cdot \nabla_{\mathbf{r}_i} U, \quad (2)$$

where  $\mathbf{r}_i$  is the position of the  $i$ th particle. Note that  $W$  has dimension energy. For a pair interaction we have

<sup>a)</sup>Electronic mail: nbailey@ruc.dk.

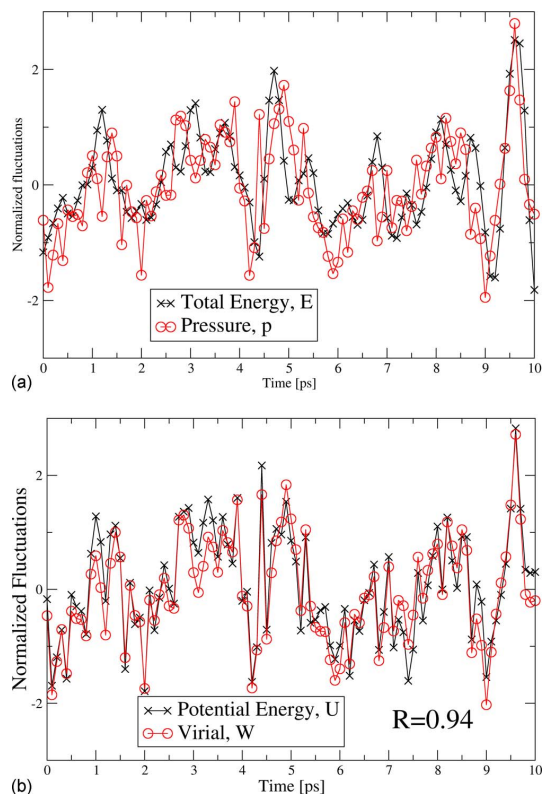


FIG. 1. (Color online) Equilibrium fluctuations of (a) pressure  $p$  and energy  $E$  and (b) virial  $W$  and potential energy  $U$ , in a single-component Lennard-Jones system simulated in the  $NVT$  ensemble at  $\rho=34.6$  mol/l and  $T=80$  K (argon units). The time-averaged pressure was close to zero (1.5 MPa). The correlation coefficient  $R$  between  $W$  and  $U$  is 0.94, whereas the correlation coefficient is only 0.70 between  $p$  and  $E$ . Correlation coefficients were calculated over the total simulation time (10 ns).

$$U_{\text{pair}} = \sum_{i<j} v(r_{ij}), \quad (3)$$

where  $r_{ij}$  is the distance between particles  $i$  and  $j$  and  $v(r)$  is the pair potential. The expression for the virial [Eq. (2)] becomes<sup>4</sup>

$$W_{\text{pair}} = -\frac{1}{3} \sum_{i<j} r_{ij} v'(r_{ij}) = -\frac{1}{3} \sum_{i<j} w(r_{ij}), \quad (4)$$

where for convenience we define

$$w(r) \equiv r v'(r). \quad (5)$$

Figure 1(a) shows normalized instantaneous values of  $p$  and  $E$ , shifted and scaled to have zero mean and unit variance, as a function of time for the standard SCLJ liquid, while Fig. 1(b) shows the corresponding fluctuations of  $W$  and  $U$ . We quantify the degree of correlation by the standard correlation coefficient  $R$ , defined by

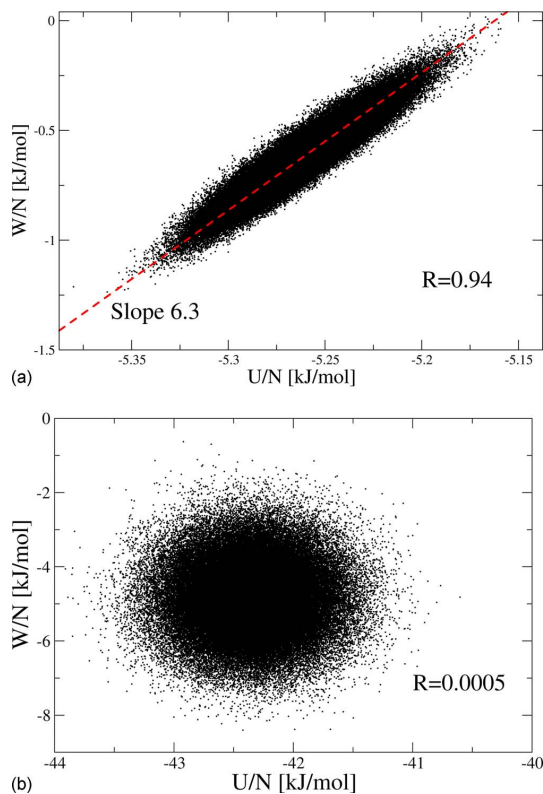


FIG. 2. (Color online) (a) Scatter plot of instantaneous virial  $W$  and potential energy  $U$  from the simulation of Fig. 1. The dashed line is a guide to the eyes, with a slope determined by the ratio of standard deviations of  $W$  and  $U$  [Eq. (7)]. (b) Example of a system with almost no correlation between  $W$  and  $U$ : TIP5P water at  $T=12.5$  °C and density of 1007.58 kg/m<sup>3</sup> ( $NVT$ ). This system has Coulomb, in addition to Lennard-Jones, interactions.

$$R = \frac{\langle \Delta W \Delta U \rangle}{\sqrt{\langle (\Delta W)^2 \rangle} \sqrt{\langle (\Delta U)^2 \rangle}}. \quad (6)$$

Here the angle brackets  $\langle \rangle$  denote thermal averages while  $\Delta$  denotes deviation from the average value of the given quantity. The correlation coefficient is ensemble dependent, but our main focus—the  $R \rightarrow 1$  limit—is not. Most of the simulations reported below were carried out in the  $NVT$  ensemble. Another important characteristic quantity is the “slope”  $\gamma$ , which we define as the ratio of standard deviations as follows:

$$\gamma \equiv \frac{\sqrt{\langle (\Delta W)^2 \rangle}}{\sqrt{\langle (\Delta U)^2 \rangle}}. \quad (7)$$

Considering the “total” quantities,  $p$  and  $E$  [Fig. 1(a)], there is some correlation; the correlation coefficient is 0.70. For the configurational parts,  $W$  and  $U$ , on the other hand [Fig. 1(b)], the degree of correlation is much higher,  $R=0.94$  in this case. Another way to exhibit the correlation is a scatter plot of  $W$  against  $U$ , as shown in Fig. 2(a).

Is this correlation surprising? Actually, there are some interatomic potentials for which there is a 100% correlation

between virial and potential energy. If we have a pair potential of the form  $v(r) \propto r^{-n}$ , an inverse power law, then  $w(r) = -nv(r)$  and  $W_{\text{pair}} = (n/3)U_{\text{pair}}$ , holds exactly. In this case the correlation is 100% and  $\gamma = n/3$ .

Conversely, suppose a system is known to be governed by a pair potential and that there is 100% correlation between  $W$  and  $U$ . We can write both  $U$  and  $W$  at any given time  $t$  as integrals over the instantaneous radial distribution function defined<sup>4</sup> as

$$g(r, t) \equiv \frac{2}{N\rho} \sum_{i < j} \delta(r - r_{ij}(t)) / (4\pi r^2), \quad (8)$$

from which

$$U(t) = \frac{N}{2} \rho \int_0^\infty dr 4\pi r^2 g(r, t) v(r) \quad (9)$$

and

$$W(t) = -\frac{N}{6} \rho \int_0^\infty dr 4\pi r^2 g(r, t) w(r). \quad (10)$$

Here the factor of  $\frac{1}{2}$  is to avoid double counting, and  $\rho = N/V$  is the number density. 100% correlation means that  $W(t) = \gamma U(t)$  holds for arbitrary  $g(r, t)$  (a possible additive constant could be absorbed into the definition of  $U$ ). In particular, we could consider  $g(r, t) = \delta(r - r_0)$ .<sup>6</sup> Substituting this into the above expressions, the integrals go away and we find  $w(r_0) = -3\gamma v(r_0)$ . Since  $r_0$  was arbitrary,  $v'(r) = -3\gamma v(r)/r$ , which has the solution  $v(r) \propto r^{-3\gamma}$ . This connection between an inverse power-law potential and perfect correlations suggests that strong correlations can be attributed to an *effective inverse power-law potential*, with exponent given by three times the observed value of  $\gamma$ . This will be detailed in Paper II, which shows that while this explanation is basically correct, matters are somewhat more complicated than this. For instance, the fixed volume condition, under which the strong correlations are observed, imposes certain constraints on  $g(r, t)$ .

The celebrated Lennard-Jones potential is given<sup>7</sup> by

$$v_{\text{LJ}}(r) = 4\epsilon \left[ \left( \frac{\sigma}{r} \right)^{12} - \left( \frac{\sigma}{r} \right)^6 \right]. \quad (11)$$

One might think that in the case of the Lennard-Jones potential the fluctuations are dominated by the repulsive  $r^{-12}$  term, but this naive guess leads to a slope of 4, rather than the 6.3 seen in Fig. 2(a). Nevertheless the observed correlation and the above mentioned association with inverse power-law potentials suggest that an effective inverse power-law description (involving short distances), with a more careful identification of the exponent, may apply. In fact, the presence of the second, attractive, term increases the steepness of the repulsive part, thus increasing the slope of the correlation, or equivalently the effective inverse power-law exponent (Fig. 3). Note the distinction between repulsive term and repulsive part of the potential: The latter is the region where  $v(r)$  has a negative slope; thus, the region  $r < r_m$  ( $r_m$  being the distance where the pair potential has its minimum,  $2^{1/6}\sigma$  for  $v_{\text{LJ}}$ ). This region involves both the repulsive and attractive terms (see

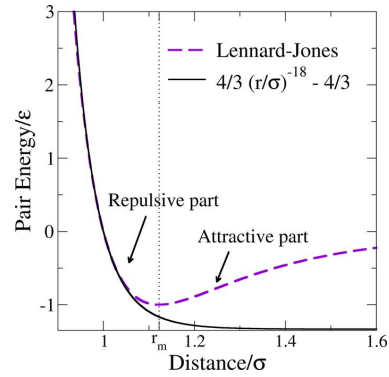


FIG. 3. (Color online) Illustration of the “effective inverse power law” chosen in this case to match the Lennard-Jones potential and its first two derivatives at the point  $r = \sigma$ . The vertical line marks the division into the repulsive and attractive parts of the Lennard-Jones potential.

Fig. 3, which also illustrates the approximation of the repulsive part by a power law with exponent 18). The same division was made by Weeks, Chandler, and Andersen in their noted paper of 1971,<sup>8</sup> in which they showed that the thermodynamic and structural properties of the Lennard-Jones fluid were dominated by the repulsive part at high temperatures and also at low temperatures for high densities. Ben-Amotz and Stell<sup>9</sup> noted that the repulsive core of the Lennard-Jones potential may be approximated by an inverse power law with  $n \sim 18-20$ . The approximation by an inverse power law may be directly checked by computing the potential and virial with an inverse power-law potential for configurations drawn from actual simulations using the Lennard-Jones potential. The agreement (apart from additive constants) is good; see Paper II.

Consider now a system with different types of pair interactions, for example, a binary Lennard-Jones system with  $AA$ ,  $BB$ , and  $AB$  interactions, or a hydrogen-bonding system modeled via both Lennard-Jones and Coulomb interactions. We can write arbitrary deviations of  $U$  and  $W$  from their mean values, denoted  $\Delta U$  and  $\Delta W$ , as a sum over types (indexed by  $i$ ; sums over pairs of a given type are implicitly understood) as follows:

$$\Delta U = \sum_i \Delta U_i, \quad \Delta W = \sum_i \Delta W_i. \quad (12)$$

Now, supposing there is near-perfect correlation for the individual terms with corresponding slopes  $\gamma_i$ , we can rewrite  $\Delta W$  as

$$\Delta W = \sum_i \gamma_i \Delta U_i. \quad (13)$$

If the  $\gamma_i$  are all more or less equal to a single value  $\gamma$ , then this can be factored out and we get  $\Delta W \approx \gamma \Delta U$ . Thus the existence of different Lennard-Jones interactions in the same system does not destroy the correlation, since they have  $\gamma_i \sim 6$ . On the other hand the slope for Coulomb interaction, which as an inverse power law has perfect  $W$ ,  $U$ -correlations, is  $1/3$ , so we cannot expect overall strong correlation in this case [Fig. 2(b)]. Indeed such reasoning also accounts for the

reduction of correlation when the total pressure and energy are considered:  $\Delta E = \Delta U + \Delta K$ , while (for a large atomic system)  $V\Delta p = \gamma\Delta U + (2/3)\Delta K$ . The fact that  $\gamma$  is (for the Lennard-Jones potential) quite different from  $2/3$  implies that the  $p$ ,  $E$ -correlation is significantly weaker than that of  $W$ ,  $U$  (Fig. 1). Even in cases of unequal slopes, however, there can be circumstances under which one kind of term, and therefore one slope, dominates the fluctuations. In this case strong correlations will be observed. Examples include the high-temperature limits of hydrogen-bonded liquids (Sec. III D) and the time-averaged (total) energy and pressure in viscous liquids (Paper II).

Some of the results detailed below were published previously in letter form;<sup>10</sup> the aim of the present contribution is to make a comprehensive report covering more systems, while Paper II contains a detailed analysis and discusses applications. In the following section, we describe the systems simulated. In Sec. III we present the results for all the systems investigated, in particular, the degree of correlation (correlation coefficient  $R$ ) and the slope. Section IV gives a summary.

## II. SIMULATED SYSTEMS

A range of simulation methods, thermodynamic ensembles, and computational codes were used. One reason for this was to eliminate the possibility that strong correlations are an artifact of using a particular ensemble or code. In addition, no code can simulate the full range of systems presented. Most of the data we present are from molecular dynamics (MD) simulations, although some are from Monte Carlo<sup>11</sup> (MC) and event-driven<sup>12</sup> (ED) simulations. Most of the MD simulations (and of course all MC simulations), had fixed temperature (*NVT*), while some had fixed total energy (*NVE*). Three MD codes were used: GROMACS (GRO),<sup>13,14</sup> ASAP (ASAP),<sup>15</sup> and DIGITALMATERIAL (DM).<sup>16</sup> Homemade (HM) codes were used for the MC and ED simulations.

We now list the 13 systems studied, giving each a code name for future reference. The systems include monatomic systems interacting with pair potentials, binary atomic systems interacting with pair potentials, molecular systems consisting of Lennard-Jones particles joined rigidly together in a fixed configuration (here the Lennard-Jones interaction models the van der Waals forces), molecular systems that have Coulomb as well as Lennard-Jones interactions, metallic systems with a many-body potential, and a binary system interacting with a discontinuous “square-well” potential. Included with each system is a list specifying which simulation method(s), which ensemble(s), and which code(s) were used [semicolons separate the method(s) from the ensemble(s) and the ensemble(s) from the code(s)]. Details of the potentials are given in Appendix A.

CU: Pure liquid Cu simulated using the many-body potential derived from effective medium theory (EMT),<sup>17,18</sup> (MD; *NVE*; ASAP).

DB: Asymmetric “dumbbell” molecules<sup>19</sup> consisting of two unlike Lennard-Jones spheres connected by a rigid bond; (MD; *NVT*; GRO).

DZ: The potential introduced by Dzугutov<sup>20</sup> as a candi-

date for a monatomic glass-forming system. Its distinguishing feature is a peak in  $v(r)$  around  $1.5\sigma$ , after which it decays exponentially to zero at a finite value of  $r$ ; (MD; *NVT*, *NVE*; DM).

EXP: A system interacting with a pair potential with exponential repulsion and a van der Waals attraction; (MC; *NVT*; HM).

KABLJ: The Kob–Andersen binary Lennard-Jones liquid;<sup>21</sup> (MD; *NVT*, *NVE*; GRO, DM).

METH: The GROMOS (Ref. 22) three-site model for methanol; (MD; *NVT*; GRO).

MGCU: A model of the metallic alloy Mg<sub>85</sub>Cu<sub>15</sub> using an EMT-based potential;<sup>23</sup> (MD; *NVE*; ASAP).

OTP: A three-site model of the fragile glass-former orthoterphenyl (OTP);<sup>24</sup> (MD; *NVT*; GRO).

SCLJ: The standard single-component Lennard-Jones system with the interaction given in Eq. (11); (MD, MC; *NVT*, *NVE*; GRO, DM).

SPC/E: The SPC/E model of water;<sup>25</sup> (MD; *NVT*; GRO).

SQW: A binary model with a pair interaction consisting of an infinitely hard core and an attractive square well;<sup>12,26</sup> (ED; *NVE*; HM).

TIP5P: A five-site model for liquid water, which reproduces the density anomaly;<sup>27</sup> (MD; *NVT*; GRO).

TOL: A seven-site united-atom model of toluene; (MD; *NVT*; GRO).

The number of particles (atoms or molecules) was in the range 500–2000. Particular simulation parameters ( $N$ ,  $\rho$ ,  $T$ , duration of simulation) are given when appropriate in Sec. III.

## III. RESULTS

### A. The standard single-component Lennard-Jones system

SCLJ is the system we have most completely investigated.  $W$ ,  $U$ -plots are shown for a range of thermodynamic state points in Fig. 4. Here the ensemble was *NVT* with  $N = 864$ , and each simulation consisted of a 10 ns run taken after 10 ns of equilibration; for all SCLJ results so-called “argon” units are used ( $\sigma = 0.34$  nm,  $\epsilon = 0.997$  kJ/mol). Each elongated oval in Fig. 4 is a collection of  $W$ ,  $U$  pairs for a given state point. Varying temperature at fixed density moves the oval parallel to itself, following an almost straight line as indicated by the dashed lines. Different densities correspond to different lines, with almost the same slope. In a system with a pure inverse power-law interaction, the correlation would be exact, and moreover the data for all densities would fall on the same straight line [see the discussion immediately after Eq. (5)]. Our data, on the other hand, show a distinct dependence on volume, but for a given volume, because of the strong correlation, the variation in  $W$  is almost completely determined by that of  $U$ .

Values of correlation coefficient  $R$  for the state points of Fig. 4 are listed in Table I, along with the slope  $\gamma$ . In Fig. 5 we show the temperature dependence of both  $R$  and  $\gamma$  for different densities. Lines have been drawn to indicate isochores and one isobar ( $p = 0$ ). Note that when we talk of an isobar here, we mean a set of *NVT* ensembles with  $V$ ,  $T$

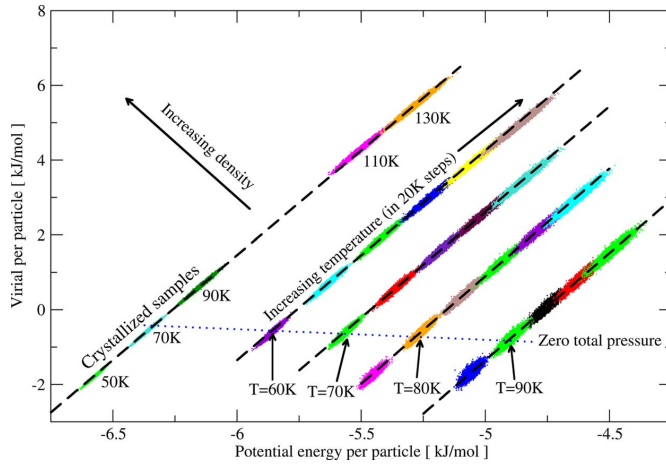


FIG. 4. (Color online) Scatter plots of the configurational parts of pressure and energy—virial vs potential energy—for several state points of the SCLJ liquid ( $NVT$ ). Each oval represents simulations at one particular temperature and density where each data point marks instantaneous values of virial and potential energy. The dashed lines mark constant density paths with the highest density to the upper left (densities: 39.8, 37.4, 36.0, 34.6, and 32.6 mol/l). State points on the dotted line have zero average pressure. The plot includes three crystallized samples (lower left corner), discussed at the end of Sec. III A and, in more detail, in Paper II (reproduced from Ref. 10).

chosen so that the thermal average of  $p$  takes on a given value, rather than fixed-pressure ensembles. This figure makes it clear that for fixed density,  $R$  increases as  $T$  increases, while it also increases with density for fixed temperature; the slope slowly decreases in these circumstances. In fact, it eventually reaches 4, the value expected for a pure

TABLE I. Correlation coefficients  $R$  and effective slopes  $\gamma$  for the SCLJ system for the state points in Fig. 4.  $p$  is the thermally averaged pressure. The last five states were chosen to approximately follow the isobar  $p=0$ .

$\rho$ (mol/l)	$T$ (K)	$p$ (MPa)	Phase	$R$	$\gamma$
42.2	12	2.6	Glass	0.905	6.02
39.8	50	-55.5	Crystal	0.987	5.85
39.8	70	-0.5	Crystal	0.989	5.73
39.8	90	54.4	Crystal	0.990	5.66
39.8	110	206.2	Liquid	0.986	5.47
39.8	150	309.5	Liquid	0.988	5.34
37.4	60	-3.7	Liquid	0.965	6.08
37.4	100	102.2	Liquid	0.976	5.74
37.4	140	192.7	Liquid	0.981	5.55
37.4	160	234.3	Liquid	0.983	5.48
36.0	70	-0.7	Liquid	0.954	6.17
36.0	110	90.3	Liquid	0.969	5.82
36.0	150	169.5	Liquid	0.977	5.63
36.0	190	241.4	Liquid	0.981	5.49
36.0	210	275.2	Liquid	0.982	5.44
34.6	60	-42.5	Liquid	0.900	6.53
34.6	100	41.7	Liquid	0.953	6.08
34.6	140	114.5	Liquid	0.967	5.80
34.6	200	211.0	Liquid	0.977	5.57
32.6	70	-35.6	Liquid	0.825	6.66
32.6	90	-0.8	Liquid	0.905	6.42
32.6	110	31.8	Liquid	0.929	6.22
32.6	150	91.7	Liquid	0.954	5.95
32.6	210	172.7	Liquid	0.968	5.68
37.4	60	-3.7	Liquid	0.965	6.08
36.0	70	-0.7	Liquid	0.954	6.17
34.6	80	1.5	Liquid	0.939	6.27
32.6	90	00	Liquid	0.905	6.42
42.2	12	2.6	Glass	0.905	6.02

$r^{-12}$  interaction (e.g., at  $\rho=34.6$  mol/l,  $T=1000$  K,  $\gamma=4.61$ , see Ref. 10). This is consistent with the idea that the repulsive part, characterized by an effective inverse power law, dominates the fluctuations: Increasing either temperature or density increases the frequency of short-distance encounters while reducing the typical distances of such encounters. On the other hand, along an isobar, these two effects work against each other, since as  $T$  increases, the density decreases. The density effect “wins” in this case, which is equivalent to a statement about the temperature and volume derivative of  $R$ : Our simulations imply that

$$\left(\frac{\partial R}{\partial T}\right)_p = \left(\frac{\partial R}{\partial T}\right)_V + \left(\frac{\partial R}{\partial V}\right)_T \left(\frac{\partial V}{\partial T}\right)_p < 0, \quad (14)$$

which is equivalent to

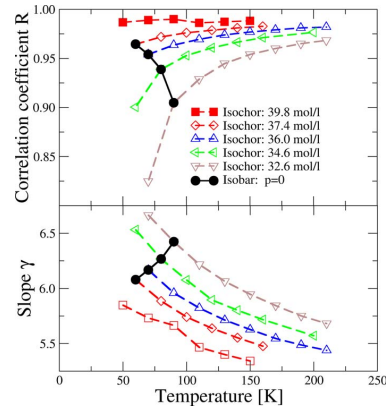


FIG. 5. (Color online) Upper plot, correlation coefficient  $R$  for the SCLJ system as a function of temperature for several densities ( $NVT$ ). This figure makes clear the different effects of density and temperature on  $R$ . Lower plot, effective slope  $\gamma$  as a function of  $T$ . Simulations at temperatures higher than those shown here indicate that the slope slowly approaches the value 4 as  $T$  increases. This is to be expected because as collisions become harder, involving shorter distances, the effective inverse power-law exponent approaches the 12 from the repulsive term of the Lennard-Jones potential.

$$\left(\frac{\partial R}{\partial T}\right)_V < -\left(\frac{\partial R}{\partial V}\right)_T V\alpha_p = \rho\left(\frac{\partial R}{\partial \rho}\right)_T \alpha_p, \quad (15)$$

where  $\alpha_p \equiv (\partial V / \partial T)_p / V$  is the thermal expansivity at constant pressure and  $\rho$  is the particle density. This can be recast in terms of logarithmic derivatives [valid whenever  $(\partial R / \partial \rho)_T > 0$ ] as follows:

$$\frac{\left(\frac{\partial R}{\partial \ln(T)}\right)_V}{\left(\frac{\partial R}{\partial \ln(\rho)}\right)_T} < T\alpha_p. \quad (16)$$

Thus what we observe in the simulations, namely, that the correlation becomes stronger as temperature is reduced at fixed pressure, is *a priori* more to be expected when the thermal expansivity is large [since then the right hand side of Eq. (16) is large]. This has particular relevance in the context of supercooled liquids, which we discuss in Paper II, because these are usually studied by lowering temperature at fixed pressure. On the other hand if the expansivity becomes small, as for example, when a liquid passes through the glass transition, inequality (16) is *a priori* less likely to be satisfied. We have, in fact, observed this in a simulation of OTP: Upon cooling through the (computer) glass transition, the correlation became weaker with further lowering of temperature at constant pressure.

Remarkably, the correlation persists when the system has crystallized, as seen in the data for the highest density—the occurrence of the first-order phase transition can be inferred from the gap between the data for 90 and 110 K, but the data fall on the same line above and below the transition. One would not expect the dynamical fluctuations of a crystal, which are usually assumed to be well described by a harmonic approximation, to resemble those of the high-temperature liquid. In fact, for a one-dimensional crystal of particles interacting with a harmonic potential  $v(r) = \frac{1}{2}k(r - r_m)^2$ , it is easy to show (Paper II) that there is a negative correlation with slope equal to  $-2/3$ . To investigate whether the harmonic approximation ever becomes relevant for the correlations, we prepared a perfect fcc crystal of SCLJ particles at zero temperature and simulated it at increasing temperatures, from 0.02 to 90 K in argon units, along a constant density path. The results are shown in Fig. 6. Clearly the correlation is maintained right down to zero temperature. The harmonic approximation is therefore useless for dealing with the pressure fluctuations even as  $T \rightarrow 0$ , because the slope is far from  $-2/3$ . The reason for this is that the dominant contribution to the virial fluctuations comes from the third-order term, as shown in Paper II.

### B. A case with little correlation: The Dzugutov system

Before presenting data for all the systems studied, it is useful to see what it means for the correlation not to hold. In this subsection we consider the Dzugutov system,<sup>20</sup> whose potential contains a peak at the second-neighbor distance (Fig. 7, see Appendix A for details) whose presence might be expected to interfere with the effectiveness of an inverse power-law description. In the next subsection we show how

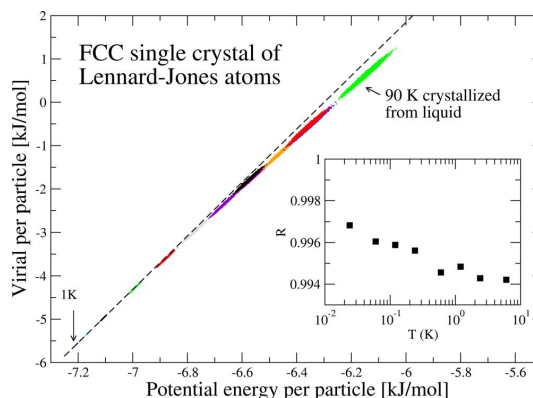


FIG. 6. (Color online) Scatter plot of the  $W, U$ -correlations for a perfect face-centered-cubic (fcc) crystal of Lennard-Jones atoms at temperatures 1, 2, 3, 5, 10, 20, 30, 40, 50, 60, 70, and 80 K, as well as for defective crystals (i.e., crystallized from the liquid) at temperatures 50, 70, and 90 K (NVT). The dashed line gives the best fit to the (barely visible) lowest-temperature data ( $T=1$  K). The inset shows the temperature dependence of  $R$  at very low temperatures. The crystalline case is examined in detail in Paper II, where we find that  $R$  does not converge to unity at  $T=0$ , but rather to a value very close to unity. All state points refer to the highest density of Fig. 4, 39.8 mol/l.

in a specific model of water the lack of correlation can be explicitly seen to be the result of competing interactions. Figure 8 shows  $W, U$ -plots for the Dzugutov system for two nearby temperatures at the same density. The ovals are much less elongated than was the case for SCLJ, indicating a significantly weaker correlation—the correlation coefficients here are 0.585 and 0.604, respectively. In Paper II it is shown explicitly that the weak correlation is due to contributions arising from the second peak. Note that the major axes of the ovals are not aligned with the line joining the state points, given by the mean values of  $W$  and  $U$ , here identifiable as the intersection of the dashed and straight lines. On the other hand, the lines of best fit from linear regression, indicated by the dashed lines in each case, *do* coincide with the line connecting state points. This holds generally, a fact which follows from statistical mechanics (Appendix B). The interesting thing is rather that the major axes point in different directions, whereas in the SCLJ case they are also aligned

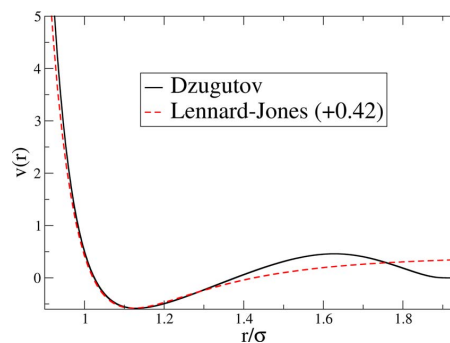


FIG. 7. (Color online) A plot of the Dzugutov pair potential, with the Lennard-Jones potential (shifted by a constant) shown for comparison.

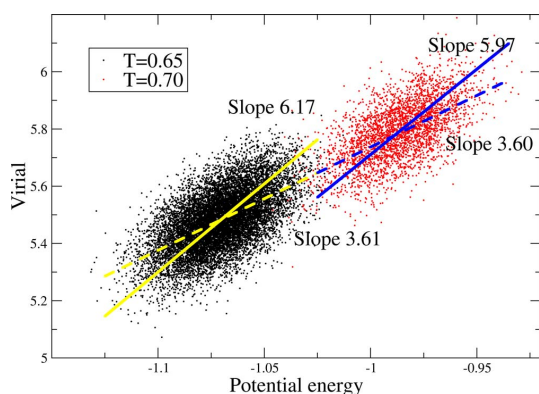


FIG. 8. (Color online) Scatter plot of  $W, U$ -correlations for the Dzugutov system at density 0.88 and temperatures 0.65 and 0.70 (NVE). The dashed lines indicate the best-fit line using linear regression. These are consistent with the temperature dependence of the mean values of  $\langle W \rangle$  and  $\langle U \rangle$ , as they should be (see Appendix B), but they clearly do not represent the direction of greatest variance. The full lines have slopes equal to the ratio of standard deviations of the two quantities [Eq. (7)]. The correlation coefficient is 0.585 and 0.604 for  $T=0.65$  and  $T=0.70$ , respectively.

with the state-point line. The linear-regression slope, being equal to  $\langle \Delta U \Delta W \rangle / \langle (\Delta U)^2 \rangle$ , treats  $W$  and  $U$  in an asymmetric manner by involving  $\langle (\Delta U)^2 \rangle$ , but not  $\langle (\Delta W)^2 \rangle$ . This is because a particular choice of independent and dependent variables is made. If instead we plotted  $U$  against  $W$ , we would expect the slope to be simply the inverse of the slope in the  $W, U$ -plot, but, in fact, the new slope is  $\langle \Delta U \Delta W \rangle / \langle (\Delta W)^2 \rangle$ . This equals the inverse of the original slope only in the case of perfect correlation, where  $\langle \Delta U \Delta W \rangle^2 = \langle (\Delta W)^2 \rangle \langle (\Delta U)^2 \rangle$ . For our purposes a more symmetric estimate of the slope is desired, one which agrees with the linear-regression slope in the limit of perfect correlation. We use simply the ratio of standard deviations  $\sqrt{\langle (\Delta W)^2 \rangle} / \sqrt{\langle (\Delta U)^2 \rangle}$  [Eq. (7)]. This slope was used to plot the dashed line in Fig. 2(a) and the full lines in Fig. 8, where it clearly represents the orientation of the data better.<sup>28</sup>

### C. When competition between van der Waals and Coulomb interactions kills the correlation: TIP5P water

As we shall see in the next section, the systems that show little correlation include several, which involve both van der Waals and hydrogen bonding, modeled by Lennard-Jones and Coulomb interactions, respectively. As noted already, the latter, being a pure inverse power law ( $n=1$ ), by itself exhibits perfect correlation with slope  $\gamma=1/3$ , while the Lennard-Jones part has near perfect correlation. However, the significant difference in slopes means that no strong correlation is seen for the full interaction. To check explicitly that this is the reason the correlation is destroyed we have calculated the correlation coefficients for the Lennard-Jones and Coulomb parts separately in a model of water. Water is chosen because the density of hydrogen bonds is quite high. Simulations were done with the TIP5P model of water,<sup>27</sup> which has the feature that the density maximum is reason-

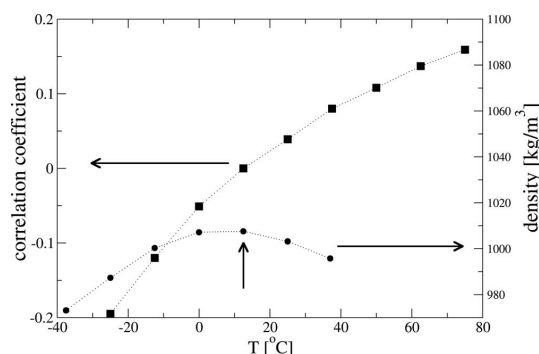


FIG. 9. Plot of  $R$  for TIP5P water in  $NVT$  simulations with densities chosen to give an average pressure of 1 atm. Not only is the magnitude of  $R$  low (less than 0.2) in the temperature range shown, but it changes sign around the density maximum. The vertical arrow indicates the state point used for Fig. 2(b).

ably well reproduced. This existence of the density maximum is, in fact, related to pressure and energy becoming uncorrelated, as we shall see.

Figure 9 shows the correlation coefficients and slopes for a range of temperatures; the correlation is almost nonexistent, passing through zero around where the density attains its maximum value. We have separately determined the correlation coefficient of the Lennard-Jones part of the interaction; it ranges from 0.9992 at  $-25$  °C to 0.9977 at 75 °C, even larger than we have seen in the SCLJ system. The reason for this is that the (attractive) Coulomb interaction forces the centers of the Lennard-Jones interaction closer together than they would be otherwise; thus, the relevant fluctuations are occurring higher up the repulsive part of the Lennard-Jones pair potential. Correspondingly the slope from this interaction ranges between 4.45 and 4.54, closer to the high- $T$ , high density limit of 4 than was the case for the SCLJ system. This is confirmed by inspection of the oxygen-oxygen radial distribution function in Ref. 27 where it can be seen that the first peak lies entirely to the left of the  $v_{LJ}=0$  distance  $\sigma = 0.312$  nm. Finally note that the near coincidence between the vanishing of the correlation coefficient and the density maximum, which is close to the experimental value of 4 °C, is not accidental: The correlation coefficient is proportional to the configurational part of the thermal pressure coefficient  $\beta_V$  (Paper II). The full  $\beta_V$  vanishes exactly at the density maximum (4 °C), but the absence of the kinetic term means that the correlation coefficient vanishes at a slightly higher temperature ( $\sim 12$  °C).

### D. Results for all systems

In Fig. 10 we summarize the results for the various systems. Here we plot the numerator of Eq. (6) against the denominator, including factors of  $1/(k_B T V)$  in both cases to make an intensive quantity with units of pressure. Since  $R$  cannot be greater than unity, no points can appear above the diagonal. Being exactly on the diagonal indicates perfect correlation ( $R=1$ ), while being significantly below indicates poor correlation. Different types of symbols indicate differ-

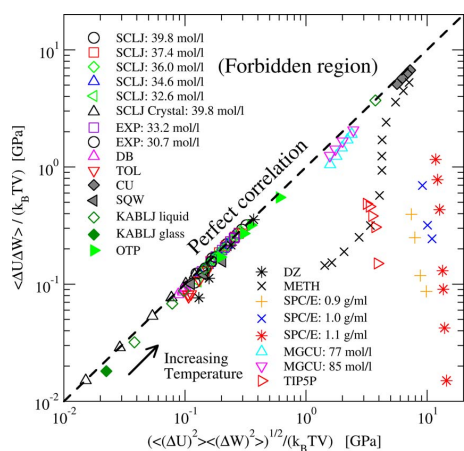


FIG. 10. (Color online)  $W, U$ -correlations for all simulated liquids;  $\langle \Delta W \Delta U \rangle / (k_B TV)$  plotted vs  $((\langle \Delta W \rangle)^2 \langle (\Delta U)^2 \rangle)^{1/2} / (k_B TV)$ . Both quantities correspond to a pressure, which is given in units of GPa; for model systems not specifically corresponding to real systems, such as SCLJ, KABLJ, and SQW, argon units were used to set the energy and length scales. If the correlation is perfect ( $R=1$ ) the data fall on the diagonal marked by a dashed line. For the TIP5P model of water only temperatures with  $R > 0$  are included; volumes were chosen to give a pressure close to zero.

ent systems, as well as different densities for the same system, while symbols of the same type correspond to different temperatures.

All of the simple liquids, SCLJ, KABLJ, EXP, DB, and TOL, show strong correlations, while METH, SPC/E, and TIP5P show little correlation. Values of  $R$  and  $\gamma$  at selected state points for all systems are listed in Table II. What determines the degree of correlation? The Dzugotov and TIP5P cases have already been discussed. The poor correlation for METH and SPC/E is (presumably) because these models, like TIP5P, involve both Lennard-Jones and Coulomb interactions. In systems with multiple Lennard-Jones species, but without any Coulomb interaction, there is overall a strong correlation because the slope is almost independent of the parameters for a given kind of pair.

As the temperature is increased, the data for the most poorly correlated systems, which are all hydrogen-bonding organic molecules, slowly approach the perfect-correlation line. This is consistent with the idea that this correlation is observed when fluctuations of both  $W$  and  $U$  are dominated by close encounters of pairs of neighboring atoms; at higher temperature there are increasingly many such encounters, which therefore come to increasingly dominate the fluctuations. Also because the Lennard-Jones potential rises much more steeply than the Coulomb potential, the latter becomes less important as short distances dominate more. Although not obvious in the plot, we find that increasing the density at fixed temperature generally increases the degree of correlation, as found in the SCLJ case; this is also consistent with the increasing relevance of close encounters or collisions.

A system quite different from the others presented so far is the binary square-well system, SQW, with a discontinuous potential combining hard-core repulsion and a narrow attractive well (Fig. 11; see Appendix A for details). Such a po-

TABLE II. Correlation coefficients and slopes at selected state points for all investigated systems besides SCLJ. Argon units were used for DZ, EXP, KABLJ, and SQW by choosing the length parameter (of the larger particle when there were two types) to be 0.34 nm and the energy parameter to be 0.997 kJ/mol. The phase is indicated as liquid or glass. SQW data involve time averaging over periods 3.0, 3.0, 8.0, and 9.0, respectively, for the four listed state points. A minus sign has been included with the slope when  $R < 0$ ; note that the  $\gamma$  values only really make sense as slopes when  $|R|$  is close to unity. The ensemble was  $NVT$  except for CU, DZ, MGCU, and SQW, where it was  $NVE$ .

System	$\rho$ (mol/l)	$T$ (K)	Phase	$R$	$\gamma$
CU	125.8	1500	Liquid	0.907	4.55
CU	125.8	2340	Liquid	0.926	4.15
DB	11.0	130	Liquid	0.964	6.77
DB	9.7	300	Liquid	0.944	7.45
DZ	37.2	78	Liquid	0.585	3.61
EXP	30.7	96	Liquid	0.908	5.98
EXP	33.2	96	Liquid	0.949	5.56
KABLJ	50.7	30	Glass	0.858	6.93
KABLJ	50.7	70	Liquid	0.946	5.75
KABLJ	50.7	240	Liquid	0.995	5.10
METH	31.5	150	Liquid	0.318	22.53
METH	31.5	600	Liquid	0.541	6.88
METH	31.5	2000	Liquid	0.861	5.51
MGCU	85.0	640	Liquid	0.797	4.74
MGCU	75.6	465	Liquid	0.622	6.73
OTP	4.65	300	Liquid	0.913	8.33
OTP	4.08	500	Liquid	0.884	8.78
OTP	3.95	500	Liquid	0.910	7.70
SPC/E	50.0	200	Liquid	0.016	208.2
SPC/E	55.5	300	Liquid	0.065	48.6
SQW	60.8	48	Liquid	-0.763	-50.28
SQW	60.8	79	Liquid	-0.833	-49.11
SQW	60.8	120	Liquid	-0.938	-52.02
SQW	59.3	120	Liquid	-0.815	-30.07
TIP5P	55.92	273	Liquid	-0.051	-2.47
TIP5P	55.94	285.5	Liquid	0.000	2.51
TOL	10.5	75	Glass	0.877	7.59
TOL	10.5	300	Liquid	0.961	8.27

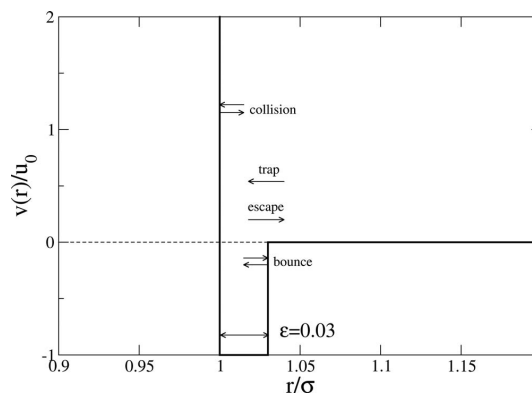


FIG. 11. Illustration of the square-well potential, indicating the four microscopic processes, which contribute to the virial.

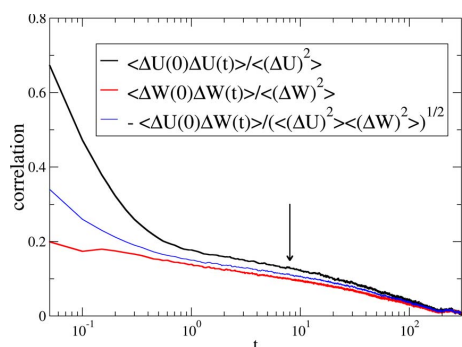


FIG. 12. (Color online) Energy-energy, virial-virial, and energy-virial correlation functions for SQW at packing fraction  $\phi=0.595$  and temperature  $T=1.0$  (normalized to unity at  $t=0$ ). The cross correlation has been multiplied by  $-1$ . The arrow marks the time  $t=8$ , roughly  $1/10$  of the relaxation time (determined from the long-time part of the energy-virial cross-correlation function). This time was used for averaging.

tential models attractive colloidal systems,<sup>12</sup> one of whose interesting features, predicted from simulations and theory, is the existence of two different glass phases, termed the “repulsive” and “attractive” glasses.<sup>29</sup> The discontinuous potential not only makes the simulations substantially different from a technical point of view, but there are also conceptual differences—in particular, the instantaneous virial is a sum of delta functions in time. The dynamical algorithm employed in the simulations is ED, where events involve a change in the relative velocity of a pair of particles due to hitting the hard-core inner wall of the potential or crossing the potential step. The algorithm must detect the next event, advance time by the appropriate amount, and adjust the velocities of all particles appropriately. There are four kinds of events (illustrated in Fig. 11): (1) “collisions,” involving the inner repulsive core; (2) “bounces,” involving bouncing off the outer (attractive) wall of the potential; (3) “trapping,” involving the separation going below the range of the outer wall; and (4) “escapes,” involving the separation increasing beyond the outer wall. To obtain meaningful values of the virial a certain amount of time averaging must be done—we can no longer consider truly instantaneous quantities. As shown in Appendix C the time-averaged virial may be written as the following sum over all events that take place in the averaging interval  $t_{av}$ :

$$\bar{W} = \frac{1}{3t_{av}} \sum_{e \text{ events}} m_{r,e} \mathbf{r}_e \cdot \Delta \mathbf{v}_e. \quad (17)$$

Here  $\mathbf{r}_e$  and  $\mathbf{v}_e$  refer to the relative position and velocity for the pair of particles participating in event  $e$ , while  $\Delta$  indicates the change taking place in that event. Positive contributions to  $\bar{W}$  come from collisions; the three other event types involve the outer wall, which, as is easy to see, always gives a negative contribution. The default  $t_{av}$  in the simulation was 0.05. Strong correlations emerge only at longer averaging times, however. An appropriate  $t_{av}$  may be chosen by considering the correlation functions (auto- and cross-) for virial and potential energy, plotted in Fig. 12, where the “instantaneous” values  $E(t)$  and  $W(t)$  correspond to averaging

over 0.05 time units. We choose  $t_{av} \approx \tau_\alpha/10$ , where  $\tau_\alpha$  is the relaxation time determined from the cross-correlation function  $\langle \Delta U(0)\Delta W(t) \rangle$ . Data for a few state points are shown in Table II. Remarkably, this system, so different from the continuous potential systems, also exhibits strong  $W, U$ -correlations, with  $R=0.94$  in the case  $T=1.0$ ,  $\phi=0.595$  (something already hinted at in Fig. 12 in the fact that the curves coincide). There is a notable difference, however, compared to continuous systems: The correlation is negative.

The reason for the negative correlation is that at high density, most of the contributions to the virial are from collisions: A particle will collide with neighbor 1, recoil, and then collide with neighbor 2 before there is a chance to make a bounce event involving neighbor 1. The number of collisions that occur in a given time interval is proportional to the number of bound pairs that is exactly anticorrelated with the energy. The effective slope  $\gamma$  has a large (negative) value of order  $-50$ , which does not seem to depend strongly on temperature. This example is interesting because it shows that strong pressure-energy correlations can appear in a wider range of systems that might first have been guessed. Note, however, that the ordinary hard-sphere system cannot display such correlations, since potential energy does not exist as a dynamical variable in this system, i.e., it is identically zero. The idea of correlations emerging when quantities are averaged over a suitable time interval is one we shall meet again in Paper II in the context of viscous liquids.

#### IV. SUMMARY

We have demonstrated a class of model liquids whose equilibrium thermal fluctuations of virial and potential energy are strongly correlated. We have presented detailed investigations of the presence or absence of such correlations in various liquids, with extra detail presented for the standard SCLJ case. One notable aspect is how widespread these correlations are, appearing not just in Lennard-Jones potentials or in potentials that closely resemble the Lennard-Jones one, but also in systems involving many-body potentials (CU and MGCU) and discontinuous potentials (SQW). We have seen how the presence of different types of terms in the potential, such as Lennard-Jones and Coulomb interactions, spoil the correlations, even though each by itself would give rise to a strongly correlating system. Most simulations were carried out in the  $NVT$  ensemble;  $R$  is not ensemble independent, but the  $R \rightarrow 1$  limit is.

Several of the hydrocarbon liquids studied here were simulated using simplified “united-atom” models where groups such as methyl groups or even benzene rings were represented by Lennard-Jones spheres. These could also be studied using more realistic “all-atom” models, where every atom (including hydrogen atoms) is included. It would be worth investigating whether the strength of the correlations is reduced by the associated Coulomb terms in such cases.

In Paper II we provide a detailed analysis for the SCLJ case, including consideration of contributions beyond the effective inverse power-law approximation and the  $T \rightarrow 0$  limit of the crystal. There we also discuss some consequences,

including a direct experimental verification of the correlations for supercritical argon and consequences of strong pressure-energy correlations in highly viscous liquids and biomembranes.

#### ACKNOWLEDGMENTS

Useful discussions with Søren Toxværd are gratefully acknowledged. Center for viscous liquid dynamics “Glass and Time” is sponsored by The Danish National Research Foundation.

#### APPENDIX A: DETAILS OF INTERATOMIC POTENTIALS

Here we give more detailed information about the interatomic potentials used. These details have been published elsewhere as indicated, except for the case of EXP and TOL.

CU: Pure liquid Cu simulated using the many-body potential derived from EMT.<sup>17,18</sup> This is similar to the embedded atom method of Daw and Baskes,<sup>30</sup> where the energy of a given atom  $i$ ,  $E_i$ , is some nonlinear function (the “embedding function”) of the electron density due to the neighboring atoms. In the EMT, it is given as the energy of an atom in an equivalent reference system, the “effective medium,” plus a correction term,  $E_i = E_{C,i}(n_i) + \frac{1}{2}[\sum_{j \neq i} v_{ij}(r_{ij}) - \sum_{j \neq i}^{ref} v_{ij}(r_{ij})]$ . Specifically, the reference system is chosen as a fcc crystal of the given kind of atom, and “equivalent” means that the electron density is used to choose the lattice constant of the crystal. The correction term is an ordinary pair potential involving a simple exponential, but notice that the corresponding sum in the reference system is subtracted (guaranteeing that the correct reference energy is given when the configuration is in fact, the reference configuration). The parameters were  $E_0 = -3.510$  eV,  $s_0 = 1.413$  Å,  $V_0 = 2.476$  eV,  $\eta_2 = 3.122$  Å<sup>-1</sup>,  $\kappa = 5.178$ ,  $\lambda = 3.602$ , and  $n_0 = 0.0614$  Å<sup>-3</sup>.

DB: Asymmetric dumbbell molecules,<sup>19</sup> consisting of two unlike Lennard-Jones spheres, labelled P and M, connected by a rigid bond. The parameters were  $\epsilon_p = 5.726$  kJ/mol,  $\sigma_p = 0.4963$  nm,  $m_p = 77.106$  u,  $\epsilon_m = 0.66944$  kJ/mol,  $\sigma_m = 0.3910$  nm, and  $m_m = 15.035$  u; the bond length was  $d = 0.29$  nm. Cross interactions,  $\epsilon_{pm}$  and  $\sigma_{pm}$ , were set equal to the geometric and arithmetic means of the  $p$  and  $m$  parameters, respectively (Lorentz–Berthelot mixing rule<sup>31</sup>).

DZ: A monatomic liquid introduced by Dzугutov as a candidate for a monatomic glass-forming system.<sup>20</sup> The potential is a sum of two parts,  $v(r) = v_1(r) + v_2(r)$ , with  $v_1(r) = A(r^m - B)\exp(c/(r-a))$  for  $r < a$  and zero otherwise, and  $v_2(r) = B \exp(d/(r-b))$  for  $r < b$ , zero otherwise. The parameters are chosen to match the location and curvature of the Lennard-Jones potential:  $m = 16$ ,  $A = 5.82$ ,  $c = 1.1$ ,  $a = 1.87$ ,  $B = 1.28$ ,  $d = 0.27$ , and  $b = 1.94$ .

EXP: A system interacting with a pair potential with exponential repulsion  $U(r) = (\epsilon/8)[6 \exp(-14(r/\sigma - 1)) - 14(\sigma/r)^6]$ . Note that the attractive term has the same form as the Lennard-Jones potential.

KABLJ: The Kob–Andersen binary Lennard-Jones liquid,<sup>21</sup> a mixture of two kinds of particles  $A$  and  $B$ , with  $A$  making 80% of the total number. The energy and length pa-

rameters are  $\epsilon_{AA} = 1.0$ ,  $\epsilon_{BB} = 0.5$ ,  $\epsilon_{AB} = 1.5$ ,  $\sigma_{AA} = 1.0$ ,  $\sigma_{BB} = 0.88$ , and  $\sigma_{AB} = 0.8$ . The masses are both equal to unity. We use the standard density  $\rho = 1.2\sigma_{AA}^{-3}$ .

METH: The GROMOS three-site model for methanol.<sup>32</sup> The sites represent the methyl ( $M \equiv \text{CH}_3$ ) group ( $m = 15.035$  u), the O atom ( $m = 15.999$  u), and the O-bonded H atom ( $m = 1.008$  u). The charges for Coulomb interactions are, respectively,  $0.176e$ ,  $-0.574e$ , and  $0.398e$ . The  $M$  and O groups additionally interact via Lennard-Jones forces, with parameters  $\epsilon_{MM} = 0.9444$  kJ/mol,  $\epsilon_{OO} = 0.8496$  kJ/mol,  $\epsilon_{MO} = 0.9770$  kJ/mol,  $\sigma_{MM} = 0.3646$  nm,  $\sigma_{OO} = 0.2955$  nm, and  $\sigma_{MO} = 0.3235$  nm. Lennard-Jones interactions are smoothly cutoff between 0.9 and 1.1 nm. The  $M$ –O and O–H distances are fixed at 0.136 and 0.1 nm, respectively, while the  $M$ –O–H bond angle is fixed at  $108.53^\circ$ .

MGCU: A model of the metallic alloy  $\text{Mg}_{85}\text{Cu}_{15}$ , simulated by EMT with parameters as in Ref. 23. In this potential there are seven parameters for each element. However, some of the Cu parameters were allowed to vary from their original values in the process of optimizing the potential for the Mg–Cu system. The parameters for Cu were  $E_0 = -3.510$  eV,  $s_0 = 1.413$  Å,  $V_0 = 1.994$  eV,  $\eta_2 = 3.040$  Å<sup>-1</sup>,  $\kappa = 4.944$ ,  $\lambda = 3.694$ , and  $n_0 = 0.0637$  Å<sup>-3</sup>, while those for Mg were  $E_0 = -1.487$  eV,  $s_0 = 1.766$  Å,  $V_0 = 2.230$  eV,  $\eta_2 = 2.541$  Å<sup>-1</sup>,  $\kappa = 4.435$ ,  $\lambda = 3.293$ , and  $n_0 = 0.0355$  Å<sup>-3</sup>. It should be noted that there is an error in Ref. 23: The parameter  $s_0$  for Cu is given in units of bohr instead of Å.

OTP: The Lewis–Wahnström three-site model of OTP (Ref. 24) consisting of three identical Lennard-Jones spheres located at the apices  $A$ ,  $B$ , and  $C$  of an isosceles triangle. Sides  $AB$  and  $BC$  are 0.4830 nm long, while the  $ABC$  angle is  $75^\circ$ . The Lennard-Jones interaction parameters are  $\epsilon = 4.989$  kJ/mol and  $\sigma = 0.483$  nm, while the mass of each sphere, not specified in Ref. 24, was taken as one-third of the mass of an OTP molecule,  $m = 76.768$  u.

SCLJ: The standard single-component Lennard-Jones system with potential given by Eq. (11).

SPC/E: The SPC/E model of water,<sup>25</sup> in which each molecule consists of three rigidly bonded point masses, with an OH distance of 0.1 nm and the HOH angle equal to the tetrahedral angle. Charges on O and each H are equal to  $-0.8476e$  and  $+0.4238e$ , respectively. O atoms interact with each other via a Lennard-Jones potential with  $\epsilon = 2.601$  kJ/mol and  $\sigma = 0.3166$  nm.

SQW: A binary model with a pair interaction consisting of an infinitely hard core and an attractive square well:<sup>12,26</sup>  $v_{ij}(r) = \infty$ ,  $r < \sigma_{ij}$ ,  $v_{ij}(r) = -u_0$ ,  $\sigma_{ij} < r < \sigma_{ij}(1 + \epsilon)$ ,  $v_{ij}(r) = 0$ , and  $r > \sigma_{ij}(1 + \epsilon)$ . The radius parameters are  $\sigma_{AA} = 1.2$ ,  $\sigma_{BB} = 1$ , and  $\sigma_{AB} = 1.1$ , while  $\epsilon = 0.03$  and  $u_0 = 1$ . The composition was equimolar, and the masses of both particles were equal to unity.

TIP5P: In this water model<sup>27</sup> there are five sites associated with a single water molecule. One for the O atom, one for each H, and two to locate the centers of negative charge corresponding to the electron lone pairs on the O. The OH bond length and the HOH bond angle are fixed at the gas-phase experimental values  $r_{\text{OH}} = 0.09572$  nm and  $\theta_{\text{HOH}} = 104.52^\circ$ . The negative charge sites are located symmetrically along the lone-pair directions at distance  $r_{\text{OL}}$

=0.07 nm and with an intervening angle  $\theta_{LOL}=109.47^\circ$ . A charge of  $+0.241e$  is located on each hydrogen site, while charges of equal magnitude and opposite sign are placed on the lone-pair sites. O atoms on different molecules interact via the Lennard-Jones potential with  $\sigma_O=0.312$  nm and  $\epsilon_O=0.669$  kJ/mol.

TOL: A seven site united-atom model of toluene, consisting of six “ring” C atoms and a methyl group (H atoms are not explicitly represented). In order to handle the constraints more easily, only three mass points were used; one at the ring C attached to the methyl group ( $m=40.065$  u), and one at each of the two “meta” C atoms ( $m=26.038$ ) (note that with this mass distribution, the moment of inertia is not reproduced correctly). Parameters were derived from the information in Ref. 33:  $\epsilon_{\text{ring}}=0.4602$  kJ/mol,  $\epsilon_{\text{methyl}}=0.6694$  kJ/mol,  $\sigma_{\text{ring}}=0.375$  nm, and  $\sigma_{\text{methyl}}=0.391$  nm. The Lorentz–Berthelot rule was used for cross interactions.<sup>33</sup>

## APPENDIX B: CONNECTING FLUCTUATIONS TO THERMODYNAMIC DERIVATIVES

If  $A$  is a dynamical quantity that depends only on the configurational degrees of freedom, then its average in the canonical ensemble ( $NVT$ ) is given by (where, for convenience, we use a discrete-state notation, with  $A_i$  referring to the value of  $A$  in the  $i$ th microstate, etc.)

$$\langle A \rangle = \frac{\sum_i A_i \exp(-\beta U_i)}{\sum_i \exp(-\beta U_i)} = \frac{\sum_i A_i \exp(-\beta U_i)}{Q}, \quad (\text{B1})$$

where  $\beta=1/k_B T$  and  $Q$  is the configurational partition function. Then the inverse temperature derivative of  $\langle A \rangle$  can be written in terms of equilibrium fluctuations as follows:

$$\left( \frac{\partial \langle A \rangle}{\partial \beta} \right)_V = - \frac{\sum_i A_i \exp(-\beta U_i) U_i}{Q} + \frac{\sum_i A_i \exp(-\beta U_i) \sum_j \exp(-\beta U_j) U_j}{Q^2} \quad (\text{B2})$$

$$= - \langle (AU) - \langle A \rangle \langle U \rangle \rangle \quad (\text{B3})$$

$$= - \langle \Delta A \Delta U \rangle. \quad (\text{B4})$$

Now taking  $A=W$  and  $A=U$  successively we find that

$$\left( \frac{\partial \langle W \rangle}{\partial T} \right)_V \bigg/ \left( \frac{\partial \langle U \rangle}{\partial T} \right)_V = \left( \frac{\partial \langle W \rangle}{\partial \beta} \right)_V \bigg/ \left( \frac{\partial \langle U \rangle}{\partial \beta} \right)_V = \frac{\langle \Delta W \Delta U \rangle}{\langle (\Delta U)^2 \rangle}. \quad (\text{B5})$$

This last expression is precisely the formula for the slope obtained by linear regression when plotting  $W$  against  $U$ .

Consider now volume derivatives. Because volume dependence comes in through the microstate values,  $A_i$  and  $U_i$ , and the volume derivatives of these are not necessarily re-

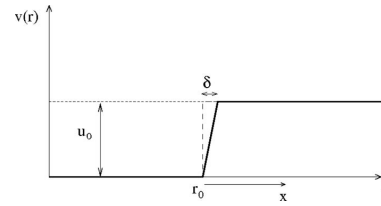


FIG. 13. Illustration of replacement of discontinuous step by a finite slope for the square-well potential for the purpose of calculating the virial. The limit  $\delta \rightarrow 0$  is taken at the end.

lated in a simple way, the corresponding expression is not as simple: The derivative of  $\langle W \rangle$  with respect to volume at fixed temperature is given by

$$\left( \frac{\partial \langle W \rangle}{\partial V} \right)_T = \frac{\partial}{\partial V} (\langle p \rangle V - Nk_B T)_T \quad (\text{B6})$$

$$= \langle p \rangle + V \left( \frac{\partial \langle p \rangle}{\partial V} \right)_T = \langle p \rangle - K_T, \quad (\text{B7})$$

where  $K_T$  is the isothermal bulk modulus. The derivative of  $U$  can be obtained by writing pressure as the derivative of Helmholtz free energy  $F$  ( $K$  is kinetic energy) as follows:

$$\langle p \rangle = - \left( \frac{\partial F}{\partial V} \right)_T = - \left( \frac{\partial (\langle U \rangle + \langle K \rangle - TS)}{\partial V} \right)_T \quad (\text{B8})$$

$$= - \left( \frac{\partial \langle U \rangle}{\partial V} \right)_T + T \left( \frac{\partial S}{\partial V} \right)_T. \quad (\text{B9})$$

Then using the thermodynamic identity  $(\partial S/\partial V)_T = (\partial \langle p \rangle/\partial T)_V \equiv \beta_V$ , we obtain the ratio of volume derivatives of  $\langle W \rangle$  and  $\langle U \rangle$  as follows:

$$\left( \frac{\partial \langle W \rangle}{\partial V} \right)_T \bigg/ \left( \frac{\partial \langle U \rangle}{\partial V} \right)_T = - \frac{K_T - \langle p \rangle}{T\beta_V - \langle p \rangle}, \quad (\text{B10})$$

which becomes  $-K_T/(T\beta_V)$  when the pressure is small compared to the bulk modulus. As discussed in Paper II,  $\beta_V$  can be expressed in terms of  $\langle \Delta U \Delta W \rangle$  again, but the fluctuation expression for  $K_T$  is more complicated. Thus we cannot simply identify the lines of constant  $T$ , varying  $V$ , on a  $\langle W \rangle$ ,  $\langle U \rangle$ -plot, as we could with lines of fixed  $V$ , varying  $T$ , by examining the fluctuations at fixed  $V, T$ .

## APPENDIX C: VIRIAL FOR SQUARE-WELL SYSTEM

Here we derive the expression for the time-averaged virial, Eq. (17), as a convenience for the reader. The idea is to replace the step  $u_0$  in the potential with a finite slope  $u_0/\delta$  over a range  $\delta$ , and take the limit  $\delta \rightarrow 0$ . We start by replacing a two-body interaction in three dimensions with the equivalent one-dimensional, one-body problem using the radial separation  $r$  and the reduced mass  $m_r$ . Let the potential step be at  $r=r_s$  and define  $x=r-r_s$  (see Fig. 13). We consider an “escape event” over a positive step, so that an initial (relative) velocity  $v_0$  becomes a final velocity  $v_1$  and  $r$  goes from a value less than  $r_0$  to a value greater than  $r_0+\delta$ . The resulting formula also applies for the other kinds of events.

The contribution to the time integral of the virial from this event is given by

$$\Delta = \int_0^{t_\delta} \frac{(r_0 + x)}{3} F dt = - \int_0^{t_\delta} \frac{(r_0 + x)u_0}{3\delta} dt, \quad (\text{C1})$$

where  $F$  is the (constant) force in the region  $0 < x < \delta$  and  $t_\delta$  is the time taken for the “particle” (the radial separation) to cross this region. The trajectory  $x(t)$  is given by the standard formula for uniform acceleration

$$x(t) = v_0 t - \frac{1}{2} \frac{u_0}{\delta m_r} t^2, \quad (\text{C2})$$

which by setting  $x(t_\delta) = \delta$  gives the following expression for  $t_\delta$ :

$$t_\delta = \delta \left( \frac{m_r v_0}{u_0} - \sqrt{\left( \frac{m_r v_0}{u_0} \right)^2 - \frac{2m_r}{u_0}} \right); \quad (\text{C3})$$

here we have taken the negative root, appropriate for a positive  $u_0$  (we want the smallest positive  $t_\delta$ ). Returning to  $\Delta$ , it can be split into two parts as follows:

$$\Delta = - \int_0^{t_\delta} \frac{r_0 u_0}{3\delta} dt - \int_0^{t_\delta} \frac{x(t) u_0}{3\delta} dt. \quad (\text{C4})$$

Consider the second term: Using the expression for  $x(t)$  from Eq. (C2), we see that the result of the integral will involve a term proportional to  $t_\delta^2$  and one proportional to  $t_\delta^3$ . Using Eq. (C3) to replace  $t_\delta \propto \delta$ , and noting the  $\delta$  in the denominator, the terms will have linear and quadratic dependences on  $\delta$ , respectively. Thus they will vanish in the limit  $\delta \rightarrow 0$ . On the other hand, the first term gives

$$\begin{aligned} \Delta &= - \frac{r_0 u_0}{3\delta} t_\delta = - \frac{r_0 u_0}{3} \left( \frac{m_r v_0}{u_0} - \sqrt{\left( \frac{m_r v_0}{u_0} \right)^2 - \frac{2m_r}{u_0}} \right) \\ &= \frac{r_0 m_r}{3} (\sqrt{v_0^2 - 2u_0/m_r} - v_0). \end{aligned} \quad (\text{C5})$$

This expression can be simplified by writing it in terms of the change of velocity  $\Delta v \equiv v_1 - v_0$ . In the one-body problem conservation of momentum does not hold, and  $v_1$  is given by energy conservation

$$\frac{1}{2} m_r v_0^2 = \frac{1}{2} m_r v_1^2 + u_0, \quad (\text{C6})$$

from which  $\Delta v$  is obtained as

$$\Delta v \equiv v_1 - v_0 = \sqrt{v_0^2 - 2u_0/m_r} - v_0; \quad (\text{C7})$$

thus, the expression for  $\Delta$  becomes

$$\Delta = \frac{r_0 m_r}{3} \Delta v = \frac{m_r}{3} \mathbf{r} \cdot \Delta \mathbf{v}, \quad (\text{C8})$$

where in the last expression a switch to three-dimensional notation was made, recognizing that for central potentials  $\Delta \mathbf{v}$  will be parallel to the displacement vector between the two particles. This expression, derived for escape events, must also hold for capture events since these are time-reverses of each other, and the virial is fundamentally a configurational quantity, independent of dynamics (the above expression is time-reversal invariant because the change in the radial com-

ponent of velocity is the same either way, since although the “initial” and “final” velocities are swapped, they also have opposite sign). Bounce and collision events may be treated by dividing the event into two parts at the turning point (where the relative velocity is zero), noting that each may be treated exactly as above, then adding the results back together. If we now consider all events that take place during an averaging time  $t_{\text{av}}$ , we get the time-averaged virial as

$$\bar{W} = \frac{1}{3t_{\text{av events } e}} \sum m_{r,e} \mathbf{r}_e \cdot \Delta \mathbf{v}_e. \quad (\text{C9})$$

- <sup>1</sup>L. D. Landau and E. M. Lifshitz, *Statistical Physics, Part I* (Pergamon, London, 1980).
- <sup>2</sup>J. P. Hansen and I. R. McDonald, *Theory of Simple Liquids*, 2nd ed. (Academic, New York, 1986).
- <sup>3</sup>L. E. Reichl, *A Modern Course in Statistical Physics*, 2nd ed. (Wiley, New York, 1998).
- <sup>4</sup>M. P. Allen and D. J. Tildesley, *Computer Simulation of Liquids* (Oxford University Press, Oxford, 1987).
- <sup>5</sup>N. P. Bailey, U. R. Pedersen, N. Gnan, T. B. Schröder, and J. C. Dyre, *J. Chem. Phys.* **129**, 184508 (2008).
- <sup>6</sup>If this seems unphysical, the argument could be given in terms of arbitrary deviations from equilibrium,  $\Delta g(r, t) \equiv g(r, t) - \langle g(r) \rangle$ . See, however, Paper II.
- <sup>7</sup>J. E. Lennard-Jones, *Proc. Phys. Soc. London* **43**, 461 (1931).
- <sup>8</sup>J. D. Weeks, D. Chandler, and H. C. Andersen, *J. Chem. Phys.* **54**, 5237 (1971).
- <sup>9</sup>D. Ben-Amotz and G. Stell, *J. Chem. Phys.* **119**, 10777 (2003).
- <sup>10</sup>U. R. Pedersen, N. P. Bailey, T. B. Schröder, and J. C. Dyre, *Phys. Rev. Lett.* **100**, 015701 (2008).
- <sup>11</sup>D. P. Landau and K. Binder, *A Guide to Monte Carlo Simulations in Statistical Physics*, 2nd ed. (Cambridge University Press, Cambridge, 2005).
- <sup>12</sup>E. Zaccarelli, G. Foffi, K. A. Dawson, S. V. Buldyrev, F. Sciortino, and P. Tartaglia, *Phys. Rev. E* **66**, 041402 (2002).
- <sup>13</sup>H. J. C. Berendsen, D. van der Spoel, and R. van Drunen, *Comput. Phys. Commun.* **91**, 43 (1995).
- <sup>14</sup>E. Lindahl, B. Hess, and D. van der Spoel, *J. Mol. Model.* **7**, 306 (2001).
- <sup>15</sup>Asap, Asap home page, see <http://wiki.fysik.dtu.dk/asap> for more information on MD codes.
- <sup>16</sup>N. P. Bailey, T. Cretegnny, J. P. Sethna, V. R. Coffman, A. J. Dolgert, C. R. Myers, J. Schiøtz, and J. J. Mortensen, e-print arXiv:cond-mat/0601236.
- <sup>17</sup>K. W. Jacobsen, J. K. Nørskov, and M. J. Puska, *Phys. Rev. B* **35**, 7423 (1987).
- <sup>18</sup>K. W. Jacobsen, P. Stoltze, and J. K. Nørskov, *Surf. Sci.* **366**, 394 (1996).
- <sup>19</sup>U. R. Pedersen, T. Christensen, T. B. Schröder, and J. C. Dyre, *Phys. Rev. E* **77**, 011201 (2008).
- <sup>20</sup>M. Dzugutov, *Phys. Rev. A* **46**, R2984 (1992).
- <sup>21</sup>W. Kob and H. C. Andersen, *Phys. Rev. Lett.* **73**, 1376 (1994).
- <sup>22</sup>W. R. P. Scott, P. H. Hunenberger, I. G. Tironi, A. E. Mark, S. R. Billeter, J. Fennen, A. E. Torda, T. Huber, P. Kruger, and W. van Gunsteren, *J. Phys. Chem. A* **103**, 3596 (1999).
- <sup>23</sup>N. P. Bailey, J. Schiøtz, and K. W. Jacobsen, *Phys. Rev. B* **69**, 144205 (2004).
- <sup>24</sup>L. J. Lewis and G. Wahnström, *Phys. Rev. E* **50**, 3865 (1994).
- <sup>25</sup>H. J. C. Berendsen, J. R. Grigera, and T. P. Straatsma, *J. Phys. Chem.* **91**, 6269 (1987).
- <sup>26</sup>E. Zaccarelli, F. Sciortino, and P. Tartaglia, *J. Phys.: Condens. Matter* **16**, 4849 (2004).
- <sup>27</sup>M. W. Mahoney and W. L. Jorgensen, *J. Chem. Phys.* **112**, 8910 (2000).
- <sup>28</sup>Choosing this measure of the slope is equivalent to diagonalizing the correlation matrix (the covariance matrix where the variables have been scaled to have unit variance) to identify the independently fluctuating variable. This is often done in multivariate analysis (see, e.g., Ref. 34), rather than diagonalizing the covariance matrix, when different variables have widely differing variances.
- <sup>29</sup>F. Sciortino, *Nature Mater.* **1**, 145 (2002).
- <sup>30</sup>M. R. Daw and M. I. Baskes, *Phys. Rev. B* **29**, 6443 (1984).
- <sup>31</sup>J. P. Hansen and I. R. McDonald, *Liquid and Liquid Mixtures* (Butterworths, London, 1969).

184507-13 Pressure-energy correlations in liquids. I.

J. Chem. Phys. **129**, 184507 (2008)

<sup>32</sup>W. F. van Gunsteren, S. R. Billeter, A. A. Eising, P. H. Hünenberger, P. Krüger, A. E. Mark, W. R. P. Scott, and I. G. Tironi, *Biomolecular Simulation: The GROMOS96 Manual and User Guide* (Hochschul-Verlag AG an der ETH Zürich, Zürich, 1996).

<sup>33</sup>W. L. Jorgensen, J. D. Madura, and C. J. Swenson, *J. Am. Chem. Soc.* **106**, 6638 (1984).

<sup>34</sup>K. H. Esbensen, D. Guyot, F. Westad, and L. P. Houmøller, *Multivariate Data Analysis—In Practice*, 5th ed. (Camo, Oslo, 2002).



## Pressure-energy correlations in liquids. II. Analysis and consequences

Nicholas P. Bailey,<sup>a)</sup> Ulf R. Pedersen, Nicoletta Gnan, Thomas B. Schröder, and Jeppe C. Dyre

DNRF Center "Glass and Time," IMFUFA, Department of Sciences, Roskilde University, P.O. Box 260, DK-4000 Roskilde, Denmark

(Received 3 July 2008; accepted 25 August 2008; published online 14 November 2008)

We present a detailed analysis and discuss consequences of the strong correlations of the configurational parts of pressure and energy in their equilibrium fluctuations at fixed volume reported for simulations of several liquids in the previous paper [N. P. Bailey *et al.*, J. Chem. Phys. **129**, 184507 (2008)]. The analysis concentrates specifically on the single-component Lennard-Jones system. We demonstrate that the potential may be replaced, at fixed volume, by an effective power law but not simply because only short-distance encounters dominate the fluctuations. Indeed, contributions to the fluctuations are associated with the whole first peak of the radial distribution function, as we demonstrate by an eigenvector analysis of the spatially resolved covariance matrix. The reason the effective power law works so well depends crucially on going beyond single-pair effects and on the constraint of fixed volume. In particular, a better approximation to the potential includes a linear term, which contributes to the mean values of potential energy and virial, but little to their fluctuations, for density fluctuations which conserve volume. We also study in detail the zero temperature limit of the (classical) crystalline phase, where the correlation coefficient becomes very close, but not equal, to unity, in more than one dimension; in one dimension the limiting value is exactly unity. In the second half of the paper we consider four consequences of strong pressure-energy correlations: (1) analyzing experimental data for supercritical argon we find 96% correlation; (2) we discuss the particular significance acquired by the correlations for viscous van der Waals liquids approaching the glass transition: For strongly correlating viscous liquids knowledge of just one of the eight frequency-dependent thermoviscoelastic response functions basically implies knowledge of them all; (3) we reinterpret aging simulations of *ortho*-terphenyl carried out by Mossa *et al.* [Eur. Phys. J. B **30**, 351 (2002)], showing their conclusions follow from the strongly correlating property; and (4) we briefly discuss the presence of the correlations (after appropriate time averaging) in model biomembranes, showing that significant correlations may be present even in quite complex systems. © 2008 American Institute of Physics.

[DOI: 10.1063/1.2982249]

### I. INTRODUCTION

In the companion paper<sup>1</sup> to this work, referred to as Paper I, we detailed the existence of a strong correlation between the equilibrium fluctuations of the configurational parts of pressure and energy in several model liquids. Recall that (instantaneous) pressure  $p$  and energy  $E$  have contributions both from particle momenta and positions,<sup>2</sup>

$$p = Nk_B T(\mathbf{p}_1, \dots, \mathbf{p}_N)/V + W(\mathbf{r}_1, \dots, \mathbf{r}_N)/V, \quad (1)$$

$$E = K(\mathbf{p}_1, \dots, \mathbf{p}_N) + U(\mathbf{r}_1, \dots, \mathbf{r}_N), \quad (2)$$

where  $K$  and  $U$  are the kinetic and potential energies, respectively, and  $T(\mathbf{p}_1, \dots, \mathbf{p}_N)$  is the "kinetic temperature,"<sup>2</sup> proportional to the kinetic energy per particle. The configurational contribution to pressure is the virial  $W$ , which for a translationally invariant potential-energy function  $U$  is defined<sup>2</sup> by

$$W = -\frac{1}{3} \sum_i \mathbf{r}_i \cdot \nabla_{\mathbf{r}_i} U, \quad (3)$$

where  $\mathbf{r}_i$  is the position of the  $i$ th particle. Note that  $W$  has dimension energy. In the case of a pair potential  $U_{\text{pair}} = \sum_{i<j} v(r_{ij})$ , the expression for the virial becomes<sup>2</sup>

$$W_{\text{pair}} = -\frac{1}{3} \sum_{i<j} r_{ij} v'(r_{ij}) = -\frac{1}{3} \sum_{i<j} w(r_{ij}), \quad (4)$$

where  $w(r) \equiv r v'(r)$ .

It is the correlation between  $U$  and  $W$  that we are interested in, quantified by the correlation coefficient

$$R = \frac{\langle \Delta W \Delta U \rangle}{\sqrt{\langle (\Delta W)^2 \rangle} \sqrt{\langle (\Delta U)^2 \rangle}}. \quad (5)$$

Paper I documented the correlation in many systems, showing that this is often quite strong, with correlation coefficient  $R > 0.9$ , while in some other cases it was found to be weak or almost nonexistent. The latter included in particular models with additional significant Coulombic interactions. The purpose of this paper is twofold. First we give a comprehensive

<sup>a)</sup>Electronic mail: nbailey@ruc.dk.

analysis of the source of the correlation in the simplest “strongly correlating” model liquid, the standard single-component Lennard-Jones (SCLJ) fluid. Paper I presented briefly an explanation in terms of an effective inverse power-law potential. Here we elaborate on that in greater detail and go beyond it. Second we discuss a few observable consequences and applications of the strong correlations. These range from their measurement in a real system to applications to systems as diverse as supercooled liquids and biomembranes.

In Sec. II we present a detailed analysis for the SCLJ case, first in terms of an effective inverse power law with exponent  $\sim 18$ . This accounts for the correlation at the level of individual pair encounters by assuming that only the repulsive part of the potential, corresponding to distances less than the minimum of the potential  $r_m$ , is relevant for fluctuations, and that this may be well approximated by an inverse power law. The value 18 is significant since this explains the “slope”  $\gamma$  defined as

$$\gamma \equiv \sqrt{\frac{\langle(\Delta W)^2\rangle}{\langle(\Delta U)^2\rangle}}, \quad (6)$$

observed to be  $\sim 6$  for Lennard-Jones systems (Paper I). The slope is exactly  $n/3$  for a pure inverse power-law potential with exponent  $n$ , a case with perfect  $W, U$  correlation (Paper I). Section II continues with a discussion of the SCLJ crystal, which is also strongly correlating. This would seem to invalidate the dominance of the repulsive part since only presumably distances around and beyond the potential minimum are important, at least at low and moderate pressure. In this case the correlation can be explained only when summation over all pairs is taken into account, thus the correlation emerges as a collective effect. There is a connection between the slope obtained in this way and that given by the effective inverse power law, in fact, they are quite similar. The third subsection in Sec. II gives a more systematic analysis of which regions dominate the fluctuations in the liquid phase using an eigenvector decomposition of the spatially resolved covariance matrix. This matrix represents the contributions to the (co-)variances of potential energy and virial from different pair separations. It is demonstrated that the region around the minimum of the potential plays a substantial role. The final subsection in Sec. II provides a synthesis of the insights from the previous subsections, resulting in an “extended effective power-law approximation,” which includes a linear term. The main point is that a linear term in the pair potential will contribute to the mean values, but not to fluctuations, of  $W$  and  $U$ , if the volume is constant.

In Sec. III we discuss some consequences, starting by considering whether the instantaneous correlations can be related to a measurable quantity in the normal liquid state, and demonstrating this with data for supercritical argon, finding a correlation coefficient of 0.96. Next we focus on consequences for highly viscous liquids, where time-scale separation implies that instantaneous correlation between virial and potential energy can be related to a correlation between the time-averaged pressure and energy. The third subsection dis-

cusses consequences for aging, while the fourth briefly discusses connections with recent work by Heimburg and Jackson on biomembranes.

Finally, Sec. IV concludes with an outlook reflecting on the broader significance of strong correlation and its implications for the understanding of liquids, particularly in the context of viscous liquids (which has been our main motivation throughout this work).

## II. ANALYSIS

### A. The effective inverse power law

In this section we consider the SCLJ system in the hope that it is simple enough that a fairly complete understanding of the cause of strong correlations is possible. Recall that  $R > 0.9$  for a wide range of states (Paper I). In order to understand the numerology better we consider a generalized Lennard-Jones potential, denoted by  $\text{LJ}(a, b)$  ( $a > b$ ),

$$v_{\text{LJ}}^{a,b}(r) \propto (\sigma/r)^a - (\sigma/r)^b, \quad (7)$$

although the standard  $\text{LJ}(12,6)$  case will be used for most examples. Starting from the idea that short distances dominate fluctuations and that the observed correlations are suggestive of a power-law interaction, we show that at a given density, the LJ potential may be approximated by a single effective inverse power law over a range from a little less than  $\sigma$  (where  $v_{\text{LJ}}$  changes sign) to around  $r_m$ , the location of the potential minimum [ $r_m = 2^{1/6}\sigma$  for  $\text{LJ}(12,6)$ ], covering an energy range of approximately  $-\epsilon$  to  $+2\epsilon$ , where  $\epsilon$  is the well-depth. At first sight, one might expect that if this were at all the case, the effective power would be less than  $a$ , somehow a mixture of the two exponents  $a$  and  $b$ . It was noticed by Ben-Amotz and Stell,<sup>3</sup> however, that the repulsive core of the  $\text{LJ}(12,6)$  potential may be approximated by an inverse power law with an exponent of  $\sim 18$ , in agreement with our data (Paper I). To see how we get an exponent greater than  $a$ , note that the exponent  $n$  in an inverse power law can be extracted from different ratios of derivatives,

$$v_{\text{PL}}(r) = Ar^{-n} + B, \quad (8)$$

where  $B$  is a constant. This implies that

$$n = \frac{-rv'_{\text{PL}}(r)}{(v_{\text{PL}}(r) - B)} = \frac{-rv''_{\text{PL}}(r)}{v'_{\text{PL}}(r)} - 1 = \frac{-rv'''_{\text{PL}}(r)}{v''_{\text{PL}}(r)} - 2 = \dots \quad (9)$$

since successive differentiation gives factors of  $n$ , then  $n+1$ , etc. For a potential  $v(r)$ , which is not an inverse power law, these expressions provide different definitions of a local effective power-law exponent [assuming  $v(r) \rightarrow 0$  as  $r \rightarrow \infty$ ],

$$\begin{aligned} n^{(0)}(r) &\equiv -rv'(r)/v(r), \\ n^{(1)}(r) &\equiv -rv''(r)/v'(r) - 1, \\ n^{(2)}(r) &\equiv -rv'''(r)/v''(r) - 2, \\ n^{(p)}(r) &\equiv -rv^{(p+1)}(r)/v^{(p)}(r) - p. \end{aligned} \quad (10)$$

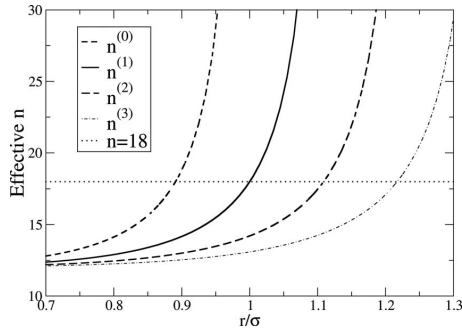


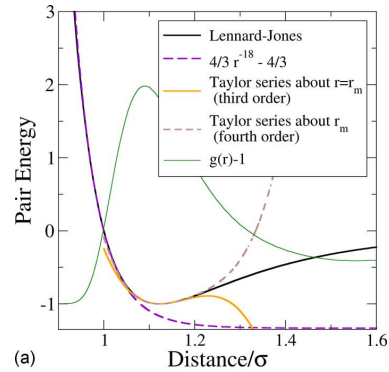
FIG. 1. Effective power-law exponents defined by derivative ratios of different orders [Eqs. (10)] for the standard Lennard-Jones potential LJ(12,6). All converge to 12 at small  $r$ ; they diverge when the derivative in the denominator vanishes, which happens for larger  $r$ , the higher the order of this derivative. The term “effective inverse power law” in this paper refers to a power law chosen to match  $n^{(1)}$  at some point  $r_0 < r_m \sim 1.12\sigma$ , the potential minimum where  $n^{(1)}$  diverges. A convenient choice is to match at  $r = \sigma$ , giving 18. In Secs. II B and II C we show that  $n^{(2)}(r)$  plays an important role in the understanding of fluctuations associated with pair distances close to the potential minimum ( $r_m \sim 1.12\sigma$ ).

A plot of the first four of these is shown in Fig. 1 for LJ(12,6). All converge to  $a=12$  at short  $r$ , as they must. All increase with increasing  $r$  until the denominator vanishes, but more slowly, the higher the order  $p$ . In particular, when  $n^{(p)}$  diverges it is straightforward algebra to show that  $n^{(p+1)}$  has the value  $a+b+p$ . So  $n^{(0)}$  diverges at  $r = \sigma$  where the potential is zero, and is therefore unsuitable for characterizing the range which we expect to dominate the fluctuations, from energy  $+\epsilon$  to energy  $-\epsilon$  (it is also sensitive to the presence of an additive constant, unlike the others). Instead we use  $n^{(1)}$ , which at  $r = \sigma$  (the zero of  $v$  and the divergence of  $n^{(0)}$ ) takes the value  $a+b$ , or 18 for the LJ(12,6). Taking the factor 3 in the denominator of the virial into account, this would explain the slope  $\sim 6$  observed in the simulations (Paper I). However first we should see how well an inverse power law with this exponent actually fits the LJ potential. We denote the point matching point  $r_0$ . With the exponent fixed, we are free to choose the multiplicative constant  $A$  and the additive one  $B$  to match the slope and value at  $r = \sigma = r_0$ ; the resulting expression is  $(4/3)((r/\sigma)^{-18} - 1)$ . This is plotted in Fig. 2(a) along with  $v_{LJ}$ . We can match at different values of  $r$  by finding the expression for  $n^{(1)}(r)$  for the generalized LJ potential,

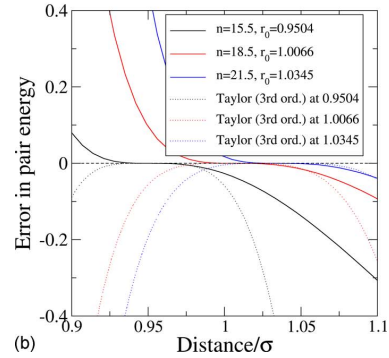
$$n^{(1)}(r) = b + \frac{a-b}{1 - (b/a)(r/\sigma)^{a-b}}, \quad (11)$$

which becomes  $6 + 12/(2 - (r/\sigma)^6)$  for LJ(12,6).<sup>4</sup>

The fact that we can choose a function (an inverse power law in this case) to match a given function and its first two derivatives is nothing special by itself; after all, a Taylor series does the same. Examples of matching power laws and Taylor series up to fourth order, at different values of  $r_0$ , are shown in Fig. 2(b), where the errors  $v_{LJ}(r) - v_{PL}(r)$  or  $v_{LJ}(r) - v_{Taylor}(r)$  are plotted. The magnitude of the errors are similar in the range of  $r$  shown but note that in Taylor series it was necessary to match third derivatives at  $r_0$  to achieve



(a)



(b)

FIG. 2. (Color online) (a) The Lennard-Jones potential  $v_{LJ}(r)$  fitted by an effective power-law potential  $v_{PL}(r) = Ar^{-n} + B$  covering the most important part of the repulsive part of the potential. The exponent  $n$  was chosen to be 18, which optimizes agreement at  $r_0 = \sigma$ , where the effective power law exactly matches not just  $v_{LJ}$  but also its first two derivatives. Also shown are the Taylor series expansions of  $v_{LJ}(r)$  about  $r = r_m$  up to third and fourth orders. The RDF  $g(r) - 1$  (at  $T = 80$  K,  $p = 0$ ) is also shown as a convenient reference for thinking about where contributions to potential energy and virial fluctuations come from. (b) Error made in approximating  $v_{LJ}(r)$  with different effective power laws matched at different points  $r_0$  and with Taylor expansions up to third order about the same point.

this, so the inverse power-law description is more compact. Moreover the power-law representation is much more useful when it comes to representing the fluctuations of total energy and virial because an inverse power law (and therefore the error) flattens out at a constant value at larger  $r$ , whereas the polynomial nature of the Taylor expansion means that away from the point of expansion, the error diverges rapidly [Fig. 2(a)].

We can test the validity of the power-law approximation for representing fluctuations in  $W$  and  $U$  as follows. For the purpose of computing the energy and virial of a configuration due to a pair interaction, all necessary information is contained in the instantaneous radial distribution function (RDF) (Ref. 2)

$$g(r, t) \equiv \frac{2}{N\rho} \sum_{i < j} \delta(r - r_{ij}(t)) / (4\pi r^2), \quad (12)$$

where  $\rho = N/V$  with  $N$  and  $V$  being the number of particles and the system volume, respectively. From this  $U$  and  $W$  may be computed as

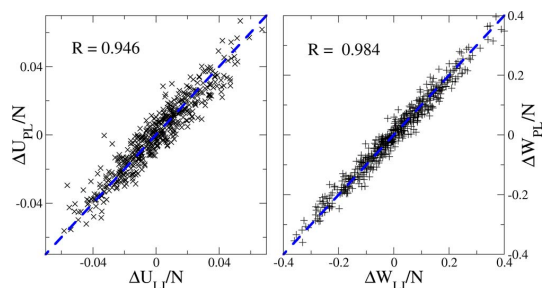


FIG. 3. (Color online) Scatter plot of true and reconstructed potential energy and virial fluctuations (dimensionless units) for the LJ liquid, where the reconstructed values  $U_{PL}$  and  $W_{PL}$  were calculated from the true configurations, assuming an inverse power-law potential with exponent of 19.2; mean values have been subtracted off. The state point is the same as in Fig. 1 of Paper I (zero average pressure,  $NVT$  ensemble). The correlation coefficients are displayed in the figures; the dashed lines indicate slope unity. The fact that actual and reconstructed fluctuations correlate strongly, and with slopes close to unity, support the idea that the  $W, U$  correlation is derived from an effective inverse power-law potential dominating fluctuations.

$$U_{LJ}(t) = \frac{N}{2} \rho \int_0^\infty dr 4\pi r^2 g(r, t) v_{LJ}(r), \quad (13)$$

$$W_{LJ}(t) = -\frac{N}{6} \rho \int_0^\infty dr 4\pi r^2 g(r, t) w_{LJ}(r). \quad (14)$$

Now,  $U_{LJ}(t)$  is rewritten as an inverse power-law potential plus a difference term,  $U_{LJ}(t) = U_{PL}(t) + U_{diff}(t)$ , where

$$U_{PL}(t) = \frac{N}{2} \rho \int_0^\infty dr 4\pi r^2 g(r, t) v_{PL}(r), \quad (15)$$

$$U_{diff}(t) = \frac{N}{2} \rho \int_0^\infty dr 4\pi r^2 g(r, t) (v_{LJ}(r) - v_{PL}(r)), \quad (16)$$

and similarly  $W_{LJ}(t) = W_{PL}(t) + W_{diff}(t)$ . We do not include the additive constant with the power-law approximation; for practical reasons the potential function should be close to zero at a cutoff distance  $r_c$  (adding a constant to  $v_{PL}$  would only add an overall constant to  $U_{PL}$ ). We refer to  $U_{PL}(t)$  and  $W_{PL}(t)$  as “reconstructed” potential energy and virial, respectively, to emphasize that the configurations are drawn from a simulation using the LJ potential, but these quantities are calculated using the inverse power law. In Fig. 3, we show a scatter plot of the true and reconstructed values of  $U$  and  $W$  for the same state point ( $p=0$ ,  $T=80$  K) as was shown in Figs. 1 and 2(a) of Paper I. Here the inverse power-law exponent was chosen to minimize the variances of the difference quantities  $\langle (\Delta U_{diff})^2 \rangle$  and  $\langle (\Delta W_{diff})^2 \rangle$ . These are minimized for  $n=19.3$  and  $19.1$ , respectively, so we choose the value 19.2, which corresponds to matching the potentials at the distance of  $1.015\sigma$ . Note that what are actually plotted are the deviations from the respective mean values—the means  $\langle U_{LJ} \rangle$  and  $\langle U_{PL} \rangle$ , for example, do not coincide. However the fluctuations are clearly highly correlated, and the data lie quite close to the blue dashed lines, marking slope unity. Specifically, the correlation coefficients are 0.946 for the potential energy and 0.984 for the virial. We can also

check how much of the variance of  $U_{LJ}$  is accounted for by  $U_{PL}$ ,  $\langle (\Delta U_{PL})^2 \rangle / \langle (\Delta U_{LJ})^2 \rangle$ , and similarly for  $W$ . This is a sensible quantity because the “PL” and “diff” parts are almost uncorrelated for the choice  $n=19.2$  (cross terms account for less than 1% of the total variance in each case). We find 92% for  $U$  and 95% for  $W$ . Thus we see that the power law gives to a quite good approximation the fluctuations of  $W$  and  $U$ . The correlation follows from this with  $\gamma$  given by one-third of the effective inverse power-law exponent, or 6.4 for this state point. The measured slope [Eq. (6)] was 6.3, corresponding to an effective exponent of 18.9, about 2% smaller than the 19.3. A simpler way to determine the exponent would be three times the slope, although for some applications it could be advantageous to optimize the fit as described here.

## B. Low-temperature limit: Anharmonic vibrations of a crystal

We turn our attention now to the fact that the correlation persists even for the crystallized samples (seen in Paper I in the lower left part of Fig. 4 and in Fig. 6). This is not trivial because the physics of solids, both crystalline and amorphous systems, is generally dominated by fluctuations about mechanically stable structures, and therefore presumably (except perhaps at very high pressure) by the form of the potential near its minimum  $r_m$ , i.e., including distances larger than the minimum. Thus the idea of the effective inverse power law would seem to be inappropriate here, in particular, since the effective exponent  $n^{(1)}$  diverges at  $r_m$ —and there is apparently no reason why one should get a correlation as strong as in the liquid and with so similar a slope. In fact, there is an interval of  $r$  between  $r_m$  and the minimum of the pair virial  $-w(r)/3$  where  $v(r)$  increases and  $-w(r)/3$  decreases, which would lead, if anything, to a negative correlation between  $W$  and  $U$ , when considering individual pair interactions. Moreover, one would expect that a harmonic approximation of the potential near the ground-state configuration would be an accurate representation of the dynamics in the low-temperature limit, but as we will see, the harmonic approximation actually implies negative  $W, U$  correlation, which is not observed. In this subsection we show why the strong positive correlation persists, and why the slope  $\gamma$  changes little going from liquid to crystal (at constant volume). Although the classical dynamics of a crystal is apparently of little importance, since in reality quantum effects dominate, it turns out to be very instructive to consider the low-temperature ( $T \rightarrow 0$ ) classical limit since what we find has significance also in the liquid phase (Sec. II C). The key ideas are (1) that the positive correlation emerges only after summing over all interactions—it is therefore a collective effect rather than a single-pair effect, and (2) the constraint of fixed volume—it is important to recall from Paper I that the virial-potential-energy correlation only appears under fixed-volume conditions; different volumes give approximately the same slope but different offsets (Fig. 4 in Paper I).

### 1. The one-dimensional crystal

For maximum clarity we start by considering the simplest possible case, a one-dimensional (1D) crystal with periodic boundary conditions and only nearest-neighbor interactions. We also suppose that the lattice spacing  $a_c$  is equal to the minimum of the potential; this assumption is not made in the subsequent treatment of the three-dimensional (3D) crystal. In a crystal the particles stay close to their equilibrium positions. It therefore makes sense to expand the pair energy (we have in mind a general pair potential with a single minimum) as a Taylor series, leaving out constant terms but keeping third order terms,

$$\begin{aligned} U &= \sum_i \left( \frac{1}{2} k_2 (r_{i,i+1} - r_m)^2 + \frac{1}{6} k_3 (r_{i,i+1} - r_m)^3 \right) \\ &\equiv \frac{1}{2} k_2 S_2 + \frac{1}{6} k_3 S_3, \end{aligned} \quad (17)$$

where  $r_{i,i+1}$  is the distance between particles  $i$  and  $i+1$ ,  $k_p$  is the  $p$ th derivative of the pair potential at  $r=r_m$ , and we introduce the notation

$$S_p \equiv \sum_i (r_{i,i+1} - r_m)^p.$$

The virial is

$$W = -\frac{1}{3} \sum_i \left( k_2 r_{i,i+1} (r_{i,i+1} - r_m) + \frac{k_3 r_{i,i+1}}{2} (r_{i,i+1} + r_m)^2 \right), \quad (18)$$

which, by writing  $r_{i,i+1} = r_m + (r_{i,i+1} - r_m)$ , can be rewritten as

$$W = -\frac{1}{3} \left( k_2 r_m S_1 + k_2 S_2 + \frac{k_3 r_m}{2} S_2 + \frac{k_3}{2} S_3 \right). \quad (19)$$

Note that  $U$  involves  $S_2$  and  $S_3$  while  $W$  also has a first-order term with  $S_1$ . Evaluating the sum  $S_1$  is very simple:  $r_{i,i+1}$  can be expressed in terms of displacements from the equilibrium positions  $u_i$  as  $r_{i,i+1} = r_m + u_{i+1} - u_i$ , giving for  $S_1$

$$S_1 = \sum_i (u_{i+1} - u_i). \quad (20)$$

Such a sum of consecutive relative displacements gives the change in separation of the two end particles. However the total sum must vanish because by periodic boundary conditions the “end particles” are the same particle (it does not matter which one), therefore  $S_1=0$ . In fact, periodic boundary conditions are not necessary, only that the length is fixed. Since both  $U$  and  $W$  involve at lowest order  $S_2$ , which is positive semidefinite, at sufficiently low temperature we may drop the  $S_3$  terms. Combining Eqs. (17) and (19) we find

$$W = -\frac{1}{3} \frac{k_2 + k_3 r_m/2}{k_2/2} U = \frac{n^{(2)}(r_m)}{3} U, \quad (21)$$

where we have written the coefficient in terms of the  $p=2$  effective power-law exponent defined in Eq. (10). For LJ(a, b) the coefficient evaluates to  $(a+b+1)/3$ , which is 6.33 for LJ(12,6), similar to the observed slope. This short calculation demonstrates the main point: summing over all interactions makes the first-order term in the virial vanish, and the

second-order term is proportional to the second-order term in the potential energy. It is also worth noting that for a purely harmonic crystal we can take  $k_3=0$ , in which case Eq. (21) implies that there is perfect negative correlation, with a slope of  $-2/3$ .

### 2. The three-dimensional crystal

We now generalize this to 3D crystals, which means allowing for transverse displacements. The calculation involves breaking overall sums into sums over 1D chains within the crystal. We also relax the condition that the lattice constant coincides with the potential minimum, which is only realistic at low pressures. We still assume only nearest-neighbor interactions are relevant (this will be justified in the next subsection). Generalization to a disordered (amorphous) solid<sup>5</sup> should be possible, since we observe the correlation to hold also in that case. The calculation would necessitate, however, some kind of disorder averaging, which is beyond the scope of this paper.<sup>6</sup>

We start by considering a simple cubic (sc) crystal of lattice constant  $a_c$ , with interactions only between nearest neighbors, so that the equilibrium bond length is  $a_c$  for all bonds. The fact that such a crystal is mechanically unstable is irrelevant for the calculation. We shall see later that the result applies also to, for instance, a face-centered-cubic (fcc) crystal. We have the same kind of expansions about  $r=a_c$  as above for  $U$  and  $W$ , except a linear term is now included since we no longer assume that  $a_c=r_m$ . An index  $b$  is used to represent nearest-neighbor bonds, and as for the 1D case, we define

$$S_p \equiv \sum_b (r_b - a_c)^p. \quad (22)$$

We then have for  $U$  and  $W$

$$U = \sum_{p=1}^{\infty} \frac{k_p}{p!} \sum_{\text{bonds } b} (r_b - a_c)^p = \sum_{p=1}^{\infty} \frac{k_p}{p!} S_p, \quad (23)$$

$$\begin{aligned} 3W &= \sum_{p=1}^{\infty} -\frac{k_p}{(p-1)!} \sum_{\text{bonds } b} r_b (r_b - a_c)^{p-1} \\ &= -\sum_{p=1}^{\infty} \frac{k_p a_c}{(p-1)!} S_{p-1} - \sum_{p=1}^{\infty} \frac{k_p}{(p-1)!} S_p \\ &= -k_1 a_c S_0 - \sum_{p=1}^{\infty} \left( \frac{k_p}{(p-1)!} + \frac{k_{p+1} a_c}{p!} \right) S_p, \end{aligned} \quad (24)$$

where  $k_p$  is the  $p$ th derivative of the pair potential at  $r=a_c$ . It is convenient to define coefficients  $C_p^U$  and  $C_p^W$  of the dimensionless quantities  $S_p/a_c^p$ ,

$$C_p^U \equiv \frac{k_p a_c^p}{p!}, \quad (25)$$

$$C_p^W \equiv -\left( \frac{k_p a_c^p}{(p-1)!} + \frac{k_{p+1} a_c^{p+1}}{p!} \right). \quad (26)$$

Dropping the constant term  $-k_1 a_c S_0$  in  $W$ , since it plays no role for the fluctuations, we then have

$$U = \sum_{p=1}^{\infty} C_p^U \frac{S_p}{a_c^p}, \quad (27)$$

$$3W = \sum_{p=1}^{\infty} C_p^W \frac{S_p}{a_c^p}. \quad (28)$$

The ratio of the corresponding coefficients is given by the  $p$ th order effective inverse power-law exponent,

$$C_p^W/C_p^U = -\left(p + \frac{k_{p+1}a_c}{k_p}\right) = n^{(p)}(a_c). \quad (29)$$

Thus for in the limit of small  $a_c$ , where these are all similar and close to the repulsive exponent in the potential (Fig. 1), the two expansions will be proportional to each other to an infinite order. Also worth noting for later use is that the  $C_p$ 's in each series increase with  $p$ . For example,

$$C_2^U/C_1^U = \frac{k_2 a_c}{2k_1} = -\frac{1}{2}(n^{(1)}(a_c) + 1), \quad (30)$$

$$C_2^W/C_1^W = \frac{k_2 a_c + k_3 a_c^2/2}{k_1 + k_2 a_c} = -\frac{1}{2}(n^{(1)}(a_c) + 1) \frac{n^{(2)}(a_c)}{n^{(1)}(a_c)}. \quad (31)$$

For  $a_c$  between  $\sigma$  and  $r_m$ , for LJ(12,6), the absolute values of these ratios lie in the intervals 9.5– $\infty$  and 6.7–9.5, respectively.

From dimensional considerations the variance of  $S_p$  is proportional to  $N\sigma_u^{2p}$ , where  $\sigma_u^2 \propto T$  is the variance of single-particle displacements. At low  $T$ , therefore, we expect the  $S_1$  terms to dominate, which causes a problem since  $k_1$  changes its sign at  $r_m$ , corresponding to the divergence of  $n^{(1)}$ . In 1D this was avoided by the exact vanishing of  $S_1$ . In 3D  $S_1$  does not vanish exactly but retains terms second order in displacements, and so contributes similarly to  $S_2$ . It turns out (see below) that  $S_1$  and  $S_2/a_c$  have similar variances and significant positive correlation, but in view of Eqs. (30) and (31) this is not even necessary for a strong  $W$ ,  $U$  correlation—the coefficients of the  $S_1$  are relatively small so that it is still the  $S_2$  terms that dominate. That is essentially the explanation of the strong correlations in the crystal, but we now continue the analysis in more detail in order to investigate how good it becomes in the limit  $T \rightarrow 0$ . These general considerations will be of use again in the following subsection, where we make a similar expansion of the fluctuations in the liquid state.

We need to evaluate  $S_1$  and  $S_2$  in terms of the relative displacements  $\mathbf{u}_b$  of the pair of particles involved in bond  $b$ .<sup>7</sup> We keep only terms up to second order in displacements since we are interested in the limit of low temperatures, so all  $S_3$  terms in the expansion are dropped. In a sc crystal, all nearest-neighbor bonds are parallel to one of the coordinate (crystal) axes. Consider all bonds along the  $x$ -axis. These may be grouped into rows of collinear bonds. The sum along a single row is almost analogous to the 1D case except that the bond length  $r_b$  now also involves transverse displacements,

$$S_p^{\text{row}} = \sum_{b, \text{row}} (r_b - a_c)^p. \quad (32)$$

We write  $r_b$  explicitly in terms of the relative displacements and expand the resulting square root, dropping terms of higher order than the second in  $u$ ,

$$\begin{aligned} r_b - a_c &= ((a_c + u_{b,x})^2 + u_{b,y}^2 + u_{b,z}^2)^{1/2} - a_c \\ &= a_c \left( 1 + \frac{2u_{b,x}}{a_c} + \frac{u_{b,x}^2}{a_c^2} + \frac{u_{b,y}^2 + u_{b,z}^2}{a_c^2} \right)^{1/2} - a_c \\ &= a_c \left( 1 + \frac{1}{2} \left( \frac{2u_{b,x}}{a_c} + \frac{u_{b,x}^2 + u_{b,y}^2 + u_{b,z}^2}{a_c^2} \right) \right. \\ &\quad \left. - \frac{1}{8} \left( \frac{2u_{b,x}}{a_c} \right)^2 \right) - a_c \\ &= u_{b,x} + \frac{u_{b,y}^2 + u_{b,z}^2}{2a_c}. \end{aligned} \quad (33)$$

Now, the sum over bonds in a given row of the parallel displacements  $u_{b,x}$  vanishes for the same reasons as in the 1D case. However when we sum the contributions to  $S_1$  over the row, there are also second-order terms coming from the transverse displacements. Extending the sum to all bonds parallel to the  $x$ -axis, we have part of  $S_1$ , denoted as  $S_1^x$ ,

$$S_1^x = \sum_{b,x} \frac{u_{b,y}^2 + u_{b,z}^2}{2a_c} = \sum_{b,x} \frac{|\mathbf{u}_{b,\perp}|^2}{2a_c}, \quad (34)$$

where  $\perp$  indicates the component of the relative displacement vector perpendicular to the bond direction. Writing it this way allows us to easily include the bonds parallel to the  $y$ - and  $z$ -axes, and the total  $S_1$  is given by

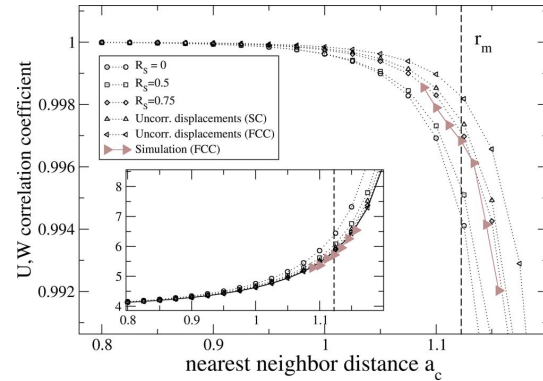


FIG. 4. (Color online) Plots of predicted  $W$ ,  $U$  correlation coefficient for  $T \rightarrow 0$  for a crystal of LJ(12,6) particles for different degrees of correlation between the quantities  $S_1 a_c$  and  $S_2$ , and of low-temperature simulation data. The first three curves (counting from the bottom) assume that the variances of  $S_1 a_c$  and  $S_2$  are equal, and that their correlation coefficients  $R_s$  are 0, 0.5, and 0.75, respectively. The fourth curve (up triangles) results from considering an sc lattice and assuming individual particles have uncorrelated Gaussian-distributed displacements, leading to specific values for the variances and covariance of  $S_1 a_c$  and  $S_2$ . The fifth (left triangles) shows the same estimate for a fcc lattice. The right triangles are data from an NVT simulation of a perfect fcc crystal at  $T=0.0002$  K. The conclusion from this figure is that  $R$  does not tend to unity as  $T \rightarrow 0$ , although it becomes extremely close. The inset shows the corresponding slopes  $\gamma$  [Eq. (6)].

$$S_1 = \sum_b \frac{|\mathbf{u}_{b,\perp}|^2}{2a_c}. \quad (35)$$

Next we calculate  $S_2$  to second order in the relative displacements  $\mathbf{u}_b$ . Starting with  $S_2^x$ , the part containing only bonds in the  $x$ -direction, using Eq. (33) we get

$$S_2^x = \sum_{b,x} u_{b,x}^2 = \sum_{b,x} |\mathbf{u}_{b,\parallel}|^2, \quad (36)$$

where  $\parallel$  means the part of the relative displacement that is parallel to the bond. Including all bonds,

$$S_2 = \sum_b |\mathbf{u}_{b,\parallel}|^2. \quad (37)$$

Now we can return to our expressions for the potential-energy fluctuations [Eqs. (23) and (24)], keeping only terms in  $S_1$  and  $S_2$ ,

$$\Delta U = k_1 S_1 + \frac{k_2}{2} S_2 = \frac{k_1}{2a_c} \sum_b |\mathbf{u}_{b,\perp}|^2 + \frac{k_2}{2} \sum_b |\mathbf{u}_{b,\parallel}|^2. \quad (38)$$

Similarly, for the virial

$$\begin{aligned} 3W &= -k_2 a_c S_1 - \frac{k_3 a_c}{2} S_2 - k_1 S_1 - k_2 S_2 \\ &= -\left(\frac{k_1}{2a_c} + \frac{k_2}{2}\right) \sum_b |\mathbf{u}_{b,\perp}|^2 - \left(k_2 + \frac{k_3 a_c}{2}\right) \sum_b |\mathbf{u}_{b,\parallel}|^2. \end{aligned} \quad (39)$$

### 3. Statistics of $S_1$ and $S_2$

It is clear that the  $\parallel$  and  $\perp$  sums are not equal, although they must be correlated to some extent. If written in terms of

single-particle displacements rather than relative displacements for bonds, a term such as  $|\mathbf{u}_{b,\parallel}|^2$  for a bond in the  $x$ -direction becomes

$$(u_{\mathbf{R}+a_c \hat{x}} - u_{\mathbf{R},x})^2 = u_{\mathbf{R}+a_c \hat{x}}^2 + u_{\mathbf{R},x}^2 - 2u_{\mathbf{R}+a_c \hat{x}} u_{\mathbf{R},x}, \quad (40)$$

where  $\mathbf{R}$  is a lattice vector used to index particles. Summing over bonds gives

$$S_2 = 2 \sum_{\mathbf{R}} |\mathbf{u}_{\mathbf{R}}|^2 - 2 \sum (\text{para. cross terms}), \quad (41)$$

where the cross terms are products of the parallel components of displacements on neighboring particles. For  $S_1$  we have something similar,

$$S_1 a_c = 2 \sum_{\mathbf{R}} |\mathbf{u}_{\mathbf{R}}|^2 - 2 \sum (\text{perp. cross terms}), \quad (42)$$

where here the cross terms involve transverse components. Since the term  $\sum_{\mathbf{R}} |\mathbf{u}_{\mathbf{R}}|^2$  appears in both  $S_1$  and  $S_2$ , these are correlated to some extent, but not 100% since different cross terms appear (note that if it were 100%, then  $W$  and  $U$  would both be proportional to  $S_2 \propto S_1$  and also correlated 100%). Before considering as to what extent they are correlated, let us see how much of a difference it makes. Suppose the quantities  $S_1 a_c$  and  $S_2$  have variances  $\sigma_1^2$  and  $\sigma_2^2$ , respectively, and are correlated with correlation coefficient  $R_S$ . Using the coefficients introduced in Eqs. (25) and (26)

$$U a_c^2 = C_1^U (S_1 a_c) + C_2^U S_2, \quad (43)$$

$$3W a_c^2 = C_1^W (S_1 a_c) + C_2^W S_2.$$

From this we obtain an expression for the  $W, U$  correlation coefficient by forming the appropriate products and taking averages,

$$R = \frac{C_1^U C_1^W \sigma_1^2 + C_2^U C_2^W \sigma_2^2 + (C_1^U C_2^W + C_1^W C_2^U) \sigma_1 \sigma_2 R_S}{\sqrt{(C_1^U)^2 \sigma_1^2 + (C_2^U)^2 \sigma_2^2 + 2C_1^U C_2^U \sigma_1 \sigma_2 R_S} \sqrt{(C_1^W)^2 \sigma_1^2 + (C_2^W)^2 \sigma_2^2 + 2C_1^W C_2^W \sigma_1 \sigma_2 R_S}}. \quad (44)$$

This estimation of  $R$  is plotted in Fig. 4 as a function of lattice constant for  $R_S=0, 0.5$  and  $0.75$ , for the case  $\sigma_1=\sigma_2$ . Clearly the value of  $R_S$  makes little difference in the region of interest,  $a_c \sim r_m$  or less, where  $R$  is above 0.99. Note that all curves drop dramatically as the lattice constant approaches the inflection point ( $k_2=0$ ) of the potential (the precise value at which  $R$  becomes zero depends on the statistics of  $S_1 a_c$  and  $S_2$ ). In this regime, however, higher-order terms in displacements, including  $S_3, S_4$ , etc., become more important, and because of Eq. (29) their inclusion tends to restore  $R$  to a high value (we have not calculated their effect in detail). Also plotted is the estimation of  $R$  obtained by assuming that particle displacements are uncorrelated and Gaussian distributed with variance  $\sigma_u^2$  for each (Cartesian) component, corresponding to an Einstein model of the vibrational dynamics. In this case tedious but straightforward al-

gebra allows the means and (co-)variances of  $S_1 a_c$  and  $S_2$  to be calculated explicitly for a given lattice. The results for sc and fcc are given in Table I. Notice that the variance of  $S_2$  is somewhat larger than that of  $S_1 a_c$ , while their means are equal. This can be traced to the fact that the latter contains

TABLE I. Statistics of  $S_1 a_c$  and  $S_2$  assuming uncorrelated particle displacements with variance  $\sigma_u^2$  for each Cartesian component, for sc and fcc lattices.

	sc	fcc
$\langle S_1 a_c \rangle$	$6N\sigma_u^2$	$12N\sigma_u^2$
$\langle S_2 \rangle$	$6N\sigma_u^2$	$12N\sigma_u^2$
$\text{var}(S_1 a_c)$	$30N\sigma_u^4$	$108N$
$\text{var}(S_2)$	$36N\sigma_u^4$	$120N$
$\text{cov}(S_1 a_c, S_2)$	$24N\sigma_u^4$	$96N$
$R_S$	0.73	0.84

twice as many cross terms as the former, and a factor of  $1/2$ , so the contribution from such terms to the mean is the same in both cases, while the contribution to the variance is smaller for  $S_1 a_c$ . From the (co-)variances we find the correlation coefficient  $R_S=0.73$  and  $R_S=0.84$  for the sc and fcc cases, respectively. These are also plotted in Fig. 4. A more exact calculation would take into account the true normal modes of the crystal but would yield little of use: Data from the crystal simulations at very low temperature, also plotted in Fig. 4 agree within estimated numerical errors with both the sc and fcc estimates. The key point of this figure—that  $R$  is close to but less than 1—apparently would change little by taking the true crystal dynamics into account. In particular, it is important to note that if  $R=1$  exactly, then this would be true no matter what kind of weighted average of configurations is taken (what kind of ensemble), so a value less than unity in the Einstein approximation is sufficient to disprove the hypothesis that  $R \rightarrow 1$  as  $T \rightarrow 0$ .

#### 4. The role of the coefficients $C_{1,2}^{U,W}$

Since the detailed statistics of  $S_1$  and  $S_2$  have little effect on the  $W, U$  correlation, it must be mainly due to the numerical values of the coefficients  $C_{1,2}^{U,W}$ . We can estimate the effect of these by assuming that  $S_1 a_c$  and  $S_2$  have equal variance and are uncorrelated ( $R_S=0$ ). Then according to Eq. (44) the  $W, U$  correlation coefficient is

$$R = \frac{C_1^U C_1^W + C_2^U C_2^W}{\sqrt{(C_1^U)^2 + (C_2^U)^2} \sqrt{(C_1^W)^2 + (C_2^W)^2}}, \quad (45)$$

which has the form of the cosine of the angle between two vectors  $\mathbf{C}^U \equiv (C_1^U, C_2^U)$  and  $\mathbf{C}^W \equiv (C_1^W, C_2^W)$ . Thus the closeness of  $R$  to unity indicates that these vectors are nearly parallel. The tangents of the angles these vectors make with the  $C_1$  axis in  $(C_1, C_2)$ -space are given by Eqs. (30) and (31); clearly the two angles become equal in the limit of small  $a_c$ , where  $n^{(1)}$  and  $n^{(2)}$  converge. On the other hand, for  $a_c \sim r_m$  where  $k_1=0$  and  $n^{(1)}$  diverges, the two vectors are

$$\begin{aligned} \mathbf{C}^U &= (0, k_2/2) a_c^2, \\ \mathbf{C}^W &= -(k_2, k_2 + k_3 a_c/2) a_c^2 \\ &= -k_2 a_c^2 \left(1, 1 - \frac{1}{2}(n^{(2)} + 2)\right) \\ &= k_2 a_c^2 \left(-1, \frac{n^{(2)}}{2}\right). \end{aligned} \quad (46)$$

Clearly  $\mathbf{C}^U$  is parallel to the  $C_2$  axis, while  $\mathbf{C}^W$  deviates from it by an angle of the order of  $2/n^{(2)} \sim 1/10$ . The  $W, U$  correlation coefficient is then  $R = \cos(1/10) \sim 1 - \frac{1}{2}(1/10)^2 \sim 0.995$ , in agreement with the bottom curve (circles) in the main part of Fig. 4. In this case ( $a_c = r_m$ ,  $k_1=0$ ,  $S_1 a_c$  and  $S_2$  uncorrelated with equal variance), we can obtain a simple expression for the slope

$$\begin{aligned} \gamma &= \sqrt{\frac{(C_1^W)^2 + (C_2^W)^2}{(C_1^U)^2 + (C_2^U)^2}} \\ &= \frac{k_2}{3} \sqrt{\frac{1 + (n^{(2)}/2)^2}{(k_2/2)^2}} \\ &= \frac{2}{3} \sqrt{1 + (n^{(2)}/2)^2} \sim \frac{n^{(2)}}{3} \end{aligned} \quad (47)$$

consistent with the result from the 1D case.

Thus when we look at the “collective” correlations in the crystal, we naturally get a slope involving the effective power-law exponent  $n^{(2)}$ . Since the latter evaluated at the potential minimum is similar to  $n^{(1)}$  at the zero of the potential, the slope is similar to that seen in the liquid phase. On the other hand, it is more typical to think about crystal dynamics starting from a harmonic approximation, adding in anharmonic terms when necessary for higher accuracy. How does it work here? If we set  $k_3=0$  as well as  $k_1=0$ , so we consider the purely harmonic system with the nearest-neighbor distance at the minimum of the potential, then we have  $\mathbf{C}^U = (0, k_2/2)$  and  $\mathbf{C}^W = -(k_2/3)(1, 1)$ . These are not close to being parallel, so the correlation will be weaker (coming mainly from that of  $S_1$  and  $S_2$ ) but more particularly, it will be negative, thus qualitatively different from the anharmonic case. Thus the presence of the  $k_3$  affects the results at arbitrarily low temperature, so the harmonic approximation is never good enough. This is reminiscent of thermal expansion, which does not occur for a purely harmonic crystal. In fact, the Grüneisen parameter for a 1D crystal with nearest neighbor interactions may be shown<sup>8</sup> to be equal to  $1 + n^{(2)}(a_c)/2$ .

Finally we consider the more realistic fcc crystal. First note that Eqs. (35) and (37) are unchanged as long as  $a_c$  is now interpreted as the nearest-neighbor distance rather than the cubic lattice spacing: Each position in a fcc lattice has 12 nearest neighbors, four located in each of three mutually orthogonal planes. Taking the  $xy$  and parallel planes first, the neighbors are located along the diagonal directions with respect to the cubic crystal axes. As before we can do the sum first over bonds forming a row, then over all parallel rows. For a given plane there are two orthogonal sets of rows, but the form of the sums in Eqs. (35) and (37) includes all bonds. The results of the calculation of (co-)variances of  $S_1$  and  $S_2$  in the Einstein model of the dynamics are changed in a way that, in fact, increases their mutual correlation and therefore the  $W, U$  correlation, as shown in Table I and Fig. 4.

To summarize this subsection, the correlation in the crystal is an anharmonic effect that persists in the limit  $T \rightarrow 0$ . It works because (1) the constraint of fixed volume causes the terms in  $U$  and  $W$  that are first order in particle displacements to cancel and (2) the coefficients of the “transverse” second-order terms are small compared to those of the “parallel” ones, a fact which can be traced to the resemblance of the potential to a power law at distances shorter than the potential minimum. “Small” here means of the order of  $1/10$ , which leads to over 99% correlation because  $R$  is essentially the cosine of this quantity. In one dimension there

are no transverse displacements and the correlation is 100% as  $T \rightarrow 0$ ; in more than one dimension as  $T \rightarrow 0$  the correlation is very close to unity but never 100%.

To gain a more complete insight into the fluctuations, we next present an analysis that clarifies exactly the contributions to fluctuations from different distances, without approximations, now again with the liquid case in mind.

### C. Fluctuation modes

In the last two subsections we considered single-pair effects (associated with  $r < r_m$ ) and collective effects (associated with  $r \sim r_m$ ), respectively. In this section we focus on contributions from particular pair separations without keeping track of which actual particles are involved. We identify the contributions to  $U$  and  $W$  coming from all pairs whose separation lies within a fixed small interval of separations  $r$ ; fluctuations in the number of such pairs generate fluctuations in the contributions. By considering all intervals we can systematically analyze the variances and covariances of  $U$  and  $W$  in terms of pair separation, which is the purpose of this section.

The instantaneous values of  $U$  and  $W$  are given by Eq. (13) and (14), generalized to an arbitrary pair potential. By taking a time (or ensemble) average we get the corresponding expressions for  $\langle U \rangle$  and  $\langle W \rangle$  in terms of  $g(r) \equiv \langle g(r, t) \rangle$ , the usual thermally averaged RDF. Now we consider the variances  $\langle (\Delta U)^2 \rangle$  and  $\langle (\Delta W)^2 \rangle$ , and the covariance  $\langle \Delta U \Delta W \rangle$ . Starting with, for example,  $\Delta U(t) = 4\pi\rho N/2 \int_0^\infty dr r^2 v(r) \Delta g(r, t)$ , where  $\Delta g(r, t) \equiv g(r, t) - g(r)$ , averaging and taking everything except  $\Delta g(r, t)$  outside the average, we have

$$\begin{aligned} \langle (\Delta U)^2 \rangle &= (4\pi\rho N/2)^2 \int_0^\infty dr_1 r_1^2 \int_0^\infty dr_2 r_2^2 v(r_1)v(r_2) \\ &\quad \times \langle \Delta g(r_1, t) \Delta g(r_2, t) \rangle, \end{aligned} \quad (48)$$

$$\begin{aligned} \langle (\Delta W)^2 \rangle &= (4\pi\rho N/2)^2 \int_0^\infty dr_1 r_1^2 \int_0^\infty dr_2 r_2^2 w(r_1)w(r_2) \\ &\quad \times \langle \Delta g(r_1, t) \Delta g(r_2, t) \rangle, \end{aligned} \quad (49)$$

$$\begin{aligned} \langle \Delta U \Delta W \rangle &= (4\pi\rho N/2)^2 \int_0^\infty dr_1 r_1^2 \int_0^\infty dr_2 r_2^2 v(r_1)w(r_2) \\ &\quad \times \langle \Delta g(r_1, t) \Delta g(r_2, t) \rangle. \end{aligned} \quad (50)$$

Clearly the quantity, which contains the essential statistical information about the fluctuations, is  $\langle \Delta g(r_1, t) \Delta g(r_2, t) \rangle$ , the covariance of the RDF with itself. Its magnitude is inversely proportional to  $N$ , so that  $\langle (\Delta U)^2 \rangle$  is proportional to  $N$ , as it should be. The variances of  $U$  and  $W$  and their covariance are integrals of this function with different weightings. To make further progress, we integrate the integrands for the variances over  $M \times M$  “blocks” in  $r_1, r_2$ -space. This is equivalent to considering the energy, say, as the following sum of  $M$  interval energies,

$$U(t) = \sum_{a=1}^M U_a(t), \quad (51)$$

where the interval energy  $U_a(t)$  is defined as the integral between boundaries  $r_a$  and  $r_{a+1}$ ,

$$U_a(t) \equiv \frac{N}{2} \rho \int_{r_a}^{r_{a+1}} dr 4\pi r^2 g(r, t) v(r). \quad (52)$$

The virial can be similarly represented as a sum of contributions from the same  $r$ -intervals,  $W(t) = \sum_{a=1}^M W_a(t)$ . From now on we consider the primary fluctuating quantities to be  $U_a(t)$  and  $W_a(t)$  and seek to understand the correlation between their respective sums in terms of correlations between particular  $U_a$ s and  $W_a$ s. In order to achieve a reasonable degree of spatial resolution, we do not make the intervals (blocks) too big, and choose an interval width of 0.05. This gives  $M=42$  intervals:  $U_1$  is the contribution to the energy coming from pairs with separation in the range of 0.85–0.9, marking the lower limit of nonzero RDF, while  $U_{42}$  refers to the range 2.9–2.95, marking the cutoff distance of the potential used here. We shall see explicitly that only distances up to around 1.4 contribute significantly to the fluctuations. We denote deviations from the mean as, e.g.,  $\Delta U_a = U_a - \langle U_a \rangle$  with the angle brackets representing the time (or ensemble) average.

We are interested in the covariance of the  $U_a$ 's with themselves (including  $\langle \Delta U_a \Delta U_b \rangle$ ,  $a \neq b$ ), the  $W_a$ 's with themselves, and the  $U_a$ 's with the  $W_a$ 's. These covariances are just what is obtained by integrating the integrands in Eqs. (48)–(50) over the block defined by the corresponding intervals for  $r_1$  and  $r_2$ . These values are conveniently represented using matrices  $\Delta^{UU}$ ,  $\Delta^{WW}$ , and  $\Delta^{UW}$  defined as

$$(\Delta^{UU})_{ab} = \langle \Delta U_a \Delta U_b \rangle, \quad (53)$$

$$(\Delta^{WW})_{ab} = \langle \Delta W_a \Delta W_b \rangle, \quad (54)$$

and

$$(\Delta^{UW})_{ab} = \langle \Delta U_a \Delta W_b \rangle. \quad (55)$$

Note that the sum of all elements of  $\Delta^{UU}$  is the energy variance since it reproduces the double integral of Eq. (48); similarly, for the other two matrices

$$\langle (\Delta U)^2 \rangle = \sum_{a,b} (\Delta^{UU})_{ab}, \quad (56)$$

$$\langle (\Delta W)^2 \rangle = \sum_{a,b} (\Delta^{WW})_{ab}, \quad (57)$$

$$\langle \Delta U \Delta W \rangle = \sum_{a,b} (\Delta^{UW})_{ab}. \quad (58)$$

At this point we make one further transformation. Define new matrices  $\Delta^{UU*}$ ,  $\Delta^{WW*}$ , and  $\Delta^{UW*}$  by

$$\Delta^{UU*} \equiv \Delta^{UU} / \langle (\Delta U)^2 \rangle, \quad (59)$$

$$\Delta^{WW*} \equiv \Delta^{WW} / \langle (\Delta W)^2 \rangle, \quad (60)$$

and

TABLE II. First ten eigenvalues of the supercovariance matrix [Eq. (65)], their fractional contributions to the three (co-)variances [Eqs. (62)–(64)], and their effective slopes [Eq. (67)] for the SCLJ liquid with parameters as in Fig. 1 of Paper I ( $\rho=34.6$  mol/l,  $T=80$  K). Contributions from the dominant four eigenvectors are in boldface. The last three rows list sums of the third, fourth, and fifth columns over, respectively, the dominant four, the first ten, and all  $2M$  eigenvectors. The sum of the fifth column over all eigenvectors should be compared [see Eq. (64)] to the  $R=0.939$  listed in Table I of Paper I.

Index	Eigenvalue	$U$ -var. contr.	$W$ -var. contr.	Corr. coeff. contr.	Effective slope
1	1.73	0.01	0.01	0.01	5.38
2	1.55	0.04	0.06	0.05	7.63
3	<b>1.11</b>	<b>0.24</b>	<b>0.15</b>	<b>0.19</b>	<b>4.98</b>
4	<b>0.87</b>	<b>0.25</b>	<b>0.25</b>	<b>0.25</b>	<b>6.34</b>
5	<b>0.78</b>	<b>0.20</b>	<b>0.14</b>	<b>0.17</b>	<b>5.27</b>
6	<b>0.58</b>	<b>0.11</b>	<b>0.17</b>	<b>0.13</b>	<b>7.80</b>
7	0.34	0.02	0.05	0.03	10.14
8	0.23	0.01	0.03	0.01	13.67
9	0.13	0.00	0.01	0.00	116.19
10	0.10	0.01	0.00	−0.00	−3.63
$\Sigma_{3,\dots,6}$	...	0.797	0.709	0.742	...
$\Sigma_{1,\dots,10}$	...	0.884	0.877	0.849	...
$\Sigma_{1,\dots,2M}$	...	1.000	1.000	0.938	...

$$\Delta^{UW*} \equiv \Delta^{UW} / \sqrt{\langle(\Delta U)^2\rangle\langle(\Delta W)^2\rangle}. \quad (61)$$

This is equivalent to normalizing the  $U_a$ 's by the standard deviation  $\sqrt{\langle(\Delta U)^2\rangle}$  and the  $W_a$ 's by  $\sqrt{\langle(\Delta W)^2\rangle}$ , respectively. The elements of  $\Delta^{UU*}$ ,  $\Delta^{WW*}$ , and  $\Delta^{UW*}$  can be thought of as representing, in some sense, what fraction of the total (co-)variance is contributed by the corresponding block. Normalized in this way, the sum over all elements of  $\Delta^{UU*}$  and  $\Delta^{WW*}$  is exactly unity and that for  $\Delta^{UW*}$  equals the correlation coefficient  $R$ ,

$$\sum_{a,b} (\Delta^{UU*})_{ab} = 1, \quad (62)$$

$$\sum_{a,b} (\Delta^{WW*})_{ab} = 1, \quad (63)$$

$$\sum_{a,b} (\Delta^{UW*})_{ab} = R. \quad (64)$$

To make a direct analysis of all possible covariances, we now construct a larger  $2M \times 2M$  matrix by placing  $\Delta^{UU*}$  and  $\Delta^{WW*}$  on the diagonal blocks, and  $\Delta^{UW*}$  and its transpose on the off-diagonal blocks,

$$\Delta^{\text{Sup}} \equiv \begin{bmatrix} \Delta^{UU*} & \Delta^{UW*} \\ (\Delta^{UW*})^T & \Delta^{WW*} \end{bmatrix}. \quad (65)$$

This “supercovariance” matrix contains all the information about the covariance of the contributions of energy and virial with each other. This symmetric and positive semidefinite<sup>9</sup> matrix can be separated into additive contributions by spectral decomposition as

$$\Delta^{\text{Sup}} = \sum_{\alpha} \lambda_{\alpha} v_{\alpha} v_{\alpha}^T, \quad (66)$$

where  $v_{\alpha}$  is the normalized eigenvector whose (non-negative) eigenvalue is  $\lambda_{\alpha}$ —this follows from the diagonalization of the matrix. Thus we decompose the supercovariance into a sum of parts. This method of accounting for the

variance of many variables is the basis of the technique known as principal component analysis (PCA), which is a workhorse of multivariate data analysis.<sup>10</sup> The eigenvectors represent statistically independent “modes of fluctuation;” the corresponding eigenvalue is the part of the variance within the  $2M$ -dimensional space accounted for by the mode. PCA is most effective when the eigenvectors associated with the largest few eigenvectors account for most of the variance in the set of fluctuating quantities. For example, in the extreme case where one eigenvector accounts for over 99% of the variance, we could claim that all the different apparently random fluctuations of the different contributions to energy and virial were moving in a highly coordinated way, such that a single parameter (say, the value of any one of them) would be enough to give the values of all.

In our case we are not necessarily interested in the modes with the largest eigenvalues: a large eigenvalue could describe a fluctuation mode where the individual  $U_a$ 's and  $W_a$ 's change a lot but their respective sums do not; this would correspond to the contributions from one interval increasing while those in others decrease, in such a way that the total is roughly constant. What we really want are those modes that contribute a lot to the variance in energy and virial and to their covariance. This is easy to do by summing all elements in the appropriate block of the matrix  $\lambda_{\alpha} v_{\alpha} v_{\alpha}^T$ , where  $v_{\alpha}$ ,  $\lambda_{\alpha}$  are the normalized eigenvector and eigenvalue in question.<sup>11</sup> In Table II we list the first ten eigenvalues in decreasing order, along with their contributions to the normalized variances of energy, virial, and their covariance—the normalized covariance being equal to  $R_{WU}$ . In addition, an “effective slope” for each mode is obtained from the  $\alpha$ th eigenvector as

$$\gamma_{\alpha} = \sqrt{\frac{\langle(\Delta W)^2\rangle \sum_{a=M+1}^{2M} (v_{\alpha})_a}{\langle(\Delta U)^2\rangle \sum_{b=1}^M (v_{\alpha})_b}} = \gamma \frac{\sum_{a=M+1}^{2M} (v_{\alpha})_a}{\sum_{b=1}^M (v_{\alpha})_b}, \quad (67)$$

where the numerator gives the sum of virial contributions for that mode, and the denominator the sum of energy contribu-

tions. The factor in front, which is numerically equal to the overall slope  $\gamma$ , accounts for the standard deviation that we normalized the  $U_a$ 's and  $W_a$ 's to define the matrices  $\Delta^{UU*}$ ,  $\Delta^{WW*}$ , and  $\Delta^{UW*}$ .

In the above equation, it looks like  $\gamma_\alpha$  is determined by the overall  $\gamma$ , whereas we could expect more the opposite, that the overall slope is somehow an average of the individual effective mode slopes. It looks like this because of the normalization choice we made in determining the decomposition. We can relate the  $\gamma_\alpha$  to the  $\gamma$  in a more meaningful way by writing the sums in Eqs. (62) and (63) in terms of the spectral decomposition Eq. (66),

$$1 = \frac{\sum_{a,c} \Delta_{a,c}^{WW}}{\sum_{b,d} \Delta_{b,d}^{UU}} = \frac{\sum_{\alpha} \sum_{a,c > M} \lambda_{\alpha} (v_{\alpha})_a (v_{\alpha})_c}{\sum_{\beta} \sum_{b,d \leq M} \lambda_{\beta} (v_{\beta})_b (v_{\beta})_d} \quad (68)$$

$$= \frac{\sum_{\alpha} \lambda_{\alpha} (\sum_{a > M} (v_{\alpha})_a)^2}{\sum_{\beta} \lambda_{\beta} (\sum_{b \leq M} (v_{\beta})_b)^2} \quad (69)$$

$$= \frac{\sum_{\alpha} \lambda_{\alpha} (\gamma_{\alpha} / \gamma)^2 (\sum_{a \leq M} (v_{\alpha})_a)^2}{\sum_{\beta} \lambda_{\beta} (\sum_{b \leq M} (v_{\beta})_b)^2}, \quad (70)$$

where in the last step Eq. (67) was used. Multiplying both sides by  $\gamma^2$  we get an expression for the latter as a weighted average of the squares of the  $\gamma_{\alpha}$ ,

$$\gamma^2 = \frac{\sum_{\alpha} X_{\alpha} \gamma_{\alpha}^2}{\sum_{\beta} X_{\beta}}, \quad (71)$$

where the weight of a given mode slope  $\gamma_{\alpha}$  is (apart from normalization)  $X_{\alpha} \equiv \lambda_{\alpha} (\sum_{a \leq M} (v_{\alpha})_a)^2$ , combining the eigenvalue and the square of the summed “energy part” of the corresponding eigenvector.

Now we can notice that the third, fourth, fifth, and sixth eigenvectors, to be referred to respectively as EV3, EV4, EV5, and EV6, account for most of the (co-)variances (totalling 0.80 out of 1.00, 0.71 out of 1.00, and 0.74 out of 0.94 for variance of  $U$ , variance  $W$ , and correlation coefficient, respectively). These four eigenvectors are represented in Fig. 5. We observe that, as expected, most of the fluctuations are associated with pair separations well within the first peak of the RDF, which extends to nearly  $r = 1.6\sigma$  [see Fig. 2(a)]. In fact, not much takes place beyond  $r = 1.3\sigma$ . Interestingly, of the four, EV5, accounting for less than 20% of the variances, is the only one that directly fits the idea that the fluctuations take place at short distances, while the other modes extend out to  $r \sim 1.3\sigma$ , beyond even the inflection point of the potential (around  $1.24\sigma$ ).

It is instructive to repeat the fluctuation mode analysis for a nonstrongly correlating liquid, the Dzugutov liquid at  $T = 0.65$ . We do not show the full results here but they can be summarized as follows. There are two modes that are concentrated at distances less than and around the first minimum of the potential. These have slopes of 5.73 and 5.01 and contribute a total of about 0.35–0.4 to the variances and correlation coefficient. Since the latter is 0.585 at this temperature, these modes account for most of it. There are four more modes that contribute more than 5% to the variances, but the slopes are quite different:  $-9.34$ ,  $7.20$ ,  $28.43$ , and  $-0.67$ . These four modes all include significant contributions at dis-

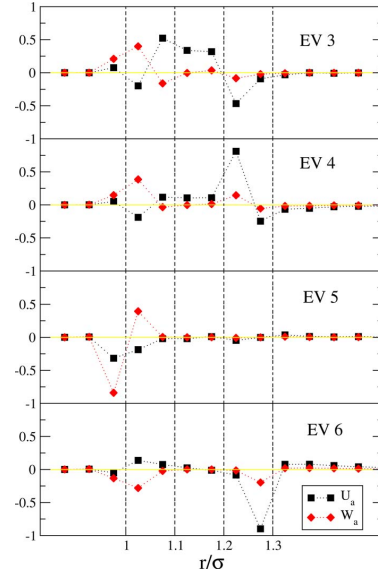


FIG. 5. (Color online) Representations of the eigenvectors 3, 4, 5, and 6 of the supercovariance matrix. Squares represent variation in  $U_a$  values for a mode; diamonds represent variation in  $W_a$  values.

tances corresponding to the peak in  $v(r)$ ; clearly this extra peak in the potential and the associated peak in the pair-virial  $w(r)$  give rise to components in the fluctuations which cannot be related in the manner of an effective inverse power law, even though fluctuations occurring around the minimum can. As a result the overall correlation is rather weak.

#### D. Synthesis: Why the effective power law works even at longer distances

We can apply ideas similar to those used in the crystal analysis to understand why the correlation holds even for modes active at separations larger than the minimum, why the slopes are similar to the effective power-law slopes, and why the effective power law works as well as it does. Recall the essential ingredients of the crystal analysis: the importance of summing over all pairs, the fixed-volume constraint, and the increase in the magnitude of coefficients of the Taylor expansion with order. These are equally valid here, but now we use them to constrain the allowed deviations in  $g(r)$  from its equilibrium value, instead of displacements from a fixed equilibrium configuration. Define the resolved pair-density  $\rho(r)$  by

$$\rho(r) \equiv (N/2) 4\pi r^2 \rho g(r). \quad (72)$$

The requirement that this integrates to the total number of pairs in the system,  $\int_0^\infty \rho(r) dr = N(N-1)/2$ , gives a global constraint on fluctuations of  $\rho(r)$ ,

$$\int_0^\infty \Delta \rho(r) dr = 0. \quad (73)$$

A typical fluctuation will have peaks around the peaks of  $g(r)$ , but only those near the first peak will significantly af-

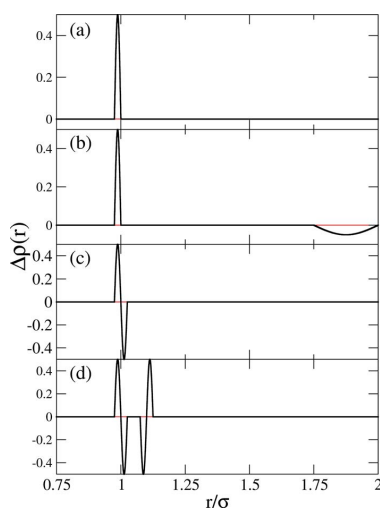


FIG. 6. (Color online) Intuitive picture of allowed and disallowed fluctuations in  $\rho(r)$ : (a) is not allowed because it violates the global constraint  $\int \Delta\rho(r)dr=0$ ; (b) satisfies the global constraint but not locality; (c) could correspond, for instance, to a single bond becoming shorter, but this is inconsistent with fixed volume (vanishing first moment—such a change cannot happen in isolation); and (d) is allowed—it corresponds, for example, to a single particle being displaced toward one neighbor and away from another. Thus one bond shortens and one lengthens.

fect the potential energy and virial (Sec. II C). We can assume that, for a dense liquid not close to a phase transition, almost any configuration  $\Gamma$  may be mapped to a nearby reference configuration  $\Gamma_{\text{ref}}$  whose RDF is identical to the thermal average  $g(r)$ . “Nearby” implies that the particle displacements relating the  $\Gamma$  and  $\Gamma_{\text{ref}}$  are small compared to the interparticle spacing.<sup>12</sup> These displacements define the deviation  $\Delta\rho(r)$  of  $\rho(r)$  from its equilibrium value. Mapping to  $\Gamma_{\text{ref}}$  gets around the absence of a unique equilibrium configuration as in the crystal case.

Let us consider what restriction this places on  $\Delta\rho(r)$ ; these are illustrated in Fig. 6. Because the displacements are small,  $\Delta\rho(r)$  must be local: a peak in  $\Delta\rho(r)$  at some  $r$  must be compensated by an opposite peak at a nearby location  $r_{\text{ref}}$  rather than one far away [thus example (b) in the figure is not allowed]—this corresponds to a bond having length  $r$  in the actual configuration and length  $r_{\text{ref}}$  in  $\Gamma_{\text{ref}}$  [Fig. 6(c)]. Finally fixed volume implies that a fluctuation cannot involve any substantial change in the mean nearest-neighbor bond length. This may be expressed mathematically as the near vanishing of the first moment of  $\Delta\rho(r)$ ,

$$\int_{\text{first peak}} r\Delta\rho(r)dr \cong 0. \quad (74)$$

Thus, if a particle is displaced toward a neighbor on one side, it is displaced away from a neighbor on the opposite side, thus the resulting fluctuation is expected to look like Fig. 6(d), which is characterized by vanishing zeroth and first moments. Note that we restrict the integral to the first peak. The principle that fluctuations of  $\Delta\rho(r)$  must be local allows us to write a version of Eq. (73) similarly restricted:

$$\int_{\text{first peak}} \Delta\rho(r)dr = 0. \quad (75)$$

Equations (74) and (75) cannot be literally true, since there must be contributions from fluctuations at whatever cut-off distance is used to define the boundary of the first peak. For instance, there could be a fluctuation such as Fig. 6(d) centered just to the right of this cutoff, so that only the first positive part was included in the integrals. We can ignore these contributions if we assume that the potential is truncated and shifted to zero at the boundary, as is standard in practice (although usually at larger distances). Then fluctuations right at the boundary do not contribute to the potential energy. The fact that the only contributions to the integral are at the boundary is a restatement of the locality of fluctuations.<sup>13</sup>

Now we make a Taylor series expansion of  $v(r)$  around the maximum  $r_M$  of the first peak of  $g(r)$ , using  $U = \int_0^\infty \rho(r)v(r)dr$ ,

$$\begin{aligned} \Delta U &= \int_{\text{first peak}} \Delta\rho(r) \left( v(r_M) + k_1(r - r_M) \right. \\ &\quad \left. + \frac{1}{2}k_2(r - r_M)^2 + \dots \right) \\ &\equiv \sum_p \frac{k_p}{p!} M_p. \end{aligned} \quad (76)$$

As for the crystal  $k_p$  is the  $p$ th derivative of  $v(r)$  at the expansion point ( $r_M$  here), while  $M_p$  is the  $p$ th moment of  $\Delta\rho(r)$ ,

$$M_p \equiv \int_{\text{first peak}} \Delta\rho(r)(r - r_M)^p dr. \quad (77)$$

A similar series exists for  $W$ , with coefficients given by Eq. (26),

$$3\Delta W = \sum_p \frac{C_p^W}{(r_M)^p} M_p. \quad (78)$$

The moments play a role exactly analogous to the sums  $S_p$  in the analysis of the crystal. The near vanishing of  $M_1$  corresponds to that of  $S_1$  in the crystal case, both following from the fixed-volume constraint; as there, it probably holds only to first order in particle displacements (except in one dimension where it is exact), but we have not tried to make a detailed estimate as we did with the crystal. Recalling that the extra contributions to the  $M_2$  terms will be small anyway, in view of Eqs. (30) and (31), we simply set  $M_1=0$ , so the two series become (noting that  $M_0=0$  also)

$$\begin{aligned} \Delta U &= \sum_{p=2}^{\infty} C_p^U \frac{M_p}{r_M^p}, \\ 3\Delta W &= \sum_{p=2}^{\infty} C_p^W \frac{M_p}{r_M^p}, \end{aligned} \quad (79)$$

where the coefficients  $C_p^{U,W}$  are those defined in Eqs. (25) and (26), but with  $r_M$  replacing  $a_c$ . The points made in

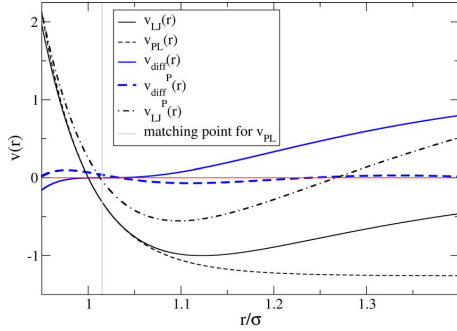


FIG. 7. (Color online) The true potential  $v_{LJ}(r)$ , the best effective power law  $v_{PL}(r)$  (in the sense that the fluctuations in potential energy and virial and reproduced most faithfully), and their difference  $v_{diff}(r)$ . Also shown are the projected versions  $v_{LJ}^P(r)$  and  $v_{diff}^P(r)$  where the constant and linear terms (determined over the interval  $0.95\sigma$  to  $1.4\sigma$ ) have been subtracted off. It is the projected functions that should be compared in order to make a statement about the smallness of  $v_{diff}(r)$  relative to  $v_{LJ}(r)$  since only the projected functions contribute to fluctuations of total potential energy.

Sec. II B regarding the relation between the two series are equally valid here. At orders  $p=2$  and higher, corresponding coefficients are related by the  $n^{(p)}(r_M)$ , which are always all above  $a=12$ . We expect from dimensional considerations that the variance of  $M_p$  is proportional to  $Nw_{FP}^{2p}$ , where  $w_{FP} \sim 0.3r_M$  is the width of the first peak of  $g(r)$ . Thus moments of higher order should contribute less, and therefore  $M_2$  should dominate, implying that the proportionality between  $\Delta U$  and  $\Delta W$  is essentially  $n^{(2)}(r_M)$ . This is in the range of 15–24 for  $r_M$  in the range of  $1.05\sigma$ – $1.15\sigma$ , giving slopes between 5 and 8, similar to those observed in the fluctuation modes. Unlike the low- $T$  limit of the crystal, we cannot assume that the fluctuations are particularly localized around  $r_M$ , so it is not surprising that a range of slopes show up. Notice that we do not see arbitrarily high mode slopes corresponding to the divergence of  $n^{(2)}(r)$  at the inflection point of the potential. Rather, for modes centered there, the assumption that we can neglect higher moments of the fluctuations no longer holds and there is an interpolation between  $n^{(2)}(r)$  and  $n^{(3)}(r)$  which is smaller (but still greater than  $a=12$ ).

We can now understand also why the potential and virial fluctuations, as “reconstructed” using the effective power-law potential (Fig. 3), agree so well with the true fluctuations, even though the fluctuation mode analysis shows that there are significant contributions from distances around and beyond the minimum, well away from the matching point  $r = 1.015\sigma$ . Figure 7 shows the LJ(12,6) potential, the  $n = 19.2$  power law (which gave the best fit in Sec. II A), and their difference,  $v_{diff}(r) \equiv v_{LJ}(r) - v_{PL}(r)$ . The latter is obviously very small and flat near the matching point but grows significantly in an approximately linear fashion at distances larger than  $r \sim 1.05\sigma$ . In view of Eqs. (16) and (72), a fluctuation of  $U_{diff}$  can be written as

$$\Delta U_{diff} = \int_0^{\infty} v_{diff}(r) \Delta \rho(r) dr, \quad (80)$$

which has the form of an inner product of functions. Vanishing fluctuations of  $U_{diff}$  follows if either (1)  $v_{diff}$  is identically

zero, or (2) it is nonzero, but orthogonal to the space of allowed  $\Delta \rho(r)$ . Given that  $v_{diff}$  is not particularly small except close to the matching point (see Fig. 7), the fact that  $U_{diff}$  fluctuations are relatively small even though they are associated with distances away from the matching point indicates that point (2) must hold approximately. Since allowed  $\Delta \rho(r)$  functions are those with no constant or linear term [see Eqs. (73) and (74)], functions orthogonal to these are those with only a constant and linear term:  $f(r) = Cf_0(r) + Df_1(r)$ , where  $f_0(r)$  is a constant function and  $f_1(r)$  is a linear function with zero mean over the range of interest. It is clear in Fig. 7 that  $v_{diff}$  is not exactly of this form, but it can be well approximated by such a function. This approximation can be checked by standard methods of the linear algebra of function spaces. First we choose a range  $(r_1, r_2)$  over which functions are to be defined. For purposes this should include the range of significant contributions to  $W$  and  $U$  (Fig. 5). We choose  $r_1 = 0.95\sigma$  and  $r_2 = 1.4\sigma$ . The normalized, mutually orthogonal basis vectors  $f_0(r)$  and  $f_1(r)$  are then given by

$$f_0(r) = 1/\sqrt{r_2 - r_1}, \quad (81)$$

$$f_1(r) = \sqrt{\frac{12}{(r_2 - r_1)^3}}(r - (r_1 + r_2)/2).$$

The part of  $v_{diff}(r)$  that is spanned by these basis functions is  $v_0 f_0 + v_1 f_1$ , where  $v_i \equiv \int_{r_1}^{r_2} f_i(r) v_{diff}(r) dr$  is the inner product of  $v_{diff}(r)$  and the corresponding basis vector. We define  $v_{diff}^P(r)$  as the part of  $v_{diff}(r)$  projected onto the space of allowed functions,

$$v_{diff}^P(r) = v_{diff}(r) - v_0 f_0(r) - v_1 f_1(r). \quad (82)$$

This function is also plotted in Fig. 7, where it can be seen that it is certainly small compared to  $v_{diff}(r)$  itself. More importantly, it is also small compared to the projected part of  $v_{LJ}(r)$ ,  $v_{LJ}^P(r)$ , defined analogously, because it is this that explains why the fluctuations of  $U_{diff}$  are small compared to those of  $U_{LJ}$  (or equivalently  $U_{PL}$ ). This may be quantified by noting that the ratio of their norms is 0.09, which indicates how orthogonal  $v_{diff}(r)$  is to the space of allowed  $\Delta \rho(r)$ . If we projected out only the constant term from  $v_{diff}(r)$  and  $v_{LJ}^P(r)$  (the *a priori* more obvious way to compare the size of two functions) the ratio of norms would be 0.50, and it would not be obvious why  $v_{PL}$  does as good a job as it does. Thus, again, constant-volume constraint, implying Eq. (74), is important.

The above discussion applies equally well to the virial. We can now write a more accurate approximate expression for  $v_{LJ}(r)$ , which we call the extended effective inverse power-law approximation,

$$v_{LJ}(r) \approx Ar^{-n} + B + Cr, \quad (83)$$

where  $A$ ,  $B$ , and  $C$  are constants. The associated pair virial ( $w(r) \equiv rv'(r)$ ) is then

$$w_{LJ}(r) \approx -nAr^{-n} + Cr, \quad (84)$$

which has the same form. In both cases the term  $Cr$  contributes to the mean value but not the fluctuations because  $\int r \rho(r) dr$  is nonzero, while  $\int r \Delta \rho(r) dr \equiv 0$  for those  $\Delta \rho(r)$

which are allowed at fixed volume. Note also that the contribution to the mean values from  $Cr$  will depend on volume because  $g(r)$  and, hence,  $\rho(r)$  do. Thus we can see that although there are significant contributions to fluctuations away from the matching point where the power law fits the true potential well, these are essentially equal for both the power law and the true potential because the difference between the two potentials in this region is almost orthogonal to the allowed fluctuations in  $\rho(r)$ . This also explains why the fluctuation only holds at fixed volume (which would not be explained by the assumption that short-distance encounters dominate the fluctuations).

The extended power-law approximation, determined empirically by the projection procedure, provides an alternative way to understand why the effective exponent  $n^{(1)}$  evaluated at  $r \sim \sigma$  agrees well with  $n^{(2)}$  evaluated around the minimum  $r_m$ . For the extended effective power-law approximate [Eq. (83)], we get

$$\begin{aligned} n^{(1)}(r) &= \frac{-n(n+1)Ar^{-(n+1)}}{-nAr^{-(n+1)} + C} - 1, \\ n^{(2)}(r) &= \frac{n(n+1)(n+2)Ar^{-(n+2)}}{n(n+1)Ar^{-(n+2)}} - 2 = n. \end{aligned} \quad (85)$$

Note that  $n^{(2)}(r)$  is constant and equal to the exponent  $n$  of the power law, while  $n^{(1)}(r)$  only approaches  $n$  when  $r$  is small enough that  $C$  in the denominator can be neglected [for the true potential  $n^{(2)}(r)$  increases with  $r$  and eventually diverges (see Fig. 1)]. This emphasizes the greater usefulness of  $n^{(2)}$  in identifying the effective power-law exponent. Recall also that our analysis earlier in this section indicates that  $n^{(2)}(r)$ , involving that the second and third derivatives of  $v(r)$  near its minimum, is more fundamentally the cause of the  $W, U$  correlations, explaining something like 80% of the correlation in the liquid phase and over 99% in the crystal phase. The fact that Eq. (83) is a good approximation for the Lennard-Jones potential pushes the correlation to over 90% also in the liquid phase.

To summarize the last two subsections, we have shown here that the source of the fluctuations is indeed pair separations within the first peak, although only a relatively small fraction of the variances come from the short- $r$  region where the approximation of the pair potential by a power law is truly valid. We have also seen how the Taylor-series analysis (which involves the crucial step of taking a sum over all pairs) may be extended to cover the whole first peak area, with all terms giving roughly the same effective slope, given essentially by the second-order effective exponent:  $\gamma \sim n^{(2)}(r_m)/3$ . The fact that this matches the first-order effective exponent at the shorter distance  $r \sim \sigma$  is equivalent to the extended effective power-law approximation [Eq. (83)], which given a constant volume is what justifies the replacement of the potential by a power law (empirically demonstrated in Fig. 3).

### III. SOME CONSEQUENCES OF STRONG PRESSURE-ENERGY CORRELATIONS

This section gives examples of consequences of strong pressure-energy correlations. The purpose is to show that these are important, whenever present. Clearly, more work needs to be done to identify and understand all consequences of strong pressure-energy correlations.

#### A. Measurable consequences of instantaneous $W, U$ correlations

The observation of strong  $W, U$  correlations is of limited interest if it can only ever be observed in simulations. How can we make a comparison with experiment? In general, fluctuations of dynamical variables are related to thermodynamic response functions,<sup>14–16</sup> for example, those of  $U$  are related to the configurational part of the specific heat,  $C_V^{\text{conf}}$ . The latter is obtained by subtracting off the appropriate kinetic term, which for a monatomic system such as argon is  $3Nk_B/2$ . The virial fluctuations, however, although related to the bulk modulus, are not directly accessible because of another term that appears in the equation, the so-called hypervirial, which is not a thermodynamic quantity.<sup>2</sup> Fortunately this difficulty can be handled.

Everything in this section refers to the  $NVT$  ensemble. First we define the various response functions and configurational counterparts, the isothermal bulk modulus  $K_T$ ,  $C_V$ , and the “pressure coefficient,”  $\beta_V$ ,

$$\begin{aligned} K_T &\equiv -V \left( \frac{\partial p}{\partial V} \right)_T, & K_T^{\text{conf}} &\equiv K_T - \frac{Nk_B T}{V}, \\ C_V &\equiv \left( \frac{\partial E}{\partial T} \right)_V, & C_V^{\text{conf}} &\equiv C_V - \frac{3}{2}Nk_B, \\ \beta_V &\equiv \left( \frac{\partial p}{\partial T} \right)_V, & \beta_V^{\text{conf}} &\equiv \beta_V - \frac{Nk_B}{V}, \\ p^{\text{conf}} &\equiv p - \frac{Nk_B T}{V} = \frac{W}{V}. \end{aligned} \quad (86)$$

We also define  $c_V \equiv C_V/V$ . The following fluctuation formulas are standard (see, for example, Ref. 2)

$$\frac{\langle (\Delta W)^2 \rangle}{k_B T V} = \frac{Nk_B T}{V} + \frac{\langle W \rangle}{V} - K_T + \frac{\langle X \rangle}{V}, \quad (87)$$

$$\frac{\langle (\Delta U)^2 \rangle}{k_B T^2} = C_V - \frac{3}{2}Nk_B = C_V^{\text{conf}}, \quad (88)$$

$$\frac{\langle \Delta U \Delta W \rangle}{k_B T^2} = V\beta_V - Nk_B = V\beta_V^{\text{conf}}. \quad (89)$$

Here  $X$  is the so-called “hypervirial,” which gives the change in virial upon an instantaneous volumetric scaling of positions. It is not a thermodynamic quantity and cannot be determined experimentally, although it is easy to compute in simulations. For a pair potential  $v(r)$ ,  $X$  is a pair-sum,

$$X = \sum_{\text{pairs}} x(r)/9, \quad (90)$$

where  $x(r) = rw'(r)$ . If we use the extended effective power-law approximation (including the linear term) discussed in the last section, then from Eq. (84) we get  $x(r) \approx n^2 Ar^{-n} + Cr$ . Summing over all pairs, and recalling that when the volume is fixed the  $Cr$  term gives a constant, we have a relation between the total virial and total hypervirial,

$$X = (n/3)W + \text{const.} \quad (91)$$

This constant survives, of course, when we take the thermal average  $\langle X \rangle$ , as do the corresponding constants in  $\langle U \rangle, \langle W \rangle$ . To get rid of these constants, one possibility would be to take derivatives with respect to  $T$ , but this can be problematic when analyzing experimental data. Instead we simply compare quantities at any temperature to those at some reference temperature  $T_{\text{ref}}$ ; this effectively subtracts off the unknown constants. Taking first the square of the correlation coefficient, we have

$$R^2 = \frac{\langle (\Delta U \Delta W)^2 \rangle}{\langle (\Delta U)^2 \rangle \langle (\Delta W)^2 \rangle}, \quad (92)$$

which implies

$$R^2 \frac{\langle (\Delta W)^2 \rangle}{k_B T V} = \frac{1}{k_B T V} \frac{\langle (\Delta U \Delta W)^2 \rangle}{\langle (\Delta U)^2 \rangle}. \quad (93)$$

Inserting the fluctuation formulas [Eqs. (87) and (89)] gives

$$R^2 \left( \langle p \rangle - K_T + \frac{\langle X \rangle}{V} \right) = \frac{1}{k_B T V} \frac{(k_B T^2 V \beta_V^{\text{conf}})^2}{k_B T^2 C_V^{\text{conf}}} \quad (94)$$

$$= T \frac{(\beta_V^{\text{conf}})^2}{c_V^{\text{conf}}}. \quad (95)$$

Defining quantities  $\tilde{A} \equiv \langle p \rangle - K_T + \langle X \rangle / V$  and  $B \equiv T(\beta_V^{\text{conf}})^2 / c_V^{\text{conf}}$  (the reason for the tilde on  $A$  will become clear), we have  $R^2 \tilde{A} = B$ . This is an exact relation. To deal with the hypervirial we first take differences with the quantities at  $T_{\text{ref}}$ ; assuming that the variation in  $R$  is much smaller than the  $\tilde{A}$  and  $B$  variations:

$$R^2(\tilde{A} - \tilde{A}_{\text{ref}}) = B - B_{\text{ref}}, \quad (96)$$

where  $\tilde{A}_{\text{ref}} = \tilde{A}(T_{\text{ref}})$ , etc.  $\tilde{A} - \tilde{A}_{\text{ref}}$  written out explicitly is

$$\tilde{A} - \tilde{A}_{\text{ref}} = (\langle p \rangle - K_T) - (\langle p \rangle_{\text{ref}} - K_{T_{\text{ref}}}) + \frac{\langle X \rangle - \langle X \rangle_{\text{ref}}}{V}. \quad (97)$$

Next we use the power-law approximation to replace  $\langle X \rangle - \langle X_{\text{ref}} \rangle$  with  $(n/3)(\langle W \rangle - \langle W_{\text{ref}} \rangle)$ . This is the crucial point: whereas it is often not a good approximation that  $\langle X \rangle = (n/3)\langle W \rangle$  due to the unknown additive constants discussed above, subtracting two state points considers *changes* in  $\langle X \rangle$  and  $\langle W \rangle$  with temperature. Recall from Sec. III B of Paper I that the changes in mean values  $\Delta \langle W \rangle$  and  $\Delta \langle X \rangle$  between (nearby) temperatures are related as the linear regression of the fluctuations of those quantities at one (nearby or intermediate) temperature. The linear relation between subtracted mean values holds if the instantaneous  $W$  and  $X$  are strongly

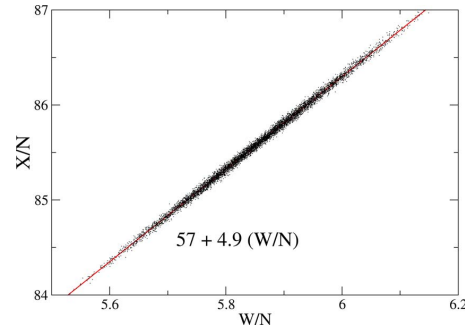


FIG. 8. (Color online) Scatter plot of instantaneous virial and hypervirial (in dimensionless units) for a SCLJ system at  $\rho=1.0$ ,  $T=0.80$  (NVE). The correlation coefficient between these quantities is 0.998. The hypervirial is the main contribution to the configurational part of the bulk modulus; it gives (after dividing by volume) the change in virial for a given relative change in volume. The sizable constant term in the linear fit shows that Eq. (91) is a poor approximation. The slope is 4.9, about 10% smaller than  $\gamma \sim 5.4$  for this state point. The difference reflects the limit of the validity of the power-law description—in fact, a more detailed analysis shows that the relation between  $W$  and  $X$  is dominated by  $n^{(3)}(r)$ , which is smaller than  $n^{(2)}(r)$  (Fig. 1).

correlated in the region of interest. The latter is confirmed by our simulations; indeed the correlation of instantaneous values of  $X$  and  $W$  is even stronger than for  $W$  and  $U$ , with approximately the same slope (Fig. 8). Thus Eq. (97) becomes

$$\tilde{A} - \tilde{A}_{\text{ref}} \approx (\langle p \rangle - K_T) - (\langle p \rangle_{\text{ref}} - K_{T_{\text{ref}}}) + \frac{n \langle W \rangle - \langle W \rangle_{\text{ref}}}{3V} \quad (98)$$

$$= A - A_{\text{ref}}, \quad (99)$$

where  $A \equiv \langle p \rangle - K_T + (n/3)(\langle W \rangle / V)$  (no tilde) contains quantities that are all directly accessible to experiment except for the effective power-law exponent  $n$ . This can be obtained by noting that if there were perfect correlation, one could interchange  $\Delta W$  and  $(n/3)\Delta U$ ; thus,

$$\frac{\beta_V^{\text{conf}}}{C_V^{\text{conf}}/V} = \frac{\beta_V^{\text{conf}}}{c_V^{\text{conf}}} = \frac{\langle \Delta U \Delta W \rangle}{\langle (\Delta U)^2 \rangle} = \frac{n}{3}, \quad (100)$$

which gives for  $A$

$$A = \langle p \rangle - K_T + \frac{\langle p \rangle_{\text{ref}} \beta_V^{\text{conf}}}{c_V^{\text{conf}}}. \quad (101)$$

Thus to compare with experiment one should plot  $B - B_{\text{ref}}$  against  $A - A_{\text{ref}}$ ; the prediction, in the case of near perfect correlation,  $R^2 \approx 1$ , is a straight line with slope close to unity. Figure 9 shows data for argon for  $T$  between 200 and 660 K. Argon was chosen because as a monatomic system there are no rotational or vibrational modes contributing to the heat capacity and it is therefore straightforward to subtract off the kinetic part. Also we restrict to a relatively high temperature to avoid quantum effects. The correlation coefficient  $R$  given as the square root of the slope of a linear fit is 0.96. Note that the assumed constancy of  $R$  is confirmed (going to lower temperatures there are increasingly large de-

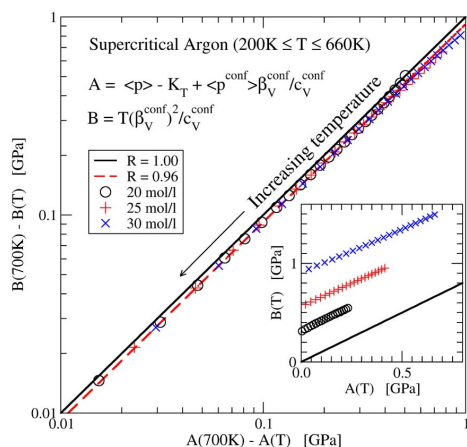


FIG. 9. (Color online) Data from the NIST database (Ref. 45) for supercritical argon at three different densities covering the temperature range of 200 K–660 K showing a strong virial-potential-energy correlation ( $R=0.96$ ) (reproduced from Ref. 4). Here  $K_T = -V(\partial p/\partial V)_T$ ,  $p^{conf} = p - Nk_B T/V = W/V$ ,  $\beta_V^{conf} \equiv (\partial p/\partial T)_V - Nk_B/V$ , and  $c_V^{conf} \equiv C_V/V - (3/2)Nk_B/V$ . The diagonal line corresponds to perfect correlation. The inset shows “unsubtracted” values for  $A$  and  $B$ ; the fact that the data do not fall on the solid line indicates that a power-law description does not hold for the full thermodynamics.

viations). The importance of subtracting from a reference state point is highlighted by the inset, which shows that  $A(T)=B(T)$  does not hold: There is a correlation in the fluctuations which is not present in the full equation of state.<sup>4</sup>

### B. Time averaging: Pressure-energy correlations in highly viscous liquids

We have observed and discussed in Paper I that when volume is held constant, the correlations tend to become more perfect with increasing  $T$ , while along an isobar (considering still fixed-volume simulations, choosing the volume to give a prescribed average pressure) they become more perfect with decreasing  $T$ . This fact makes the presence of correlations highly relevant for the physics of highly viscous liquids approaching the glass transition. Basic questions such as the origins of nonexponential relaxations and non-Arrhenius temperature dependence are still vigorously debated in this field of research.<sup>17–20</sup> Instantaneous correlations of the kind discussed in this work would seem to be relevant only to the high frequency properties of a highly viscous liquid; their relevance to the long time scales on which structural relaxation occurs follows from the separation of time scales as explained below.

A question that is not actively debated in this research field (but see, e.g., Refs. 21–23) is whether a single parameter is enough to describe a highly viscous liquid. The consensus for more than 30 years is that with few exceptions these liquids require more than just one parameter, a conclusion scarcely surprising given their complexity. The meaning of “having a single parameter” can be understood as follows. Following a sudden change in volume, both pressure and energy relax to their equilibrium values over a time scale of

minutes or even hours, sufficiently close to the glass transition. If a single parameter governs the internal relaxation of the liquid, then both pressure and energy relax with the same time scale, and, in fact, the normalized relaxation functions are identical.<sup>21,23</sup> This behavior can be expressed in the frequency domain, as a certain quantity, the dynamic Prigogine–Defay ratio, being equal to unity.<sup>23</sup> A key feature of highly viscous liquids is the separation of time scales between the slow structural (“alpha”) relaxation (up to order seconds) and the very short times (of order picoseconds) characterizing the vibrational motion of the molecules. This separation allows a more direct experimental consequence of  $W, U$  correlations than that described in the previous subsection: Suppose a highly viscous liquid has perfectly correlated  $W, U$  fluctuations. When  $W$  and  $U$  are time averaged over, say, one-tenth of the alpha relaxation time  $\tau_\alpha$ ,<sup>24</sup> they still correlate 100%. Since the kinetic contribution to pressure is fast, its time average over  $\tau_\alpha/10$  is just its thermal average, and thus the time-averaged pressure equals the time average of  $W/V$  plus a constant. Similarly, the time-averaged energy equals the time-averaged potential energy plus a constant. Thus the fluctuations of the time-averaged  $W$  and  $U$  equal the slowly fluctuating parts of pressure and energy, so these slow parts will also correlate 100% in their fluctuations. In this way we get from the nonobservable quantities  $W$  and  $U$  to the observable ones  $E$  and  $p$  (we similarly averaged to observe the correlation in the SQW system in Paper I). The upper part of Fig. 10 shows normalized fluctuations of energy and pressure for the commonly studied Kob–Andersen binary Lennard-Jones system<sup>25</sup> (referred to as KABLJ in Paper I), time averaged over one-tenth of  $\tau_\alpha$ . In the lower part we show the dynamic Prigogine–Defay ratio,<sup>12</sup> which in the  $NVT$  ensemble is defined as follows:

$$\Lambda_{TV}(\omega) \equiv - \frac{c_V''(\omega)(1/\kappa_T(\omega))''}{T[\beta_V''(\omega)]^2}. \quad (102)$$

Here  $\kappa_T = 1/K_T$  is the isothermal compressibility and  $''$  denotes the imaginary part of the complex frequency-dependent response function. A way to interpret this quantity can be found by considering the fluctuation-dissipation theorem expressions for the response functions. For example the frequency-dependent constant-volume specific heat  $c_V(\omega)$  is given<sup>26</sup> by

$$c_V(\omega) = \frac{\langle(\Delta E)^2\rangle}{k_B T^2} - \frac{i\omega}{k_B T^2} \int_0^\infty \langle\Delta E(0)\Delta E(t)\rangle \exp(-i\omega t) dt, \quad (103)$$

where  $E$  is the total energy. Taking the imaginary part we have

$$c_V''(\omega) = - \frac{\omega}{k_B T^2} (\mathcal{L}\{\langle\Delta E(0)\Delta E(t)\rangle\})', \quad (104)$$

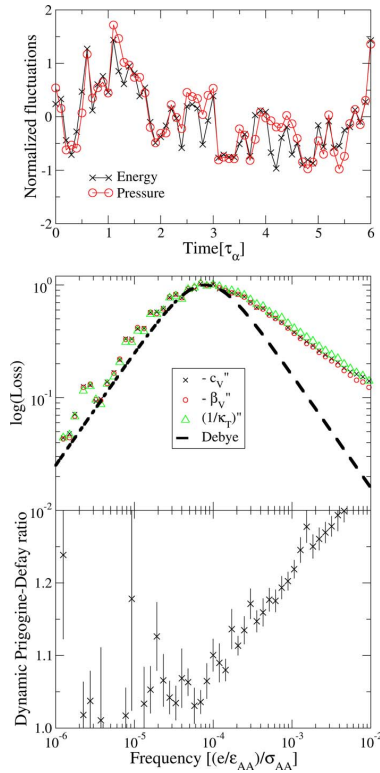


FIG. 10. (Color online) Upper panel, time-averaged (over  $\tau_\alpha/10$ , where  $\tau_\alpha$  is the structural relaxation time) normalized fluctuations of  $E$  and  $p$  in  $NVT$  simulations of the Kob–Andersen (Ref. 20) binary Lennard–Jones (KABLJ) system, plotted against time in units of  $\tau_\alpha \sim 10^3 \sigma_{AA} \sqrt{m/\epsilon_{AA}}$ . The density was  $1.2\sigma_{AA}^{-3}$ , and the temperature was  $0.474\epsilon_{AA}$ . Middle panel, imaginary parts of the three response functions  $-c_v''(\omega)$ ,  $-\beta_v''(\omega)$ , and  $1/\kappa_T''(\omega)$ , scaled to the maximum value. Lower panel, dynamic Prigogine–Defay ratio for the same simulation. The approach toward unity at frequencies smaller than the loss-peak frequency ( $\sim 1/\tau_\alpha$ ) is exactly equivalent to the correlation between time-averaged quantities shown in the upper panel (reproduced from Ref. 19).

where we use  $\mathcal{L}$  to represent Laplace transformation. Similarly,

$$(1/\kappa_T)''(\omega) = \frac{\omega V}{k_B T} (\mathcal{L}\{\langle \Delta p(0) \Delta p(t) \rangle\})' \quad (105)$$

and

$$\beta_v''(\omega) = -\frac{\omega}{k_B T^2} (\mathcal{L}\{\langle \Delta E(0) \Delta p(t) \rangle\})'. \quad (106)$$

Forming the Prigogine–Defay ratio then gives, after cancelling factors of  $k_B$ ,  $T$ ,  $V$ , and  $\omega$ ,

$$\Lambda_{TV}(\omega) = \frac{(\mathcal{L}\{\langle \Delta E(0) \Delta E(t) \rangle\})' (\mathcal{L}\{\langle \Delta p(0) \Delta p(t) \rangle\})'}{(\mathcal{L}\{\langle \Delta E(0) \Delta p(t) \rangle\})'^2}. \quad (107)$$

We can see that the right-hand side has a similar structure to a correlation coefficient, if we take the inverse square root. So in a loose sense the dynamic Prigogine–Defay ratio can

be thought of as the inverse square of a correlation coefficient, referred to a particular time scale. This gives an intuitive reason for why it is in general greater or equal to unity, with equality only achieved in the case of perfect correlation.<sup>23</sup> The lower panel of Fig. 10 shows this quantity for a range of frequencies for the KABLJ system. It clearly approaches one at low frequencies and stays within 20% of one in the main relaxation region. In the sense above, this corresponds to  $R > 0.9$ , or strongly correlation.

The line of reasoning presented here opens for a new way of utilizing computer simulations to understand ultraviscous liquids. Present-day computers are barely able to simulate 1  $\mu$ s of real-time dynamics, making it difficult to predict the behavior of liquids approaching the laboratory glass transition. We find that pressure-energy correlations are almost independent of viscosity, however, which makes it possible to make predictions regarding the relaxation properties even in the second or hour range of characteristic times. Thus if a glass-forming liquid at high temperatures (low viscosity) has very strong pressure-energy correlations ( $R \sim 1$ ), its eight thermoviscoelastic response functions at ultraviscous conditions may basically be expressed in terms of just one, irrespective of temperature (or viscosity).

### C. Aging and energy landscapes

We now discuss the significance of the present results for the interesting results reported in 2002 by Mossa *et al.*<sup>27</sup> who studied the inherent states (ISs) visited by the Lewis–Wahnström model<sup>28</sup> of the glass-forming liquid *ortho*-terphenyl (OTP) during aging, i.e., the approach to equilibrium. An IS is a local minimum of the so-called potential-energy landscape (PEL) to which a given configuration is mapped by steepest-descent minimization.<sup>29,30</sup> The PEL formalism involves modeling the distributions and averages of properties of the IS in the hope of achieving a compact description of the thermodynamics of glass-forming liquids.<sup>31,32</sup> The thesis of Mossa *et al.*<sup>27</sup> and of the previous work<sup>33</sup> is that an equation of state can be derived using this formalism which is valid even for nonequilibrium situations. This involves including an extra parameter, namely, the average IS (potential) energy,  $\langle e_{IS} \rangle$ , so that the equation of state takes the form

$$p(T, V, \langle e_{IS} \rangle) = p_{IS}(\langle e_{IS} \rangle, V) + p_{\text{vib}}(T, V, \langle e_{IS} \rangle), \quad (108)$$

where  $p_{IS}$  is the ensemble averaged IS pressure—for a given configuration it is the pressure of the corresponding IS—and  $p_{\text{vib}} \equiv p - p_{IS}$ . The usefulness of splitting in this way lies in the fact that  $p_{IS}$  does not explicitly depend on  $T$ .

At equilibrium  $\langle e_{IS} \rangle$  is determined by  $V$  and  $T$ . The conclusion of Ref. 22 is that knowledge of  $\langle e_{IS} \rangle$  in nonequilibrium situations is enough to predict the corresponding pressure (given also  $T$  and  $V$ ). This was based on the extensive simulations of various aging schedules. Thus the authors concluded that the ISs visited by the system while out of equilibrium must be in some sense the “same” ones sampled during equilibrium conditions. Same is effectively defined by their results that averages of various IS properties ( $V$ ,  $e_{IS}$ ,  $p_{IS}$ , as well as a measure of the IS curvature) are all related to

each other the same way under nonequilibrium conditions as under equilibrium conditions. It was similarly found that the volume could be determined from  $\langle e_{\text{IS}} \rangle$  following a pressure jump in a pressure-controlled simulation. On the other hand, subsequent work by the same group found that this was not at all possible for glassy water during compression/decompression cycles.<sup>34</sup>

Now, our results (Paper I) for the same OTP model show that it is a strongly correlating liquid. Thus we expect a general correlation between individual, not just average, values of  $p_{\text{IS}}$ , the inherent state pressure (which lacks a kinetic term and therefore equals the inherent state virial divided by volume) and  $e_{\text{IS}}$ , for a given volume. Therefore, for any given collection of ISs with the same volume—not just equilibrium ensembles—the mean values of  $U$  and  $W$  will fall on the same straight line as the instantaneous values. Note that this would not hold if the correlation was nonlinear. Correspondingly, for a given  $p_{\text{IS}}$ , there is a general correlation between individual values of  $e_{\text{IS}}$  and  $V$ . In fact, any two of these quantities determine the third with high accuracy, and this is true at the level of individual configurations, including ISs.

To see how this works for cases involving fixed volume, we write the total (instantaneous) pressure as a sum of an IS part, which involves the virial at the corresponding IS, plus a term involving the difference in the true virial from the IS virial, plus the kinetic term:

$$p = \frac{W_{\text{IS}}}{V} + \frac{W - W_{\text{IS}}}{V} + \frac{Nk_B T}{V}. \quad (109)$$

The first term is linearly related to the IS energy for a strongly correlating liquid. Moreover, the difference term is similarly expressed in terms of the corresponding energy difference,  $W - W_{\text{IS}} = \gamma(U - e_{\text{IS}})$ . Taking averages over the (possibly nonequilibrium, although we assume equilibrium within a given potential-energy basin) ensemble, we expect that  $\langle U - e_{\text{IS}} \rangle$  depends only on  $T$  and  $V$  (a slight  $e_{\text{IS}}$  dependence can appear in  $\gamma$  since this is slightly state-point dependent). Thus it follows that  $p$  can be reconstructed from a knowledge of (average)  $e_{\text{IS}}$ ,  $V$ , and  $T$ , without any assumptions about the nature of the ISs visited. In particular, no conclusion can be drawn regarding the latter. The failure of the pressure reconstruction in the case of water<sup>23</sup> is not surprising since water models are generally not strongly correlating (which as we saw in Paper I is linked to the existence of the density maximum).

#### D. Biomembranes

A completely different area of relevance for the type of correlations reported here relates to the recent work of Heimburg and Jackson,<sup>35</sup> who proposed a controversial new theory of nerve signal propagation. Based on experiment and theory they suggest that a nerve signal is not primarily electrical but a soliton sound wave.<sup>36</sup> Among other things this theory explains how anaesthesia works (and why one can dope people with the inert gas xenon): anaesthesia works simply by a freezing-point depression that changes the membrane phase transition temperature and affects its ability to carry the soliton sound wave. A crucial ingredient of the

TABLE III. Data from  $NpT$  simulations of fully hydrated phospholipid membranes of 1,2-dimyristoyl-sn-glycero-3-phosphocholine (DMPC), 1,2-dimyristoyl-sn-glycero-3-phospho-L-serine with sodium as counter ion (DMPS-Na), hydrated DMPS (DMPSH), and DPPC (Refs. 40 and 44). The columns list temperature, correlation coefficient between volume and energy, average lateral area per lipid, simulation time in equilibrium, and total simulation time.

	$T$ (K)	$R_{\text{EV}}$	$A_{\text{lip}}$ ( $\text{\AA}^2$ )	$t$ (ns)	$t_{\text{tot}}$ (ns)
DMPC	310	0.885	53.1	60	114
DMPC	330	0.806	59.0	50	87
DMPS-Na	340	0.835	45.0	22	80
DPPC	325	0.866	67.3	13	180

theory is the postulate of proportionality between volume and enthalpy of microstates, i.e., that their thermal equilibrium fluctuations should correlate perfectly. This should apply even through the first-order membrane *melting* transition. The theory was justified in part from previous experiments by Heimburg showing proportionality between compressibility and specific heat through the phase transition.<sup>37</sup> The postulated correlation—including the claim that it survives a first-order phase transition—fits precisely the pattern found in our liquid simulations.

By re-examining existing simulation data<sup>38,39</sup> as well as carrying out extensive new simulations,<sup>40</sup> we have investigated whether the correlations are also found in several model membrane systems, five of which are listed in Table III. The simulations involved a layer of phospholipid membrane surrounded by water, in the  $L_{\alpha}$  phase (that is, at temperatures above the transition to the gel-state), at constant  $p$  and  $T$ . When  $p$ , rather than  $V$ , is constant, the relevant quantities that may correlate are energy and volume. As with viscous liquids (Sec. III B) and the square well system (Paper I), time averaging is necessary for a correlation to emerge, where now

$$\overline{\Delta E(t)} \approx \gamma^{\text{vol}} \overline{\Delta V(t)}. \quad (110)$$

When an averaging time of 1 ns is chosen, a significant correlation emerges, with correlations between 0.8 and 0.9 (Table III; note these  $R_{\text{EV}}$  values fall slightly short of our criterion of 0.9 for “strong correlations”). The time series of time-averaged normalized  $E$  and  $V$  for one case are shown in Fig. 11. The necessity of time averaging stems from the presence of water, which we know does not exhibit strong correlations. Since the membrane dynamics are much slower than those of the water, they can be isolated by time averaging.

#### IV. CONCLUSIONS AND OUTLOOK

In Paper I and this work we have demonstrated several cases of strongly correlating liquids and some cases where the correlation is weak or absent (at least under normal conditions of pressure and temperature). An important next step is to continue to document the existence or nonexistence of correlations, particularly in different kinds of model systems, such as nonpair potential systems and systems with interactions computed using quantum mechanics (e.g., by density functional theory). It is noteworthy in this respect that after

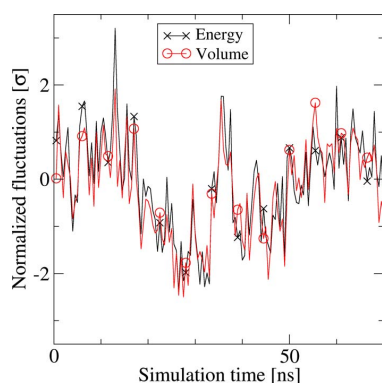


FIG. 11. (Color online) Normalized fluctuations of energy ( $\times$ ) and volume ( $\circ$ ) for a 1,2-dipalmitoyl-sn-glycero-3-phosphocholine (DPPC) membrane at 325 K (Ref. 44). Each data point represents a 0.5 ns average. Energy and volume are correlated with a correlation coefficient of  $R=0.87$  ( $NpT$ ).

suitable time averaging the correlations may appear in systems where they are otherwise unexpected. One example was the square-well (SQW) case, where the correlation was between the time-averaged virial and potential energy. In the case of viscous liquids time averaging allowed a correlation to appear between the more accessible energy and pressure, while for the biomembranes it made it possible to remove the nonstrongly correlating contributions from the water. In all cases time averaging is relevant because of a separation of time scales: the SQW system because the time scale over which the average number of neighbors changes is long compared to the time between collisions; viscous liquids because the vibrational dynamics (which includes the kinetic contributions) is fast compared to the slow configurational dynamics; biomembranes because the membrane dynamics is slow compared to those of the water. Note that in this case it was necessary to consider an  $NpT$  ensemble and study the correlations between energy and volume because only a part of the system is strongly correlating, and this part cannot be constrained to a particular volume. It is worth noting that even with fixed volume, the correlation coefficient depends on whether the ensemble is  $NVT$  or  $NVE$ , although the strongly correlating limit of  $R \rightarrow 1$  is independent of ensemble.

A point which has been mentioned, but which is worth emphasizing again, is that the replacement of the potential by an appropriate inverse power law can only reproduce the fluctuations, and not the mean values of (potential) energy and virial, nor their first derivatives with respect to  $T$  and  $V$ . These determine the equation of state, in particular features such as the van der Waals loop that are absent in a pure power-law system, even if changes in the exponent are allowed. The generalization to the extended effective inverse power-law approximation, however, allows in principle such features to be described.

Finally, consider again viscous liquids, which are typically deeply supercooled. The most common way of classifying them involves the fragility parameter introduced by Angell,<sup>41</sup> related to the departure from Arrhenius behavior of

the temperature dependence of the viscosity. Strong liquids, having the most Arrhenius behavior, have traditionally been considered the easiest ones to understand because Arrhenius temperature dependence is well-understood. However it may well be that strongly correlating liquids are in fact the simplest.<sup>42</sup> The connection with the long-discussed question of whether a single-order parameter describes highly viscous liquids has been discussed briefly in Sec. III B and is discussed further in Ref. 21. As an example, a direct application of the strongly correlating property concerns diffusion in supercooled liquids. Recent work of Coslovich and Roland<sup>43</sup> has shown that the diffusion constant in viscous binary Lennard-Jones mixtures may be fitted by an expression  $D = F(\rho^\gamma/T)$ , where  $\gamma$  reflects the effective inverse power of the repulsive core. “Density scaling” has also been observed experimentally.<sup>46–49</sup> It is natural, given the results of Coslovich and Roland, to hypothesize that the scaling exponent is connected to pressure-energy correlations, and in Ref. 4 it was conjectured that density scaling applies if and only if the liquid is strongly correlating. We have recently studied the relationship between the two quantitatively<sup>50</sup> and have found that (1) density scaling does indeed hold to the extent that the liquids are strongly correlating, and (2) the scaling exponent is given accurately by the slope  $\gamma$  of the correlations (hence our use of the same symbol). This finding supports the conjecture that strongly correlating liquids may be simpler than liquids in general.

In summary, the property of strong correlation between the equilibrium fluctuations of virial and potential energy allows a new way to classify liquids. It is too soon to tell how fruitful this will turn out in the long term, but judging from the applications briefly presented here, it seems at least plausible that it will be quite useful.

## ACKNOWLEDGMENTS

Useful discussions with Søren Toxværd are gratefully acknowledged. Center for viscous liquid dynamics “Glass and Time” is sponsored by The Danish National Research Foundation.

<sup>1</sup>N. P. Bailey, U. R. Pedersen, N. Gnan, T. B. Schröder, and J. C. Dyre, *J. Chem. Phys.* **129**, 184507 (2008).

<sup>2</sup>M. P. Allen and D. J. Tildesley, *Computer Simulation of Liquids* (Oxford University Press, Oxford, 1987).

<sup>3</sup>D. Ben-Amotz and G. Stell, *J. Chem. Phys.* **119**, 10777 (2003).

<sup>4</sup>U. R. Pedersen, N. P. Bailey, T. B. Schröder, and J. C. Dyre, *Phys. Rev. Lett.* **100**, 015701 (2008).

<sup>5</sup>K. Binder and W. Kob, *Glassy Materials and Disordered Solids: An Introduction to Their Statistical Mechanics* (World Scientific, Singapore, 2005).

<sup>6</sup>The analysis of fluctuations in the liquid in Sec. II C can be applied to the case of a disordered solid, explaining the high correlation also there, but it is not accurate enough to get as good an estimate for the low-temperature limit as we do our analysis of the crystal.

<sup>7</sup>“Displacement” refers to the displacement of a given particle from its equilibrium position, while the “relative displacement” is the difference in this quantity for the given pair of particles.

<sup>8</sup>N. W. Ashcroft and N. D. Mermin, *Solid State Physics* (Saunders College, Rochester, 1976).

<sup>9</sup>This follows since if  $v$  is an arbitrary vector and  $A_{ab} = \langle \Delta x_a \Delta x_b \rangle$  is the covariance matrix of a set  $\{x_a\}$  of random variables, then  $v^T A v$  is the variance of the random variable  $w = \sum_a v_a x_a$ , and thus non-negative.

<sup>10</sup>K. H. Esbensen, D. Guyot, F. Westad, and L. P. Houmøller, *Multivariate*

- Data Analysis—In practice*, 5th ed. (Camo, Oslo, 2002).
- <sup>11</sup>The sums over the diagonal blocks are non-negative since  $\lambda_\alpha$  is, and the sum over the first (last) components of  $v_\alpha v_\alpha^T$  is the dot product of the first (last) half of  $v_\alpha$  with itself, which is also non-negative.
- <sup>12</sup>The configuration  $\Gamma_{\text{ref}}$  is analogous to the inherent state configuration often used to describe viscous liquid dynamics (Refs. 29 and 30), which is obtained by minimizing the potential energy starting from configuration  $\Gamma$ .
- <sup>13</sup>We have checked the statements that the zeroth and first moments of  $\rho(r)$  over the first peak are constant apart from contributions at the cutoff by computing orthogonalized versions of them (using Legendre polynomials defined on the interval from  $0.8\sigma$  to  $1.4\sigma$ ) and showing that they are strongly correlated (correlation coefficient 0.9) with a slope corresponding to the cutoff itself.
- <sup>14</sup>L. D. Landau and E. M. Lifshitz, *Statistical Physics, Part 1* (Pergamon Press, London, 1980).
- <sup>15</sup>J. P. Hansen and I. R. McDonald, *Theory of Simple Liquids*, 2nd ed. (Academic, New York, 1986).
- <sup>16</sup>L. E. Reichl, *A Modern Course in Statistical Physics*, 2nd ed. (Wiley, New York, 1998).
- <sup>17</sup>W. Kauzmann, *Chem. Rev. (Washington, D.C.)* **43**, 219 (1948).
- <sup>18</sup>S. Brawer, *Relaxation in Viscous Liquids and Glasses* (American Ceramic Society, Columbus, 1985).
- <sup>19</sup>C. A. Angell, K. L. Ngai, G. B. McKenna, P. F. McMillan, and S. W. Martin, *J. Appl. Phys.* **88**, 3113 (2000).
- <sup>20</sup>J. C. Dyre, *Rev. Mod. Phys.* **78**, 953 (2006).
- <sup>21</sup>N. P. Bailey, T. Christensen, B. Jakobsen, K. Niss, N. B. Olsen, U. R. Pedersen, T. B. Schröder, and J. C. Dyre, *J. Phys.: Condens. Matter* **20**, 244113 (2008).
- <sup>22</sup>J. W. P. Schmelzer and I. Gutzow, *J. Chem. Phys.* **125**, 184511 (2006).
- <sup>23</sup>N. L. Ellegaard, T. Christensen, P. V. Christiansen, N. B. Olsen, U. R. Pedersen, T. B. Schröder, and J. C. Dyre, *J. Chem. Phys.* **126**, 074502 (2007).
- <sup>24</sup>U. R. Pedersen, T. Christensen, T. B. Schröder, and J. C. Dyre, *Phys. Rev. E* **77**, 011201 (2008).
- <sup>25</sup>W. Kob and H. C. Andersen, *Phys. Rev. Lett.* **73**, 1376 (1994).
- <sup>26</sup>J. K. Nielsen and J. C. Dyre, *Phys. Rev. B* **54**, 15754 (1996).
- <sup>27</sup>S. Mossa, E. La Nave, F. Sciortino, and P. Tartaglia, *Eur. Phys. J. B* **30**, 351 (2002).
- <sup>28</sup>L. J. Lewis and G. Wahnström, *Phys. Rev. E* **50**, 3865 (1994).
- <sup>29</sup>M. Goldstein, *J. Chem. Phys.* **51**, 3728 (1969).
- <sup>30</sup>F. H. Stillinger, *Science* **267**, 1935 (1995).
- <sup>31</sup>F. Sciortino, *J. Stat. Mech.: Theory Exp.* **2005**, 35.
- <sup>32</sup>A. Heuer, *J. Phys.: Condens. Matter* **20**, 373101 (2008).
- <sup>33</sup>E. La Nave, S. Mossa, and F. Sciortino, *Phys. Rev. Lett.* **88**, 225701 (2002).
- <sup>34</sup>N. Giovambattista, H. E. Stanley, and F. Sciortino, *Phys. Rev. Lett.* **91**, 115504 (2003).
- <sup>35</sup>T. Heimburg and A. D. Jackson, *Proc. Natl. Acad. Sci. U.S.A.* **102**, 9790 (2005).
- <sup>36</sup>T. Heimburg and A. D. Jackson, *Biophys. J.* **92**, 3159 (2007).
- <sup>37</sup>H. Ebel, P. Grabitz, and T. Heimburg, *J. Phys. Chem. B* **105**, 7353 (2001).
- <sup>38</sup>U. R. Pedersen, C. Leidy, P. Westh, and G. H. Peters, *Biochim. Biophys. Acta* **1758**, 573 (2006).
- <sup>39</sup>U. R. Pedersen, G. H. Peters, and P. Westh, *Biophys. Chem.* **125**, 104 (2007).
- <sup>40</sup>U. R. Pedersen, G. H. Peters, T. B. Schröder, and J. C. Dyre, *AIP Conf. Proc.* **982**, 407 (2008).
- <sup>41</sup>C. A. Angell, in *Relaxations in Complex Systems*, edited by K. L. Ngai and G. B. Wright (U.S. GPO, Washington, D.C., 1985), p. 3.
- <sup>42</sup>A. Le Grand, C. Dreyfus, C. Bousquet, and R. M. Pick, *Phys. Rev. E* **75**, 061203 (2007).
- <sup>43</sup>D. Coslovich and C. M. Roland, *J. Phys. Chem. B* **112**, 1329 (2008).
- <sup>44</sup>U. R. Pedersen, G. H. Peters, T. B. Schröder, and J. C. Dyre (unpublished).
- <sup>45</sup>E. W. Lemmon, M. O. McLinden, and D. G. Friend, in *NIST Chemistry WebBook, NIST Standard Reference Database Number 69*, edited by P. J. Linstrom and W. G. Mallard (NIST, Gaithersburg, 2005), URL <http://webbook.nist.gov>.
- <sup>46</sup>G. Tarjus, D. Kivelson, S. Mossa, and C. Alba-Simionesco, *J. Chem. Phys.* **120**, 6135 (2004).
- <sup>47</sup>C. Dreyfus, A. L. Grand, J. Gapinski, W. Steffen, and A. Patkowski, *Eur. Phys. J. B* **42**, 309 (2004).
- <sup>48</sup>R. Casalini and C. M. Roland, *Phys. Rev. E* **69**, 062501 (2004).
- <sup>49</sup>C. Roland, S. Hensel-Bielowka, M. Paluch, and R. Casalini, *Rep. Prog. Phys.* **68**, 1405 (2005).
- <sup>50</sup>T. B. Schröder, U. R. Pedersen, and J. C. Dyre, e-print arXiv:0803.2199.

## Pressure-energy correlations in liquids. III. Statistical mechanics and thermodynamics of liquids with hidden scale invariance

Thomas B. Schröder,<sup>a)</sup> Nicholas P. Bailey,<sup>b)</sup> Ulf R. Pedersen,<sup>c)</sup> Nicoletta Gnan,<sup>d)</sup> and Jeppe C. Dyre<sup>e)</sup>

*DNRF Center "Glass and Time," IMFUFA, Department of Sciences, Roskilde University, P.O. Box 260, DK-4000 Roskilde, Denmark*

(Received 29 May 2009; accepted 15 September 2009; published online 17 December 2009)

In this third paper of the series, which started with Bailey *et al.* [J. Chem. Phys. **129**, 184507 (2008); *ibid.* **129**, 184508 (2008)], we continue the development of the theoretical understanding of strongly correlating liquids—those whose instantaneous potential energy and virial are more than 90% correlated in their thermal equilibrium fluctuations at constant volume. The existence of such liquids was detailed in previous work, which identified them, based on computer simulations, as a large class of liquids, including van der Waals liquids but not, e.g., hydrogen-bonded liquids. We here discuss the following: (1) the scaling properties of inverse power-law and extended inverse power-law potentials (the latter includes a linear term that “hides” the approximate scale invariance); (2) results from computer simulations of molecular models concerning out-of-equilibrium conditions; (3) ensemble dependence of the virial/potential-energy correlation coefficient; (4) connection to the Grüneisen parameter; and (5) interpretation of strong correlations in terms of the energy-bond formalism. © 2009 American Institute of Physics. [doi:10.1063/1.3265955]

### I. INTRODUCTION

In a series of papers published last year,<sup>1–5</sup> we introduced the concept of strongly correlating liquids and demonstrated by computer simulations that this includes a large class of model liquids. Specifically, the fluctuations, which are in many cases strongly correlated, are those of the configurational parts of pressure and energy, i.e., the parts in addition to the ideal gas terms, coming from the interatomic forces. Recall that for any microscopic state, energy  $E$  and pressure  $p$  have contributions both from particle momenta and positions,

$$E = K(\mathbf{p}_1, \dots, \mathbf{p}_N) + U(\mathbf{r}_1, \dots, \mathbf{r}_N), \quad (1)$$

$$p = Nk_B T(\mathbf{p}_1, \dots, \mathbf{p}_N)/V + W(\mathbf{r}_1, \dots, \mathbf{r}_N)/V.$$

Here,  $K$  and  $U$  are the kinetic and potential energies, respectively, and  $T(\mathbf{p}_1, \dots, \mathbf{p}_N)$  is the “kinetic temperature,” proportional to the kinetic energy per particle.<sup>6</sup> The configurational contribution to pressure is the virial  $W$ , which is defined<sup>6</sup> by

$$W = -\frac{1}{3} \sum_i \mathbf{r}_i \cdot \nabla_{\mathbf{r}_i} U. \quad (2)$$

For a liquid with pair interactions, if  $v(r)$  is the pair potential and  $r_{ij}$  is the distance between particles  $i$  and  $j$ , we have

$$U_{\text{pair}} = \sum_{i < j} v(r_{ij}), \quad (3)$$

$$W_{\text{pair}} = -\frac{1}{3} \sum_{i < j} r_{ij} v'(r_{ij}). \quad (4)$$

Strong  $W$ ,  $U$  correlation, if present at all, is observed under conditions of fixed volume, as illustrated in Fig. 1(a). The degree of correlation is quantified by the standard correlation coefficient  $R$ , defined<sup>1,4</sup> by

$$R = \frac{\langle \Delta W \Delta U \rangle}{\sqrt{\langle (\Delta W)^2 \rangle} \sqrt{\langle (\Delta U)^2 \rangle}}. \quad (5)$$

Here and henceforth, unless otherwise specified, angular brackets  $\langle \rangle$  denote thermal  $NVT$  ensemble averages and  $\Delta$  denotes deviation from the average value of the quantity in question. We call liquids with  $R > 0.9$  strongly correlating. Another characteristic quantity is the “slope”  $\gamma$ , which we here define<sup>1,4</sup> as the ratio of standard deviations,

$$\gamma = \frac{\sqrt{\langle (\Delta W)^2 \rangle}}{\sqrt{\langle (\Delta U)^2 \rangle}}. \quad (6)$$

In the limit of perfect correlation ( $R \rightarrow 1$ ),  $\gamma$  becomes equal to the slope of average  $W$  as a function of average  $U$  at fixed volume,  $\gamma = (\partial W / \partial U)_V$ .

In Paper I (Ref. 4) of this series, it was shown that strongly correlating liquids are typically those with van der Waals type attraction and steep repulsion, which in simulations are often modeled by combinations of one or more Lennard-Jones (LJ)-type potentials. Typical slope values for the latter are of the order of 6, depending slightly on the state point (in the limit of very high density or temperature, the slope converges slowly to 4).

It is worth noting that the class of strongly correlating liquids does not simply correspond to radially symmetric

<sup>a)</sup>Electronic mail: tbs@ruc.dk.

<sup>b)</sup>Electronic mail: nbailey@ruc.dk.

<sup>c)</sup>Electronic mail: urp@ruc.dk.

<sup>d)</sup>Electronic mail: ngnan@ruc.dk.

<sup>e)</sup>Electronic mail: dyre@ruc.dk.

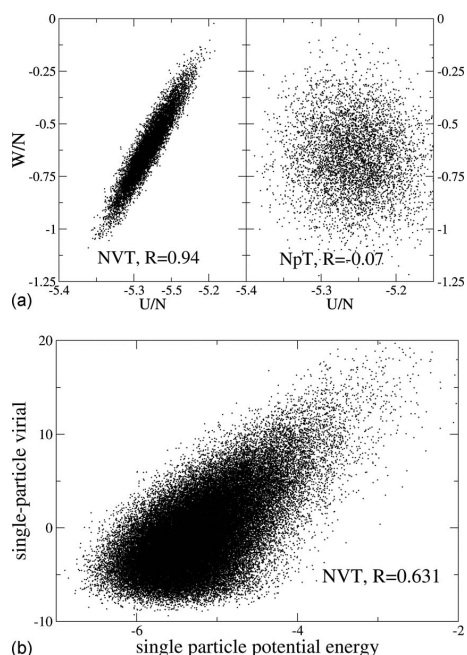


FIG. 1. (a) Scatter plot of total virial and potential energy (in LJ units) for the standard single-component LJ liquid at  $T=80$  K (argon units) and near-zero pressure, simulated at constant volume (density  $\rho=34.6$  mol/l, argon units, left panel) and constant pressure (1.5 MPa, argon units, right panel). (b) Scatter plot of single-particle virial and potential energy for the same simulation as in the left panel of (a). The single-particle  $WU$  correlation is much weaker,  $R=0.63$ , showing that collective effects are crucial for the correlation.

pair potentials. Firstly, two metallic systems with many-body potentials were found to be strongly correlating; we believe metallic systems in general are strongly correlating, although this needs to be confirmed. Also many molecular liquids are strongly correlating. In fact, any potential with an inverse power-law (IPL) dependence on distances (not necessarily based on pair interactions) is perfectly correlating. Secondly, there exist radially symmetric pair potentials that are not strongly correlating, for example, the Dzugutov system.<sup>4,7</sup> One reason for strong correlation not to hold in some molecular systems is the presence of Coulombic terms in the potential. By themselves these would give 100% correlation, but their combination with LJ forces typically leads to a weak correlation. This was detailed in Paper I, which presented results from simulations of 13 different model liquids. In our present understanding based on these simulations, liquids with two length scales in their potentials are rarely strongly correlating.

Paper II (Ref. 5) in this series analyzed the case of the standard single-component LJ liquid in detail. Building on the fact that IPL potentials  $\propto r^{-n}$  are perfectly correlating, the results of this analysis can be summarized as follows: (1) almost all of the fluctuations in  $W$  and  $U$  come from interparticle separations in the region of the first peak of the radial distribution function  $g(r)$ ; (2) in this region, the LJ potential is approximated very well by the sum of an IPL with

exponent  $n \sim 18$  and a linear term  $B+Cr$ ; and (3) when volume is fixed, the parts of  $W$  and  $U$  that come from the linear term are almost constant. Our initial and simpler explanation of strong  $WU$  correlations<sup>1</sup> was based on the dominance of close encounters, i.e., that it is only the nature of the repulsive part of the potential that matters for the strong correlations. This explanation, however, is only adequate at high pressure/density. It does not explain the requirement of fixed volume, nor the fact that strong correlation is observed even at zero pressure, as well as for the low-temperature/low-pressure (classical) crystal. To see that an explanation at the individual pair interaction level is generally inadequate, consider Fig. 1(b) which shows a scatter plot of single-particle energy and virial. These are sums over the pair interactions a given particle has with its neighbors; summing over all particles gives the total potential energy and virial, respectively. If strong correlation held at the level of single pair interactions, it would also hold at the particle level, but it clearly does not. This emphasizes that strong correlation is a collective effect, as detailed in Paper II.

In this paper, we elaborate on the statistical mechanics and thermodynamics of strongly correlating liquids and report results from computer simulations, showing that strong virial/potential energy correlations are present even in non-equilibrium processes. The purpose is to present a number of new results supplementing those of Paper II in order to broadly illuminate the properties of strongly correlating liquids. Together Papers II and III give a fairly complete characterization of the properties of a strongly correlating liquid at one state point, as well as at different state points with the same density. Paper IV<sup>8</sup> in this series goes on to consider varying-density curves of “isomorphic” state points in the phase diagram, which are characterized by several invariants; such curves exist only for strongly correlating liquids. Paper IV also discusses how and why there are, in fact, other numbers close to the  $\gamma$  of Eq. (6) that reflect a liquid’s hidden scale invariance. For any strongly correlating liquid, these numbers are close to each other, so for simplicity throughout this paper we shall only use one  $\gamma$ , namely the one defined by Eq. (6) (in Paper IV the definition of  $\gamma$  changes to a slightly smaller number).

The organization of the paper is as follows. Section II begins with a discussion of the scaling properties of systems with IPL potentials, the natural starting point for a discussion of the hidden scaling properties of strongly correlating liquids. This is followed by a generalization to allow an extra term in the free energy depending on the volume only. Some, but not all, scaling properties of IPL systems are inherited by this generalization. Following this, in Sec. III we discuss the “extended inverse-power law” (eIPL) potential introduced in Paper II, which includes the above-mentioned linear term. We illustrate with simulation results the key property that the linear term contributes significantly to the virial and potential energy fluctuations when the volume may fluctuate, but little when it is fixed. Hence, it gives rise, approximately, to a volume-dependent term in the free energy of the type discussed in the previous subsection. This leads to an inherited approximate scaling property, which we refer to as “hidden scale invariance” since it is not immediately obvious from

the intermolecular potential. The argument about how and why hidden scale invariance causes strong  $WU$  correlations makes no assumption about equilibrium. To emphasize this point, Sec. IV presents results from nonequilibrium computer simulations of strongly correlating molecular liquids, in particular, aging following a temperature jump, and crystallization, both at constant volume. The property of strong correlation is shown to apply even in these out-of-equilibrium situations. Section V discusses ensemble dependence; it is shown here that the virial/potential energy correlation is always stronger in the  $NVT$  ensemble than in the  $NVE$  one. The last main section, Sec. VI, comprises of two topics under the heading “thermodynamics of strongly correlating liquids.” First, we discuss the relation of pressure-energy correlations to the thermodynamic Grüneisen parameter  $\gamma_G$ , showing that the slope  $\gamma$  [Eq. (6)] is larger than  $\gamma_G$  by roughly a factor involving the ratio of excess (configurational) to total constant-volume specific heat. This ratio is around 2 for many simple liquids.<sup>9</sup> The second part formulates the property of strong correlation in the energy-bond language known as “network thermodynamics.”<sup>10</sup>

## II. PROPERTIES OF IPL SYSTEMS AND GENERALIZATIONS

The purpose of this section is to summarize the properties of IPL potentials and identify which of these properties are inherited by strongly correlating liquids and which are not.

### A. IPL potentials

IPL potentials—sometimes referred to as soft-sphere potentials—have been used in liquid state theory for many years as convenient model systems.<sup>11–18</sup> Such potentials have a number of simple properties. IPL potentials have, however, been considered unrealistic because their predicted equation of state is quite unrealistic and because they have no stable low-pressure liquid phase and no van der Waals loop, problems that derive from the fact that IPL potentials are purely repulsive. Moreover, the correct IPL exponent fitting the LJ liquid is around 18 (Papers I and II, Refs. 16, 19, and 20), not 12 as one might naively guess from the repulsive  $r^{-12}$  term of the LJ potential; this may have confused people searching from an effective IPL description of the LJ liquid. A major point made in this series of papers is that, when interpreted correctly, IPL potentials are much more realistic than generally thought because they describe well a number of properties of strongly correlating liquids. For reference, we now briefly summarize the long established properties of IPL liquids.

Consider  $N$  identical particles in volume  $V$  interacting by a pair potential of the form  $v(r)=Ar^{-n}$ ; we make the pair assumption for simplicity but note that the argument below generalizes immediately to any potential that is an Euler homogeneous function of the position coordinates. From the standard partition function, the (Helmholtz) free energy  $F$  is conveniently written<sup>6,21</sup> as the ideal gas term plus the non-trivial “excess” free energy,  $F=F_{id}+F_{ex}$ . The first term is the free energy of an ideal gas at the same volume and tempera-

ture,  $F_{id}=Nk_B T \ln(\rho\Lambda^3/e)$ , where  $\rho=N/V$  is the particle number density and  $\Lambda=h/\sqrt{2\pi mk_B T}$  is the thermal de Broglie wavelength. The excess free energy is given<sup>6,21</sup> by

$$e^{-F_{ex}/k_B T} = \int \frac{d\mathbf{r}_1}{V} \dots \frac{d\mathbf{r}_N}{V} e^{-U(\mathbf{r}_1, \dots, \mathbf{r}_N)/k_B T}. \quad (7)$$

Whenever  $n > 3$ , this expression leads to a free energy with a well-defined extensive thermodynamic limit ( $N \rightarrow \infty$ ).<sup>11,12</sup>

It follows from Eq. (7) that the excess free energy of an IPL liquid is given as follows in terms of a function of density  $\rho$  to the power  $n/3$  over temperature  $T$ ,  $\phi(\rho^{n/3}/T)$  (Klein’s theorem<sup>11,12</sup>):

$$F_{ex,IPL} = Nk_B T \phi(\rho^{n/3}/T). \quad (8)$$

Equation (8) implies that a number of derived quantities are also functions of  $\rho^{n/3}/T$ . As important examples, recall the following standard identities: the excess entropy:  $S_{ex} = -(\partial F_{ex}/\partial T)_V$ , the potential energy:  $U = F_{ex} + TS_{ex}$ , the virial  $W = -V(\partial F_{ex}/\partial V)_T$ , the excess isothermal bulk modulus:  $K_T^{ex} = V(\partial^2 F_{ex}/\partial V^2)_T$ , the excess isochoric specific heat per unit volume:  $c_V^{ex} = -(T/V)(\partial^2 F_{ex}/\partial T^2)_V$ , the excess pressure coefficient:  $\beta_V^{ex} = (1/V)(\partial W/\partial T)_V = -\partial^2 F_{ex}/\partial T \partial V$ . These quantities are all functions of the single variable  $\rho^{n/3}/T$ ; more accurately, one has [where  $f_1(x) = x\phi'(x) - \phi(x)$ ,  $f_2(x) = x\phi'(x)$ ,  $f_3(x) = (n/3)^2 x^2 \phi''(x) + [(n/3) + (n/3)^2] x\phi'(x)$ , and  $f_4(x) = -x^2 \phi''(x)$ ],

$$S_{ex,IPL} = Nk_B f_1(\rho^{n/3}/T), \quad (9)$$

$$U_{IPL} = Nk_B T f_2(\rho^{n/3}/T), \quad (10)$$

$$W_{IPL} = \frac{n}{3} Nk_B T f_3(\rho^{n/3}/T), \quad (11)$$

$$K_{T,IPL}^{ex} = \rho k_B T f_3(\rho^{n/3}/T), \quad (12)$$

$$c_{V,IPL}^{ex} = \rho k_B f_4(\rho^{n/3}/T), \quad (13)$$

$$\beta_{V,IPL}^{ex} = \frac{n}{3} \rho k_B f_4(\rho^{n/3}/T). \quad (14)$$

The functions  $\phi$  and  $f_1, \dots, f_4$  all depend on  $n$ , but, for simplicity of notation, we have not indicated this explicitly. Dividing across by the dimensional factors on the right hand side (for example,  $k_B T$  in the case of potential energy and virial), one arrives at dimensionless forms of the excess entropy, potential energy, etc., which are functions of  $\rho^{n/3}/T$  only.

Turning now to the dynamics, consider the standard molecular dynamics (MD) case where the equations of motion are Newton’s equations. Suppose  $\mathbf{r}_i(t)$  ( $i=1, \dots, N$ ) is a solution to Newton’s equations. Then, it is straightforward to show that  $\mathbf{r}_i^{(1)}(t) = \alpha \mathbf{r}_i(\lambda t)$  is also a solution if  $\alpha^{-(n+2)} = \lambda^2$ . In particular, if  $\mathbf{r}_i(t)$  refers to equilibrium ( $NVE$  or  $NVT$ ) dynamics at a state point with density  $\rho_0$  and temperature  $T_0$ , then  $\mathbf{r}_i^{(1)}(t) = \alpha \mathbf{r}_i(\lambda t)$  refers to equilibrium dynamics at density  $\rho_1 = \rho_0/\alpha^3$  and temperature  $T_1 = T_0 \alpha^2 \lambda^2$  (temperature

scales as the mean-square velocity and velocities get a factor  $\alpha\lambda$ ). Using the above relation between  $\alpha$  and  $\lambda$ , this implies that

$$T_1 = \alpha^{-n} T_0 = \left(\frac{\rho_1}{\rho_0}\right)^{n/3} T_0. \quad (15)$$

This means that two states with different densities and temperatures but the same  $\rho^{n/3}/T$  have dynamics that scale into one another by simple scalings of space and time. In particular, if for any quantity  $A$  one defines the relaxation time  $\tau_A$  via  $\tau_A = \int_0^\infty \langle A(0)A(t) \rangle dt / \langle A^2 \rangle$ , it follows that any two states with same  $\rho^{n/3}/T$  have the same “reduced” (dimensionless) relaxation time  $\tilde{\tau}_A$ , if this quantity is defined by  $\tilde{\tau}_A = \tau_A/t_0$  where the characteristic time  $t_0$  is defined by  $t_0 = \rho^{-1/3} \sqrt{m/k_B T}$ . Similarly, if one defines the reduced diffusion constant  $\tilde{D}$  by  $\tilde{D} = D/D_0$ , where  $D_0 = \rho^{-2/3}/t_0 = \rho^{-1/3} \sqrt{k_B T/m}$ , then  $\tilde{D}$  is the same for the two states. Summarizing,

$$\tilde{\tau} = f_5(\rho^{n/3}/T), \quad (16)$$

$$\tilde{D} = f_6(\rho^{n/3}/T). \quad (17)$$

Finally, we note that it follows from the above scaling property that

$$\frac{U_{\text{IPL}}(\mathbf{r}_1^{(1)}, \dots, \mathbf{r}_N^{(1)})}{k_B T_1} = \frac{U_{\text{IPL}}(\mathbf{r}_1, \dots, \mathbf{r}_N)}{k_B T_0}. \quad (18)$$

Thus, the Boltzmann factors of the two microscopic configurations are the same. Consequently, the scaling of the dynamics holds also for stochastic dynamics. This observation, in a generalized form, is the starting point of Paper IV in this series. By the same argument, the structure of states with the same  $\rho^{n/3}/T$  are identical provided that lengths are scaled by  $\rho^{-1/3}$ .

### B. Inheritance of scaling properties by generalized IPL potentials

This section discusses how a potential may have a number of IPL properties to a good approximation, thus justifying the term “hidden scale invariance.” Consider a general potential between particles  $i$  and  $j$ , rewriting it (as can always be done) as a sum of an IPL potential plus the difference, denoted as “diff,”

$$v_{ij}(r_{ij}) = \epsilon_{ij} \left(\frac{\sigma_{ij}}{r_{ij}}\right)^n + v_{ij}^{\text{diff}}(r_{ij}). \quad (19)$$

For any microscopic configuration  $(\mathbf{r}_1, \dots, \mathbf{r}_N)$ , the potential energy is then the sum of an IPL term and a “diff” term, and the excess free energy is given by

$$e^{-F_{\text{ex}}/k_B T} = \int \frac{d\mathbf{r}_1}{V} \dots \frac{d\mathbf{r}_N}{V} e^{-U_{\text{IPL}}(\mathbf{r}_1, \dots, \mathbf{r}_N)/k_B T} e^{-U_{\text{diff}}(\mathbf{r}_1, \dots, \mathbf{r}_N)/k_B T}. \quad (20)$$

We now investigate consequences of the crucial assumption (see Paper II and Sec. III) that  $U_{\text{diff}}$  to a good approximation is only a function of volume:  $U_{\text{diff}}(\mathbf{r}_1, \dots, \mathbf{r}_N) \cong f(V)$ —at least for states that carry Boltzmann weights of any significance. The approximate identity  $U_{\text{diff}}(\mathbf{r}_1, \dots, \mathbf{r}_N) = f(V)$

means that the second exponential can be moved outside the integral, and we get

$$e^{-F_{\text{ex}}/k_B T} = e^{-f(V)/k_B T} \int \frac{d\mathbf{r}_1}{V} \dots \frac{d\mathbf{r}_N}{V} e^{-U_{\text{IPL}}(\mathbf{r}_1, \dots, \mathbf{r}_N)/k_B T}. \quad (21)$$

From this follows directly that

$$F_{\text{ex}} = f(V) + F_{\text{ex,IPL}} = f(V) + Nk_B T \phi(\rho^{n/3}/T). \quad (22)$$

This implies that

$$S_{\text{ex}} = S_{\text{ex,IPL}} = Nk_B f_1(\rho^{n/3}/T), \quad (23)$$

$$U = f(V) + U_{\text{IPL}} = f(V) + Nk_B T f_2(\rho^{n/3}/T), \quad (24)$$

$$W = -Vf'(V) + W_{\text{IPL}} = -Vf'(V) + \frac{n}{3} Nk_B T f_2(\rho^{n/3}/T), \quad (25)$$

$$K_T^{\text{ex}} = Vf''(V) + K_{T,\text{IPL}}^{\text{ex}} = Vf''(V) + \rho k_B T f_3(\rho^{n/3}/T), \quad (26)$$

$$c_V^{\text{ex}} = c_{V,\text{IPL}}^{\text{ex}} = \rho k_B f_4(\rho^{n/3}/T), \quad (27)$$

$$\beta_V^{\text{ex}} = \beta_{V,\text{IPL}}^{\text{ex}} = \frac{n}{3} \rho k_B f_4(\rho^{n/3}/T). \quad (28)$$

While the systems under consideration here have the same excess entropy as their “hidden” IPL systems, several other quantities have contributions from the  $f(V)$  term. These quantities do not obey IPL scaling. In contrast, the scaling behavior for dynamics and structure *is* inherited. To see this, consider two state points with the same  $\rho^{n/3}/T$ . For the pure IPL system [ $f(V)=0$ ], the two state points have the same dynamics and structure as argued in the previous section. Letting  $f(V) \neq 0$  simply shifts the energy surface, which changes neither the dynamics nor the structure.<sup>22,23</sup> This scenario—scaling of the dynamics, but not the equation of state—is exactly what is experimentally observed for a large number of viscous liquids. For example, in van der Waals liquids relaxation times are found to be a function of  $\rho^{n/3}/T$  (using  $n$  as an empirical parameter),<sup>24,25</sup> but the scaling does not apply to the (excess) pressure with the exponent determined from the scaling of relaxation time, as required for IPL scaling.<sup>24,26</sup>

In Sec. III we provide numerical evidence that there are indeed systems that to a good approximation fulfill the assumption introduced above that  $U_{\text{diff}}$  is a function of volume only.

### III. LJ AS A GENERALIZED IPL POTENTIAL: THE eIPL POTENTIAL APPROXIMATION

In this section we examine the extent to which the LJ potential may be approximated by an eIPL potential [including a linear term, Eq. (33), below] by considering the fluctuations at a particular state point of the LJ liquid. We choose a state point whose pressure is near zero because here it is particularly clear that single-pair effects are insufficient to explain the strong  $WU$  correlation (Fig. 1).

The analysis of Paper II took its starting point in assuming that the approximating IPL should match the potential

closely at a particular value of the interparticle separation. An important conclusion of the analysis was, however, that the success of the IPL approximation is derived not from its behavior near any particular  $r$ -value, but rather from the fact that the difference from the real potential is close to linear over the whole first-peak region. In this section we reexamine the idea that the fluctuations are well described by an IPL potential and the argument for why the difference term almost does not fluctuate. We show explicitly that the latter contributes little to the fluctuations at constant volume, but significantly when the volume is allowed to fluctuate as in the  $NpT$  ensemble. This demonstrates that the LJ potential is of the type considered in the previous subsection.

We wish to determine to what extent the LJ potential

$$v_{\text{LJ}}(r) = 4\epsilon((\sigma/r)^{12} - (\sigma/r)^6) \quad (29)$$

can be matched, for the purpose of describing fluctuations of potential energy and virial at fixed volume, by an IPL

$$v_{\text{IPL}}(r) = Ar^{-n}[+B]. \quad (30)$$

Here,  $B$  indicates an optional constant. To start with, how should the exponent  $n$  and the coefficients  $A$  and  $B$  be chosen? An obvious choice, followed in the first part of Paper II, is to require that the two potentials,  $v_{\text{LJ}}$  and  $v_{\text{IPL}}$ , should agree as much as possible around a particular value of  $r$ , denoted  $r_0$ . Given  $r_0$ , if we require the functions and their first two derivatives to match at  $r_0$ , this determines all three parameters  $A$ ,  $n$ , and  $B$ . The exponent  $n$  is given (Paper II) by

$$n = n^{(1)}(r_0) \equiv -\frac{r_0 v_{\text{LJ}}''(r_0)}{v_{\text{LJ}}'(r_0)} - 1. \quad (31)$$

Here, the notation  $n^{(1)}(r_0)$  refers to one kind of  $r$ -dependent effective IPL exponent, based on the ratio of the second and first derivatives. For  $v_{\text{IPL}}(r)$  this simply returns  $n$ . Otherwise, it gives a local matching of the  $v_{\text{LJ}}(r)$  to  $v_{\text{IPL}}(r)$ . This leaves effectively one parameter to vary, namely  $r_0$ , which must be less than the location of the minimum of the LJ potential  $r_m = 2^{1/6}\sigma$ , where  $n^{(1)}$  diverges. The parameter  $r_0$  may be chosen to optimize the match of the fluctuations in the total energy and virial. For an  $NVT$  simulation at  $T=80$  K and near-zero pressure, the best fit was obtained with  $n=19.2$  (while the exponent implied by the slope [Eq. (6)],  $\gamma=6.3$ , was slightly smaller, 18.9).

Later in Paper II, it was demonstrated that there is no particular reason why the potentials should match close at a particular value of  $r$  since the fluctuations have contributions from the whole first-peak region, including beyond the potential minimum. The reason that any kind of matching is possible over this region—where  $v_{\text{LJ}}$  clearly does not resemble a power law—is that a linear term may be added to the power-law potential almost without affecting the fluctuations as long as the volume is held constant. The analysis of Paper II, which also included an in-depth treatment of the perfect LJ (fcc) crystal which is also strongly correlating, showed that the more relevant  $r$ -dependent effective exponent is the higher order  $n^{(2)}$  defined by

$$n^{(2)}(r_0) \equiv -\frac{r_0 v_{\text{LJ}}'''(r_0)}{v_{\text{LJ}}''(r_0)} - 2. \quad (32)$$

This also returns  $n$  for  $v_{\text{IPL}}(r)$ , but since it does not involve the first derivative, it returns  $n$  even if a linear function of  $r$  is added to the potential as in the eIPL potential defined by

$$v_{\text{eIPL}} = Ar^{-n} + B + Cr. \quad (33)$$

This potential fits the LJ potential very well around its minimum (Paper II) and thus includes some of its attractive part.

There are several possible ways of choosing the “best” eIPL to match the real potential. These will give slightly different exponents and coefficients  $A$ ,  $B$ , and  $C$ . We do not investigate them here; rather the purpose is to validate the basic idea of the eIPL approximation. Therefore, we choose a simple matching scheme, whereby we match the fluctuations to those of the IPL potential, without including a linear term, in order to determine  $n$  and  $A$ . For simplicity, we take the exponent directly from the observed fluctuations:  $n=3\gamma$ , where  $\gamma$  is defined in Eq. (6). To fix the coefficient  $A$ , agreement with the potential energy and virial fluctuations is optimized by proceeding as follows. For a given configuration generated in a LJ MD simulation, we calculate the LJ potential energy  $U_{\text{LJ}}$  and the power-law potential energy  $U_{\text{IPL}}$ , similarly the corresponding virials  $W_{\text{LJ}}$  and  $W_{\text{IPL}}$ . The difference quantities  $U_{\text{diff}}$  and  $W_{\text{diff}}$  are defined as

$$U_{\text{diff}} = U_{\text{LJ}} - U_{\text{IPL}}, \quad (34)$$

$$W_{\text{diff}} = W_{\text{LJ}} - W_{\text{IPL}}. \quad (35)$$

A perfect match of the fluctuations would mean that  $U_{\text{diff}}$  and  $W_{\text{diff}}$  have zero variance. Therefore, we choose  $A$  to minimize the sum of the relative diff variances,

$$\frac{\langle(\Delta U_{\text{diff}})^2\rangle}{\langle(\Delta U_{\text{LJ}})^2\rangle} + \frac{\langle(\Delta W_{\text{diff}})^2\rangle}{\langle(\Delta W_{\text{LJ}})^2\rangle}. \quad (36)$$

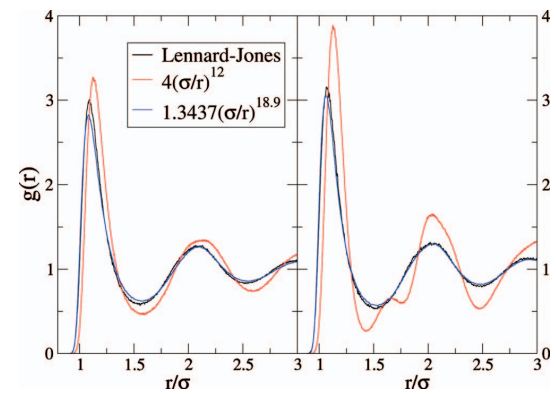


FIG. 2. Comparison of  $g(r)$  for simulations using the LJ potential and two IPL potentials: the  $r^{-12}$  repulsive term in  $v_{\text{LJ}}(r)$  and the IPL potential that optimizes the agreement in the fluctuations of potential energy and virial by minimizing Eq. (36). The left panel shows these at a density of 0.82 and a temperature of 0.67 (LJ units), the right one at a density of 0.90 and a temperature of 0.80 (where the  $r^{-12}$  potential leads to crystallization).

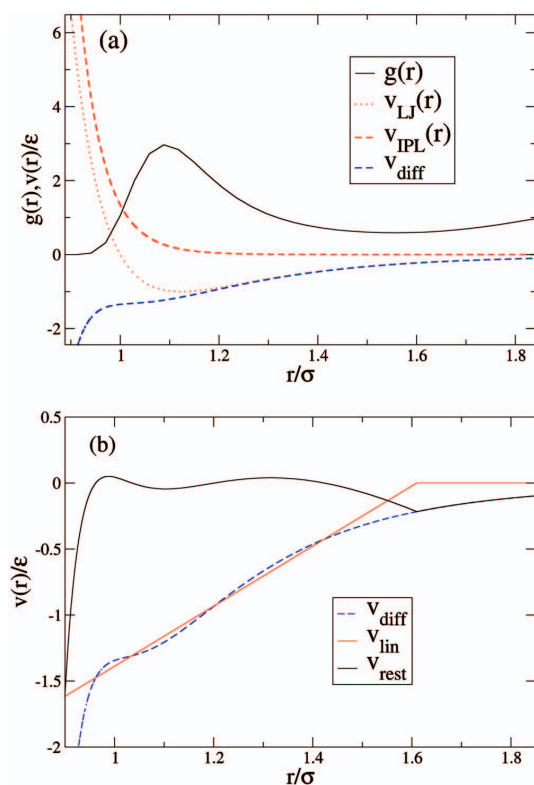


FIG. 3. (a) Illustration of the difference between the LJ potential  $v_{LJ}(r)$ , the empirically matched IPL potential  $v_{IPL}(r)$  with  $A=1.3437\epsilon\sigma^n$  and  $n=18.9$ , and their difference  $v_{diff}(r)$ . (b) Linear fit,  $v_{lin}(r)=\min(0, -3.6635 + 2.2756r/\sigma)$ , to  $v_{diff}$  between  $0.95\sigma$  and  $1.5\sigma$ , and the remainder  $v_{rest}(r) \equiv v_{diff}(r) - v_{lin}(r)$  (full black curve).

For the near-zero pressure state point used in Fig. 1 of Paper I, the exponent determined from  $\gamma$  is  $n=3\gamma=18.9$  and the optimal value of  $A$  is  $1.3437\epsilon\sigma^n$ . Before examining the difference potential, what do we get if we simulate with the matched IPL potential? Figure 2 shows the radial distributions  $g(r)$  obtained for the above state point and another with a higher density and temperature, for three potentials: LJ, the repulsive  $r^{-12}$  term of the LJ potential, and the optimal IPL potential with  $n=18.9$ . We used the same IPL potential at both state points (i.e., we did not adjust  $A$  and  $n$  to match the second state point). The first thing to note is that the  $n=18.9$  potential gives a structure much closer to that of the LJ potential than does the repulsive  $n=12$  term alone, in particular, the latter system has crystallized at the higher density and temperature. The second point is that there is still a difference between the LJ and the  $n=18.9$  IPL, present in both state points. The first peak in the LJ system is slightly higher and narrower, although its position is barely altered. Thus, the real potential gives a slight increase in order—however, the difference in the coordination number is less than 0.1 (integrating to the first minimum after the peak).

Figure 3(a) shows the LJ potential, the IPL potential with parameters optimized as described above, their difference,

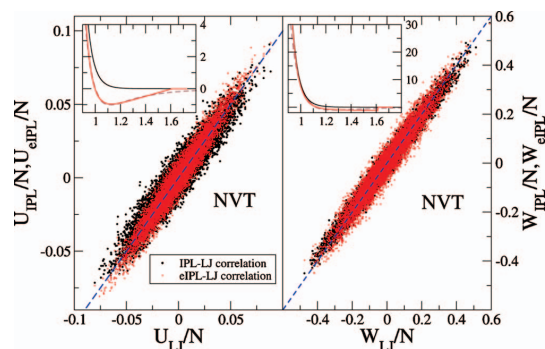


FIG. 4. Effect on fixed-volume fluctuations of adding a linear term to the IPL potential. The linear term is that shown in Fig. 3(b). Configurations were generated by an NVT simulation using the LJ potential, and the different determinations of energy (LJ, IPL, and eIPL) and virial were computed on these configurations. The dashed lines indicate a perfect match. Including the linear term when computing the energy improves the match to the true (LJ) fluctuations (the correlation coefficient goes from 0.950 to 0.970), while it reduces the match to the virial (the correlation coefficient goes from 0.987 to 0.971, which is probably related to the fact that the pair virial is discontinuous at  $r_c$ —we find that smoothing the linear part around  $r_c$  restores the match somewhat). The insets show the pair potentials and virials: brown dashed lines, LJ; black lines, IPL; and red lines, eIPL. The overall conclusion from Fig. 4 is that the addition of the linear term induces little change in the fluctuations.

and the radial distribution function. As shown in Fig. 3(b), the main part of the difference potential  $v_{diff}(r)$  is nearly linear. Thus, a good approximation to the real potential is the eIPL potential of Eq. (33) for  $r$  less than a cutoff  $r_c$  and zero otherwise. Neglecting the small value of  $v_{IPL}(r_c) \sim 10^{-5}\epsilon$ , the cutoff is given by  $r_c = -B/C$ . For the fit shown in Fig. 3(b),  $r_c = 1.61\sigma$ .

What are the implications of the linear term? A linear term in the pair potential contributes a term proportional to the sum of all bond lengths to the total potential energy. It was shown in Paper II that at constant volume, this sum is a constant in one dimension, and it was argued that it is approximately constant in three dimensions. The difference is because of two things. First, in three dimensions, there are contributions to bond-length changes from transverse components of relative displacements between the two particles defining a bond; second, within the eIPL the potential is only linear up to  $r_c$ , which means that argument that the linear term contributes little to the fluctuations depends on all bond lengths being less than  $r_c$ . In one dimension, at moderate temperatures, a single-component system has a rather well-defined nearest-neighbor distance, which, at densities where the pressure is not too negative, will be less than  $r_c$ . In a three-dimensional liquid, however, the nearest-neighbor distance is not as well defined—the radial distribution function does not go to zero after the first peak. Therefore, there will always be fluctuations at  $r_c$  as the lengths of bonds fluctuate back and forth across  $r_c$ , so the sum of bond lengths, which are less than  $r_c$ , will fluctuate. In Paper II, it was shown that for a three-dimensional (classical) crystal at low temperature—where this is not an issue because  $g(r)$  does go to zero after the peak—the correlation coefficient  $R$  becomes very high, over 99.5%, as  $T \rightarrow 0$  (but not 100%).

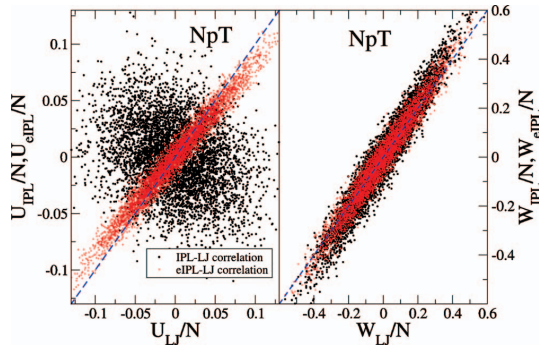


FIG. 5. Comparison of potential energy calculated using  $v_{LJ}(r)$ ,  $v_{IPL}(r)$  (black points), and  $v_{eIPL}(r)$  (red points) for configurations drawn from an  $NpT$  simulation using the LJ potential for the same state as in Fig. 4. The potential energy, in particular, is very poorly represented by the inverse power-law contribution when the volume is allowed to fluctuate. In fact, the correlation between  $U_{IPL}$  and  $U_{LJ}$  is not only weak, it is negative. Including the linear term makes a huge difference here, yielding a correlation coefficient of 0.977 between  $U_{eIPL}$  and  $U_{LJ}$  (changed from  $-0.201$ ). The slope is somewhat less than unity, indicating that there are significant contributions from pair distances beyond  $r_c$  (i.e., from the “rest” part of the potential). The linear term affects the virial fluctuations much less presumably because the derivative of the potential is dominated by the IPL term.

We can check directly the effect of adding the linear term to the IPL. Figure 4 shows scatter plots of IPL (black) and eIPL (red) energy and virial plotted against the true LJ values. These were calculated for a set of configurations drawn from an  $NVT$  simulation using the true (LJ) potential. Including the linear term makes little difference. It somewhat improves the match to the energies, though not to the virials (possibly due to the discontinuity in the pair virial at  $r_c$ ). The  $WU$  correlation coefficient of the eIPL potential energy and virial is 0.917 [compare to the true (LJ) value of 0.938 and the pure IPL value of 1.0].

It is instructive to repeat the above for configurations drawn from an  $NpT$  simulation at the same state point, i.e., with pressure chosen as the average pressure of the corresponding  $NVT$  simulation. The results are shown in Fig. 5. Here, it is clear that the IPL potential represents the potential energy fluctuations very poorly (black points), while adding the linear term makes a substantial difference (red points). As in the  $NVT$  case, the linear term affects the virial fluctuations much less. This is presumably because when taking the derivative to form the virial, the IPL term gets multiplied by  $n \gg 1$ , while the linear term gets multiplied by  $-1$  and is thus reduced considerably in significance (cf. the insets of Fig. 4).

The size of the variances of the different terms are com-

pared in Table I. We do not make a detailed analysis of the variance (taking into account cross correlations, etc). In the  $NVT$  case, the IPL contributions are of similar size to the full (LJ) fluctuations—naturally since we explicitly optimized this—and the diff contributions are small compared to the IPL ones. In the  $NpT$  case, on the other hand, the diff contributions to the fluctuations of  $U$  are more than double the IPL ones; this is not the case for the diff contributions to  $W$ , though they are still a larger fraction of the total than in the  $NVT$  case. These numbers are consistent with Fig. 5. The diff contributions to the energy must be larger than the IPL ones because the latter is negatively correlated with the true energy. The fact that the variance of  $U_{diff}$  is smaller than the sum of those of  $U_{lin}$  and  $U_{rest}$ , in the  $NVT$  case, indicates that the latter two are negatively correlated. This is presumably due to bond lengths around  $r_c$  which alternately are counted as part of  $U_{lin}$  and as part of  $U_{rest}$  as they fluctuate. This effect is less noticeable in the  $NpT$  case; there we see clearly that fluctuations in  $U_{lin}$  account for most of those in  $U_{rest}$ .

Based on the above, we can now answer the question: Is it possible to predict whether or not a liquid is strongly correlating by inspection of its potential (i.e., without simulating virial and potential energy fluctuations)? For liquids with particles interacting by pair potentials, the answer is in the affirmative: the liquid is strongly correlating if the potential around the first peak of the structure factor (the typical interparticle distance) may be fitted well by an eIPL and if the potential involves only one characteristic length. For more general potentials, the situation is more complex. Thus, it is possible to construct many-body potentials with angular dependencies which scale like IPL pair potentials; these have 100%  $WU$  correlation because this property follows whenever the potential is an Euler homogeneous function. In most realistic cases, however, systems with angular dependencies are not expected to be strongly correlating. An example is the coarse-grained model of water using a short-range many-body potential recently introduced by Molinero and Moore,<sup>27</sup> a model that reproduces water’s properties with surprising accuracy. This potential is not strongly correlating because close to water’s density maximum the virial/potential energy correlation coefficient  $R$  must be close to zero (Paper I). Examples of potentials with two length scales, that for this reason are not strongly correlating, are the Jagla potential<sup>28</sup> and the Dzugutov potential.<sup>7</sup> Likewise, the addition of Coulomb terms to a LJ-type potential generally ruins strong correlations (Paper I).

TABLE I. Variances of potential energy  $U$  and virial  $W$ , and of various contributions to  $U$  and  $W$ , of two different ensembles at the LJ state point given by  $\rho=0.82$  and  $T=0.67$  (dimensionless units).

Ensemble	Quantity	LJ	IPL	diff	lin	rest
$NVT$	$U$	0.0231	0.0225	0.0075	0.0085	0.0063
	$W$	0.1468	0.1402	0.0227	0.0301	0.0350
$NpT$	$U$	0.0484	0.0320	0.0665	0.0539	0.0144
	$W$	0.1704	0.1997	0.0589	0.0417	0.0430

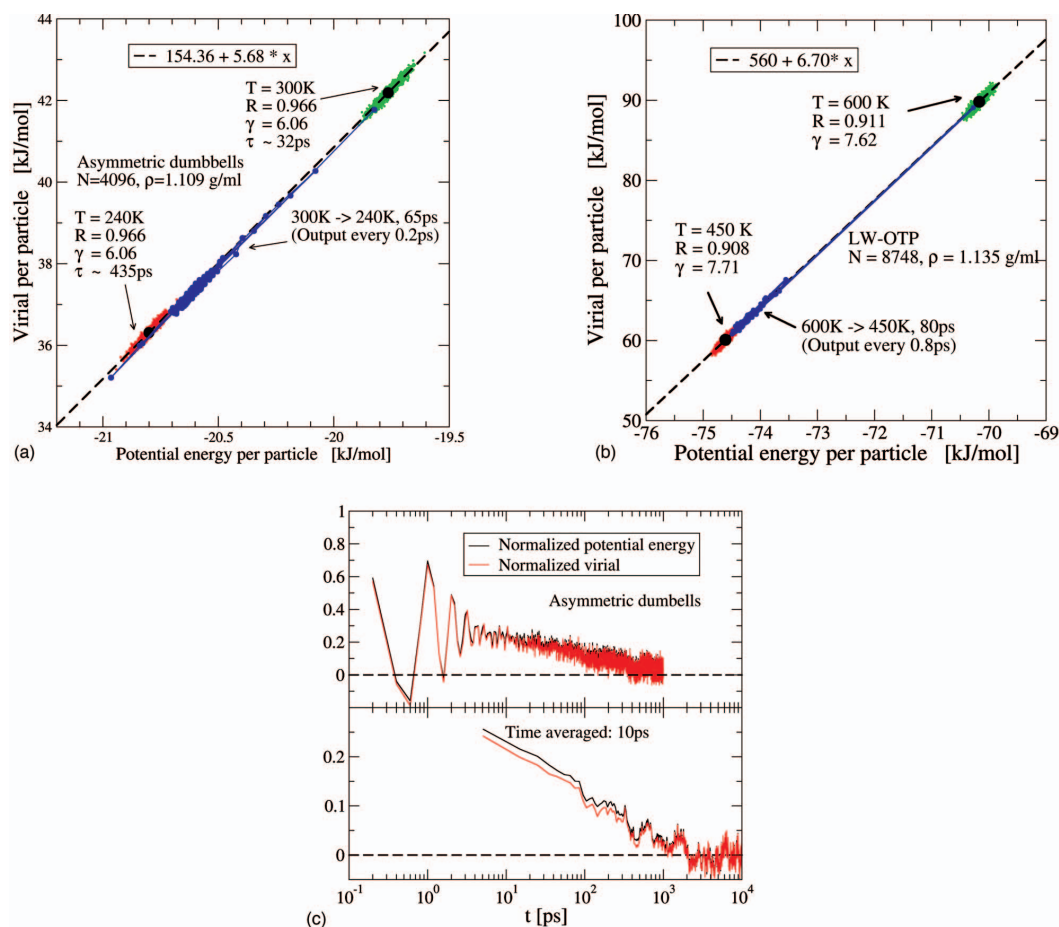


FIG. 6. Computer simulations of virial and potential energy during the aging of two strongly correlating molecular liquids following temperature down-jumps at constant volume (*NVT* simulations). (a) The asymmetric dumbbell model at a density of  $\rho = 1.109$  g/ml. The liquid was first equilibrated at  $T = 300$  K. Here, simultaneous values of virial and potential energy are plotted, producing the green ellipse, the elongation of which directly reflects the strong *WU* correlation. Temperature was then changed to  $T = 240$  K where the red ellipse marks the equilibrium fluctuations. The aging process itself is given by the blue points. These points follow the line defined by the two equilibrium simulations, showing that virial and potential energy correlate also out of equilibrium. (b) Similar temperature down-jump simulation of the LW OTP system (Ref. 30). Again, green marks the high-temperature equilibrium ( $T = 600$  K), red the low-temperature equilibrium ( $T = 450$  K), and blue the aging toward equilibrium. In both (a) and (b), the slope of the dashed line is not precisely the number  $\gamma$  of Eq. (6) because the liquids are not perfectly correlating; the line slope is  $\langle \Delta U \Delta W \rangle / \langle (\Delta U)^2 \rangle$  (see Paper I, Appendix B), a number that is close to  $\gamma$  whenever the liquid is strongly correlating. (c) Virial and potential energy for the asymmetric dumbbell model as functions of time after the temperature jump of (a); in the lower subfigure, data were averaged over 10 ps. Virial and potential energy clearly correlate closely, both on short and long time scales.

#### IV. OUT-OF-EQUILIBRIUM DYNAMICS IN MOLECULAR MODELS

According to the eIPL explanation detailed in Sec. III, strong *WU* correlations characterize all configurations of the LJ liquid at a given volume. This means that the correlations should be there also under nonequilibrium conditions if the volume is kept constant. In this section we present numerical evidence that this prediction is indeed fulfilled, even for molecular liquids, provided that they are strongly correlating in their equilibrium *WU* fluctuations.

##### A. Temperature down-jump simulations of three molecular model liquids

Figure 6(a) shows the results for a temperature down-

jump at constant volume, starting and ending in equilibrium (*NVT* simulations).<sup>29</sup> The system studied is an asymmetric dumbbell liquid consisting of two different-sized LJ particles glued together by a bond of fixed length, with parameters chosen to mimic toluene.<sup>2</sup> The system was first equilibrated at 300 K. The green ellipse is the scatter plot of simultaneous values of *U* and *W* in equilibrium at  $T = 300$  K. The strong *WU* correlation is revealed by the elongation of the ellipse ( $R = 0.97$ ;  $\gamma = 6.1$ ). When the liquid is similarly equilibrated at 240 K, the red blob appears. To test for correlation in an out-of-equilibrium situation, we changed temperature abruptly from the 300 K equilibrium situation to 240 K. The blue points show how virial and potential energy evolve following the temperature down-jump. Clearly, strong *WU* cor-

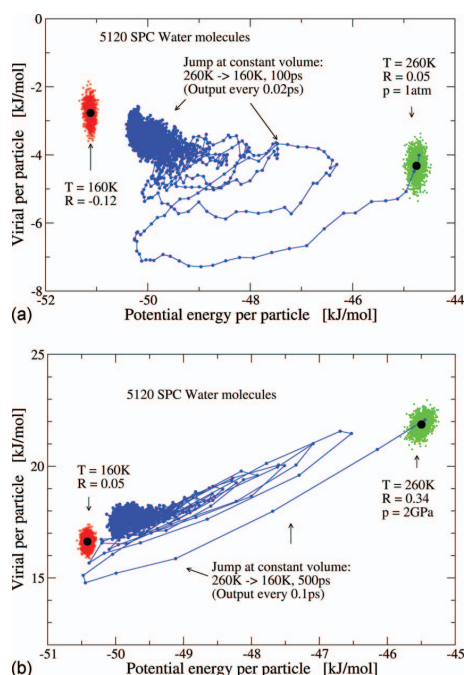


FIG. 7. Virial vs potential energy after a temperature down-jump at constant volume applied to SPC water, which is not strongly correlating (colors as in Fig. 6). (a) SPC water at 1 atm equilibrated at  $T=260$  K, subsequently subjected to an isochoric temperature down jump to  $T=160$  K. Clearly,  $W$  and  $U$  are not strongly correlated during the aging process. (b) Same procedure starting from a 2 GPa state point.

relations are also present during the aging toward equilibrium. Figure 6(b) shows the same phenomenon for the Lewis–Wahnström *ortho*-terphenyl (LW OTP) model, which consists of three LJ spheres at fixed length and angle with parameters optimized to mimic *ortho*-terphenyl.<sup>30</sup> This liquid is also strongly correlating ( $R=0.91$ ;  $\gamma=7.6$ ). The colors are as in Fig. 6(a): green gives a high-temperature equilibrium state ( $T=600$  K), red gives a low-temperature equilibrium state ( $T=450$  K), and the blue points show the aging toward equilibrium after changing temperature from 600 to 450 K. The picture is the same as in Fig. 6(a). The blue points follow the dashed line. Thus, virial and potential energy correlate strongly also for far-from-equilibrium states. Figure 6(c) plots  $W(t)$  and  $U(t)$  after the temperature jump for the data in Fig. 6(a) for the asymmetric dumbbell liquid.  $W(t)$  and  $U(t)$  follow each other closely on the picosecond time scale as well as in their slow, overall drift to equilibrium.

What happens when the same simulation scheme is applied to a liquid that is not strongly correlating? An example is SPC water, where the hydrogen bonds are mimicked by Coulomb interactions.<sup>31</sup> Figure 7 shows results of simulations of SPC water at two different densities, corresponding to (a) low pressure and (b) very high pressure. In the first case, virial and potential energy are virtually uncorrelated ( $R=0.05$ ,  $T=260$  K); in the second case, correlations are somewhat stronger ( $R=0.34$ ,  $T=260$  K), though still weak. As in Fig. 6, green denotes the initial, high-temperature equi-

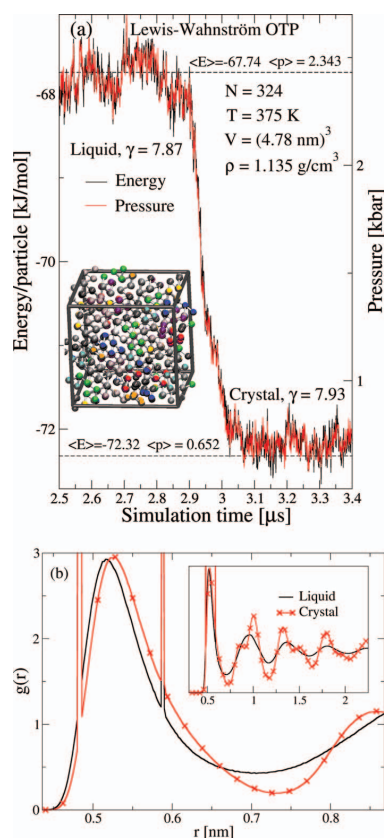


FIG. 8. Crystallization of the supercooled LW OTP liquid where each molecule consists of three LJ spheres with fixed bond lengths and angles (Ref. 30). (a) Pressure (right) and energy (left) monitored as functions of time during crystallization at constant volume. Both quantities were averaged over 1 ns; on this time scale the pressure/energy fluctuations directly reflect the virial/potential energy fluctuations (Paper II). The horizontal dashed lines indicate the liquid (upper line) and crystal (lower line), the averages of which were obtained from the simulation by averaging over times 0–2 and 5–10  $\mu$ s, respectively. Both liquid and crystal show strong correlations, and the correlations are also present during the crystallization. Inset: crystal structure from the simulation. (b) Radial distribution functions of liquid and crystalline phases. The two spikes present in both phases come from the fixed bond lengths.

librium, red denotes the low-temperature equilibrium, and blue denotes the aging toward equilibrium. Clearly, for this system,  $W$  and  $U$  are not closely linked to one another during the relaxation toward equilibrium.

## B. Pressure and energy monitored during crystallization of a supercooled liquid: The LW OTP model

A different far-out-of-equilibrium situation is that of crystallization of a supercooled liquid monitored at fixed volume and temperature. To the best of our knowledge, crystallization of the LW OTP model has not been reported before, but Fig. 8 shows that for simulations over microseconds the supercooled liquid crystallizes at  $T=375$  K and  $\rho=1.135$  g/cm<sup>3</sup>. In the crystal, the LJ spheres

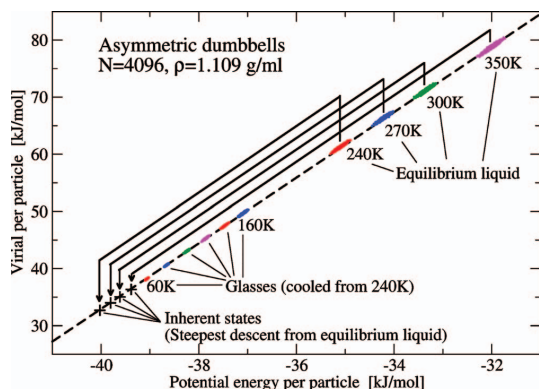


FIG. 9.  $WU$  plot for the asymmetric dumbbell model for various states at the same volume. The upper right corner shows data for simultaneous values of virial and potential energy for four equilibrium simulations ( $T=240$ – $350$  K). When quenching each of these to zero temperature in order to identify the inherent states, the crosses are arrived at. The intermediate points are glasses prepared by different cooling rates: out-of-equilibrium systems generated by cooling in 1 ns from 240 K to the temperature in question. This plot confirms the findings of Figs. 6 and 8 that strong virial/potential energy correlations are not limited to thermal equilibrium situations.

are arranged in a slightly deformed bcc lattice where the molecules have otherwise random orientation. The crystal is shown in the inset of Fig. 8(a). Figure 8(a) shows how time-averaged pressure and energy develop during crystallization. Contributions to pressure and energy from the momentum degrees of freedom are virtually constant after averaging over 1 ns, so strong  $WU$  correlations manifest themselves in strong averaged pressure/averaged energy correlations. Clearly, averaged pressure and averaged energy follow each other closely before, during, and after the crystallization. This confirms the above finding, as well as those of Paper I, that strong correlations apply also for the crystalline phase of a strongly correlating liquid. Note that the slope  $\gamma$ , the proportionality constant between virial and potential energy fluctuations, is virtually unaffected by the crystallization. The persistence of strong virial/potential energy correlations during crystallization—and the insignificant change in  $\gamma$ —is noticeable because physical characteristics are rarely unaffected by a first-order phase transition. These simulations show that the property of strong virial/potential energy correlations pertains to the intermolecular potential, not to the particular mi-

croscopic configurations under study. Figure 8(b) shows the radial distribution functions for the liquid and crystalline phases.

### C. Glasses and inherent states

The above out-of-equilibrium simulations show that the property of strong  $WU$  correlation is not confined to thermal equilibrium. This is consistent with the  $\epsilon$ IPL description given in the previous section, but was shown here to apply even for molecular models. It appears that strongly correlating liquids have a particularly simple potential energy surface. These results have significance for any out-of-equilibrium situation. Consider the potential energy landscape picture of viscous liquid dynamics<sup>32–35</sup> according to which each configuration has an underlying inherent state defined via a deepest-descent quench, a state that contains most information relevant to the slow dynamics, which may be regarded as jumps between different inherent states.<sup>32–35</sup> Figure 9 shows a  $WU$  plot of the asymmetric dumbbell model in different situations at same density: equilibrium states (upper right) and their corresponding inherent states (lower left, one quench per temperature), and glasses at different temperatures in between. A glass is an out-of-equilibrium state, of course, and inherent states may be regarded as zero-temperature glasses. The plot shows, once again, that strong correlations are present also far from equilibrium.

### V. ENSEMBLE DEPENDENCE OF THE CORRELATION COEFFICIENT

Most of the simulations of Paper I were done in the  $NVT$  ensemble. An obvious question is how the correlations differ between ensembles. This section develops the necessary theory needed to answer this question and compares first the  $NVT$  and  $NVE$  ensembles, then the  $NVT$  and  $NpT$  ensembles.

It is well known that although simple thermodynamic averages are independent of ensemble,<sup>36</sup> fluctuations are generally ensemble dependent. Consider two ensembles, one with extensive variable  $F$  held fixed and one with its conjugate intensive variable  $f$  held fixed (defined so their product is dimensionless). The other parameters defining the ensembles are the same. The covariance of observables  $A$  and  $B$  in the two ensembles are then related as<sup>6,37</sup>

$$\langle \Delta A \Delta B \rangle_F = \langle \Delta A \Delta B \rangle_f + \left( \frac{\partial f}{\partial F} \right) \left( \frac{\partial}{\partial f} \langle A \rangle_f \right) \left( \frac{\partial}{\partial f} \langle B \rangle_f \right). \quad (37)$$

TABLE II. Check of relation (47) between  $R_T$  and  $R_E$  for the LJ and the Kob–Andersen binary Lennard-Jones (KABLJ) liquids. The units for  $\rho$  and  $T$  are defined in terms of the length and energy parameters  $\sigma$  and  $\epsilon$  for the interactions of the large particles. The excess isochoric heat capacity was calculated from the potential energy fluctuations in the  $NVT$  ensemble.

System	$\rho$	$T$	$R_T$	$C_V^e/N$	$R_E$ [Eq. (47)]	$R_E$ (measured)
LJ	1.00	1.00	0.991	1.5	0.982	0.983
LJ	1.00	0.80	0.991	1.7	0.981	0.981
LJ	0.82	0.80	0.943	0.90	0.912	0.918
LJ	0.82	0.67	0.949	1.3	0.909	0.904
KABLJ	1.2	0.47	0.936	2.1	0.859	0.862

### A. *NVT* versus *NVE*

To compare the *NVT* and *NVE* ensembles, we take  $F$  and  $f$  as the energy  $E$  and the inverse temperature  $\beta=1/(k_B T)$ , respectively, keeping the volume fixed. Noting that  $\partial/\partial\beta=-k_B T^2 \partial/\partial T$  and  $(\partial\beta/\partial E)_V=1/(-k_B T^2 C_V)$ , where  $C_V$  is the extensive isochoric specific heat,  $C_V=Vc_V$ , the covariance of  $U$  and  $W$  is given by

$$\langle\Delta U\Delta W\rangle_{NVE}=\langle\Delta U\Delta W\rangle_{NVT}-\frac{k_B T^2}{C_V}\frac{\partial\langle U\rangle_{NVT}}{\partial T}\frac{\partial\langle W\rangle_{NVT}}{\partial T} \quad (38)$$

$$=\langle\Delta U\Delta W\rangle_{NVT}-k_B T^2 C_V^{\text{ex}} V \beta_V^{\text{ex}}/C_V. \quad (39)$$

Here, we have introduced the excess parts of the isochoric specific heat and pressure coefficient,  $C_V^{\text{ex}}$  and  $\beta_V^{\text{ex}}$ , respectively (note the change in notation from Paper II where the

superscript “conf” was used—“ex” is, however, more standard in liquid state theory). These two quantities are given by (for monatomic liquids)

$$C_V^{\text{ex}}=\left(\frac{\partial\langle U\rangle}{\partial T}\right)_V=C_V-\frac{3}{2}Nk_B, \quad (40)$$

$$\beta_V^{\text{ex}}=\left(\frac{\partial\langle W/V\rangle}{\partial T}\right)_V=\beta_V-\frac{Nk_B}{V}. \quad (41)$$

For the variances, one has

$$\langle(\Delta U)^2\rangle_{NVE}=\langle(\Delta U)^2\rangle_{NVT}-k_B T^2(C_V^{\text{ex}})^2/C_V, \quad (42)$$

$$\langle(\Delta W)^2\rangle_{NVE}=\langle(\Delta W)^2\rangle_{NVT}-k_B T^2(V\beta_V^{\text{ex}})^2/C_V. \quad (43)$$

The above implies that the *NVE*  $WU$ -correlation coefficient  $R_E$  (in the following subscripts  $E$  or  $T$  indicate the *NVE* or *NVT* ensemble, respectively) is given by

$$R_E=\frac{\langle\Delta U\Delta W\rangle_{NVT}-k_B T^2 C_V^{\text{ex}} V \beta_V^{\text{ex}}/C_V}{\sqrt{\langle(\Delta U)^2\rangle_{NVT}-k_B T^2(C_V^{\text{ex}})^2/C_V}\sqrt{\langle(\Delta W)^2\rangle_{NVT}-k_B T^2(V\beta_V^{\text{ex}})^2/C_V}}. \quad (44)$$

We wish to express the right side in terms of the *NVT* coefficient  $R_T$ . The definition of  $R_T$  implies that

$$\langle(\Delta W)^2\rangle_{NVT}=\frac{\langle\Delta U\Delta W\rangle_{NVT}^2}{R_T^2\langle(\Delta U)^2\rangle_{NVT}}. \quad (45)$$

Inserting this into Eq. (44) and making use of the fluctuation relations  $\langle\Delta U\Delta W\rangle_{NVT}=k_B T^2 V \beta_V^{\text{ex}}$  and  $\langle(\Delta U)^2\rangle_{NVT}=k_B T^2 C_V^{\text{ex}}$  (see, e.g., Appendix B of Paper I) gives

$$R_E=\frac{k_B T^2 V \beta_V^{\text{ex}}-k_B T^2 C_V^{\text{ex}} V \beta_V^{\text{ex}}/C_V}{\sqrt{k_B T^2 C_V^{\text{ex}}-k_B T^2(C_V^{\text{ex}})^2/C_V}\sqrt{\frac{(k_B T^2 V \beta_V^{\text{ex}})^2}{R_T^2 k_B T^2 C_V^{\text{ex}}}-k_B T^2(V\beta_V^{\text{ex}})^2/C_V}}. \quad (46)$$

After squaring and cancelling factors of  $k_B T^2$  and  $V\beta_V^{\text{ex}}$ , we get an expression relating  $R_E$  to  $R_T$ ,

$$R_E^2=\frac{1-C_V^{\text{ex}}/C_V}{1/R_T^2-C_V^{\text{ex}}/C_V}. \quad (47)$$

To get a feel for the relation, divide by  $R_T^2$ . This yields

$$\left(\frac{R_E}{R_T}\right)^2=\frac{1-C_V^{\text{ex}}/C_V}{1-R_T^2 C_V^{\text{ex}}/C_V}. \quad (48)$$

First one notes that when  $R_T=1$ , the denominator on the right side becomes equal to the numerator and  $R_E=1$ . That is, the property of perfect correlation is independent of (fixed volume) ensemble. When  $R_T<1$ , the denominator becomes greater than the numerator, and so  $R_E^2<R_T^2$ . That is, the correlation coefficient is smaller in the *NVE* ensemble than in the *NVT* one. How can we understand this? Consider the set of  $WU$  points sampled by the system during an *NVE* trajectory; this is an elongated blob in the  $WU$  diagram. Changing the energy will cause the blob to move along a line almost parallel with the long axis of the blob (Paper I). Switching to the *NVT* ensemble is equivalent to superposing several of these collinear blobs on top of each other—the result is nec-

essarily longer, but not wider. This corresponds to higher correlation.

Simulation data confirming relation (47) are presented in Table II.

### B. *NVT* versus *NpT*

In the *NpT* ensemble, where volume is allowed to fluctuate, we must consider different variables. The natural variables to correlate are the excess enthalpy  $H_{\text{ex}}\equiv U+pV$  and the volume  $V$ . We use again Eq. (37), but now take  $F$  as  $V$  and  $f$  as  $p\beta$ , the pressure times inverse temperature, keeping temperature constant. Equation (37) becomes

$$\langle\Delta A\Delta B\rangle_{NVT}=\langle\Delta A\Delta B\rangle_{NpT}-\frac{k_B T K_T}{V}\left(\frac{\partial}{\partial p}\langle A\rangle\right)_T\left(\frac{\partial}{\partial p}\langle B\rangle\right)_T. \quad (49)$$

The details of the calculation, which are somewhat tedious, are given in the Appendix. The result for the  $H_{\text{ex}}V$  correlation coefficient is

$$R_{H_{\text{ex}},V,NpT} = \frac{1}{\sqrt{1 + b^2/a^2}}, \quad (50)$$

where

$$a = \langle \Delta U \Delta W \rangle_{NVT} + N(k_B T)^2 \quad (51)$$

and

$$b^2 = K_T V k_B T \langle (\Delta U)^2 \rangle_{NVT}. \quad (52)$$

Notice that  $R_{H_{\text{ex}},V,NpT}$  is strictly less than unity—even for perfectly correlating liquids (that is, with perfect  $WU$  correlations in the  $NVT$  and  $NVE$  ensembles). For the LJ simulation of Fig. 1(b),  $R_{H_{\text{ex}},V,NpT} = 0.86$  (the  $NVT$   $WU$  correlation coefficient for the same state point is 0.94). Unlike the situation when comparing the  $NVT$  and  $NVE$  ensembles, there does not seem to be a simple relation between the two correlation coefficients. It seems likely, though, that the  $H_{\text{ex}}V$  correlation in the  $NpT$  ensemble is generally smaller than the  $WU$  correlation in the  $NVT$  ensemble; thus, the property of strong correlation is less evident in the  $NpT$  ensemble.

## VI. THERMODYNAMICS OF STRONGLY CORRELATING LIQUIDS

The property of strong virial/potential energy correlation does not just refer to microscopic properties that are only accessible in simulation, it also has consequences for the liquid's thermodynamics. The first subsection below relates the slope [Eq. (6)] to the Grüneisen parameter, the second subsection shows how to give a general thermodynamic formulation of the property of strong correlations.

### A. Relation to the Grüneisen parameter

The Grüneisen parameter was originally introduced to characterize the volume dependence of normal modes of a crystal,<sup>38,39</sup>

$$\gamma_i = - \frac{d \ln(\omega_i)}{d \ln(V)}, \quad (53)$$

where  $\omega_i$  is the frequency of the  $i$ th normal mode. By assuming that  $\gamma_i$  is the same for all modes and denoting the common value by  $\gamma_G$ , one can derive the Mie–Grüneisen equation of state<sup>38</sup> as

$$p + \frac{du}{dv} = \gamma_G \frac{E_{\text{vib}}}{V}. \quad (54)$$

Here,  $p$  is the pressure,  $u(v)$  with  $v = V/N$  is the “static” energy of the crystal per atom (the energy of the force-free configuration about which vibrational motion occurs), and  $E_{\text{vib}}$  is the vibrational energy. In general  $\gamma_G$  depends on volume, but this dependence is typically small enough that it can be neglected. From Eq. (54) it follows that, if  $E$  is the total, thermally averaged internal energy, one has  $(\partial p / \partial T)_V = (\gamma_G / V) (\partial E_{\text{vib}} / \partial T)_V = (\gamma_G / V) (\partial E / \partial T)_V$ , i.e.,

$$\gamma_G = V \left( \frac{\partial p}{\partial E} \right)_V. \quad (55)$$

This expression is the slope of the pressure versus energy curve at fixed volume, analogous to the  $\gamma$  of Eq. (6) but for the presence of the kinetic terms (recall that for an IPL liquid  $\gamma = n/3 = (\partial W / \partial U)_V$ ). If  $\alpha_p$  is the coefficient of thermal expansion,  $K_T$  is the isothermal bulk modulus, and  $c_V = C_V / V$  is the isochoric specific heat per unit volume, Eq. (55) implies via standard thermodynamic identities

$$\gamma_G = \frac{\alpha_p K_T}{c_V}. \quad (56)$$

This relation allows  $\gamma_G$  to be determined from experimentally accessible quantities; in fact, Eq. (56) can be taken as a thermodynamic definition of  $\gamma_G$ .<sup>40</sup>

There have been suggestions of how to connect the so-called density scaling exponent<sup>24,25</sup>—the one controlling the relaxation time via the variable  $\rho^*/T$ —with the Grüneisen parameter, notably by Roland and co-workers.<sup>41–43</sup> In Ref. 41, equality of  $\gamma_G$  and  $\gamma$  was argued theoretically by reference to the Avramov model. More recently, Roland and Casalini showed<sup>43</sup> that equality is not consistent with experimental results; rather  $\gamma_G$  is smaller than  $\gamma$  by a factor of order 3. This discrepancy was reconciled in the context of the entropy model for relaxation (by which the relaxation time is a unique function of the so-called configurational entropy  $S_c$ ), by introducing an excess or corrected Grüneisen parameter defined via

$$\gamma_G^{\text{corr}} = \frac{\alpha_p K_T}{\Delta c_V}. \quad (57)$$

Here,  $\Delta c_V$  is the difference in the isochoric specific heats per unit volume between the liquid and the glass. Because  $\Delta c_V$  is smaller than  $c_V$ , one has  $\gamma_G^{\text{corr}} > \gamma_G$ . By arguing from the experimental data that the nonconfigurational part of the entropy (associated with vibrations, equal to the entropy of the glass) is independent of volume and assuming that  $\Delta c_V$  is constant, Roland and Casalini derive

$$S_c = \Delta C_V \ln(TV^{\gamma_G^{\text{corr}}}) + \text{const.} \quad (58)$$

Hence,  $\gamma_G^{\text{corr}}$  is the density-scaling exponent.

We take a different approach to connecting the Grüneisen parameter with the slope  $\gamma$  (which provides a good estimate of the density scaling exponent, see Ref. 22 and Paper IV). Instead of splitting the entropy, we split the pressure into potential and kinetic parts and get from  $\gamma_G = V(\partial p / \partial E)_V$

$$\gamma_G = V \frac{\left( \frac{\partial p}{\partial T} \right)_V}{\left( \frac{\partial E}{\partial T} \right)_V} = \frac{\left( \frac{\partial W}{\partial T} \right)_V + Nk_B}{\left( \frac{\partial E}{\partial T} \right)_V}. \quad (59)$$

Expressing the temperature derivatives in terms of fluctuations (Appendix B of Paper I) gives

$$\gamma_G = \frac{\langle \Delta U \Delta W \rangle / k_B T^2 + N k_B}{C_V}. \quad (60)$$

In the limit of strong correlation, one can replace  $\langle \Delta U \Delta W \rangle$  with  $\gamma(\Delta U)^2$ . Writing the resulting expression in terms of the excess (configurational) specific heat  $C_V^{\text{ex}}$  gives

$$\gamma_G = \frac{\gamma C_V^{\text{ex}} + N k_B}{C_V}. \quad (61)$$

In the harmonic approximation, good for many simple liquids close to their melting point,<sup>9</sup>  $C_V^{\text{ex}} = (3/2)Nk_B$  (while it is generally larger in the supercooled state). Thus, the term  $Nk_B$  in the numerator is expected to be roughly a factor of 10 smaller than the other term; we drop it and arrive at

$$\frac{\gamma_G}{\gamma} \cong \frac{C_V^{\text{ex}}}{C_V}. \quad (62)$$

This ratio is around one-half in the harmonic approximation, otherwise larger.

## B. Energy-bond formulation of the strongly correlation property

This section derives a general thermodynamic condition of the property of strong  $WU$  correlations, a condition which linearly constrains small variations in entropy, volume, temperature, and pressure [Eq. (72), below]. It is convenient to approach the problem from a general point of view. The energy-bond formalism provides an abstract description of the interactions between a system and its surroundings.<sup>10,44–49</sup> An energy bond has an “effort” variable  $e(t)$  and a “flow” variable  $f(t)$ , where  $e(t)f(t)$  is the free energy transferred into the system per unit time. The “displacement”  $q(t)$  is the time-integrated flow, i.e.,  $\dot{q}(t) = f(t)$ . The energy-bond formalism is general, but we only discuss the linear case where it is most useful. Thus, we consider a system that is slightly perturbed from equilibrium. It is assumed that the underlying microscopic dynamics is described by a stochastic equation, i.e., inertial forces are ignored. This is believed to be a good approximation whenever the highly viscous phase is approached; thus the below results are mainly of relevance to viscous liquids.

Linear-response theory is characterized by the fluctuation-dissipation (FD) theorem, which in the energy-bond formalism is given as follows. Consider a situation with  $n$  energy bonds and external control of the effort variables. If  $\langle f_i(0)f_j(t') \rangle_0$  is the equilibrium flow autocorrelation function, the average flow at time  $t$  is given by

$$f_i(t) = \frac{1}{k_B T} \sum_{j=1}^n \int_0^\infty \langle f_j(0)f_i(t') \rangle_0 e_j(t-t') dt'. \quad (63)$$

If the arbitrary additive constants of the displacements are chosen such that  $q_i = 0$  on average, the time-integrated version of this is

$$q_i(t) = -\frac{1}{k_B T} \sum_{j=1}^n \int_0^\infty \langle q_i(0)f_j(t') \rangle_0 e_j(t-t') dt'. \quad (64)$$

If the flow variables are externally controlled, the FD theorem is

$$e_i(t) = \frac{1}{k_B T} \sum_{j=1}^n \int_0^\infty \langle e_i(0)e_j(t') \rangle_0 f_j(t-t') dt'. \quad (65)$$

In most cases, efforts are invariant under time reversal and flows change sign. The Onsager reciprocity relation is  $\langle f_i(0)f_j(t) \rangle_0 = \langle f_j(0)f_i(t) \rangle_0$  (or  $\langle e_i(0)e_j(t) \rangle_0 = \langle e_j(0)e_i(t) \rangle_0$ , depending on which variables are externally controlled and which are free to fluctuate). From the FD theorem, expressions for the frequency-dependent response functions are easily derived. Consider, for instance, the compliances  $J_{ij}(\omega)$ , defined by  $J_{ij}(\omega) = q_i(\omega)/e_j(\omega)$  for a periodic situation with infinitesimal perturbations around equilibrium,  $e(t) = \text{Re}[e(\omega)\exp(i\omega t)]$ , etc. For these quantities, the FD theorem implies

$$J_{ij}(\omega) = -\frac{1}{k_B T} \int_0^\infty \langle q_i(0)f_j(t') \rangle_0 \exp(-i\omega t') dt'. \quad (66)$$

The case relevant to strongly correlating liquids is that of two energy bonds that are not independent, as we now proceed to show. The two energy bonds are those of standard thermodynamics, reflecting the fundamental relation  $dE = TdS - pdV$ .<sup>50,51</sup> These two energy bonds are given as follows. The thermal energy bond has temperature variation as the effort variable and entropy variation as the displacement variable ( $e_1(t) = \delta T(t)$ ,  $q_1(t) = \delta S(t)$ ), the mechanical energy bond has pressure variation as the effort variable and the negative volume variation as the displacement variable ( $e_2(t) = \delta p(t)$ ,  $q_2(t) = -\delta V(t)$ ). Usually, the two standard thermodynamic energy bonds are independent, but we are here interested in the case when they are not.

Treating the problem of two constrained energy bonds from a general perspective, we shall prove that the following four criteria are equivalent.

- (1) The variables of the two energy bonds are linearly constrained as follows:

$$aq_1(t) + bq_2(t) = ce_1(t) + de_2(t). \quad (67)$$

- (2) The system's relaxing properties, i.e., its noninstantaneous responses, are described<sup>50</sup> by a single variable  $\epsilon(t)$  as follow:

$$\begin{aligned} q_1(t) &= J_{11}^\infty e_1(t) + J_{12}^\infty e_2(t) + \gamma_1 \epsilon(t), \\ q_2(t) &= J_{21}^\infty e_1(t) + J_{22}^\infty e_2(t) + \gamma_2 \epsilon(t). \end{aligned} \quad (68)$$

In these equations the  $J^\infty$ 's are the compliances referring to the short-time, nonrelaxing response (the high-frequency response). Note that  $J_{12}^\infty = J_{21}^\infty$  by the FD theorem.

- (3) The relaxing parts of the correlation functions entering into Eq. (66) are proportional. More precisely, the correlation functions obey

$$\begin{aligned} \langle q_1(0)f_1(t) \rangle_0 &\propto \langle q_1(0)f_2(t) \rangle_0 \propto \langle q_2(0)f_1(t) \rangle_0 \\ &\propto \langle q_2(0)f_2(t) \rangle_0 \quad (t \neq 0) \end{aligned} \quad (69)$$

and

$$\begin{aligned} \langle q_1(0)f_1(t) \rangle_0 \langle q_2(0)f_2(t) \rangle_0 \\ = \langle q_1(0)f_2(t) \rangle_0 \langle q_2(0)f_1(t) \rangle_0 \quad (t \neq 0). \end{aligned} \quad (70)$$

Note that by differentiation, Eq. (69) implies for  $t \neq 0$  that  $\langle f_1(0)f_1(t) \rangle_0 \propto \langle f_1(0)f_2(t) \rangle_0 \propto \langle f_2(0)f_1(t) \rangle_0 \propto \langle f_2(0)f_2(t) \rangle_0$ .

- (4) The dynamic Prigogine–Defay ratio<sup>50</sup>  $\Lambda(\omega)$  is unity at all frequencies (where double prime denotes the imaginary part),

$$\Lambda(\omega) \equiv \frac{J''_{11}(\omega)J''_{22}(\omega)}{(J''_{12}(\omega))^2} = 1. \quad (71)$$

*Proof that 1  $\Leftrightarrow$  2.* By elimination of the variable  $\epsilon$  from Eq. (68), 2 implies 1. To prove the reverse implication, suppose that Eq. (67) applies and fix the dimensions such that the constants  $c$  and  $d$  are dimensionless. Define  $J''_{11} = (1+c)/a$ ,  $J''_{12} = J''_{21} = -1/b$ , and  $J''_{22} = (db+a)/b^2$ . Introducing the variables  $\epsilon_1 = q_1 - J''_{11}e_1 - J''_{12}e_2$  and  $\epsilon_2 = q_2 - J''_{21}e_1 - J''_{22}e_2$ , it follows that  $a\epsilon_1 + b\epsilon_2 = 0$ . This means that we are in the situation described by Eq. (68) with a common relaxing variable to the two energy bonds,  $\epsilon(t) \propto \epsilon_1(t) \propto \epsilon_2(t)$ , and symmetric short-time compliances,  $J''_{12} = J''_{21}$ .

*Proof that 2  $\Rightarrow$  3.* In terms of functional derivatives with respect to the efforts at an earlier time ( $t' < t$ ) since  $\epsilon(t)$  for small variations in the effort variables is linear in these, via the FD theorem time-reversal invariance implies that  $\delta q_1(t) / \delta e_2(t') = \delta q_2(t) / \delta e_1(t')$ . Thus, Eq. (68) implies that  $\delta \epsilon(t) / \delta e_2(t') \propto \delta \epsilon(t) / \delta e_1(t')$ . From this, Eqs. (69) and (70) now follow via the FD theorem and Eq. (68).

*Proof that 3  $\Rightarrow$  4.* According to the FD theorem, the compliance matrix imaginary parts are given by  $J''_{ij}(\omega) = (1/k_B T) \int_0^\infty \langle q_i(0)f_j(t') \rangle_0 \sin(\omega t') dt'$ . In conjunction with Eqs. (69) and (70), this implies that  $\Lambda(\omega) = 1$  at all frequencies.

*Proof that 4  $\Rightarrow$  2.* We refer to calculations of Ref. 50 which considered a system described by stochastic dynamics, i.e., with no inertial forces. Generalization of the arguments given there for the two standard thermodynamic energy bonds to the case of two arbitrary energy bonds proves the required implication.

This completes the proof of the equivalence of points (1)–(4). For the case where the two energy bonds are the two standard thermodynamic bonds, the constraint Eq. (67) translates into (changing here the sign of  $b$ )

$$a\delta S(t) + b\delta V(t) = c\delta T(t) + d\delta p(t). \quad (72)$$

How does this all relate to strong  $WU$  correlations in liquids? Via the equivalence of Eq. (72) to Eq. (68) and to unity dynamic Prigogine–Defay ratio [Eq. (71)], the results derived in Refs. 1–3 imply that Eq. (72) describes a 100% correlating liquid subjected to small perturbations from equilibrium. Generally, for any strongly correlating liquid Eq. (72) is obeyed with good accuracy. Thus, Eq. (72) gives the

required thermodynamic formulation of the hidden scale invariance characterizing strongly correlating liquids.

Equation (72) implies that for strongly correlating liquids, the four thermodynamic variables, entropy, volume, temperature, and pressure, cannot vary independently. Referring to Eq. (68), it is clear that for certain simultaneous changes in the four thermodynamic variables, the relaxing part is left unchanged; this suggests that for such changes, the system is taken to a state where it is immediately in thermal equilibrium. This observation inspired the works leading to Paper IV where “isomorphs” are introduced. These are curves in the phase diagram along which several quantities are invariant, and along which jumps from equilibrium at one state point take the system to a new state that is instantaneously in thermal equilibrium.

Finally, we would like to draw attention to an analog of strongly correlating liquids. Consider a relaxing dielectric such as, e.g., a highly viscous dipolar liquid placed in a metal capacitor. This system’s interaction with its surroundings may be described by two energy bonds: one energy bond is defined by the capacitor charge (electronic plus induced) and the voltage across the capacitor, the other energy bond is the induced dielectric charge at the capacitor surface and a fictive electric field only coupling to the liquid’s dipoles. Because of Gauss’ law, these two energy bonds are not independent, but constrained by a linear displacement-field relation of the form Eq. (67). Thus, from the energy-bond formalism point of view, a strongly correlating liquid is analogous to the standard measuring cell used for probing  $\epsilon(\omega)$  of dipolar viscous liquids, with the strong virial/potential energy correlations reflecting one of Maxwell’s four equations.

## VII. CONCLUDING REMARKS

We have illuminated a number of features of strongly correlating liquids’ hidden scale invariance. The linear term in the eIPL potential, which hides the approximate scale invariance, contributes little to the thermal fluctuations at fixed volume; this is why strongly correlating liquids inherit a number of IPL properties. As shown in previous papers,<sup>1–5</sup> the hidden scale invariance has important experimental consequences, including that of density scaling.<sup>22,57</sup> The general physical picture is that van der Waals liquids and metallic liquids—because they are strongly correlating—are simpler than hydrogen-bonding liquids, ionic liquids, and covalently bonded liquids, which are not strongly correlating.

Paper IV further investigates the consequences of a liquid being strongly correlating. This is done by defining so-called isomorphs in the liquid’s phase diagram and showing that a number of properties to a good approximation are invariant along an isomorph. The isomorph definition does not refer to  $WU$  correlations. Only strongly correlating liquids have isomorphs, however; this is because the existence of isomorphs is a direct consequence of the hidden scale invariance characterizing strongly correlating liquids.

**ACKNOWLEDGMENTS**

We thank Tage Christensen and Søren Toxværd for helpful input. The center for viscous liquid dynamics “Glass and Time” is sponsored by the Danish National Research Foundation (DNRF).

**APPENDIX: CALCULATING THE  $H_{\text{ex}}V$  CORRELATION COEFFICIENT IN THE  $NpT$  ENSEMBLE**

Here, we provide the details of the calculation of the correlation coefficient between volume and excess enthalpy in the  $NpT$  ensemble. We apply Eq. (49) with  $A, B \in \{U, V\}$ . First, we need the pressure derivatives at constant temperature of  $\langle U \rangle$  and  $\langle V \rangle$ . Taking  $U$  first, we have (noting that for simple averages like  $\langle U \rangle$ , it is not necessary to specify the ensemble because of equivalence of ensembles)

$$\left. \frac{\partial \langle U \rangle}{\partial p} \right|_T = \left. \frac{\partial \langle V \rangle}{\partial p} \right|_T \left. \frac{\partial \langle U \rangle}{\partial V} \right|_T \quad (\text{A1})$$

$$= - \frac{\langle V \rangle}{K_T} \left. \frac{\partial \langle U \rangle}{\partial V} \right|_T. \quad (\text{A2})$$

Note that  $V$  in the derivative is without averaging signs since there it is a parameter of the relevant ensemble ( $NVT$ ). The volume derivative of  $\langle U \rangle$  is calculated as follows. The excess (configurational) partition function  $Z(V, T)$  is the integral (where  $\beta = 1/k_B T$ )

$$Z(V, T) = \int_{\Gamma} \exp(-\beta U(\Gamma, V)) d\Gamma. \quad (\text{A3})$$

Here,  $\Gamma$  indexes points in configuration space and  $d\Gamma = d^{3N}r/V^N$ . In the following, we use the configuration space identity  $\partial U/\partial V = -W/V$  valid for changes that scale the coordinates of the microscopic configurations, corresponding to fixed so-called reduced coordinates (compare Appendix A of Paper IV); constant temperature is implicit, as is the dependence of  $U$  on  $\Gamma$  and  $V$ ,

$$\left. \frac{\partial \langle U \rangle}{\partial V} \right|_T = \frac{\partial}{\partial V} \left( Z^{-1} \int_{\Gamma} U \exp(-\beta U) d\Gamma \right) \quad (\text{A4})$$

$$= Z^{-1} \int_{\Gamma} \left( \frac{\partial U}{\partial V} + U(-\beta) \frac{\partial U}{\partial V} \right) \exp(-\beta U) d\Gamma - \frac{1}{Z^2} \left( \int_{\Gamma} U \exp(-\beta U) d\Gamma \right) \frac{\partial Z}{\partial V} \quad (\text{A5})$$

$$= \left\langle \frac{\partial U}{\partial V} \right\rangle - \beta \left\langle U \frac{\partial U}{\partial V} \right\rangle - \langle U \rangle Z^{-1} \int_{\Gamma} (-\beta) \frac{\partial U}{\partial V} \times \exp(-\beta U) d\Gamma \quad (\text{A6})$$

$$= \left\langle \frac{\partial U}{\partial V} \right\rangle - \beta \left\langle U \frac{\partial U}{\partial V} \right\rangle + \beta \langle U \rangle \left\langle \frac{\partial U}{\partial V} \right\rangle \quad (\text{A7})$$

$$= \left\langle \frac{\partial U}{\partial V} \right\rangle - \beta \left\langle \Delta U \Delta \left( \frac{\partial U}{\partial V} \right) \right\rangle \quad (\text{A8})$$

$$= \frac{1}{V} (-\langle W \rangle + \beta \langle \Delta U \Delta W \rangle). \quad (\text{A9})$$

Thus we have (adding the subscript  $NVT$  to the fluctuation expression since this is ensemble dependent)

$$\left. \frac{\partial \langle U \rangle}{\partial p} \right|_T = \frac{\langle W \rangle}{K_T} - \frac{\langle \Delta U \Delta W \rangle_{NVT}}{k_B T K_T}. \quad (\text{A10})$$

The pressure dependence of  $\langle V \rangle$  is given by

$$\left. \frac{\partial \langle V \rangle}{\partial p} \right|_T = - \frac{\langle V \rangle}{K_T}. \quad (\text{A11})$$

To keep the notation simple, averaging signs are henceforth omitted from simple averages such as  $\langle V \rangle$ ,  $\langle W \rangle$ , etc. We can write expressions for the variances of  $U$  and  $V$  in the  $NpT$  ensemble using Eq. (49),

$$\langle (\Delta U)^2 \rangle_{NpT} = \langle (\Delta U)^2 \rangle_{NVT} + \frac{k_B T K_T}{V} \left( \frac{W}{K_T} - \frac{\langle \Delta U \Delta W \rangle_{NVT}}{k_B T K_T} \right)^2, \quad (\text{A12})$$

$$\langle (\Delta V)^2 \rangle_{NpT} = 0 + \frac{k_B T K_T V^2}{V K_T^2} = \frac{V k_B T}{K_T}. \quad (\text{A13})$$

We need also the covariance

$$\langle \Delta U \Delta V \rangle_{NpT} = 0 + \frac{k_B T K_T}{V} \left( \frac{W}{K_T} - \frac{\langle \Delta U \Delta W \rangle_{NVT}}{k_B T K_T} \right) \frac{-V}{K_T} \quad (\text{A14})$$

$$= - \frac{k_B T W}{K_T} + \frac{\langle \Delta U \Delta W \rangle_{NVT}}{K_T}. \quad (\text{A15})$$

Now we have all we need to construct the  $H_{\text{ex}}V$  correlation coefficient in the  $NpT$  ensemble where  $H_{\text{ex}} = U + pV$ . The covariance between  $H_{\text{ex}}$  and  $V$  is

$$\langle \Delta H_{\text{ex}} \Delta V \rangle_{NpT} = \langle \Delta U \Delta V \rangle_{NpT} + p \langle (\Delta V)^2 \rangle_{NpT} \quad (\text{A16})$$

$$= \frac{\langle \Delta U \Delta W \rangle_{NVT}}{K_T} - \frac{k_B T W}{K_T} + p \frac{V k_B T}{K_T} \quad (\text{A17})$$

$$= \frac{\langle \Delta U \Delta W \rangle_{NVT}}{K_T} + \frac{k_B T (N k_B T)}{K_T}, \quad (\text{A18})$$

where we have used  $pV = N k_B T + W$ . The variance of  $H_{\text{ex}}$  is more tedious,

$$\langle(\Delta H_{\text{ex}})^2\rangle_{NpT} = \langle(\Delta U)^2\rangle_{NpT} + p^2\langle(\Delta V)^2\rangle_{NpT} + 2p\langle\Delta U\Delta V\rangle_{NpT} \quad (\text{A19})$$

$$= \langle(\Delta U)^2\rangle_{NVT} + \frac{k_B T K_T}{V} \left( \frac{W}{K_T} - \frac{\langle\Delta U\Delta W\rangle_{NVT}}{k_B T K_T} \right)^2 + \frac{p^2 V k_B T}{K_T} + \frac{2p}{K_T} (-k_B T W + \langle\Delta U\Delta W\rangle_{NVT}) \quad (\text{A20})$$

$$= \langle(\Delta U)^2\rangle_{NVT} + \frac{k_B T}{V K_T} \left( W^2 - \frac{2W\langle\Delta U\Delta W\rangle_{NVT}}{k_B T} + \frac{\langle\Delta U\Delta W\rangle_{NVT}^2}{(k_B T)^2} + (pV)^2 - 2pVW + \frac{2pV\langle\Delta U\Delta W\rangle_{NVT}}{k_B T} \right). \quad (\text{A21})$$

Again using  $pV = Nk_B T + W$  allows some simplification,

$$\langle(\Delta H_{\text{ex}})^2\rangle_{NpT} = \langle(\Delta U)^2\rangle_{NVT} + \frac{k_B T}{V K_T} \left( W^2 - \frac{2W\langle\Delta U\Delta W\rangle_{NVT}}{k_B T} + \frac{\langle\Delta U\Delta W\rangle_{NVT}^2}{(k_B T)^2} + W^2 + 2WNk_B T + (Nk_B T)^2 - 2W^2 - 2Nk_B T W + \frac{2W\langle\Delta U\Delta W\rangle_{NVT}}{k_B T} + 2N\langle\Delta U\Delta W\rangle_{NVT} \right) \quad (\text{A22})$$

$$= \langle(\Delta U)^2\rangle_{NVT} + \frac{\langle\Delta U\Delta W\rangle_{NVT}^2}{k_B T V K_T} + \frac{N^2 (k_B T)^3}{V K_T} + \frac{2Nk_B T}{V K_T} \langle\Delta U\Delta W\rangle_{NVT}. \quad (\text{A23})$$

Now we can form the  $H_{\text{ex}}V$  correlation coefficient,

$$R_{H_{\text{ex}}V, NpT} = \frac{\langle\Delta H_{\text{ex}}\Delta V\rangle_{NpT}}{\sqrt{\langle(\Delta H_{\text{ex}})^2\rangle_{NpT}\langle(\Delta V)^2\rangle_{NpT}}} \quad (\text{A24})$$

$$= \frac{\langle\Delta U\Delta W\rangle_{NVT} + N(k_B T)^2/K_T}{\sqrt{\langle(\Delta U)^2\rangle_{NVT} + \frac{\langle\Delta U\Delta W\rangle_{NVT}^2}{k_B T V K_T} + \frac{N^2 (k_B T)^3}{V K_T} + \frac{2Nk_B T}{V K_T} \langle\Delta U\Delta W\rangle_{NVT}} \sqrt{\frac{V k_B T}{K_T}} \quad (\text{A25})$$

$$= \frac{\langle\Delta U\Delta W\rangle_{NVT} + N(k_B T)^2}{\sqrt{K_T V k_B T \langle(\Delta U)^2\rangle_{NVT} + \langle\Delta U\Delta W\rangle_{NVT}^2 + N^2 (k_B T)^4 + 2N\langle\Delta U\Delta W\rangle_{NVT} (k_B T)^2}} \quad (\text{A26})$$

$$= \frac{a}{\sqrt{b^2 + a^2}} = \frac{1}{\sqrt{1 + b^2/a^2}} \quad (\text{A27})$$

where  $a = \langle\Delta U\Delta W\rangle_{NVT} + N(k_B T)^2$  and  $b^2 = K_T V k_B T \langle(\Delta U)^2\rangle_{NVT}$ .

<sup>1</sup>U. R. Pedersen, N. P. Bailey, T. B. Schröder, and J. C. Dyre, *Phys. Rev. Lett.* **100**, 015701 (2008).

<sup>2</sup>U. R. Pedersen, T. Christensen, T. B. Schröder, and J. C. Dyre, *Phys. Rev. E* **77**, 011201 (2008).

<sup>3</sup>N. P. Bailey, T. Christensen, B. Jakobsen, K. Niss, N. B. Olsen, U. R. Pedersen, T. B. Schröder, and J. C. Dyre, *J. Phys.: Condens. Matter* **20**, 244113 (2008).

<sup>4</sup>N. P. Bailey, U. R. Pedersen, N. Gnan, T. B. Schröder, and J. C. Dyre, *J. Chem. Phys.* **129**, 184507 (2008) (Paper I).

<sup>5</sup>N. P. Bailey, U. R. Pedersen, N. Gnan, T. B. Schröder, and J. C. Dyre, *J. Chem. Phys.* **129**, 184508 (2008) (Paper II).

<sup>6</sup>M. P. Allen and D. J. Tildesley, *Computer Simulation of Liquids* (Clarendon, Oxford, 1987).

<sup>7</sup>M. Dzugutov, *Phys. Rev. A* **46**, R2984 (1992).

<sup>8</sup>N. Gnan, T. B. Schröder, U. R. Pedersen, N. P. Bailey, and J. C. Dyre, *J. Chem. Phys.* **131**, 234504 (2009) (Paper IV).

<sup>9</sup>E. D. Chisolm and D. C. Wallace, *J. Phys.: Condens. Matter* **13**, R739 (2001).

<sup>10</sup>G. Oster, A. Perelson, and A. Katchalsky, *Nature (London)* **234**, 393 (1971).

<sup>11</sup>O. Klein, *Medd. Vetenskapskad. Nobelinst.* **5**, 1 (1919).

<sup>12</sup>T. H. Berlin and E. W. Montroll, *J. Chem. Phys.* **20**, 75 (1952).

<sup>13</sup>W. G. Hoover, M. Ross, K. W. Johnson, D. Henderson, J. A. Barker, and B. C. Brown, *J. Chem. Phys.* **52**, 4931 (1970).

<sup>14</sup>W. G. Hoover, S. G. Gray, and K. W. Johnson, *J. Chem. Phys.* **55**, 1128 (1971).

<sup>15</sup>Y. Hiwatari, H. Matsuda, T. Ogawa, N. Ogita, and A. Ueda, *Prog. Theor. Phys.* **52**, 1105 (1974).

<sup>16</sup>D. Ben-Amotz and G. J. Stell, *J. Chem. Phys.* **119**, 10777 (2003).

<sup>17</sup>C. DeMichele, F. Sciortino, and A. Coniglio, *J. Phys.: Condens. Matter* **16**, L489 (2004).

<sup>18</sup>P. E. Ramirez-Gonzalez and M. Medina-Noyola, *J. Phys.: Condens. Matter* **21**, 075101 (2009).

<sup>19</sup>S. M. Stishov, *Sov. Phys. Usp.* **17**, 625 (1975).

<sup>20</sup>J. D. Weeks and J. Q. Broughton, *J. Chem. Phys.* **78**, 4197 (1983).

<sup>21</sup>J. P. Hansen and I. R. McDonald, *Theory of Simple Liquids*, 2nd ed. (Academic, New York, 1986).

<sup>22</sup>T. B. Schröder, U. R. Pedersen, and J. C. Dyre, e-print arXiv:0803.2199.

<sup>23</sup>T. B. Schröder, U. R. Pedersen, N. P. Bailey, S. Toxvaerd, and J. C. Dyre, *Phys. Rev. E* **80**, 041502 (2009).

<sup>24</sup>C. Alba-Simionesco, A. Cailliaux, A. Alegria, and G. Tarjus, *Europhys. Lett.* **68**, 58 (2004).

<sup>25</sup>C. M. Roland, S. Hensel-Bielowka, M. Paluch, and R. Casalini, *Rep. Prog. Phys.* **68**, 1405 (2005).

<sup>26</sup>A. Grzybowski, M. Paluch, and K. Grzybowska, *J. Phys. Chem. B* **113**, 7419 (2009).

<sup>27</sup>V. Molinero and E. B. Moore, *J. Phys. Chem. B* **113**, 4008 (2009).

<sup>28</sup>E. A. Jagla, *J. Chem. Phys.* **111**, 8980 (1999).

<sup>29</sup>The system consisted of 512 asymmetric dumbbell molecules modeled as two LJ spheres connected by a rigid bond. The dumbbells were parameterized to mimic toluene. A large sphere (mimicking a phenyl group) was

- taken from the Lewis-Wahnström OTP model (Ref. 30) with the parameters  $m_p=77.106$  u,  $\sigma_p=0.4963$  nm, and  $\epsilon_p=5.726$  kJ/mol. A small sphere (mimicking a methyl group) was taken from UA-OPLS having  $m_m=15.035$  u,  $\sigma_m=0.3910$  nm, and  $\epsilon_m=0.66944$  kJ/mol. The bonds were kept rigid with a bond length of  $d=0.29$  nm. The volume was  $V=77.27$  nm<sup>3</sup>, giving an average pressure of approximately 1 atm. The temperature was held constant at  $T=130$  K using the Nosé–Hoover thermostat. *NVT* simulations were carried out using GROMACS software (Refs. 52 and 53) using the Nosé–Hoover thermostat (Refs. 54 and 55). Molecules were kept rigid using the LINCS algorithm (Ref. 56).
- <sup>30</sup>L. J. Lewis and G. Wahnström, *Phys. Rev. E* **50**, 3865 (1994).
- <sup>31</sup>H. J. C. Berendsen, J. R. Grigera, and T. P. Straatsma, *J. Phys. Chem.* **91**, 6269 (1987).
- <sup>32</sup>M. Goldstein, *J. Chem. Phys.* **51**, 3728 (1969).
- <sup>33</sup>F. H. Stillinger and T. A. Weber, *Phys. Rev. A* **28**, 2408 (1983).
- <sup>34</sup>F. H. Stillinger, *Science* **267**, 1935 (1995).
- <sup>35</sup>T. B. Schröder, S. Sastry, J. C. Dyre, and S. C. Glotzer, *J. Chem. Phys.* **112**, 9834 (2000).
- <sup>36</sup>In particular, averages of quantities which are the sums of single-particle functions (Ref. 6).
- <sup>37</sup>J. L. Lebowitz, J. K. Perkus, and L. Verlet, *Phys. Rev.* **153**, 250 (1967).
- <sup>38</sup>M. Born and K. Huang, *Dynamical Theory of Crystal Lattices* (Oxford University Press, Oxford U.K., 1954).
- <sup>39</sup>N. W. Ashcroft and N. D. Mermin, *Solid State Physics* (Holt, Rinehart and Wiston, New York, 1976).
- <sup>40</sup>D. C. Wallace, *Thermodynamics of Crystals* (Dover, New York, 1972).
- <sup>41</sup>R. Casalini, U. Mohanty, and C. M. Roland, *J. Chem. Phys.* **125**, 014505 (2006).
- <sup>42</sup>C. M. Roland, J. L. Feldman, and R. Casalini, *J. Non-Cryst. Solids* **352**, 4895 (2006).
- <sup>43</sup>C. M. Roland and R. Casalini, *J. Phys.: Condens. Matter* **19**, 205118 (2007).
- <sup>44</sup>H. Paynter, *Analysis and Design of Engineering Systems* (MIT, Cambridge, MA, 1961).
- <sup>45</sup>G. F. Oster, A. S. Perelson, and A. Katchalsky, *Q. Rev. Biophys.* **6**, 1 (1973).
- <sup>46</sup>P. V. Christiansen, *Dynamik og Diagrammer* (1978), IMFUFA Text No. 8, Roskilde.
- <sup>47</sup>P. V. Christiansen, *Semiotik og Systemegenskaber* (1979), IMFUFA Text No. 22, Roskilde.
- <sup>48</sup>D. C. Mikulecky, *Applications of Network Thermodynamics to Problems in Biomedical Engineering* (New York University, New York, 1993).
- <sup>49</sup>D. C. Karnopp, D. L. Margolis, and R. C. Rosenberg, *System Dynamics: Modeling and Simulation of Mechatronic Systems* (Wiley, New York, 2006).
- <sup>50</sup>N. L. Ellegaard, T. Christensen, P. V. Christiansen, N. B. Olsen, U. R. Pedersen, T. B. Schröder, and J. C. Dyre, *J. Chem. Phys.* **126**, 074502 (2007).
- <sup>51</sup>T. Christensen and J. C. Dyre, *Phys. Rev. E* **78**, 021501 (2008).
- <sup>52</sup>H. J. C. Berendsen, D. van der Spoel, and R. van Drunen, *Comput. Phys. Commun.* **91**, 43 (1995).
- <sup>53</sup>E. Lindahl, B. Hess, and D. van der Spoel, *J. Mol. Model.* **7**, 306 (2001).
- <sup>54</sup>S. Nosé, *Mol. Phys.* **52**, 255 (1984).
- <sup>55</sup>W. G. Hoover, *Phys. Rev. A* **31**, 1695 (1985).
- <sup>56</sup>B. Hess, H. Bekker, H. J. C. Berendsen, and J. G. E. M. Fraaije, *J. Comput. Chem.* **18**, 1463 (1997).
- <sup>57</sup>D. Coslovich and C. M. Roland, *J. Chem. Phys.* **130**, 014508 (2009).



## Pressure-energy correlations in liquids. IV. “Isomorphs” in liquid phase diagrams

Nicoletta Gnan,<sup>a)</sup> Thomas B. Schröder,<sup>b)</sup> Ulf R. Pedersen,<sup>c)</sup> Nicholas P. Bailey,<sup>d)</sup> and Jeppe C. Dyre<sup>e)</sup>

*DNRF Center “Glass and Time,” IMFUFA, Department of Sciences, Roskilde University, P.O. Box 260, DK-4000 Roskilde, Denmark*

(Received 29 May 2009; accepted 27 October 2009; published online 17 December 2009)

This paper is the fourth in a series devoted to identifying and explaining the properties of strongly correlating liquids, i.e., liquids where virial and potential energy correlate better than 90% in their thermal equilibrium fluctuations in the *NVT* ensemble. For such liquids we here introduce the concept of “isomorphic” curves in the phase diagram. A number of thermodynamic, static, and dynamic isomorph invariants are identified. These include the excess entropy, the isochoric specific heat, reduced-unit static and dynamic correlation functions, as well as reduced-unit transport coefficients. The dynamic invariants apply for both Newtonian and Brownian dynamics. It is shown that after a jump between isomorphic state points the system is instantaneously in thermal equilibrium; consequences of this for generic aging experiments are discussed. Selected isomorph predictions are validated by computer simulations of the Kob–Andersen binary Lennard-Jones mixture, which is a strongly correlating liquid. The final section of the paper relates the isomorph concept to phenomenological melting rules, Rosenfeld’s excess entropy scaling, Young and Andersen’s approximate scaling principle, and the two-order parameter maps of Debenedetti and co-workers. This section also shows how the existence of isomorphs implies an “isomorph filter” for theories for the non-Arrhenius temperature dependence of viscous liquids’ relaxation time, and it explains isochronal superposition for strongly correlating viscous liquids. © 2009 American Institute of Physics. [doi:10.1063/1.3265957]

### I. INTRODUCTION

How much does knowledge of a system’s thermal equilibrium fluctuations at one state point tell us about its behavior at other state points? In principle, complete knowledge of the fluctuations provides enough information to determine the density of states, from which the free energy at other state points may be calculated. In practice, only second-order moments of the fluctuations may be determined reliably. These generally give little knowledge of the system’s properties away from the state point in question. It was recently shown that a large class of liquids exhibits strong correlations between their virial and potential energy *NVT* thermal equilibrium fluctuations.<sup>1–6</sup> Such liquids have a hidden (approximate) scale invariance.<sup>5,7</sup> Because of this, important global information about the system may be obtained from knowledge of the virial and potential energy fluctuations’ second-order moments at a single state point. This unusual situation in statistical mechanics is the background of the present paper, which is the fourth in a series<sup>3–5</sup> devoted to identifying and explaining the properties of strongly correlating liquids.

Paper I (Ref. 3) of the series presented results from computer simulations of 13 different liquids. The results show

that van der Waals and metallic liquids are strongly correlating, whereas hydrogen-bonding liquids such as methanol and water are not. Likewise, covalent and ionic liquids are not expected to be strongly correlating because competing interactions generally spoil the correlations. Paper II (Ref. 4) gave a thorough analysis of the cause of the strong correlations, which is briefly recapitulated below. It was shown how to qualify the simple explanation of the correlations given in our first publication (Ref. 1), where strong correlations were argued to derive from particle-particle close encounters probing only the repulsive part of the potential, which is in many cases well approximated by an inverse power law (IPL). This explanation must be qualified in order to explain the occurrence of strong correlations at low and moderate temperatures and/or low pressures, as well as in the crystalline state. A number of consequences of strong virial/potential energy correlations were also discussed in Paper II. Paper III (Ref. 5) published in tandem with this paper, gives further theoretical results on the statistical mechanics and thermodynamics of the hidden scale invariance that characterizes strongly correlating liquids. Paper III also presents results from computer simulations demonstrating that strong virial/potential energy correlations are present even in nonequilibrium situations.

The present paper introduces the new concept of “isomorphs” in the phase diagram of a strongly correlating liquid and derives a number of isomorph characteristics. The existence of isomorphs distills the properties of strongly correlat-

<sup>a)</sup>Electronic mail: ngnan@ruc.dk.

<sup>b)</sup>Electronic mail: tbs@ruc.dk.

<sup>c)</sup>Electronic mail: urp@ruc.dk.

<sup>d)</sup>Electronic mail: nbailey@ruc.dk.

<sup>e)</sup>Electronic mail: dyre@ruc.dk.

ing liquids into one single concept and its immediate consequences, a concept that is defined without reference to correlations.

In order to recapitulate the definition of a strongly correlating liquid, recall<sup>8</sup> that for a system of  $N$  particles in volume  $V$  at temperature  $T$ , the pressure  $p$  is a sum of the ideal gas term  $Nk_B T/V$  and a term reflecting the interactions,  $W/V$ , where  $W$  is the so-called virial, i.e.,

$$pV = Nk_B T + W. \quad (1)$$

This equation is usually thought of as describing thermodynamic averages, but it also applies for the instantaneous values. The instantaneous ideal-gas pressure term is a function of the particle momenta, giving the  $Nk_B T$  term. The instantaneous virial  $W$  is the function of particle positions defined<sup>8</sup> by  $W(\mathbf{r}_1, \dots, \mathbf{r}_N) \equiv -(1/3) \sum_i \mathbf{r}_i \cdot \nabla_{\mathbf{r}_i} U(\mathbf{r}_1, \dots, \mathbf{r}_N)$ , where  $U(\mathbf{r}_1, \dots, \mathbf{r}_N)$  is the potential energy function. If  $\Delta U$  is the instantaneous potential energy minus its thermodynamic average and  $\Delta W$  the same for the virial, at any given state point the  $WU$  correlation coefficient  $R$  is defined by (sharp brackets here and henceforth denote equilibrium  $NVT$  ensemble averages)

$$R = \frac{\langle \Delta W \Delta U \rangle}{\sqrt{\langle (\Delta W)^2 \rangle \langle (\Delta U)^2 \rangle}}. \quad (2)$$

By the Cauchy–Schwarz inequality the correlation coefficient obeys  $-1 \leq R \leq 1$ . We define strongly correlating liquids by the condition  $R > 0.9$  (Paper I). The correlation coefficient is state-point dependent, but for all liquids we have studied by computer simulation<sup>3</sup>  $R$  is either above 0.9 in a large part of the phase diagram, or not at all. In all cases the correlation coefficient quickly decreases when pressure becomes negative, but strongly correlating liquids generally remain so at zero pressure.

Strongly correlating liquids include<sup>1–4,6,9</sup> the standard Lennard–Jones (LJ) liquid, the Kob–Andersen binary LJ mixture as well as other binary LJ-type mixtures, a “dumbbell” liquid consisting of two different LJ spheres with fixed bond length, a system with exponential repulsion, a seven-site united-atom toluene model, the Lewis–Wahnström orthoterphenyl model, and an attractive square-well binary mixture. Strongly correlating liquids have simpler physics than liquids in general. This has particular significance for the highly viscous phase.<sup>10–21</sup> Thus to a good approximation strongly correlating viscous liquids have all eight fundamental frequency-dependent thermoviscoelastic response functions<sup>22–24</sup> given in terms of just one,<sup>2</sup> i.e., they are single-order-parameter liquids in the sense of having dynamic Prigogine–Defay ratio<sup>22</sup> close to unity.<sup>2,4,23</sup> Moreover, strongly correlating viscous liquids obey density scaling, i.e., their average relaxation time  $\tau$  varies with density  $\rho = N/V$  and temperature according to  $\tau = F(\rho^\gamma/T)$ .<sup>7,25–29</sup> Even complex systems like biomembranes may exhibit significant correlations for their slow thermodynamic degrees of freedom; this was shown by all-atom computer simulations of five phospholipid membranes which exhibit strong correlations of the energy-volume fluctuations in the  $NpT$  ensemble.<sup>30</sup>

When instantaneous values of virial and potential energy are plotted against each other for a strongly correlating liquid

in thermal equilibrium at constant volume, an elongated ellipse appears.<sup>1,3,4,6</sup> The slope of this ellipse is  $\sqrt{\langle (\Delta W)^2 \rangle / \langle (\Delta U)^2 \rangle}$ . As detailed in Sec. II D this quantity, which is weakly state-point dependent, is to a good approximation the exponent  $\gamma$  of the density-scaling relation  $\tau = F(\rho^\gamma/T)$ .<sup>7,9</sup> Thus for a strongly correlating liquid knowledge of the equilibrium fluctuations at one state point provides information about how the relaxation time varies with density and temperature.

What causes the strong  $WU$  correlations of some liquids? A hint comes from the well-known fact that an IPL pair potential<sup>31–42</sup>  $v(r) \propto r^{-n}$ , where  $r$  is the distance between two particles, implies 100% correlation (Paper II). In this case the slope is  $n/3$ .<sup>115</sup> In simulations of the standard LJ liquid we found slopes around 6, corresponding to  $n \approx 18$ .<sup>1</sup> Although this may seem puzzling given the expression defining the LJ potential  $v_{LJ}(r) = 4\epsilon[(r/\sigma)^{-12} - (r/\sigma)^{-6}]$ , if one wishes to fit the repulsive part of the this potential by an IPL, an exponent around 18 is indeed required.<sup>1,4,43</sup> The reason is that the attractive  $r^{-6}$  term makes the repulsion considerably steeper than the bare repulsive  $r^{-12}$  term would imply.

Paper II gave a thorough discussion of the  $WU$  correlations with a focus on the standard single-component LJ liquid; this included also a treatment of the (classical) LJ crystal where one finds  $0.99 < R < 1$  at low temperature. According to Paper II the  $r$ -dependent effective exponent  $n$  which controls the correlation is not simply that coming from fitting the repulsive part of the potential, but rather  $n^{(2)}(r) \equiv -2 - r v'''(r)/v''(r)$ . This number is 18–19 around the LJ minimum. In fact, the LJ potential may here be fitted very well with an “extended IPL” potential (Papers II and III), i.e.,  $v_{LJ}(r) \approx A r^{-n} + B + C r$  with  $n$  of order 18. For this potential  $n^{(2)}(r) = n$ . At constant volume the linear term contributes little to the virial and potential energy fluctuations: when one nearest-neighbor interatomic distance increases, another decreases in such a way that their sum remains almost constant (Paper II). This means that virtually correct canonical probabilities are arrived at by using the IPL approximation, an observation which inspired us to the definition of isomorphs given below.

For an IPL liquid several quantities are invariant along the curves in the phase diagram given by  $\rho^{n/3}/T = \text{const}$ . Paper III (Ref. 5) summarizes the thermodynamic IPL invariants, which include for instance Helmholtz free energy over temperature, excess entropy, average potential energy over temperature, isothermal bulk modulus over density times temperature, and virial over temperature. In reduced units the dynamics of an IPL liquid is also invariant along the  $\rho^{n/3}/T = \text{const}$  curves (Paper III). The present paper shows that some IPL invariants give rise to general “isomorph invariants” of strongly correlating liquids. Not all IPL invariants generalize, however, and, e.g., the equation of state of a strongly correlating liquid is usually poorly represented by the IPL approximation (Paper II).

We demonstrate below several implications of one single assumption: the existence of curves in the phase diagram on which for any two state points there is a one-to-one correspondence between their respective microscopic configura-

tions, such that corresponding configurations have identical configurational  $NVT$  canonical probabilities. These curves in the phase diagrams are referred to as *isomorphs*. Section II defines isomorphs and summarizes their properties classified into thermodynamic, structural, equilibrium dynamic, and aging properties. Most isomorph properties come in the form of isomorph invariants. In Sec. II we also discuss how to identify isomorph curves in the phase diagram. Section III presents results from computer simulations of (mainly) the Kob–Andersen binary LJ mixture, validating some of the isomorph predictions. Section IV relates the isomorph concept to selected topics of current liquid state theory and experiment. Section V gives a brief conclusion.

## II. ISOMORPHS

This section introduces the concept of isomorphs in the phase diagram of a strongly correlating liquid. Although the definition of an isomorph refers neither to IPL potentials nor to strong  $WU$  correlations, only strongly correlating liquids have isomorphs. This is because the existence of isomorphs reflects the hidden scale invariance characterizing strongly correlating liquids (Paper III).

### A. Isomorph definition

Assuming that the origin of the coordinate system is centered in the liquid, for any microscopic configuration  $(\mathbf{r}_1, \dots, \mathbf{r}_N)$  of a thermodynamic state point with density  $\rho$ , the “reduced” (dimensionless) coordinates are defined by

$$\tilde{\mathbf{r}}_i \equiv \rho^{1/3} \mathbf{r}_i. \quad (3)$$

Using reduced coordinates corresponds to switching to a scaled coordinate system where the density is unity. We term a microscopic configuration *physically relevant* with respect to a given thermodynamic state point if the configuration’s contribution to the partition function at that state point is not *a priori* negligible. For instance, no configurations where all particles occupy the left half of the system’s volume are physically relevant for ordinary liquid states.

State points (1) and (2) with temperatures  $T_1$  and  $T_2$  and densities  $\rho_1$  and  $\rho_2$  are *isomorphic* if they obey the following: whenever two of their physically relevant microscopic configurations  $(\mathbf{r}_1^{(1)}, \dots, \mathbf{r}_N^{(1)})$  and  $(\mathbf{r}_1^{(2)}, \dots, \mathbf{r}_N^{(2)})$  have identical reduced coordinates (i.e.,  $\tilde{\mathbf{r}}_i^{(1)} = \tilde{\mathbf{r}}_i^{(2)}$ ), they have proportional configurational  $NVT$  Boltzmann factors:

$$e^{-U(\mathbf{r}_1^{(1)}, \dots, \mathbf{r}_N^{(1)})/k_B T_1} = C_{12} e^{-U(\mathbf{r}_1^{(2)}, \dots, \mathbf{r}_N^{(2)})/k_B T_2}. \quad (4)$$

It is understood that the constant  $C_{12}$  depends only on the state points (1) and (2), not on the microscopic configurations. *Isomorph curves* in the phase diagram are defined as curves on which any two state points are isomorphic.

An IPL liquid with interactions scaling with distance  $\propto r^{-n}$  trivially obeys Eq. (4) with  $C_{12}=1$  for states with  $\rho_1^{n/3}/T_1 = \rho_2^{n/3}/T_2$ . No other systems obey Eq. (4) rigorously, but we show in Sec. III from simulations of a strongly correlating liquid that the existence of isomorphs is a good approximation. Although only IPL liquids have exact isomor-

phs, we shall generally say that a liquid “has isomorphs” if isomorph curves exist to a good approximation in the liquid’s phase diagram.

The isomorph definition does not refer to  $WU$  correlations, but only strongly correlating liquids have isomorphs. Appendix A proves in detail that all strongly correlating liquids have isomorphs and *vice versa*. It is illuminating here to briefly sketch why the existence of isomorphs for a liquid implies that it must be strongly correlating. Consider a liquid with two isomorph state points that are infinitesimally close to each other. If  $\delta$  represents the variation between two infinitesimally close microscopic configurations with same reduced coordinates of the two state points, the logarithm of Eq. (4) implies  $\delta(U/T) = \text{const}$  where the constant is infinitesimal. The differentiation leads to a relation of the form  $\delta U = (da)U + db$  where  $da$  and  $db$  are infinitesimals. Since  $\delta U$  is the potential energy difference between two microscopic configurations differing by  $\delta \mathbf{r}_i \propto \mathbf{r}_i$ , one has  $\delta U \propto W$  with an infinitesimal proportionality constant (Appendix A). Altogether we get  $W = AU + B$  for some constants  $A$  and  $B$ . This implies 100% correlation of the  $WU$  fluctuations—recall, however, that the existence of isomorphs is itself an approximation. Thus liquids having isomorphs (to a good approximation) must be strongly correlating.

A number of properties characterize isomorph curves in the phase diagram of a strongly correlating liquid. Most isomorph properties come in the form of isomorph invariants. These are consequences of the fact that for any two isomorph state points there is a one-to-one correspondence between the state points’ physically relevant microscopic configurations, such that corresponding configurations have the same  $NVT$  canonical probabilities. This one-to-one correspondence motivates the name isomorph (“same form”), which is fundamental throughout mathematics. Here two objects are termed isomorphic if they are structurally equivalent, i.e., if a structure-preserving bijective mapping between them exists. In physics and chemistry isomorphic crystals by definition have symmetry groups that are mathematically isomorphic—such crystals have the same structure, but different constituents.

### B. Isomorph properties

We briefly recall well-known facts of the statistical mechanics of classical liquids in the  $NVT$  canonical ensemble.<sup>8,44–47</sup> The Helmholtz free energy  $F$  is the sum of an ideal gas term and an “excess” free energy term reflecting the molecular interactions,  $F = F_{\text{id}} + F_{\text{ex}}$ . The first term is the free energy of an ideal gas at the same density and temperature,  $F_{\text{id}} = Nk_B T \ln(\rho \Lambda^3/e)$ , where  $\Lambda = h/\sqrt{2\pi m k_B T}$  is the thermal de Broglie wavelength. The excess free energy is given by

$$e^{-F_{\text{ex}}/k_B T} = \int \frac{d\mathbf{r}_1}{V} \dots \frac{d\mathbf{r}_N}{V} e^{-U(\mathbf{r}_1, \dots, \mathbf{r}_N)/k_B T}. \quad (5)$$

The integral involves only the configurational degrees of freedom. This separation of the configurational degrees of freedom from the momenta should be kept in mind throughout this paper. Thus when we refer to the canonical ensemble

and canonical probabilities, only the configurational part of phase space is implied. Likewise, the microcanonical ensemble refers to the uniform probability distribution on the constant potential energy surface in configuration space.

The configuration space probability distribution normalized to the above dimensionless integral is given by

$$P(\mathbf{r}_1, \dots, \mathbf{r}_N) = e^{-[U(\mathbf{r}_1, \dots, \mathbf{r}_N) - F_{\text{ex}}]/k_B T}. \quad (6)$$

The excess entropy  $S_{\text{ex}}$  is defined by  $S_{\text{ex}} = -\partial F_{\text{ex}}/\partial T$ . Since the entropy in the canonical ensemble is generally given by  $-k_B \langle \ln P \rangle$ , we have

$$S_{\text{ex}} = -k_B \int \frac{d\mathbf{r}_1}{V} \dots \frac{d\mathbf{r}_N}{V} P(\mathbf{r}_1, \dots, \mathbf{r}_N) \ln P(\mathbf{r}_1, \dots, \mathbf{r}_N). \quad (7)$$

The inequality  $-P \ln P \leq 1 - P$  implies that  $S_{\text{ex}}$  is always negative, a fact that is physically obvious since any liquid is more ordered than an ideal gas at the same volume and temperature.

Most isomorph invariants are consequences of two fundamental isomorph properties, Eqs. (8) and (9) below. Equation (4) implies that the normalized reduced-coordinate canonical probability distribution is invariant along an isomorph

$$\tilde{P}(\tilde{\mathbf{r}}_1, \dots, \tilde{\mathbf{r}}_N) \text{ is an isomorph invariant.} \quad (8)$$

The notation  $\tilde{P}$  is introduced to distinguish from the  $P$  of Eq. (6);  $\tilde{P}$  is normalized via  $\int \tilde{P}(\tilde{\mathbf{r}}_1, \dots, \tilde{\mathbf{r}}_N) d\tilde{\mathbf{r}}_1 \dots d\tilde{\mathbf{r}}_N = 1$  which implies  $\tilde{P}(\tilde{\mathbf{r}}_1, \dots, \tilde{\mathbf{r}}_N) = N^{-N} P(\mathbf{r}_1, \dots, \mathbf{r}_N)$ . The second fundamental isomorph property is that an isomorph  $I$  is characterized by two functions  $f_I(\tilde{\mathbf{r}}_1, \dots, \tilde{\mathbf{r}}_N)$  and  $g(Q)$ , where  $Q$  denotes the state point, such that for any physically relevant microscopic configuration of state point  $Q$ ,

$$U(\mathbf{r}_1, \dots, \mathbf{r}_N; \rho) = k_B T f_I(\tilde{\mathbf{r}}_1, \dots, \tilde{\mathbf{r}}_N) + g(Q). \quad (9)$$

This follows from the isomorph definition equation (4). In this formulation the potential energy function is formally regarded as density dependent, reflecting the fact that Eq. (9) only applies for physically relevant microscopic configurations, i.e., configurations that fill out the volume.

Before deriving the isomorph properties we note two multidimensional geometric isomorph characterizations. Recall that the potential energy landscape is the graph of the potential energy function, i.e., a subset of  $R^{3N+1}$ . The first geometric property is that isomorph state points have potential energy landscapes which, when restricted to the physically relevant states, are identical except for a vertical displacement and scaling by the inverse temperature, and a horizontal scaling to unit density. This follows from the isomorph definition equation (4), and this is what Eq. (9) expresses. The second geometric isomorph characterization relates to the hypersurface  $\Omega$  in  $R^{3N}$  where the potential energy equals the average potential energy of the state point in question: in reduced coordinates this “constant potential energy hypersurface,” denoted by  $\tilde{\Omega}$ , is invariant along an isomorph. This follows from the first geometric property in conjunction with the isomorph definition equation (4). For details, please

consult Appendix A, which proves that a liquid is strongly correlating if and only if it has isomorphs, and that this happens if and only if the liquid has curves in the phase diagram along which  $\tilde{\Omega}$  is invariant.

## 1. Thermodynamics

A number of thermodynamic quantities are invariant along isomorph curves in the phase diagram of a strongly correlating liquid.

- 1a. The excess entropy  $S_{\text{ex}}$  is invariant along an isomorph. Equation (7) implies that  $S_{\text{ex}} = -k_B \int \tilde{P} \ln \tilde{P} d\tilde{\mathbf{r}}_1 \dots d\tilde{\mathbf{r}}_N + \text{const}$ , from which property 1a follows because of the invariance of  $\tilde{P}$ . Property 1a may also be derived by referring to the microcanonical ensemble where the excess entropy is  $k_B$  times the logarithm of the area of  $\tilde{\Omega}$  plus a constant: because  $\tilde{\Omega}$  is an isomorph invariant, so is the excess entropy.
- 1b. The configurational entropy  $S_{\text{conf}}$  is invariant along an isomorph. The term “configurational entropy,” not to be confused with  $S_{\text{ex}}$ , is used here in the sense of Adam and Gibbs and subsequent workers, who related  $S_{\text{conf}}$  to the temperature dependence of viscous liquids’ average relaxation time.<sup>14,16,48</sup> The configurational entropy is  $k_B$  times the logarithm of the “density of states” of potential energy minima, the so-called inherent states, evaluated at the state point’s average inherent state energy.<sup>18,20</sup> Property 1b follows from the identity of the scaled potential energy landscapes of two isomorph state points.
- 1c. When a liquid is heated along an isomorph, the measured specific heat equals the ideal-gas specific heat. Since the specific heat is  $dS/d \ln T$  and property 1a implies  $dS_{\text{ex}} = 0$  along an isomorph, the measured specific heat equals the specific heat that would be measured for an ideal gas subjected to the same process.
- 1d. The isochoric specific heat is invariant along an isomorph. If the liquid’s extensive excess isochoric specific heat is denoted by  $C_V^{\text{ex}}$ , in terms of the variable  $X = U/k_B T$  Einstein’s expression  $C_V^{\text{ex}} = \langle (\Delta U)^2 \rangle / k_B T^2$  becomes  $C_V^{\text{ex}} = k_B \langle (\Delta X)^2 \rangle$ . Equation (9) implies that for two isomorph state points pairs of microscopic configurations with same reduced coordinates obey  $X_1 = X_2 + \text{const}$ , i.e., for the fluctuations  $\Delta X_1 = \Delta X_2$ . Since  $\Delta X$  depends only on the reduced coordinates and  $\tilde{P}(\tilde{\mathbf{r}}_1, \dots, \tilde{\mathbf{r}}_N)$  is isomorph invariant, it follows that the excess isochoric specific heat is an isomorph invariant. This implies invariance of the full  $C_V$  because the contribution to  $C_V$  from the momentum degrees of freedom is state-point independent.

## 2. Structure

Particle distribution functions are generally invariant along an isomorph when quoted in reduced coordinates.

TABLE I. Reduced units. The energy and length units refer to state-point properties only, the time unit refers also to the dynamics. Once these fundamental units have been defined, transport and other properties have uniquely defined dimensionless versions, denoted by a tilde. The table gives three examples of such properties.

Quantity	Newtonian dynamics	Brownian dynamics
Energy unit ( $E_0$ )	$k_B T$	$k_B T$
Length unit ( $l_0$ )	$\rho^{-1/3}$	$\rho^{-1/3}$
Time unit ( $t_0$ )	$\frac{\sqrt{m/k_B T}}{\rho^{1/3}}$	$\frac{1}{\rho^{2/3} \mu k_B T}$
Diffusion constant:		
$\tilde{D} = D/(l_0^2/t_0)$	$\tilde{D} = (\rho^{1/3} \sqrt{m/k_B T}) D$	$\tilde{D} = \frac{1}{\mu k_B T} D$
Viscosity:		
$\tilde{\eta} = \eta/(E_0 t_0/l_0^3)$	$\tilde{\eta} = \frac{1}{\rho^{2/3} \sqrt{m k_B T}} \eta$	$\tilde{\eta} = \frac{\mu}{\rho^{1/3}} \eta$
Heat conductivity:		
$\tilde{\kappa} = \kappa/(k_B/l_0 t_0)$	$\tilde{\kappa} = \frac{\sqrt{m k_B T}}{\rho^{2/3} k_B} \kappa$	$\tilde{\kappa} = \frac{1}{\rho \mu k_B^2 T} \kappa$

- 2a. Reduced-coordinate radial distribution function(s), as well as higher-order equilibrium particle probability distributions, are invariant along an isomorph. Property 2a follows from Eq. (8); note that it applies for liquids with any number of different particles.
- 2b. The multiparticle entropies  $S_2, S_3, \dots$  are invariant along an isomorph. The equilibrium particle distributions give rise to  $n$ -particle entropies<sup>49,50</sup> contributing to the total entropy as follows:  $S_{\text{ex}} = S_2 + S_3 + \dots$ . In terms of the radial distribution function for a system of identical particles  $g(r)$ , the pair-correlation contribution  $S_2$  is given by  $S_2/N = -(\rho k_B/2) \int d\mathbf{r} [g(r) \ln g(r) + 1 - g(r)]$ . When this expression, as well as the more involved expressions defining  $S_3$ , etc., is rewritten in terms of reduced coordinates, it becomes clear that property 2b is a consequence of Eq. (8). We considered here only the case of identical particles, but property 2b holds for systems with any number of different particles.

### 3. Equilibrium dynamics

Like the static isomorph invariants, dynamic invariants also derive from the fact that for all physically relevant microscopic configurations the potential energy landscapes of isomorphic state points are identical—except for additive constants and overall scalings that do not affect the reduced-unit dynamics. For reference, Table I summarizes the definition of the basic units and gives examples of some reduced quantities.

- 3a. Both  $NVE$  and  $NVT$  Newtonian dynamics are isomorph invariant when described in reduced units. Consider first standard energy-conserving Newtonian dynamics, the  $NVE$  ensemble. If the mass of particle  $i$  is  $m_i$ , Newton's second law is  $m_i \ddot{\mathbf{r}}_i = \mathbf{F}_i$ , where  $\mathbf{F}_i = -\nabla_{\mathbf{r}_i} U$  is the force on the  $i$ th particle. We rewrite this in terms of reduced units as follows. If the average particle mass

is  $m$ , the reduced mass of the  $i$ th particle is defined by  $\tilde{m}_i = m_i/m$ . The reduced potential energy is defined by  $\tilde{U} = U/k_B T$  and the reduced force by  $\tilde{\mathbf{F}}_i = -\nabla_{\tilde{\mathbf{r}}_i} \tilde{U}$ . We also define a reduced time  $\tilde{t} = t/t_0$  where  $t_0 = \rho^{-1/3} \sqrt{m/k_B T}$ . In terms of these reduced variables Newton's second law becomes  $\tilde{m}_i \ddot{\tilde{\mathbf{r}}}_i = \tilde{\mathbf{F}}_i$ . The isomorph invariance now follows from Eq. (9), which implies that the reduced force is the same function of the reduced particle positions for all state points on a given isomorph. Proceeding to Newtonian dynamics in the  $NVT$  ensemble realized via the Nosé–Hoover thermostat,<sup>51,52</sup> recall that the forces here have the additional term  $-\zeta m_i \dot{\mathbf{r}}_i$  with a “friction constant”  $\zeta$  obeying  $\dot{\zeta} = (K/K_0 - 1)/\tau_0^2$ , where  $K$  is the kinetic energy,  $K_0$  its average, and  $\tau_0$  the thermostat time constant. These equations become isomorph invariant when rewritten in terms of the same reduced units as the  $NVE$  Newtonian equations, if the thermostat time constant is adjusted to be the same in reduced units; otherwise, only the long-time  $NVT$  dynamics is isomorph invariant.

- 3b. Brownian dynamics is isomorph invariant when described in reduced units. The Brownian (Langevin) equations of motion are first-order stochastic equations. These equations obey detailed balance, ensuring consistency with the canonical ensemble. The Brownian equation of motion is  $\dot{\mathbf{r}}_i = \mu \mathbf{F}_i + \boldsymbol{\xi}(t)$ , where  $\mu$  is the “mobility” (velocity/force) and  $\boldsymbol{\xi}(t)$  is a Gaussian white-noise vector term characterized by  $\langle \boldsymbol{\xi}_m(t) \boldsymbol{\xi}_n(t') \rangle = 2\mu k_B T \delta_{mn} \delta(t-t')$  ( $m, n = 1, 2, 3$ ). The path-probability functional is given<sup>53</sup> by  $P \propto \exp[-1/(4\mu k_B T) \sum_{i,j} \int_{-\infty}^{\infty} (\dot{\mathbf{r}}_i - \mu \mathbf{F}_i)^2 dt]$ . We rewrite this in terms of reduced variables with  $\tilde{U} = U/k_B T$  as above, but the reduced time is now defined via  $\tilde{t} = t/t_0$  where  $t_0 = \rho^{-2/3} / \mu k_B T$ . This leads to  $P \propto \exp[-1/4 \sum_{i,j} \int_{-\infty}^{\infty} (\dot{\tilde{\mathbf{r}}}_i - \tilde{\mathbf{F}}_i)^2 d\tilde{t}]$ . Since the reduced force is isomorph invariant for microscopic configurations with same reduced coordinates, it follows that reduced-time Brownian dynamics is isomorph invariant.
- 3c. Normalized time-autocorrelation functions, as well as normalized higher-order time correlation functions, are invariant along an isomorph when quoted in reduced units. Consider the time-autocorrelation function or higher-order time-correlation functions of some variable  $A$  referring to constant-volume dynamics. Properties 3a and 3b imply that for both Newtonian and Brownian dynamics time-autocorrelation functions of  $A$  are invariant as functions of the reduced time if they are normalized by dividing by  $\langle A^2 \rangle$ . Normalization of any higher-order time-correlation function similarly makes it isomorph invariant as a function of the reduced times defining the correlation function.
- 3d. Average relaxation times are isomorph invariant when quoted in reduced units. For any variable  $A$  with zero mean a generic definition of its average relaxation time is  $\tau_A = \int_0^{\infty} \langle A(0)A(t) \rangle dt / \langle A^2 \rangle$ . In reduced units this becomes  $\tilde{\tau}_A = \int_0^{\infty} \langle \tilde{A}(0)\tilde{A}(\tilde{t}) \rangle d\tilde{t} / \langle \tilde{A}^2 \rangle$ . By property 3c this expression is isomorph invariant.

- 3e. Reduced transport coefficients such as the diffusion constant, the viscosity, etc. are invariant along an isomorph. By the fluctuation-dissipation (FD) theorem the diffusion constant is given by  $D = \int_0^\infty \langle v_x(0)v_x(t) \rangle dt$ , where  $v_x$  is the  $x$  component of a particle's velocity. The reduced diffusion constant  $\tilde{D}$  is defined by  $\tilde{D} = (\rho^{1/3} \sqrt{m/k_B T}) D$  for Newtonian and  $\tilde{D} = D / (\mu k_B T)$  for Brownian dynamics (Table I). In both cases one has  $\tilde{D} = \int_0^\infty \langle \tilde{v}_x(0)\tilde{v}_x(t) \rangle dt$ , implying that  $\tilde{D}$  is an isomorph invariant because both dynamics are isomorph invariant. Similarly, if  $\eta$  is the viscosity, the reduced viscosity is defined by  $\tilde{\eta} = (\rho^{-2/3} / \sqrt{mk_B T}) \eta$  for Newtonian and  $\tilde{\eta} = (\mu \rho^{-1/3}) \eta$  for Brownian dynamics. When rewritten as a reduced-time integral over the reduced shear-stress autocorrelation function, the required result follows. Similar results apply for the heat conductivity and other dc transport coefficients.
- 3f.  $G_\infty / T\rho$  is invariant along an isomorph where  $G_\infty$  is the instantaneous shear modulus. If  $S_{xy} = \sum_i x_i F_{i,y}$  where  $x_i$  is the  $x$ -coordinate of the  $i$ th particle and  $F_{i,y}$  is the  $y$ -component of the force acting on it, the FD expression for the instantaneous shear modulus<sup>54</sup> is  $G_\infty = \rho k_B T + \langle S_{xy}^2 \rangle / V k_B T$ . In terms of reduced variables one has  $x_i F_{i,y} = -k_B T \tilde{x}_i \partial \tilde{U} / \partial \tilde{y}_i$  leading to  $G_\infty / \rho k_B T = 1 + \langle (\sum_i \tilde{x}_i \partial \tilde{U} / \partial \tilde{y}_i)^2 \rangle / N$ . The required isomorph invariance now follows. Note that, because of the density dependence of the potential energy in Eq. (9), the analog expression with the instantaneous bulk modulus replacing the instantaneous shear modulus is not a general isomorph invariant.

#### 4. Aging

Not all isomorph properties come in the form of invariants. This section discusses a different type of consequence of the existence of isomorphs for strongly correlating liquids. It is assumed that the externally controlled variables are volume and temperature.

- 4a. A jump between two isomorphs starting from equilibrium takes the system instantaneously to equilibrium. This is because the normalized Boltzmann probability factors for microscopic configurations with same reduced coordinates are identical for the two systems. Thus isomorphs are predicted to be a kind of “wormholes” in the phase diagram along which one can jump instantaneously from equilibrium to equilibrium, even when the states are characterized by long relaxation times.
- 4b. Jumps from any two isomorphs to a third state point lead to the same aging behavior for all physical quantities. Note first that a jump between two arbitrary state points starting from equilibrium,  $1 \rightarrow 3$ , has the same relaxation pattern as the jump  $2 \rightarrow 3$ , where state point (2) is isomorph with state point (1) and has the same density as state point (3). To see this, suppose that instead of the  $1 \rightarrow 3$  jump we first impose

the isomorph jump to state point (2) with the correct final density and then, immediately thereafter, jump to state point (3). On the one hand, the system does not “register” it spent a tiny amount of time at state point (2). On the other hand, the  $1 \rightarrow 2$  jump took the system instantaneously to equilibrium at state point (2) (property 4a). Consequently, the  $1 \rightarrow 3$  and  $2 \rightarrow 3$  jumps must have the same relaxation toward equilibrium for all physical quantities. It now follows that if state point (1) is replaced by an isomorph state point (1'), the  $1 \rightarrow 3$  and  $1' \rightarrow 3$  relaxations are identical.

A concise way of summarizing the aging properties of strongly correlating liquids is that isomorph state points are equivalent during any aging scheme.

#### C. IPL invariants and general isomorph invariants

As mentioned, an IPL liquid has exact isomorphs. These are the curves in the phase diagram given by the equation  $\rho^{n/3} / T = \text{const}$ . All above isomorph properties apply exactly to IPL liquids (single component or multicomponent, as long as the exponent is the same for all interactions). However, only some of the IPL invariants along the curves given by  $\rho^{n/3} / T = \text{const}$  give rise to general isomorph invariants. Examples of IPL invariants that do not generalize are  $F_{\text{ex}} / T$ ,  $U / T$ ,  $W / T$ , the excess pressure coefficient over density  $\beta_V^{\text{ex}} / \rho = (\partial(W/V) / \partial T)_V / \rho$ , and  $K_T / T\rho$ , where  $K_T$  is the isothermal bulk modulus. One way to see that not all IPL thermodynamic properties give rise to general isomorph invariants is to refer to the approximate equation for the excess free energy derived in Paper III. Here it was shown that the hidden scale invariance of a strongly correlating liquid implies that one may write  $F_{\text{ex}}(V, T) = f(V) + N k_B T \phi(\rho^\gamma / T)$  to a good approximation. For an IPL liquid  $f(V) = 0$ , which, however, does not apply generally. The  $f(V)$  term implies that IPL properties involving volume derivatives do not give rise to general isomorph invariants.

#### D. Identifying isomorphs

How to identify the isomorphs in a strongly correlating liquid's phase diagram? As we just saw, for an IPL liquid the answer is simple: all static and dynamic IPL invariants refer to the curves given by  $\rho^\gamma / T = \text{const}$  where  $\gamma = n/3$ . For an IPL liquid the virial and potential energy equilibrium fluctuations from their average values obey  $\Delta W = \gamma \Delta U$ , and the number  $\gamma$  may be expressed in terms of equilibrium fluctuation averages in three simple ways:  $\gamma = \langle \Delta W \Delta U \rangle / \langle (\Delta U)^2 \rangle = \sqrt{\langle (\Delta W)^2 \rangle / \langle (\Delta U)^2 \rangle} = \langle (\Delta W)^2 \rangle / \langle \Delta W \Delta U \rangle$ . This applies only for a 100% correlating liquid, however. For a general strongly correlating liquid there are three slightly different corresponding gammas,

$$\gamma_1 = \frac{\langle \Delta W \Delta U \rangle}{\langle (\Delta U)^2 \rangle}, \quad \gamma_2 = \sqrt{\frac{\langle (\Delta W)^2 \rangle}{\langle (\Delta U)^2 \rangle}}, \quad \gamma_3 = \frac{\langle (\Delta W)^2 \rangle}{\langle \Delta W \Delta U \rangle}. \quad (10)$$

It follows from the definition of the correlation coefficient  $R$  [Eq. (2)] that

$$\gamma_1 = R\gamma_2 = R^2\gamma_3. \quad (11)$$

Thus  $\gamma_2$  is the geometric mean of  $\gamma_1$  and  $\gamma_3$ , and (since  $R > 0$  for a strongly correlating liquid)

$$\gamma_1 \leq \gamma_2 \leq \gamma_3. \quad (12)$$

Although for any strongly correlating liquid the three gammas are quite similar, the question is which gamma to use to identify the isomorphs. The answer is that there is no unique gamma common to all the isomorph invariants. To see this, note that in complete generality any quantity  $q$  of any liquid defines a state-point dependent exponent  $\gamma_q(Q)$  with the following property. An infinitesimal change away from state point  $Q$  conserves  $q$  whenever the quantity  $\rho^{\gamma_q(Q)}/T$  is kept constant [thus,  $\gamma_q(Q) = (\partial \ln T / \partial \ln \rho)_q(Q)$ ]. Strongly correlating liquids are characterized by the particular property that these  $\gamma$ 's are very similar for all the isomorph invariants.

In the simulations reported in Sec. III we used the excess entropy's "density scaling exponent"  $\gamma$  derived as follows. Along a configurational adiabatic curve  $0 = dS_{\text{ex}} = (\partial S_{\text{ex}} / \partial V)_T dV + (\partial S_{\text{ex}} / \partial T)_V dT$ . The volume-temperature Maxwell relation for the configurational degrees of freedom implies  $(\partial S_{\text{ex}} / \partial V)_T = (\partial(W/V) / \partial T)_V$ . Thus a configurational adiabat is characterized by  $(d \ln \rho)(\partial W / \partial T)_V = (d \ln T)T(\partial S_{\text{ex}} / \partial T)_V = (d \ln T)(\partial U / \partial T)_V$ , i.e.,

$$\gamma = \left( \frac{d \ln T}{d \ln \rho} \right)_{S_{\text{ex}}} = \left( \frac{\partial W}{\partial T} \right)_V = \frac{\langle \Delta W \Delta U \rangle}{\langle (\Delta U)^2 \rangle}. \quad (13)$$

This is  $\gamma_1$  of Eq. (10); the last equality is a standard thermodynamic fluctuation identity derived, e.g., in Appendix B of Paper I. Since it is convenient to think of the density scaling exponent as a generic quantity, we will not refer to it as  $\gamma_1$ , but simply as  $\gamma$ . Note that  $\gamma = (\partial W / \partial U)_V$ , which implies that  $\gamma$  is the slope of the lines of average virial versus average potential energy at constant density (compare, e.g., Fig. 4 in Paper I).

We propose to use the excess entropy's density scaling exponent because, on the one hand, it rigorously reproduces property 1a and, on the other hand, it may be calculated from equilibrium fluctuations at any given state point. Furthermore, it may be shown that for a given infinitesimal density change the optimal temperature change leading to a mean-square best fit of the logarithm of Eq. (4) is obtained by using this  $\gamma$  (Appendix B). Finally, note that this  $\gamma$  is also the one suggested by taking the ratio of Eqs. (28) and (27) in Paper III:  $\gamma = \beta_V^{\text{ex}} / c_V^{\text{ex}}$  where  $\beta_V^{\text{ex}} = (\partial(W/V) / \partial T)_V$  is the excess pressure coefficient and  $c_V^{\text{ex}}$  is the excess isochoric specific heat per unit volume.

It is now clear how to step-by-step map out an isomorph which is realized as a configurational adiabat. At any given

state point one calculates  $\gamma$  from the equilibrium fluctuations using Eq. (13). For a slight density change Eq. (13) determines the corresponding temperature change. This identifies a new state point that is isomorphic with the initial one. At the new state point a new value of  $\gamma$  is calculated from the equilibrium fluctuations, etc. We used this method in the simulations reported below, but found, notably, almost as good agreement with predictions using  $\gamma_2$  ( $\gamma_3$  was not tested).

In the below simulations, as well as in previous simulations, we generally found only rather weak state-point dependence of the density scaling exponent  $\gamma$ . As shown in Appendix B, for a strongly correlating liquid any variation in  $\gamma$  with state point can only come via a density dependence:  $\gamma = \gamma(\rho)$ . This result is derived from the isomorph identity between the curves in the phase diagram of constant excess entropy and those of constant isochoric specific heat. Our simulations are consistent with this result in the sense that  $\gamma$  generally varies significantly less along isochores than otherwise throughout the phase diagram. The conclusion is that in the isomorph approximation, any isomorph invariant is a function of  $\rho^{\gamma(\rho)}/T$ , i.e., it may be written as a function of a variable of the form  $e(\rho)/T$ . Interestingly, this was precisely the recipe for collapsing dielectric relaxation measurements at different pressures and temperatures, which was proposed by Alba-Simionesco and her co-workers in their pioneering paper on density scaling.<sup>27</sup>

### III. COMPUTER SIMULATIONS

This section presents results from computer simulations investigating some of the predicted isomorph properties. The purpose is to document the existence of isomorphs for a typical strongly correlating liquid. Results are reported for molecular dynamics (MD) simulations of the standard Kob-Andersen<sup>55,56</sup> 80:20 binary Lennard-Jones (KABLJ) liquid with  $N=8000$  particles simulated using the GROMACS package.<sup>57,58</sup> The KABLJ system is a strongly correlating liquid (Paper I) which is easily supercooled without crystallizing.<sup>59</sup> Its density scaling exponent  $\gamma$  varies slightly with state point, but at low and moderate pressure and temperature  $\gamma$  stays between 5 and 6 (at extremely high pressure and temperature  $\gamma$  converges to the value of 4, which a purely repulsive  $r^{-12}$  potential would imply). The simulations were performed in the  $NVT$  ensemble using the Nosé-Hoover thermostat with characteristic time of 0.5 in MD units. Collections of isomorphic state points were identified as described above.

#### A. Direct isomorph check

It is possible to check directly the proportionality between Boltzmann factors which defines an isomorph. This is done as follows. At one state point of the equilibrium KABLJ liquid the simulation generates a time sequence of microscopic configurations. We now ask: For a given density change, does a temperature exist at which the new density state point is isomorphic to the initial one? If yes, what is this temperature? These questions are answered by plotting the potential energy of each microscopic configuration against

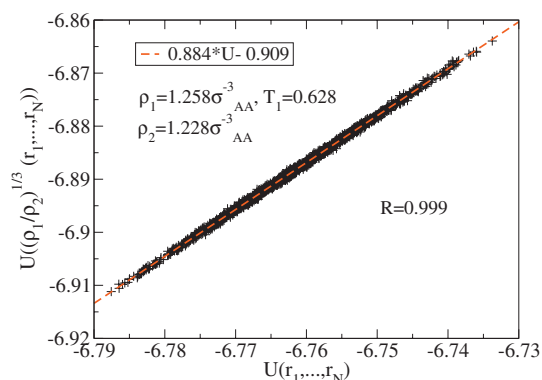


FIG. 1. Direct check of the isomorph condition equation (4) for the KABLIJ liquid with 8000 particles (energies are given per particle). The MD algorithm generates a time sequence of equilibrium microscopic configurations at the state point (1) given by  $\rho_1=1.258$  and  $T_1=0.628$  in standard LJ units. For each configuration the potential energy is plotted on the  $x$ -axis, while the  $y$ -axis gives the potential energy of the same microscopic configuration scaled to density  $\rho_2=1.228$ . Clearly these two quantities are highly correlated, which is the requirement for an isomorph. The slope of 0.884 implies that state point  $(\rho_2, T_2)$  is isomorph with state point  $(\rho_1, T_1)$  if  $T_2=0.884T_1=0.555$ . In comparison, the exponent of Eq. (13) evaluated from the fluctuations at state point (1) is  $\gamma=5.018$ , and the temperature at state point (2) keeping  $\rho^\gamma/T=\text{const}$  is  $T_2=0.556$ . The nonzero offset of the best fit line (of  $-0.909$ ) reflects the fact that the constant  $C_{12}$  in Eq. (4) differs from unity.

the potential energy of the same configuration scaled to the new density. In Fig. 1 density was decreased by 2.4%, which corresponds to a decrease in the relaxation time by more than a factor of 4 if temperature is not changed. The two potential energies are 99.9% correlated. This shows that a temperature does exist at which the isomorph condition equation (4) is fulfilled to a very good approximation. When the density change goes to zero, the correlation goes to 100%, of course, but the high correlation is nevertheless noteworthy given the fact that the slope of the stretched oval in the figure is not very close to unity (the slope is 0.884). The interpretation of the slope is that the two state points are isomorph if the temperature at the new density is 0.884 times the old temperature. Appendix C details how the correlation coefficient of Fig. 1 relates to the standard *WU* correlation coefficient of Eq. (2).

One might think that Fig. 1 proves that all the isomorph invariants apply to a good approximation for the KABLIJ liquid, but this is not necessarily the case. Consider for instance the dynamics. This becomes increasingly barrier dominated as temperature is lowered,<sup>60</sup> and the increasingly unlikely event of a barrier transition determines the relaxation time. Even if almost all microscopic configurations of significant weight in the canonical ensemble obey the isomorph definition equation (4) very well, this does not ensure that the barriers scale in the same way. Consequently we need more simulations to validate the isomorph concept.

## B. Equilibrium properties: Statics and dynamics

Denoting the large LJ particles as A, Fig. 2(a) gives the AA radial distribution functions for six isomorph state

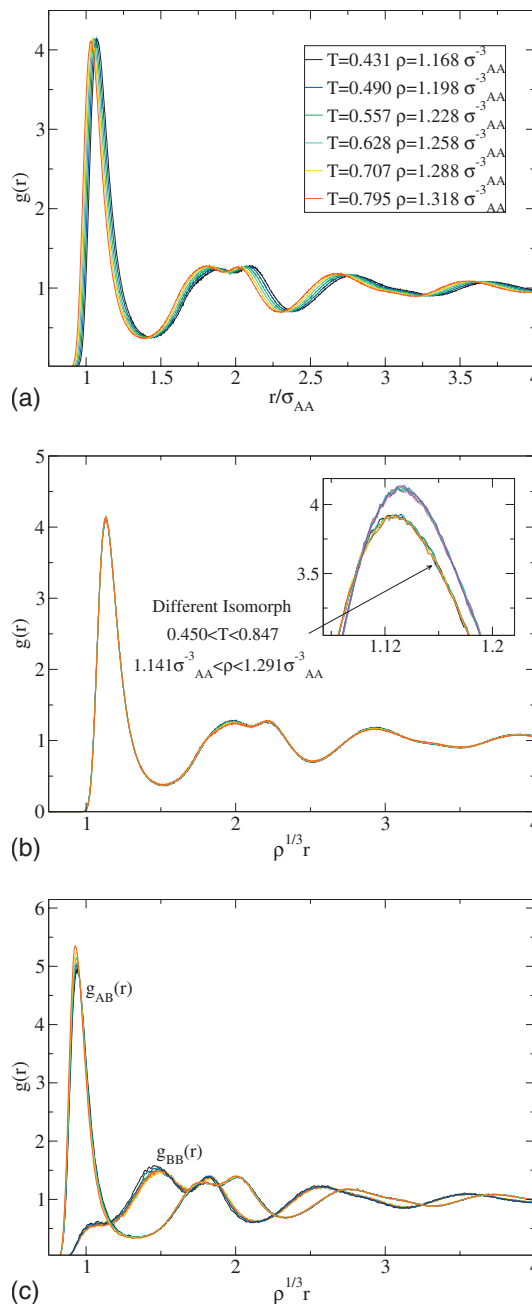


FIG. 2. (a) AA particle radial distribution functions for the KABLIJ liquid at six isomorph state points. (b) The same radial distribution functions plotted as functions of the reduced distance, showing very good data collapse. The inset focuses on the first peak and includes results for a second location of isomorph state points. (c) AB and BB radial distribution functions in reduced units for the six isomorph state points of (a). There is good data collapse, but with larger deviations than for the AA distribution function. This shows that isomorph properties are not exact.

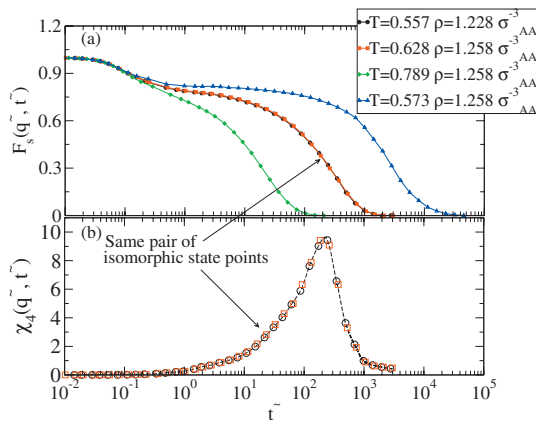


FIG. 3. (a) The self-part of the intermediate scattering functions at the wave vector corresponding to the first peak of the static structure factor as a function of the reduced time  $\tilde{t}$  for four state points of the KABLJ liquid. Two of the state points are isomorphous (red and black curves); these two state points have virtually indistinguishable self-part of the intermediate scattering functions. (b) The four-point dynamic susceptibility  $\chi_4(\tilde{t})$  for the two isomorphous state points of (a). This quantity, which measures the degree of dynamic heterogeneity, is predicted to be an isomorph invariant. The dashed curve is a cubic spline fit to the black data points.

points of the KABLJ system. The temperature varies by almost a factor of 2; nevertheless there is good collapse of the curves when these are plotted as functions of the reduced distance [Fig. 2(b)]. The inset of (b) zooms in on the peak of the radial distribution function. We added here data for a second collection of isomorphous state points, showing that different isomorphs have different structures. That the isomorph invariants are, after all, not exact is evident from Fig. 2(c), which shows the scaled AB and BB radial distribution functions of the isomorphous state points of (a).

Turning to the dynamics, Fig. 3(a) shows the AA self part of the intermediate scattering functions  $F_s(\vec{q}, \tilde{t})$  at the reduced wave vector corresponding to the first peak of the static structure factor, where  $\tilde{t}$  is time scaled by the characteristic time  $t_0 = \rho^{-1/3}(m/k_B T)^{1/2}$  (Table I). The figure shows results for four state points at two densities. Two of the four state points are isomorphous. These two state points (black and red curves) have virtually identical relaxation behavior, including the short-time ‘‘cage rattling.’’ Figure 3 thus confirms isomorph properties 3c and 3d. For the two isomorphous state points of Fig. 3(a), Fig. 3(b) shows the four-point dynamic susceptibility defined<sup>61</sup> by  $\chi_4(\tilde{t}) = N \langle (\Delta F_s(\vec{q}, \tilde{t}))^2 \rangle$ , i.e., the mean-square fluctuation of the self-part of the intermediate scattering functions. The quantity  $\chi_4(\tilde{t})$  measures the degree of dynamic heterogeneity on a given time scale. By the predicted isomorph invariance of time-correlation functions as functions of reduced time (property 3c)  $\chi_4(\tilde{t})$  is predicted to be invariant, which is indeed the case.<sup>62,63</sup>

As shown briefly in Sec. II and in detail in Appendix A, only strongly correlating liquids have isomorphs. A system that is not strongly correlating (Paper I) is the SPC water model, where the hydrogen bonds are mimicked using Coulomb interactions and the oxygen atoms interact via a LJ potential.<sup>64</sup> The fact that this model has near zero  $WU$  cor-

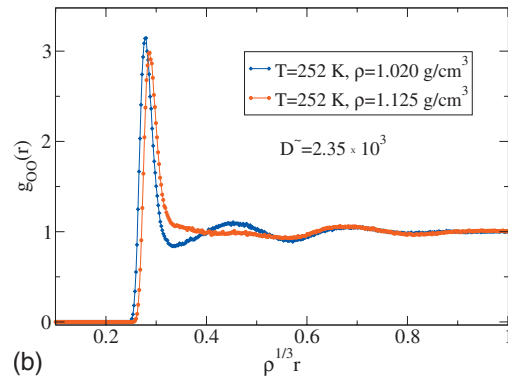
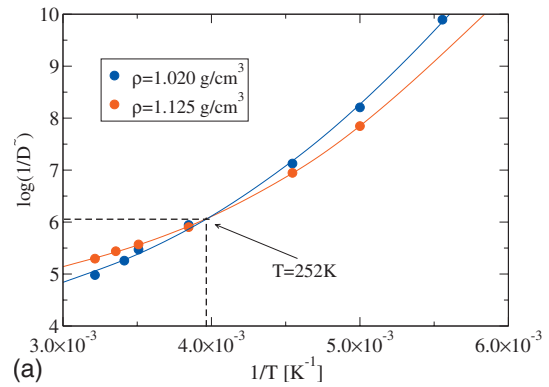


FIG. 4. (a) Reduced diffusion constants for two sets of isochoric state points of the SPC water model, which is not strongly correlating. The data were fitted by a polynomial in order to identify the temperature where the two densities have the same reduced diffusion constant ( $T=252 \text{ K}$ ). (b) Oxygen-oxygen radial distribution functions as functions of reduced distance for the two state points of SPC water identified in (a) with same temperature and same reduced diffusion constant, but different density. If water had isomorphs, the two radial distribution functions would be virtually identical in reduced units, compare Fig. 2.

relation reflects (Paper I) water’s density maximum. In order to prove that SPC water does not have isomorphs, suppose that it did. Then state points with the same reduced diffusion constant would have same structure. Figure 4(a) shows the reduced diffusion constant as a function of temperature for two sets of isochoric state points. Interpolation with a polynomial was done in order to identify the temperature where the two densities have the same reduced diffusion constant ( $T=252 \text{ K}$ ). Figure 4(b) shows the radial distribution functions of these two state points. Clearly, SPC water does not have isomorphs.

### C. Out-of-equilibrium properties: Aging

We showed by example that isomorphous state points have the same scaled static and dynamic correlation functions, but all properties tested so far were equilibrium properties. What happens when a strongly correlating liquid is taken out of equilibrium? To answer this we simulated temperature/density jumps from equilibrium, i.e., instantaneous changes of these two variables to new values. All

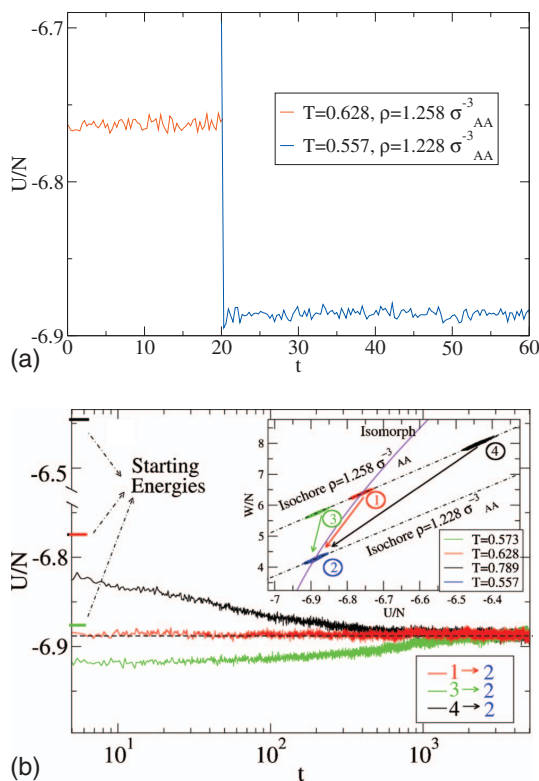


FIG. 5. (a) Results from simulating an instantaneous temperature and density jump applied to the KABLIJ liquid, starting from equilibrium and jumping to a state which is isomorphic with the initial state (LJ units). Except for the transient no relaxation is associated with the jump, showing that the system is instantaneously in equilibrium. (b) Potential energy relaxation toward equilibrium for the KABLIJ liquid for different jumps:  $1 \rightarrow 2$ ,  $3 \rightarrow 2$ , and  $4 \rightarrow 2$  (see the inset). The  $1 \rightarrow 2$  jump is the isomorphic jump of (a), the two other jumps are not between isomorphic state points. The results shown in (a) and (b) are averaged over ten independent simulations.

states involved in the “aging experiments” belong to the state points whose self-intermediate scattering functions are plotted in Fig. 3(a).

Figure 5(a) shows the time evolution of the potential energy when a jump is made from equilibrium, bringing the KABLIJ liquid to a new state point which is isomorphic to the initial state. The jump was performed as follows: we instantaneously increased the box volume without changing particle positions (the initial overshoot is due to this) and simultaneously changed the thermostat temperature to the final temperature. There are no signs of slow relaxation after the jump. Thus the system is immediately in equilibrium, as predicted for jumps between isomorphic state points (property 4a).

The horizontal (red) line in Fig. 5(b) shows the data of Fig. 5(a), now on a logarithmic scale with time shifted such that the jump occurs at  $t=0$ . Here it is even more clear that jumps between isomorphic state points preserve equilibrium. In contrast, the  $3 \rightarrow 2$  and  $4 \rightarrow 2$  jumps both age slowly toward equilibrium, where all three initial states (1), (3), and (4)

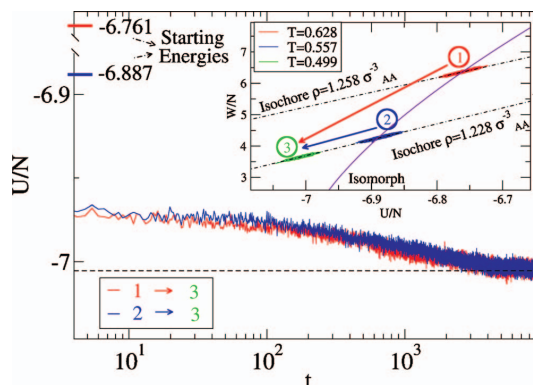


FIG. 6. Potential energy relaxation toward equilibrium for the KABLIJ liquid comparing jumps  $1 \rightarrow 3$  and  $2 \rightarrow 3$  (see the inset). The two relaxations are predicted to be identical because state points (1) and (2) are isomorphic. The results shown are averaged over ten independent simulations.

have the same density. Clearly, instantaneous equilibration is a feature of jumps between isomorphic points only.

The preservation of equilibrium for jumps between isomorphic state points has important consequences for general jumps (Fig. 6). Consider first the inset of Fig. 6. Suppose we start in equilibrium at state point (1) and change temperature and density to  $T_3$  and  $\rho_3$ . According to property 4b, if state point (2) is isomorphic to state point (1), the observed relaxation behavior for the  $2 \rightarrow 3$  jump should be the same as for the  $1 \rightarrow 3$  jump. The simulations confirm this prediction.

We can now understand why the  $3 \rightarrow 2$  jump in Fig. 5(b) approaches the equilibrium potential energy from below, although state point (3) has an average potential energy which is slightly *higher* than that of state point (2) [compare the inset of Fig. 5(b)]. This is because whenever a jump is performed, the system makes an instantaneous isomorphic jump to the new density to relax from here to the final state point by moving on the given isochore. Thus in Fig. 5(b), the  $3 \rightarrow 2$  jump is first an isomorphic jump to the state with correct density, a state that has lower average potential energy than state (2). Only thereafter the system relaxes toward state (2).

In most real experiments pressure, not density, is controlled. The only difference is that an instantaneous isomorphic jump goes to a new pressure, instead of to a new density, and that the subsequent relaxation follows an isobar instead of an isochore. Thus relabeling the dashed lines in the insets of Figs. 5(b) and 6 to isobars would qualitatively illustrate an experimental temperature and pressure jump.

#### IV. RELATING ISOMORPHS TO SELECTED TOPICS OF LIQUID STATE THEORY AND EXPERIMENT

This section discusses some connections between the isomorph concept and current liquid state theory and experiment. No subject is treated in depth; the purpose is merely to show by example that isomorphs fit nicely into a number of previous findings. In most cases we demonstrate how these are *consistent* with the isomorph concept, but in a few cases a previous finding is shown to be a *consequence* of the existence of isomorphs for strongly correlating liquids.

### A. Phenomenological melting rules

Melting is an old subject of condensed-matter physics. There has long been a good understanding of the statistical mechanics of melting via the density functional theory of Ramakrishnan and Yussouff.<sup>65</sup> Supplementing this are a number of phenomenological melting rules. Perhaps the most famous is the Lindemann criterion, according to which melting takes place when the crystal's vibrational root-mean-square displacement is about 10% of the nearest-neighbor distance.<sup>66,67</sup>

For a strongly correlating liquid the melting curve in the phase diagram must be parallel to nearby liquid and crystalline isomorphs (the isomorph concept applies to the crystalline phase as well as to the liquid). This is because if an isomorph were to cross the melting curve, the Boltzmann factors favoring crystalline order would dominate one part of that isomorph and be negligible on another part; this contradicts the isomorph structure invariance. For strongly correlating liquids the invariance of the crystalline excess entropy along the melting line implies, as is easy to show, pressure invariance of the Lindemann melting criterion. Moreover, since both crystalline and liquid excess entropy are invariant along the melting curve, the melting entropy must be pressure independent.

There are other consequences of melting curves being isomorphs for strongly correlating liquids. Thus along the melting curve, slightly to the liquid side, a number of properties are predicted to be invariant: the reduced viscosity, the reduced surface tension, the reduced diffusion constant, the reduced heat conductivity—in fact all isomorph invariants. There are several theoretical and experimental works pointing in these directions.<sup>68–73</sup> For instance, the reduced-unit static structure factor of liquid iron measured by x-ray scattering is invariant along the melting curve for pressures up to 58 GPa.<sup>74</sup> Finally, note that the Hansen–Verlet<sup>75</sup> criterion, according to which melting takes place when the liquid structure factor peak is 2.85, due to the invariance of the structure factor in reduced coordinates, is also consistent with the melting curve being an isomorph for strongly correlating liquids.

### B. Rosenfeld's excess entropy scaling

Rosenfeld<sup>76,77</sup> presented in 1977 an interesting observation: for a large class of model systems the reduced transport coefficients (Table I) appear to be functions of the excess entropy only. He justified what is now known as “excess entropy scaling” by reference to variational hard-sphere thermodynamic perturbation theory.<sup>76</sup> He emphasized that excess entropy scaling is a semiquantitative model, rather than a theory, and referred to excess entropy scaling as a principle of corresponding states. For any given strongly correlating liquid excess entropy scaling follows from the isomorph properties derived in Sec. II, although this does not explain why the functional excess entropy dependence appears to be quasiuniversal.<sup>76,77</sup> Recent simulations of the Gaussian core model by Truskett and co-workers<sup>78</sup> provide an example

where Rosenfeld's excess entropy scaling fails. This is not surprising, since this model due to the soft core is not expected to be strongly correlating.

A scaling procedure that is similar in spirit to Rosenfeld's excess entropy scaling was discussed by Dzугutov<sup>79</sup> in 1996. He showed from simulations that the reduced diffusion constant follows  $\tilde{D} \propto \exp(S_2/Nk_B)$  for a number of systems, where  $S_2$  is the two-particle entropy. This relation is also consistent with the isomorph concept, because  $\tilde{D}$  and  $S_2$  are both isomorph invariants (properties 3e and 2b).

From the isomorph viewpoint there is no reason to expect Rosenfeld's or Dzугutov's equations to hold for liquids that are not strongly correlating. While genuine Rosenfeld scaling seems to fail for liquids that are not strongly correlating, it appears that related excess entropy scaling procedures hold for many such liquids (see, e.g., Refs. 80 and 81). Why this is so is an important question for future research.

### C. Young and Andersen's approximate scaling principle

In 2003 Young and Andersen<sup>82,83</sup> conjectured an approximate scaling principle according to which two liquids have similar dynamical properties if they at two same-density state points have similar static pair-correlation functions—even if their potentials are quite different and the temperatures differ. This was confirmed by simulations comparing the LJ liquid to the same system with a Weeks–Chandler–Andersen (WCA) cutoff (where only the repulsive part of the potential is kept). At same density the latter system required lower temperature in order to have almost identical pair-correlation functions. When temperature was properly adjusted, however, the two liquids were shown to have similar coherent and incoherent intermediate scattering functions, as well as similar velocity and current autocorrelation functions. This confirms the authors' proposed approximate scaling principle for the single-component LJ liquid (in contrast, Berthier and Tarjus<sup>84</sup> very recently showed that the WCA approximation applied to the KABLJ liquid does not reproduce this liquid's dynamics).

As pointed out by Young and Andersen, if not only the pair-correlation but all higher-order correlation functions are identical for two liquids, they must have proportional  $NVT$  Boltzmann statistical weights for all microscopic configurations. This suggests generalizing the isomorph concept to an equivalence relation between *different* liquids. One may define two liquids to be isomorphic if (1) they are both strongly correlating and (2) a pair of state points exists such that Eq. (4) is obeyed for all physically relevant microscopic configurations with same reduced coordinates (in the form generalized to two different potential energy functions,  $U_1$  and  $U_2$ ). Clearly when this is obeyed, the entire system of isomorphic curves of one liquid maps onto that of the other liquid.

### D. Two-order parameter maps of Debenedetti and co-workers

In a series of publications Debenedetti and co-workers<sup>85–90</sup> studied liquid structure in terms of a translational order parameter  $t$  and a system-dependent orientational

order parameter that may be, for instance, the often used quantity  $Q_6$ . The translational order parameter is defined as  $t = \int_0^{\tilde{r}_c} |g(\tilde{r}) - 1| d\tilde{r}$ , where  $g(\tilde{r})$  is the reduced-coordinate pair distribution function and  $\tilde{r}_c = \rho^{1/3} r_c$  is a cutoff;  $Q_6$  is defined from sixth-order spherical harmonics involving the “bonds” to the 12 particles nearest a given particle (averaged over all particles).

The general picture one finds by plotting  $t$  versus  $Q_6$  in so-called ordering maps is that for the LJ liquid and related systems there is a striking collapse, showing that “bond-orientational order and translational order are not independent for simple spherically symmetric systems at equilibrium.”<sup>89</sup> For water,<sup>87,90</sup> and silica,<sup>88</sup> on the other hand, there is no such collapse; here the order parameters cover a two-dimensional region of order-parameter space. These results may be explained by reference to isomorphs: since both order parameters are isomorph invariants, they cannot vary independently for strongly correlating liquids like the LJ liquid and related systems. Water and silica are not strongly correlating (Paper I), so there is no reason to expect their two order parameters to follow each other.

### E. Viscous liquid dynamics

The dynamics of viscous liquids is a long-time focus of our research at the DNRF “Glass and Time” center, and the class of strongly correlating liquids was identified in our efforts to understand the properties of single-order-parameter viscous liquids.<sup>1,2,22,23</sup> As shown below, the isomorph concept throws new light on facts and puzzles of the physics of viscous liquids.

#### 1. Cause of the non-Arrhenius relaxation time: The “isomorph filter”

A major puzzle concerning viscous liquids approaching the glass transition is the origin of the non-Arrhenius temperature dependence of their average relaxation time  $\tau$ .<sup>10,12–21,91–93</sup> In many cases the relaxation-time increase is truly dramatic, with a factor of 10 or more slowing down if temperature is decreased by just 1%. There are several theories for this. Although it is not obvious that any universal theory exists, most workers in the field assume this to be the case. A universal theory must apply also to strongly correlating liquids, of course. This implies a criterion which we shall refer to as the isomorph filter. The idea is the following. Since the reduced average relaxation time is an isomorph invariant, this quantity can only be controlled by a quantity that is also an isomorph invariant. All theories relate  $\ln \tau$  to some quantity. For any viscous liquid, as regards variation with state point one may assume that  $\ln \tau \cong \ln \tilde{\tau}$ , because the temperature variation in the average relaxation time dominates completely over the reduced time unit’s  $\sqrt{T}$  temperature dependence. Thus the average relaxation time must be controlled by an isomorph invariant. Consider now some examples.

According to the Adam–Gibbs model<sup>48,94</sup> the relaxation time  $\tau$  varies as  $\ln \tau \propto 1/TS_{\text{conf}}(\rho, T)$ , where  $S_{\text{conf}}(\rho, T)$  is the configurational entropy discussed in connection with isomorph property 1b. Adam and Gibbs wrote the proportional-

ity constant as the product of a critical configurational entropy  $s_c^*$  and a term  $\Delta\mu$  which is “largely the potential energy hindering the cooperative rearrangement per monomer segment,” and they argued that the state-point dependence of these terms can be neglected. This is also what is usually done in comparing with experiments. In this case, however, since  $\tilde{\tau}$  and  $S_{\text{conf}}(\rho, T)$  are both invariant along an isomorph, the model is inconsistent with the isomorph invariance due to the extra factor  $T$ . Thus in this version the model cannot apply to strongly correlating liquids. Alternatively, the proportionality constant must be allowed to vary with state point. Indeed, simulations of Sastry<sup>95</sup> of the KABLJ liquid show good agreement with the Adam–Gibbs model if the constant is density dependent, a density dependence which, in order not to violate isomorph invariance, must be—and to a good approximation is—given by a factor proportional to  $\rho^\gamma$ . Although the original Adam–Gibbs model cannot apply for strongly correlating liquids (van der Waals and metallic liquids), it should be noted that for very fragile liquids the temperature dependence of  $S_{\text{conf}}(\rho, T)$  dominates over the  $T$  factor in the Adam–Gibbs expression;<sup>48</sup> for these liquids the model may work fairly well in practice. Another possibility is that  $S_{\text{conf}}(\rho, T)$  alone controls the relaxation time. Interestingly, this was suggested by Bestul and Chang<sup>96</sup> in a paper preceding Adam–Gibbs by one year, which showed data consistent with a universal value of the excess entropy at the glass transition for several liquids. Much more recently, Truskett and co-workers<sup>97</sup> suggested that the excess entropy  $S_{\text{ex}}$  controls the relaxation time in the spirit of Rosenfeld<sup>76,77</sup> scaling; this is also consistent with isomorph invariance. As a final example of a theory where entropy controls the relaxation time, consider the random first-order transition (RFOT) theory of Wolynes and co-worker (reviewed in Ref. 98). According to this theory and its generalization by Bouchaud and Biroli,<sup>99</sup> for some exponents  $x$  and  $y$  the relaxation time is given by  $\ln \tau \propto (Y/T)^x S_{\text{conf}}^{-y}(\rho, T)$ , where  $Y$  is a surface tension at the molecular scale. This expression is isomorph invariant only if  $Y \propto T$ . This is, however, precisely what was predicted in 2000 on different grounds by Xia and Wolynes,<sup>100</sup> so the RFOT passes the isomorph filter.

The free-volume model of Cohen and Grest predicts that  $\ln \tau \propto 1/v_f(\rho, T)$ , where  $v_f(\rho, T)$  is the free volume. As it stands, this model does not survive the isomorph filter because the proportionality constant is state-point independent and, although the free volume definition is not obvious,  $v_f(\rho, T)$  is hardly an isomorph invariant. If one imagines  $v_f$  to be a geometrically determined quantity measured in units of  $1/\rho$ , however, the model prediction is invariant along an isomorph. Thus, while  $v_f(\rho, T)$  cannot determine the relaxation time, the quantity  $v_f(\rho, T)\rho$  can possibly. The shoving model<sup>21,101,102</sup> predicts that  $\ln \tau \propto G_\infty(\rho, T)V_c/k_B T$ , where  $V_c$  is a characteristic volume which in experiments is of order of the molecular volume. This model, which is one of several related “elastic” models,<sup>21</sup> is consistent with the existence of isomorphs if  $V_c$  is geometrically determined: in this case  $V_c \propto 1/\rho$ , and because  $G_\infty(\rho, T)/T\rho$  is an isomorph invariant (property 3f), this implies that  $G_\infty(\rho, T)V_c/k_B T$  is isomorph invariant. The vibrational mean-square displacement version of the elastic models  $\ln \tau \propto a^2/\langle x^2 \rangle$  is not isomorph invariant

if  $a$  is assumed to be independent of density,<sup>103</sup> but it does survive the isomorph filter if the reasonable assumption is made<sup>104</sup> that  $a \propto \rho^{-1/3}$ . As a final example, we note that the entropic barrier hopping theory of Schweizer and co-workers<sup>105,106</sup> in a certain limit predicts that  $\ln \tau \propto d^2 \langle F^2 \rangle / (k_B T)^2$ , where  $d$  is an effective hard-sphere diameter and  $\langle F^2 \rangle$  is the short-time-averaged single-particle mean-square force. This expression is not isomorph invariant, but the modest modification of it obtained by replacing  $d$  by  $\rho^{-1/3}$  leads to an isomorph invariant expression, as is easily shown from Eq. (9).

## 2. Isochronal superposition

Building on earlier works by Roland *et al.*,<sup>107</sup> in 2005 Ngai *et al.*<sup>108</sup> published a paper entitled “Do theories of the glass transition, in which the structural relaxation time does not define the dispersion of the structural relaxation, need revision?” The authors showed here that for many viscous liquids and polymers the average relaxation time determines the shape of the dielectric loss peak. Thus whether the average relaxation time is increased by lowering temperature or by increasing pressure or a combination thereof, the effect is the same on the relaxation time distribution as monitored via the dielectric loss. This result, which we, for brevity, refer to as “isochronal superposition,” was puzzling at the time (at least to us). Isochronal superposition now appears as a consequence of the existence and properties of isomorphs: any strongly correlating liquid must obey isochronal superposition because according to properties 3c and 3d, both the average relaxation time and the dielectric spectrum are isomorph invariants (when given in reduced units, but as mentioned their use makes little difference for viscous liquids). Thus, no matter how the thermodynamic conditions are changed to bring the liquid to a state with a certain relaxation time, all such states are isomorphic. Consequently, they have the same relaxation spectra for quantities probed by linear response experiments (property 3c). In Ref. 108 hydrogen-bonding liquids were quoted explicitly as exceptions to isochronal superposition; this is consistent with the fact that these liquids are not strongly correlating (Paper I).

## 3. How many parameters are needed for describing a viscous liquid?

In the early days of glass science it was actively debated whether one or more “order parameters” are required to describe glass structure and the glass transition. Note that the term order parameter has a slightly different use in traditional glass science than in the theory of critical phenomena. The original considerations of Prigogine and Defay,<sup>109</sup> Davies and Jones,<sup>110,111</sup> and others referred to the glass transition as a second-order phase transition in the Ehrenfest sense. It was recently shown that strongly correlating liquids are precisely the liquids that to a good approximation may be regarded as single-order-parameter liquids;<sup>1,22</sup> a review of the connection was given in Ref. 23. Strongly correlating liquids have isomorphs, so it should be possible to link isomorphs directly to the single-order-parameter scenario. Indeed, by labeling the collection of isomorphic curves in the

phase diagram with a continuously varying real number, a formal single-order-parameter description throughout the phase diagram is arrived at. This suggests a generic way of defining the single-order-parameter scenario that is implicit in the old works. The isomorph label is not unique, obviously; it may be chosen as any property that is isomorph invariant, for instance  $S_{\text{ex}}$  or  $C_V$ .

## F. Some further potential isomorph connections

(1) In 1989 Baranya and Evans<sup>50</sup> reported from simulations that the excess entropy of the LJ liquid to a good approximation equals the two-particle entropy  $S_2$  plus a constant. This is consistent with the existence of isomorphs because on an isomorph both  $S_2$  and  $S_{\text{ex}}$  are invariant. That is, because the LJ liquid is strongly correlating, if for instance  $S_{\text{ex}}$  were an isomorph invariant but  $S_2$  were not, the Baranya–Evans finding could not be correct.

(2) Saija *et al.*<sup>112</sup> in 2001 showed by simulations of both the Yukawa and the LJ liquids that the scaled radial distribution functions are identical for states where the excess entropy equals the two-particle entropy. This is consistent with the fact that these liquids are both strongly correlating because scaled radial distribution function, excess entropy, and two-particle entropy are all isomorph invariants.

(3) The basic idea of mode-coupling theory—that statics determines the dynamics—is consistent with the existence of isomorphs: for any strongly correlating liquid, if two state points have the same reduced pair-correlation functions, they are isomorphic. This means that they have the same (reduced) dynamics, so in this sense the pair correlation function “determines” the dynamics. From the isomorph perspective mode-coupling theory may be expected to work best for strongly correlating liquids.

(4) Recently, Roland briefly reviewed characteristic times and their invariance to thermodynamic conditions from a general point of view, including also systems that are not liquids.<sup>113</sup> He showed that quite different transitions in systems with slow relaxations—onset of activated dynamics, dynamic crossover in viscous liquids and polymers, order-disorder transitions in liquid crystals, vitrification—at varying temperature and pressure all take place at state points with the same value of the relaxation time. The conclusion is that<sup>113</sup> “the control parameter driving these transitions has the same functional dependence on  $T$ ,  $p$ , and  $V$  as the relaxation time.” For strongly correlating liquids and solids, this follows from the existence of isomorphs.

(5) The concept of hidden scale invariance (Paper III) may have implications beyond liquid state theory. Thus, very recently Procaccia and co-workers<sup>114</sup> studied by simulation plastic flow of amorphous solids in the athermal limit. For two-dimensional solids composed of multidisperse particles with the interaction length taken from a Gaussian distribution, they showed that stress-strain curves at different densities collapse to a master curve. This happens when stress is scaled by  $\rho^\nu$ , where  $\nu$  is 5.87 when the repulsive part of the potential can be fitted by the IPL term  $r^{-10}$ . The number 5.87 is not far from the number 5 predicted by the two-dimensional exponent  $\gamma = n/2$  for IPL potentials.<sup>115</sup>

## V. CONCLUDING REMARKS

This paper introduces the concept of isomorph curves in the phase diagram of a strongly correlating liquid. The existence of isomorphs reflects the liquid's hidden scale invariance (Paper III), and therefore the class of strongly correlating liquids is identical to the class of liquids with isomorphs (Appendix A). Isomorphs may be labeled by any of these invariants, for instance  $S_{\text{ex}}$  or  $C_V$ . The isomorph concept, in fact, may be justified by starting from the concept of an order parameter labeling curves in the phase diagram of same physical properties: suppose a liquid is described by a single order parameter in the sense that many of its properties are determined by the value of the order parameter. In this case one may draw curves in the phase diagram along which these properties are all invariant. If one asks how it is that several properties could possibly correlate in this way, the simplest answer is that for any two state points on a constant order parameter curve, the canonical probabilities are proportional to microscopic configurations that somehow correspond to each other—and the simplest possibility is that corresponding configurations are those which trivially scale into one another. This is nothing but the isomorph definition. Thus the isomorph concept may be arrived at—via some extrapolation—by postulating that single-order-parameter liquids exist and inquiring into their properties.

All isomorph invariants apply to IPL liquids. But as emphasized repeatedly, the converse is not true: not all properties that are invariant for an IPL liquid along states obeying  $\rho^{n/3}/T = \text{const}$  generalize to become isomorph invariants. The exceptions derive from the fact that the constant  $C_{12}$  of Eq. (4) generally differs from unity. Only IPL invariants that are independent of the identity  $C_{12} = 1$ , which characterizes IPL liquids, generalize to the class of strongly correlating liquids.

The present and previous papers on strongly correlating liquids show that this class of liquids is simpler than liquids in general. This is consistent with the general understanding among liquid-state specialists for many years, according to which nonassociated liquids are generally simpler than associated ones. The virial/potential energy correlation coefficient  $R$  of the  $NVT$  ensemble provides a quantitative criterion for distinguishing simple liquids from the more complex—and admittedly often more spectacular—liquids that are not strongly correlating.

## ACKNOWLEDGMENTS

When writing this paper we benefited from discussions with Hans Andersen, Austen Angell, Giulio Biroli, Simone Capaccioli, Daniele Coslovich, Pablo Debenedetti, Gregor Diezemann, Jack Douglas, Sharon Glotzer, Andreas Heuer, Valeria Molinero, Itamar Procaccia, Mike Roland, Ken Schweizer, Francesco Sciortino, Thomas Truskett, as well as in Roskilde with Morten Andersen, Ditte Gundermann, Claudio Maggi, Kristine Niss, Søren Toxværd, and Frank Vinther. This work was supported by a grant from the Danish National Research Foundation (DNRF) for funding the center for viscous liquid dynamics “Glass and Time.”

## APPENDIX A: EQUIVALENCE OF THREE CONDITIONS

This appendix proves that the following three conditions are equivalent for any liquid:

- (a) The liquid is strongly correlating.
- (b) The liquid has isomorphs.
- (c) The liquid has curves in the phase diagram along which the reduced-coordinate constant potential energy hypersurface is invariant.

Only true IPL liquids obey these conditions rigorously [i.e., with 100% correlation in (a)], and the equivalences may be stated more accurately as follows: a liquid is strongly correlating if and only if it has isomorphs to a good approximation, which happens if and only if the liquid has curves in its phase diagram along which the reduced-coordinate constant potential energy hypersurface is almost invariant. It is instructive to prove all six implications, although logically  $(a) \Rightarrow (b) \Rightarrow (c) \Rightarrow (a)$  would suffice.

Before proving the equivalences we note a few facts. If  $\delta$  denotes the variation between two infinitesimally close microscopic configurations with same reduced coordinates, we first show that

$$\delta U = (d \ln \rho) W. \quad (\text{A1})$$

For two infinitesimally close microscopic configurations with the same reduced coordinates ( $\tilde{\mathbf{r}}_i \equiv \rho^{1/3} \mathbf{r}_i$ ), one has  $0 = \delta \tilde{\mathbf{r}}_i = (\rho^{-2/3}/3)(d\rho) \mathbf{r}_i + \rho^{1/3} \delta \mathbf{r}_i$ , i.e.,  $\delta \mathbf{r}_i = -(1/3)(d \ln \rho) \mathbf{r}_i$ . The change in potential energy between the two configurations is given by  $\delta U = \sum_i \delta \mathbf{r}_i \cdot \nabla_{\mathbf{r}_i} U$ , which via the definition of the virial  $W \equiv -(1/3) \sum_i \mathbf{r}_i \cdot \nabla_{\mathbf{r}_i} U$  leads to Eq. (A1). We note further the following identity:

$$\delta \left( \frac{U}{T} \right) = \frac{(d \ln \rho) W - (d \ln T) U}{T}. \quad (\text{A2})$$

This follows by differentiation and use of Eq. (A1). Finally, note that the infinitesimal version of the isomorph condition equation (4) is

$$\delta \left( \frac{U}{T} \right) = \text{const}. \quad (\text{A3})$$

At any given state point  $Q$ , if the average potential energy is denoted by  $\langle U \rangle_Q$ , we define the constant potential energy hypersurface  $\Omega$  as the subset of  $R^{3N}$  given by

$$\Omega = \{(\mathbf{r}_1, \dots, \mathbf{r}_N) \in R^{3N} | U(\mathbf{r}_1, \dots, \mathbf{r}_N) = \langle U \rangle_Q\}. \quad (\text{A4})$$

The corresponding reduced-coordinate constant potential energy hypersurface  $\tilde{\Omega}$  is given by

$$\tilde{\Omega} = \{(\tilde{\mathbf{r}}_1, \dots, \tilde{\mathbf{r}}_N) \in R^{3N} | U(\rho^{-1/3} \tilde{\mathbf{r}}_1, \dots, \rho^{-1/3} \tilde{\mathbf{r}}_N) = \langle U \rangle_Q\}. \quad (\text{A5})$$

*Proof that (a)  $\Leftrightarrow$  (b):* A strongly correlating liquid has (near) proportionality between virial and potential energy fluctuations,  $\Delta W = \gamma \Delta U$ . Thus at any given state point,  $W = \gamma U + C$  to a good approximation for the physically relevant microscopic configurations. If density and temperature are changed infinitesimally such that  $d \ln T = \gamma d \ln \rho$ , Eq. (A2)

implies that  $\delta(U/T)=\text{const}$ , which is the isomorph condition equation (A3). Suppose conversely that a liquid has isomorphs, and let  $\Delta$  denote the difference between two arbitrary, physically relevant configurations at the state point in question. Then Eq. (A3) implies  $\Delta\delta(U/T)=0$  where  $\delta$  (as usual) refers to changes from one configuration to another infinitesimally close by with the same reduced coordinates. Via Eq. (A2) this implies  $(d \ln \rho)\Delta W=(d \ln T)\Delta U$ , i.e., the liquid is strongly correlating with  $\gamma=d \ln T/d \ln \rho$ .

*Proof that (a)  $\Leftrightarrow$  (c):* For a strongly correlating liquid  $\Delta W \propto \Delta U$  for fluctuations between physically relevant configurations at any given state point. This implies that the hypersurfaces of constant virial and constant potential energy coincide. In particular,  $W$  is constant on the state point's constant potential energy hypersurface  $\Omega$ . Accordingly, if density is changed infinitesimally, the change in potential energy between microscopic configurations with the same reduced coordinates is the same for all microscopic configurations on  $\Omega$  [Eq. (A1)]. Thus a new hypersurface of constant potential energy is arrived at by slightly scaling  $\Omega$ ; by adjusting temperature the new hypersurface is where the potential energy equals the average potential energy. Finally we note that the new and old hypersurfaces by construction have same reduced coordinates, thus the two state points have the same  $\tilde{\Omega}$ . Suppose conversely that two infinitesimally close state points have the same  $\tilde{\Omega}$ . All points on the two constant potential energy hypersurfaces differ by the same potential energy, which via Eq. (A1) implies that  $W$  must be constant on each hypersurface. In other words,  $W$  is constant on surfaces where  $U$  is. This implies 100% correlation between  $W$  and  $U$ . For large systems the fluctuations are small, relatively, and a first order Taylor expansion of the  $WU$  relationship leads to a linear relation between  $W$  and  $U$ .

*Proof that (b)  $\Leftrightarrow$  (c):* Suppose a liquid has isomorphs. For a state point  $Q$  on an isomorph  $I$  one concludes from Eq. (9) that  $\langle U \rangle_Q = k_B T \langle f_i \rangle + g(Q)$ , where the (canonical) average  $\langle f_i \rangle$  by Eq. (8) is independent of  $Q$ . Consequently,  $\tilde{\Omega} = \{(\tilde{\mathbf{r}}_1, \dots, \tilde{\mathbf{r}}_N) \in R^{3N} | k_B T f_i(\tilde{\mathbf{r}}_1, \dots, \tilde{\mathbf{r}}_N) + g(Q) = k_B T \langle f_i \rangle + g(Q)\} = \{(\tilde{\mathbf{r}}_1, \dots, \tilde{\mathbf{r}}_N) \in R^{3N} | f_i(\tilde{\mathbf{r}}_1, \dots, \tilde{\mathbf{r}}_N) = \langle f_i \rangle\}$  is invariant along the isomorph. Suppose conversely that two state points have the same  $\tilde{\Omega}$ . For these state points microcanonical averages are identical for all quantities that may be expressed as functions of the reduced coordinates. By the equivalence of the microcanonical and the canonical ensembles, for the two state points in question canonical ensemble averages are likewise identical for all quantities that are functions of the reduced coordinates. This can only be so if there is identity of the normalized canonical probability factors of any two physically relevant microscopic configurations of the two state points, which have the same reduced coordinates. This is another way of stating that the two state points are isomorphic.

## APPENDIX B: TWO PROPERTIES OF THE DENSITY SCALING EXPONENT

This appendix has two purposes: (1) to derive an optimization property of the density scaling exponent  $\gamma$  of Eq. (13) and (2) to prove that any possible state-point depen-

dence of  $\gamma$  comes from a density dependence; more accurately it is shown that  $\gamma = \gamma(\rho)$  in the isomorph approximation.

As mentioned in the main text there is no unique solution to the problem of finding the ‘‘correct’’ density scaling exponent  $\gamma$ , i.e., the exponent identifying isomorphs as the curves along which  $\rho^2/T = \text{const}$ . First of all, the exponent must be expected to vary slightly with state point. But even at a given state point, there is no unique  $\gamma$  in the sense that all isomorph invariants are mathematically constant for changes obeying Eq. (13). This is because isomorph properties are generally approximate, so for instance the curves of constant excess entropy cannot be expected to be precisely the curves of constant isochoric specific heat (or constant reduced relaxation time, etc.); this just applies to a good approximation for strongly correlating liquids.

We argued in Sec. II D that at any given state point there are three obvious gammas, the  $\gamma_1$ ,  $\gamma_2$ , and  $\gamma_3$  of Eq. (10). We recommend using  $\gamma_1$  and used this in Sec. III when comparing isomorph predictions with computer simulations. This exponent is to be preferred because it—among other things—makes the excess entropy an exact invariant. It worked very well with our simulations of the KABLJ liquid, but as noted in the main paper  $\gamma_2$  works almost equally well.

The excess entropy exponent  $\gamma_1$ , henceforth just denoted by  $\gamma$ , has an optimization property coming from answering the following question: At any given state point, suppose we change density by an infinitesimal amount, how much should temperature be changed to arrive at a new state point which is ‘‘as isomorphic as possible’’ with the original state point? To answer this we note that Eq. (A3) suggests requiring the quantity  $F \equiv \delta(U/T)$  to be as constant as possible (where the symbol  $\delta$  refers to the difference between two infinitesimally close microscopic configurations with same reduced coordinates). This is obtained by minimizing  $\langle (\Delta F)^2 \rangle$ . Since according to Eq. (A2) one has  $F \propto (d \ln \rho)W - (d \ln T)U$ , for a given density change the quantity to be minimized by varying temperature is  $\langle ((d \ln \rho)\Delta W - (d \ln T)\Delta U)^2 \rangle$ , i.e.,

$$(d \ln \rho)^2 \langle (\Delta W)^2 \rangle + (d \ln T)^2 \langle (\Delta U)^2 \rangle - 2(d \ln \rho)(d \ln T) \langle \Delta W \Delta U \rangle. \quad (\text{B1})$$

Equating to zero the derivative of this expression with respect to  $d \ln T$  leads to

$$\frac{d \ln T}{d \ln \rho} = \frac{\langle \Delta W \Delta U \rangle}{\langle (\Delta U)^2 \rangle}, \quad (\text{B2})$$

which is the excess entropy gamma of Eq. (13).

Suppose instead that one asks the complementary question: For a given infinitesimal temperature change, what is the density change giving a new state point that is as ‘‘isomorphic as possible’’ with the original state point? In this case, minimizing Eq. (B1) leads to the  $\gamma_3$  of Eq. (10). Thus, optimization arguments cannot determine which gamma to choose.

The second property of the density scaling exponent to be proved is that if the  $\gamma$  of Eq. (13) varies with state point, this variation can come only from a density dependence. More accurately, in the isomorph approximation where the

curves of constant excess entropy and constant excess isochoric specific heat coincide, one has  $\gamma = \gamma(\rho)$ . Recalling that the excess pressure coefficient  $\beta_V^{\text{ex}}$  is defined by  $\beta_V^{\text{ex}} = (\partial(W/V)/\partial T)_V$  (Papers I and III) and denoting the excess isochoric specific heat per unit volume by  $c_V^{\text{ex}}$ , Eq. (13) may be written as

$$\gamma = \frac{\beta_V^{\text{ex}}}{c_V^{\text{ex}}}. \quad (\text{B3})$$

If there is identity of the curves in the phase diagram of constant excess entropy  $S_{\text{ex}}$  and those of constant (extensive) excess isochoric specific heat  $C_V^{\text{ex}}$  ( $C_V^{\text{ex}} = Vc_V^{\text{ex}}$ ), the definition of the density scaling exponent  $\gamma = (\partial \ln T / \partial \ln \rho)_{S_{\text{ex}}}$  implies

$$\gamma = - \left( \frac{\partial \ln T}{\partial \ln V} \right)_{C_V^{\text{ex}}}. \quad (\text{B4})$$

From this we get via the mathematical identity  $(\partial x / \partial y)_z (\partial y / \partial z)_x (\partial z / \partial x)_y = -1$ ,

$$\begin{aligned} \left( \frac{\partial \ln C_V^{\text{ex}}}{\partial \ln T} \right)_V &= \frac{-1}{\gamma} \left( \frac{\partial \ln T}{\partial \ln V} \right)_{C_V^{\text{ex}}} \left( \frac{\partial \ln C_V^{\text{ex}}}{\partial \ln T} \right)_V \\ &= \frac{1}{\gamma} \left( \frac{\partial \ln C_V^{\text{ex}}}{\partial \ln V} \right)_T. \end{aligned} \quad (\text{B5})$$

Using  $C_V^{\text{ex}} = T(\partial S_{\text{ex}} / \partial T)_V$  we get via Eq. (B3),

$$\begin{aligned} \left( \frac{\partial \ln C_V^{\text{ex}}}{\partial \ln T} \right)_V &= \frac{C_V^{\text{ex}}}{V\beta_V^{\text{ex}}} \left( \frac{\partial \ln C_V^{\text{ex}}}{\partial \ln V} \right)_T \\ &= \frac{1}{\beta_V^{\text{ex}}} \left( \frac{\partial C_V^{\text{ex}}}{\partial V} \right)_T = \frac{T}{\beta_V^{\text{ex}}} \frac{\partial^2 S_{\text{ex}}}{\partial V \partial T}. \end{aligned} \quad (\text{B6})$$

The Maxwell relation  $(\partial S_{\text{ex}} / \partial V)_T = (\partial(W/V) / \partial T)_V = \beta_V^{\text{ex}}$  allows us to rewrite this as

$$\left( \frac{\partial \ln C_V^{\text{ex}}}{\partial \ln T} \right)_V = \frac{T}{\beta_V^{\text{ex}}} \left( \frac{\partial \beta_V^{\text{ex}}}{\partial T} \right)_V = \left( \frac{\partial \ln \beta_V^{\text{ex}}}{\partial \ln T} \right)_V. \quad (\text{B7})$$

Because  $d \ln c_V^{\text{ex}} = d \ln C_V^{\text{ex}}$  at constant volume this implies that

$$\left( \frac{\partial \ln \beta_V^{\text{ex}}}{\partial \ln c_V^{\text{ex}}} \right)_V = 1. \quad (\text{B8})$$

Thus at constant volume  $\beta_V^{\text{ex}}$  is proportional to  $c_V^{\text{ex}}$ , i.e.,  $\gamma$  is constant on isochores. In particular, since  $\gamma = (\partial W / \partial U)_T$  [see Eq. (13)], it follows that isochores are straight lines in the  $WU$  phase diagram.

### APPENDIX C: RELATING THE CORRELATION COEFFICIENT OF FIGURE 1 TO THE $WU$ CORRELATION COEFFICIENT $R$ OF EQUATION (2)

In order to distinguish from the  $WU$  correlation coefficient  $R$  of Eq. (2), for the ‘‘direct isomorph check’’ of Fig. 1 we denote by  $R_{\text{DI}}$  the correlation coefficient between potential energies of microscopic configurations with same reduced coordinates. Writing for a strongly correlating liquid for each microscopic configuration  $\Delta W = \gamma \Delta U + \varepsilon$ , where  $\varepsilon$  is an ‘‘error’’ term uncorrelated with  $\Delta U$ , implies by squaring and averaging

$$\langle (\Delta W)^2 \rangle = \gamma^2 \langle (\Delta U)^2 \rangle + \langle \varepsilon^2 \rangle. \quad (\text{C1})$$

Multiplying  $\Delta W = \gamma \Delta U + \varepsilon$  by  $\Delta U$ , averaging and squaring give

$$\langle \Delta W \Delta U \rangle^2 = \gamma^2 \langle (\Delta U)^2 \rangle^2. \quad (\text{C2})$$

The left hand side of this is expressed in terms of the  $WU$  correlation coefficient  $R$ , giving

$$\langle (\Delta W)^2 \rangle = \gamma^2 \langle (\Delta U)^2 \rangle / R^2. \quad (\text{C3})$$

Eliminating  $\langle (\Delta W)^2 \rangle$  between this and Eq. (C1) gives a relation between the correlation coefficient and the variance of the error term,

$$\frac{1}{R^2} - 1 = \frac{\langle \varepsilon^2 \rangle}{\gamma^2 \langle (\Delta U)^2 \rangle}. \quad (\text{C4})$$

Next consider an infinitesimal rescaling of all microscopic configurations to a new density, calling the old and new potential energies of corresponding microscopic configurations  $U^{(1)}$  and  $U^{(2)}$ , respectively. If the relative density change is small, Eq. (A1) minus its average implies for each microscopic configuration

$$\Delta U^{(2)} = \Delta U^{(1)} + (d \ln \rho) \Delta W^{(1)}, \quad (\text{C5})$$

which, using  $\Delta W = \gamma \Delta U + \varepsilon$ , becomes

$$\Delta U^{(2)} = (1 + \gamma d \ln \rho) \Delta U^{(1)} + (d \ln \rho) \varepsilon. \quad (\text{C6})$$

We can now calculate the correlation coefficient  $R_{\text{DI}}$  between the old and new potential energies of microscopic configurations with the same reduced coordinates. In fact, since this equation is identical in structure to  $\Delta W = \gamma \Delta U + \varepsilon$ , we can use the result of Eq. (C4), replacing  $\gamma$  with  $1 + \gamma d \ln \rho$  and  $\varepsilon$  with  $(d \ln \rho) \varepsilon$ ,

$$\frac{1}{R_{\text{DI}}^2} - 1 = \frac{\langle \varepsilon^2 \rangle (d \ln \rho)^2}{(1 + \gamma d \ln \rho)^2 \langle (\Delta U)^2 \rangle}. \quad (\text{C7})$$

Using Eq. (C4) to eliminate  $\langle \varepsilon^2 \rangle / \langle (\Delta U)^2 \rangle$  finally implies (using  $d \ln T = \gamma d \ln \rho$ ),

$$\frac{1}{R_{\text{DI}}^2} - 1 = (d \ln T)^2 \left( \frac{1}{R^2} - 1 \right). \quad (\text{C8})$$

Equation (C8) applies to any liquid. If the density change goes to zero ( $d \ln \rho \rightarrow 0$ ) and/or the liquid becomes 100% correlating ( $R \rightarrow 1$ ), there is a perfect correlation between the new and old potential energies ( $R_{\text{DI}} \rightarrow 1$ ), as expected. For strongly correlating liquids one has to lowest order  $1 - R_{\text{DI}} = (d \ln T)^2 (1 - R)$ . Using the correlation coefficient for the KABLJ liquid at the state point studied in Fig. 1 this predicts the observed value of 0.999 for  $R_{\text{DI}}$ .

<sup>1</sup>U. R. Pedersen, N. P. Bailey, T. B. Schröder, and J. C. Dyre, *Phys. Rev. Lett.* **100**, 015701 (2008).

<sup>2</sup>U. R. Pedersen, T. Christensen, T. B. Schröder, and J. C. Dyre, *Phys. Rev. E* **77**, 011201 (2008).

<sup>3</sup>N. P. Bailey, U. R. Pedersen, N. Gnan, T. B. Schröder, and J. C. Dyre, *J. Chem. Phys.* **129**, 184507 (2008) (Paper I).

<sup>4</sup>N. P. Bailey, U. R. Pedersen, N. Gnan, T. B. Schröder, and J. C. Dyre, *J. Chem. Phys.* **129**, 184508 (2008) (Paper II).

<sup>5</sup>T. B. Schröder, N. P. Bailey, U. R. Pedersen, N. Gnan, and J. C. Dyre, *J. Chem. Phys.* **131**, 234503 (2009) (Paper III).

<sup>6</sup>D. Coslovich and C. M. Roland, *J. Phys. Chem. B* **112**, 1329 (2008).

- <sup>7</sup>T. B. Schröder, U. R. Pedersen, N. P. Bailey, S. Toxvaerd, and J. C. Dyre, *Phys. Rev. E* **80**, 041502 (2009).
- <sup>8</sup>M. P. Allen and D. J. Tildesley, *Computer Simulation of Liquids* (Oxford Science, Oxford, 1987).
- <sup>9</sup>D. Coslovich and C. M. Roland, *J. Chem. Phys.* **130**, 014508 (2009).
- <sup>10</sup>W. Kauzmann, *Chem. Rev. (Washington, D.C.)* **43**, 219 (1948).
- <sup>11</sup>G. Harrison, *The Dynamic Properties of Supercooled Liquids* (Academic, New York, 1976).
- <sup>12</sup>S. Brawer, *Relaxation in Viscous Liquids and Glasses* (American Ceramic Society, Columbus, OH, 1985).
- <sup>13</sup>I. Gutzow and J. Schmelzer, *The Vitreous State: Thermodynamics, Structure, Rheology, and Crystallization* (Springer, New York, 1995).
- <sup>14</sup>M. D. Ediger, C. A. Angell, and S. R. Nagel, *J. Phys. Chem.* **100**, 13200 (1996).
- <sup>15</sup>R. V. Chamberlin, *Phase Transitions* **65**, 169 (1998).
- <sup>16</sup>C. A. Angell, K. L. Ngai, G. B. McKenna, P. F. McMillan, and S. W. Martin, *J. Appl. Phys.* **88**, 3113 (2000).
- <sup>17</sup>C. Alba-Simionesco, Acad. Sci., Paris, C. R. (Ser. IV) **2**, 203 (2001).
- <sup>18</sup>P. G. Debenedetti and F. H. Stillinger, *Nature (London)* **410**, 259 (2001).
- <sup>19</sup>K. Binder and W. Kob, *Glassy Materials and Disordered Solids: An Introduction to Their Statistical Mechanics* (World Scientific, Singapore, 2005).
- <sup>20</sup>F. Sciortino, *J. Stat. Mech.: Theory Exp.* **2005**, P05015.
- <sup>21</sup>J. C. Dyre, *Rev. Mod. Phys.* **78**, 953 (2006).
- <sup>22</sup>N. L. Ellegaard, T. Christensen, P. V. Christiansen, N. B. Olsen, U. R. Pedersen, T. B. Schröder, and J. C. Dyre, *J. Chem. Phys.* **126**, 074502 (2007).
- <sup>23</sup>N. P. Bailey, T. Christensen, B. Jakobsen, K. Niss, N. B. Olsen, U. R. Pedersen, T. B. Schröder, and J. C. Dyre, *J. Phys.: Condens. Matter* **20**, 244113 (2008).
- <sup>24</sup>T. Christensen and J. C. Dyre, *Phys. Rev. E* **78**, 021501 (2008).
- <sup>25</sup>A. Tölle, *Rep. Prog. Phys.* **64**, 1473 (2001).
- <sup>26</sup>C. Dreyfus, A. Aouadi, J. Gapinski, M. Matos-Lopes, W. Steffen, A. Patkowski, and R. M. Pick, *Phys. Rev. E* **68**, 011204 (2003).
- <sup>27</sup>C. Alba-Simionesco, A. Cailliaux, A. Alegria, and G. Tarjus, *Europhys. Lett.* **68**, 58 (2004).
- <sup>28</sup>R. Casalini and C. M. Roland, *Phys. Rev. E* **69**, 062501 (2004).
- <sup>29</sup>C. M. Roland, S. Hensel-Bielowka, M. Paluch, and R. Casalini, *Rep. Prog. Phys.* **68**, 1405 (2005).
- <sup>30</sup>U. R. Pedersen, G. H. Peters, T. B. Schröder, and J. C. Dyre, "Correlated volume-energy fluctuations of phospholipid membranes: A simulation study," *J. Phys. Chem. B* (in press).
- <sup>31</sup>W. G. Hoover, R. Grover, and D. A. Young, *J. Chem. Phys.* **56**, 2207 (1972).
- <sup>32</sup>Y. Hiwatari, H. Matsuda, T. Ogawa, N. Ogita, and A. Ueda, *Prog. Theor. Phys.* **52**, 1105 (1974).
- <sup>33</sup>L. V. Woodcock, *Phys. Rev. Lett.* **54**, 1513 (1985).
- <sup>34</sup>J. L. Barrat, J. P. Hansen, G. Pastore, and E. M. Waisman, *J. Chem. Phys.* **86**, 6360 (1987).
- <sup>35</sup>P. G. Debenedetti, F. H. Stillinger, T. M. Truskett, and C. J. Roberts, *J. Phys. Chem.* **103**, 7390 (1999).
- <sup>36</sup>E. La Nave, F. Sciortino, P. Tartaglia, M. S. Shell, and P. G. Debenedetti, *Phys. Rev. E* **68**, 032103 (2003).
- <sup>37</sup>R. J. Speedy, *J. Phys.: Condens. Matter* **15**, S1243 (2003).
- <sup>38</sup>M. S. Shell, P. G. Debenedetti, E. La Nave, and F. Sciortino, *J. Chem. Phys.* **118**, 8821 (2003).
- <sup>39</sup>G. Rickayzen and D. M. Heyes, *Phys. Rev. E* **71**, 061204 (2005).
- <sup>40</sup>A. C. Branka and D. M. Heyes, *Phys. Rev. E* **74**, 031202 (2006).
- <sup>41</sup>R. Casalini, U. Mohanty, and C. M. Roland, *J. Chem. Phys.* **125**, 014505 (2006).
- <sup>42</sup>D. M. Heyes and A. C. Branka, *Phys. Chem. Chem. Phys.* **9**, 5570 (2007).
- <sup>43</sup>D. Ben-Amotz and G. J. Stell, *J. Chem. Phys.* **119**, 10777 (2003).
- <sup>44</sup>L. D. Landau and E. M. Lifshitz, *Statistical Physics, Part I* (Pergamon, New York, 1980).
- <sup>45</sup>D. Chandler, *Introduction to Modern Statistical Mechanics* (Oxford University Press, New York, 1987).
- <sup>46</sup>L. E. Reichl, *A Modern Course in Statistical Physics*, 2nd ed. (Wiley, New York, 1998).
- <sup>47</sup>J. P. Hansen and J. R. McDonald, *Theory of Simple Liquids*, 3rd ed. (Academic, New York, 2005).
- <sup>48</sup>G. Adam and J. H. Gibbs, *J. Chem. Phys.* **43**, 139 (1965).
- <sup>49</sup>R. E. Nettleton and M. S. Green, *J. Chem. Phys.* **29**, 1365 (1958).
- <sup>50</sup>A. Baranyai and D. J. Evans, *Phys. Rev. A* **40**, 3817 (1989).
- <sup>51</sup>S. Nosé, *Mol. Phys.* **52**, 255 (1984).
- <sup>52</sup>W. G. Hoover, *Phys. Rev. A* **31**, 1695 (1985).
- <sup>53</sup>H. Risken, *The Fokker-Planck Equation*, 2nd ed. (Springer, New York, 1989).
- <sup>54</sup>R. Zwanzig and R. D. Mountain, *J. Chem. Phys.* **43**, 4464 (1965).
- <sup>55</sup>J. E. Lennard-Jones, *Proc. Phys. Soc. London* **43**, 461 (1931).
- <sup>56</sup>W. Kob and H. C. Andersen, *Phys. Rev. Lett.* **73**, 1376 (1994).
- <sup>57</sup>H. J. C. Berendsen, D. van der Spoel, and R. van Drunen, *Comput. Phys. Commun.* **91**, 43 (1995).
- <sup>58</sup>E. Lindahl, B. Hess, and D. van der Spoel, *J. Mol. Model.* **7**, 306 (2001).
- <sup>59</sup>S. Toxvaerd, U. R. Pedersen, T. B. Schröder, and J. C. Dyre, *J. Chem. Phys.* **130**, 224501 (2009).
- <sup>60</sup>A. Heuer, *J. Phys.: Condens. Matter* **20**, 373101 (2008).
- <sup>61</sup>C. Toninelli, M. Wyart, L. Berthier, G. Biroli, and J.-P. Bouchaud, *Phys. Rev. E* **71**, 041505 (2005).
- <sup>62</sup>D. Coslovich and C. M. Roland, *J. Chem. Phys.* **131**, 151103 (2009).
- <sup>63</sup>D. Fragiadakis, R. Casalini, and C. M. Roland, *J. Phys. Chem. B* **113**, 13134 (2009).
- <sup>64</sup>H. J. C. Berendsen, J. R. Grigera, and T. P. Straatsma, *J. Phys. Chem.* **91**, 6269 (1987).
- <sup>65</sup>T. V. Ramakrishnan and M. Yussouff, *Phys. Rev. B* **19**, 2775 (1979).
- <sup>66</sup>J. J. Gilvarry, *Phys. Rev.* **102**, 308 (1956); J. J. Gilvarry, *ibid.* **102**, 317 (1956); J. J. Gilvarry, *ibid.* **102**, 325 (1956).
- <sup>67</sup>A. R. Ubbelohde, *Melting and Crystal Structure* (Clarendon, London, 1965).
- <sup>68</sup>W. G. Hoover and M. Ross, *Contemp. Phys.* **12**, 339 (1971).
- <sup>69</sup>Y. Rosenfeld, *J. Chem. Phys.* **63**, 2769 (1975).
- <sup>70</sup>S. M. Stishov, *Sov. Phys. Usp.* **17**, 625 (1975).
- <sup>71</sup>J. P. Poirier, *Geophys. J.* **92**, 99 (1988).
- <sup>72</sup>M. D. Rutter, R. A. Secco, H. Liu, T. Uchida, M. L. Rivers, S. R. Sutton, and Y. B. Wang, *Phys. Rev. B* **66**, 060102 (2002).
- <sup>73</sup>R. M. Digilov, *Physica B* **352**, 53 (2004).
- <sup>74</sup>G. Shen, V. B. Prakapenka, M. L. Rivers, and S. R. Sutton, *Phys. Rev. Lett.* **92**, 185701 (2004).
- <sup>75</sup>J.-P. Hansen and L. Verlet, *Phys. Rev.* **184**, 151 (1969).
- <sup>76</sup>Y. Rosenfeld, *Phys. Rev. A* **15**, 2545 (1977).
- <sup>77</sup>Y. Rosenfeld, *J. Phys.: Condens. Matter* **11**, 5415 (1999).
- <sup>78</sup>W. P. Krekelberg, T. Kumar, J. Mittal, J. R. Errington, and T. M. Truskett, *Phys. Rev. E* **79**, 031203 (2009).
- <sup>79</sup>M. Dzugutov, *Nature (London)* **381**, 137 (1996).
- <sup>80</sup>W. P. Krekelberg, M. J. Pond, G. Goel, V. K. Shen, J. R. Errington, and T. M. Truskett, e-print arXiv:cond-mat/0910.0280.
- <sup>81</sup>M. J. Pond, W. P. Krekelberg, V. K. Shen, J. R. Errington, and T. M. Truskett, *J. Chem. Phys.* **131**, 161101 (2009).
- <sup>82</sup>T. Young and H. C. Andersen, *J. Chem. Phys.* **118**, 3447 (2003).
- <sup>83</sup>T. Young and H. C. Andersen, *J. Phys. Chem. B* **109**, 2985 (2005).
- <sup>84</sup>L. Berthier and G. Tarjus, *Phys. Rev. Lett.* **103**, 170601 (2009).
- <sup>85</sup>S. Torquato, T. M. Truskett, and P. G. Debenedetti, *Phys. Rev. Lett.* **84**, 2064 (2000).
- <sup>86</sup>T. M. Truskett, S. Torquato, and P. G. Debenedetti, *Phys. Rev. E* **62**, 993 (2000).
- <sup>87</sup>J. R. Errington and P. G. Debenedetti, *Nature (London)* **409**, 318 (2001).
- <sup>88</sup>M. S. Shell, P. G. Debenedetti, and A. Z. Panagiotopoulos, *Phys. Rev. E* **66**, 011202 (2002).
- <sup>89</sup>J. R. Errington, P. G. Debenedetti, and S. Torquato, *J. Chem. Phys.* **118**, 2256 (2003).
- <sup>90</sup>N. Giovambattista, P. G. Debenedetti, F. Sciortino, and H. E. Stanley, *Phys. Rev. E* **71**, 061505 (2005).
- <sup>91</sup>G. W. Scherer, *Relaxation in Glass and Composites* (Wiley, New York, 1986).
- <sup>92</sup>I. M. Hodge, *J. Non-Cryst. Solids* **169**, 211 (1994).
- <sup>93</sup>I. Avramov, *Thermochim. Acta* **280-281**, 363 (1996).
- <sup>94</sup>J. C. Dyre, T. Hecksher, and K. Niss, *J. Non-Cryst. Solids* **355**, 624 (2009).
- <sup>95</sup>S. Sastry, *Phys. Rev. Lett.* **85**, 590 (2000).
- <sup>96</sup>A. B. Bestul and S. S. Chang, *J. Chem. Phys.* **40**, 3731 (1964).
- <sup>97</sup>J. Mittal, J. R. Errington, and T. M. Truskett, *J. Chem. Phys.* **125**, 076102 (2006).
- <sup>98</sup>V. Lubchenko and P. G. Wolynes, *Annu. Rev. Phys. Chem.* **58**, 235 (2007).
- <sup>99</sup>J.-P. Bouchaud and G. Biroli, *J. Chem. Phys.* **121**, 7347 (2004).
- <sup>100</sup>X. Y. Xia and P. G. Wolynes, *Proc. Natl. Acad. Sci. U.S.A.* **97**, 2990 (2000).
- <sup>101</sup>J. C. Dyre, N. B. Olsen, and T. Christensen, *Phys. Rev. B* **53**, 2171

234504-18 Gnan *et al.*J. Chem. Phys. **131**, 234504 (2009)

- (1996).
- <sup>102</sup>D. H. Torchinsky, J. A. Johnson, and K. A. Nelson, *J. Chem. Phys.* **130**, 064502 (2009).
- <sup>103</sup>L. Larini, A. Ottochian, C. De Michele, and D. Leporini, *Nat. Phys.* **4**, 42 (2008).
- <sup>104</sup>K. Niss, C. Dalle-Ferrier, B. Frick, D. Russo, J. C. Dyre, and C. Alba-Simionesco, e-print arXiv:cond-mat/0908.2046.
- <sup>105</sup>K. S. Schweizer and G. Yatsenko, *J. Chem. Phys.* **127**, 164505 (2007).
- <sup>106</sup>M. Tripathy and K. S. Schweizer, *J. Chem. Phys.* **130**, 244907 (2009).
- <sup>107</sup>C. M. Roland, R. Casalini, and M. Paluch, *Chem. Phys. Lett.* **367**, 259 (2003).
- <sup>108</sup>K. L. Ngai, R. Casalini, S. Capaccioli, M. Paluch, and C. M. Roland, *J. Phys. Chem. B* **109**, 17356 (2005).
- <sup>109</sup>I. Prigogine and R. Defay, *Chemical Thermodynamics* (Longmans, Green, New York, 1954).
- <sup>110</sup>R. O. Davies and G. O. Jones, *Proc. R. Soc. London, Ser. A* **217**, 26 (1952).
- <sup>111</sup>R. O. Davies and G. O. Jones, *Adv. Phys.* **2**, 370 (1953).
- <sup>112</sup>F. Saija, S. Prestipino, and P. V. Giaquinta, *J. Chem. Phys.* **115**, 7586 (2001).
- <sup>113</sup>C. M. Roland, *Soft Matter* **4**, 2316 (2008).
- <sup>114</sup>E. Lerner, I. Procaccia, E. S. C. Ching, and H. G. E. Hentschel, *Phys. Rev. B* **79**, 180203 (2009).
- <sup>115</sup>Potentials consisting of IPL interactions plus an explicit function of volume also have exact isomorphs. Such volume-dependent terms are sometimes used in models of metals, although generally not in conjunction with IPL pair potentials.

## Pressure-energy correlations in liquids. V. Isomorphs in generalized Lennard-Jones systems.

Thomas B. Schröder\*, Nicoletta Gnan\*, Ulf R. Pedersen\*<sup>o</sup>, Nicholas P. Bailey\*, and Jeppe C. Dyre\*

\*DNRFC centre “Glass and Time,” IMFUFA, Department of Sciences,  
Roskilde University, Postbox 260, DK-4000 Roskilde, Denmark and

<sup>o</sup>Department of Chemistry, University of California, Berkeley, California 94720, USA

(Dated: April 28, 2010)

A liquid is termed strongly correlating if its virial and potential energy fluctuations in the NVT ensemble are more than 90% correlated [U. R. Pedersen *et al.*, Phys. Rev. Lett. **100**, 015701 (2008); N. P. Bailey *et al.*, J. Chem. Phys. **129**, 184507 (2008)]. This paper is the fifth in a series devoted to identifying and explaining the properties of strongly correlating liquids. Expressions are derived for the shape of isomorphs in the  $WU$  phase diagram for generalized Lennard-Jones (LJ) potentials. It is shown that the shape of the isomorphs only depend on the exponents of the potential, e.g., all 12-6 LJ systems have the same isomorphs, independent of the number of components and parameters of the potentials. An equation of state for generalized LJ systems is derived.

### I. INTRODUCTION

This is the fifth in a series of papers<sup>1-4</sup> investigating the properties of so-called strongly correlating liquids<sup>5</sup>, i.e., liquids that have strong correlations between constant-volume equilibrium fluctuations in potential energy,  $U$ , and virial,  $W$ . The virial gives the configurational contribution to the pressure:

$$pV = Nk_B T + W. \quad (1)$$

Letting  $\Delta$  denote instantaneous deviations from equilibrium mean values, the  $WU$  correlation is quantified by the correlation coefficient,  $R$ :

$$R = \frac{\langle \Delta W \Delta U \rangle}{\sqrt{\langle (\Delta W)^2 \rangle \langle (\Delta U)^2 \rangle}}. \quad (2)$$

Perfect correlation gives  $R = 1$ , and as a pragmatic definition we have chosen “strongly correlating liquids” to mean those liquids that have  $R \geq 0.9$  when volume,  $V$ , and temperature,  $T$ , is held constant.

Strongly correlating liquids have simpler physics than liquids in general, an observation that has particular significance for the highly viscous phase.<sup>6-17</sup> Thus it has been shown that strongly correlating viscous liquids have all eight frequency-dependent thermoviscoelastic response functions<sup>18-20</sup> given in terms of just one<sup>21</sup> (i.e. are “single-parameter liquids” in the sense of having dynamic Prigogine-Defay ratio<sup>18</sup> close to unity<sup>2,19,21</sup>). Moreover, strongly correlating viscous liquids obey density scaling<sup>22-26</sup>, i.e., their dimensionless relaxation time  $\tilde{\tau}$  depends on density  $\rho = N/V$  and temperature as  $\tilde{\tau} = F(\rho^\gamma/T)$ .<sup>27-29</sup>

Paper I<sup>1</sup> presented computer simulations of 13 different systems, indicating that van der Waals type liquids are generally strongly correlating, whereas hydrogen-bonding liquids like methanol or water are not. Strongly correlating liquids include<sup>1,2,5,21,28</sup> the standard Lennard-Jones (LJ) liquid, the Kob-Andersen binary LJ liquid as well as other binary LJ type mixtures, a dumbbell-type liquid of two different LJ spheres

with fixed bond length, a system with exponential repulsion, a seven-site united-atom toluene model, the Lewis-Wahnström OTP model, and an attractive square-well binary model.

Paper II<sup>2</sup> analyzed the cause of the correlations with a focus on the LJ potential. The strong correlations are related to the well-known fact that an inverse power-law pair potential,  $v(r) \propto r^{-n}$  where  $r$  is the distance between two particles,<sup>30-41</sup> implies perfect correlation<sup>2,5</sup> with  $\gamma = n/3$ . Around the minimum, the LJ potential can be fitted with an “extended” inverse power-law potential,<sup>2</sup>  $v_{LJ}(r) \cong Ar^{-n} + B + Cr$ . At constant volume the linear term contributes little to the virial and potential-energy fluctuations: When one nearest-neighbor interatomic distance increases, another decreases in such a way that their sum is almost constant. Thus, systems interacting via the LJ potential “inherits” strong  $WU$  correlations from the underlying apparent inverse power-law - they have a “hidden scale invariance”.<sup>3,27</sup>

Paper III<sup>3</sup> gave further numerical evidence for the explanation for strong correlations given in paper II, and further theoretical results was given on the statistical mechanics and thermodynamics of the hidden scale invariance that characterizes strongly correlating liquids. It was shown that strong virial-potential energy correlations are present even in out-of-equilibrium situations - the hidden scale invariance is a property of the potential energy surface, not just the equilibrium states.

Paper IV<sup>4</sup> introduced the concept of “isomorphs” in the phase diagram of a strongly correlating liquid. Starting from a single assumption, a number of “isomorph invariants” was derived. In particular, structure and dynamics was shown to be invariant on isomorphs, provided proper ‘reduced’ units are used. Some striking aging properties was demonstrated; Jumps between isomorphic state points (state points belonging to the same isomorph) are instantaneous, even if the equilibrium relaxation time is long, i.e., the liquid is in the viscous phase.

In the present paper further simulation results sup-

porting isomorph predictions are presented using systems interacting with the multicomponent generalized LJ potential:

$$v_{ij}(r_{ij}) = v_{ij}^{(m)}(r_{ij}) + v_{ij}^{(n)}(r_{ij}), \quad (3)$$

where  $v_{ij}^{(k)}(r_{ij})$  is an IPL potential acting between the two particles  $i$  and  $j$ :

$$v_{ij}^{(k)}(r_{ij}) \equiv \varepsilon_{ij}^{(k)} \left( \sigma_{ij}^{(k)} / r_{ij} \right)^k \quad (4)$$

For systems interacting via the generalized LJ potential, a prediction for the shape of the isomorphs in the  $WU$  phase diagram is derived, and demonstrated to fit very well to simulation results. The shape of the isomorphs only depends on the exponents  $m$  and  $n$ , thus e.g. all 12-6 LJ systems have the same isomorphs in the  $WU$  phase diagram. An equation of state giving  $U$  and  $W$  as a function of  $\rho$  and  $T$  is derived for systems interacting via generalized LJ potentials.

## II. ISOMORPHS

In this section we briefly review the isomorph definition and some of the predictions following from this. For further details the reader is referred to paper IV<sup>4</sup>.

Two state points (1) and (2) with temperatures  $T_1$  and  $T_2$  and densities  $\rho_1$  and  $\rho_2$ , respectively, are defined to be *isomorphic* if they obey the following: Any two physically relevant configurations<sup>49</sup> of state points (1) and (2),  $(\mathbf{r}_1^{(1)}, \dots, \mathbf{r}_N^{(1)})$  and  $(\mathbf{r}_1^{(2)}, \dots, \mathbf{r}_N^{(2)})$  that may be trivially scaled into one another,

$$\rho_1^{1/3} \mathbf{r}_i^{(1)} = \rho_2^{1/3} \mathbf{r}_i^{(2)} \quad (i = 1, \dots, N), \quad (5)$$

have proportional Boltzmann statistical weights:

$$e^{-U(\mathbf{r}_1^{(1)}, \dots, \mathbf{r}_N^{(1)})/k_B T_1} = C_{12} e^{-U(\mathbf{r}_1^{(2)}, \dots, \mathbf{r}_N^{(2)})/k_B T_2}. \quad (6)$$

Here  $U(\mathbf{r}_1, \dots, \mathbf{r}_N)$  is the potential energy function and  $C_{12}$  depends only on state points (1) and (2). ‘‘Isomorphs’’ are curves in the state diagram along which all state point are isomorphic.

The excess entropy,  $S_{\text{ex}} = S - S_{\text{ideal}}$ , was shown in paper IV<sup>4</sup> to be invariant on an isomorph. In the following we generate a set of state points with constant  $S_{\text{ex}}$ , and then demonstrate that other isomorph properties follow, i.e., that we (to a good approximation) have generated an isomorph. To change density and temperature while keeping  $S_{\text{ex}}$  constant, the following is utilized<sup>4</sup>:

$$\gamma \equiv - \left( \frac{\partial \ln(T)}{\partial \ln(V)} \right)_{S_{\text{ex}}} = \frac{V \left( \frac{\partial S_{\text{ex}}}{\partial V} \right)_T}{T \left( \frac{\partial S_{\text{ex}}}{\partial T} \right)_V} = \frac{V \beta_V^{\text{ex}}}{C_V^{\text{ex}}} \quad (7)$$

where  $\beta_V^{\text{ex}} \equiv \left( \frac{\partial p^{\text{ex}}}{\partial T} \right)_V = \frac{1}{V} \left( \frac{\partial W}{\partial T} \right)_V$  and a Maxwell relation was applied. Utilizing the standard fluctuation formulae we get<sup>4</sup>:

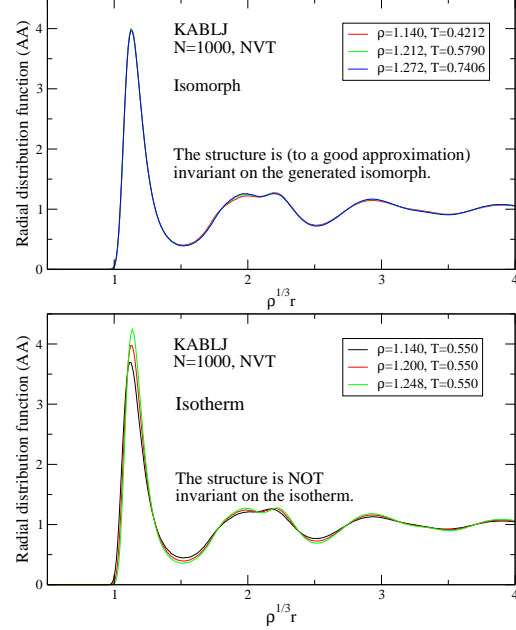


FIG. 1: a) Radial distribution function (AA interaction) for three isomorphic state points of the Kob and Andersen binary LJ mixture<sup>42</sup> (KABLJ). b) Radial distribution function for isotherm of the KABLJ mixture

$$\gamma = \left( \frac{\partial \ln(T)}{\partial \ln(\rho)} \right)_{S_{\text{ex}}} = \frac{\langle \Delta U \Delta W \rangle}{\langle (\Delta U)^2 \rangle} \quad (8)$$

The isomorphs presented below was generated by the following procedure: 1) an equilibrium NVT simulation was performed at a given state point. 2)  $\gamma$  was calculated from the fluctuations, using Eq. (8). 3) The density  $\rho$  was changed a small amount (of order 1%), and  $\gamma$  was used to calculate the corresponding change in temperature in order to keep  $S_{\text{ex}}$  constant (Eq. (8)). 4) A simulation at the new state point was performed, and the procedure was repeated.

The structure in reduced units is predicted to be invariant along an isomorph. This follows directly from Eq. (6): Configurations that are identical in reduced units have proportional Boltzmann’s factors and therefore identical probabilities since the pre-factor cancels out when normalizing by the partition function. Fig. 1(a) demonstrates the isomorph invariance of the radial distribution function for the large particles of the Kob and Andersen binary LJ mixture<sup>42</sup> (KABLJ). For comparison, Fig. 1(b) shows the same property on an isotherm with roughly the same density change as on the isomorph. Clearly, the structure is to a good approximation invariant on the isomorph, whereas this is not true on the isotherm.

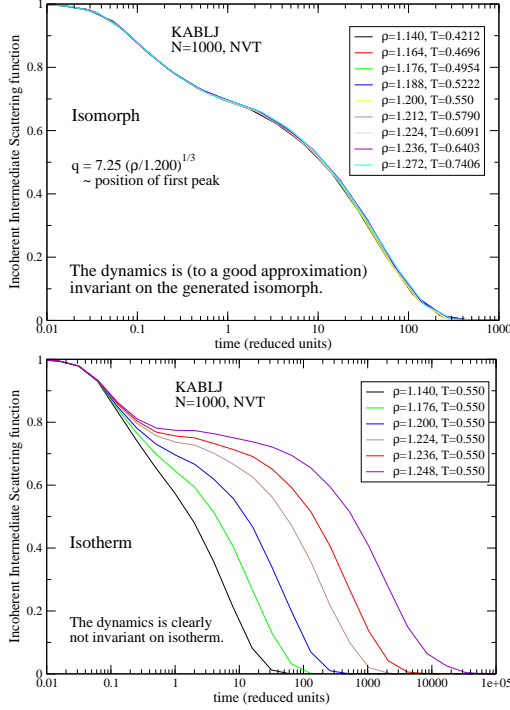


FIG. 2: a) Incoherent intermediate scattering function for the large (A) particles for isomorph state points of the KABLJ mixture. The  $q$ -vector is kept constant in reduced units. b) Same as in a), but for an isotherm.

Taking the logarithm of Eq. (6) shows that the potential energy surface in reduced units is the same for two isomorph state points - except for an additive constant. This constant does not influence the dynamics, and consequently the dynamics in reduced units is the same for the two isomorph state points, see paper IV<sup>4</sup>. Fig. 1(a) demonstrates the isomorph invariance of incoherent intermediate scattering function the large particles of the Kob and Andersen binary LJ mixture<sup>42</sup> (KABLJ). For comparison, Fig. 1(b) shows the same property on an isotherm with roughly the same density change as on the isomorph. Clearly, the dynamics is to a good approximation invariant on the isomorph - both regarding relaxation time and relaxation spectra - whereas this is far from true on the isotherm.

The  $\gamma$  calculated from Eq. (8) in general depends on the state point. Fig. 3 shows (as red squares)  $\gamma$  found from the fluctuations along the isomorph shown above. Even though temperature changes by almost a factor of two,  $\gamma$  changes less than 5%. It was shown in paper IV<sup>4</sup> that for a system with good isomorphs,  $\gamma$  should - to a good approximation - only depend on density. This is supported by Fig. 3 where  $\gamma$  on an isochore is shown to

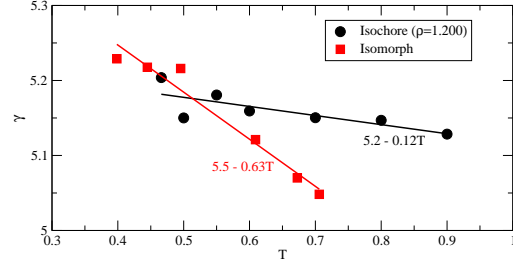


FIG. 3:  $\gamma$  calculated from equilibrium fluctuation via Eq. (8) for the KABLJ system. Red squares: state points belonging to the isomorph presented in Figs. 1 and 2. Black circles: isochoric state points. Straight lines are linear regression fits.

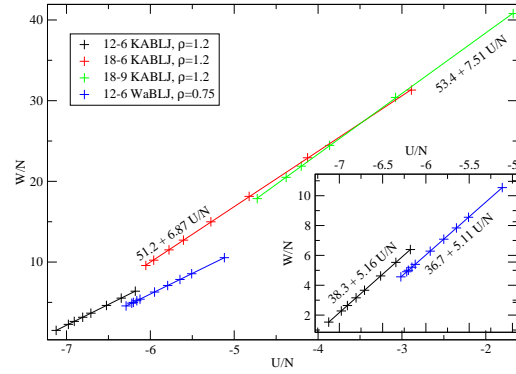


FIG. 4: Isochores for four different binary systems. 12-6 KABLJ is the Kob and Andersen binary 80:20 mixture<sup>42</sup> using the standard 12-6 LJ potential. 18-6 KABLJ is the same system, except using the generalized LJ potential ( $m = 18$ ,  $n = 6$ , Eq. (3)) with parameters chosen to place the minimum of the potential at the same distance and depth as in the 12-6 KABLJ. Likewise, 18-9 KABLJ is using the exponents  $m = 18$  and  $n = 9$ . 12-6 WaBLJ is the Wahnstrom 50:50 mixture<sup>43</sup> using the standard 12-6 LJ potential. Straight lines are linear regression fits. The inset shows a zoom on the data for the two 12-6 LJ systems.

vary around 1% when temperature is changed by a factor of two.

It follows from Eq. (7) that the slope of isochores in the  $WU$  phase diagram is given by  $\gamma$ :

$$\gamma = \left( \frac{\partial W}{\partial U} \right)_V \quad (9)$$

The very small change of  $\gamma$  along isochores (black circles in Fig. 3) means that these to a good approximation are straight lines in the  $WU$  phase diagram. This is illustrated in Fig. 4 for 4 different generalized LJ systems.

### III. SHAPE OF ISOMORPHS IN THE $WU$ PHASE DIAGRAM

What is the shape of isomorphs in the  $WU$  phase diagram? This section answers this question for the multi-component generalized LJ potential. This potential is in Eq. (3) explicitly expressed as the sum of two IPL's. Correspondingly we can write the potential energy and virial as the sum of two terms (where  $\langle \dots \rangle$  denotes thermodynamic average):

$$U = U_m + U_n, \quad U_k \equiv \left\langle \sum_{i>j} v_{ij}^{(k)}(r_{ij}) \right\rangle \quad (10)$$

For pair interactions the virial is given by:

$$W \equiv -\frac{1}{3} \left\langle \sum_{i>j} r_{ij} v'_{ij}(r_{ij}) \right\rangle \quad (11)$$

From which we get:

$$W = \frac{m}{3}U_m + \frac{n}{3}U_n. \quad (12)$$

For any state point in the  $WU$  phase diagram we can solve for  $(U_m, U_n)$ :

$$U_m = \frac{3W - nU}{m - n} \quad (13)$$

$$U_n = \frac{-3W + mU}{m - n} \quad (14)$$

These equations allow us to determine what regions of the  $WU$  phase diagram are accessible to the system. Adopting the convention  $m > n$ , we restrict ourselves to  $\epsilon_{ij}^{(m)} > 0$ , in order to have a repulsive core for all interactions. This leads to  $U_m > 0$  for all configurations, and therefore also for thermodynamic averages. Combining this with Eq. (13) leads to  $W > \frac{n}{3}U$ . If all interactions have an attractive part ( $\epsilon_{ij}^{(n)} < 0$ ) we have  $U_n < 0$  which in combinations with Eq. (14) gives  $W > \frac{m}{3}U$ . The region of the  $WU$  phase diagram accessible to the standard 12-6 LJ potential is thus given by  $W > 4U$  and  $W > 2U$  (the later inequality being relevant for  $U \leq 0$ ).

#### A. Parametric description isomorphs

Along isomorphs the structure is invariant in reduced units ( $\tilde{r} \equiv r\rho^{1/3}$ ) as demonstrated in Fig. 1. From this follows directly that  $\langle U_m \rangle / \rho^{m/3}$ , is also invariant on an isomorph:

$$\frac{U_m}{\rho^{m/3}} = \frac{1}{\rho^{m/3}} \left\langle \sum_{i>j} \epsilon_{ij}^{(m)} \left( \frac{\sigma_{ij}^{(m)}}{\tilde{r}_{ij}\rho^{-1/3}} \right)^m \right\rangle \quad (15)$$

$$= \left\langle \sum_{i>j} \epsilon_{ij}^{(m)} \left( \frac{\sigma_{ij}^{(m)}}{\tilde{r}_{ij}} \right)^m \right\rangle \quad (16)$$

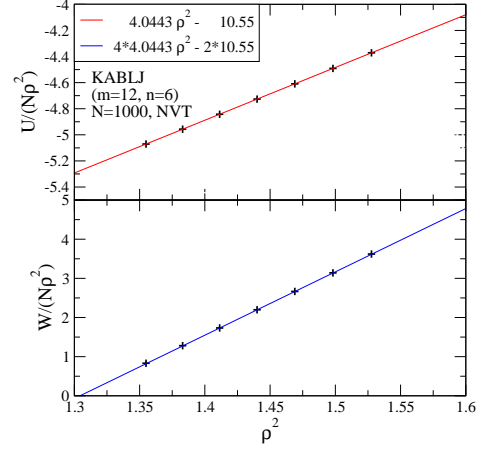


FIG. 5: Test of KABLJ ( $m = 12$ ,  $n = 6$ ) isomorph generated from  $\gamma$  (Eq. 8). Top panel:  $U$  fitted to Eq. (20) using  $\rho_* = 1$ . Bottom panel:  $W$  compared to Eq. (21), using the parameters  $U_m^*$  and  $U_n^*$  found from  $U$  (top panel), i.e., without fitting again.

If we let “\*” denote a reference-point,  $(W_*, U_*)$ , we can use Eqs. (13) and (14) to get  $(U_m^*, U_n^*)$  and we find for other state points on the same isomorph:

$$U_m = \left( \frac{\rho}{\rho_*} \right)^{m/3} U_m^* = \tilde{\rho}^{m/3} U_m^* \quad (17)$$

where  $\tilde{\rho} \equiv \rho/\rho_*$ . Combining Eq. (17) with Eqs. (10) and (12) we obtain a one-parameter parametric description of an isomorph in the  $WU$  phase diagram:

$$U = \tilde{\rho}^{m/3} U_m^* + \tilde{\rho}^{n/3} U_n^* \quad (18)$$

$$W = \frac{m}{3} \tilde{\rho}^{m/3} U_m^* + \frac{n}{3} \tilde{\rho}^{n/3} U_n^*. \quad (19)$$

For a given isomorph  $U_m^*$  and  $U_n^*$  can be found from a single reference state point using Eqs. (13) and (14), or by linear regression from:

$$\frac{U}{\tilde{\rho}^{n/3}} = \tilde{\rho}^{(m-n)/3} U_m^* + U_n^* \quad (20)$$

$$\frac{W}{\tilde{\rho}^{n/3}} = \frac{m}{3} \tilde{\rho}^{(m-n)/3} U_m^* + \frac{n}{3} U_n^*. \quad (21)$$

This is done in Fig. 5 for the 12-6 KABLJ isomorph shown in the previous section. The potential energies were fitted by linear regression to Eq. (20) giving a very nice fit. The virials were compared to Eq. (21) using the parameters estimated from the potential energies, i.e., without performing a new fit. The agreement is striking.

We note here two consequences of the above. 1) If the reference state point  $(U_*, W_*)$  generates the isomorph  $(U(\rho), W(\rho))$ , then the reference state point  $(aU_*, aW_*)$

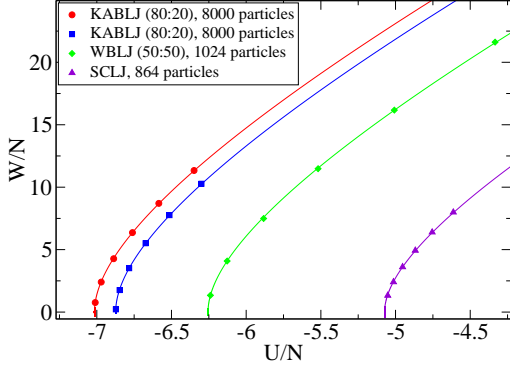


FIG. 6: Four different isomorphs in the  $U$ - $W$  plane. Two isomorphs belongs to the same system (KABLJ) while the third is a result from simulations of Wahnström binary LJ liquid<sup>43</sup> (WaBLJ), and the fourth (SCLJ) is the single component LJ liquid.

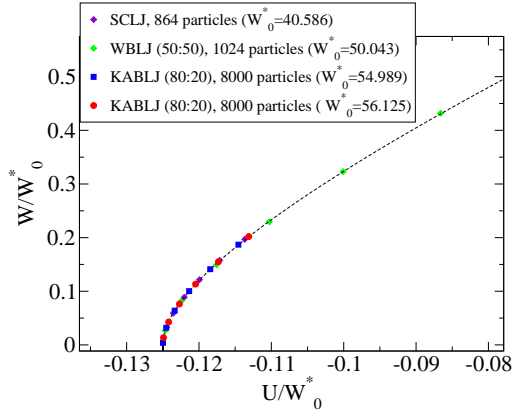


FIG. 7: The “master isomorph”: collapsing isomorphs from Fig. 6 by scaling with  $W_0^*$  defined as the virial on the same isomorph when  $U = 0$ .

generates the isomorph  $(aU(\rho), aW(\rho))$ . This means all the isomorphs for a given system have the same shape, and can be scaled onto each other with a single scaling parameter. 2) The shape of the isomorphs only depend on the exponents,  $m$  and  $n$ , e.g all 12-6 LJ systems have the same isomorphs in the  $WU$  phase diagram.

Fig. 6 shows isomorphs in the  $WU$  phase diagram for three different 12-6 LJ systems. Fig. 7 shows the same isomorph scaled onto a master isomorph”. Fig. 8 shows an isomorph for the 18-6 KABLJ system and compares it to a 12-6 LJ isomorph.

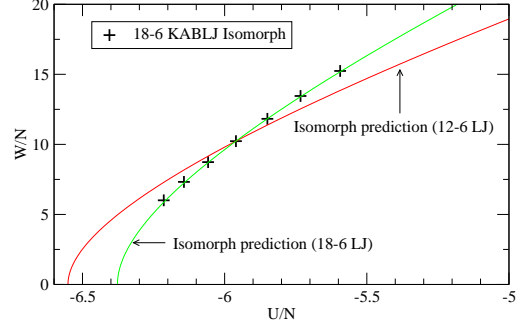


FIG. 8: Isomorph of the 18-6 KABLJ liquid compared to the theoretical prediction. For reference, also the prediction for 12-6 LJ systems is included

## B. Equation description of isomorphs

Combining Eq. (17) with Eqs. (13) and (14) we get

$$\bar{\rho}^{n/3} = \frac{U_n}{U_n^*} = \frac{3W - mU}{3W_* - mU_*} \quad (22)$$

$$\bar{\rho}^{m/3} = \frac{U_m}{U_m^*} = \frac{3W - nU}{3W_* - nU_*} \quad (23)$$

Eliminating the density and rearranging, we find an invariant for the isomorph:

$$\frac{(W - \frac{m}{3}U)^m}{(W - \frac{n}{3}U)^n} = \frac{(W_* - \frac{m}{3}U_*)^m}{(W_* - \frac{n}{3}U_*)^n} \quad (24)$$

Choosing a reference point with zero potential energy ( $U_* = 0, W_* = W_0^*$ ) we get:

$$\frac{(W - \frac{m}{3}U)^m}{(W - \frac{n}{3}U)^n} = (W_0^*)^{m-n} \quad (25)$$

$W_0^*$  is a unique number identifying the isomorph. The isomorph is the solution to

$$\left( \frac{W}{W_0^*} - \frac{m}{3} \frac{U}{W_0^*} \right)^{m/n} = \left( \frac{W}{W_0^*} - \frac{n}{3} \frac{U}{W_0^*} \right) \quad (26)$$

For  $m = 2n$  (as is the case e.g. for the standard 12-6 LJ potential) the solution to this quadratic equation is:

$$2 \frac{W}{W_0^*} = 1 + 4 \frac{n}{3} \frac{U}{W_0^*} \pm \sqrt{1 + 4 \frac{n}{3} \frac{U}{W_0^*}} \quad (27)$$

which has real solution(s) for  $U/W_0^* \geq -\frac{3}{4n}$ , where the equal sign gives the solution to  $W = 0$ , which is also where the slope of the isomorph is infinite.

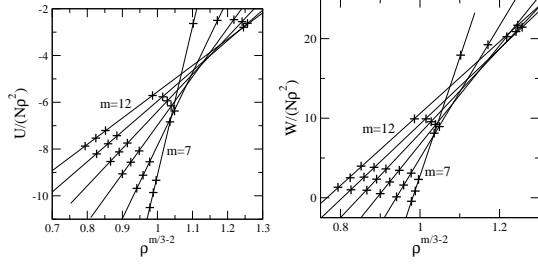


FIG. 9: Test of isomorph prediction (Eqs. (20) and (21)) for the liquid side of solid-liquid coexistence of single component generalized LJ potential. Data points are simulation results from Ahmed and Sadus<sup>44</sup>, straight lines are linear regression fits.

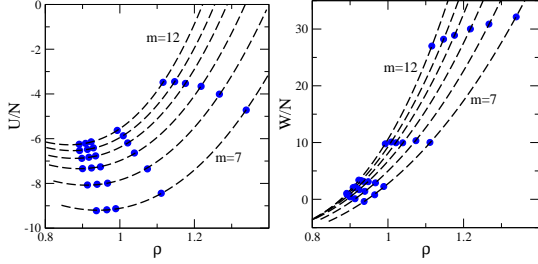


FIG. 10: Same data as in Fig. 9, plotting potential energy versus density (left panel) and virial versus density (right panel). Dashed lines: Isomorph predictions (Eqs. (18) and (19)), using the parameters determined in Fig. 9.

### C. Solid-liquid coexistence

In paper IV it was argued that solid-liquid co-existence lines are isomorphs; the Boltzmann probability of all microscopic configurations are invariant along an isomorph, and therefore so is the phase-behavior. Ahmed and Sadus presented in a recent paper<sup>44</sup> a method for determining solid-liquid co-existence. They reported results for the generalized LJ potential (Eq. 3) with the repulsive exponent  $n = 6$  (they termed the repulsive exponent  $m$ , we are here keeping the notation of Eq. (3)). Fig. 9 shows the state points reported by Ahmed et al. for the liquid side of solid-liquid coexistence, compared to the isomorph predictions as expressed in Eqs. (20) and (21). Fig. 10 shows the same data, now plotting simply respectively potential energy (left panel) and virial (right panel) versus density.

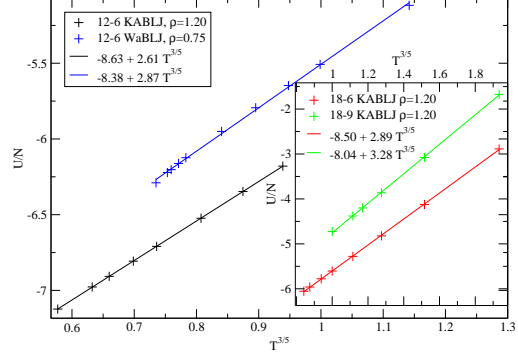


FIG. 11: Test of Rosenfeld-Tarazona scaling (Eq. (28)) for the systems investigated in Fig. 4.

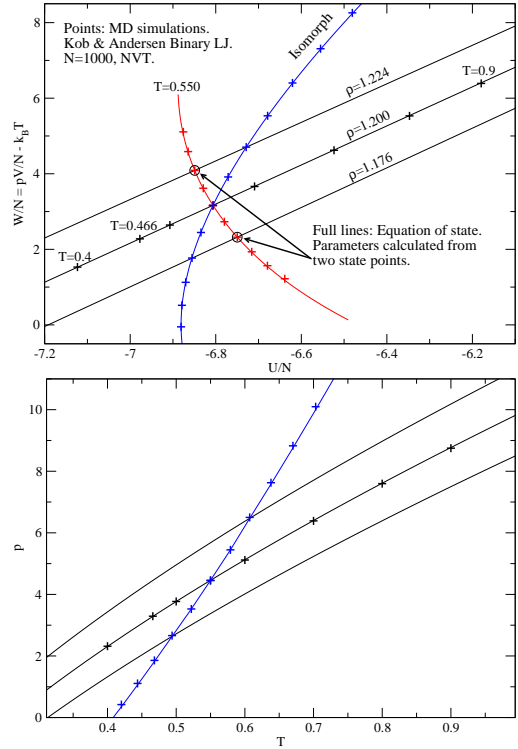


FIG. 12: Upper panel: Test of derived equation of state in  $WU$  phase diagram. Lines: theoretical prediction (three isochores, an isomorph and an isotherm). Data point: simulations of the KABLJ mixture. Lower panel: Same data for the isomorph and the three isochores in a  $p$ - $T$  diagram.

#### IV. EQUATION OF STATE FOR GENERALIZED LJ SYSTEMS

Eqs. (18) and (19) gives the potential energy and virial as a function of density on an isomorph. The temperature on the isomorph can be found by integrating Eq. (8). Since  $\gamma$  changes only weakly, it will in many situations be a sufficient approximation to assume it constant, leading to the relation  $T = \bar{\rho}^\gamma T_*$ , where  $T_*$  is the temperature at the reference point. Taken together Eqs. (18), (19), and (8) thus means that from a single reference point  $(\rho_*, T_*, U_*, W_*)$  we have a prediction for  $(\rho, T, U, W)$  on the isomorph to which the reference point belongs.

Fig. 4 demonstrated that in the  $WU$  phase diagram, isochores to a very good approximation are straight lines with slope  $\gamma$ , i.e., we can write  $W(\rho, T) = W_0 + \gamma U(\rho, T)$ . The only ingredient missing to generate a full equation of state (expressed as  $U(\rho, T)$  and  $W(\rho, T)$ ) is a relation between temperature and either potential energy or virial on an isochore.

Rosenfeld and Tarazona<sup>45</sup> derived from density functional theory an expression for the potential energy on an isochore (where the coefficients  $U_0$  and  $\alpha$  depend on the density,  $\rho_*$ ):

$$U(\rho_*, T) = U_0 + \alpha T^{3/5} \quad (28)$$

Eq. (28) has since been confirmed to be an excellent approximation for several models, including the KABLJ model<sup>46,47</sup>. Fig. 11 tests the Rosenfeld-Tarazona prediction (Eq. (28)) for the systems investigated in Fig. 4. The prediction works well, *except* for the Wahnstrom system<sup>48</sup>.

Combining Eq. 28 with our results on isomorphs and isochores, we can make an equation of state for generalized LJ systems. The idea is to map any state point  $(\rho, T, U, W)$  to the corresponding isomorph state point on the reference isochore  $(\rho_*, T_*, U_*, W_*)$ :

$$T_*(\rho, T) = T \bar{\rho}^{-\gamma}, \quad \bar{\rho} \equiv \rho/\rho_* \quad (29)$$

$$U_*(\rho, T) = U_0 + \alpha (T \bar{\rho}^{-\gamma})^{3/5} \quad (30)$$

$$W_*(\rho, T) = W_0 + \gamma U_*(\rho, T) \quad (31)$$

From  $(U_*, W_*)$  we can calculate the contribution to the potential energy from the two IPL terms of the potential:

$$U_{m,*}(\rho, T) = \frac{3W_*(\rho, T) - nU_*(\rho, T)}{m-n} \quad (32)$$

$$= \frac{3W_0 - (n-3\gamma)U_*(\rho, T)}{m-n} \quad (33)$$

$$U_{n,*}(\rho, T) = \frac{-3W_*(\rho, T) + mU_*(\rho, T)}{m-n} \quad (34)$$

$$= \frac{-3W_0 + (m-3\gamma)U_*(\rho, T)}{m-n} \quad (35)$$

Finally we use isomorphic scaling to go back to the  $(\rho, T, U, W)$  state point:

$$U(\rho, T) = \bar{\rho}^{n/3} U_{n,*}(\rho, T) + \bar{\rho}^{m/3} U_{m,*}(\rho, T) \quad (36)$$

$$W(\rho, T) = \frac{n}{3} \bar{\rho}^{n/3} U_{n,*}(\rho, T) + \frac{m}{3} \bar{\rho}^{m/3} U_{m,*}(\rho, T) \quad (37)$$

The derived equation of state contains 4 parameters ( $W_0, \gamma, U_0, \alpha$ ) and a reference density  $\rho_*$ . The parameters can be calculated from  $U, W, C_v^{ex}$ , and  $\beta v^{ex}$  at a single state point. A more convenient way of estimating the parameters might be: i) for a collection of  $(\rho, T, U, W)$  state points (at least two non-isomorphic), use isomorphic scaling (Eqs. (36) and (37)) to get the corresponding  $(U_*, W_*)$  at the chosen reference density, and fit them to Eq. (31) to get  $W_0$  and  $\gamma$ . ii) Fit to Eq. (30) get  $U_0$  and  $\alpha$ .

To put the derived equation of state to the test, the procedure described above was used to determine the four parameters ( $W_0, \gamma, U_0, \alpha$ ) for the 12-6 KABLJ system using two state points. The resulting equation of state is shown as full lines in Fig. 12, where it is compared to simulation results shown as data points.

#### ACKNOWLEDGMENTS

URP is supported by the Danish Council for Independent Research in Natural Sciences. The center for viscous liquid dynamics 'Glass and Time' is sponsored by the Danish National Research Foundation DNRF.

<sup>1</sup> N. P. Bailey, U. R. Pedersen, N. Gnan, T. B. Schröder, and J. C. Dyre, J. Chem. Phys. **129**, 184507 (2008) [paper I].

<sup>2</sup> N. P. Bailey, U. R. Pedersen, N. Gnan, T. B. Schröder, and J. C. Dyre, J. Chem. Phys. **129**, 184508 (2008) [paper II].

<sup>3</sup> T. B. Schröder, N. P. Bailey, U. R. Pedersen, N. Gnan, and J. C. Dyre, J. Chem. Phys. **131**, 234503 (2009) [paper III].

<sup>4</sup> N. Gnan, T. B. Schröder, U. R. Pedersen, N. P. Bailey, and J. C. Dyre, J. Chem. Phys. **131**, 234504 (2009) [paper IV].

<sup>5</sup> U. R. Pedersen, N. P. Bailey, T. B. Schröder, and J. C.

Dyre, Phys. Rev. Lett. **100**, 015701 (2008).

<sup>6</sup> W. Kauzmann, Chem. Rev. **43**, 219 (1948).

<sup>7</sup> G. Harrison, *The Dynamic Properties of Supercooled Liquids* (Academic, New York, 1976).

<sup>8</sup> S. Brawer, *Relaxation in Viscous Liquids and Glasses* (American Ceramic Society, Columbus, OH, 1985).

<sup>9</sup> I. Gutzow and J. Schmelzer, *The Vitreous State: Thermodynamics, Structure, Rheology, and Crystallization* (Springer, Berlin, 1995).

<sup>10</sup> M. D. Ediger, C. A. Angell, and S. R. Nagel, J. Phys. Chem. **100**, 13200 (1996).

<sup>11</sup> R. V. Chamberlin, Phase Transitions **65**, 169 (1999).

<sup>12</sup> C. A. Angell, K. L. Ngai, G. B. McKenna, P. F. McMillan,

- and S. W. Martin, *J. Appl. Phys.* **88**, 3113 (2000).
- <sup>13</sup> C. Alba-Simionesco, *C. R. Acad. Sci. Paris (Ser. IV)* **2**, 203 (2001).
- <sup>14</sup> P. G. Debenedetti and F. H. Stillinger, *Nature* **410**, 259 (2001).
- <sup>15</sup> K. Binder and W. Kob, *Glassy Materials and Disordered Solids: An Introduction to their Statistical Mechanics* (World Scientific, Singapore, 2005).
- <sup>16</sup> F. Sciortino, *J. Stat. Mech.* P05015 (2005).
- <sup>17</sup> J. C. Dyre, *Rev. Mod. Phys.* **78**, 953 (2006).
- <sup>18</sup> N. L. Ellegaard, T. Christensen, P. V. Christiansen, N. B. Olsen, U. R. Pedersen, T. B. Schröder, and J. C. Dyre, *J. Chem. Phys.* **126**, 074502 (2007).
- <sup>19</sup> N. P. Bailey, T. Christensen, B. Jakobsen, K. Niss, N. B. Olsen, U. R. Pedersen, T. B. Schröder, and J. C. Dyre, *J. Phys.: Condens. Matter* **20**, 244113 (2008).
- <sup>20</sup> T. Christensen and J. C. Dyre, *Phys. Rev. E* **78**, 021501 (2008).
- <sup>21</sup> U. R. Pedersen, T. Christensen, T. B. Schröder, and J. C. Dyre, *Phys. Rev. E* **77**, 011201 (2008).
- <sup>22</sup> A. Tölle, *Rep. Prog. Phys.* **64**, 1473 (2001).
- <sup>23</sup> C. Dreyfus, A. Aouadi, J. Gapinski, M. Matos-Lopes, W. Steffen, A. Patkowski, R. M. Pick, *Phys. Rev. E* **68**, 011204 (2003).
- <sup>24</sup> C. Alba-Simionesco, A. Cailliaux, A. Alegria, and G. Tarjus, *Europhys. Lett.* **68**, 58 (2004).
- <sup>25</sup> R. Casalini and C. M. Roland, *Phys. Rev. E* **69**, 062501 (2004).
- <sup>26</sup> C. M. Roland, S. Hensel-Bielowka, M. Paluch, and R. Casalini, *Rep. Prog. Phys.* **68**, 1405 (2005).
- <sup>27</sup> T. B. Schröder, U. R. Pedersen, N. P. Bailey, S. Toxvaerd, and J. C. Dyre, *arXiv:0812.4960* (2008); *arXiv:0803.2199* (2008).
- <sup>28</sup> D. Coslovich and C. M. Roland, *J. Phys. Chem. B* **112**, 1329 (2008).
- <sup>29</sup> D. Coslovich and C. M. Roland, *J. Chem. Phys.* **130**, 014508 (2009).
- <sup>30</sup> W. G. Hoover, D. A. Young, and E. Grover, *J. Chem. Phys.* **56**, 2207 (1972).
- <sup>31</sup> Y. Hiwatari, H. Matsuda, T. Ogawa, N. Ogita, and A. Ueda, *Prog. Theor. Phys.* **52**, 1105 (1974).
- <sup>32</sup> L. V. Woodcock, *Phys. Rev. Lett.* **54**, 1513 (1985).
- <sup>33</sup> J. L. Barrat, J. P. Hansen, G. Pastore, E. M. Waisman, *J. Chem. Phys.* **86**, 6360 (1987).
- <sup>34</sup> P. G. Debenedetti, F. H. Stillinger, T. M. Truskett, and C. J. Roberts, *J. Phys. Chem.* **103**, 7390 (1999).
- <sup>35</sup> E. La Nave, F. Sciortino, P. Tartaglia, M. S. Shell, and P. G. Debenedetti, *Phys. Rev. E* **68**, 032103 (2003).
- <sup>36</sup> R. J. Speedy, *J. Phys.: Condens. Matter* **15**, S1243 (2003).
- <sup>37</sup> M. S. Shell, P. G. Debenedetti, E. La Nave, and F. Sciortino, *J. Chem. Phys.* **118**, 8821 (2003).
- <sup>38</sup> G. Rickayzen and D. M. Heyes, *Phys. Rev. E* **71**, 061204 (2005).
- <sup>39</sup> A. C. Branka and D. M. Heyes, *Phys. Rev. E* **74**, 031202 (2006).
- <sup>40</sup> R. Casalini, U. Mohanty, and C. M. Roland, *J. Chem. Phys.* **125**, 014505 (2006).
- <sup>41</sup> D. M. Heyes and A. C. Branka, *Phys. Chem. Chem. Phys.* **9**, 5570 (2007).
- <sup>42</sup> W. Kob and H. C. Andersen, *Phys. Rev. Lett.* **73**, 1376 (1994).
- <sup>43</sup> G. Wahnström, *Phys. Rev. A* **44**, 3752 (1991).
- <sup>44</sup> A. Ahmed and R. J. Sadus, *J. Chem. Phys.* **131**, 174504 (2009).
- <sup>45</sup> Y. Rosenfeld and P. Tarazona, *Mol. Phys.* **95**, 141 (1998).
- <sup>46</sup> F. Sciortino, W. Kob, and P. Tartaglia, *J. Phys.: Condens. Matter* **12**, 6525 (2000).
- <sup>47</sup> B. Coluzzi B, G. Parisi, P. Verrocchio, *J. Chem. Phys.* **112**, 2933 (2000).
- <sup>48</sup> U. R. Pedersen, T. B. Schröder, J. C. Dyre, and P. Harrowell, *Phys. Rev. Lett.* **104**, 105701 (2010)
- <sup>49</sup> A configuration is termed “physically relevant“ if its contribution to the partition function is not a priori negligible. E.g., a configuration where all particles occupy the left half of the system’s volume is not physically relevant for ordinary liquid states.

## Strongly correlating liquids and their isomorphs

Ulf R. Pedersen

*Department of Chemistry, University of California, Berkeley, California 94720, USA*

Nicoletta Gnan, Nicholas P. Bailey, Thomas B. Schröder, and Jeppe C. Dyre  
*DNRF Center “Glass and Time”, IMFUFA, Dept. of Sciences,  
 Roskilde University, P.O. Box 260, DK-4000 Roskilde, Denmark*

(Dated: April 9, 2010)

This paper summarizes the properties of strongly correlating liquids, i.e., liquids with strong correlations between virial and potential energy equilibrium fluctuations at constant volume. We proceed to focus on the experimental predictions for strongly correlating glass-forming liquids. These predictions include i) density scaling, ii) isochronal superposition, iii) that there is a single function from which all frequency-dependent viscoelastic response functions may be calculated, iv) that strongly correlating liquids are approximately single-parameter liquids with close to unity Prigogine-Defay ratio, and v) that the fictive temperature initially decreases for an isobaric temperature up jump. The “isomorph filter”, which allows one to test for universality of theories for the non-Arrhenius temperature dependence of the relaxation time, is also briefly discussed.

### I. INTRODUCTION

After the initial reports in early 2008 of the existence of a class of strongly correlating liquids [1, 2], these liquids were described in four comprehensive publications that appeared later in 2008 and in 2009 in the Journal of Chemical Physics [3–6]. This paper briefly summarizes the properties and characteristics of strongly correlating liquids as detailed in Refs. 3–6 and present a number of new computer simulations. We list a number of experimental predictions for strongly correlating liquids, focusing on glass-forming liquids since this volume constitutes the proceedings of the Rome conference held in September 2009 (6IDMRCS). The main message is that the class of strongly correlating liquids, which includes the van der Waals and metallic liquids, are simpler than liquids in general. This explains, for instance, the long known observation that hydrogen-bonded liquids have several peculiar properties.

### II. STRONG VIRIAL / POTENTIAL ENERGY CORRELATIONS IN LIQUIDS

Consider a system of  $N$  particles in volume  $V$  at temperature  $T$ . The virial  $W$  is defined by writing the pressure  $p$  is a sum of the ideal gas term  $Nk_B T/V$  and a term reflecting the interactions as follows

$$pV = Nk_B T + W. \quad (1)$$

If  $U(\mathbf{r}_1, \dots, \mathbf{r}_N)$  is the potential energy function, the virial, which has dimension of energy, is given [7–11] by

$$W(\mathbf{r}_1, \dots, \mathbf{r}_N) = -1/3 \sum_i \mathbf{r}_i \cdot \nabla_{\mathbf{r}_i} U(\mathbf{r}_1, \dots, \mathbf{r}_N). \quad (2)$$

Equation (1) describes thermodynamic averages, but it also applies for the instantaneous values if the virial is

defined by Eq. (2) and the temperature is defined from the kinetic energy in the usual fashion [7–11].

If  $\Delta U$  is the instantaneous potential energy minus its average and  $\Delta W$  the same for the virial at any given state point, the  $WU$  correlation coefficient  $R$  is defined by (where sharp brackets denote equilibrium NVT ensemble averages)

$$R = \frac{\langle \Delta W \Delta U \rangle}{\sqrt{\langle (\Delta W)^2 \rangle \langle (\Delta U)^2 \rangle}}. \quad (3)$$

By the Cauchy-Schwarz inequality the correlation coefficient obeys  $-1 \leq R \leq 1$ . We define *strongly correlating liquids* by the condition  $R > 0.9$  [3]. The correlation coefficient is state-point dependent, but for all of the several liquids we studied by simulation [3, 5, 12]  $R$  is either above 0.9 in a large part of the state diagram, or not at all.

Figure 1 shows two examples of constant-volume thermal equilibrium fluctuations of virial and potential energy for two model systems, the standard Lennard-Jones (LJ) liquid and the Wahnström binary Lennard-Jones mixture [13]. In both cases there are strong virial / potential energy correlations. In (b) one sees striking dips in the potential energy; these dips reflect the existence of transient clusters in the liquid characterized by the same short range order as the crystal [14]. During the dips virial and potential energy also correlate strongly. Actually, the correlation even survives crystallization [4]. Thus the property of strong virial / potential energy correlations is quite robust; even complex systems like biological membranes may exhibit strong correlations [15].

One way to illuminate the correlations is to plot instantaneous values of virial and potential energy versus one another in so-called scatter plots. Figure 2(a) shows an example of this with data taken from a simulation of the Kob-Andersen binary Lennard-Jones (KABLJ) liquid [16]. This has become the standard liquid for studying

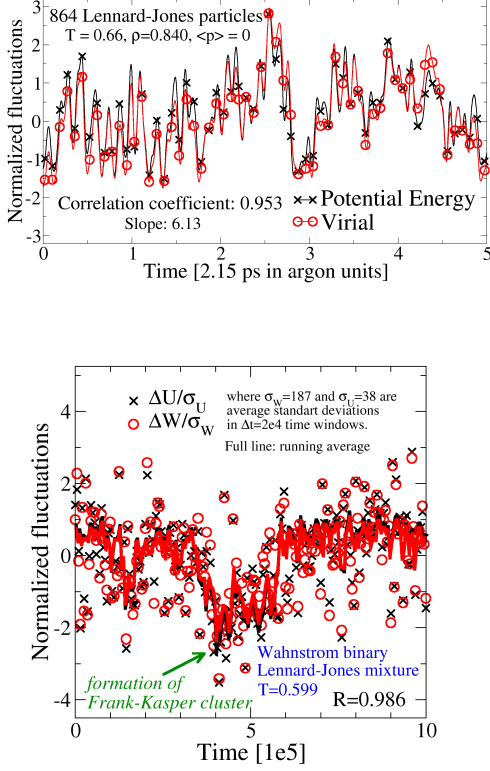


FIG. 1: (a) Instantaneous normalized equilibrium fluctuations of virial and potential energy in the standard single-component Lennard-Jones liquid at constant volume (NVT simulation).  $W(t)$  and  $U(t)$  correlate strongly. (b) The same for the supercooled Wahnström binary Lennard-Jones mixture [13]; here  $W(t)$  and  $U(t)$  correlate strongly even during the formation of a so-called Frank-Kaspers cluster [14].

viscous liquid dynamics, because it is difficult to crystallize (this requires simulating for more than 100 microseconds (Argon units)[17]). The “slope”  $\gamma$  of the scatter plot gives the proportionality constant of the fluctuations according to

$$\Delta W(t) \cong \gamma \Delta U(t). \quad (4)$$

The number  $\gamma$ , which varies slightly with state point, is roughly 6 for the standard LJ liquid, roughly 5 for the KABLJ liquid, and roughly 8 for the OTP model studied below in Fig. 7.

Since viscous liquid dynamics consists of long-time vibrations around potential energy minima – the so-called inherent states [18] – followed by rapid transitions between the inherent states [19, 20], it is interesting to study

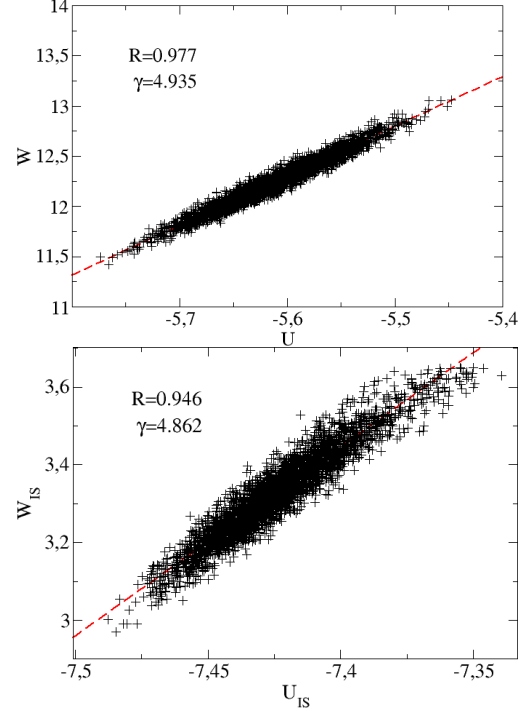


FIG. 2: (a) Virial / potential energy correlations for the Kob-Andersen binary Lennard-Jones liquid (1000 particles studied by Monte Carlo simulation,  $\rho = 1.264$ ,  $T = 1.24$  in standard LJ units). (b) Inherent state energies and virials of the simulation in (a); the correlation is still high. The slope  $\gamma$  defined by  $\Delta W(t) \cong \gamma \Delta U(t)$  is slightly different, but comparable to that of the true dynamics.

the inherent dynamics analogue of Fig. 2(a). This is done in Fig. 2(b), which gives the same simulation data after minimizing the configurations’ potential energy using the conjugate gradient method. The correlations are still present and the “slope”  $\gamma$  doesn’t change very much – even though the virial decreased by more than 60% going from (a) to (b). This confirms the robustness of virial / potential energy correlations.

A convenient way to get an overview of a liquid’s  $WU$  thermal equilibrium fluctuations at constant volume is to collect scatter plots for several state points in a common diagram. Figure 3 (top) shows such a plot for the standard LJ liquid. Each state point is represented by one color. As in Fig. 2 the strong correlation is reflected in the fact that the ovals are highly elongated. For each value of the density the ovals form almost straight lines with slope close to 6 (in Ref. 4 it was shown that during and after constant-volume crystallization the system’s scatter plots fall on the extension of the line). The bottom three figures show the correlation coefficient  $R$  (Eq.

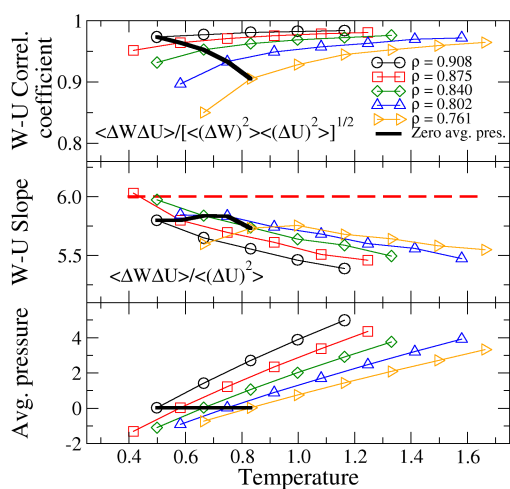
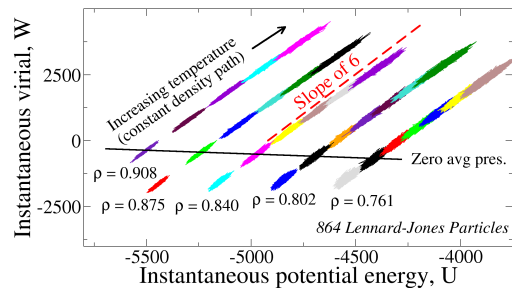


FIG. 3: (a) Scatter plot of the  $WU$  thermal equilibrium fluctuations at constant volume for the standard single-component LJ liquid, and (b) plots of various quantities as functions of temperature for the different densities studied. The full black line marks state points of zero average pressure.

(3)), the “slope”  $\gamma$ , and the average pressure as functions of temperature for the different densities. Clearly, both  $R$  and  $\gamma$  are somewhat state-point dependent. At a given density  $R$  increases with temperature whereas  $\gamma$  decreases; at a given temperature  $R$  increase with increasing density. The thick black lines mark state points of zero average pressure. Note that the density effect of increasing  $R$  “wins” over the temperature effect of decreasing  $R$  upon cooling at constant low pressure. Thus one expects higher correlations upon supercooling a liquid, which is an important observation when it comes to focusing on glass-forming liquids.

How common are strong  $WU$  correlations? In Ref. 3

we reported simulations of 13 different model liquids. All liquids with van-der-Waals type interactions were found to be strongly correlating ( $R > 0.9$ ), whereas models of the two hydrogen-bonding liquids water and methanol were not. Although much remains to be done by means of theory and simulation, it has now been established without reasonable doubt that liquids can be classified into two classes: (i) The class of strongly correlating liquids, which includes the van der Waals and metallic liquids; this liquid class has a number of regularities and simple properties. (b) All remaining liquids – the hydrogen-bonded, the covalently bonded, and (strongly) ionic liquids – which are much more complicated.

### III. CAUSE OF STRONG VIRIAL / POTENTIAL ENERGY CORRELATIONS

Before discussing the consequences of strong virial / potential energy correlations we briefly reflect on the cause of the correlations. The starting point is the well-known fact [7–11] that for any liquid in which the particles (of one or more types) interact with purely repulsive inverse power-law forces,  $v(r) \propto r^{-n}$ , there is 100% correlation between  $W$  and  $U$ :  $W(t) = \gamma U(t)$  where

$$\gamma = \frac{n}{3}. \quad (5)$$

From the values of  $\gamma$  close to 6 observed for the LJ liquid one would expect that, if the LJ liquid somehow corresponds to an IPL liquid, the exponent  $n$  is close to 18. Although at first sight this may seem strange given the  $r^{-6}$  and  $r^{-12}$  terms that enter into the definition of the LJ potential, a potential proportional to  $r^{-18}$  does indeed give a good fit to the repulsive part of the LJ potential (Fig. 4 (a)). The reason that a much larger exponent than 12 is required is that the attractive  $r^{-6}$  term makes the LJ repulsion much steeper than that of the  $r^{-12}$  term alone. Figure 4 (b) shows that both potential energy and virial fluctuations of the LJ liquid are well represented by those of an  $r^{-18}$  IPL potential.

In our first publications on strongly correlating liquids [1, 2] it was suggested that the strong correlations derive from particle close encounters taking the intermolecular distance to values below the LJ potential minimum, at which the IPL potential is a good approximation. It quickly became clear, however, that this is not the full explanation; thus this can explain neither the existence of strong correlations in the crystal (above 99% at low temperatures [4]), nor the existence of correlations at low pressures at which nearest-neighbor interparticle distances fluctuate around the LJ potential’s minimum distance. Also, the original explanation is a single-pair explanation, which would imply that the strong correlations should be present as well in constant pressure ensembles. This contradicts our finding that switching from constant volume to constant pressure reduces  $R$  from values above 0.9 to values around 0.1 [5].

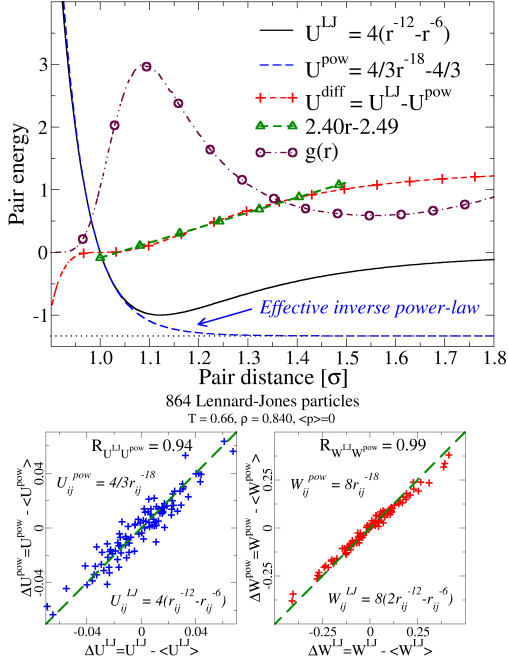


FIG. 4: (a) Approximation of the LJ potential by an effective inverse power law (IPL) potential  $\propto r^{-18}$ . The blue dotted curve marks the IPL potential, which approximates the LJ potential well at small interparticle spacing. The red open circles mark the radial distribution function at a typical low-pressure state point. The difference between the LJ potential and the IPL potential is approximately linear in  $r$ ; this fact forms the basis for the “extended inverse power law” (eIPL) approximation (Eq. (6)) [4, 5]. (b) Two figures demonstrating that the LJ potential and its virial in their thermal equilibrium fluctuations correlate strongly to the same quantities for the  $r^{-18}$  IPL potential.

References 4 and 5 detail the more complete explanation of the cause of strong correlations. The difference between the IPL potential and the LJ potential is plotted in Fig. 4 (a) as the red dashed curve. The green dashed curve is a straight line, which approximates the red dashed curve well around the LJ minimum (i.e., over the entire first peak of the structure factor). Thus over the most important intermolecular distances an “extended” inverse power law potential, eIPL, defined by

$$v_{\text{eIPL}}(r) = Ar^{-n} + B + Cr \quad (6)$$

gives a good approximation to the LJ potential,  $v_{\text{LJ}}(r) \cong v_{\text{eIPL}}(r)$ . It has been shown by simulation that the linear “quark confining” term of the eIPL potential gives a contribution to the total potential energy that fluctuates

little *at constant volume* [4, 5]. Thus as regards *fluctuations*, the pure IPL gives representative results. This explains why the IPL approximation works so well and why the strong correlations disappear when going to constant pressure ensembles. This also explains why several IPL liquid properties are not shared by LJ-type liquids (e.g., the IPL equation of state is generally quite wrong and does not allow for low-pressure stable liquid states, and the IPL free energy and bulk modulus are quite wrong).

While the eIPL approximation explanation of strong  $WU$  correlations for physically realistic cases, there are also strong correlations in the purely repulsive Weeks-Chandler-Andersen [21] version of the KABLJ liquid [16, 22, 23]. The slope  $\gamma$  here varies quite a lot (from 5.0 to 7.5) over the range of densities and temperatures in which  $\gamma$  is fairly constant for the KABLJ liquid. Our simulations show that the strong correlations for the WCA case is a single-particle-pair effect, not the cooperative effect that only applies at constant volume conditions, observed for LJ-type liquids. More work is needed to illuminate the correlation properties of this interesting (but physically unrealistic) potential.

#### IV. ISOMORPHS: CURVES OF INVARIANCE IN THE PHASE DIAGRAM

This section defines isomorphs and summarizes their invariants. As shown in Ref. 6 a liquid has isomorphs if and only if the liquid is strongly correlating. An isomorph is a curve in the phase diagram along which a number of properties are invariant.

For any microscopic configuration  $(\mathbf{r}_1, \dots, \mathbf{r}_N)$  of a thermodynamic state point with density  $\rho$ , the “reduced” coordinates are defined by  $\tilde{\mathbf{r}}_i \equiv \rho^{1/3} \mathbf{r}_i$ . State points (1) and (2) with temperatures  $T_1$  and  $T_2$  and densities  $\rho_1$  and  $\rho_2$  are said to be *isomorphic* [6] if, whenever two microscopic configurations  $(\mathbf{r}_1^{(1)}, \dots, \mathbf{r}_N^{(1)})$  and  $(\mathbf{r}_1^{(2)}, \dots, \mathbf{r}_N^{(2)})$  have identical reduced coordinates, to a good approximation they have proportional configurational NVT Boltzmann probability factors:

$$e^{-U(\mathbf{r}_1^{(1)}, \dots, \mathbf{r}_N^{(1)})/k_B T_1} = C_{12} e^{-U(\mathbf{r}_1^{(2)}, \dots, \mathbf{r}_N^{(2)})/k_B T_2}. \quad (7)$$

The constant  $C_{12}$  here depends only on the state points (1) and (2), not on the microscopic configurations. *Isomorphic curves* in the state diagram are defined as curves for which any two state points are isomorphic. The property of having isomorphs is generally approximate – only IPL liquids have exact isomorphs. For this reason Eq. (7) should be understood as obeyed to a good approximation for the physically relevant configurations, i.e., those that do not have negligible canonical probabilities [6].

Figure 5 illustrates Eq. (7) by checking the logarithm of this equation, where (a) gives simulation data for the KABLJ liquid. We consider a number of configurations of the state point with density and temperature

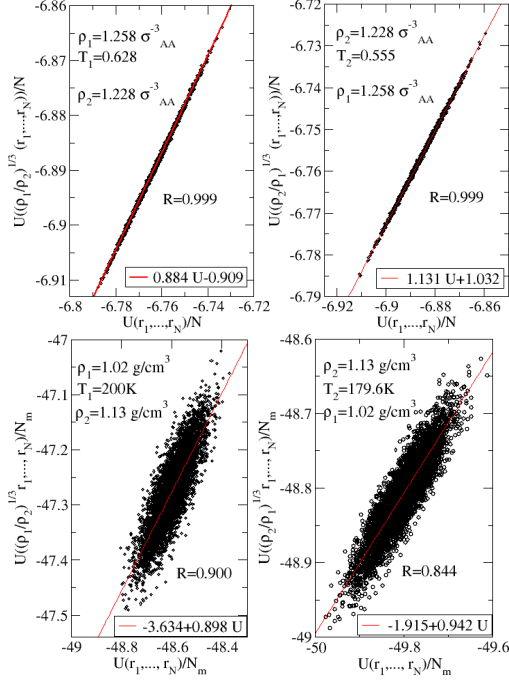


FIG. 5: Direct check of the isomorph condition for the KABLJ liquid (8000 particles), which is strongly correlating (a), and for the SPC water model (5120 molecules), which is not (b). For both liquids the consistency of the isomorph condition is checked by jumping from one to a different density and back. This works well for the KABLJ liquid but not for SPC water; details are given in the text.

$(\rho_1, T_1) = (1.258, 0.628)$  in standard LJ units. For these configurations the total potential energy was evaluated. In order to investigate whether the state point has an isomorph state point at density  $\rho_2 = 1.228$  we scaled the simulated configurations of the first state point to density  $\rho_2$ . For the scaled configurations the potential energies are plotted against the original energies of state point 1 (top figure). According to the isomorph definition Eq. (7) the best fit slope gives the ratio between the temperatures of the isomorph state points; in this way we estimate that  $T_2 = 0.555$ .

The right panel of Fig. 5(a) investigates the consistency of this procedure by reversing it in order to check whether the original temperature  $T_1$  is arrived at. Indeed, when this is done one does find the original temperature to be 0.628. Two things should be noted. The first is the very strong correlation between scaled configurations, as required for having good isomorphs. The second notable fact is that the best fit lines do not pass through (0,0). This shows that the constant  $C_{12}$  of Eq. (7) is not unity, as it would be for an IPL liquid ( $C_{12}$  is

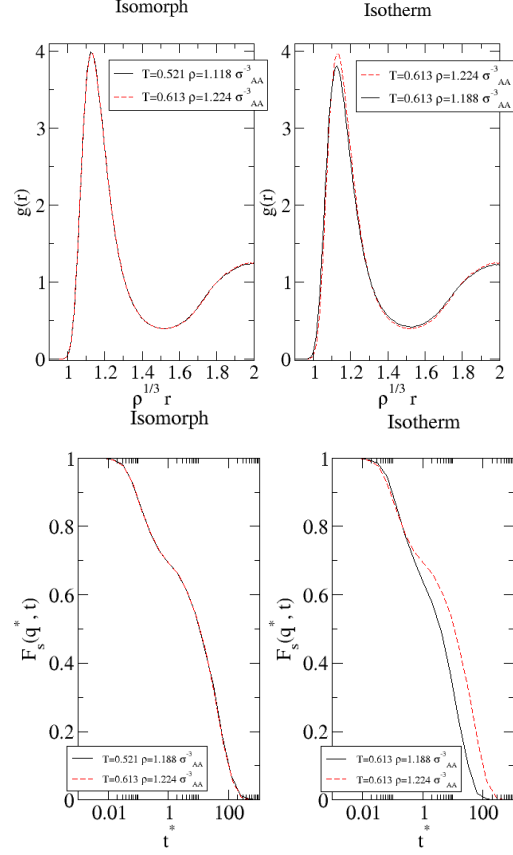


FIG. 6: (a) AA particle radial distribution function of the KABLJ liquid for two isomorph state points (left) and for the same temperature at the two densities (right). The isomorph state points have the same radial distribution functions. (b) The same for the AA incoherent intermediate scattering function at the  $q$ -vector corresponding to the first peak of the radial distribution function. The two isomorph state points have the same dynamics (in reduced units, as used here).

determined by the contribution to the partition function coming from the linear term of the eIPL, and thus  $C_{12}$  reflects the deviation from true IPL behavior).

Figure 5(b) makes this “direct isomorph test” for the non-strongly correlating liquid SPC water, starting from temperature  $T_1 = 200$  K. From the slope of the left panel we find  $T_2 = 179.6$  K. When the reverse jump is performed, however, one does not come back to the initial state point, but to a predicted temperature of 166.36 K. This shows that water does not have isomorphs, consistent with the fact that it is not a strongly correlating liquid.

For the practical identification of an isomorph in the phase diagram the above method may be used. Alternatively, it has been shown [6] that to a good approximation isomorphs are characterized by

$$\frac{\rho^\gamma}{T} = \text{Const.} \quad (8)$$

Here  $\gamma$  is the above discussed ‘‘slope’’ characterized by  $\Delta W(t) \cong \gamma \Delta U(t)$ . As shown in Ref. 6 this quantity may be calculated to a good approximation from equilibrium fluctuations via the expression (giving the least-squared linear-regression best-fit slope of  $WU$  scatter plots, compare Appendix B of Ref. 3)

$$\gamma = \frac{\langle \Delta W \Delta U \rangle}{\langle (\Delta U)^2 \rangle}. \quad (9)$$

Several physical quantities are invariant along a strongly correlating liquid’s isomorphs to a good approximation. These include: 1) Thermodynamic properties like the excess entropy (i.e., in excess of the ideal gas entropy at same density and temperature) and the excess isochoric specific heat, 2) static averages like radial distribution function(s) in reduced coordinates, 3) dynamic quantities like the reduced diffusion constant, viscosity, and heat conductivity, time-autocorrelation functions in properly reduced units, average reduced relaxation times, etc.

Figure 6 shows results of simulations of the KABLIJ liquid at two isomorphic state points (left subfigures) and isothermal state points (right subfigures) of the AA particle radial distribution functions and the AA incoherent intermediate scattering functions, respectively. These figures confirm the prediction that isomorphic state points have identical static distribution functions and identical dynamics.

Since the isochoric specific heat is an isomorph invariant, this quantity should be a function of  $\rho^\gamma/T$  for a strongly correlating liquid. Figure 7 confirms this for the Lewis-Wahnström OTP model consisting of three LJ spheres [24].

The theory further predicts that jumps between two isomorphic state points should take the system instantaneously to equilibrium, because the Boltzmann statistical factors of two isomorphic state points by definition are proportional [6]. More generally, isomorphic state points are equivalent during any aging scheme. We recently showed that the isomorph concept can be used to throw light on the concept of an effective temperature [26]. In particular, the theory implies that for strongly correlating liquids the effective temperature after a jump to a new (low) temperature and a new density, depends only on the new density (Fig. 8(a)). We showed also that this does not apply for the non-strongly correlating monatomic Lennard-Jones Gaussian liquid, confirming the general conjecture that strongly correlating liquids have simpler physics than liquids in general. Figure 8 (b) shows a result confirming the finding of Ref.

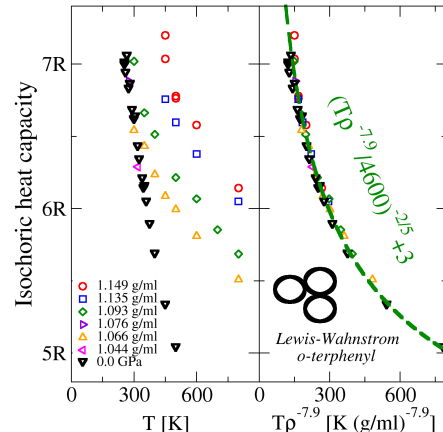


FIG. 7:  $c_V$  per particle for the Lewis-Wahnström model [24] of ortho-terphenyl consisting of three LJ spheres arranged with fixed bond lengths. The left panel shows the raw simulation data, The right panel shows the same data replotted as function of  $\rho^{7.9}/T$  in which the exponent 7.9 was determined from the proportionality between equilibrium virial and potential energy fluctuations [12]. This model follows the Rosenfeld-Tarazona prediction of  $c_V$  varying with temperature as  $T^{-2/5}$  [25].

26 that the effective temperature concept for a strongly correlating liquid makes good sense physically. On the x-axis the inherent state energies of given state points are shown as the system fell out of equilibrium. The arrested phase is characterized by an effective temperature  $T_{\text{eff}}$ , which can be calculated in the standard way from the violation of the fluctuation-dissipation theorem [26]. On the y-axis is shown the inherent energies found from an *equilibrium* simulation with temperature equal to  $T_{\text{eff}}$  for the corresponding arrested phase. The red points give data for the strongly correlating KABLIJ liquid, the green points give data for the non-strongly correlating monatomic Lennard-Jones Gaussian liquid. Clearly, the latter system fell out of equilibrium by freezing into a part of phase space that is not characterized by  $T_{\text{eff}}$ .

## V. THE EQUATION OF STATE OF A STRONGLY CORRELATING LIQUID

This section shows that the Helmholtz free energy for any strongly correlating liquid is of the form

$$F_{\text{ex}}/N = T\psi(Tf(\rho)) + g(\rho). \quad (10)$$

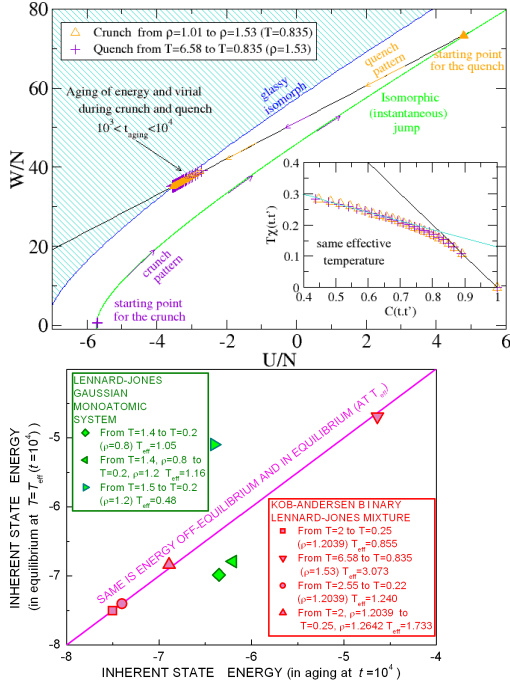


FIG. 8: (a) Virial versus potential energy for the KABLJ liquid during a temperature quench and a crunch [26]. A crunch increases the density and keeps the temperature constant; this is equivalent to first an instantaneous jump along an isomorph (green curve) to the right density followed by a temperature quench (black curve). The inset shows that the crunch and the quench have the same fluctuation-dissipation violation factors, i.e., result in the same effective temperature. (b) Inherent state energies for several state points of the KABLJ liquid as the system falls out of equilibrium and freezes versus the equilibrium inherent state energy at the effective temperature (details are given in Ref. 26).

For simplicity we shall not indicate “excess” quantities explicitly,  $V$  is used as variable instead of the  $\rho$ , and the  $N$  is ignored since it is fixed; thus we shall prove that

$$F = T\psi(Tf(V)) + g(V). \quad (11)$$

Suppose a given strongly correlating liquid’s isomorphs are labeled by the variable  $x$ , i.e., that its isomorphs are curves of constant  $x$  for which  $x = x(T, V)$ . Isomorphs are curves of constant (excess) entropy, as well as curves of constant (excess)  $C_V$  [6]. This means that for some functions  $\phi_1(x)$  and  $\phi_2(x)$  one may write

$$S = \phi_1(x), \quad C_V = \phi_2(x). \quad (12)$$

Since  $C_V = T(\partial S/\partial T)_V = T\phi_1'(x)(\partial x/\partial T)_V$ , if we define  $m(x) \equiv \phi_2(x)/\phi_1'(x)$ , one has  $T(\partial x/\partial T)_V = m(x)$ . Along an isochore this implies that  $dx/m(x) = d\ln T$ . When integrated along the isochore this gives  $h(x) \equiv \int_{x_0}^x dx'/m(x') = \ln T + \alpha(V)$ , implying  $\exp(h(x)) = Tf(V)$  where  $f(V) = \exp(\alpha(V))$ . In other words, lines of constant  $x$  have constant  $Tf(V)$ . Since  $x$  is merely used for labeling the isomorphs, this means that we can redefine  $x$  as follows  $x \equiv Tf(V)$ . Integrating now  $S = \phi_1(x) = -(\partial F/\partial T)_V$  along an isochore gives

$$F = -\int_{T_0}^T \phi_1(x')dT' + g(V) = -\frac{T}{x} \int_{x_0}^x \phi_1(x')dx' + g(V). \quad (13)$$

The integral is some function of  $x$ , and we have thus derived Eq. (11).

As mentioned the slope  $\gamma$  may vary with state point. The equation of state gives information about which variables  $\gamma$  may depend on:

$$S = -\left(\frac{\partial F}{\partial T}\right)_V = -\psi(Tf(V)) - T\psi'(Tf(V))f(V) \quad (14)$$

implies that

$$U = F + TS = -T^2\psi'(Tf(V))f(V) + g(V). \quad (15)$$

We also have

$$\frac{W}{V} = -\left(\frac{\partial F}{\partial V}\right)_T = -T^2\psi'(Tf(V))f'(V) - g'(V). \quad (16)$$

Combining these equations leads to

$$W = V\frac{f'(V)}{f(V)}(U - g(V)) - Vg'(V). \quad (17)$$

Summarizing,

$$W = \gamma(V)U + h(V), \quad (18)$$

where

$$\gamma(V) = \frac{d\ln f}{d\ln V} \quad (19)$$

and

$$h(V) = -g(V)\frac{d\ln(fg)}{d\ln V}. \quad (20)$$

Thus if  $\gamma$  varies with state point, it may only depend on volume [6]. As shown in Ref. 6 this result is consistent with the original experimentally based formulation of the

so-called “density scaling” due to Alba-Simionesco and co-workers [27]. Figure 3(b) shows that  $\gamma$  is not rigorously constant along isochores as predicted by Eq. (18), although it varies only of order 10% when temperature is tripled. This serves to emphasize that isomorphs are only approximate constructs and so are their predicted invariants (only IPL liquids have exact isomorphs).

The equation of state Eq. (18) is of the Mie-Grüneisen form for the excess variables (excess pressure:  $W/V$ , and excess energy:  $U$ ) [28]

$$p_{\text{ex}} = \frac{W}{V} = \frac{\gamma(V)}{V}U + \psi(V). \quad (21)$$

In the Mie-Grüneisen equation of state for solids  $\gamma(V) = -d \ln \omega / d \ln V$  where  $\omega$  is a phonon mode eigenfrequency,  $U$  is the vibrational potential energy, and  $\psi(V)$  relates to the volume derivative of the energy per atom (i.e., of the energy of the force-free configuration about which the vibrational motion occurs). Further discussion of the relation of strong  $WU$  correlations to the Mie-Grüneisen equation of state is given in Ref. 5.

## VI. SOME EXPERIMENTAL PREDICTIONS FOR STRONGLY CORRELATING GLASS-FORMING LIQUIDS

Strongly correlating liquids have a number of since long described properties. For instance, since the melting line in the phase diagram is an isomorph [6], strongly correlating liquids have several invariants along their melting lines, including the radial distribution function and dimensionless transport coefficients. Such regularities have been observed in simulation and experiment; we refer to the reader to Ref. 6 for more details. This section focuses on predictions for highly viscous liquids, for which the strong-correlation property implies several experimental predictions.

### 1. Density scaling

In the last decade, in particular since 2005, many papers appeared dealing with the so-called density scaling, which is the finding that for several glass-forming liquids the relaxation time  $\tau$  at varying pressure and temperature is some function of the quantity  $\rho^\gamma/T$ , in which the exponent  $\gamma$  is an empirical fitting parameter:

$$\tau = F(\rho^\gamma/T). \quad (22)$$

Neither the function  $F$  nor  $\gamma$  are universal. The isomorph theory [6, 12] shows that all strongly correlating glass formers obey density scaling with the exponent  $\gamma$  given by the equilibrium fluctuations at one state point (Eq. (9)) (provided  $\gamma$  is fairly constant over the relevant part of phase space).

This has not yet been tested experimentally, but it is consistent with the finding that density scaling works well for van der Waals liquids [29], but not for hydrogen-bonded liquids [30–33]. Meanwhile, density scaling has been shown to apply in computer simulations of strongly correlating liquids with  $\gamma$  given by Eq. (9) to a good approximation [12, 34].

### 2. Isochronal superposition

Isochronal scaling is the further, fairly recent finding that for varying pressures and temperatures the dielectric loss as a function of frequency depends only on the loss-peak frequency [35, 36]. This is trivial if the liquid obeys time-temperature-pressure superposition (TTPS) in which case nothing changes. But many liquid do not obey TTPS, and for such liquids isochronal superposition is a new and striking regularity that works generally for van der Waals liquids, but rarely for hydrogen-bonding liquids [36]. Since both the relaxation time and the entire relaxation spectrum are isomorph invariants, isochronal superposition must apply for any strongly correlating liquid: If temperature and pressure for two state points are such that their relaxation times are the same, the two points must belong to the same isomorph and thus have same relaxation time spectra for any observables, in particular the dielectric loss as function of frequency should be the same.

### 3. Frequency-dependent viscoelastic response functions

There are eight fundamental complex, frequency-dependent linear thermoviscoelastic response functions like, e.g., the frequency-dependent isochoric or isobaric specific heat, the frequency-dependent isobaric expansion coefficient, and the frequency-dependent adiabatic or isothermal compressibility [37]. Standard linear irreversible thermodynamic arguments, where the Onsager relations play the role of the Maxwell relations of usual thermodynamics, show that there are only three independent frequency-dependent response functions. If moreover stochastic dynamics is assumed as is realistic for highly viscous liquids [38], there are only two independent response functions [39–41]. For strongly correlating liquids the further simplification appears that there is just a single independent response function [1, 37, 42]. Since there are explicit expressions linking the different response functions (depending on the ensemble considered [37]), this can be tested experimentally. Unfortunately it is difficult to measure thermoviscoelastic functions properly; to the best of our knowledge there are yet no reliable data for a complete set of three or more such response functions on any liquid.

### 4. The Prigogine-Defay ratio: Strongly correlating liquids as approximate single-parameter liquids

After many years of little interest the Prigogine-Defay (PD) ratio [43–45] has recently again come into focus in the scientific discussion about glass-forming liquids [37, 46–49]. From a theoretical point of view the PD ratio is poorly defined since it involves extrapolations from the liquid and glass phases to a common temperature [37, 42]. It is possible to overcome this problem by modifying the PD ratio by referring exclusively to linear response experiments; here the traditional difference between liquid and glass responses is replaced by a difference between low- and high-frequency values of the relevant frequency-dependent thermoviscoelastic response function [37]. In this formulation, the property of strong virial / potential energy correlations manifests itself as a PD ratio close to unity. Actually, an extensive compilation of data showed that van der Waals bonded liquids and polymers have PD ratios close to unity [50] – even though as mentioned the traditional PD ratio is poorly defined, there are good reasons to assume that it approximates the rigorously defined “linear” PD ratio.

The theoretical developments of Refs. 2, 4, 37 show that in any reasonable sense of the old concept “single-order-parameter liquid”, strongly correlating liquids are precisely the single-order-parameter liquids. The isomorph concept makes this even more clear: State points along an isomorph have so many properties in common that they are identical from many viewpoints. In the two-dimensional phase diagram this leaves just one parameter to classify which isomorph the state point is on; thus a liquid with (good) isomorphs is an (approximate) single-parameter liquid. Note that this is consistent with the old viewpoint that single-parameter liquids should have unity PD ratio [43–45].

5. *Cause of the relaxation time’s non-Arrhenius temperature dependence: The isomorph filter*

Since the relaxation time  $\tau$  is an isomorph invariant for any strongly correlating liquid, any universally valid theory predicting  $\tau$  to depend on some physical quantity must give  $\tau$  as a function of another isomorph invariant (we do not distinguish between the relaxation time and the reduced relaxation time since their temperature dependencies are virtually identical). This gives rise to an “isomorph filter” [6], showing that several well-known models cannot be generally valid. For instance, the entropy model cannot apply in the form usually used by experimentalists:  $\tau \propto \exp(C/S_{\text{conf}}T)$  where  $C$  is a constant and  $S_{\text{conf}}$  is the configurational entropy; it can only be correct if  $C$  varies with density as  $C \propto \rho^\gamma$ . Likewise, the free volume model does not survive the isomorph filter. If the characteristic volume  $V_c$  of the shoving model (predicting that  $\tau \propto \exp(V_c G_\infty / k_B T)$  [51–53]) varies with density as  $V_c \propto 1/\rho$ , this model is consistent with the iso-

morph filter.

6. *Fictive temperature variations following a temperature jump*

Any jump from equilibrium at some density and temperature to another density and temperature proceeds as if the system first jumped along an isomorph to equilibrium at the final density and then, immediately starting thereafter, jumped to the final temperature (Fig. 8(a)): The first isomorph jump takes the system instantaneously to equilibrium. This property, which applies for all strongly correlating liquids, means that glass-forming van der Waals and metallic liquids are predicted to have simpler aging behavior than, e.g., covalently bonded liquids like ordinary oxide glasses [26].

In traditional glass science the concept of “fictive temperature” is used as a structural characteristic that by definition gives the temperature at which the structure would be in equilibrium [54–59]. For any aging experiment, in glass science one assumes that the fictive temperature adjusts itself monotonically from the initial temperature to the final temperature. Consider, however, a sudden temperature increase applied at ambient pressure. In this case there is first a rapid thermal expansion before any relaxation takes place. This “instantaneous isomorph” takes the system initially to a state with canonical (Boltzmann) probability factors corresponding to a *lower* temperature. In other words, immediately after the temperature up jump the system has a structure which is characteristic of a temperature that is *lower* than the initial temperature. With any reasonable definition of the fictive temperature, this quantity thus initially must decrease during an isobaric positive temperature jump – at least for all strongly correlating liquids.

## VII. SUMMARY

The class of strongly correlating liquids includes the van der Waals and metallic liquids, but excludes the hydrogen-bonded, the covalently bonded, and the (strongly) ionic liquids. Due to their “hidden scale invariance” – the fact that they inhering a number of IPL properties – strongly correlating liquids are simpler than liquids in general. Strongly correlating liquids have isomorphs, curves along which a number of physical properties are invariant when given in properly reduced units. In particular, for glass-forming liquids the property of strong virial / potential energy correlations in the equilibrium fluctuations implies a number of experimental predictions. Some of these, like density scaling and isochronal superposition, are well-established experimental facts for van der Waals liquid and known not apply for hydrogen-bonded liquids. This is consistent with our predictions. Some of the predicted properties have not

yet been tested, for instance that the density scaling exponent can be determined by measuring the linear thermoviscoelastic response functions at a single state point, or that jumps between isomorphic state points take the system instantaneously to equilibrium, no matter how long is the relaxation time of the liquid at the relevant state points. – We hope this paper may inspire to new experiments testing the new predictions.

### Acknowledgments

URP is supported by the Danish Council for Independent Research in Natural Sciences. The centre for viscous liquid dynamics “Glass and Time” is sponsored by the Danish National Research Foundation (DNRF).

- 
- [1] U. R. Pedersen, N. P. Bailey, T. B. Schröder, and J. C. Dyre, *Phys. Rev. Lett.* **100**, 015701 (2008).
- [2] U. R. Pedersen, T. Christensen, T. B. Schröder, and J. C. Dyre, *Phys. Rev. E* **77**, 011201 (2008).
- [3] N. P. Bailey, U. R. Pedersen, N. Gnan, T. B. Schröder, and J. C. Dyre, *J. Chem. Phys.* **129**, 184507 (2008).
- [4] N. P. Bailey, U. R. Pedersen, N. Gnan, T. B. Schröder, and J. C. Dyre, *J. Chem. Phys.* **129**, 184508 (2008).
- [5] T. B. Schröder, N. P. Bailey, U. R. Pedersen, N. Gnan, and J. C. Dyre, *J. Chem. Phys.* **131**, 234503 (2009).
- [6] N. Gnan, T. B. Schröder, U. R. Pedersen, N. P. Bailey, and J. C. Dyre, *J. Chem. Phys.* **131**, 234504 (2009).
- [7] D. Chandler, *Introduction to Modern Statistical Mechanics* (Oxford University Press, 1987).
- [8] L. D. Landau and E. M. Lifshitz, *Statistical Physics, Part I* (Pergamon Press, London, 1980).
- [9] M. P. Allen and D. J. Tildesley, *Computer Simulation of Liquids* (Oxford Science Publications, Oxford, 1987).
- [10] L. E. Reichl, *A Modern Course in Statistical Physics* (Wiley, New York, 1998), 2nd ed.
- [11] J. P. Hansen and J. R. McDonald, *Theory of Simple Liquids*, 3rd edition (Academic, New York, 2005).
- [12] T. B. Schröder, U. R. Pedersen, N. P. Bailey, S. Toxvaerd, and J. C. Dyre, *Phys. Rev. E* **80**, 041502 (2009).
- [13] G. Wahnström, *Phys. Rev. A* **44**, 3752 (1991).
- [14] U. R. Pedersen, T. B. Schröder, J. C. Dyre, and P. Harrowell, *Phys. Rev. Lett.* **104**, 105701 (2010).
- [15] U. R. Pedersen, G. H. Peters, T. B. Schröder, and J. C. Dyre, *J. Phys. Chem. B* **114**, 2124 (2010).
- [16] W. Kob and H. C. Andersen, *Phys. Rev. Lett.* **73**, 1376 (1994).
- [17] S. Toxvaerd, U. R. Pedersen, T. B. Schröder, and J. C. Dyre, *J. Chem. Phys.* **130**, 224501 (2009).
- [18] F. H. Stillinger and T. A. Weber, *Phys. Rev. A* **28**, 2408 (1983).
- [19] M. Goldstein, *J. Chem. Phys.* **51**, 3728 (1969).
- [20] T. B. Schröder, S. Sastry, J. C. Dyre, and S. C. Glotzer, *J. Chem. Phys.* **112**, 9834 (2000).
- [21] J. D. Weeks, D. Chandler, and H. C. Andersen, *J. Chem. Phys.* **54**, 5237 (1971).
- [22] L. Berthier and G. Tarjus, *Phys. Rev. Lett.* **103**, 170601 (2009).
- [23] D. Coslovich and C. M. Roland, *J. Chem. Phys.* **131**, 151103 (2009).
- [24] L. J. Lewis and G. Wahnström, *Phys. Rev. E* **50**, 3865 (1994).
- [25] Y. Rosenfeld and P. Tarazona, *Mol. Phys.* **95**, 141 (1998).
- [26] N. Gnan, C. Maggi, T. B. Schröder, and J. C. Dyre, *Phys. Rev. Lett.* **104**, 125902 (2010).
- [27] C. Alba-Simionesco, A. Caillaux, A. Alegria, and G. Tarjus, *Europhys. Lett.* **68**, 58 (2004).
- [28] M. Born and K. Huang, *Dynamical Theory of Crystal Lattices* (Oxford University Press, Oxford U.K., 1954).
- [29] C. M. Roland, S. Hensel-Bielowka, M. Paluch, and R. Casalini, *Rep. Prog. Phys.* **68**, 1405 (2005).
- [30] A. Grzybowski, K. Grzybowska, J. Ziolo, and M. Paluch, *Phys. Rev. E* **74**, 041503 (2006).
- [31] C. M. Roland, S. Bair, and R. Casalini, *J. Chem. Phys.* **125**, 124508 (2006).
- [32] A. Le Grand, C. Dreyfus, C. Bousquet, and R. M. Pick, *Phys. Rev. E* **75**, 061203 (2007).
- [33] C. M. Roland, R. Casalini, R. Bergman, and J. Mattsson, *Phys. Rev. B* **77**, 012201 (2008).
- [34] D. Coslovich and C. M. Roland, *J. Chem. Phys.* **130**, 014508 (2009).
- [35] C. M. Roland, R. Casalini, and M. Paluch, *Chem. Phys. Lett.* **367**, 259 (2003).
- [36] K. L. Ngai, R. Casalini, S. Capaccioli, M. Paluch, and C. M. Roland, *J. Phys. Chem. B* **109**, 17356 (2005).
- [37] N. L. Ellegaard, T. Christensen, P. V. Christiansen, N. B. Olsen, U. R. Pedersen, T. B. Schröder, and J. C. Dyre, *J. Chem. Phys.* **126**, 074502 (2007).
- [38] T. Gleim, W. Kob, and K. Binder, *Phys. Rev. Lett.* **81**, 4404 (1998).
- [39] J. Meixner and H. G. Reik, *Principien der Thermodynamik und Statistik* (Handbuch der Physik) vol 3, ed. S. Flügge (Springer, Berlin, 1959) p. 413.
- [40] P. K. Gupta and C. T. Moynihan, *J. Chem. Phys.* **65**, 4136 (1976).
- [41] J. I. Berg and A. R. Cooper, *J. Chem. Phys.* **68**, 4481 (1978).
- [42] N. P. Bailey, T. Christensen, B. Jakobsen, K. Niss, N. B. Olsen, U. R. Pedersen, T. B. Schröder, and J. C. Dyre, *J. Phys.: Condens. Matter* **20**, 244113 (2008).
- [43] I. Prigogine and R. Defay, *Chemical Thermodynamics* (London, Longman, 1954).
- [44] R. O. Davies and G. O. Jones, *Proc. Roy. Soc.* **217**, 26 (1952).
- [45] R. O. Davies and G. O. Jones, *Adv. Phys.* **2**, 370 (1953).
- [46] Th. M. Nieuwenhuizen, *Phys. Rev. Lett.* **79**, 1317 (1997).
- [47] J. W. P. Schmelzer and I. Gutzow, *J. Chem. Phys.* **125**, 184511 (2006).
- [48] L. Wondraczek and H. Behrens, *J. Chem. Phys.* **127**, 154503 (2007).
- [49] R. M. Pick, *J. Chem. Phys.* **129**, 124115 (2008).
- [50] U. R. Pedersen, Ph. D. thesis, Roskilde University (2009) [available at <http://www.urp.dk/phdthesis.htm>].
- [51] J. C. Dyre, N. B. Olsen, and T. Christensen, *Phys. Rev. B* **53**, 2171 (1996).
- [52] J. C. Dyre, *Rev. Mod. Phys.* **78**, 953 (2006).
- [53] D. H. Torchinsky, J. A. Johnson, and K. A. Nelson, *J. Chem. Phys.* **130**, 064502 (2009).

- [54] A. J. Kovacs, Fortschr. Hochpoly.-Forsch. **3**, 394 (1963).
- [55] C. T. Moynihan *et al.*, Ann. NY Acad. Sci. **279**, 15 (1976).
- [56] O. V. Mazurin, J. Non-Cryst. Solids **25**, 129 (1977).
- [57] L. C. E. Struik, *Physical Aging in Amorphous Polymers and Other Materials* (Elsevier, Amsterdam, 1978).
- [58] G. B. McKenna, J. Res. Natl. Inst. Stand. Technol. **99**, 169 (1994).
- [59] I. M. Hodge, Science **267**, 1945 (1995).



## Aging effects manifested in the potential energy landscape of a model glass former

Christian Rehwald<sup>1</sup>, Nicoletta Gnan<sup>2</sup>, Andreas Heuer<sup>1</sup>, Thomas Schröder<sup>2</sup>, Jeppe C. Dyre<sup>2</sup> and Gregor Diezemann<sup>3</sup>

<sup>1</sup>*Institut für Physikalische Chemie, Universität Münster, Corrensstr. 30, 48149 Münster, FRG*

<sup>2</sup>*Department of Sciences, DNRF Centre 'Glass and Time', IMFUFA, Roskilde University, P.O. Box 260, DK-4000 Roskilde, Denmark*

<sup>3</sup>*Institut für Physikalische Chemie, Universität Mainz, Welderweg 11, 55099 Mainz, FRG*

*We present molecular dynamics simulations of a model glass-forming liquid (the binary Kob-Anderson Lennard-Jones model) and consider the distributions of inherent energies and metabasins during aging. In addition to the typical protocol of performing a temperature jump from a high temperature to a low destination temperature, we consider the temporal evolution of the distributions after an 'up-jump', i.e. from a low to a high temperature. In this case the distribution of megabasin energies exhibits a transient two-peak structure. Our results can qualitatively be rationalized in terms of a trap model with a Gaussian distribution of trap energies. The analysis is performed for different system sizes. A detailed comparison with the trap model is possible only for a small system because of major averaging effects for larger systems.*

### I. Introduction

The primary relaxation of supercooled liquids still poses challenging questions regarding its mechanism, and a detailed theoretical understanding of the often dramatic temperature dependence of the relaxation time is still lacking. In the past decade it has been shown that the  $\alpha$ -relaxation has to be viewed as dynamically heterogeneous[1, 2].

The present paper focuses on one particular aspect of the primary relaxation, namely the response of the system to an abrupt change in temperature. The out-of-equilibrium dynamics of glassy systems has been studied for a long time, for a review see[3]. Many investigations were devoted to the study of violations of the fluctuation-dissipation theorem[4]. In particular, the question regarding a meaningful definition of an effective temperature remains to be answered as there are still conflicting results (for a recent investigation see[5] and the literature therein). Apart from the theoretically challenging possibility of a description of the off-equilibrium dynamics in terms of an effective thermodynamics, the aging behavior of glassy systems is of huge interest, both theoretically and for practical reasons. Accordingly, it has been studied for a long time. In particular, the rotational and translational dynamics has been investigated with the result that the aging properties of glass-forming liquids are determined by the primary relaxation, cf. ref.[6, 7], albeit there are still some discussions about the detailed analysis of the corresponding data.

In addition to these investigations of the aging behavior, also the interesting question regarding

the detailed interrelation of the aging properties of supercooled liquids and the nature of the dynamic heterogeneities is yet to be answered. In the simplest conceivable picture the heterogeneous dynamics, as well as the aging properties, are governed by a distribution of activation energies. Various theories and models of the glass transition deal with such distributions in one way or the other. A detailed analysis of the temperature- and time-dependent properties of this distribution should be helpful in discriminating among different models.

If computer simulations on models for viscous liquids are considered, one has to face the problem of identifying a relevant distribution of activation energies. Even though this point does not appear to be resolved completely, there seems to be growing evidence that the inherent structure (IS) energies or - in a more detailed picture - the metabasin (MB) energies are relevant for the determination of the activation energies[8]. This view partly emerges from the comparison of the results of molecular dynamics simulations with the predictions of a simple trap model with a Gaussian density of states[9]. This Gaussian trap model qualitatively captures some relevant features of the energy landscape of simulated glassy systems[8, 9, 10]. The comparison can be made more quantitative if a slightly extended version of the trap model is employed in the analysis[11]. From this analysis it appears that the IS- or MB-energies are intimately related to the relevant activation energies.

The aging behavior of the distribution of IS-energies of the Kob-Andersen binary mixture Lennard Jones (KABLJ) model[12, 13] was investigated by Saika-Vovoid and Sciortino[14]. These authors found that after a quench from a high temperature to some low temperature the mean SI-energy drops continuously and monotonously from its initial to the final value. Furthermore, the width of the distribution of IS-energies decreases and then increases again as a function of the time that has elapsed after the quench. An analysis of the aging behavior of the distribution of the energies in the Gaussian trap model shows a very similar behavior, cf. ref.[9, 15]. Also the single-particle dynamics of a simulated glass-forming liquid immediately after a temperature jump are fully compatible with the predictions of the Gaussian trap model[16].

For a more quantitative analysis of the dynamics of simulated supercooled liquids the use of MBs rather than ISs has proven advantageous. The reason is that IS trajectories are dominated by a large and temperature-dependent fraction of correlated forward-backward jumps. In contrast, the MB trajectories can be interpreted in terms of a random-walk in configuration space with a temperature independent jump-length[8, 17]. The complexity of the dynamics, giving rise, e.g., to the existence of dynamic heterogeneities, is fully reflected by the broad waiting time distribution. This picture of a broad distribution of independent random jumps among different configurations presents the physical basis of the trap model.

In the present paper we study the temporal evolution of the IS-energies and the MB-energies of the KABLJ[12, 13] system after temperature jumps. For a jump from a high to a low temperature, our results closely resemble those obtained by Saika-Vovoid and Sciortino[14]. Motivated by the finding that for the trap model after an 'up-jump' in temperature the energy-distribution exhibits a two-peak structure[9], we show that this feature is also found in MD-simulations. We discuss our findings with particular emphasis on their relevance to possible experimental realizations.

After a brief review of the aging-properties of the energy distributions in the Gaussian trap model[9, 18], we will discuss the results of a temperature jump. Guided by the fact noted above

that a trap model can - at least qualitatively - be used to describe the relaxation of the MB-energies of simulated supercooled liquids, we will study the behavior of the IS- and MB-energies of the Kob-Andersen KABLJ liquid.

## II. Energy relaxation in the Gaussian trap model

In the trap model one considers a collection of traps, to be termed 'states' in the following, characterized by their energies. The temporal evolution of the population of these states is determined by simple kinetic rules. After the activated transition out of a given state, the destination trap/state is chosen at random, i.e. according to the prescribed density of states (DOS)  $\rho(\epsilon)$  of trap energies  $\epsilon$ . The escape rate for the transitions out of the state characterized by  $\epsilon$  is given by the Arrhenius law  $\kappa_T(\epsilon) = \kappa_\infty e^{\beta\epsilon}$  where  $\kappa_\infty$  denotes the attempt frequency and  $\beta = (k_B T)^{-1}$  with the Boltzmann constant  $k_B$ . The master equation for the populations is given in the Appendix for the convenience of the reader.

Different realizations of the trap model have been considered in the past. Often, one considers the model with an exponential distribution of trap energies[19]. This model shows a phase transition into a low-temperature phase where equilibrium can never be reached. However, when discussing canonical glasses one usually deals with systems that reach equilibrium in the long run as in the Gaussian trap model[8, 9, 10, 15].

In the following, we briefly review the results that one obtains for this model in order to motivate the MD-simulations presented afterwards.

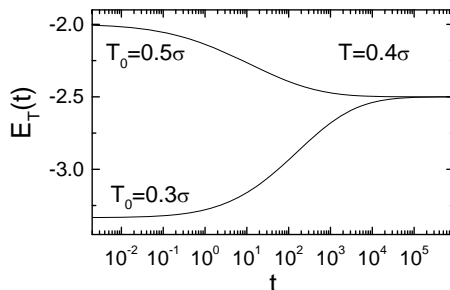


Figure 1: Temporal evolution of the mean energy  $E_T(t)$  for a jump from  $T_0 = 0.3\sigma$  to  $T = 0.4\sigma$  and for  $T_0 = 0.5\sigma$  to  $T = 0.4\sigma$ .  $E_T(t)$  is calculated according to eq.(A.6) using the numerical solution of the master equation, eq.(A.1). The time is measured in units of the attempt frequency  $\kappa_\infty$ .

We start with considering the relaxation of the energy after a sudden change from some initial temperature  $T_0$  to a destination temperature  $T$ . In Fig.1 we show results for both, a quench and an up-jump. It is obvious that the value of the mean energy,  $E_T(t)$ , changes monotonously from  $E_{T_0}^{\text{eq}} = -\beta_0\sigma^2$  to  $E_T^{\text{eq}} = -\beta\sigma^2$  in both cases. If one compares the behavior for the quench and the up-jump, there is an asymmetry in the relaxation[20]. This asymmetry reflects the fact that linear-response theory cannot be applied for the interpretation of such large temperature jumps

(in linear-response, the curves are symmetric). The relaxation of the energy looks very similar to the curves shown in Fig.1 if other initial and final temperatures are considered.

In the present context the temporal evolution of the distributions of the energies,  $p_T(\epsilon, t)$ , is more important than its moments. Therefore, in the following we will discuss the behavior of  $p_T(\epsilon, t)$  after a temperature jump, cf.[15]. In Fig.2 we show the evolution of  $p_T(\epsilon, t)$  after a quench starting from two different initial temperatures  $T_0$ . It is evident immediately that the Gaussian is centered at  $E_T(t = 0) = -\beta_0\sigma^2$  directly after the quench and at  $E_T(t = \infty) = -\beta\sigma^2$  after the system has relaxed to the final temperature. The full lines correspond to the numerical solution of the master equation, while the dotted lines are based on the following approximation. Neglecting

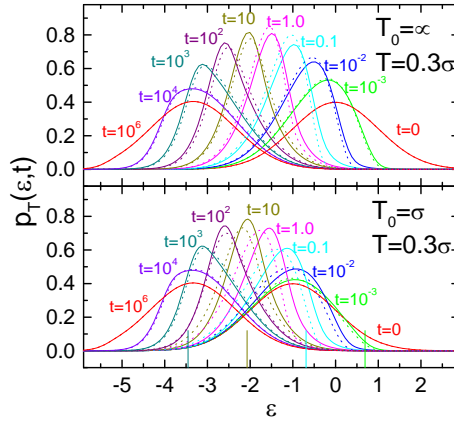


Figure 2: Trap populations  $p_T(\epsilon, t)$  for different times (measured in units of the attempt frequency  $\kappa_\infty$ ) after a quench from  $T_0 = \infty$  (upper panel) and  $T_0 = \sigma$  (lower panel) to  $T = 0.3\sigma$ . The full lines represent the numerical solution of the master equation, eq.(A.1). The dotted lines are obtained from the approximative solution given in eq.(1) and the vertical lines in the lower panel denote the demarcation energy  $\epsilon_D$  for  $t = 10^{-3}, 10^{-1}, 10^1, 10^3$  (from right to left)

any correlations in the energies of the initial and final trap of a transitions, one can assume that the initial distribution  $p_{T_0}^{\text{eq}}$  diminishes due to escape-transitions according to  $p_{T_0}^{\text{eq}}(\epsilon)e^{-\kappa_T(\epsilon)t}$ . Similarly, the distribution at the destination temperature,  $p_T^{\text{eq}}$ , is built up independently according to  $p_T^{\text{eq}}(\epsilon)(1 - e^{-\kappa_T(\epsilon)t})$ . These considerations allow us to write:

$$p_T^{\text{ap.}}(\epsilon, t) = N(t)^{-1} [p_{T_0}^{\text{eq}}(\epsilon)e^{-\kappa_T(\epsilon)t} + p_T^{\text{eq}}(\epsilon)(1 - e^{-\kappa_T(\epsilon)t})] \quad (1)$$

where

$$N(t) = 1 + \int d\epsilon [p_{T_0}^{\text{eq}}(\epsilon) - p_T^{\text{eq}}(\epsilon)] e^{-\kappa_T(\epsilon)t}$$

is a constant that ensures the normalization of  $p_T^{\text{ap.}}(\epsilon, t)$ . Actually, one can show that eq.(1) follows from the long-time limit of the solution of the master equation, eq.(A.1). It is intriguing how well this simple approximation represents the numerical solution of the master equation. The quality of the approximation (1) is similar for other  $T_0$  and  $T$ . Eq.(1) can be further interpreted in the following way. At a given time the states can be divided into two classes, those that have

undergone an escape-transition, i.e. those that have relaxed, and those that are still frozen. The latter are low-energy states with  $e^{-\kappa_T(\epsilon)t} \sim 1$  and for the former one has  $e^{-\kappa_T(\epsilon)t} \sim 0$ . This distinction between frozen and relaxed states can be quantified via the definition of the so-called demarcation energy via  $\kappa_T(\epsilon_D) = 1/t$ , i.e.

$$\epsilon_D(t) = -\beta^{-1} \ln(\kappa_\infty t) \quad (2)$$

The meaning of  $\epsilon_D$  is that, due to the activated nature of the dynamics, most states with  $\epsilon < \epsilon_D$  are frozen at time  $t$ , while those with  $\epsilon > \epsilon_D$  essentially have reached equilibrium[9, 21, 22]. Eq.(1) also allows a simple interpretation of the temporal evolution of the moments of the distribution. For a given time states with  $\epsilon < \epsilon_D$  are still represented by  $p_{T_0}^{\text{eq}}(\epsilon)$  while those with larger energy have already relaxed and are represented already by  $p_T^{\text{eq}}(\epsilon)$ . The different weights of the initial and final Gaussian give rise to a narrowing of the distribution at intermediate times, as observed in the quoted simulations[14].

The situation changes completely if instead of a quench from a high to a low temperature the opposite case of an up-jump from  $T_0 < T$  is considered, cf. Fig.3. In this case,  $p_{T_0}^{\text{eq}}(\epsilon)$  is centered

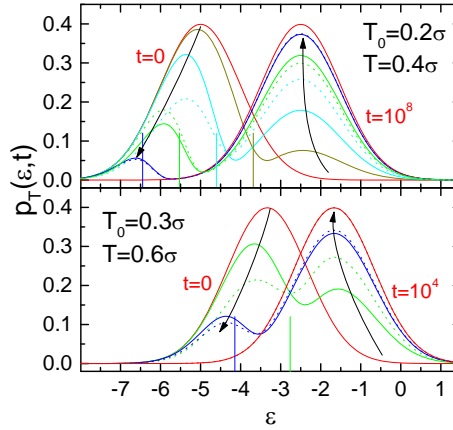


Figure 3:  $p_T(\epsilon, t)$  for different times after a temperature up-jump from  $T_0 = 0.2\sigma$  to  $T = 0.4\sigma$  (upper panel;  $t = 0, 10^2, 10^3, 10^4, 10^5, 10^8$ s) and from  $T_0 = 0.3\sigma$  to  $T = 0.6\sigma$  (lower panel;  $t = 0, 1, 10, 10^4$ s). The solid lines are the numerical solution of the master equation and the dotted lines represent the approximation (1). The vertical lines show the demarcation energies for the various times. Note that with increasing time  $\epsilon_D$  decreases meaning that less states are frozen for longer times.

at lower energy than  $p_T^{\text{eq}}(\epsilon)$  which means that it is the slowly relaxing part of the distribution that dominates the dynamics. Put differently, the high energy tail of  $p_{T_0}^{\text{eq}}(\epsilon)$  relaxes quickly and thus 'moves' to higher energies, while the low energy part is trapped for a very long time. Thus, one has a distribution that can be viewed as a weighted superposition of the two involved equilibrium distributions, separated roughly by the demarcation energy, cf. the vertical lines in Fig.3. This scenario gives rise to a two-peak structure, cf. Fig.3, that was discussed earlier by one

of us[9]. The dotted lines are the approximate solution, eq.(1). It is evident that the quality of the approximation increases with increasing time. Also the behavior of the moments of  $p_T(\epsilon, t)$  for an up-jump is evident from Fig.3. The two-peak behavior already indicates that here the second moment will show a maximum at some intermediate time.

In Fig.4 we show the variance of  $p_T(\epsilon, t)$  for both, various quenches and up-jumps. We scaled the time by the relaxation time  $\tau_{\text{rel}}$ . This relaxation time is determined from the temporal evolution

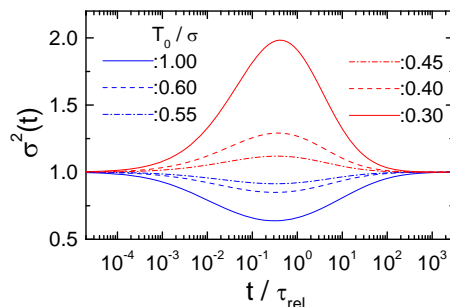


Figure 4:  $\sigma^2(t)$  for a temperature jump with different initial temperatures  $T_0$  to  $T = 0.5\sigma$  versus time scaled by the temperature-dependent relaxation time  $\tau_{\text{rel}}$ ; quench:  $T_0/\sigma = 1.0, 0.6, 0.55$  (blue) and up-jump:  $T_0/\sigma = 0.3, 0.4, 0.45$  (red)

of  $E_T(t)$ , cf. Fig.1, as the  $1/e$ -decay time of the normalized energy-relaxation function  $(E_T(t) - E_T^{\text{eq}})/(E_{T_0}^{\text{eq}} - E_T^{\text{eq}})$  and roughly divides the energies into those that have and those that have not relaxed until  $t = \tau_{\text{rel}}$ . Accordingly, the maximum/minimum width is found for  $t \sim \tau_{\text{rel}}$  (more precisely around  $t/\tau_{\text{rel}} \sim 0.3 \dots 0.4$ ).

Given the fact that the equilibrium behavior of simulated glass-forming liquids and the aging dynamics following a quench can qualitatively be understood in terms of a Gaussian trap model we anticipate that it should be possible to observe the two-peak structure in the distributions following an up-jump also in simulations.

### III. Energy relaxation in the KABLJ liquid

We now discuss the results of molecular dynamics simulations of the KABLJ liquid[12, 13]. We start with a jump from high to low temperatures very similar to what has already been considered by Saika-Vovoid and Sciortino[14], and afterwards we will show that one indeed can observe a double-peak structure when a jump from a low to a high temperature is considered.

The simulations of what will be called the *large system* have been carried out on a KABLJ system of 1000 particles. All simulation were performed in the NVT ensemble, and time and temperatures are in reduced units (the density is 1.204). Temperature was controlled using a Nose-Hoover thermostat and a time step of 0.001 was used. The distributions of the inherent state energies were obtained by averaging over 1500 independent runs (each of length 4000) both for the up-jumps and the quenches.

In order to investigate the distributions of metabasin (MB) energies, we additionally performed simulations on a *small system*. We use a KABLJ system of 65 particles (and a reduced cut-off radius  $r_c = 1.8$ ) in the NVT ensemble at a density of 1.2. We determined the distribution of MB-energies as described in detail in ref.[23]. For the up-jump we used 4600 trajectories of length 10000 and for the quench we used 3000 trajectories of length 70000. The LJ-system with the shorter cutoff has slightly different properties compared to using the larger cutoff. However, the modifications are small ( $T_c$ , e.g., is roughly modified by 2%). Since we do not compare absolute values of energies, this modification is of little relevance for the present work.

We have checked[10] that the distribution of MB and IS is nearly identical in the temperature range of interest for this work. This is not surprising, because during the stay in a given MB the system is mainly residing in the IS with the lowest energy. Thus, considerable differences between IS and MB only come into play when analyzing the dynamics (see below).

## 1. Large system

In Fig.5 we present results from simulations of a quench from  $T_0 = 0.6$  to  $T = 0.45$ . The results

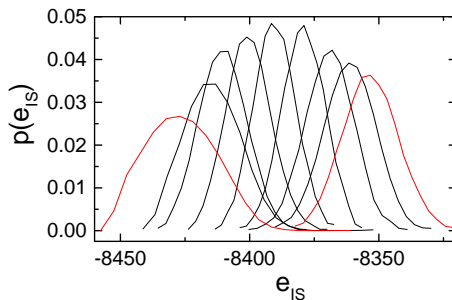


Figure 5:  $p(e_{IS})$  or the large system for different waiting times,  $t=9.6, 27.0, 76.8, 614.4, 868.8, 1737.6, 3475.8$  from right to left after a quench from  $T_0 = 0.6$  to  $T = 0.45$  (black lines). The red lines are the equilibrium distributions at the initial and the final temperature.

are very similar to those of Saika-Vovoid and Sciortino[14]. The distribution moves from high energies at high temperature to lower energies as a function of the time elapsed after the quench, and the width of the distribution diminishes for intermediate times. The overall behavior is very similar to what is observed in the trap model, cf. Fig.2, with the difference that the widths of the equilibrium distributions are temperature-dependent as opposed to the situation in the Gaussian trap model.

The moments of the distribution are shown in Fig.6. In particular the monotonous decay of the mean and the drop in the variance for intermediate times are clearly displayed.

We have seen that the simulation data for a quench can qualitatively be understood in terms of a Gaussian trap model. From this model we expect a bimodal distribution to show up for intermediate waiting times, reflecting the different relaxation behavior of states below and above the demarcation energy if an up-jump in temperature is considered instead of a quench.

In Fig.7 we present  $p(e_{IS})$  for an up-jump from  $T_0 = 0.45$  to  $T = 0.6$ . Even though one

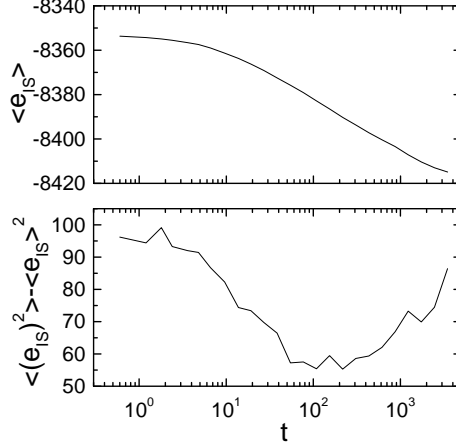


Figure 6: First and second moment of  $p(e_{IS})$  for the large system as obtained from MD simulations after a quench from  $T_0 = 0.6$  to  $T = 0.45$ , for details see the main text.

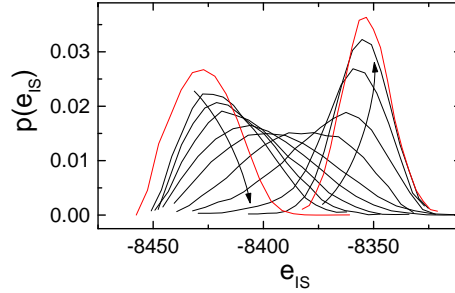


Figure 7:  $p(e_{IS})$  for the large system for different waiting times,  $t=27.0, 38.4, 54.6, 76.8, 108.6, 153.6, 217.2, 307.2, 434.2$  (black lines, in the order indicated by the arrows) after a temperature jump from  $T_0 = 0.45$  to  $T = 0.6$ . The red lines correspond to the equilibrium distributions at the respective temperatures.

cannot observe a bimodal distribution it is obvious that the distribution broadens tremendously for intermediate times, cf. the curves for  $t=108.5$  and  $t=153.6$ . Low-energy states relax extremely slowly, while states with higher IS-energy move towards the equilibrium distribution at the higher temperature much more rapidly. This means that for short times only a few (high-energy) states are relaxed, while for long times there are still some low-energy states that are not yet relaxed.

The corresponding moments are shown in Fig.8. These curves nicely reflect the fact that the variance reaches its maximum value roughly when the time elapsed after the up-jump coincides with the relaxation time of  $E_T(t)$ , indicating that about half of the inherent structures are relaxed at this time while the others still are frozen at their low-temperature values. These simulations indicate that the predictions of the trap model might be helpful in the interpretation not only of the equilibrium properties but also the aging behavior of the system studied. However, for the up-jump we do not observe a two-peak structure of the distributions of IS-energies. The reason

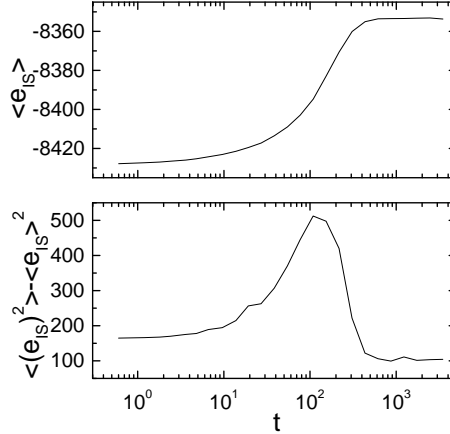


Figure 8: First and second moments of  $p(e_{IS})$  for the large system for an up-jump from  $T_0 = 0.45$  to  $T = 0.6$

will be outlined below.

## 2. Small system

In the following we present simulation results for the small systems. The system size of 65 particles is small enough to allow the identification of the MBs and we will concentrate on the temporal evolution of the distribution of MB-energies,  $p(e_{MB})$ , after sudden temperature changes.

In order to compare the behavior of the IS-energies to the corresponding behavior of the MB-energies, we show the evolution of  $p(e_{MB})$  for the same quench from  $T_0 = 0.6$  to  $T = 0.45$  for the small system in Fig.9. Apart from the smaller values of the MB-energies the overall features

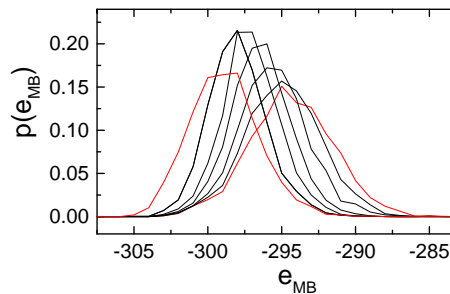


Figure 9:  $p(e_{MB})$  of the small system for different waiting times,  $t=4, 32, 152, 392, 1992, 15992$  (from right to left) after a quench from  $T_0 = 0.6$  to  $T = 0.45$  (black lines). Red lines:  $p_T^{\text{eq}}(e_{MB})$

like the shift of the distribution and the narrowing at intermediate times are very similar to the observations made for the large system in Fig.5. In Fig.10 we plot the moments of the distribution as a function of the waiting time. This plot shows that also the moments of  $p(e_{MB})$  behave very much in the same way as those of the distributions of the IS-energies in the large system. The

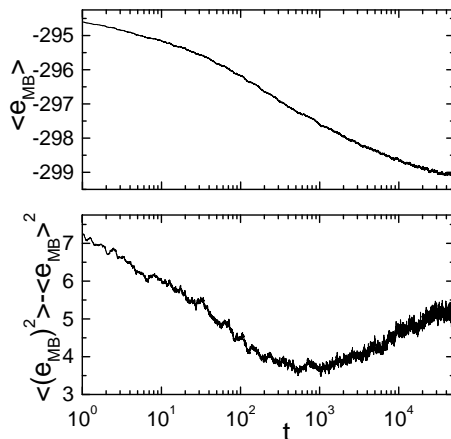


Figure 10: First and second moment of  $p(e_{MB})$  for the small for a quench from  $T_0 = 0.6$  to  $T = 0.45$ .

most prominent differences are the better statistics and the increase in the overall relaxation time of roughly one decade in case of the small system.

We have seen that the evolution of both, the IS-energies or the MB-energies again qualitatively follow the predictions of the trap model with a Gaussian DOS. Thus, the dependence of the moments on the waiting time can be understood in terms of the demarcation energy, which separates low-energy states that up to the given time are frozen from high-energy states, which at the same time have reached the new equilibrium already.

Next, we consider the same up-jump from  $T_0 = 0.45$  to  $T = 0.6$  as for the large system. We present the distributions  $p(e_{MB})$  for various times after the up-jump in Fig.11. In this case we

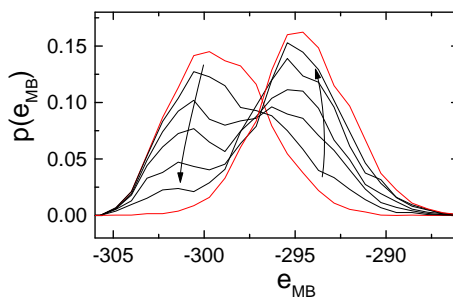


Figure 11:  $p(e_{MB})$  for the small system for different waiting times,  $t=115, 240, 390, 740, 1490$  after an up-jump from  $T_0 = 0.45$  to  $T = 0.6$  (black lines, in the order indicated by the arrows). Red lines:  $p_T^{\text{eq}}(e_{MB})$

really observe a two-peak structure in the distribution for intermediate waiting times. This effect is most prominent for times on the order of the relaxation time, i.e. on the order of  $300 \dots 400$ , cf. Fig.12.

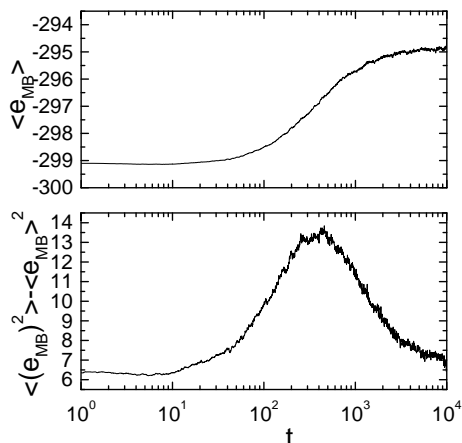


Figure 12: First and second moment of  $p(e_{IS})$  for an up-jump from  $T_0 = 0.45$  to  $T = 0.6$

One may wonder why the small system displays a two-peak structure but not the large system. To clarify this point we compare the case of a single trap model ( $N=1$ ) with the case of two superimposed trap models ( $N=2$ ), see Fig.13. To render the superposition more realistic we have

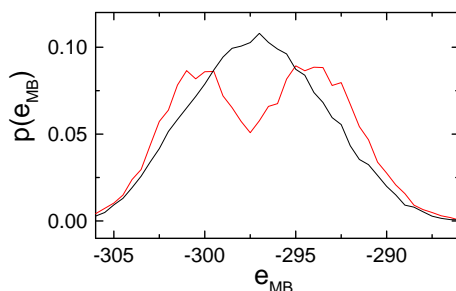


Figure 13:  $p(e)$  for the extended trap model with  $N = 1$  (red line) and  $N = 2$  (black line) small systems after a temperatur jump from  $T = 0.45$  to  $T = 0.6$ . The waiting times correspond to the time when the variance reaches its maximum value.

adopted the dynamic coupling as described in ref.[11]. As shown in that reference, a LJ system of 65 particles should indeed be considered as a superposition of 2-3 elementary trap models, reflecting the fact that the elementary relaxation processes, i.e. MB transitions, are on average localized to 20-30 particles. Interestingly, explicit simulations of the  $N=2$  case does not yield a two-peak structure, cf. Fig.13. Thus, it is not at all surprising that also the much larger system discussed above does not display this feature. One should rather wonder why the real 65-particle system displays a two-peak structure. Note that it is less pronounced than for the  $N=1$  case shown in Fig.13. A possible reason is as follows. The degree of localization of the MB transition can vary from case to case. Thus, for some transitions the total system may be described as one elementary system, i.e.  $N=1$ , whereas in other cases larger values of  $N$  may characterize the

present configuration. The average over the different situations, i.e. an average over a two-peak and a single-peak distribution, can yield a two-peak distribution albeit with a less pronounced separation between both peaks. Stated differently, we interpret the emergence of the two peaks as a consequence of the presence of different spatial extensions for different MB transitions. From this observation we conclude that for a small system as considered here couplings among different 'regions' are of minor relevance only and that a description of the aging dynamics in terms of a Gaussian trap model captures the most important dynamic features.

A more quantitative comparison with the trap model is possible by comparing the time scale of energy equilibration  $\tau_{\text{eq}}$  after a temperature jump with the time scale to escape an IS or an MB ( $\tau_{IS}$  or  $\tau_{MB}$ , respectively) in their dependence of the initial energy. For the trap model a single jump yields full decorrelation of the energy. As shown in Fig.14 for the whole energy range one roughly has  $\tau_{\text{eq}}(e) \approx 2\tau_{MB}(e)$ . At first glance this result contradicts the trap model predictions, but can qualitatively be explained in the following way. As explained in ref.[11] the reason for the remaining deviations may be related to the fact that even the small system with just 65 particles has to be regarded as a superposition of two subsystems. Thus, a single relaxation process does not necessarily decorrelate the whole system. As a result one gets  $\tau_{\text{eq}} > \tau_{MB}(e)$ . Actually, the more quantitative analysis in ref.[11] shows that roughly 10 MB transitions are necessary for energy equilibration. How does this agree with the behavior of the relaxation times shown in Fig.14? For low initial energies the energy attained after a single transition on average is already significantly higher than the starting value. Thus, the second jump occurs much faster than the initial one. The same behavior is found for the following MB transitions and as a consequence the resulting MB transitions take place on a time scale  $\tau_{MB}(e)$ , giving rise to  $\tau_{\text{eq}}/\tau_{MB}(e) \approx 2$ . For  $e > -296$ , however, this statement is no longer true because the first jump already is relatively fast. Here, the complete factor of roughly 10 shows up in the ratio  $\tau_{\text{eq}}/\tau_{MB}(e)$ .

In contrast, comparison of  $\tau_{\text{eq}}(e)$  with  $\tau_{IS}(e)$  clearly shows that for low energies the deviations are as large as an order of magnitude. This observation reflects the fact that at low temperatures and low IS energies the system displays many forward-backward processes between different IS which do not contribute to the energy relaxation. It is for this reason that the MB trajectories are better suited for a direct comparison with the trap model.

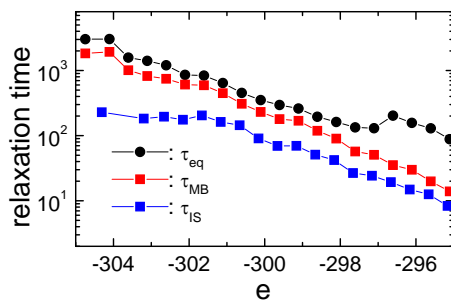


Figure 14: Time scale of energy relaxations  $\tau_{\text{eq}}$  vs. escape time  $\tau_{IS}$  and  $\tau_{MB}$  after a temperature jump from  $T = 0.45$  to  $T = 0.6$ ; see text for the definition of the various relaxation times.

## IV. Conclusions

We presented molecular dynamics simulations of the temporal evolution of the distribution of inherent structure energies (of a large system) and the metabasin energies (of a small system) after sudden temperature changes in a model glass-forming liquid. While simulations for a quench from a high temperature to some low temperature exist already, we present new results for an up-jump from low to high temperature.

Both sets of results can qualitatively be understood in terms of the relaxation properties of the trap energies in a Gaussian trap model. In particular, the concept of a demarcation energy separating frozen states (lower energies) from states that are already relaxed (higher energies) is extremely helpful in rationalizing the data. It allows to explain the behavior of the second moment in rather general terms.

Our most important result is that for an up-jump we find a two-peak structure in the distribution of MB-energies in case of the small system for times on the order of the relaxation time. This finding shows that the concept of the demarcation energy appears to qualitatively reflect the real behavior of the simulated system. When the IS-energies in a large system are considered, one already sees the trend towards this bimodality in terms of extremely broad distributions. As discussed above, the fact that a large system is to be viewed as consisting of a number of (weakly interacting) sub-systems is responsible for the smearing of the effect that is so nicely visible in the small system. This averaging of course is to be expected on the basis of the central limit theorem.

Of course, the trap model is a very simplistic mean-field model of the relaxation in glassy systems. From our simulation results, however, we can speculate that a behavior similar to the one observed here might be rather generic for any Markovian model of collective energy jumps in systems with many degrees of freedom whenever a random walk description of the dynamics appears appropriate, i.e. if the correlations among the different energies decay fast. Actually, recently the behavior of a large system has been described as a superposition of dynamically coupled elementary systems[24], i.e. a collection of trap models (using the present notation). The present results suggest that a similar description might also work in non-equilibrium situations.

An asymmetry akin to the one discussed above between cooling and heating has been observed in experiments. In 1989 Bokov and Andreev[25] reported anomalously high intensity of (static) light scattering (at 90 degrees) from vitreous  $B_2O_3$  during heating, but only at intermediate times when the system goes through the glass transition. Thus the previous cooling that produced the borate glass produced no such anomalous signal. Since the static light scattering intensity is proportional to the density fluctuations, the implication is that a glass upon heating temporarily goes through a phase characterized by anomalously large density fluctuations. Moynihan, Schroeder, and coworkers[26, 27] pointed out that this behavior is consistent with the presence of nanoscale density fluctuations which relax at different rates. If, as suggested by Brawer[28], energy and density correlate locally such that low density corresponds to high energy, the trap model provides a simple way to understand these phenomena[9]. In this "volume-energy correlation" model the anomalous light scattering signals are direct proof of the above discussed two-peak structure in the energy distribution upon heating.

If we assume that the energies considered in our present study (either IS- or MB-energies)

can directly be related to activation energies relevant for the dynamics of supercooled liquids, we can speculate about possible implications of our findings. As mentioned in the Introduction, the primary relaxation appears to be the driving force for the aging dynamics. Furthermore, it has been found by a thorough analysis of probe rotation and translation data that the width of the distribution of relaxation times appears to decrease for intermediate times during aging after a quench[6]. This finding is in accord with the fact that the distribution of activation energies shows the same time-dependence. Our results for an up-jump thus suggest that the width of the relaxation time distribution should broaden and then narrow again as a function of the time elapsed after the up-jump.

As another experimental technique that possibly can show a intermittent narrowing for a quench and a broadening for an up-jump is provided by measurements of the enthalpy relaxation following sudden temperature changes. However, we have to point out here that at the same time the relaxation time decreases which may make it difficult to observe the effect of a broadening.

Other interesting implications of our results might arise when one compares different theoretical approaches to the glass transition problem that in equilibrium might give rise to very similar results. We hope that our findings will stimulate calculations of the details of the aging dynamics for different models and probably help to discriminate among them.

## Acknowledgment

We thank Roland Böhmer and Gerald Hinze for fruitful discussions. Financial support of the work in Münster by the Deutsche Forschungsgemeinschaft via the SFB 458 is acknowledged. The centre for viscous liquid dynamics "Glass and Time" is sponsored by the Danish National Research Foundation (DNRF).

## Appendix: The trap model

The trap model was introduced into glass science in 1987[21]. The temporal evolution of the population of a considered trap is determined by the escape rate  $\kappa_T(\epsilon) = \kappa_\infty e^{\beta\epsilon}$  which depends only on the trap-energy. (The rate  $\kappa_\infty$  gives the overall time scale. Throughout the calculations the time is measured in units of  $\kappa_\infty$ .) After the escape from a given trap the destination trap is chosen at random. In a continuous formulation, the populations obey the following master equation:

$$\dot{p}_T(\epsilon, t) = -\kappa_T(\epsilon)p_T(\epsilon, t) + \rho(\epsilon) \int d\epsilon' \kappa_T(\epsilon') p_T(\epsilon', t) \quad (\text{A.1})$$

We have used the subscript  $T$  to emphasize that  $p_T(\epsilon, t)$  depends on temperature  $T = 1/\beta$ . Throughout the calculations the DOS is chosen to be Gaussian

$$\rho(\epsilon) = \frac{1}{\sqrt{2\pi}\sigma} e^{-\epsilon^2/(2\sigma^2)} \quad (\text{A.2})$$

with  $\sigma = 1$ . This choice for the DOS guarantees that the system reaches equilibrium at all temperatures (temperatures are measured in units of  $\sigma$ ). The corresponding equilibrium populations

at a given temperature  $T$  are found to be Gaussian:

$$p_T^{\text{eq}}(\epsilon) = \frac{1}{\sqrt{2\pi}\sigma} e^{-(\epsilon - \bar{\epsilon}_T)^2 / (2\sigma^2)} \quad \text{with} \quad \bar{\epsilon}_T = -\beta\sigma^2 \quad (\text{A.3})$$

The solution of eq.(A.1) allows the computations of all quantities of interest. For instance, the population of the trap with trap energy  $\epsilon$  is given by

$$p_T(\epsilon, t) = \int d\epsilon_0 G_T(\epsilon, t - t_0 | \epsilon_0) p(\epsilon_0, t_0) \quad (\text{A.4})$$

where  $p(\epsilon_0, t_0)$  denotes the population at the initial time  $t_0$  and  $G_T(\epsilon, t - t_0 | \epsilon_0)$  is the conditional probability to find the system in trap  $\epsilon$  at time  $t$  provided it started in  $\epsilon_0$  at  $t_0$ . The initial population is usually taken as the equilibrium population at the initial temperature  $T_0$ ,

$$p(\epsilon_0, t_0) = p_{T_0}^{\text{eq}}(\epsilon_0), \quad (\text{A.5})$$

cf. eq.(A.3). From eq.(A.4), one can obtain all further quantities like the observables, for example the moments of the energy distribution

$$E_T^n(t) = \int d\epsilon \epsilon^n p_T(\epsilon, t). \quad (\text{A.6})$$

We solely consider instantaneous changes of temperature  $T_0 \rightarrow T$ , changes with a finite cooling or heating rate can be considered in a similar way, by assuming constant temperatures in small time-intervals. As the populations reach equilibrium for long times,  $p(\epsilon, t \rightarrow \infty) = p_T^{\text{eq}}(\epsilon)$ , we find after a temperature jump from  $T_0$  to  $T$  that the energy evolves according to eq.(A.6) with  $n = 1$  and that  $E(t = 0) = E_{T_0}^{\text{eq}} = -\beta_0\sigma^2$  and the final value  $E(\infty) = E_T^{\text{eq}} = -\beta\sigma^2$ .

## References

- [1] H. Sillescu, J. Non-Cryst. Solids **243**, 81 (1999).
- [2] M. Ediger, Annu. Rev. Phys. Chem. **51**, 99 (2000).
- [3] J.-P. Bouchaud, L. Cugliandolo, and M. Mezard, *in: Spin Glasses and Random Fields*, Editor: A.P. Young, World Scientific, Singapore, 1998.
- [4] A. Crisanti and F. Ritort, J. Phys. A-Math. Gen. **36**, R181 (2003).
- [5] S. Jabbari-Farouji et al., Europhys. Lett. **84**, 20006 (2008).
- [6] C. Thureau and M. Ediger, J. Chem. Phys. **116**, 9089 (2002).
- [7] P. Lunkenheimer, R. Wehn, U. Schneider, and A. Loidl, Phys. Rev. Lett. **95**, 055702 (2005).
- [8] A. Heuer, J. Phys.: Condens. Mat. **20**, 373101 (2008).

- [9] J. C. Dyre, Phys. Rev. B **51**, 12276 (1995).
- [10] R. Denny, D. Reichman, and J. Bouchaud, Phys. Rev. Lett. **90**, 025503 (2003).
- [11] A. Heuer, B. Doliwa, and A. Saksangwijit, Phys. Rev. E **72**, 021503 (2005).
- [12] W. Kob and H. C. Andersen, Phys. Rev. E **51**, 4626 (1995).
- [13] W. Kob and H. C. Andersen, Phys. Rev. E **52**, 4134 (1995).
- [14] I. Saika-Vovoid and F. Sciortino, Phys. Rev. E **70**, 041202 (2004).
- [15] G. Diezemann, J. Chem. Phys. **123**, 204510 (2005).
- [16] M. Warren and J. Rottler, Europhys. Lett. **88**, 58005 (2009).
- [17] B. Doliwa and A. Heuer, Phys. Rev. E **67**, 031506 (2003).
- [18] G. Diezemann, J. Phys.: Condens. Mat. **19**, 205107 (2007).
- [19] C. Monthus and J. Bouchaud, J. Phys. A-Math. Gen. **29**, 3847 (1996).
- [20] C. Angell, K. Ngai, G. McKenna, P. McMillan, and S. Martin, J. Appl. Phys. **88**, 3113 (2000).
- [21] J. C. Dyre, Phys. Rev. Lett. **58**, 792 (1987).
- [22] V. Arkhipov, M. Iovu, A. Rudenko, and S. Shutov, Phys. Status Solidi (a) **54**, 67 (1979).
- [23] S. Buchner and A. Heuer, Phys. Rev. Lett **84**, 2168 (2000).
- [24] C. Rehwald, O. Rubner, and A. Heuer, arXiv:1003.0781 (2010).
- [25] N. Bokov and N. Andreev, Sov. J. Glass Phys. Chem. **15**, 243 (1989).
- [26] C. T. Moynihan and J. Schroeder, J. Non-Cryst. Solids **160**, 52 (1993).
- [27] J. Schroeder, M. Lee, S. K. Saha, J. H. Wang, and C. T. Moynihan, J. Non-Cryst. Solids **203**, 186 (1996).
- [28] S. A. Brawer, J. Chem. Phys. **81**, 954 (1981).

## Predicting the Effective Temperature of a Glass

Nicoletta Gnan,\* Claudio Maggi, Thomas B. Schröder, and Jeppe C. Dyre

*DNRF Center “Glass and Time,” IMFUFA, Department of Sciences, Roskilde University, P.O. Box 260, DK-4000 Roskilde, Denmark*  
(Received 23 December 2009; published 24 March 2010)

We explain the findings by Di Leonardo *et al.* [Phys. Rev. Lett. **84**, 6054 (2000)] that the effective temperature of a Lennard-Jones glass depends only on the final density in the volume and/or temperature jump that produces the glass. This is not only a property of the Lennard-Jones liquid, but a feature of all strongly correlating liquids. For such liquids data from a single quench simulation provide enough information to predict the effective temperature of any glass produced by jumping from an equilibrium state. This prediction is validated by simulations of the Kob-Andersen binary Lennard-Jones liquid and shown not to apply for the nonstrongly correlating monatomic Lennard-Jones Gaussian liquid.

DOI: 10.1103/PhysRevLett.104.125902

PACS numbers: 65.20.-w

Condensed matter is frequently found in out-of-equilibrium states. For example, for systems like supercooled liquids, dense colloids, spin systems, etc., the (off-equilibrium) glass state occurs naturally after cooling or compression from a state of thermal equilibrium. An effective temperature describes the nonequilibrium properties of a glass, and the possibility of connecting the effective temperature with the observed violation of the fluctuation-dissipation theorem (FDT) [1] has opened new ways of inquiry [2–6]. In 2000, Di Leonardo *et al.* [5] studied the off-equilibrium dynamics of the single-component Lennard-Jones (LJ) liquid (with a small many-body term added to the potential to prevent crystallization). This system was subjected to sudden temperature decreases at constant density (quenches) as well as to sudden density increases at constant temperature (crunches). From the violation of the FDT, the effective temperature was determined. Surprisingly, it was observed that the effective temperature  $T_{\text{eff}}$  is independent of the particular path in the temperature-density plane crossing the glass transition line:  $T_{\text{eff}}$  depends only on the final density. In this Letter we demonstrate that the findings of Di Leonardo *et al.* hold generally for strongly correlating liquids (defined below). We further argue and demonstrate that—for this class of liquids—from a single quench simulation one can predict the effective temperature for any off-equilibrium jump.

Reference [7] documented the existence of a large class of liquids characterized by strong correlations between virial ( $W \equiv pV - Nk_B T$ ) and potential energy ( $U$ ) thermal equilibrium fluctuations at fixed volume,  $\Delta W(t) \cong \gamma \Delta U(t)$ . Strongly correlating liquids have a hidden (approximate) scale invariance, which implies that they inherit many—but not all—of the scaling properties of liquids interacting via inverse power-law potentials. Strongly correlating liquids include van der Waals-type liquids but not, e.g., hydrogen-bonding liquids. Strongly correlating liquids have curves in their phase diagrams—“isomorphs”—along which several static and dynamic prop-

erties are invariant [8]. These invariants derive from the fact that two microscopic configurations of two isomorphic state points, which scale into one another, to a good approximation have identical canonical probabilities. If the density is denoted by  $\rho$ , an isomorph is given by  $\rho^\gamma/T = \text{const}$ . The exponent  $\gamma$ —which may be slightly state-point dependent—can be calculated from equilibrium fluctuations at one state point or from a single quench simulation utilizing the relation between the relaxing averages,  $\langle W(t) \rangle \cong \gamma \langle U(t) \rangle + W_0$ .

Because the canonical probabilities of scaled configurations belonging to the same isomorph are identical, a jump between two isomorphic state points takes the system instantaneously to equilibrium [property (i)][8]. Moreover, jumps from isomorphic state points to the same final state point show identical aging behavior [property (ii)] [8]. In view of these properties the results of Di Leonardo *et al.* [5] may be understood as follows. A crunch from density  $\rho_1$  to density  $\rho_2$  can be ideally decomposed into two parts (Fig. 1): First, the system jumps instantaneously from its initial state to the corresponding isomorphic state at the final density (i.e., the state which has the same  $\rho^\gamma/T$  as the initial state); see Fig. 1. This is an equilibrium state [8]. Thereafter the system at constant density begins to approach the equilibrium state defined by the temperature. If the crunch is made to a state with very high density, the thermalization takes an extremely long time and the effective temperature may be determined from the FDT violation as detailed below. In this way any crunch corresponds to a quench to the final density with the same relaxation pattern. In particular, these two transformations should have identical FDT violation factors and identical effective temperatures.

These arguments should apply to any strongly correlating liquid, not just the single-component LJ system. To confirm this we simulated the Kob-Andersen binary Lennard-Jones (KABLJ) liquid [9,10]. Following Di Leonardo *et al.* [5] we subjected the KABLJ liquid to a number of instantaneous quenches and crunches and

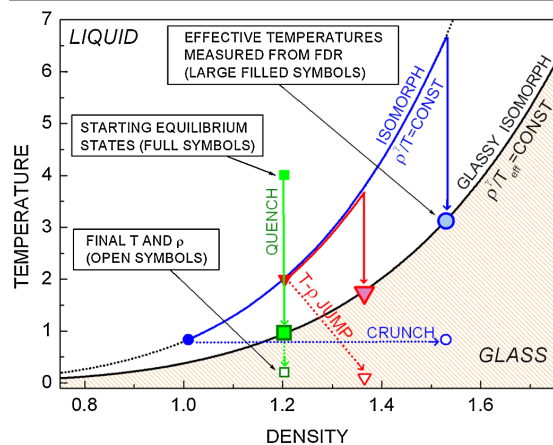


FIG. 1 (color online). Patterns followed by the KABLJ liquid in different off-equilibrium density and/or temperature jumps. Consider, for example, the case of a crunch (horizontal dotted line), where the system is densified at constant temperature. This transformation is equivalent to a quench (right-most vertical line) from an isomorphic state point having the final density of the crunch. Thus the  $T_{\text{eff}}$  (large filled circle) is identical for these transformations. In all processes represented here the liquid undergoes a glass transition characterized by an effective temperature that can be measured from the fluctuation-dissipation relation (FDR) Eq. (1).  $T_{\text{eff}}$  versus (final) density constitutes an isomorph, as discussed later in the text.

calculated the effective temperatures from the fluctuation-dissipation relation (FDR). Recall that for off-equilibrium systems the FDR in  $k_B = 1$  units is [11–15]

$$T \partial_{t'} \chi(t, t') = -X(t, t') \partial_{t'} C(t, t'). \quad (1)$$

Here  $C = \langle A(t)B(t') \rangle$  is the correlation function of the variables  $A$  and  $B$  in the unperturbed situation, the perturbing contribution to the Hamiltonian is  $\delta H = -\epsilon B$ ,  $\chi(t, t') = \langle A(t) \rangle / \epsilon |_{\epsilon \rightarrow 0}$  is the response of  $A$  to the perturbation applied at time  $t' < t$ , and  $X$  is the FDT violation factor. This is unity at short times  $(t - t')/t' \ll 1$ , while  $X < 1$  in the long-time limit  $(t - t')/t' \gg 1$ . We chose as dynamic variables  $A_{\mathbf{k}}(t) = N^{-1} \sum_j \eta_j \cos[\mathbf{k} \cdot \mathbf{r}_j(t)]$  and  $B_{\mathbf{k}}(t) = 2NA_{\mathbf{k}}(t)$ , where the sum is extended to all  $N$  particles of the system and  $\eta_j = \pm 1$  is a random variable with zero mean. With this choice the correlation function  $C(t, t')$  is the self-intermediate scattering function.

For quenches to low enough temperatures, at long times an effective temperature of the slow degrees of freedom is associated with the FDT violation factor:  $T_{\text{eff}} = T/X$  [12–16]. The effective temperature reflects the slow structural rearrangements in the sense that the aging system behaves as if it were thermalized at  $T_{\text{eff}}$  [16]. We obtained  $X$  by calculating the correlation function and the response function in the nonequilibrium regime by means of  $X = X(t) = -T \partial_{t'} \chi(t, t') / \partial C(t, t')$ , which applies at long times (note

that the correct  $X$  is found by taking this derivative at fixed  $t$ , not at fixed  $t'$  [17]).

Recently Berthier introduced a new method for calculating the response without applying an external field for an off-equilibrium Monte Carlo simulation of the KABLJ [17]. Using his procedure Fig. 2 shows the FD plots for the KABLJ liquid during a number of temperature-density jumps. In Fig. 2 we test the construction of equivalent crunches and quenches argued above: a crunch and a quench from initially isomorphic states (i.e., with the same  $\rho^2/T$ ) to the same final  $T$  and  $\rho$  (red circles and red squares). Clearly the crunch overlaps well with the quench; in fact, they follow the same aging pattern. The exponent  $\gamma$  was estimated by a linear fit of the parameter plot  $\langle W(t) \rangle$  vs  $\langle U(t) \rangle$  when the system is relaxing after a temperature jump from  $T = 2.55$  to  $T = 0.3192$  at fixed  $\rho = 1.264$ . The resulting value is  $\gamma = 5.01$  (for details, refer to Ref. [10]). Figure 3 shows the linear relation that connects  $\langle W(t) \rangle$  and  $\langle U(t) \rangle$  during two “isomorphic” quenches.

Identical responses and correlations do not only appear when a strongly correlating liquid is taken from two isomorphic states to the same state point. Supplementing properties (i) and (ii), strongly correlating liquids have a

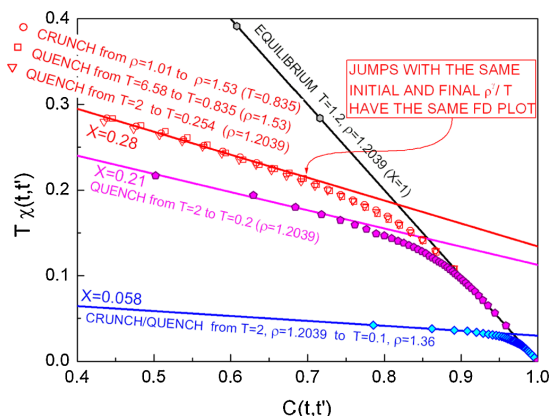


FIG. 2 (color online). Response versus correlation function for several density or temperature jumps for the KABLJ liquid. All FD plots have fixed  $t = 10^4$  (Monte Carlo steps) and  $t'$  varying from  $10^3$  to  $10^4$ . All functions plotted here have the same reduced  $k$ -vector (referring to the final density) and the same reduced microscopic time. In the crunch (○) we set  $|\mathbf{k}| = 7.81$  corresponding to the reduced  $k$ -vector  $|\bar{\mathbf{k}}| = 6.78$  (see Ref. [10] for details). The crunch (○) overlaps very well with the quench (□) that takes the system from an initial state isomorphic to the one of the crunch to the same final state. Note also the good superposition of the additional quench (▽) that takes the system from a state isomorphic to the initial state of (○) to a state isomorphic to the final one of (○). The full lines have the slopes predicted from the density-scaling relation Eq. (2) for  $T_{\text{eff}}$ .

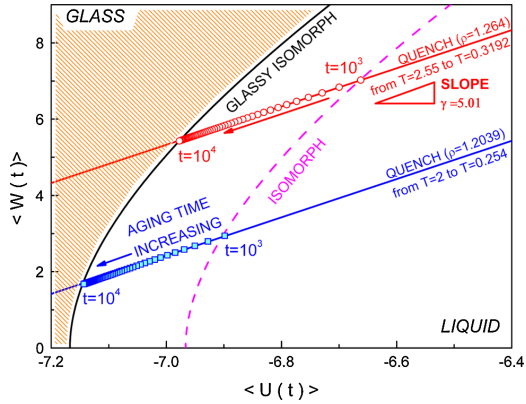


FIG. 3 (color online). Average virial versus potential energy per particle during aging in two quenches for the KABLJ liquid. These quenches were performed between states with same initial and final  $\rho^\gamma/T$ . At each time the off-equilibrium states are connected by an isomorph (e.g., the dashed line). In these two jumps the FDT violation factor  $X$  should be identical. The slope of the  $\langle W(t) \rangle$  vs  $\langle U(t) \rangle$  plot is  $\gamma$ . The analytical equation used for drawing the isomorphs in the  $W$ - $U$  plot here is reported in Ref. [20].

third interesting aging property (iii): For two jumps  $(T_1, \rho_1) \rightarrow (T_2, \rho_2)$  and  $(T_3, \rho_3) \rightarrow (T_4, \rho_4)$  between mutually isomorphic initial and final states (i.e.,  $\rho_1^\gamma/T_1 = \rho_3^\gamma/T_3$  and  $\rho_2^\gamma/T_2 = \rho_4^\gamma/T_4$ ), the systems follow the same path in configuration space in reduced units [10] because the dynamical equations governing the evolution of the particle trajectories are identical in reduced units. Accordingly, the responses and correlations of two such jumps must be identical in reduced units. In Fig. 2 we show the reduced unit  $C$  and  $\chi$  of a quench between initial and final states that are isomorphic, respectively, to the initial and final states of the crunch described above (red triangles). The overlap between the functions is good. Figure 3 shows the variables  $\langle W(t) \rangle$  vs  $\langle U(t) \rangle$  in two such isomorphic jumps; they are connected by an isomorph at each time during the relaxation.

A further consequence of property (iii) is the following. Because the reduced-unit evolution is the same for the system in the two jumps, their FDR violation factors must also be identical,  $X_2 = X_4$ . Combining this equation with  $\rho_2^\gamma/T_2 = \rho_4^\gamma/T_4$  and expressing  $X$  via the effective temperature, we find  $\rho_2^\gamma/T_{\text{eff},2} = \rho_4^\gamma/T_{\text{eff},4}$ , i.e.,

$$\rho^\gamma/T_{\text{eff}} = \text{const.} \quad (2)$$

This equation identifies the glass transition curve in the  $(T, \rho)$  plane defined in terms of the FDR effective temperature with an isomorph. This is consistent with the findings of Ref. [5] and the standard way of defining the glass transition, because the standard glass line in the  $(T, \rho)$  plane is located where the equilibrium relaxation

time reaches a certain (high) value of order the inverse cooling rate. For strongly correlating liquids an isomorph is also an “isochronal” curve along which the (reduced) relaxation time is constant [8]. Figure 2 shows the slopes predicted by Eq. (2) (lines); clearly the prediction is fulfilled.

It is well known (see, for example, Refs. [4,17]) that the effective temperature is independent of the initial and final temperature if the initial temperature is high (the system is in a warm liquid state) and if the quenching temperature is low enough (i.e., in the regime where  $X = T/T_{\text{eff}}$  with constant  $T_{\text{eff}}$ ). Consequently, Eq. (2) predicts the effective temperatures for all possible jumps ending at density  $\rho$ . The exponent  $\gamma$  and the constant may both be calculated from the results of one single aging simulation. In Fig. 4 we compare  $T_{\text{eff}}$  identified from several crunches and quenches (not only involving isomorphic initial and final state points) with the prediction of Eq. (2). The agreement is very good.

The above discussed simple aging properties are only expected to apply for liquids with isomorphs, i.e., strongly correlating liquids. To validate this we simulated the non-equilibrium dynamics of the monatomic Lennard-Jones Gaussian (MLJG) model [18]. The pair potential of the MLJG has an additional Gaussian attractive well compared to the LJ liquid (see the inset of Fig. 5); details about the model’s potential and its glassy behavior can be found in Ref. [18]. The MLJG liquid has  $WU$  fluctuations which correlate less than 2% at the state points studied here. As is clear from Fig. 5, two jumps to the same final density lead to quite different effective temperatures. Thus, this system provides a counterexample to the observation by

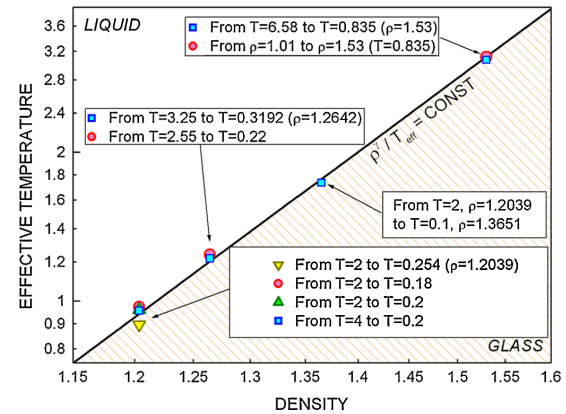


FIG. 4 (color online). Effective temperature as a function of density in several crunch and/or quenches (in double log scale) for the KABLJ liquid. The effective temperature is computed from the violation factor:  $T/T_{\text{eff}} = X = -T\partial\chi(t, t')/\partial C(t, t')|_t$ . The scaling exponent  $\gamma$  is computed from potential energy-virial relaxation (see Fig. 3) as described in the text. The full line is the prediction of the density scaling equation (2) for  $T_{\text{eff}}$ .

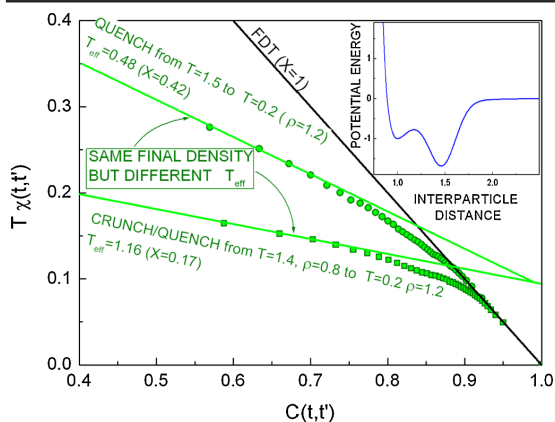


FIG. 5 (color online). FD plot for two jumps of the MLJG liquid ending at same final density and temperature. The potential defining this model is shown in the inset. In this case the two effective temperatures are very different.

Di Leonardo *et al.* [5] that the effective temperature depends only on the final density.

We also investigated the relation between the inherent state energies in aging and at equilibrium for the KABLJ and the MLJG liquids (see Ref. [10] for more details). Only for the strongly correlating liquid KABLJ can one interpret  $T_{\text{eff}}$  as an indicator of which part of the energy landscape is visited during aging, confirming a suggestion by Sciortino and Tartaglia in [19].

In conclusion, the existence of isomorphs for strongly correlating liquids explains the previously reported result [5] for the LJ liquid that the effective temperature depends only on the final density of any jump (when temperature and density are the externally controlled variables). We presented simulations of the aging dynamics of another strongly correlating liquid, the KABLJ liquid, as well as simulations of aging of a liquid without strong virial or potential energy correlations (the MLJG liquid). For strongly correlating liquids it is always possible to produce equivalent density or temperature transformations connected by the density-scaling relation. Moreover, for this class of liquids the effective temperature satisfies the density-scaling equation (2). Since the exponent  $\gamma$  and the constant of Eq. (2) may both be identified from a single quench simulation, the implication is that for a strongly

correlating liquid the effective temperature of an arbitrary glass may be calculated from the results of a single jump simulation.

The center for viscous liquid dynamics *Glass and Time* is sponsored by the Danish National Research Foundation (DNRF).

\*ngnan@ruc.dk

- [1] J.-P. Hansen and I.R. Mc-Donald, *Theory of Simple Liquids* (Academic, New York, 2006).
- [2] G. Parisi, Phys. Rev. Lett. **79**, 3660 (1997).
- [3] M. Sellitto, Eur. Phys. J. B **4**, 135 (1998).
- [4] W. Kob and J.L. Barrat, Europhys. Lett. **46**, 637 (1999).
- [5] R. Di Leonardo, L. Angelani, G. Parisi, and G. Ruocco, Phys. Rev. Lett. **84**, 6054 (2000).
- [6] R.L. Jack, M.F. Hagan, and D. Chandler, Phys. Rev. E **76**, 021119 (2007).
- [7] U.R. Pedersen *et al.*, Phys. Rev. Lett. **100**, 015701 (2008); Phys. Rev. E **77**, 011201 (2008); N.P. Bailey *et al.*, J. Chem. Phys. **129**, 184507 (2008); **129**, 184508 (2008); T.B. Schröder *et al.*, Phys. Rev. E **80**, 041502 (2009).
- [8] N. Gnan, T.B. Schröder, U.R. Pedersen, N.P. Bailey, and J.C. Dyre, J. Chem. Phys. **131**, 234504 (2009).
- [9] W. Kob and H.C. Andersen, Phys. Rev. Lett. **73**, 1376 (1994); L. Berthier and W. Kob, J. Phys. Condens. Matter **19**, 205130 (2007).
- [10] See supplementary material at <http://link.aps.org/supplemental/10.1103/PhysRevLett.104.125902> for simulation details, definitions of the reduced units, and the study of the off-equilibrium landscape in the two systems studied.
- [11] U.M. Marconi, A. Puglisi, L. Rondoni, and A. Vulpiani, Phys. Rep. **461**, 111 (2008).
- [12] J. Kurchan, Nature (London) **433**, 222 (2005).
- [13] A. Crisanti and R. Ritort, J. Phys. A **36**, R181 (2003).
- [14] L.F. Cugliandolo, *Slow Relaxations and Nonequilibrium Dynamics in Condensed Matter*, Dynamics of Glassy Systems Course 7 (Springer, Berlin, 2004).
- [15] C. Chamon and L.F. Cugliandolo, J. Stat. Mech. (2007) P07022.
- [16] L. Leuzzi, J. Non-Cryst. Solids **355**, 686 (2009).
- [17] L. Berthier, Phys. Rev. Lett. **98**, 220601 (2007).
- [18] V. Van Hoang and T. Odagaki, Physica (Amsterdam) **403B**, 1803 (2008).
- [19] F. Sciortino and P. Tartaglia, Phys. Rev. Lett. **86**, 107 (2001).
- [20] N. Gnan *et al.*, arXiv:0905.3497v1.